# GEOLOGICAL SURVEY RESEARCH 1966

# Chapter B

GEOLOGICAL SURVEY PROFESSIONAL PAPER 550-B

*Scientific notes and summaries of investigations by members of the Conservation, Geologic, Topographic, and Water Resources Divisions in geology, hydrology, and related fields*

UNITED STATES GOVERNMENT PRINTING OFFICE, WASHINGTON: 1966

UNITED STATES DEPARTMENT OF THE INTERIOR

STEWART L. UDALL, Secretary

GEOLOGICAL SURVEY

William T. Pecora, Director

For sale by the Superintendent of Documents, U.S. Government Printing Office,
Washington, D.C., 20402 - Price $2.00

# CONTENTS

## GEOLOGIC STUDIES

# GEOLOGICAL SURVEY RESEARCH 1966

This collection of 43 short papers is the first published chapter of "Geological Survey Research 1966." The papers report on scientific and economic results of current work by members of the Conservation, Geologic, Topographic, and Water Resources Divisions of the U.S. Geological Survey.

Chapter A, to be published later in the year, will present a summary of significant results of work done during fiscal year 1966, together with lists of investigations in progress, reports published, cooperating agencies, and Geological Survey offices.

"Geological Survey Research 1966" is the seventh volume of the annual series Geological Survey Research. The six volumes already published are listed below, with their series designations.

Geological Survey Research 1960—Prof. Paper 400
Geological Survey Research 1961—Prof. Paper 424
Geological Survey Research 1962—Prof. Paper 450
Geological Survey Research 1963—Prof. Paper 475
Geological Survey Research 1964—Prof. Paper 501
Geological Survey Research 1965—Prof. Paper 525

# UNCONFORMITY BETWEEN GNEISSIC GRANODIORITE AND OVERLYING YAVAPAI SERIES (OLDER PRECAMBRIAN), CENTRAL ARIZONA

By P. M. BLACET, Beltsville, Md.

*Abstract.*—Granodiorite older than isoclinally folded schists of the Yavapai Series is uniquely exposed in the core of an upfaulted anticline at Brady Butte southeast of Prescott, Ariz. A folded unconformity at the base of the Alder Group of the Yavapai Series is well exposed in an area of about 3 square miles, providing the only known exposure of the depositional contact between the older Precambrian Yavapai Series and a still older basement. The herein named Brady Butte Granodiorite predates the Mazatzal revolution, during which the overlying Alder Group was metamorphosed, and represents a plutonic event older than any previously recognized in Arizona.

Detailed geologic mapping has revealed the occurrence of gneissic granodiorite unconformably below the older Precambrian [1] Yavapai Series (Yavapai Schist of former usage) in the Bradshaw Mountains, Yavapai County, central Arizona. The granodiorite is exposed along a high ridge approximately 15 airline miles southeast of Prescott and 6 miles southwest of Mayer (fig. 1). This gneissic granodiorite is well exposed at Brady Butte, the most prominent geographic feature in the area, and the name Brady Butte Granodiorite is here introduced for this unit. A continuous section through the granodiorite is provided by the canyon of Wolf Creek immediately northeast of Brady Butte; this area serves as the type locality of the formation.

The unconformity between the gneissic granodiorite and basal arkosic metasedimentary rocks of the Yavapai Series represents a major break in the stratigraphic record of the older Precambrian in Arizona. This unconformity is marked by a coarse basal conglomerate that contains large subangular blocks of gneiss indistinguishable from the underlying Brady Butte Granodiorite. The unconformity is exposed in an area of less than 3 square miles, and is the only known exposure of the depositional contact at the base of the Yavapai Series. The Brady Butte Granodiorite represents part of an ancient basement upon which the older Precambrian schists of central Arizona were deposited.

The Yavapai Series consists of metamorphosed sedimentary, pyroclastic, and other volcanic rocks, which are largely included within the greenschist facies. In the Jerome area, Anderson and Creasey (1958, p. 9) have divided the Yavapai Series into the Ash Creek Group and the Alder Group, and have recognized about a dozen formations on the basis of relict textures and structures. In keeping with their usage, the prefix "meta" has been omitted from descriptive terminology used for these older Precambrian rocks.

## STRUCTURAL SETTING

The Brady Butte Granodiorite is exposed in the core of a major faulted anticline that plunges gently north-northeast, and that trends approximately parallel to the strike of foliation in the granodiorite and in the overlying Alder Group (fig. 1). The surface trace of the unconformity between the granodiorite and the Alder Group has a general northwest trend, where it is well exposed along the northeastern wall of the canyon of Wolf Creek for a distance of about 2 miles downstream from the confluence with Little Wolf Creek. North of Brady Butte, along Wolf Creek, the unconformity has been tightly folded, with attenuation of the fold limbs evidenced by flattening and elongation of cobbles in the basal conglomerate. The Brady Butte Granodiorite was mylonitized in the area of tight folding.

Southeastward from locality 46, about 0.8 mile north-northeast of Brady Butte, the folds rapidly diminish in amplitude, and relict sedimentary textures and structures are remarkably preserved in the conglomerate and arkose above the unconformity; the granodiorite beneath is only slightly foliated. The intensity of deformation increases rapidly northeastward away from

[1] The age designation "older Precambrian" has only local significance, and is used in Arizona to distinguish older metamorphic and plutonic rocks from the overlying, unmetamorphosed "younger Precambrian" sedimentary rocks of the Apache Group and the Grand Canyon Series.

U.S. GEOL. SURVEY PROF. PAPER 550-B, PAGES B1-B5

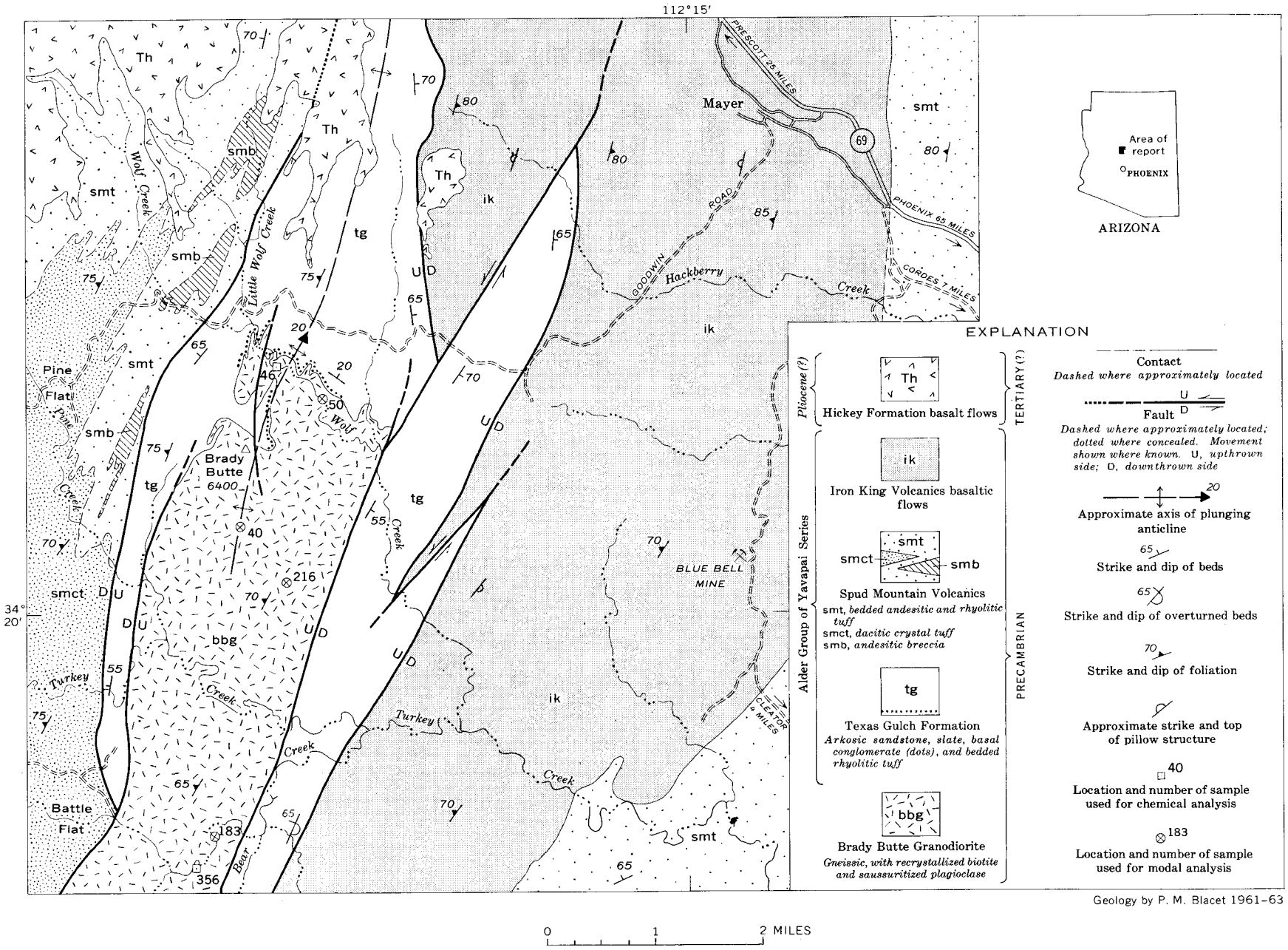


FIGURE 1.—Generalized geologic map of the Brady Butte area, Yavapai County, central Arizona, illustrating the unconformity between the gneissic Brady Butte Granodiorite and the overlying Texas Gulch Formation. Distribution of the deformed basal conglomerate is indicated by stippling along the folded unconformity.

this segment of the unconformity. The remarkable preservation of the rocks near this part of the unconformity indicates that this small area was shielded from the stresses that intensely deformed the adjacent rocks. This small region of low strain directly overlies the relatively undeformed interior of the granodiorite core, which apparently acted as a rigid block deflecting tectonic stresses during metamorphism.

Except where the unconformity is exposed north and northeast of Brady Butte, the contacts between the Brady Butte Granodiorite and the overlying Texas Gulch Formation of the Alder Group are steeply dipping, north-northeast-trending faults. The fault bounding the granodiorite on the west either dies out northward, west of Brady Butte, or diverges from the contact and is undetected within the schists of the Texas Gulch Formation. The fault east of the granodiorite has a left-lateral separation of about 1½ miles, where it offsets the shear zone constituting the contact between the Texas Gulch Formation and the Iron King Volcanics.

The anticlinal block, consisting of the granodiorite and overlying sedimentary rocks, has apparently been squeezed upward along two shear zones which bound the Texas Gulch Formation on the east and west. The displacements on these two major faults are unknown, but the minimum stratigraphic throw along the eastern fault probably exceeds 10,000 feet. Structural and stratigraphic relationships within the isoclinally folded Alder Group suggest that the upfaulted anticline has been elevated several miles with respect to the adjacent volcanic rocks. Erosion has breached the anticlinal core at Brady Butte, providing a unique exposure of the ancient basement beneath schists of the Yavapai Series.

South of the map area (fig. 1), the Brady Butte Granodiorite is truncated by large plutons which are intrusive into the Alder Group. Northward, the Texas Gulch Formation, crudely defining the anticlinal axis, narrows to form a schistose belt several hundred feet wide and disappears beneath Tertiary sedimentary rocks about 10 miles north of Brady Butte (C. A. Anderson and Blacet, unpub. data).

The summit of Brady Butte lies approximately along the axis of the anticline, and a thin cover of arkosic sandstone and the basal conglomerate is draped over the northern shoulder of the butte, between the summit and locality 46 (fig. 1). The unconformity near the summit of Brady Butte is 1,100 feet above its altitude in the canyon of Wolf Creek, indicating that here the anticline plunges approximately 28° north-northeast. Axes of the minor folds in the overlying Texas Gulch Formation generally plunge approximately parallel to the main anticlinal axis.

## BASAL CONGLOMERATE

A remarkable exposure of boulder conglomerate lying directly on the Brady Butte Granodiorite is found 1,000 feet east of the summit of Brady Butte, at an elevation of 6,000 feet. In most places the conglomerate above the unconformity is less than 10 feet thick, but here its thickness is more than 30 feet. Well-rounded cobbles and boulders of leucocratic granophyre as much as 18 inches in diameter are abundant and are mixed with even larger subangular gneissic blocks indistinguishable from the underlying granodiorite (fig. 2). Clasts of chert, argillite, siltstone, and quartzite are also abundant and are commonly flattened or elongated, contrasting with the tough nearly spherical granophyre clasts, which have apparently escaped shear deformation by rotation within the schistose matrix. In the attenuated limbs of the tight folds, north of Brady Butte, the length-to-width ratios of the deformed clasts are commonly as high as 8:1, with the granophyre clasts retaining their original sphericity.

The matrix of the basal conglomerate is poorly sorted arkosic sandstone with angular to subrounded relict grains of quartz, plagioclase, and microcline. Muscovite is the predominant metamorphic mineral, but green biotite is abundant. Foliation is generally apparent and is nearly parallel to the long dimension of deformed clasts, to the foliation in the gneissic blocks, and to the foliation in the Brady Butte Granodiorite.

The basal conglomerate, although widespread, is not evenly distributed along the unconformity, and may have been deposited in channels and depressions on the

FIGURE 2.—Boulder conglomerate at the base of the Texas Gulch Formation exposed on a high spur 1,000 feet east of Brady Butte. The compass rests about 5 feet stratigraphically above the Brady Butte Granodiorite. Light-colored, well-rounded granophyre and felsite clasts are in a schistose matrix of poorly sorted arkose. The compass points to a large angular block of gneissic granodiorite indistinguishable from the Brady Butte Granodiorite.

ancient erosion surface beneath the Alder Group. Southeastward along the main trace of the unconformity, north of Wolf Creek, the basal conglomerate gradually diminishes in thickness and clast size. North of locality 50 (fig. 1) it is a pebble conglomerate 3 feet thick, which grades southeastward into coarse-grained arkose. East-southeast of locality 50 there are a few probable remnants of a Precambrian weathered zone several feet thick at the top of the Brady Butte Granodiorite.

## BRADY BUTTE GRANODIORITE

The granitoid basement beneath the Yavapai Series in the vicinity of Brady Butte has undergone varying degrees of alteration and deformation. On the west flank and north of Brady Butte, the granodiorite has been mylonitized, with intense granulation of the altered plagioclase and preferential preservation of quartz augen. In general, the Brady Butte Granodiorite is somewhat gneissic with a medium- to coarse-grained hypidiomorphic-granular texture. In the field it is characterized by the fine-grained granular biotite, which occurs in crudely oriented patches, and by turbid plagioclase, which is sometimes difficult to distinguish from granulated quartz. The freshest and least deformed rocks are found along watercourses in the interior of the anticlinal core. Recrystallization of the original plutonic mafic minerals is thorough, so that ragged crudely lenticular patches of olive-green biotite, with lesser amounts of epidote, sphene, magnetite, and muscovite constitute the present mafic and accessory constituents. Quartz occurs as large, strained or recrystallized patches which, like microcline, are interstitial to subhedral plagioclase. The plagioclase is invariably altered to a turbid aggregate of clinozoisite and sericite in an albite base; some calcite is present. Twinning is largely obscured by saussuritization and it is impossible to determine the original composition of the plagioclase. Modal analyses of four relatively fresh and undeformed samples of the Brady Butte Granodiorite plot near the center of the granodiorite field on a triangular diagram (fig. 3). Modal analyses were made by point counting polished slabs which were stained for both plagioclase (albite) and potassium feldspar. The average mode of these 4 rocks is as follows: quartz, 27.2 percent; microcline, 15.6 percent; saussuritized plagioclase, 44 percent; and total mafic and accessory minerals (largely biotite), 13.2 percent.

Chemical analyses of mylonitized and of relatively undeformed Brady Butte Granodiorite are presented in table 1. The mylonitized sample (No. 46, fig. 1) was obtained from a fresh exposure along Wolf Creek, approximately 200 feet stratigraphically below the unconformity. Sample 356 represents relatively fresh,

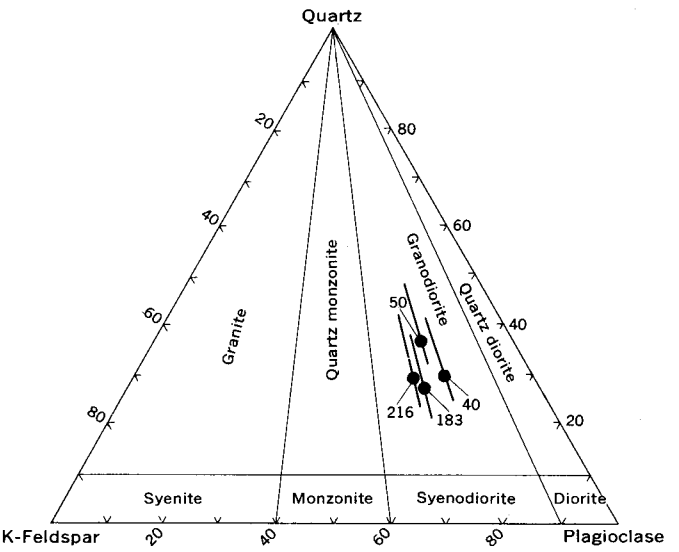


FIGURE 3.—Diagram of modal analyses of the Brady Butte Granodiorite. Length of the inclined lines represents percentage of essential constituents (mostly biotite) not otherwise indicated on the diagram. Numbers refer to sample locations plotted on figure 1.

TABLE 1.—*Chemical analyses and molecular norms of Brady Butte Granodiorite*

[Analyzed by X-ray fluorescence supplemented by methods described by Shapiro and Brannock (1962). Analysts: Paul Elmore, Sam Botts, Gillison Chloe, Lowell Artis, and H. Smith]

| Constituent or normative mineral | Sample (field No.) | |
|---|---|---|
| | 46 | 356 |
| **Chemical analyses** | | |
| $SiO_2$ | 70.5 | 70.8 |
| $Al_2O_3$ | 14.4 | 15.1 |
| $Fe_2O_3$ | .84 | 1.0 |
| FeO | 1.6 | 1.6 |
| MgO | 1.2 | .75 |
| CaO | 2.0 | 1.7 |
| $Na_2O$ | 4.0 | 3.7 |
| $K_2O$ | 3.2 | 3.3 |
| $H_2O^-$ | .06 | .13 |
| $H_2O^+$ | .79 | .78 |
| $TiO_2$ | .21 | .24 |
| $P_2O_5$ | .09 | .31 |
| MnO | .07 | .06 |
| $CO_2$ | 1.0 | .12 |
| **Molecular norms** | | |
| Quartz | 29.7 | 31.6 |
| Orthoclase | 19.1 | 18.8 |
| Albite | 36.2 | 34.0 |
| Anorthite | 3.1 | 5.3 |
| Corundum | 3.5 | 4.1 |
| Magnetite | .88 | 1.0 |
| Ferrosilite | 1.6 | 1.5 |
| Enstatite | 3.3 | 2.1 |
| Ilmenite | .30 | .34 |
| Apatite | .18 | .67 |
| Calcite | 2.5 | .50 |

46. Mylonitized granodiorite, on Wolf Creek 1 mile north of Brady Butte; lab. No. 163347.
356. Undeformed granodiorite, on Tuscumbia Creek 4 miles south of Brady Butte; lab. No. 163348.

undeformed granodiorite collected 5 miles south of locality 46 (fig. 1). Molecular norms, calculated by Barth's (1962) modification of the Niggli method, accompany the chemical analyses. The chemical analyses of these two contrasting samples of Brady Butte Granodiorite are similar, indicating that mylonitization was not accompanied by significant changes in bulk composition. Addition of $CO_2$ in the mylonitized phase is the most apparent chemical variation and reflects the abundance of calcite, commonly occurring as granular fringes along the boundaries of albitized plagioclase augen.

## AGE OF THE BRADY BUTTE GRANODIORITE

Geologic mapping demonstrates that the gneissic granodiorite at Brady Butte lies unconformably below the Texas Gulch Formation, which is the oldest formation in the Alder Group of the Yavapai Series. The bulk of geologic and radiometric data on the older Precambrian of Arizona suggests a widespread regional metamorphic and plutonic episode about 1,700 million years ago. This orogeny, named the Mazatzal revolution by Wilson (1939), is the most intense and widespread metamorphic event recorded in the geologic history of Arizona. The type locality of the Alder Group is in the Mazatzal Mountains about 60 miles east of Brady Butte (Anderson and Creasey, 1958, p. 20). Recent U-Pb isotopic work on zircon from the older Precambrian complex of the Mazatzal Mountains gives the age of rhyolite in the Yavapai Series as $1,715 \pm 15$ m.y., and that of postdeformational granite as $1,660 \pm 15$ m.y. (Silver, 1965). These ages place the date of the type-Mazatzal orogeny within the interval 1,660 to 1,715 m.y., which corresponds to the age of metamorphism of the Pinal Schist in southeastern Arizona (Silver and Deutsch, 1963). The stratigraphic relations, combined with radiometric dating of the Mazatzal orogeny, indicate that the Brady Butte Granodiorite is older than 1,700 m.y. Isotopic lead dating of zircon from the Brady Butte Granodiorite has confirmed its minimum age as 1,700 m.y. (Anderson, 1963, p. 180).

## DISCUSSION

The occurrence of granodiorite unconformably beneath older Precambrian schists of the Yavapai Series has two principal implications: (1) that a crust of continental character has underlain central Arizona for more than 1,700 m.y.; and (2) that direct evidence now exists in Arizona for a plutonic, and probably orogenic, event predating the Mazatzal revolution. The existence of large volumes of quartzofeldspathic sedimentary and silicic igneous rocks within the older Precambrian of Arizona has long suggested the presence of older granitoid rocks, but the granodiorite at Brady Butte constitutes the first known exposure of this ancient basement.

## REFERENCES

Anderson, C. A., 1963, Simplicity in structural geology, *in* Albritton, C. C., Jr., The fabric of geology: Reading, Mass., Addison-Wesley, p. 175–183.

Anderson, C. A., and Creasey, S. C., 1958, Geology and ore deposits of the Jerome area, Yavapai County, Arizona: U.S. Geol. Survey Prof. Paper 308, 184 p.

Barth, T. F. W., 1962, Theoretical petrology: New York, John Wiley and Sons, Inc., 416 p.

Shapiro, Leonard, and Brannock, W. W., 1962, Rapid analysis of silicate, carbonate, and phosphate rocks: U.S. Geol. Survey Bull. 1144–A, p. A1–A56.

Silver, L. T., 1965, Mazatzal orogeny and tectonic episodicity [abs.]: Geol. Soc. America Spec. Paper 82, p. 185–186.

Silver, L. T., and Deutsch, Sarah, 1963, Uranium-lead isotopic variation in zircon—a case study: Jour. Geology, v. 71, no. 6, p. 721–758.

Wilson, E. D., 1939, Pre-Cambrian Mazatzal revolution in central Arizona: Geol. Soc. America Bull., v. 50, p. 1113–1164.

# TECTONIC MOVEMENT IN THE GRAPEVINE AREA, KERN COUNTY, CALIFORNIA

By BEN E. LOFGREN, Sacramento, Calif.

*Work done in cooperation with the California Department of Water Resources*

*Abstract.*—Tectonic movements during the destructive Arvin-Tehachapi earthquake of 1952 caused a differential uplift of as much as 2 feet in the Tehachapi Mountains south of Wheeler Ridge. Periodic releveling since 1952 indicates an axis of continuing flexure 2 miles south of Grapevine, at the northern edge of the Tehachapi Mountains. Differential movement of bench marks during the period 1953–62 was 0.32 foot, about 7 times the maximum allowable surveying error. It is not known, however, whether the axis area is rising or the areas north and south of the axis are subsiding. In either case, tectonic movement in the mountains evidently is continuing.

Movement along the White Wolf fault south of Bakersfield, in southern California, on July 21, 1952, caused one of California's major earthquakes (magnitude 7.7 on the Richter scale). This was the strongest disturbance in California since the 1906 San Francisco earthquake (Buwalda, 1954, p. 137), and accounted for the loss of 14 lives and estimated property damage of more than $60 million in Kern and Los Angeles Counties (Oakeshott, 1955a, p. 11).

Figure 1 shows the relation of the area of this study to the three principal areas of subsidence in the San Joaquin Valley (Poland and Davis, 1956; Lofgren, 1963). The southern end of the San Joaquin Valley is bounded on the east by the foothills of the Sierra Nevada, on the south by the Tehachapi and San Emigdio Mountains, and on the west by the Temblor Range.

Along most of the northeastern half of its trace, the White Wolf fault traverses or borders intrusive rocks of the Sierra Nevada. Steep mountain slopes facing the valley mark the fault zone, along which as much as 10,000 feet of vertical displacement has occurred since Pliocene time (Dibblee, 1955, p. 30). Along this reach, surface scarps and ruptures developed throughout a fault zone a mile wide and about 17 miles long. Although the position of the fault along the southeastern part of its trace is obscured by Recent valley alluvium,

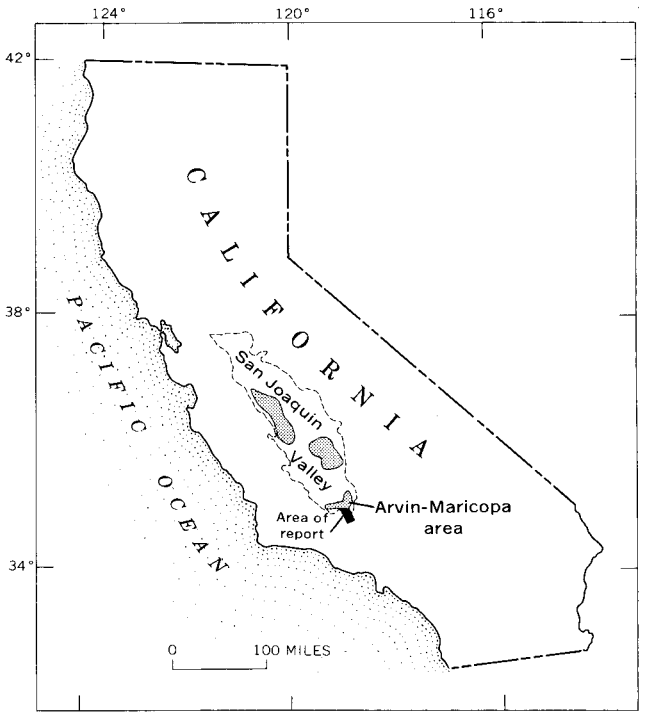


FIGURE 1.—Principal areas of subsidence (shaded) in the San Joaquin Valley, Calif., and the area of this study.

subsurface evidence (Dibblee, 1955, p. 31) indicates that the fault trace continues S. 50° W. and that the fault plane passes at depth under Wheeler Ridge and the San Emigdio foothills. According to Oakeshott (1955b, p. 20) the 1952 earthquake centered at a depth of about 10 miles at lat 35°00′ N. and long 119°02′ W., near Wheeler Ridge. Following the earthquake a complex pattern of cracks and flexures gave evidence of underlying disturbances at a considerable distance from the fault trace. Although the White Wolf fault was considered inactive prior to the 1952 earthquake, movement along it had been recent enough to cause a

major ground-water barrier to form in the valley alluvium (Wood and Dale, 1964, fig. 7 and p. 68).

Soon after the destructive 1952 earthquake, triangulation and leveling networks in the affected areas were resurveyed to determine the direction and amount of surface movement that had occurred. Between October 1952 and March 1953 the U.S. Coast and Geodetic Survey reestablished the position of triangulation stations that had been established the previous winter and also releveled a network of bench marks which had been last surveyed in 1947. These surveys indicated that lateral movement and differential uplift had occurred south of the White Wolf fault.

Subsequent periodic releveling by the U.S. Coast and Geodetic Survey indicates that tectonic movement probably is continuing in the mountainous area south of the White Wolf fault. The possibility of continuing tectonic readjustments is of prime concern in the design and construction of major engineering structures, including a 2,000-foot pump-lift system and several miles of tunnels of the large California Aqueduct.

All the leveling data utilized in the following discussion are from the surveys made by the U.S. Coast and Geodetic Survey.

## TECTONIC MOVEMENT

The displacements attributed by Whitten (1955, fig. 4) to the 1952 earthquake are shown graphically in figure 2; horizontal displacement is shown by vectors and vertical movement by lines of equal change of altitude of the land surface. Although most of the triangulation stations on the mountain block southeast of the fault indicated movement of 1 to 2 feet toward the north-northeast, several stations on the southwestern part of the block indicated movement toward the northwest. Major upwarping occurred south of the fault, with maximum uplift of about 2 feet at Wheeler Ridge near the earthquake epicenter. The extensive depression of the valley west of Arvin, which was first attributed to the 1952 earthquake, has since been shown on the basis of more adequate data to be of nontectonic origin (Lofgren, 1960).

Figure 3 shows the vertical movement of bench mark G 54 for the period 1926–59, based on adjusted altitudes of the U.S. Coast and Geodetic Survey. This bench mark is in the Tehachapi Mountains, about 5 miles south-southeast of Grapevine (fig. 8). As shown, two surveys before and three surveys after the 1952 earthquake indicate that, except for an uplift of 0.45 foot between the 1943 and 1953 levelings, this bench mark has remained at relatively constant elevation. It is assumed that the uplift occurred during the 1952 earthquake.

The vertical movement of bench mark M 54, 2 miles north-northwest of Grapevine, for the period 1926–62, is shown in figure 4. Graph *A* is a direct plot of the published Coast and Geodetic Survey leveling data. The marked uplift that occurred between the 1947 and 1953 leveling is readily apparent. A subsidence trend that preceded 1947 and has continued since 1953 also is clearly shown. Graph *B* is an interpretation of the vertical movement at bench mark M 54. As shown, the movement has been resolved into two components: (1) a general downward trend that has resulted in about 0.45 foot of subsidence (relative to an assumed unchanging datum), and (2) a vertical uplift of 1.77 feet apparently directly related to the 1952 earthquake. In this graphical analysis, the slope of the interpolated curve from 1947 to 1953 is constructed as an average slope between the earlier and later parts of the curve. Although the slow relative subsidence indicated through

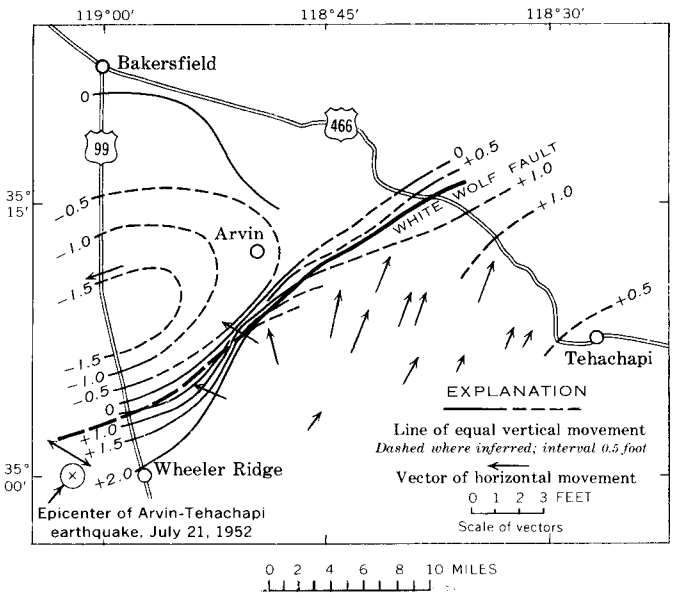


FIGURE 2.—Measurements of earth movement, Arvin-Tehachapi area (after Whitten, 1955, fig. 4).

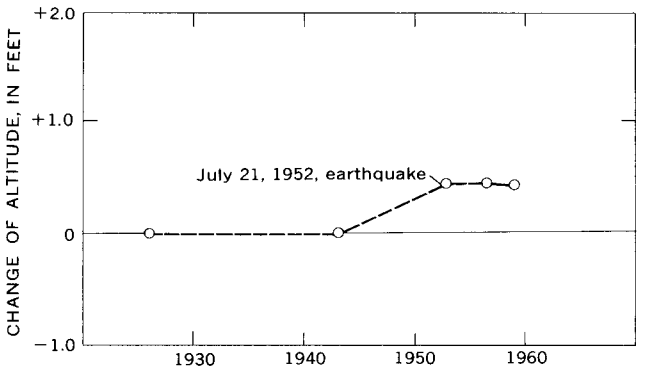


FIGURE 3.—Vertical movement of bench mark G 54, 5 miles south-southeast of Grapevine, 1926–59.

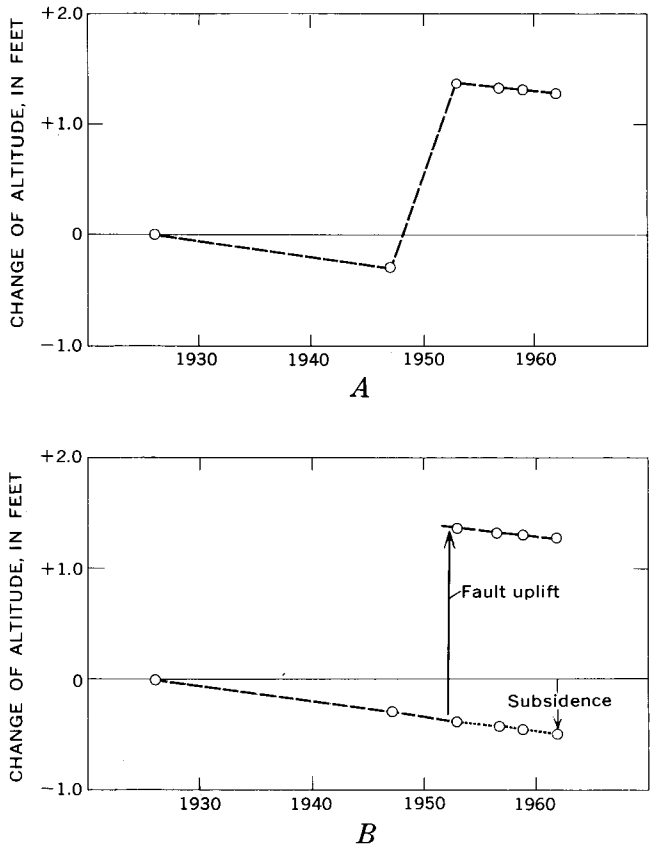


FIGURE 4.—Vertical movement of bench mark M 54, 2 miles north-northwest of Grapevine, 1926–62. *A*, direct plot of U.S. Coast and Geodetic Survey data; *B*, interpretation of movement.

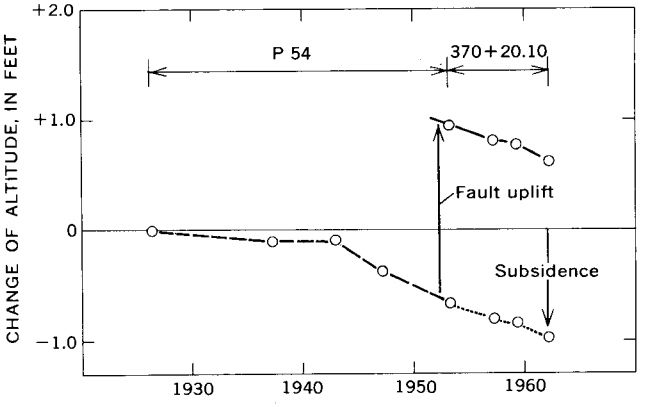


FIGURE 5.—Vertical movement of bench marks P 54 and nearby 370+20.10, about 7 miles north-northwest of Grapevine, 1926–62.

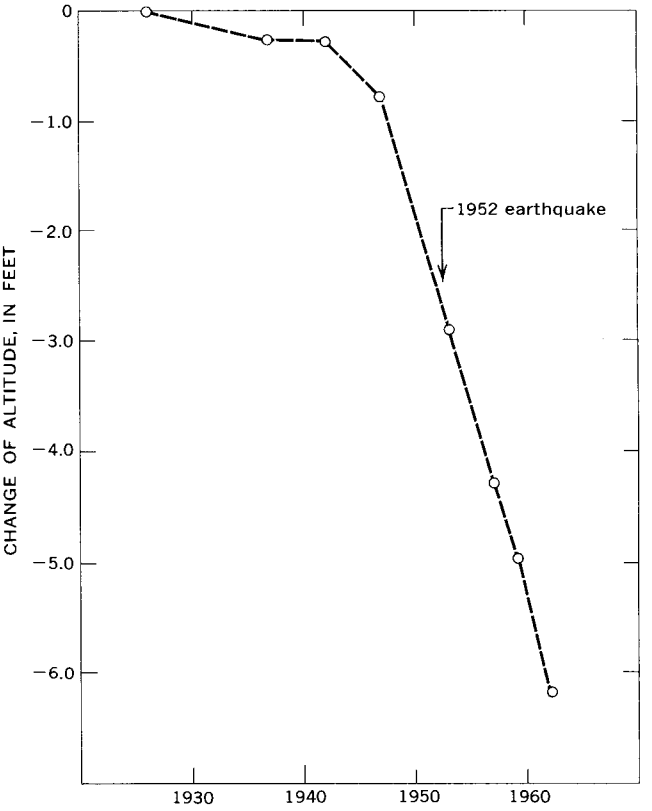


FIGURE 6.—Subsidence trend 14 miles north-northwest of Grapevine, as determined by changes in altitude of three closely spaced bench marks, S 54 (1926–43), A 608 (1943–59) and 713+39.54 (1959–62).

the period of record probably is real, it is possible that the reference bench marks to which the various surveys have been tied are rising at a continuing slow rate. It is noteworthy that the subsidence trend was not interrupted by the 1952 earthquake.

Figure 5 shows the interpreted two components of vertical movement of bench marks P 54 and 370+20.10 just south of the White Wolf fault trace. Bench mark P 54 was last surveyed, and 370+20.10 was first surveyed, in 1953. The data indicate about 0.96 foot of subsidence from 1926 to 1962, and an uplift of 1.61 feet that is attributed to the 1952 earthquake.

Figure 6 shows the trend of subsidence since 1926 in an area of intensive ground-water pumping about 7 miles north-northwest of bench mark 370+20.10 and 14 miles north-northwest of Grapevine. Subsidence at this location, as determined by the change in elevation of three closely spaced bench marks, shows a markedly different trend from that at locations south of the fault. Because rapid subsidence in this area began about 1940 and maintained a steep downward trend through 1962, without apparent interruption by the 1952 earthquake disturbance, it is assumed that no appreciable uplift occurred during the 1952 earthquake. If the leveling data of 1957, 1959, and 1962 were not available it would be difficult to analyze the 1947–53 subsidence without relating it to the 1952 earthquake. These subsequent points on the curve, however, indicate that the 2.1 feet of subsidence that occurred between 1947 and 1953 conformed to the long-term subsidence trend at the bench mark and apparently is directly related to

declining ground-water levels in the area and not to tectonic readjustments.

By means of the method of graphical analysis shown in figures 4 through 6, the vertical displacement attributed to the 1952 earthquake was computed for each bench mark that lies along U.S. Highway 99 from Mettler to Gorman and was leveled prior to and after the 1952 earthquake. Figure 7 shows this computed tectonic uplift. As shown, the up-arching of the mountain block south of the fault between Mettler and Gorman, resulting in a maximum differential uplift of 2 feet, 2–4 miles south of the fault, is in agreement with Whitten's earlier work (fig. 2). A short distance north of the White Wolf fault, however, the effect of the 1952 earthquake is not discernible in bench-mark plots. As noted earlier, the subsidence north of the fault, earlier attributed to tectonic adjustment, is directly related to the accelerated decline of ground-water levels which began in the late 1930's (Lofgren, 1963). It is significant that the maximum computed tectonic uplift along U.S. 99 occurred at bench marks nearest the earthquake epicenter, 2–4 miles south of the White Wolf fault trace; also, that the amount of uplift decreased abruptly to the north and to the south.

Figure 8 shows the measured vertical displacement in the Grapevine area since 1953. The map (*A*), based on releveling of bench marks along U.S. Highway 99 and throughout the contoured area, shows the amount of subsidence that occurred from 1953 to 1962. Changes in altitude of all available bench marks, based on published 1953 leveling data and tentatively adjusted 1962 data, were used in constructing this map. As shown, the 0.1- and 0.2-foot lines of equal subsidence pass through the deformed rocks of Wheeler Ridge. Also, the 0.5- and 1.0-foot lines of equal subsidence apparently cross the trace of the White Wolf fault without interruption.

The upper graph (*B*) in figure 8 shows the measured subsidence along U.S. Highway 99 during the 6 years following the 1952 earthquake. As much as 2.5 feet of subsidence occurred during this period north of the White Wolf fault owing to water-level decline. Also, a differential subsidence occurred along the line of bench marks south of the fault trace. As shown, no subsidence was indicated at bench mark D 367, in the mountains 2 miles south of Grapevine, but relative subsidence occurred both north and south of this axis of flexure. It is noteworthy that this axis is about 6 miles south of the area of maximum uplift during the 1952 earthquake.

The lower graph (*C*) in figure 8 shows the vertical displacement of bench marks along U.S. Highway 99 that occurred during the 3-year period 1959–62. Bench mark H 537, which was the starting reference bench mark for the 1962 leveling, was first leveled in 1957 and for the 1959 and 1962 surveys was considered stable. Leveling data show no change in altitude of bench mark D 367 from 1953, when first leveled, to 1962. The nontectonic subsidence caused by water-level decline extended south about to the trace of the White Wolf fault, and possibly beyond it. In the heavily pumped area north of the White Wolf fault it continued at a maximum annual rate of about 0.5 foot per year. South of the fault, subsidence during the 3-year period decreased from 0.15 foot near the fault to zero at bench mark H 537. Although the observed subsidence south from bench mark 422+24.04 about to U 824 may in part be due to water-level decline, the tectonic subsid-

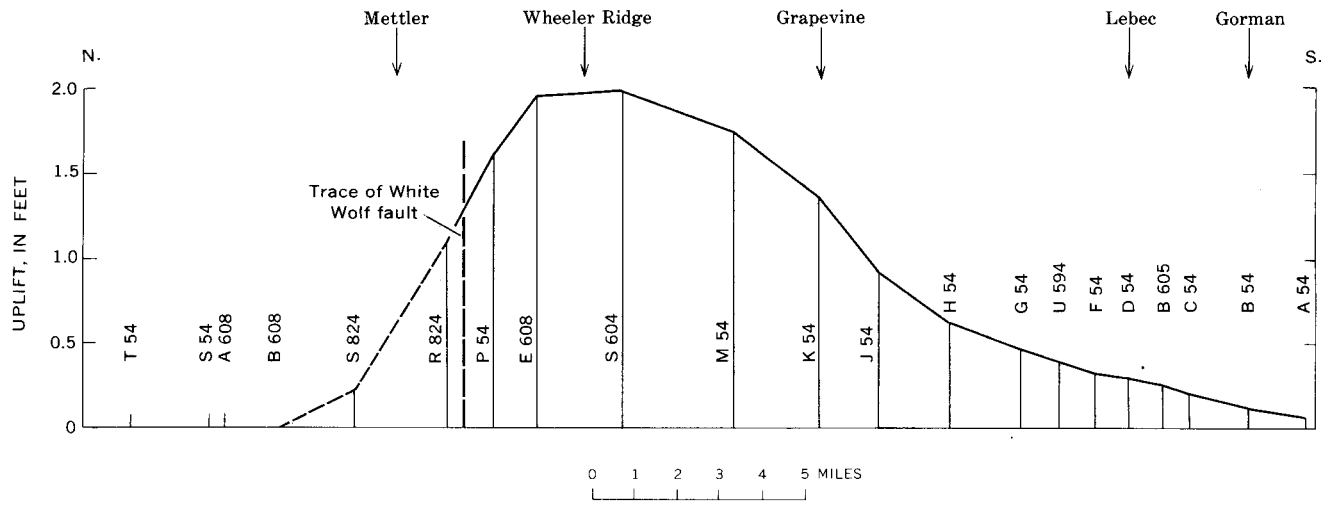


FIGURE 7.—Tectonic uplift along U.S. Highway 99, between Mettler and Gorman, Calif., that is attributed to the 1952 earthquake. Uplift determined by graphical analysis of data according to method illustrated by figures 4–6. Numbers refer to bench marks (location shown on fig. 8).

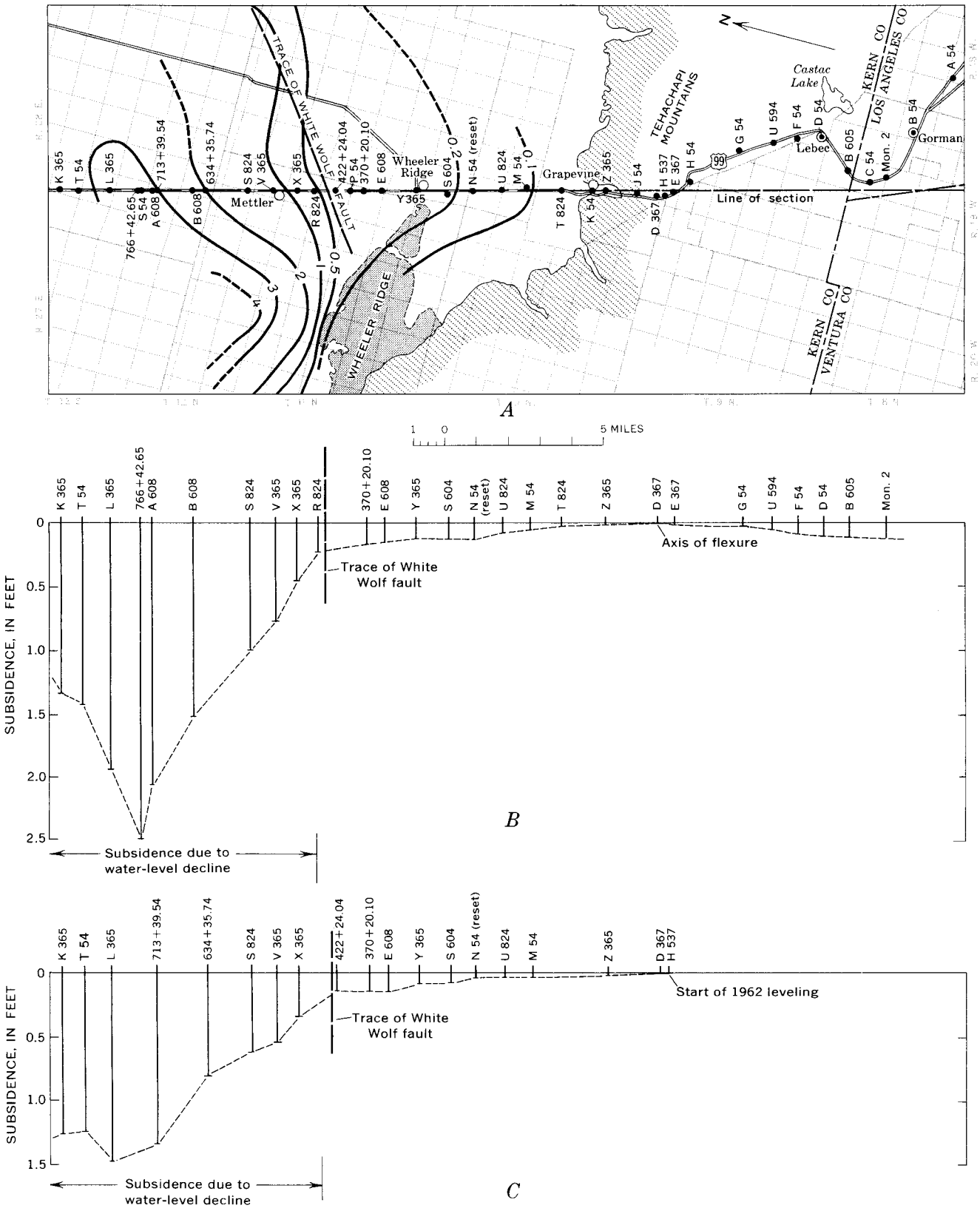


FIGURE 8.—Vertical movement of bench marks along U.S. Highway 99 in the Grapevine area, 1953–62. *A*, Lines of equal subsidence, in feet, 1953–62; *B*, subsidence profile, 1953–59; and *C*, subsidence profile, 1959–62. The vertical movement of some bench marks in *A* is shown on figure 7.

ence occurring on the Wheeler Ridge mountain mass to the west was of the same order of magnitude, suggesting that the subsidence south of the fault between the cited bench marks was largely if not wholly tectonic.

## ACCURACY OF LEVELING DATA

The maximum allowable error for precision leveling (first order) by the U.S. Coast and Geodetic Survey is equal to 0.017 foot times the square root of the distance of the level line in miles. In bringing absolute altitudes into the Grapevine area from a distant tidal bench mark such as San Pedro, 110 miles away, a difference of a few tenths of a foot in bench-mark altitudes as determined from successive levelings would be within first-order limits. The adjusted altitudes of bench marks in the area, therefore, may depart from absolute values by that amount. In traversing the 10-mile distance from the trace of the White Wolf fault to the axis of flexure south of Grapevine, however, a maximum error of only 0.05 foot would be allowed. Thus, change in the difference in altitude of bench marks at these two locations of 0.32 foot (bench mark 422+24.04), or by about 7 times the maximum permissible error, from 1953 to 1962 (fig. 8 *B*, *C*) is fully consistent with the suggestion that tectonic movement has occurred. Instrument error can account for only a small part of the measured change.

## CONCLUSIONS

The evidence appears conclusive that tectonic warping is occurring in the Tehachapi Mountains south of the White Wolf fault. Observed differential subsidence of bench marks between the fault and the axis of flexure, from 1953 to 1962, is 0.32 foot, or about 7 times the order of accuracy of first-order leveling. The long-term trend (figs. 4 and 5) is convincing evidence of continuing relative subsidence. Although adjusted leveling data indicate differential subsidence of bench marks north and south of the axis of flexure, the reference bench marks along the axis actually may have been rising progressively at a slow rate. The Coast and Geodetic Survey recently (1964 and 1965) has releveled lines from this area to a tide gage at San Pedro for the purpose of resolving this problem.

## REFERENCES

Buwalda, J. P., 1954, Geology of the Tehachapi Mountains, California, *in* chap. 2 *of* Jahns, R. H., ed., Geology of southern California: California Dept. Nat. Resources, Div. Mines Bull. 170, p. 131–142.

Dibblee, T. W., Jr., 1955, Geology of the southeastern margin of the San Joaquin Valley, California, *in* pt. 1 *of* Oakeshott, G. B., ed., Earthquakes in Kern County, California, during 1952: California Dept. Nat. Resources, Div. Mines Bull. 171, p. 23–24.

Lofgren, B. E., 1960, Land subsidence adjacent to the White Wolf fault near Bakersfield, California [abs.]: Geol. Soc. America Bull., v. 71, p. 1918.

——— 1963, Land subsidence in the Arvin-Maricopa area, San Joaquin Valley, California: Art. 47 *in* U.S. Geol. Survey Prof. Paper 475-B, p. B171–B175.

Oakeshott, G. B., ed., 1955a, Earthquakes in Kern County, California, during 1952: California Dept. Nat. Resources, Div. Mines Bull. 171, 283 p.

——— 1955b, The Kern County earthquakes in California's geologic history, *in* pt. 1 *of* Oakeshott, G. B., ed., Earthquakes in Kern County, California, during 1952: Calif. Dept. Nat. Resources, Div. Mines Bull. 171, p. 15–22.

Poland, J. F., and Davis, G. H., 1956, Subsidence of the land surface in the Tulare-Wasco (Delano) and Los Banos-Kettleman City area, San Joaquin Valley, California: Am. Geophys. Union Trans., v. 37, no. 3, p. 287–296.

Whitten, C. A., 1955, Measurements of earth movements in California, *in* pt. 1 *of* Oakeshott, G. B., ed., Earthquakes in Kern County, California, during 1952: California Dept. Nat. Resources, Div. Mines Bull. 171, p. 75–80.

Wood, P. R., and Dale, R. H., 1964, Geology and ground-water features of the Edison-Maricopa area, Kern County, California: U.S. Geol. Survey Water-Supply Paper 1656, 108 p.

797-218 O—66——2

# CATTLE CREEK ANTICLINE, A SALT DIAPIR NEAR GLENWOOD SPRINGS, COLORADO

By W. W. MALLORY, Denver, Colo.

*Abstract.*—The Cattle Creek anticline, 7 miles south of Glenwood Springs, Garfield County, Colo., is determined by vertical dip in gypsum of the Eagle Valley Evaporite on the west side of the Roaring Fork Valley and by gentle dip in the Maroon Formation on the east side. A well 3,060 feet deep near the axis of the structure penetrates a thick section of gypsum, anhydrite, and halite probably older than beds exposed at the surface. Presence of an isolated arch of halite only 2,100 feet below the surface in a strongly expressed anticline indicates diapiric structure. Potash and oil or gas may be present at depth.

## REGIONAL SETTING

The Cattle Creek anticline, a salt diapir near Glenwood Springs in western Colorado, is in the northeast corner of the Colorado Plateaus physiographic province, near the western edge of the Southern Rocky Mountains province. It is in a generally synclinal area between the White River Plateau on the northwest and the Sawatch Range on the southeast (fig. 1), and is flanked on the southwest by a prominent hogback of Pennsylvanian to Cretaceous rocks that forms the eastern rim of the Piceance Creek basin. The principal stream is the Roaring Fork River which flows northwesterly from the vicinity of Aspen to Glenwood Springs. Dips are low except locally where faulting or monoclinal flexure is present. In terms of Pennsylvanian paleogeography the region lay in an evaporite pan in the west-central part of the Eagle basin (fig. 2).

The Maroon is the most conspicuous and widespread formation exposed in the valley of the Roaring Fork and vicinity. It consists in general of several thousand feet of brilliant red coarse clastic rocks of Pennsylvanian and Permian age. Below the Maroon is the yellow and gray Eagle Valley Evaporite (Lovering and Mallory, 1962), a sequence of halite-gypsum-anhydrite and of siltstone of similar age.

The contact between the Eagle Valley and the overlying Maroon Formation is gradational at most places. In general the rugged interfluvial areas are developed

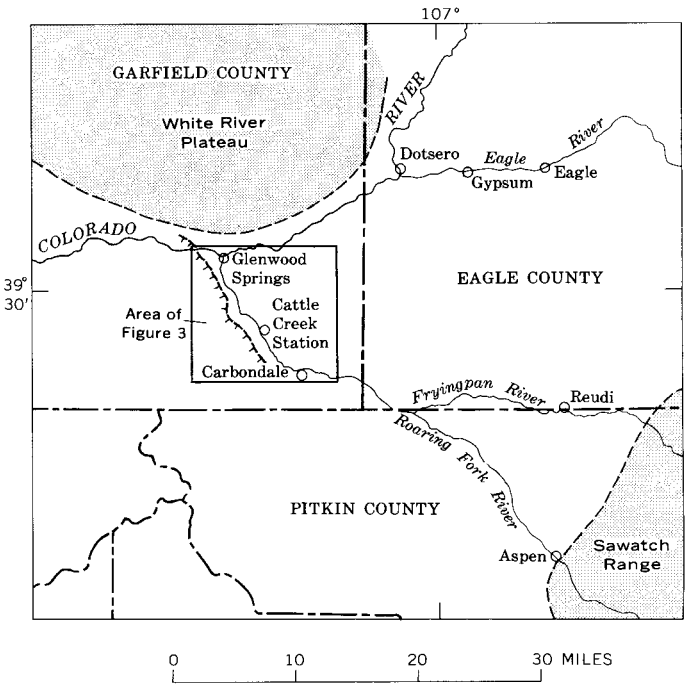


FIGURE 1.—Map of part of western Colorado, showing principal geographic features and location of figure 3. The Sawatch Range is part of the Southern Rocky Mountains physiographic province; the remainder of the area is in the Colorado Plateaus province. Line of hachures marks a southeastward continuation of the hogback which forms the western and southwestern margins of the White River Plateau.

on the Maroon Formation; in the major valleys the Maroon has been removed by erosion and the Eagle Valley Evaporite is exposed where it is not covered by glacial gravels and alluvium. It typically appears as grotesquely contorted and eroded beds and chaotic masses, especially where it is uncontaminated with mudstone or interbedded clastic strata.

## STRUCTURE AT CATTLE CREEK STATION

At Cattle Creek Station, on the Aspen spur of the Denver and Rio Grande Railroad 7 miles south of

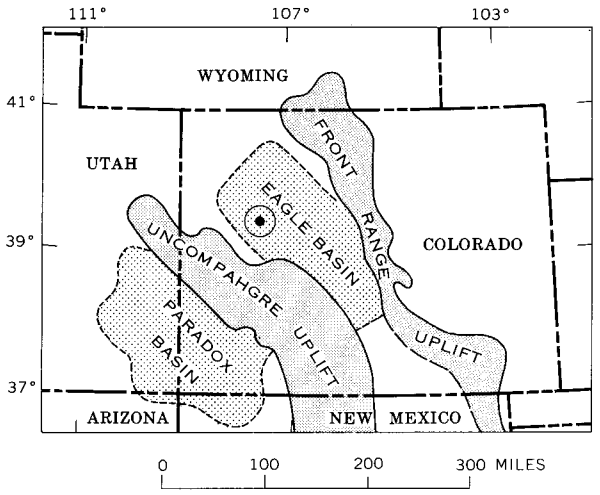


FIGURE 2.—Location of Cattle Creek anticline (circled point) and major paleogeographic features of Middle Pennsylvanian time in Colorado and adjacent States.

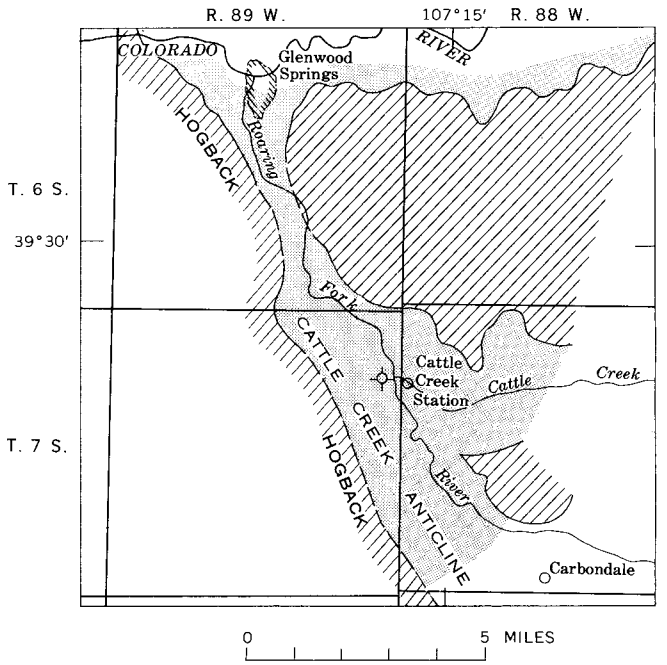


FIGURE 3.—Generalized bedrock geology of the Glenwood Springs–Cattle Creek Station area, Colorado. Line pattern, Pennsylvanian and Permian Maroon Formation and scattered Tertiary and Quaternary volcanic rocks; stipple, Pennsylvanian and Permian Eagle Valley Evaporite (extensively covered by Quaternary alluvium in the Roaring Fork valley). Dry-hole symbol is location of Shannon 1 Rose well. Geology in northern part after Bass and Northrop (1963, pl. 1).

Glenwood Springs, the Roaring Fork flows northwest in a valley about a mile wide which is floored by Pleistocene and Recent river terraces. The valley walls, which rise abruptly on either side, are composed of Eagle Valley Evaporite overlain by the Maroon Formation (fig. 3). On the west side of the valley, vertical beds of gypsum form a prominent scarp. About half a mile west of the valley margin the gypsum grades upward into light-colored micaceous siltstone which in turn grades upward into typical Maroon Formation. In the vicinity of the lithologic transition zones, the westward dip becomes progressively more gentle. On the east side of the valley, soft complexly contorted gypsum beds underlie competent strata of the Maroon Formation, which dips gently eastward away from the valley.

Observation of surface features indicates that the Roaring Fork River has breached an asymmetrical anticline whose steep limb is on the west, adjacent to a prominent hogback. Northward the anticline plunges gently to structural closure just south of Glenwood Springs townsite (Bass and Northrop, 1963, pl. 1, SW¼); its southern terminus is masked by a cover of alluvial gravel. The visible structure is about 8 miles long and 1½ miles wide.

In 1960 the Shannon Oil Co. drilled its No. 1 Rose well in the central part of the anticline (center NW¼-SE¼, sec. 12, T. 7 S., R. 89 W.) (American Stratigraphic Co., 1960). The well passed through 60 feet of alluvial gravel, and 2,065 feet of gypsum, anhydrite, and micaceous siltstone of the Eagle Valley Evaporite. At a depth of 2,125 feet the drill entered halite with minor interbeds of anhydrite and siltstone, and it remained in halite to the total depth at 3,060 feet. The total thickness of the halite at the wellsite is therefore unknown but is at least 935 feet. The presence of halite at relatively shallow depth calls to mind the diapirs of the Paradox basin, in southwestern Colorado and east-central Utah (fig. 2), a basin whose origin and history resemble those of the Eagle basin in many ways.

The conclusion that the Cattle Creek anticline is also a salt diapir seems unavoidable. Evidence for diapir structure is provided by: (1) the steep dip on the west side of the anticline a few tenths of a mile from the wellsite, (2) the absence of halite or any indication of its former presence in the gypsum section in the valley walls, or at other exposures in the vicinity, (3) the shallow depth to the top of the halite body in the anticline, and (4) local intrusive relations on the east side of the valley.

Regional dip of the hogback near Glenwood Springs is in the neighborhood of 56° (Bass and Northrop, 1963, pl. 1, SW¼). The local 90° dip in the Cattle Creek area is attributed to vertical movement and horizontal stress exerted by upwelling and expanding evaporites in the Cattle Creek anticline. The lack of chaotic crumpling in the thick gypsum sections which forms the vertical west limb of the anticline is an unusual occurrence in the Eagle basin. It may be that high confining pressure exerted by the rising mass of evaporitic rocks in the anticlinal core prevented these beds from becoming distorted. On the east side of the valley,

adjacent to State highway 82 about a mile southeast of the bridge over Cattle Creek, the Eagle Valley Evaporite can be observed locally in intrusive contact with the Maroon Formation.

## CORRELATION OF SURFACE AND SUBSURFACE STRATA

The 2,000 feet of gypsum exposed in vertical section west of the wellsite contains thin but conspicuous beds of calcareous, fine-grained sandstone and a few beds of black shale and shaly carbonate rock. The 2,125 feet of gypsum, anhydrite, and siltstone beds which overlie the halite section in the Rose well contain several thin carbonate beds. The carbonate markers in the well cannot be identified in the surface section, and the calcareous sandstone beds on the surface do not seem to be present in the well. Hence the stratigraphic and structural relations of the highest gypsum beds in the well to those of the base of the surface section west of the wellsite are unknown. Furthermore, the attitude of the gypsum beds in the well is not known, but it is probable that they are contorted like the gypsum beds on the east side of the valley and in most other outcrops in the area. Moreover, the sulfate-and-clastic section lying above the halite in the Rose well may have contained halite which has since been removed by solution. Hence a sequence of evaporite strata of unknown thickness between the lowermost bed on the surface and the highest bed in the well may have been removed by erosion and solution. Additional removal may have occurred by solution of salt at depth (Omer B. Raup, U.S. Geol. Survey, oral commun., 1964).

## TIME AND MECHANICS OF DEFORMATION

It is difficult to establish the time of initial movement of the Cattle Creek anticline. An obvious possibility is that it originated in the Laramide orogeny when major structural features of the Western United States were developed. Recent work (Elston and Landis, 1960) has shown, however, that the Paradox basin diapirs began to form soon after deposition of the salt and that movement continued for a long time. It may therefore be that upward movement at Cattle Creek Station began in late Paleozoic time. If so, renewal or intensification of movement in Laramide time is also probable.

Whether the structure is of ancient or more recent origin, it is likely that as arching progressed, erosion removed surficial strata, streams breached the structure, the Eagle Valley Evaporite was exposed to meteoric water, and anhydrite was hydrated to gypsum. The degree of expansion which accompanies the hydration of anhydrite to gypsum is not accurately known, but it seems to range from 30 to 58 percent, and the pressure exerted by hydration has been estimated at 300 to 10,000 pounds per square inch (Brune, 1965, p. 30). Three significant factors, therefore, favored flowage of halite at depth from marginal into crestal areas: (1) removal of overburden from the crest of the anticline, (2) weight of thousands of feet of Maroon Formation on the flanks of the structure, and (3) the high hydration pressure of anhydrite.

Depth of folding is not known. If regional tectonic movements caused initial arching it seems probable that the entire sedimentary column and basement rocks were involved. If the structure is due only to evaporite-tectonic factors, arching could have been limited only to Pennsylvanian and younger strata. A combination of both circumstances seems probable. High gravel terraces of probable Pleistocene age on the west side of the valley of the Roaring Fork near the town of Carbondale slope gently west, away from the Roaring Fork, instead of gently east, toward the river, as would be expected. This observation implies that upwelling of halite at depth has tilted the terraces in post-Pleistocene time, and that movement may therefore still be taking place.

The Cattle Creek anticline may be only one of several examples of the occurrence of salt arching in the Glenwood Springs area. Benson and Bass (1955) reported that in the valley of the Eagle River, between Dotsero and Gypsum (fig. 1), an anticlinal axis roughly coincides with the course of the river. Moreover, at the town of Eagle, halite was logged by the American Stratigraphic Co. (1965) in the Champlin 1 Black Well (NE¼NE¼NE¼ sec. 4, T. 5 S., R. 84 W.). These circumstances suggest the possible presence in the Eagle Valley of salt movement. Also, at Reudi on the Fryingpan River (fig. 1), solution sinks of very recent origin apparently in gypsum, and blebs of halite in shallow drill cores nearby suggest the presence of salt intrusion.

## ECONOMIC POTENTIAL

The presence of more than 935 feet of halite in the core of the Cattle Creek anticline suggests by analogy with potash-halite associations in the Paradox basin (Hite, 1961), that potash salts may also be present in the Cattle Creek anticline. If adequate structural closure is present at depth on the northern and southern termini of the Cattle Creek anticline, oil and gas may be present in strata of Cambrian, Ordovician, Devonian, or Mississippian age beneath the salt.

## REFERENCES

American Stratigraphic Company, 1960, Sample log of Shannon No. 1 Rose, 12–7S–89W, Garfield County, Colorado.

——— 1965, Sample log of Champlin No. 1 Black, 4–5S–84W, Eagle County, Colorado.

Bass, N. W., and Northrop, S. A., 1963, Geology of Glenwood Springs quadrangle and vicinity, northwest Colorado: U.S. Geol. Survey Bull. 1142–J, p. 1–71.

Benson, J. C., and Bass, N. W., 1955, Eagle River anticline, Eagle County, Colorado: Am. Assoc. Petroleum Geologists Bull., v. 39, no. 1, p. 103–106.

Brune, Gunnar, 1965, Anhydrite and gypsum problems in engineering geology: Eng. Geology, v. 2, no. 1, p. 26–38.

Elston, D. P., and Landis, E. R., 1960, Pre-Cutler unconformities and early growth of the Paradox Valley and Gypsum Valley salt anticlines, Colorado: Art. 118 *in* U.S. Geol. Survey Prof. Paper 400–B, p. B261–B265.

Hite, R. J., 1961, Potash-bearing evaporite cycles in the salt anticlines of the Paradox basin, Colorado and Utah: Art. 337 *in* U.S. Geol. Survey Prof. Paper 424–D, p. D135–D138.

Lovering, T. S., and Mallory, W. W., 1962, The Eagle Valley Evaporite and its relation to the Minturn and Maroon Formations, northwest Colorado: Art. 132 *in* U.S. Geol. Survey Prof. Paper 450–D, p. D45–D48.

Mallory, W. W., 1960, Outline of Pennsylvanian stratigraphy of Colorado, *in* Rocky Mountain Association of Geologists, Guide to the geology of Colorado: Denver, p. 23–33.

# DOMES IN THE ATLANTIC COASTAL PLAIN EAST OF TRENTON, NEW JERSEY

By JAMES P. MINARD and JAMES P. OWENS,
Washington, D.C.

*Abstract.*—The presence of two elongate domes in the coastal-plain formations east of Trenton, N.J., has been established by detailed mapping. They were delineated by plotting the tops of 2 formations of Late Cretaceous age as determined in 85 outcrops and auger holes. Formations as young as Miocene seem to be involved in the folding. Other similar structures or folds may be present along the inner edge of the coastal plain in this area. Such structures may be suitable for underground gas storage.

Detailed geologic mapping recently completed in the Roosevelt and Allentown 7½-minute quadrangles, in the Coastal Plain province east of Trenton, N.J. (fig. 1), has shown the presence of two small domes in formations of Cretaceous and Tertiary age. The authors began geologic-quadrangle mapping in the coastal plain of New Jersey in 1957 at a larger scale (1:24,000) than any mapping previously undertaken over a comparable area in the coastal-plain area. Twelve 7½-minute quadrangles have been completed to date, ten of which are in the vicinity of Trenton. As mapping progressed it showed that the formations are folded locally and do not trend uniformly northeast-southwest (about N. 45° E.) nor dip toward the southeast within the range of about 10 to 65 feet per mile as reported by earlier workers. This was particularly evident in the southwest part of the Roosevelt quadrangle (Minard, 1964) and in the southeast part of the Allentown quadrangle (Owens and Minard, unpub. data). Upon completion of mapping in the two quadrangles it was possible to delineate the domes.

Two other workers have referred to similar warps in the general area. Woollard (1941, p. 65–67) shows a minor anticlinal fold in the vicinity of Lakewood (fig. 1) and a syncline near Jacksons Mills, about 7 miles northwest of Lakewood. Olsson [1] noted a structural anomaly in the vicinity of Emleys Hill and postulated the existence of a northeast-southwest trending anticline, but did not present a map of the structure.

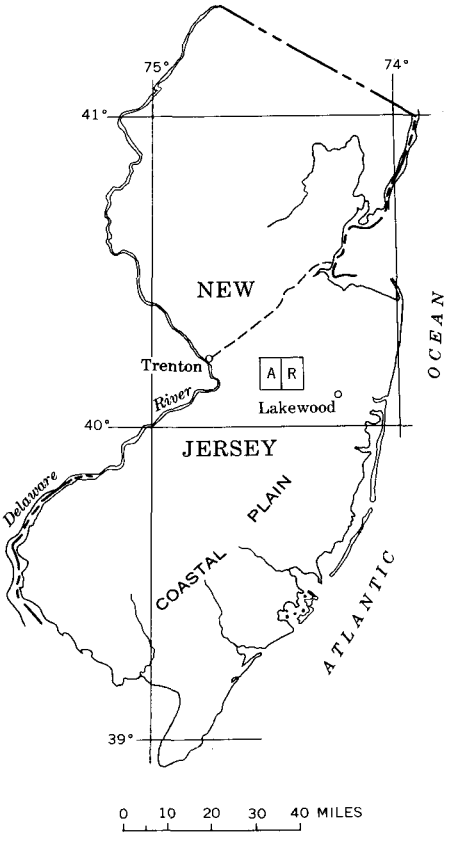


FIGURE 1.—Index map showing location of the Allentown (A) and Roosevelt (R) quadrangles, in the northern part of the coastal plain in New Jersey. Dashed line extending northeast from Trenton *indicates inner boundary of coastal plain.*

[1] Fox, S. K., and Olsson, R. K., 1960, Stratigraphic problems of the latest Cretaceous and earliest Tertiary sediments in New Jersey: Atlantic Coastal Plain Geol. Assoc. Guidebook, 1st Ann. Field Conf.: [Duplicated report] 31 p.

## STRATIGRAPHIC SUMMARY

The sedimentary formations underlying the surface at and in the vicinity of the domes are an alternating sequence of sands and clays of Upper Cretaceous and Tertiary age (fig. 2). Other than the Raritan Formation, which is 200 to 300 feet thick, and the Englishtown Formation, which is about 90 feet thick, the formations range between 10 and 50 feet in thickness. The Merchantville, Marshalltown, and Navesink Formations, the basal part of the Red Bank Sand, and the Hornerstown Sand each has a high glauconite content (the Marshalltown, Navesink, and Hornerstown are mostly or nearly all glauconite), and forms a conspicuous marker bed in an otherwise largely quartz-sand sequence. The two horizons which are structure contoured, the tops of the Englishtown Formation and Mount Laurel Sand, are distinct and easily discerned in the field. The Englishtown is a quartz sand containing clay interbeds, overlain by the quartz-glauconite sand of the Marshalltown. The Mount Laurel is a quartz sand overlain by the glauconite sand of the Navesink.

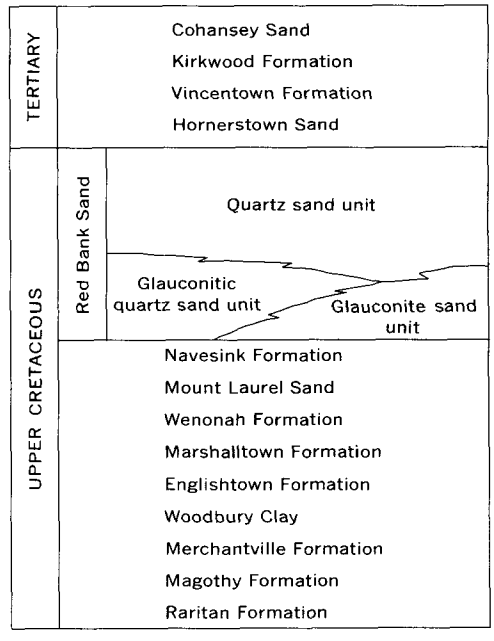


FIGURE 2.—Sedimentary marine and continental formations which underlie the ground surface over or near the domes. The Raritan Formation rests on the basement complex of Precambrian age. The total thickness of the sedimentary sequence is about 750 feet in the vicinity of the domes.

## MAPPING

### Method

Altitudes of the tops of the Englishtown Formation and Mount Laurel Sand in outcrop were plotted on parts of the Allentown and Roosevelt 7½-minute topographic maps (10-foot contour interval). The contacts between the Marshalltown and Englishtown Formations (top of the Englishtown) and Navesink Formation and Mount Laurel Sand (top of the Mount Laurel) can be seen at about 25 to 30 places in the area shown in figure 3. In addition, about 60 auger holes were put down through these contacts in this area or near it. Most of these holes were shallow and penetrated the contacts within 30 feet below the surface. The outcrops and auger holes provided 85 to 90 control points from which to plot the structure contours outlining the domes. Two horizons instead of one (the tops of the Englishtown and Mount Laurel) were chosen because the Navesink Formation and Mount Laurel Sand are present over only part of the dome near Davis Station, and the top of the Englishtown Formation is too deep to provide adequate control for the dome near Emleys Hill.

### Results

The results of the detailed mapping have been the discovery of two domes. Deviations from the regional attitude, noticed in the early stages of mapping, became more evident as a larger area was completed, as better outcrops were found, and as auger techniques were perfected. The first firm evidence of folding was found in the southwest part of the Roosevelt quadrangle in 1962; there, dips are locally reversed from southeast to northwest, and steepen toward the southeast to as much as 120 feet per mile. This folding was particularly evident from altitudes of points on the top of the Mount Laurel Sand.

When the Allentown quadrangle was mapped in 1964, the formational attitudes in the southern part of the quadrangle were found to diverge markedly from the regional trends. For example, the Marshalltown Formation, a unit only 10 to 15 feet thick, could be traced nearly horizontally along Crosswicks Creek (which flows nearly due west) for a distance of 2 miles. The strike of this unit and of the other formations exposed here shifts markedly from the regional northeast-southwest trend. The Marshalltown-Englishtown contact was traced northeastward from Walnford to just northwest of Davis Station (fig. 3), and was found at progressively higher elevations. Near Davis Station this contact was 20 feet higher than at Walnford. Traced farther northeastward from Davis Station to Imlaystown, the contact descended to the same elevation as that at Walnford. This traverse had nearly paralleled the long axis of the western dome.

An even more noticeable deviation from the general trend is found in the eastern dome where the contact between the Navesink Formation and the underlying Mount Laurel Sand is outlined in the southeast corner

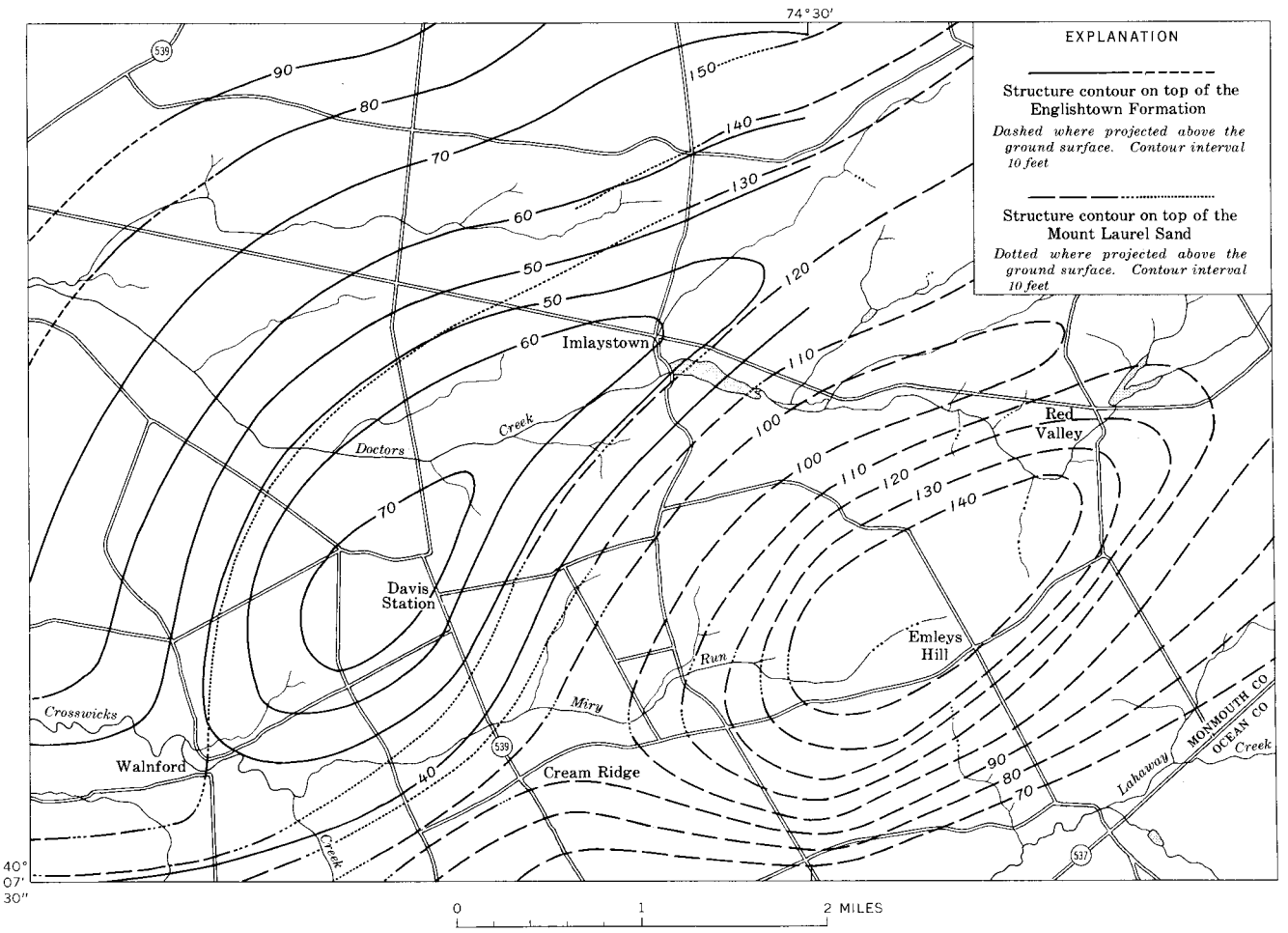


FIGURE 3.—Structure-contour map of the southeast part of the Allentown quadrangle and the southwest part of the Roosevelt quadrangle. Lat 40°07'30" N. is the southern boundary of both quadrangles; long 74°30' E. is the boundary between them.

of the Allentown quadrangle. This contact can be seen at an altitude of about 105 feet in the south bank of Miry Run, just east of the road north to Imlaystown. Traced due east in the bank of Miry Run—that is, diagonally down the direction of the normal regional dip—the contact rises progressively upstream, instead of descending. About a quarter of a mile to the east the contact is 15 feet higher (altitude 120 feet), and this rise continues eastward into the Roosevelt quadrangle (fig. 3). This conforms to the pattern previously established (largely by augering) in the southwest part of the Roosevelt quadrangle (Minard, 1964).

## DESCRIPTION OF THE DOMES

The domes are elliptical in surface plan, and the long axes are oriented northeast-southwest (fig. 3). One, shown by the structure contours on the top of the Englishtown Formation, lies in the southeast part of the Allentown quadrangle (fig. 3). It has a maximum vertical closure of slightly more than 20 feet and maximum horizontal closures of about 1.6 and 4.5 miles. The long axis trends along a slightly curved line extending from Walnford northeast through Imlaystown. The other dome, outlined by structure contours on top of the Mount Laurel Sand, lies mostly in the southwest part of the Roosevelt quadrangle but extends into the southeast corner of the Allentown quadrangle (fig. 3). It has a maximum vertical closure of slightly more than 40 feet and maximum horizontal closures of about 1.8 and 4 miles. The long axis trends along a line extending from Cream Ridge northeast, passing between Emleys Hill and Red Valley.

The youngest formation on the crest of the western dome is the Wenonah; erosion has breached both it and the Marshalltown on the southwest nose, and exposed the upper part of the Englishtown. The Navesink Formation and Red Bank Sand flank the southeast side. The youngest formation on the crest of the eastern dome is the Navesink; it is breached by erosion at the west end, exposing the upper part of the Mount Laurel Sand. The Red Bank, Hornerstown, Vincentown, Kirkwood, and Cohansey Formations flank the

sides. Thus, units as young as Miocene seem to be involved in the folding.

Investigation into the mechanism of folding (gravity gliding, basement warping, or other causes) would necessitate detailed knowledge of the distribution and thicknesses of formations at depth. That information was not obtained because of the limited capacity of the power auger used in the routine mapping.

## POTENTIAL ECONOMIC SIGNIFICANCE OF THE DOMES

In recent years there has been an extensive search in the subsurface of the New Jersey coastal plain for sites suitable for storage of natural gas. As far as the authors know, these efforts to date have been unsuccessful.

At a typical underground-storage site in unconsolidated deposits, an impervious layer (composed largely of very clayey sediments) overlies a bed of more porous sediment (largely well-sorted sands), and the beds have been folded into an anticline of sufficient storage capacity. The coastal plain in New Jersey is underlain by an alternating sequence of clayey formations and sandy formations which, if folded, could form many possible traps. In the Allentown area the lower part of the stratigraphic section appears to offer the best potential for storage sites. Here the very clayey Woodbury and Merchantville Formations (fig. 2) are about 100 feet thick, and they overlie several hundred feet of the much more sandy Magothy and Raritan Formations. The presence of the domes at Allentown would involve these sediments if the structures mapped on the surface persist to basement.

A search for similar folds is currently being conducted west and south of Trenton. Preliminary indications are that many other folds exist. These warps, however, are less obvious than the Allentown domes, mainly because they are masked by a widespread alluvial cover along the Delaware River drainage system. A much more extensive drilling program is needed to delineate these structures. An interesting feature of some of these folds is that they are downdip from the Allentown domes and involve a thicker section of sediment. These folds may ultimately prove to be larger and perhaps better traps than the Allentown domes, and therefore to have even greater economic potential.

## REFERENCES

Minard, J. P., 1964, Geology of the Roosevelt quadrangle, New Jersey: U.S. Geol. Survey Geol. Quad. Map GQ–340.

Woollard, G. P., 1941, Geophysical methods of exploration and their application to geological problems in New Jersey: New Jersey Dept. Conserv. and Devel., Geol. Ser. Bull. 54, 89 p.

# REGIONAL UNCONFORMITY IN LATE CRETACEOUS, WYOMING

By JAMES R. GILL and WILLIAM A. COBBAN, Denver, Colo.

*Abstract.*—An important unconformity, present throughout much of Wyoming at the base of the Teapot Sandstone Member of the Mesaverde Formation and its lateral equivalents—the Pine Ridge Sandstone Member of the Mesaverde Formation and the upper part of the Ericson Sandstone, is the result of erosion that took place about 72 million years ago following broad regional uplift. The Teapot equivalents rest on progressively older rocks from east to west. Possibly as much as 3,600 feet of strata was eroded from the western part of the State.

A widespread unconformity at the base of the Teapot Sandstone Member of the Mesaverde Formation and of its lateral equivalents has recently been proved by stratigraphic and faunal data at several localities in Wyoming. This unconformity increases in magnitude from east to west. It has been recognized in the Powder River, Bighorn, Great Divide, and Hanna basins; it seems to be present in the Wind River and Washakie basins and along the margins of the Rock Springs uplift also, although confirming data are sparse. A minimum of 2,000 feet of nonmarine and marine beds of Late Cretaceous age was eroded from the western part of the Bighorn basin following this uplift and prior to deposition of the Teapot Sandstone Member. Uplift and erosion also seem to have occurred in south-central Wyoming, where as much as 3,600 feet of strata may have been removed from the western part of the Rock Springs uplift prior to deposition of the Ericson Sandstone. Areas of stronger local uplift which the authors relate at least in part to pre-Teapot uplift have been described on the northeast margin of the Great Divide basin in the Lost Soldier oil field by Fath and Moulton (1924, p. 27), Zapp and Cobban (1962, p. D52), and Reynolds (1966, p. B69–B76, this chapter).

This report describes recent results of investigation of the depositional history, position of strandlines, and intertonguing relations of marine and nonmarine rocks deposited during the Santonian, Campanian, and early Maestrichtian Stages of the Upper Cretaceous in Wyoming and adjacent States. This work is a continuation of investigations initiated by Zapp (Zapp and Cobban, 1960, 1962), and incorporates data obtained during a study of the Pierre Shale and equivalent rocks in North and South Dakota, Montana, and eastern Wyoming (Tourtelot, 1962; Tourtelot and others, 1960; Gill and Cobban, 1961, 1962, 1965).

*Acknowledgments.*—L. G. Schultz assisted in measuring the Salt Creek–Teapot dome section (loc. 3, fig. 1) in 1961, and R. E. Burkholder aided in measuring the North Fork section (loc. 4, fig. 1) in 1963. C. R. Givens was of material aid in making collections of fossils and measuring sections in the Bighorn basin during the 1964 field season. James R. Davis, of the University of Wyoming, provided unpublished data on the Mesaverde Formation in central Wyoming.

## GENERAL SETTING

In the western interior region of the United States, great thicknesses of rocks accumulated in a north-trending epicontinental sea during the Cretaceous. In Wyoming as much as 19,000 feet of beds accumulated in and along the margin of this sea during the Upper Cretaceous (Reeside, 1944). The stratigraphic sequence is preserved in the form of westward-thickening wedges of nonmarine rocks intercalated with eastward-thickening bodies of marine sediments. The geologic record is more completely preserved in the eastern areas of offshore marine deposition, and the authors believe that the depositional history can be best understood by relating the faunal and stratigraphic record of the totally marine depositional environment to that of the western areas of mixed marine and nonmarine accumulation.

The Pierre Shale and its marine equivalents throughout the western interior region of the United States and Canada are abundantly fossiliferous and contain large numbers of distinctive groups of ammonites, many of which have broad geographic distribution and limited stratigraphic range. Index ammonites are invaluable aids in locating the positions of ancient shorelines, determining the sequence of depositional events, and recognizing depositional or erosional breaks in thick sections of marine shale. The ammonite zones used to document the observations presented in this paper

are shown on the right-hand side of figure 1, adjacent to the Red Bird Section (loc. 1, fig. 1), and are the same as those presented by Zapp and Cobban (1962, p. D54) except for the addition of two younger zones, *Baculites clinolobatus* and *Sphenodiscus* cf. *lenticularis*.

In Wyoming, the base of littoral marine and associated nonmarine deposits that form the Mesaverde Formation or equivalent rocks rises stratigraphically from west to east. The interfingering relation of transgressive and regressive deposits that accounts for this eastward change has been illustrated by Weimer (1961, p. 24), Zapp and Cobban (1962, p. D54), Weichman (1961, p. 30–31), Rich (1958), Severn (1961, p. 196), Barwin (1961, p. 177), and others. In the western part of the Powder River basin the Mesaverde Formation consists of three members. The Parkman Sandstone Member, which is at the base, consists of a thick regressive marine sandstone overlain by nonmarine beds. The middle or unnamed marine member represents a westward-pointing tongue of the Pierre Shale. It consists of marine sandy shales in its lower and middle parts and a thick marine sandstone of shallow-water origin at the top. The upper member is the Teapot Sandstone Member, which most workers, including the authors, regard as nonmarine. The Parkman Member has been related to a period of regression (R3 Parkman regression of Zapp and Cobban, 1962, p. D53–D54); the unnamed middle member of the Mesaverde is considered to be a transgressive unit (T3 pre-Teapot transgression of Zapp and Cobban, 1962, p. D53–D54; middle Mesaverde transgression of Rich, 1958, p. 2440); the nonmarine Teapot Sandstone Member, although somewhat anomalous in physical appearance and in its regional stratigraphic relations with enclosing strata, is commonly considered to have been deposited during the final regression of the Mesaverde (R4 Teapot regression of Zapp and Cobban, 1962, p. D53–D54).

## THE UNCONFORMITY

An angular unconformity has not been observed at the base of the Teapot Sandstone Member, nor has conglomeratic material other than clay or shale pebbles been recognized in the lower part of the Teapot. The unconformity is known to be present however, because faunal zones in the upper part of the Pierre and in the Lewis are parallel with the top of the Teapot, whereas those in the Cody and lower part of the Pierre lie at an angle to it. In the distance of 230 miles from Red Bird to Cottonwood Creek, the Teapot cuts across possibly as many as 11 faunal zones (*Baculites* sp. (smooth) to *Exiteloceras jenneyi*). The authors thus believe that a considerable part of the stratigraphic record for the upper part of the Mesaverde is missing at many localities in Wyoming. It appears likely that uplift and erosion throughout much of the State prior to deposition of the Teapot Sandstone Member of the Mesaverde Formation obliterated evidence of additional regressive and transgressive phases of deposition during the latter part of the Upper Cretaceous.

Figure 1 shows an east-west transect formed by a lien of sections extending 230 miles from Red Bird, Wyo. (fig. 1, loc. 1), in the southeastern part of the Powder River basin, to Cottonwood Creek (fig. 1, loc. 9) on the southwest margin of the Bighorn basin. Figure 2 shows the locations of the sections. The top of the Teapot Sandstone Member, used for a datum, is very nearly parallel to the index ammonite zones in the overlying Lewis and Pierre Shales. The Teapot unconformably overlies regressive marine sandstones in the upper part of the middle member of the Mesaverde in the Powder River basin, and unconformably truncates older and older beds of the lower part of the Mesaverde as it is traced westward across the Bighorn basin. In the vicinity of Zimmerman Butte and No Water Creek (locs. 6 and 5, fig. 1), rocks that are recognized as Mesaverde in the Powder River basin have been removed by pre-Teapot erosion, and the Teapot rests unconformably on parts of the Mesaverde Formation that are represented by marine shale in the Powder River basin. Diagnostic ammonites have not been found in the thin marine sandstones (locs. 5, 6, fig. 1); but these sandstones seem, on the basis of fossils in the underlying units, to lie somewhere within the range span of *Baculites asperiformis*. In the Power River basin *B. asperiformis* is found in the Cody Shale 1,100 to 1,300 feet below the base of the Teapot.

## AGE OF THE UNCONFORMITY

Stratigraphic and faunal studies of the Pierre Shale outcrops along the southern and eastern margins of the Powder River basin indicate that, although the Teapot Sandstone Member was not deposited in these areas, the part of the Pierre which normally contains the zones of *Didymoceras cheyennense*, *Baculites compressus*, and *B. cuneatus* is missing. Physical evidence for slow deposition, nondeposition, or erosion has not been observed, however. These zones are present in nearby areas in western South Dakota, southern Montana, and northern Colorado, and their absence in easternmost Wyoming is attributed to submarine planation resulting from pre-Teapot uplift and erosion. Evidence from these nearby areas indicates that a sizable portion of the stratigraphic record in the Powder River basin may have been obliterated by pre-Teapot erosion. As closely as the authors can determine, the Teapot Sandstone Member was deposited sometime during the early part of the time span of *Baculites reesidei*. The iden-

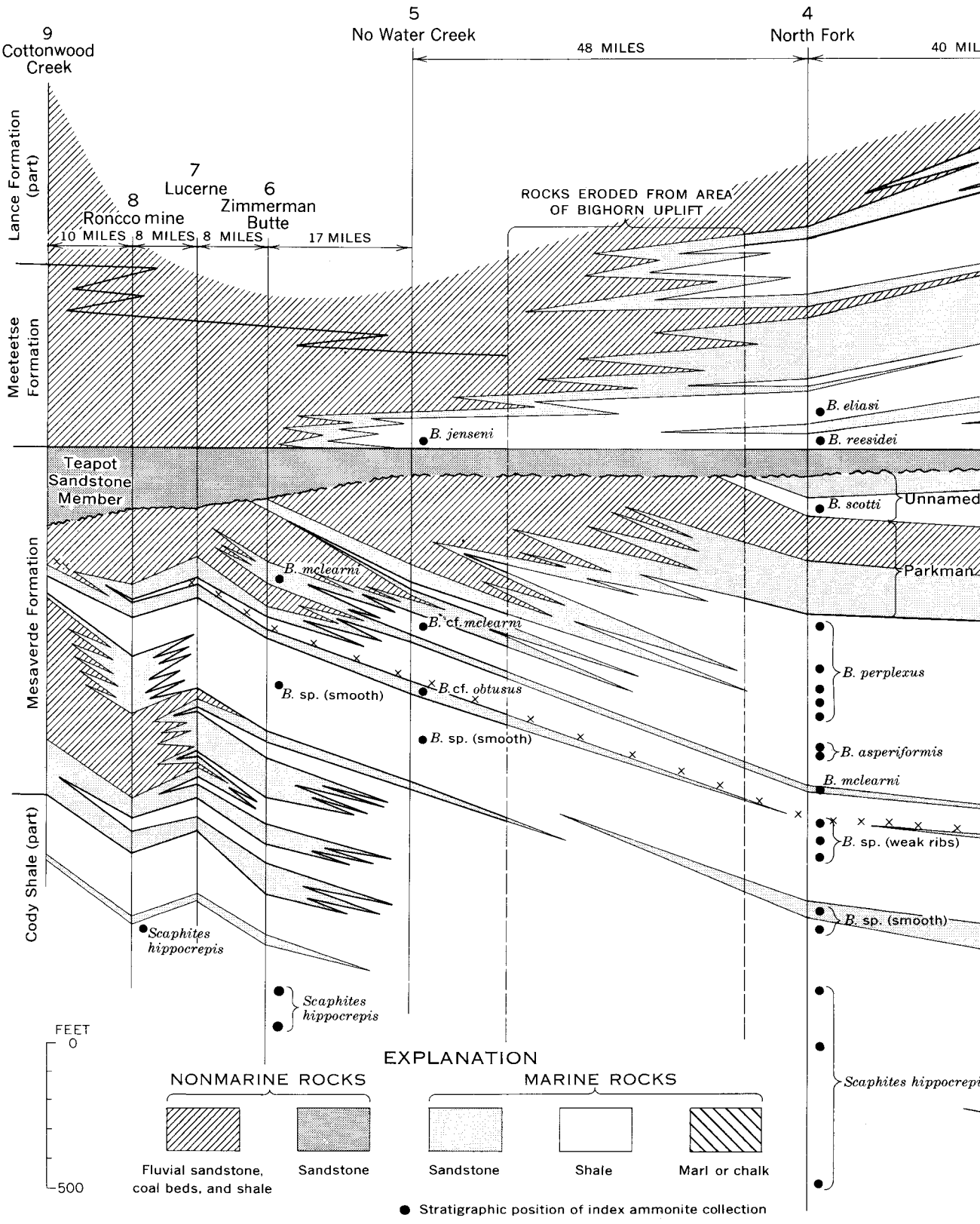


FIGURE 1.—Restored section showing relation of unconformity to other rocks of Late Cretaceous age in the Powder Ri the Salt Creek and Teapot Dome oil field, Natrona Cour

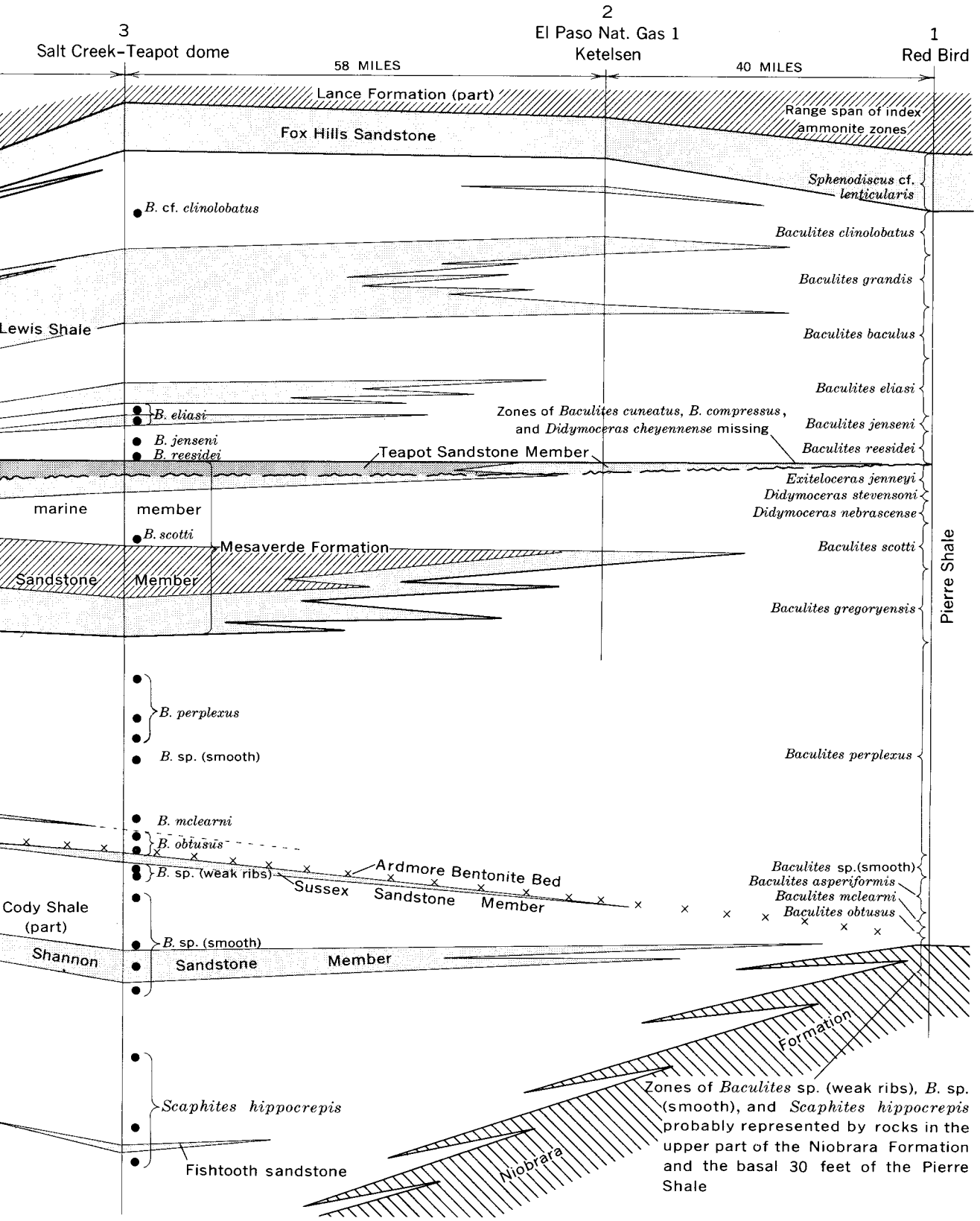


he base of the Teapot Sandstone Member of the Mesaverde Formation
nd Bighorn basins. Section at locality 3 is a composite measured in
Wyo.

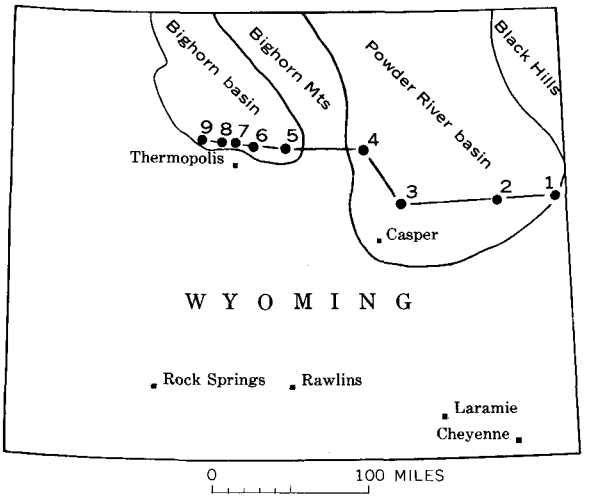


| No. (fig. 1) | Name | Section | Township N. | Range W. |
|---|---|---|---|---|
| 1 | Red Bird | 23 | 38 | 62 |
| 2 | El Paso Natural Gas 1 Ketelsen | 5 | 37 | 68 |
| 3 | Salt Creek–Teapot dome (composite) | 3, 4 | 38 | 78 |
| | | 24, 25 | 39 | 78 |
| | | 3 | 39 | 79 |
| | | 34 | 40 | 79 |
| 4 | North Fork | 23, 26 | 43 | 81 |
| | | 25, 27 | 44 | 82 |
| 5 | No Water Creek | 35 | 44 | 90 |
| 6 | Zimmerman Butte | 15 | 44 | 92 |
| | | 25 | 44 | 93 |
| 7 | Lucerne | 13, 26 | 44 | 94 |
| 8 | Roncco mine | 13, 17 | 44 | 95 |
| 9 | Cottonwood Creek | 26 | 45 | 97 |

FIGURE 2.—Index map showing location of sections on figure 1.

tity of the missing ammonite zones at Red Bird (loc. 1, fig. 1) indicates that the pre-Teapot unconformity is no older than late in the time span of *Exiteloceras jenneyi*, and no younger than early in the time span of *Baculites reesidei*. East of the Black Hills, in western South Dakota, the zones of *Didymoceras cheyennense* and *Baculites compressus* are well represented and some strata representing the zone of *B. cuneatus* are present, indicating that the unconformity must have developed late in the time span of *Baculites cuneatus* or early in the time span of *B. reesidei*.

## THE TEAPOT SANDSTONE MEMBER

The Teapot Sandstone Member of the Mesaverde Formation is a striking lithologic unit composed largely of white- to light-gray fine- to coarse-grained thin to massive and locally torrentially crossbedded nonmarine sandstone that contrasts strongly with darker contiguous strata. It contains an abundance of dark-brown to black carbonaceous material in the form of angular to rounded coaly fragments, thin laminae of carbonaceous shale, and local thin lenticular beds of impure coal. The Teapot contains an abundance of rounded to subangular grains of dark chert along with subangular to angular quartz grains and clay. In most areas the matrix appears to be clay, but locally the rock is cemented with silica. At many places the Teapot is more resistant than adjacent units and forms a ridge covered with pine trees. The type locality of the Teapot Sandstone Member is in the vicinity of the Salt Creek oil field and, prior to being formally defined by Barnett (1915, p. 113–114), it was referred to as "the sandstone forming the Little Pine Ridge" (Wegemann, 1911, p. 48). In the Powder River basin it ranges in thickness from about 50 feet at the type locality to about 125 feet at the Big Muddy oil field in the southern part of the basin near Glenrock, Wyo.

Subsurface studies indicate that the Teapot extends throughout much of the Powder River basin. Over much of this area it is interpreted to be nonmarine in the main part but bordered on the east by a narrow belt of marine sandstone. This marine sandstone is exposed only in the Lance Creek oil field, on the southeast margin of the basin, where it consists of about 50 feet of coarse-grained glauconitic sandstone that crops out about 1,300 feet below the top of the Pierre Shale. *Baculites reesidei* is present in the upper part of the Teapot and in a 60-foot interval in the overlying Pierre Shale. The marine phase of the Teapot grades eastward into shale and has not been recognized along the east margin of the Powder River basin. Along the west side of the basin the Teapot or its equivalents have been recognized as far north as Parkman, Wyo., where it forms the upper unit of Darton's (Darton and Salisbury, 1906, p. 8) type Parkman Sandstone.

Subsurface studies by Rich (1958, p. 2435) of Cretaceous rocks in the Wind River and southern Bighorn basins led him to postulate that the Teapot was present in these areas. Houston and Murphy (1962, p. 86, 89) recognized the Teapot Sandstone Member of the Mesaverde in outcrops in the southeastern part of the Bighorn basin in the vicinity of the No Water Creek section (loc. 5, fig. 1). The authors have traced the Teapot along the east, south, and west sides of the Bighorn basin. Throughout this area the Teapot rests unconformably on the older parts of the Mesaverde (fig. 1). In the southeast and eastern parts of the basin it is conformably overlain by marine shale and sandy beds equivalent to the lower part of the Lewis Shale of the western Powder River basin or to the lower tongue of the Lewis Shale as used by Rich (1958, p. 2437) in the Wind River basin. In the vicinity of the No Water Creek section (loc. 5, fig. 1),

*Baculites jenseni* was collected 50 feet above the base of the Lewis and another ammonite that has previously been found only with *Baculites eliasi* or *B. jenseni* was collected from near the top of the formation. In view of the fact that the lower 50 feet of the Lewis has not been dated and of the ambiguous age implication of the ammonite from the top of the unit, it can be postulated that the Lewis could possibly range in age from somewhere in the time span from *Baculites reesidei* to *B. eliasi* (fig. 1, right-hand column).

The physical appearance of the Teapot is as striking in the Bighorn basin as it is in the Powder River basin to the east and in the Wind River basin to the south. In the Bighorn basin the Teapot is 75 to 100 feet thick in areas where it is overlain by marine rocks of the Lewis, but it is more than 300 feet thick in western and northern areas where it is overlain by the Meeteetse Formation, a nonmarine partial equivalent of the Lewis (fig. 1). Similar thickness variations have been observed in the Wind River, Laramie, and Hanna basins.

The areal distribution of the Teapot Sandstone Member in the Wind River basin is largely unknown. The unit has been recognized and described along the southeastern part of the Basin by Rich (1958, p. 2429–2430, 2432, 2435–2436) and Barwin (1961, p. 176) and along the east side of the basin adjacent to the Casper arch by Workum (1959). In the northwest part of the basin, Keefer and Troyer (1956) described as the uppermost unit of the Mesaverde in the Shotgun Butte area a white to light-gray very fine to coarse-grained massively crossbedded sandstone that is 225 feet to 435 feet thick. Keefer and Rich (1957, p. 73) later discussed the stratigraphic relations of this sandstone and suggested that it might correlate with the Teapot.

In deference to other workers who have made extensive studies of rocks of Late Cretaceous age in this region, it should be stated that there is not complete concurrence of opinion as to the interpretation of the origin of the Teapot and its lateral equivalents—the Pine Ridge Member and upper part of the Ericson Sandstone. The authors and many others consider the Teapot and its equivalents to be of nonmarine origin, but Weimer (1960, p. 9, fig. 4) appears to regard the Teapot and the Pine Ridge (1961, p. 20, fig. 3) as transitional and marine sandstones and the Ericson a marine sandstone "* * * deposited in and marginal to the marine embayment" (Weimer, 1961, p. 27).

In the eastern half of the Bighorn basin, Severn (1961, p. 198) tentatively correlates a 192-foot-thick sandstone at the top of his Judith River Formation (Mesaverde of this report) with the Teapot Sandstone Member and regards it as "* * * combined beach, fluvial and lagoonal deposits related to a pause in the westward transgression of the Bearpaw sea." Miller and others (1965, p. 281), although not explicit, appear to regard the Teapot or its equivalent as a marine sandstone in the Bearpaw Shale.

## LATE CRETACEOUS UPLIFT AND EROSION

The interfingering of marine and nonmarine rocks of Late Cretaceous age in the Bighorn and Powder River basins is thought to be the direct result of periods of uplift alternating with periods of quiescence and subsidence along the western cordillera margin of the Late Cretaceous sea. Large eastward-pointing wedge-shaped masses of shallow-water marine and nonmarine strata are interpreted as reflecting uplift in western areas, and the interfingering westward-pointing wedges of fine-grained marine rocks appear to reflect continued basin subsidence coincident with the final stages of erosion of uplifted areas. The regressive sequences of marine and nonmarine rocks, and the enclosing transgressive deposits of fine-grained marine sediments represented by parts of the Cody, Lewis, and Pierre Shales and the Mesaverde, Meeteetse, Fox Hills, and Lance Formations, are thus thought to be a record of the pulsating nature of orogenic events that took place in a region west of the area of present study.

The Teapot Sandstone Member of the Mesaverde is also a regressive deposit that reflects orogeny, but one which differs markedly from the bulk of the regressive units found in the underlying parts of the Mesaverde or in the younger Meeteetse, Fox Hills, or Lance Formations. The detritus in these latter rocks appears to have been transported from remote western areas and deposited in and along the margins of the sea. The rate of sediment delivery exceeded the rate of basin subsidence, and the coastline slowly shifted eastward. As an example, the time involved in depositing the main mass of the Mesaverde, as it is exposed in the area between Cottonwood Creek (loc. 9, fig. 1) and North Fork (loc. 4, fig. 1), is estimated to involve the greater part of the time span of 9 ammonite zones, whereas the Teapot Sandstone Member is inferred to have been deposited in less than the time span of 1 zone, *Baculites reesidei*.

The Teapot and its lateral equivalents—the Pine Ridge Sandstone Member of the Mesaverde Formation and the upper part of the Ericson Sandstone—are considered to be postorogenic deposits derived from strongly uplifted areas in western Wyoming or eastern Idaho. These rocks differ in appearance and lithology from regressive deposits of the Mesaverde and other Cretaceous formations in Wyoming because of their somewhat different environments of deposition. The Mesaverde and similar rocks accumulated slowly in and along the margins of the regressing sea. The Teapot and its equivalents appear to have been deposited

rapidly as a broad sheetlike body of nonmarine sand on the uplifted and eroded surface of nonmarine rocks of the Mesaverde. In the western part of the Powder River basin, uplift was sufficiently intense to expose large areas of former sea bottom to subaerial erosion. In these areas the nonmarine rocks of the Teapot rest disconformably on marine sandstone or shale and are overlain by marine deposits of the Pierre or Lewis Shale.

Incipient and in some places strongly accentuated growth of structural features that later attained their maximum configuration during the Laramide orogeny appears to be related to uplift preceding deposition of the Teapot Sandstone Member of the Mesaverde. One such example of pre-Teapot structural growth in the Lost Soldier oil field, near Lamont, Wyo., has been described by Zapp and Cobban (1962, p. D52) and by Reynolds (1966, p. B69–B76, this chapter). Miller and others (1965) recently reported the results of a study of the stratigraphy and petroleum potential of rocks of latest Cretaceous age in the Bighorn basin and concluded (p. 283–284) that,

> In a number of areas anomalous thinning occurs in the Judith River section [Mesaverde of this report]. Several of these areas are in the southeastern part of the basin associated with well-known Laramide structural trends at Worland dome, Slick Creek, and Neiber. In most places the anomalous thinning of the section amounts to 100 to 150 feet and occurs in the continental deposits in the middle of the Judith River [Mesaverde of this report]. The thinning reflects the influence of either erosion or slower rates of deposition related to incipient structural upwarp during the period of maximum regression. The upper Judith River Sandstone [Teapot Sandstone Member of the Mesaverde of this report] may in some areas lie unconformably on the middle continental unit.

The authors do not concur with the stratigraphic interpretations presented by Miller and others (1965) but do consider that erosion beneath their "upper Judith River sandstone" reflects incipient structural growth which was a precursor to later structural development. The authors believe that many structural and stratigraphic traps or combinations of these were formed by pre-Teapot tectonic events throughout much of Wyoming. Some of these potential traps have been exhumed and obliterated by erosion but it seems likely that many more may exist in the present structural basins of Wyoming but remain hidden beneath thick deposits of Tertiary basin fill.

The regional tectonic and depositional history of the Teapot segment of Late Cretaceous time in the northern part of the western interior region is interesting and significant. During the period of broad uplift and erosion and of the subsequent deposition of the Teapot in Wyoming, widespread westward transgression of the sea took place in Montana and adjacent parts of southern Canada. During this interval the strandline moved westward a distance of about 350 miles and the sea lapped on the eastern margin of the Elkhorn Mountains Volcanics in western Montana. Explosive vulcanism which occurred intermittently throughout this advance of the sea is reflected by numerous thick persistent beds of bentonite in the Bearpaw Shale.

An absolute age determination of $75 \pm 2$ million years has been reported by Folinsbee and others (1961, p. 353–356) for biotite and sanidine obtained from a bentonite bed in the *Baculites compressus* zone in the Bearpaw Shale of southern Alberta. An extrapolation of this and other data currently in the process of publication by the authors indicates that the extensive transgression of the Bearpaw sea in southern Canada and Montana and the uplift, erosion, and regression of the sea as marked by the Teapot Sandstone Member in Wyoming took place approximately 72 m.y. ago.

## REFERENCES


Barnett, V. H., 1915, Possibilities of oil in the Big Muddy dome, Converse and Natrona Counties, Wyoming: U.S. Geol. Survey Bull. 581, p. 105–117.

Barwin, J. R., 1961, Stratigraphy of the Mesaverde Formation in the southern part of the Wind River Basin, Wyoming, *in* Wyoming Geol. Assoc. Guidebook, 16th Ann. Field Conf., Symposium on Late Cretaceous rocks, 1961: p. 171–179.

Darton, N. H., and Salisbury, R. D., 1906, Description of Bald Mountain and Dayton quadrangles, Wyoming: U.S. Geol. Survey Geol. Atlas, Folio 141, 15 p.

Fath, A. E., and Moulton, G. F., 1924, Oil and gas fields of the Lost Soldier–Ferris district, Wyoming: U.S. Geol. Survey Bull. 756, 57 p.

Folinsbee, R. E., Baadsgard, Halfdan, and Lipson, J., 1961, Potassium-argon dates of Upper Cretaceous ash falls, Alberta, Canada, *in* Kulp, J. L., ed., Geochronology of rock systems: New York Acad. Sci. Annals, v. 91, art. 2, p. 352–363.

Gill, J. R., and Cobban, W. A., 1961, Stratigraphy of the lower and middle parts of the Pierre shale in the northern Great Plains States: Art. 352 *in* U.S. Geol. Survey Prof. Paper 424–D, p. D185–D191.

——— 1962, Red Bird Silty Member of the Pierre Shale, a new stratigraphic unit: Art. 8 *in* U.S. Geol. Survey Prof. Paper 450–B, p. B21–B24.

——— 1965, Stratigraphy of the Pierre Shale, Valley City and Pembina Mountain areas, North Dakota: U.S. Geol. Survey Prof. Paper 392–A, p. A1–A20.

Houston, R. S., and Murphy, J. F., 1962, Titaniferous black sandstone deposits of Wyoming: Wyoming Geol. Survey Bull. 49, 120 p.

Keefer, W. R., and Rich, E. I., 1957, Stratigraphy of the Cody Shale and younger Cretaceous and Paleocene rocks in the western and southern parts of the Wind River Basin, Wyoming, *in* Wyoming Geol. Assoc. Guidebook, 12th Ann. Field Conf., Southwest Wind River Basin, 1957: p. 71–78.

Keefer, W. R., and Troyer, M. L., 1956, Stratigraphy of the Upper Cretaceous and lower Tertiary rocks of the Shotgun Butte area, Fremont County, Wyoming: U.S. Geol. Survey Oil and Gas Inv. Chart OC–56.

Miller, D. N., Jr., Barlow, J. A., and Haun, J. D., 1965, Stratigraphy and petroleum potential of latest Cretaceous rocks, Bighorn Basin, Wyoming: Am. Assoc. Petroleum Geologists Bull., v. 49, no. 3, p. 277–285.

Reeside, J. B., Jr., 1944, Map showing thickness and general character of the Cretaceous deposits of the Western Interior of the United States: U.S. Geol. Survey Oil and Gas Inv. Prelim. Map 10.

Rich, E. I., 1958, Stratigraphic relation of latest Cretaceous rocks in parts of Powder River, Wind River, and Big Horn basins, Wyoming: Am. Assoc. Petroleum Geologists Bull., v. 42, no. 10, p. 2424–2443.

Severn, W. P., 1961, General stratigraphy of the Mesaverde Group, Bighorn Basin, Wyoming, *in* Wyoming Geol. Assoc. Guidebook, 16th Ann. Field Conf., Symposium on Late Cretaceous rocks, 1961: p. 195–199.

Tourtelot, H. A., 1962, Preliminary investigation of the geological setting and chemical composition of the Pierre Shale, Great Plains region: U.S. Geol. Survey Prof. Paper 390, 74 p.

Tourtelot, H. A., Schultz, L. G., and Gill, J. R., 1960, Stratigraphic variations in mineralogy and chemical composition of the Pierre shale in South Dakota and adjacent parts of North Dakota, Nebraska, Wyoming, and Montana: Art. 205 in U.S. Geol. Survey Prof. Paper 400–B, p. B447–B452.

Wegemann, C. H., 1911, The Salt Creek oil field, Natrona County, Wyoming: U.S. Geol. Survey Bull. 452, p. 37–83.

Weichman, B. E., 1961, Regional correlation of the Mesaverde Group and related rocks in Wyoming, *in* Wyoming Geol. Assoc. Guidebook, 16th Ann. Field Conf., Symposium on Late Cretaceous rocks, 1961: p. 29–33.

Weimer, R. J., 1960, Upper Cretaceous stratigraphy, Rocky Mountain area: Am. Assoc. Petroleum Geologists Bull., v. 44, no. 1, p. 1–20.

——— 1961, Uppermost Cretaceous rocks in central and southern Wyoming, and northwest Colorado, *in* Wyoming Geol. Assoc. Guidebook, 16th Ann. Field Conf., Symposium on Late Cretaceous rocks, 1961: p. 17–28.

Workum, R. H., 1959, Stratigraphy of the Mesaverde formation of the west flank of the Casper Arch, Natrona County, Wyoming: Wyoming Univ. M.A. thesis.

Zapp, A. D., and Cobban, W. A., 1960, Some Late Cretaceous strand lines in northwestern Colorado and northeastern Utah: Art. 112, *in* U.S. Geol. Survey Prof. Paper 400–B, p. B246–B249.

——— 1962, Some Late Cretaceous strand lines in southern Wyoming: Art. 134, *in* U.S. Geol. Survey Prof. Paper 450–D, p. D52–D55.

797–218 O—66——3

# PERMIAN COLEOID CEPHALOPODS FROM THE PHOSPHORIA FORMATION IN IDAHO AND MONTANA

By MACKENZIE GORDON, JR., Washington, D.C.

*Abstract.*—Belemnite-like coleoid cephalopods belonging to the family Aulacoceratidae occur in two phosphatic shale members of the Phosphoria Formation. The Meade Peak Member of Early Permian age contains *Stenoconites idahoensis* n. gen., n. sp., at four localities in southeastern Idaho. This is the oldest Permian coleoid known. The Retort Member of Late Permian age contains *"Dictyoconites"* cf. *"D." groenlandicus* Fischer at six localities in southwestern Montana. *"D." groenlandicus* was originally described from northeastern Greenland. Both genera appear to be closely related to, but not identical with, true *Dictyoconites* of the Alpine Triassic. A fairly direct seaway connecting Greenland and southwestern Montana is implied by the distribution of *"Dictyoconites."*

The coleoid cephalopods described in this paper were collected during an intensive sampling program of the Phosphoria Formation in Montana, Idaho, Wyoming, and Utah, begun by the U.S. Geological Survey in 1947 under the direction of V. E. McKelvey. The coleoids were found in sections of the phosphatic shale members exposed in trenches dug by bulldozer to facilitate sampling of this relatively nonresistant rock. Stratigraphic data and partial chemical analyses of rocks from the sampled sections have been published in U.S. Geological Survey circulars and professional papers. Data from Idaho sections, used in this paper, are from McKelvey, Davidson, and others (1953), McKelvey, Armstrong, and others (1953), Sheldon and others (1953), and Davidson and others (1953). Data from Montana sections are from Cressman and Swanson (1964). As part of the Phosphoria investigations, paleontologic collections were taken from fossiliferous beds in sampled and measured sections. A summary report of these faunal investigations by E. L. Yochelson is now in preparation.

The first Permian coleoid found in the United States and, indeed, the first known Lower Permian one in the world, is from Idaho. It was recognized as a possible belemnite by J. E. Smedley, of the U.S. Geological Survey, who collected it in July 1948, and showed it to the writer later that year. This specimen is the type of the new genus and species described in this paper. A search for further material in the U.S. Geological Survey collections at the U.S. National Museum proved fruitless until a colleague suggested that the coleoids might have been mistaken for fish spines by those doing preliminary sorting of material. Subsequently, 15 collections containing coleoids, mostly external molds, were found among fish remains from the Phosphoria Formation. This should emphasize the possibility that other late Paleozoic coleoids may be undiscovered in museum, university, and private collections the world over.

## LOCATION AND STRATIGRAPHIC POSITION OF THE PHOSPHORIA COLEOIDS

Coleoid cephalopods in the Phosphoria Formation of Idaho that are sufficiently well preserved to identify, all of which occur in the Meade Peak Phosphatic Shale Member of Early Permian (Leonard) age, are referred to *Stenoconites idahoensis* n. gen., n. sp. The specimens from Montana are from the Retort Phosphatic Shale Member of Late Permian age. They appear likewise to be restricted to a single genus and species, here identified as *"Dictyoconites"* cf. *"D." groenlandicus* Fischer.

### Distribution of *Stenoconites*

The specimens assigned to this new genus, which is described in a later part of this report, are from 5 collections taken from 4 trenches dug in southeastern Idaho in 1948 and 1949. The location of the trenches is shown on the index map (fig. 1). *Stenoconites idahoensis* is recorded in four of these collections and is identified with question in the fifth. The localities cover an elongate area in Caribou County, southeastern Idaho, about 21 miles long in a northerly direction and as much as 5 miles wide, northeast and southeast of Soda Springs.

U.S. GEOL. SURVEY PROF. PAPER 550-B, PAGES B28-B35

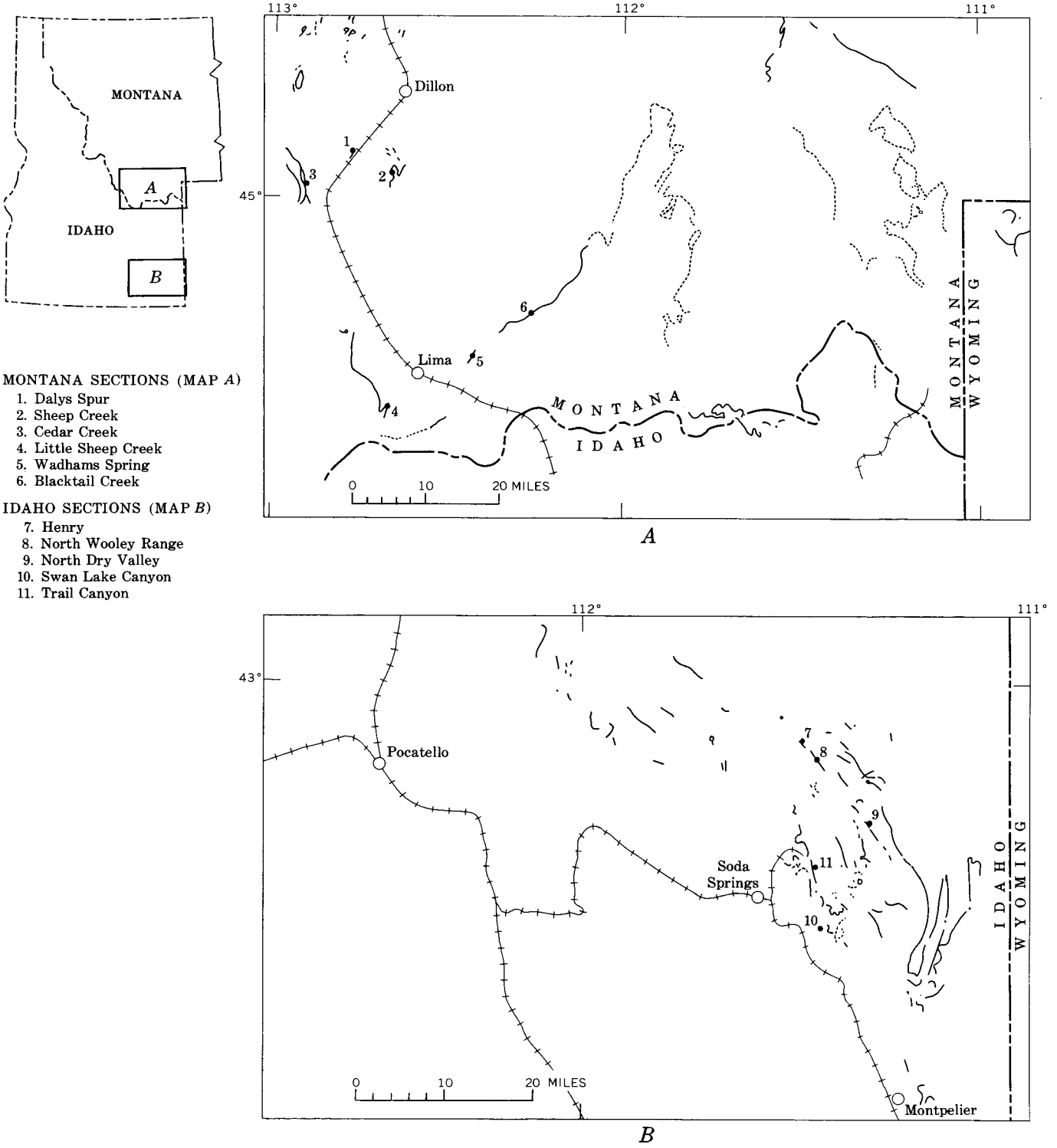


MONTANA SECTIONS (MAP *A*)

1. Dalys Spur
2. Sheep Creek
3. Cedar Creek
4. Little Sheep Creek
5. Wadhams Spring
6. Blacktail Creek

IDAHO SECTIONS (MAP *B*)

7. Henry
8. North Wooley Range
9. North Dry Valley
10. Swan Lake Canyon
11. Trail Canyon

FIGURE 1.—Index map showing localities where coleoid cephalopods were collected from measured sections of the Phosphoria Formation. Outcrop pattern (solid and dotted lines) of Phosphoria rocks and numbered locations of sections after Klepper and others (1948) and McKelvey, Davidson, and others (1953). Outcrop pattern dotted where uncertain.

The thickness of the Meade Peak Phosphatic Shale Member at each collecting locality, the thickness of the coleoid-bearing shale interval, and the distance above the base and below the top of the nearest boundary of this interval are shown in table 1. *Stenoconites idahoensis* appears to be limited to a stratigraphic interval only a few feet thick, roughly four-fifths of the way up in the phosphatic shale member at the North Wooley Range, North Dry Valley, and Swan Lake Canyon sections (locs. 8-10, fig. 1) and only a little higher in the Henry section (loc. 7). The only occurrence of a coleoid from a lower horizon in the Meade Peak Member is a poorly preserved, unidentifiable fragment of an aulacoceratid in a 2½-foot bed of slightly oolitic mudstone, 16 feet above the base of the Meade Peak Member in the Trail Canyon trench, about 8 miles northeast of Soda Springs (USGS loc. 9971-PC).

TABLE 1.—*Stratigraphic distribution of* Stenoconites *in the Meade Peak Phosphatic Shale Member of the Phosphoria Formation in Idaho*

| Section sampled | Loc. No. (fig. 1) | USGS loc. No. | Thickness of— | | Distance | |
|---|---|---|---|---|---|---|
| | | | Meade Peak Member (ft) | Coleoid-bearing interval (ft) | Above base of member (ft) | Below top of member (ft) |
| Henry | 7 | 11630-PC | 177.8 | 1.6 | 157.4 | 18.8 |
| North Wooley Range | 8 | 10434-PC | 163.1 | 4.7 | 129.8 | 28.6 |
| North Dry Valley | 9 | 10519-PC | 157.6 | 3.4 | 124.7 | 29.5 |
| Swan Lake Canyon | 10 | 10593-PC 10594-PC | 162.5 | 3.2 | 129.7 | 29.6 |

## Distribution of "*Dictyoconites*"

The Montana coleoids were found in six trenches (fig. 1) dug during the period 1947–49 in Beaverhead County, in the southwestern part of the State. Two of the trenches (locs. 1 and 2) are about 13 miles (airline) south and southwest of Dillon; another (loc. 3) is 19 miles southwest of Dillon; the fourth (loc. 4) is about 36 miles south of the northernmost locality, within a few miles of the Continental Divide. The last two (locs. 5 and 6) are in a line to the northeast of the southernmost locality, the farther one 23 miles from it. The stratigraphy and petrology of the Permian rocks in this region have been discussed in detail by Cressman and Swanson (1964); stratigraphic data used in table 2 come from their report. The thickness of the "*Dictyoconites*"-bearing Retort Member at each trenched section, the thickness of the shale interval that yielded coleoids in each section, and the distances from the limits of this interval to the top and bottom of the member are shown in table 2.

TABLE 2.—*Stratigraphic distribution of* "Dictyoconites" *in the Retort Phosphatic Shale Member of the Phosphoria Formation in Montana*

| Section sampled | Loc. No. (fig. 1) | USGS loc. No. | Thickness of— | | Distance | |
|---|---|---|---|---|---|---|
| | | | Retort Member (ft) | Coleoid-bearing interval (ft) | Above base of member (ft) | Below top of member (ft) |
| Dalys Spur | 1 | 9790-PC | 55.7 | 1.7 | 21.4 | 32.6 |
| Sheep Creek | 2 | 10901-PC 10902-PC 10906-PC 10907-PC | 60.3 | 23.9 | 27.3 | 4.5 |
| Cedar Creek | 3 | 10826-PC | 51.1+ | .3 | 8.0+ | 41.9 |
| Little Sheep Creek | 4 | 11658-PC 11659-PC | 28.4 | 7.6 | 20.8 | 0 |
| Wadhams Spring | 5 | 10848-PC | 66.9 | 3.3 | 58.8 | 4.8 |
| Blacktail Creek | 6 | 11669-PC | 61.1 | 2.7 | 56.7 | 1.7 |

The Sheep Creek trench (loc. 2) is at the type locality of the Retort Phosphatic Shale Member of the Phosphoria Formation. Here the Retort can be divided into three parts (Cressman and Swanson, 1964, p. 334): a lower unit, 26 feet thick, consisting chiefly of interbedded phosphorite and phosphatic mudstone; a middle unit, slightly over 15 feet thick, of nonphosphatic carbonaceous mudstone; and an upper unit, 19 feet thick, of phosphorite and phosphatic mudstone similar to the lower unit. At this locality the coleoid-bearing interval is nearly 24 feet thick; the coleoids are limited to the upper two units and do not occur in the top few feet. In the nearby Dalys Spur trench (loc. 1) the only coleoid, a poorly preserved fragment referred with question to "*Dictyoconites*" cf. "*D.*" *groenlandicus*, came from the middle unit. A "*Dictyoconites*" in the Cedar Creek trench (loc. 3), about 12 miles west of the Sheep Creek locality, is from the lower phosphatic unit. At the other three localities (locs. 4–6), all to the southeast, the coleoids occur in a relatively narrow interval at or near the top of the member.

## AGE OF THE COLEOID-BEARING BEDS

The Meade Peak Member of the Phosphoria Formation contains an ammonoid fauna regarded by Miller and others (1957, p. 1057) as equivalent in age to that of the Leonard Formation of Texas. The Leonard is assigned a Lower Permian age by the U.S. Geological Survey.

The Retort Member of the Phosphoria Formation has not previously been referred to a specific series within the Permian. The presence in it at several localities of "*Dictyoconites*", known elsewhere in the

late Paleozoic only in the *Posidonia*-Schiefer of east-central Greenland, suggests the approximate equivalence of the two stratigraphic units. The *Posidonia*-bearing shale beds of east-central Greenland interfinger with brachiopod-bearing limestone beds of Zechstein and Kazanian age. Biostratigraphers are generally inclined to regard them as Late Permian in age (Fischer, 1947, p. 6; Trümpy, 1960, p. 98; Dutro, 1961, p. C227). A similar age assignment for the Retort Member appears warranted.

## INTERPRETATION OF THE COLEOID DISTRIBUTION

It is not known at present what controls the locally limited stratigraphic distribution of the coleoids. Only the bed-by-bed collection of fossils in the Phosphoria Formation sample trenches has permitted recognition of the distribution shown in the tables. Coleoids are relatively rare among the fossils collected. All that is known with relative certainty is that they are limited to the phosphatic shale members.

One would expect that further local limitation of coleoid distribution, within the phosphatic shale members, might be related to salinity, pH, and other environmental chemical features of the sea water. Cressman and Swanson (1964, p. 383) suggest that subsidence occurred in southwestern Montana during Retort time. No doubt this opened a fairly direct connection with the Greenland region, permitting *"Dictyoconites"* to venture into the plankton-rich waters of the Phosphoria sea. This genus, however, is nowhere as abundant in Montana as it is in the Upper Permian rocks of Greenland.

Whatever the relationship of the coleoids to environmental chemical conditions, their distribution in the phosphatic members of the Phosphoria Formation does not appear to be governed by the content of $P_2O_5$ as expressed by the present quantities of phosphate in these rocks. However, all the coleoids occur where the average content of carbonaceous matter in the Retort Member is reported to range from 5 to 7 percent, a relatively high content of organic matter for shale.

## SYSTEMATIC PALEONTOLOGY

### Subclass COLEOIDEA
### Order AULACOCERIDA Jeletzky, 1965
### Family AULACOCERATIDAE Mojsisovics, 1882
### Genus DICTYOCONITES Mojsisovics, 1902

### "Dictyoconites" cf. "D." groenlandicus Fischer

Figure 2, *a*, *c–k*

*Dictyoconites groenlandicus* Fischer, 1947, p. 10–19, pls. 1, 2; text figs. 1–4.

All the 25 coleoid specimens from southwestern Montana are rostra or fragments of rostra and all have a subcircular to compressed elliptical cross section indented by a pair of prominent dorsolateral grooves, the *sulci geminati* of Müller-Stoll (1936, p. 177) and Fischer (1947, p. 9). Most of the rostra are preserved as external molds in shale, but two solid fragments were found, one of which has been thin sectioned transversely (fig. 2, *a*, *c*). No phragmocones or fragments thereof have been recognized.

The more complete rostra reach a maximum height (dorsoventral diameter) of 5 mm and width (lateral diameter) of 4 mm, tapering at both ends, the apicad to a blunt point and the orad to a contracted zone, probably near the apex of the phragmocone, where they were broken off. The longest of these fairly complete rostra is 38 mm (fig. 2, *d*). A larger, less complete one is 41 mm long and reaches a maximum width of 5.5 mm (fig. 2, *j*, *k*). Other rostra are less than 3 mm in height. A latex cast from an external mold of the apical end of a gerontic rostrum is also figured (fig. 2, *e*, *f*). This shows the blunt, bullet-shaped termination, its sides curving to meet at a moderately acute angle.

The rostral surface is sculptured by low, rather flat, longitudinal lirae with narrower interspaces. Some of the lirae increase by bifurcation; less commonly some pairs of lirae unite. Intercalation occurs locally but is extremely rare. Generally 6 to 8 lirae occur in the space of 1 mm, but there is some variation. As nearly as can be determined, the figured solid fragment of a rostrum (fig. 2, *h*, *i*) has 113 lirae at its wider end. The lirae are crossed by fine, faint, transverse threads, stronger over the lirae and therefore giving them a minutely beaded or granular appearance. Some groups of lirae are slightly inflated into elongate beads along transverse trends. Locally, transverse sculpture is sufficiently strong to give the surface a cancellate aspect, which probably is accentuated by weathering.

Dorsolateral grooves (*sulci geminati*) begin shallowly within 2 mm of the apex, strengthen rapidly into L-shaped grooves, and continue strongly for the full length of the rostrum in our specimens (which admittedly are incomplete, lacking the parts that surround the phragmocone). In some, a moderately coarse thread appears within each groove near the middle of the rostrum. Longitudinal lirae ornamenting the dorsum between the sulci diverge slightly so that lira after lira is gradually cut off by, or disappears into, the narrow troughs. Lirae on the ventrad side of the sulci are either subparallel to the sulcus or crowded, and appear to be cut off at their apicad end.

Transversely cut thin sections (fig. 2, *a*, *c*) show the radiating structure of the rostrum and the three dis-

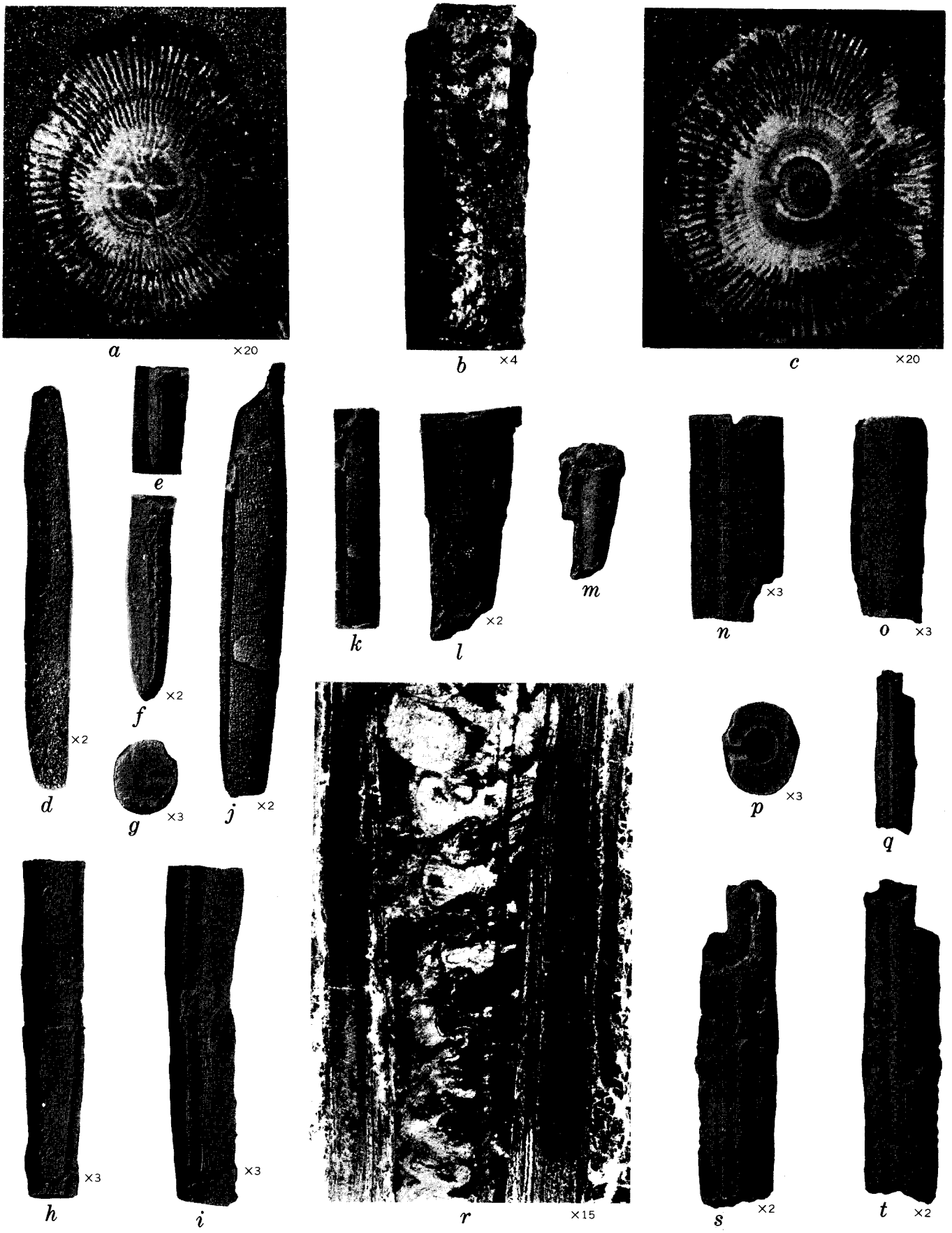


FIGURE 2.—Permian coleoid cephalopods from the Phosphoria Formation in Idaho and Montana.

tinct stages of ontogeny (Fischer, 1947, p. 13) referred to as nepionic, neanic, and ephebic-gerontic. The narrow rod-shaped nepionic rostrum is circular in cross section and without visible structure (fig. 2, *c*). The neanic stage is characterized by sharply differentiated light and dark concentric layers (*laminae pellucidae* and *laminae obscurae*) and the beginning of an elliptical cross section flattened in the position of the *sulci geminati* (fig. 2, *a*, *c*). The ephebic-gerontic stage, whose beginning is not well differentiated from the neanic one, is characterized by radial as well as lamellar structure and occupies half, or a little more, of the thickness of the rostrum.

In all their characters the Montana rostra agree reasonably well with *"Dictyoconites" groenlandicus* Fischer. Perhaps the only notable difference is that some of the Montana specimens reach a slightly greater circumference than was recorded by Fischer for the Greenland specimens. Because entire rostra and particularly phragmocones are lacking, it is impossible to make a positive identification at this time of the Greenland species.

The writer does not believe that the Greenland species is correctly assigned by Fischer to *Dictyoconites*. This is also the opinion of J. A. Jeletzky (oral commun., 1964), of the Geological Survey of Canada, and Helmuth Zapfe, of the Natural History Museum of Vienna, Austria. They plan to publish their conclusions as to the generic assignment of *Dictyoconites groenlandicus* Fischer in a joint paper. Rather than take any action that might preempt this work, the writer is merely using *"Dictyoconites"* in quotation marks.

*Figured specimens.*—USNM 146468–146472.

*Occurrence.*—Phosphoria Formation, Retort Phosphatic Shale Member, USGS locs. 9790–PC(?), 10826–PC, 10848–PC, 10901–PC, 10902–PC(?), 10906–PC, 10907–PC, 11658–PC, 11659–PC, 11669–PC(?), Beaverhead Co., Mont.

### Genus STENOCONITES Gordon, n. gen.

(Greek: *stenos*=narrow, *konos*=cone, *-ites*=rock)

*Diagnosis.*—Rostrum straight, compressed elliptical in cross section with rather prominent lateral ridge at either side a little dorsad of center; venter well rounded; dorsum a little flatter and narrower than venter. Lateral ridges set off by smooth sulcus at either side; smaller grooves may be present locally. Surface of rostrum ornamented by fine longitudinal, discontinuous to subcontinuous ramifying threads, with greatest strength and linearity on venter. Sulci that flank lateral ridges are locally smooth. Phragmocone continuous through considerable part of rostrum, circular, expanding gradually by about 1 in 10 mm in type species, with an apical angle of 6° to 7°; conothecal surface smooth; septa saucer shaped, without septal necks; sutures straight, vertical or tilted very slightly dorsorad. Cameral deposits present, episeptal ones appearing thick in some chambers, hyposeptal ones thin; both occur as circuli locally surrounding siphuncle. Siphuncle tubular, strongly execntric but not marginal.

*Type species.*—*Stenoconites idahoensis* n. sp.

*Discussion.*—The principal characters of *Stenoconites* are the compressed rostrum, the lateral ridges flanked by fairly smooth sulci, the very fine subcontinuous to discontinuous longitudinal threads, the smooth conotheca, fairly straight, vertical sutures, moderately strong cameral deposits, and the nonmarginal siphuncle. No other coleoid genus is known to have this combination of characters. The rostra of *Aulococeras*, *Bactritimimus*, and *Hematites* are much more coarsely sculptured longitudinally. Those of *Atractites*, *Calliconites*, *Metabelemnites*, and *Paleoconus* are virtually smooth. Rostra that appear closest to that of *Stenoconites* are those of *Dictyoconites* and related forms. *Dictyoconites* has a marginal siphuncle and the surface of its conotheca is longitudinally lirate. The Upper Permian shell from Greenland called *"Dictyoconites" groenlandicus* Fischer has a smooth conotheca as in *Stenoconites*, but lacks its lateral ridges and ventrad sulci, and has slightly stronger, more continuous surface sculpture and a

EXPLANATION OF FIGURE 2

*a*, *c–k*. *"Dictyoconites"* cf. *"D." groenlandicus* Fischer.
- *a*, *c*. Two transverse thin sections (× 20) of rostrum (USNM 146469) from USGS loc. 10848–PC, under dark-field illumination.
- *d*. Ventral view (× 2) of latex cast of external mold (USNM 146470) from USGS loc. 10901–PC.
- *e*, *f*. Views (× 1 and × 2) of latex cast of apical end of rostrum (USNM 146472) from USGS loc. 11658–PC, showing one of *sulci geminati*.
- *g*, *h*, *i*. Apicad, dorsal, and side views (× 3) of slightly distorted solid fragment of rostrum (USNM 146468) from USGS loc. 10826–PC, showing strong *sulci geminati*.
- *j*, *k*. Dorsal views (× 2 and × 1) of latex cast of external mold (USNM 146471) from USGS loc. 10902–PC.

*b*, *l–t*. *Stenoconites idahoensis* n. gen., n. sp.
- *b*, *q*, *s*, *t*. Ventral view (unwhitened), showing part of phragmocone ground to siphuncle (× 4), side view (× 1), and opposite side and side views (× 2) of posterior part of holotype (USNM 146473) from USGS loc. 10434–PC.
- *l*, *m*. Side view (× 2 and × 1) of anterior part of holotype showing conothecal surface of phragmocone with small area of adhering rostrum at upper right.
- *n*, *o*, *p*. Side, dorsal, and end views (× 3) of paratype (USNM 146474) from type locality.
- *r*. Longitudinal dorsoventral thin section (× 15) of paratype (USNM 146475) from USGS loc. 10594–PC, showing part of phragmocone and rostrum, siphuncle, and thick secondary deposits and club-shaped areas of secondary filling of camerae (diagrammatic sketch shown on fig. 3).

Name and location of USGS localities shown in tables 1 and 2.

marginal siphuncle and no cameral deposits in the phragmocone.

So far *Stenoconites* is known only in the Lower Permian from a restricted area in southeastern Idaho.

### Stenoconites idahoensis Gordon, n. gen., n. sp.

Figures 2, *b*, *l-t*, 3

*Diagnosis.*—*Stenoconites* with approximately 3.7 camerae in space equal to diameter of phragmocone. Thick episeptal and thin hyposeptal deposits nearly filling some chambers, appearing as circuli around siphuncle in others.

*Description.*—Holotype an incomplete phragmocone and adhering guard broken in 3 pieces, totaling 53.5 mm in length. Rostrum compressed, suboval in cross section, measuring 5.6 mm high and 5.1 mm wide at adaptical end of specimen and increasing to 7.1×6.7 mm in 20 mm adorally, an increase in height of 1 in 50 mm and in width of 1 in 40 mm. Dorsum and venter well rounded; dorsum a little narrower than venter; at adapical end of holytype, width just ventrad of dorsolateral shoulder is 4.2 mm and just dorsad of ventrolateral shoulder is 4.6 mm. Prominent rounded lateral ridge at either side of rostrum, a little dorsad of center, 1.2–1.5 mm wide at base in adapical 30 mm of specimen. Lateral ridge flanked by depressed zone at either side, dorsad one deeper and somewhat wider than ventrad one and also wider than lateral ridge. Lesser faint narrow longitudinal groove on rounded ventrolateral zone at either side of shell and at outer edge of ventrad depressed zone. Surface of rostrum fairly smooth but under moderate magnification seen to consist of fine faint subcontinuous to discontinuous, branching, reuniting, rarely intercalated, slightly granular longitudinal lirae, somewhat irregular in strength and linearity. About 11 lirae occupy space of 1 mm on dorsum. Ventrad depressed zone flanking lateral ridge smooth.

Phragmocone approximately circular, 1.3 mm in diameter at adapical end of holotype, as anterior part of guard is missing. Diameter at adoral end of specimen is 7.8 mm, where guard is only 0.3 mm thick. Rate of expansion of phragmocone 1 in 9.5 mm. Septa saucer shaped, without septal necks; camerae of moderate depth, 3.65 occurring in space equal to one diameter of phragmocone at point 30 mm from adapical end of holotype. Sutures straight, vertical, but some are tilted slightly ventrorad. Conothecal surface smooth but locally with almost imperceptible longitudinal groove.

Siphuncle tubular, strongly eccentric, not marginal; located at distance approximately equal to its own diameter dorsad of ventral margin; diameter of siphuncle 0.7 mm near middle of holotype. Siphuncle encircled by dark hyposeptal and episeptal circuli in holotype (fig. 2, *b*), which may represent ventral extension of larger hyposeptal and episeptal cameral deposits that appear to fill chambers in sectioned paratype (fig. 2, *r*).

*Discussion.*—This species is based on 5 specimens from 2 localities (3 collections), of which only the 2 from the type locality are well preserved. Some variation is present. On the holotype the deeper part of the dorsad depressed zone flanking the lateral ridge at either side of the rostrum, corresponding to the *sulci geminati*, is smooth. On the figured paratype (fig. 2, *n–p*) from the same locality, the dorsad depressed zone contains fine longitudinal lirae throughout, and in addition, both depressed zones at either side of the rostrum contain a tiny longitudinal ridge. Both specimens also show similar fine lirae or striae at a low angle to the base of the lateral ridge near the edge of the smooth zone. On the holotype these appear to form narrow linguae across the dorsad slope of the lateral ridge, but this effect may be produced partly from wear of the somewhat indistinct and slightly irregular longitudinal lirae.

The thin section of another paratype (fig. 2, *r*) leaves much to be desired, as there is a secondary filling of calcite and some fine- to medium-grained pyrite obscuring and even distorting some parts of the specimen. The coarser pyrite grains are ranged along some of the fine laminae of the rostrum. Also a fine cloudy brownish deposit that includes very fine grains of pyrite borders the siphuncle and several of the septa on its ventral side and forms a boundary between the cameral deposits and club-shaped areas of secondary calcite that have filled former cavities in the camerae. The material filling these club-shaped areas appears to have broken out from the sides of the siphuncle, which also is filled largely with secondary calcite (fig. 3).

The first three camerae in the thin section appear to be largely filled with cameral deposits, the episeptal ones fairly thick and the hyposeptal ones thin and poorly preserved. Owing to later recrystallization the boundaries cannot be distinguished. The episeptal deposits along the dorsal side of the chambers, marked by concentric bands of dark coloring matter, appear to reach nearly to the next septum. The hyposeptal deposits are thickest near the middle of the septum and toward the siphuncle. The camerae appear to be largely filled, also, on the ventral side of the siphuncle, but this is obscured by recrystallization and staining. Club-shaped cavity fillings are best developed in the 4th to 7th camerae in the thin section, each of them nearly touching the orad septum where the hyposeptal deposits are extremely thin. In subsequent camerae the deposits are much thinner and most of the space is occupied by secondary calcite. Here the septa and siphuncle are achoanitic terminating in rather sharp

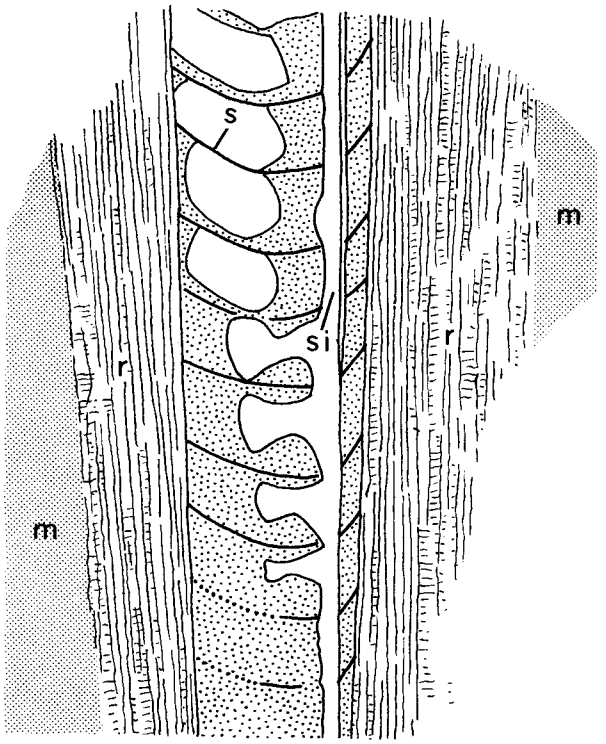


FIGURE 3.—*Stenoconites idahoensis* n. gen., n. sp. Diagrammatic sketch (× 10) of thin section along longitudinal dorsoventral axis of paratype (USNM 146475) shown also in fig. 2*r*. Sketch shows matrix (m), rostrum (r), septum (s), siphuncle (si), and two areas of secondary calcite within the phragmocone (white) occupied by material that appears to have in part moved along siphuncle, breaking through and invading some camerae; and stippled, areas believed to be occupied at least in part by secondary cameral deposits.

edges. Details of the structure of the siphuncle are obscured by the brown-stained secondary deposits.

Transverse thin sections cut further along the phragmocone show that the siphuncle enlarges somewhat and approaches a little closer to the ventral wall of the phragmocone. The rostrum, in this part of the shell at least, does not show a strong radial pattern as in the rostra of "*Dictoyoconites*." Instead, wavy or wrinkled concentric laminae are dominant, the minute wrinkles tending to line up radially to form a secondary interrupted radial pattern.

*Stenoconites idahoensis* is distinguished from the only other known Permian belemnoid "*Dictyoconites*" *groenlandicus* Fischer by the presence of a lateral ridge at either side of the rostrum, presence of smaller longitudinal grooves on some specimens, finer and less continuous longitudinal lirae on the rostral surface, and passage of the phragmocone for a considerable distance through the compressed rostrum. The phragmocone of the Greenland species (Fischer, 1947, p. 17) is without cameral deposits and has a marginal siphuncle, in contrast with the locally thick cameral deposits and the strongly excentric but not marginal siphuncle of *Stenoconites*.

*Types.*—Holotype USNM 146473, paratypes USNM 146474–146476.

*Occurrence.*—Phosphoria Formation, Meade Peak Member, USGS locs. 10434–PC (holotype and paratype), 10519–PC(?), 10493–PC (2 paratypes), 10594–PC (paratype), and 11630–PC(?), Caribou Co., Idaho.

## REFERENCES

Cressman, E. R., and Swanson, R. W., 1964, Stratigraphy and petrology of the Permian rocks of southwestern Montana: U.S. Geol. Survey Prof. Paper 313-C, p. 275–569, pls. 14–25, text figs. 87–156, 2 tables.

Davidson, O. F., Smart, R. A., Pierce, H. W., and Weisner, J. D., 1953, Stratigraphic sections of the Phosphoria Formation in Idaho, 1949, pt. 2: U.S. Geol. Survey Circ. 305, 28 p., 2 text figs.

Dutro, J. T., Jr., 1961, Correlation of the Arctic Permian: Art. 231 *in* U.S. Geol. Survey Prof. Paper 424-C, p. C225–C228, text fig. 231.1.

Fischer, A. G., 1947, A belemnoid from the Late Permian of Greenland: Meddelelser om Grønland, v. 133, no. 5, 24 p., 2 pls., 6 text figs.

Jeletzky, J. A., 1965, Taxonomy and phylogeny of fossil Coleoidea (=Dibranchiata): Geol. Survey Canada Paper 65–2.

Klepper, M. R., Honkala, F. S., Payne, O. A., and Ruppel,E. T., 1948, Stratigraphic sections of the Phosphoria Formation in Montana, 1948: U.S. Geol. Survey Circ. 260, 39 p., 2 text figs.

McKelvey, V. E., Armstrong, F. C., Gulbrandsen, R. A., and Campbell, R. M., 1953, Stratigraphic sections of the Phosphoria Formation in Idaho, 1947–48, pt. 2: U.S. Geol. Survey Circ. 301, 58 p., 2 text figs.

McKelvey, V. E., Davidson, D. F., O'Malley, F. W., and Smith, L. E., 1953, Stratigraphic section of the Phosphoria Formation in Idaho, 1947–48, pt. 1: U.S. Geol. Survey Circ. 208, 49 p., 1 pl., 2 text figs.

Miller, A. K., Furnish, W. M., Jr., and Clark, D. L., 1957, Permian ammonoids from western United States: Jour. Paleontology, v. 31, p. 1057–1068, pls. 133, 134, 6 text figs.

Mojsisovics, Edmund von, 1882, Cephalopoden der mediterranean Trias-provinz: K. K. geol. Reichanstalt, v. 10, 317 p., 94 pls.

———1902, Das Gebirge um Hallstad. Die Cephalopoden der Hallstädter Kalke. Supplement (1902): K. K. geol. Reichanstalt, v. 6, p. 175–356, pls. 1–33.

Müller-Stoll, Hans, 1936, Beiträge zur Anatomie der Belemnoidea: Nova Acta Leopoldina, N. F., v. 4, no. 20, p. 160–226, pls. 56–69, 5 text figs.

Sheldon, R. P., Warner, M. A., Thompson, M. E., and Pierce, H. W., 1953, Stratigraphic sections of the Phosphoria Formation in Idaho, 1949, pt. 1: U.S. Geol. Survey Circ. 304, 30 p., 2 text figs.

Trümpy, Rudolph, 1960, Über die Perm-Trias Grenze in Ostgrönland und über die problematik stratigraphischer Grenzen: Geol. Rundschau, v. 49, p. 97–103.

# DEVONIAN STRATIGRAPHY OF THE CONFUSION RANGE, WEST-CENTRAL UTAH

By RICHARD K. HOSE, Menlo Park, Calif.

*Abstract.*—Devonian strata in the Confusion Range, in west-central Utah, are more than a mile thick and are subdivided into four formations. In ascending order these are the Sevy Dolomite, Simonson Dolomite, Guilmette Formation, and Pilot Shale. The Sevy Dolomite is virtually unfossiliferous, but on the basis of regional considerations it is presumed to be of Devonian age. The Pilot Shale yields Devonian fossils from its lower half; however, the upper part, locally at least, contains a fauna of Early Mississippian age.

Devonian strata of the Confusion Range in western Utah are subdivided into four formational units which are, in ascending order, the Sevy Dolomite, the Simonson Dolomite, the Guilmette Formation, and the Pilot Shale. The first three formations were named by Nolan (1930, 1935) in the Gold Hill area, about 35 miles northwest of the Confusion Range; the Pilot Shale was named by Spencer (1917) in the Ely mining district, 60 miles west of the Confusion Range. Figure 1 shows the location of the Confusion Range and specific localities discussed in the text. Figure 2 is a generalized graphic section of the Devonian of the Confusion Range, showing the relative positions of critical fossils.

## SEVY DOLOMITE

Use of the term Sevy Dolomite, as is true also with the terms Simonson Dolomite and Guilmette Formation, was first extended to the Confusion Range by Campbell (1951). Subsequently Osmond (1954, 1962) made an exhaustive regional study of the Sevy and of the overlying Simonson Dolomite, and included data on one stratigraphic section in the Confusion Range.

The Sevy Dolomite crops out in the Salt Marsh Range (fig. 1, loc. 4); in the western of the two hills called Coyote Buttes (loc. 1); in the eastern flank of the Confusion Range from a point about 8 miles southeast of Cowboy Pass to the Barn Hills (locs. 7 to 14); along U.S. Route 6–50; on the southwest flank of the Confusion Range (loc. 13); and in the Conger Range (loc. 11). At localities 7 and 12 the Sevy is 1,300 feet thick; mapping in other areas in the Confusion Range indicates that this thickness is fairly representative.

The Sevy is undoubtedly one of the most homogeneous formations in western Utah and eastern Nevada. It consists of medium-gray dolomite that weathers light gray to yellowish gray, although some darker zones are present in the upper half. The rock is predominantly dense, with individual dolomite anhedra somewhat less than 0.008 mm in diameter, although the lower hundred feet or so is coarser (Osmond, 1954), and many anhedra in it are 0.02 to 0.09 mm in diameter. Within the upper few hundred feet there are also interbeds of tan medium- to coarse-textured dolomite. The thickness of the beds ranges from 6 inches to 6 feet and averages 1½ to 2 feet. Bedding and jointing are very regular, and the rock weathers to cuboidal or prismatic blocks.

In zones and thin beds in the upper 100 feet of the Sevy, scattered quartz grains are embedded in a dense dolomite matrix. The quartz grains are typically well rounded and equant to somewhat elongate, and range in diameter from 0.14 to 0.6 mm. Osmond (1954, 1962) has discussed the sand of the Sevy on a regional basis.

The contact of the Sevy Dolomite with the underlying Laketown Dolomite, of Silurian age, along the eastern edge of the Confusion Range is characterized

NAMES OF LOCALITIES ON FIGURE 1

1. West Coyote Butte; sec. 32, T. 15½ S., R. 15 W.
2. Unnamed butte; sec. 35, T. 15½ S., R. 16 W.
3. Bishop Spring anticline; sec. 8, T. 16 S., R. 17 W.
4. Salt Marsh Range; sec. 28, T. 15 S., R. 18 W.
5. Cowboy Pass; W½, T. 17 S., R. 17 W.
6. Southeast of Skunk Spring; sec. 3, T. 18 S., R. 16 W.
7. East of Cattleman's Little Valley; sec. 13, T. 18 S., R. 16 W.
8. Two miles northeast of Conger Mountain; sec. 29, T. 18 S., R. 16 W.
9. Mile and a Half Canyon; sec. 2, T. 19 S., R. 16 W.
10. East of Okelberry Pass; sec. 23, T. 19 S., R. 18 W.
11. Conger Range; sec. 28, T. 19 S., R. 18 W.
12. Central Confusion Range; secs. 14, 15, T. 20 S., R. 16 W.
13. West flank of Confusion Range; sec. 8, T. 21 S., R. 16 W.
14. Barn Hills; T. 21, 22 S., R. 14 W.

U.S. GEOL. SURVEY PROF. PAPER 550-B, PAGES B36-B41

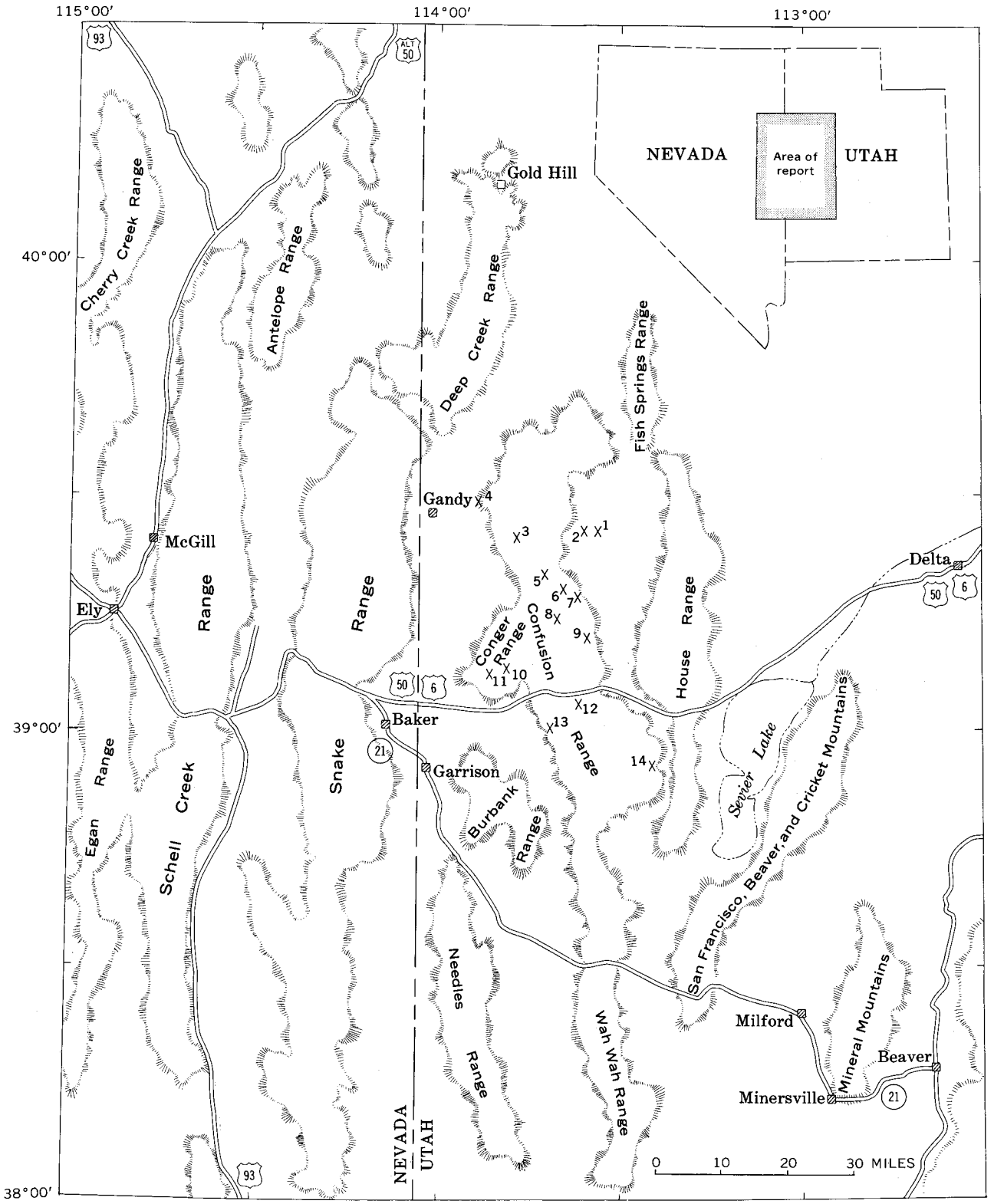


FIGURE 1.—Index map showing location of the Confusion Range and localities discussed in text.

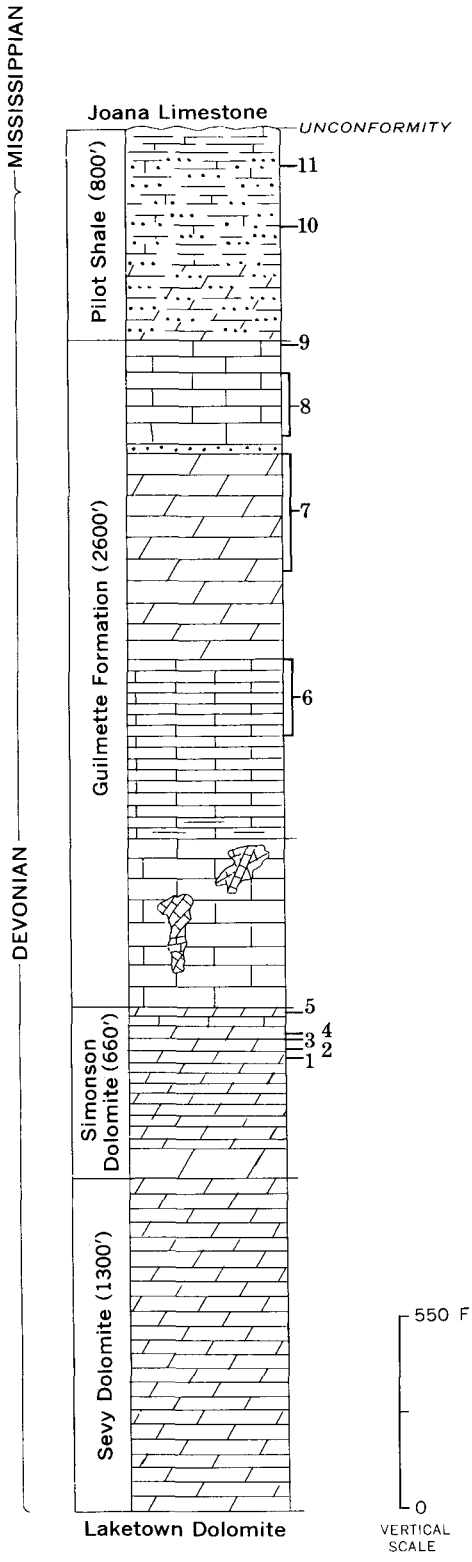


## FOSSIL COLLECTIONS

11 *Schuchertella*? sp. indet., *Chonetes* aff. *C. ornatus* Shumard, *Chonetes* sp., *Orbinaria* aff. *O. pyxidata* (Hall), *Geniculifera* sp., *Rhipidomella* cf. *R. missouriensis* (Swallow), *Stenocisma* 3 sp., *Camerotoechia* sp., *Rhynchopora*? cf. *R.*? *rowleyi* Weller, *Cranaena*? sp., *Spirifer centronatus* Winchell, *Spirifer* cf. *S. marionensis* Shumard, *Syringothyris* aff. *S. hannibalensis* (Swallow), *Torynifer cooperensis* (Swallow), *Crurithyris* sp., *Nuculana* sp., *Aviculopecten marbuti* (Rowley) var., *Cardiomorpha* sp. cf. *Naiadites* sp., *Sphenotus* sp., *Loxonema* sp., cf. *Dolorthoceras* sp., cf. *Imitoceras* sp., *Proetus (Pudoproetus)* cf. *P. (P.) missouriensis* Shumard, *Proetus* sp., horn corals

10 *Cyrtiopsis*? sp., "*Cleiothyridina*" sp.

9 *Manticoceras* sp., *Spirifer* cf. *S. strigosus* Meek, ?*Hypothyridina* sp.

8 *Thamnopora* sp., *Alveolites* sp., *Temnophyllum* or *Macgeea* n. sp., *Atrypa* cf. *missouriensis* Miller, *Productella* sp., *Disphyllum* sp., *Tenticospirifer utahensis* (Meek)

7 *Amphipora* sp., *Stromatopora* sp., *Orecopia mccoyi* (Walcott)?, *Atrypa* sp., *Orthoceras* sp., corals and bryozoans

6 *Tylothyris* sp., *Martiniopsis*? sp. or ?*Athyris* sp.

5 *Stringocephalus* sp.

4 *Dendrostella rhenana* (Frech)

3 *Cladopora* sp., *Syringopora* sp., *Mictophyllum* cf. *M. modicum* Smith, high-spired gastropods

2 *Cladopora* sp., *Favosites* sp., *Thamnopora* sp., *Alveolites* (abundant), *Atelophyllum* n. sp. A, *Atrypa* sp., ?*Athyris* sp., *Paracyclas* sp., *Productella* sp., "*Martinia*" cf. "*M.*" *sublineata* (Meek)

1 *Stromatopora* sp., *Amphipora*, ?*Atrypa* sp., *Orthoceras* sp., abundant high-spired gastropods

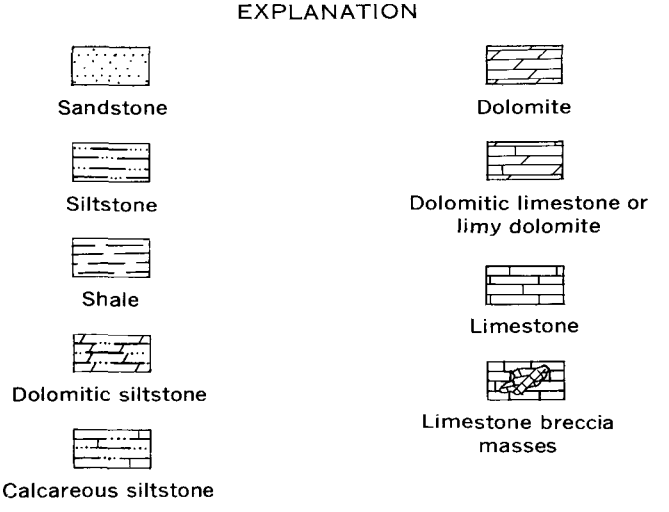


FIGURE 2.—Generalized stratigraphic section showing the relative positions of critical faunas.

by light-gray, fine-grained to dense dolomite above and by medium-dark-gray, medium- to fine-grained dolomite below. In the Conger Range the Sevy is in contact with a light-tan, massive saccharoidal dolomite of the Laketown.

Except for the occurrence of a questionable stromatoporoid biostrome just south of the Cowboy Pass quadrangle and a poorly preserved cephalopod siphuncle within that quadrangle, the Sevy Dolomite is unfossiliferous. On the basis of its stratigraphic position, but more importantly on its lithologic similarity, the Sevy is correlated with the Beacon Peak Dolomite and Oxyoke Canyon Sandstone Members of the Nevada Formation in the Eureka area, Nevada. According to C. W. Merriam (oral commun., 1965) the Beacon Peak Dolomite and Oxyoke Canyon Sandstone members of the Nevada Formation of the Eureka area are correlatives of the lower part of the Nevada Formation of Lone Mountain and the Sulphur Springs Range and are therefore of Helderberg and Oriskany age (Early Devonian).

## SIMONSON DOLOMITE

The Simonson Dolomite, like the Sevy Dolomite, is very widespread in western Utah and eastern Nevada. Its thickness of 660 feet at localities 12 and 13, in the central and western parts of the Confusion Range, is probably typical of that in areas to the north. Osmond's (1954) regional study has shown that the Simonson is divisible into four persistent subunits. This fourfold breakdown applies well in the Confusion Range.

The lowest unit of the Simonson—the coarse member of Osmond (1954)—is about 100 feet thick and consists of pale-yellowish-brown dolomite that weathers light olive gray. The rock is uniformly medium to coarsely crystalline and saccharoidal. The beds are from 3 to 4 feet thick and weather to rounded ledges.

The second unit—the lower alternating member of Osmond (1954)—is about 320 feet thick and consists of alternating beds of dense to finely crystalline dolomite and of somewhat coarser dolomite. The finer grained dolomite is virtually identical in gross lithology to the Sevy, although it is somewhat darker on a fresh fracture. The coarser material is brownish to light brownish gray, weathering pale brown to olive gray. Strong laminations such as those described by Nolan (1935) and Osmond (1954) are common. Within this unit locally are breccia masses that seem to occur as lenticular strata as well as in irregular pipes.

The third unit—the brown cliff member of Osmond (1954)—is about 40 feet thick and consists of dark-gray dolomite that weathers olive gray to pale yellowish brown. The rock is finely crystalline and occurs in beds from 6 inches to 2 feet thick. The upper part of the unit contains abundant gastropods, cephalopods, and hydrozoans (*Stromatopora* sp., *Amphipora* sp.), and sparse brachiopods. The fossils weather light yellowish gray and appear in sharp contrast to their dark matrix. About 8 miles southeast of Cowboy Pass the *Stromatopora* sp. forms a reeflike body.

The highest unit—the upper alternating member of Osmond (1954)—is about 200 feet thick south of U.S. Route 6–50 but seems somewhat thinner in the areas to the north. Dolomite is the dominant rock, but limestone is present locally. The dolomite alternates from dense or finely crystalline to coarse. Colors vary in much the same way as in Osmond's lower alternating member. Fossils from limestone in the lower part of this unit were identified as "*Martiniopsis*" sp. by C. W. Merriam, who (oral commun., 1955) regards this fossil as a temporal correlative of the *Martinia kirki* zone of central Nevada. *Stringocephalus* sp. was collected from a bed about 10 feet below the top of the Simonson in the southern part of the Cowboy Pass quadrangle. Merriam (written commun., 1960) regards this as a representative of the *Stringocephalus* zone of central Nevada. Both these zones are of Middle Devonian age, and at least the upper unit of the Simonson is correlative with the Woodpecker Limestone and Bay State Dolomite Members of the Nevada Formation of central Nevada.

The contact of the Simonson Dolomite with the Sevy Dolomite is characterized by dense medium-light-gray dolomite below and light-olive gray medium to coarsely crystalline dolomite above.

## GUILMETTE FORMATION

The Guilmette Formation is present in the Salt Marsh Range (fig. 1, loc. 4) and in an unnamed butte east of the northern part of the Confusion Range (loc. 2). It crops out along the east flank of the Confusion Range from an area about 6 miles east of Cowboy Pass southward to Mile-and-a-Half Canyon (loc. 9). Extensive outcrops are also present in the central and southern Confusion Range and in the Conger Range.

The Guilmette is about 2,600 feet thick at locality 6, about a mile southeast of Skunk Spring. However, mapping indicates that it is somewhat thinner in the Conger Range (loc. 11). The Guilmette consists of a well-defined basal unit and three additional, less well-defined units. The basal unit, which is about 650 feet thick, consists of massive to even-bedded, dark-gray to grayish-black sublithographic limestone that contains some zones of thin-bedded, somewhat laminated, dark-gray limestone. A distinctive feature of the basal unit is the presence of breccia in irregularly shaped, pipelike bodies that transect bedding for several tens of feet, and as somewhat irregular lenses. Breccia fragments

consist of limestone virtually identical with that of the unbrecciated portions. The fragments are angular and as much as 4 feet long, although most range from 2 to 7 inches in length. The similarity of the breccia clasts to the country rocks, coupled with their dissimilarity to both underlying and overlying units, suggests that the breccia was formed in part by collapse of the walls of solution cavities and in part by the washing into these cavities of material from above, at some period before or during the deposition of the next younger unit of the Guilmette.

The basal unit of the Guilmette generally forms massive rounded knolls, ridges, and cliffs.

The next younger unit of the Guilmette Formation, about 700 feet thick, consists mainly of even-bedded dark-gray limestone which weathers grayish black to very dark gray; pale-olive mottling is common in the upper half of this unit. Beds range from 6 inches to 3 feet in thickness and form minor ledges. In the lower half some zones are thin bedded and slightly argillaceous. Locally the sequence is dolomitized. C. W. Merriam identified the spiriferoid *Tylothyris* sp. from the upper half of this unit.

Next in ascending order is an 800-foot sequence of medium-gray to dark-gray dolomite that weathers light olive gray to brownish black. It is dominantly fine to medium grained, but some coarser zones of lighter colored dolomite are present. Vuggy inclusions of white, opaque crystals of calcite and of dolomite are scattered through a large portion of the rock. The unit is characterized by abundant biostromes made up of *Amphipora* and other stromatoporoids, corals, and bryozoans. Both the upper and lower boundaries are gradational.

The uppermost unit of the Guilmette Formation, 450 feet thick, consists primarily of limestone; however, it locally includes dolomite and, in the lower hundred feet or so, a few thin beds of quartz sandstone. The limestone is medium gray and weathers to olive gray. It is finely crystalline to dense. A large portion of the limestone of this topmost unit is biostromal and consists mainly of *Amphipora* or other stromatoporoids, corals, and bryozoans. Locally the limestone grades laterally into dolomite; the gradation is generally abrupt and is accompanied by an increase in grain size and a change in color from gray to brown. The sandstone is yellowish gray and weathers to yellowish gray or dark yellowish orange. It is of fine to medium grain. This unit forms resistant ridges. *Tenticospirifer utahensis* (Meek) was collected from 250 to 350 feet below the top of the Guilmette, and *Manticoceras* sp. from the uppermost few feet.

C. W. Merriam (*in* Nolan and others, 1956, p. 50–51; and 1963, p. 54–55) considers the species of *Tylothyris* to represent a temporal position between the *Stringocephalus* and *Spirifer argentarius* zones of central Nevada; he tentatively places the *Tylothyris* zone near the top of the Middle Devonian. The *Tenticospirifer utahensis* is considered correlative with the *Spirifer argentarius* zone of the Devils Gate Limestone, and the latter is a fairly reliable indicator of a widely recognized zone in the lower part of the Upper Devonian. *Manticoceras* is also of early Late Devonian age.

The contact of the Guilmette Formation with the underlying Simonson Dolomite is characterized by resistant massive thick-bedded locally brecciated limestone above and medium-bedded relatively less resistant dolomite below.

## PILOT SHALE

The term Pilot Shale was first extended to the Confusion Range by Campbell (1951). Within the Confusion Range, complete sections of the Pilot are lacking, although several well-exposed partial sections are present. The lower 200 to 300 feet is well exposed at locality 2. The core of Bishop Spring anticline (fig. 1, loc. 3) is underlain by the Pilot, and excellent exposures are present just east of Okelberry Pass in the Conger Range (loc. 10).

A moderately well exposed section was measured at locality 8, about 2 miles northeast of Conger Mountain, where the Pilot is about 830 feet thick and consists mainly of siltstone and dolomite siltstone. The latter lithology is common in the lower 300 feet or so, and thin sections indicate that about 60 percent of the rock is made up of grains of dolomite that are silt sized and generally euhedral, and of a small amount of calcite. Quartz, also of silt size, makes up about 15 percent of the rock. Interstitial material consisting of illite, chlorite, and brown pigment makes up the remaining 25 percent. The unit is olive gray, but equivalent strata of similar appearance, at locality 2 to the north, weather grayish yellow.

Siltstone higher in the section contains less carbonate and includes some shale interbeds. This siltstone is olive gray but weathers to yellowish gray and light olive gray.

A 4-foot conglomerate of limestone pebbles is present 160 feet above the base; another, about 15 feet thick, is about 450 feet above the base. A 4-foot nodular limestone underlain by 10 feet of shale that weathers to pale red is present 660 feet above the base. This limestone is the highest nodular limestone in the section. Together with the underlying shale it has been traced for 10 miles to the north. At the southernmost exposure the limestone-shale zone is about 170 feet below the top of the Pilot; at the northernmost exposure it is only 80 feet below the top; at inter-

mediate points the depth of the zone below the top changes northward from 170 to 80 feet, indicating that the Pilot Shale thins northerly in this area.

A collection of fossils from 450 feet above the base was identified by Jean M. Berdan and C. W. Merriam, who state (written commun., 1956): "This collection probably represents Zone D of Merriam (1940) on Dutch John Mountain and is considered Upper Devonian. Two of the most distinctive forms, *Cyrtiopsis*? sp. and *'Cleiothyridina'* sp., appear to be identical with specimens from Dutch John Mountain."

Collections from the highest nodular limestone unit, identified by Mackenzie Gordon, Jr., and Ellis Yochelson, include the following forms: *Schuchertella*? sp. indet., *Chonetes* aff. *C. ornatus* Shumard, *Chonetes* sp., *Orbinaria* aff. *O. pyxidata* (Hall), *Geniculifera* sp., *Rhipidomella* cf. *R. missouriensis* (Swallow), *Stenocisma* 3 sp., *Camerotoechia* sp., *Rhynchopora*? cf. *R.*? *rowleyi* Weller, *Cranaena*? sp., *Spirifer centronatus* Winchell, *Spirifer* cf. *S. marionensis* Shumard, *Syringothyris* aff. *S. hannibalensis* (Swallow), *Torynifer cooperensis* (Swallow), *Crurithyris* sp., *Nuculana* sp. *Aviculopecten marbuti* (Rowley) var., *Cardiomorpha* sp. cf. *Naiadites* sp., *Sphenotus* sp., pleuratomariid gastropods indet., *Bellerophon* sp., A, cf. *Sinautina* sp., *Loxonema* sp., cf. *Dolorthoceras* sp., cf. *Imitoceras* sp., *Proetus* (*Pudoproetus*) cf. *P.* (P.) *missouriensis* Shumard, *Proetus* sp., and horn corals.

Gordon's report (written commun., 1956) states:

"The presence of such species as *Spirifer centronatus* Winchell, *Torynifer cooperensis* (Swallow) and *Syringothyris* aff. *S. hannibalensis* (Swallow) are clear indications of the early Mississippian age of the beds. Inasmuch as this is a varied fauna and there are close similarities in different phyla and classes to species in the Louisiana Limestone of east central Missouri, we feel that there is good evidence for a rough stratigraphic equivalence of these beds to the Louisiana Limestone." From the same collections Helen Duncan (U.S. Geol. Survey, 1964, p. A104) identified *Permia* and *Rhopalolasma* which she regards as characteristic Carboniferous rugose coral genera.

Characteristically the Pilot Shale forms slopes. Its contact with the Guilmette Limestone is moderately sharp, being gradational within a few feet. Beds below the contact form resistant ridges and ledges, whereas those above form slopes.

## REFERENCES


Campbell, G. S., 1951, Stratigraphy of the House and Confusion Ranges, Millard County, Utah: Utah Geol. Soc. Guidebook, no. 6, p. 19–25.

Merriam, C. W., 1940, Devonian stratigraphy and paleontology of the Roberts Mountains region, Nevada: Geol. Soc. America Spec. Paper 25, 114 p.

——— 1963, Paleozoic rocks of Antelope Valley, Eureka and Nye Counties, Nevada: U.S. Geol. Survey Prof. Paper 423, 67 p.

Nolan, T. B., 1930, Paleozoic formations in the Gold Hill quadrangle, Utah: Washington Acad. Sci. Jour., v. 20, no. 17, p. 421–432.

——— 1935, The Gold Hill mining district, Utah: U.S. Geol. Survey Prof. Paper 177.

Nolan, T. B., Merriam, C. W., and Williams, James Steele, 1956, The stratigraphic section in the vicinity of Eureka, Nevada: U.S. Geol. Survey Prof. Paper 276, 77 p.

Osmond, J. C., 1954, Dolomites in Silurian and Devonian of east-central Nevada: Am. Assoc. Petroleum Geologists Bull., v. 38, no. 9, p. 1911–1956.

——— 1962, Stratigraphy of Devonian Sevy Dolomite in Utah and Nevada: Am. Assoc. Petroleum Geologists Bull., v. 46, no. 11, p. 2033–2056.

Spencer, A. C., 1917, The geology and ore deposits of Ely, Nevada: U.S. Geol. Survey Prof. Paper 96, 189 p.

U.S. Geological Survey, 1964, Geological Survey Research 1964: U.S. Geol. Survey Prof. Paper 501–A, 367 p.

# TERTIARY EXTRUSIVE VOLCANIC ROCKS IN MIDDLE PARK, GRAND COUNTY, COLORADO

By GLEN A. IZETT, Denver, Colo.

*Abstract.*—Middle and late Tertiary volcanism along Rabbit Ears Range, Colo., produced extrusive rocks that extend from the crest of the range into the Hot Sulphur Springs quadrangle, Middle Park, Grand County, Colo. These rocks are here divided into two units newly named in this paper: the Rabbit Ears Volcanics of Oligocene and Miocene(?) age, and the Grouse Mountain Basalt of Pliocene(?) age. The Grouse Mountain, which comprises basalt flows 0 to 500 feet thick, is locally separated from the Rabbit Ears by the Troublesome Formation of Miocene age. In the Hot Sulphur Springs quadrangle, the Rabbit Ears unconformably overlies the Middle Park Formation of Late Cretaceous and early Tertiary age and includes a lower unit of trachybasalt lavas here named the Pete Gulch Member, 0 to 200 feet thick, and an overlying unit of interlayered tuff breccia, tuffs, and latite lavas, 0 to 800 feet thick. An isotopic K–Ar age of $33 \pm 3$ million years, or Oligocene, was obtained from a rhyolite breccia near the middle of the Rabbit Ears Volcanics.

Middle to late Tertiary volcanism along the Rabbit Ears Range produced a sequence of extrusive volcanic rocks that mantle uplands in the range and extend northward into North Park and southward into Middle Park, in Grand County, Colo. A generalized map of the distribution of these volcanic rocks is shown in figure 1. In general, the rocks extend along the crest of the Rabbit Ears Range from about Sheep Mountain to near Chimney Rock. From Chimney Rock, they extend southeastward along Rabbit Ears Creek and generally east of Troublesome Creek into Middle Park as far south as Hot Sulphur Springs. The distribution north of Rabbit Ears Range is not yet known. The aggregate thickness of the rocks may be as much as 1,500 feet in the Rabbit Ears Range, but they thin to the south. The original thickness and lateral extent of the rocks are uncertain owing to extensive erosion and to the intensely dissected terrain upon which the rocks lie. The rocks belong to the alkali-calcic clan and include silicic tuffs, intermediate lavas and fragmental rocks, and basaltic lavas.

The volcanic rocks exposed in the Hot Sulphur Springs quadrangle in Middle Park have been studied as part of a mapping program of the U.S. Geological Survey. In the Hot Sulphur Springs quadrangle, the rocks form mappable units here designated the Rabbit Ears Volcanics of Oligocene and Miocene(?) age and the Grouse Mountain Basalt of Pliocene(?) age. The Rabbit Ears Volcanics locally includes a distinctive lower member composed of trachybasalt flows here named the Pete Gulch Member. The volcanic rocks in the Hot Sulphur Springs quadrangle were extruded from vents scattered along the Rabbit Ears Range.

Details of stratigraphic relations and areal extent of the volcanic rocks in the Rabbit Ears Range and North Park are currently being studied by D. M. Kinney and W. J. Hail, Jr., of the U.S. Geological Survey.

In the past, the volcanic rocks have been studied only in reconnaissance or have been mapped as part of thesis problems, and complete descriptions of the rocks have never been reported. Marvine (1874, p. 174) briefly mentioned these rocks and, later, Grout and others (1913, p. 51) mapped in reconnaissance along the Rabbit Ears Range and described intrusive and extrusive rocks that included a breccia unit composed of "an immense deposit of fragments, with some flows." Grout and others believed that the rocks were of late Eocene or younger age. Richards (1941), in an unpublished thesis, applied the name "Rabbit Ears Creek breccia" to a sequence of volcanic rocks northeast of Kremmling, Colo., and he assigned an Eocene age to the rocks. These rocks can be traced into the mass of breccia mapped by Grout and others. Tollefson (1955), Tweto (1957), Shearer (1957), and Bombolakis (1958) briefly mentioned or mapped some of the volcanic rocks in Middle Park.

## RABBIT EARS VOLCANICS

Extrusive volcanic rocks of Oligocene and Miocene(?) age are assigned to the Rabbit Ears Volcanics here named for the Rabbit Ears Range, the type area, where the rocks are extensively exposed. The formation in-

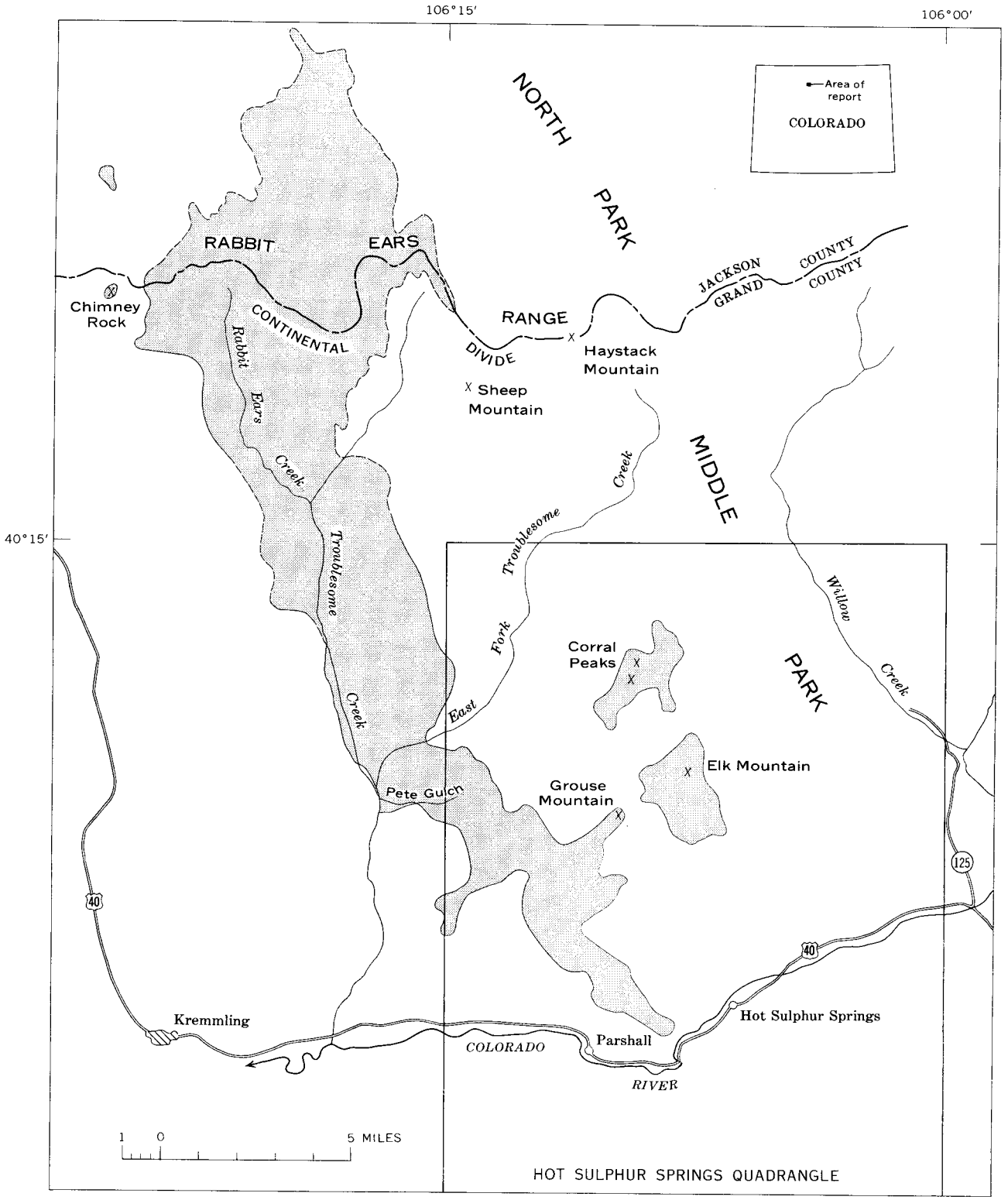


FIGURE 1.—Index map showing generalized outcrop of extrusive volcanic rocks (stippled) of middle to late Tertiary age in northern Middle Park, Colo.

797-218 O—66——4

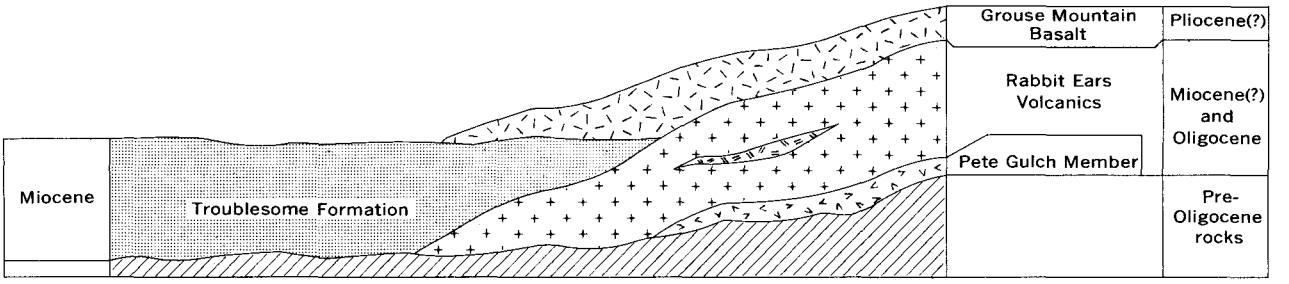


FIGURE 2.—Schematic section showing relation between extrusive volcanic rocks and Troublesome Formation in Middle Park, Colo.

cludes (1) a thin lower unit of olivine-bearing trachybasalt flows, the Pete Gulch Member of probable Oligocene age, and (2) a thick upper part composed of intercalated tuff, breccia, and lavas of silicic to intermediate composition. The Rabbit Ears rests with marked unconformity on coarse-grained sedimentary rocks of the Middle Park Formation or equivalent rocks of Late Cretaceous and early Tertiary age or on older Mesozoic sedimentary and Precambrian crystalline rocks that floor Middle Park Basin. The Rabbit Ears is locally overlain by tuffaceous basin-fill sedimentary rocks of the Miocene Troublesome Formation (Richards 1941; Lovering and Goddard, 1950, p. 41; and Izett and Lewis, 1963) or by late Tertiary olivine-bearing basalt flows, here named the Grouse Mountain Basalt of Pliocene(?) age. A schematic diagram of the relations of these rocks is shown in figure 2.

The Rabbit Ears is well exposed at Elk Mountain, Corral Peaks, and along the lower reaches of the East Fork Troublesome Creek. In these areas, the bulk of the formation comprises about 800 feet of poorly bedded and sorted breccia and tuff breccia interlayered with tuffs and lavas. Most of the fragments in the breccia and tuff breccia consist of porphyritic quartz latite, rhyodacite, and latite in various shades of gray, brown, and red. Many of these rock fragments contain large phenocrysts of feldspar and smaller phenocrysts of biotite, hornblende and pyroxene. A few of the fragments are a distinctive well-indurated slightly welded quartz rhyolite ash-flow tuff. Most of the fragments are fist sized, but blocks as large as 4 feet in diameter are common. At East Fork Troublesome Creek, the upper part of the Rabbit Ears contains lenticular rhyolite ash-flow tuffs that weather to tepee-shaped forms, and latite lava flows about 100 feet thick.

Some fragments in the breccia are petrographically similar to samples of a small pluton collected at Haystack Mountain in the Rabbit Ears Range. Haystack Mountain is one of many small intrusive bodies along the Rabbit Ears Range that probably vented during middle Tertiary time. Vents of this type were the source of part of the volcanic rocks in the Rabbit Ears Volcanics.

In most areas, the Rabbit Ears rests unconformably on a rugged erosion surface cut on the Middle Park Formation and older rocks during late Eocene and early Oligocene time. Remarkably clean exposures of the basal contact of the Rabbit Ears occur on the east face of Elk Mountain (fig. 3). In areas where the Pete Gulch Member is present, the upper contact of the Pete Gulch appears unconformable and marked by a thin concentration of pebbles of Precambrian granitic rocks probably derived from reworking of conglomerates in the Middle Park Formation.

The lavas and breccia fragments in the Rabbit Ears are varied in composition and texture. Under the microscope, the quartz latite, rhyodacite, and latite contain phenocrysts of plagioclase that range from oligoclase through andesine, and the quartz latite contains a few large phenocrysts of soda-rich sanidine. Phenocrysts of mafic minerals are biotite, hornblende, salitic augite, and hypersthene. The biotite and hornblende show thick opaque borders, the effects of

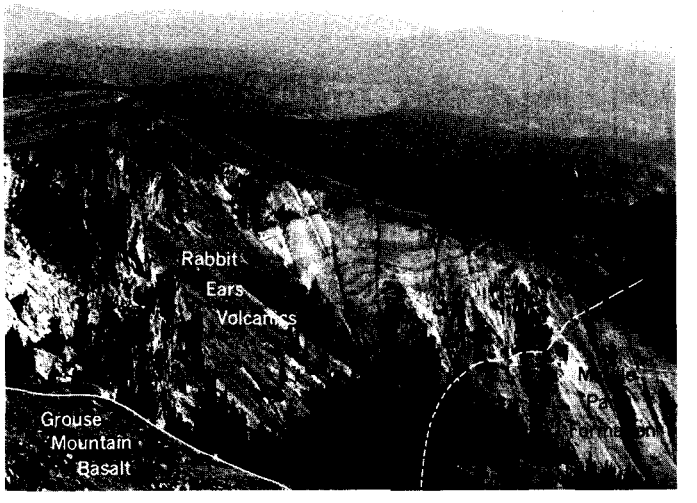


FIGURE 3.—Relation between Rabbit Ears Volcanics and the Middle Park Formation at Elk Mountain.

roasting. The groundmass usually consists of felty to trachytic feldspar and occult quartz. The phenocrysts in the rhyolite welded tuffs are embayed bipyramidal high-temperature quartz, sanidine, and oligoclase set in a matrix of slightly compacted devitrified shards. Mafic minerals in the rhyolite are sparse, but a few flakes of altered biotite are present.

The Rabbit Ears is roughly dated as middle Tertiary by its stratigraphic position above the Middle Park Formation of Late Cretaceous and early Tertiary age and below the Troublesome Formation of Miocene age. Corroborating the stratigraphic evidence of a middle Tertiary age for the Rabbit Ears is an isotopic K-Ar age of $33\pm3$ million years, or Oligocene, determined on sanidine from a rhyolite welded tuff breccia fragment collected by the writer from about the middle of the formation in the center of sec. 23, T. 2. N., R. 79 W., in the Hot Sulphur Springs quadrangle. G. C. Curtin, of the U.S. Geological Survey, separated the sanidine from the tuff, and the sample was analyzed for potassium and argon by H. H. Thomas, R. F. Marvin, and Paul Elmore, of the U.S. Geological Survey. The analytical data obtained on the sanidine separate are as follows:

| *Sample No.* | $K_2O$ *(percent)* | $K^{40}$ *(ppm)* | $*Ar^{40}$ *(ppm)* | $*Ar^{40}/Ar^{40}_{total}$ | $*Ar^{40}/K^{40}$ | *Age (m.y.)* |
|---|---|---|---|---|---|---|
| G06762___ | 8.97 | 9.09 | 0.0176 | 91 | 0.00194 | $33\pm3$ |

Decay constants: $K^{40}\lambda_\epsilon=0.585\times10^{-10}$ yr$^{-1}$.
$\lambda_\beta=4.72\times10^{-10}$ yr$^{-1}$.
Abundance: $K^{40}=1.22\times10^{-4}$ g/g K.
*radiogenic

The isotope age is probably a maximum age for the formation for three reasons: (1) the sample was a breccia fragment, and an unknown amount of time elapsed between the extrusion of the ash flow and the time it was fragmented and incorporated in the breccia; (2) the rhyolite contains rare xenocrysts of microcline that probably were derived from a rock of Precambrian age; the microcline might have contaminated the sanidine and would tend to mask the age of the welded ash-flow tuff; and (3) later metamorphism to which K-Ar ages have been found to be particularly sensitive is lacking in the area. Locally, the Rabbit Ears is overlain by the Troublesome Formation of Miocene age in seemingly gradational contact, and an early Miocene age for part of the Rabbit Ears cannot be discounted. Accordingly, the Rabbit Ears is tentatively dated as Oligocene and early Miocene(?).

### Pete Gulch Member

The Pete Gulch Member of the Rabbit Ears Volcanics of Oligocene age is here named for distinctive trachybasalt lava flows near Pete Gulch in secs. 4 and 9, T. 2 N., R. 79 W., the type locality, in the Hot Sulphur Springs quadrangle. The trachybasalt is exposed at several places in the quadrangle and ranges in thickness from 0 to 200 feet. Near Pete Gulch, the lower 70 feet of the unit is polygonally jointed and overlain by about 100 feet of massive-weathering trachybasalt. The Pete Gulch was deposited on an intensely eroded terrain cut on the Middle Park Formation. Commonly, the contact between the Pete Gulch and the older rocks is covered by talus, but where the contact was seen it is sharp and the lower part of the formation is red and scoriaceous.

In hand sample, the trachybasalt is porphyritic and is a distinctive dark-gray to black fairly dense rock characterized by conspicuous large phenocrysts of pyroxene set in an aphanitic groundmass. Smaller phenocrysts include olivine, scattered flakes of biotite about 0.5 millimeter in diameter, small tabular feldspar crystals, and hornblende(?) ghosts as much as 1 centimeter long. The large phenocrysts of pyroxene and the biotite and hornblende(?) ghosts distinguish the Pete Gulch from younger nonporphyritic basalt flows of the Grouse Mountain Basalt.

Thin sections of the rock show that the large phenocrysts of pyroxene are ferroaugite-salite ($2V_z=56$–$59°$; $n_y=1.705$–$1.715$), as much as 1 cm long. Other smaller mafic minerals are ferroaugite, olivine ($2V_x=85$–$88°$; $n_x=1.678$–$1.680$), and rare biotite. Hornblende(?) ghosts that now consist of magnetite, feldspar, clinopyroxene, and chlorophaeite are scattered through the rock. Corroded phenocrysts of plagioclase ($An_{40-45}$) are set in a flow-oriented groundmass of plagioclase ($An_{35-45}$) laths, clinopyroxene rods and granules, alkali feldspar(?), acicular apatite, and iron ore. Alteration products are analcime, saponite, chlorophaeite, and calcite.

The Pete Gulch is tentatively dated as Oligocene inasmuch as it overlies the Middle Park Formation of Late Cretaceous and early Tertiary age and seems to be spatially related to the upper part of the Rabbit Ears, a part of which has been dated as no older than Oligocene by radioisotope methods.

## GROUSE MOUNTAIN BASALT

The Grouse Mountain Basalt of Pliocene(?) age is here named for basalt lava flows at Grouse Mountain in the Hot Sulphur Springs quadrangle. The type locality is designated to be in NE¼ sec. 18, T. 2 N., R. 78 W., at Grouse Mountain. The basalt is the youngest extrusive rock in the area and caps many of the upland surfaces north of the Colorado River. The basalt is about 250 feet thick at Grouse Mountain, but elsewhere it is as much as 500 feet thick. At Grouse Mountain, the basalt flows rest unconformably on the Rabbit Ears Volcanics or the Middle Park Formation. In the main, the Grouse Mountain consists of a succes-

sion of massive to blocky lava flows that show scoriaceous tops and bottoms. Locally, thin layers of tuffaceous sedimentary rocks are intercalated between the lavas.

Hand samples of the basalt are dark brownish gray to black and contain inconspicuous small phenocrysts of olivine. The basalt is generally altered to shades of brown or gray, and some weathered surfaces show a characteristic spotted pattern. Under the microscope, the phenocrysts of olivine ($Fo_{75-80}$) are as much as 3 mm long and are set in a flow-oriented matrix of plagioclase laths ($An_{50}$), granular augite ($2V_z=55°$; $n_y=1.705$), acicular apatite, and iron ore. Alteration products include calcite, saponite, zeolites, and quartz.

The Grouse Mountain is no older than Miocene for it locally overlies the Troublesome Formation of Miocene age, but an upper age limit for the Grouse Mountain cannot be stratigraphically determined because no other rocks overlie the formation. Until the age of the Grouse Mountain can be established, it is provisionally dated as Pliocene(?).

In summary, the extrusive volcanic rocks of middle and late Tertiary age can be divided into a lower unit of interlayered lavas and fragmental rocks (Rabbit Ears Volcanics) and an upper unit of basalt flows (Grouse Mountain Basalt). In some areas, these units are separated by tuffaceous intermontane basin-fill deposits of Miocene age (Troublesome Formation).

## REFERENCES

Bombolakis, E. G., 1958, Geology of the Hot Sulphur Springs–Parshall area of Middle Park, Grand County, Colorado: Colorado School of Mines Master's thesis (available on microfilm from University Microfilms, Inc., Ann Arbor, Mich.).

Grout, F. F., Worcester, P. G., and Henderson, Junius, 1913, Reconnaissance of the geology of the Rabbit Ears region, Routt, Grand, and Jackson Counties, Colorado: Colorado Geol. Survey Bull. 5, pt. 1, p. 1–57.

Izett, G. A., and Lewis, G. E., 1963, Miocene vertebrates from Middle Park, Colorado: Art. 31 *in* U.S. Geol. Survey Prof. Paper 475–B, p. B120–B122.

Lovering, T. S., and Goddard, E. N., 1950, Geology and ore deposits of the Front Range, Colorado: U.S. Geol. Survey Prof. Paper 223, 318 p.

Marvine, A. R., 1874, Report [on the Middle Park division], *in* Hayden, F. V., Seventh Annual Report of the U.S. Geological and Geographical Survey of the Territories * * * for the year 1873: Washington, U.S. Gov't. Printing Office, p. 83–192.

Richards, Arthur, 1941, Geology of the Kremmling area, Grand County, Colorado: Michigan Univ., Ph. D. thesis (available on microfilm from University Microfilms, Inc., Ann Arbor, Mich.).

Shearer, E. M., 1957, Geology of the Hot Sulphur Springs area, Grand County, Colorado, *in* Rocky Mountain Assoc. Geologists Guidebook 9th Ann. Field Conf., North and Middle Park Basins, Colorado, 1957: p. 99–103.

Tollefson, O. W., 1955, Geology of central Middle Park, Colorado: Colorado Univ., Ph. D. thesis (available on microfilm from University Microfilms, Inc., Ann Arbor, Mich.).

Tweto, Ogden, 1957, Geologic sketch of southern Middle Park, Colorado, *in* Rocky Mountain Assoc. Geologists Guidebook 9th Ann. Field Conf., North and Middle Park Basins, Colorado, 1957: p. 18–31.

# *OKETAELLA EARGLEI*, A NEW FUSULINID SPECIES, FROM THE ADAMS BRANCH LIMESTONE MEMBER OF THE GRAFORD FORMATION OF LATE PENNSYLVANIAN AGE, BROWN COUNTY, TEXAS

By DONALD A. MYERS, Denver, Colo.

*Abstract.*—Specimens of a new fusulinid species, *Oketaella earglei*, described in this report, were collected from the Adams Branch Limestone Member of the Graford Formation (Upper Pennsylvanian) in north-central Texas. Poorly preserved specimens of this form had been questionably referred to the genus *Staffela* by Myers in 1960.

Small thin-walled fusulinids with a *Staffella*-like shape have been observed by the writer since 1952 in post-Strawn Pennsylvanian rocks in north-central Texas. Specimens with this shape were identified and figured by Myers (1960) as *Staffella*? sp. in collections from the Winchell Limestone (pl. 17, fig. 25), the Home Creek Limestone Member of the Caddo Creek Formation (pl. 17, fig. 5), and the Bluff Creek Shale and Gunsight Limestone Members of the Graham Formation (pl. 18, figs. 12, 19; pl. 19, fig. 9).

The structure of the spiral wall, or spirotheca, is a primary criterion in generic classification of fusulinids. The wall of *Staffella* is thin and is composed of four layers consisting of outer and inner tectoria, a thin tectum, and the diaphanotheca. Because the forms identified as *Staffella*? sp. have a thin spirotheca that is generally poorly preserved, their taxonomic position has been in doubt. Sections of specimens prepared recently, from U.S.G.S. loc. f10109 (fig. 1), from the Adams Branch Limestone Member of the Graford Formation, reveal a two-layered wall consisting of a thin tectum and keriotheca (fig. 2, *e*, *g*). This wall structure, plus the size and shape of the test and the character of the septa, places these fusulinids in the genus *Oketaella* Thompson, 1951.

The genus *Oketaella* was described by Thompson (1951, p. 116) for those forms with a minute and inflated shell

with convex surfaces, straight to slightly irregular axis of coiling, and sharply pointed to rounded polar ends. Mature specimens are composed generally of less than six volutions and are approximately a millimeter in maximum diameter, which is in the direction of the axis coiling. The ratio of the axial length to the width of the shell normal to the axis of coiling is greater than unit value but is less than three in all forms known. The proloculus is large in comparison to the size of the shell, and all volutions are relatively loosely coiled. The septa are thick and are unfluted throughout their length * * *. The spirotheca is relatively thick * * * and is composed of the tectum and a thick keriotheca with coarse alveoli in its lower part * * *. The tunnel is singular, and its path is straight to slightly irregular. Chomata occur throughout the shell except for the last part of the last volution. They are low and narrow in the first volution and are high, broad, and asymmetrical in outer volutions. They seem continuous with coatings on top of the spirotheca that merge with small fillings in the axial zone.

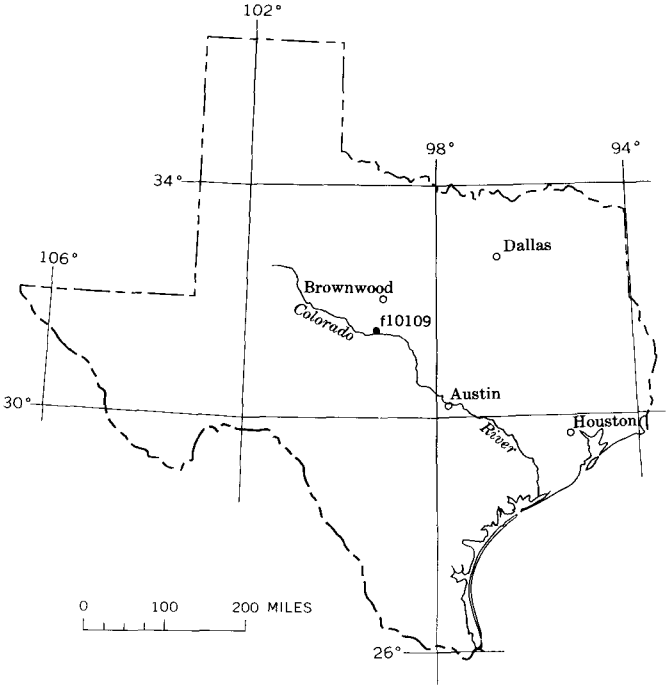


FIGURE 1.—Index map of Texas, showing location of USGS loc. f10109.

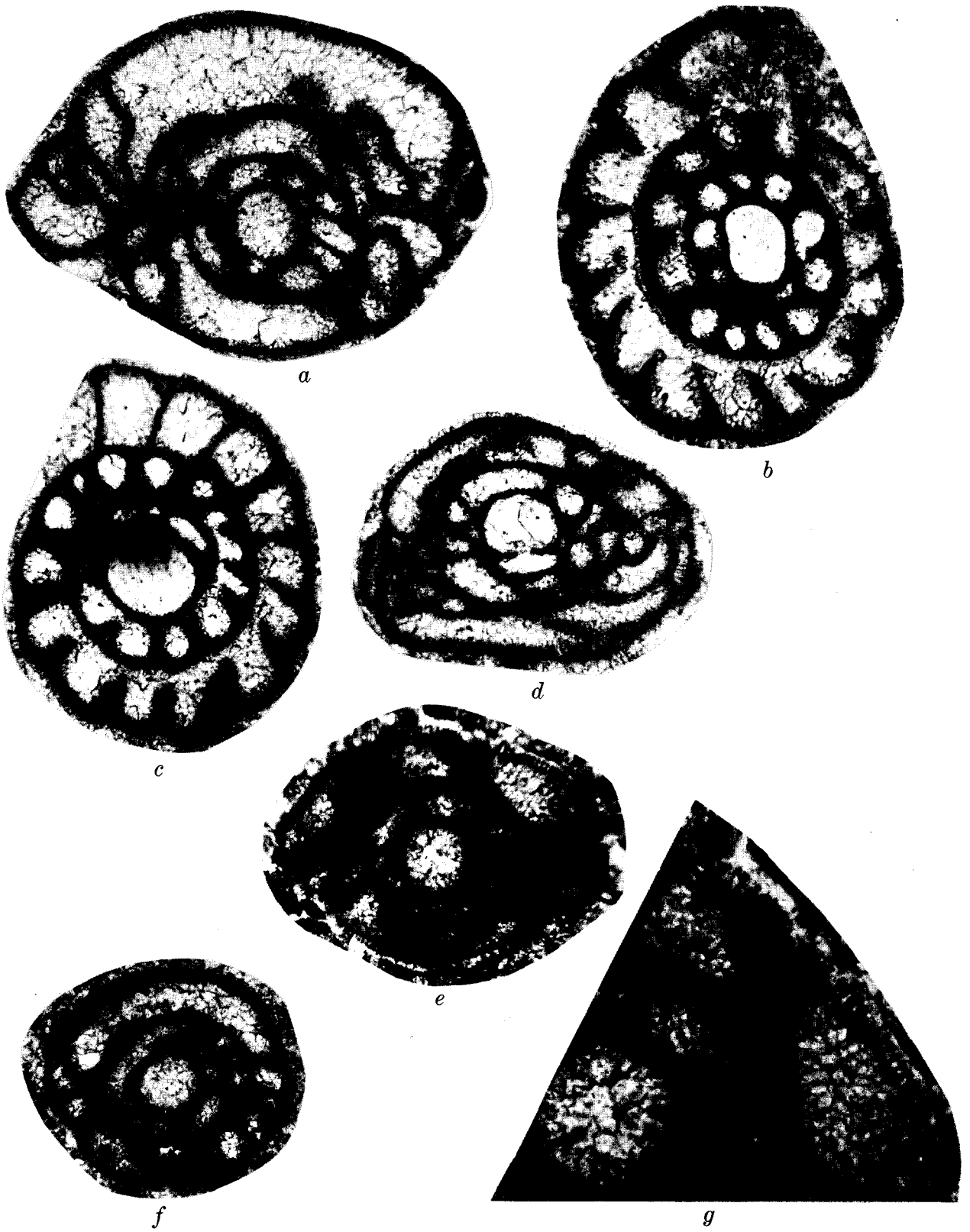


FIGURE 2.—*Oketaella earglei*, n. sp., from the Adams Branch Limestone Member of the Graford Formation, Brown County, Tex.

The type species, designated *Oketaella fryei* by Thompson (1951, p. 116) is from the Oketo Shale Member of the Barneston Limestone in Kansas, and is of middle Wolfcamp age. Since 1951, three species have been described from Lower Permian rocks and three from Pennsylvanian rocks. The Permian species, all from north-central Texas, are: *Oketaella waldripensis* Thompson, 1954, from the Waldrip Shale Member of the Pueblo Formation; *O. campensis* Thompson, 1954, from the Camp Colorado Limestone Member of the Pueblo Formation; and *O. cheneyi* Thompson, 1954, from the Coleman Junction Limestone Member of the Putnam Formation. The Pennsylvanian species are: *Oketaella lenensis* Thompson, Verville, and Lokke, 1956, from the Perry Farm Shale Member (Jewett, 1941, p. 339–340) of the Lenapah Limestone in northern Oklahoma; *O. oscurensis* Thompson, Verville, and Lokke, 1956, from the lower part of the type section of the Coane Formation of Thompson (1942) in New Mexico; and *O. inflata* Thompson and Lamerson, 1957 (*in* Thompson, 1957) from the Sniabar Limestone Member of the Hertha Limestone of Thompson (1957) near Kansas City, Mo.

## Genus OKETAELLA Thompson, 1951

### Oketaella earglei Myers, new species

Figure 2, *a–g* and table 1

*Description.*—A small, subspherical to inflated, fusiform species with rounded ends and a maximum length of about 0.9 mm and a maximum width of about 0.6 mm. Average length and width are 0.7 mm and 0.5 mm, respectively, in mature specimens of 3 volutions.

The height of the volution increases from an average of 0.037 mm in the first whorl, to 0.053 mm in the second, and to 0.090 mm in the third. The form ratio averages 1.2 in the first whorl and 1.4 in the second and third whorls.

The proloculus is larger than that of any previously described species assigned to this genus. Its external diameter averages 0.124 mm and ranges from 0.085 mm to 0.158 mm. It is generally spherical, although in a few specimens it exhibits a subquadrate cross section. The wall of the proloculus is about 0.012 mm thick, although in a few specimens it may be as thin as 0.006 mm.

The chomata are low, broad, and poorly defined. The tunnel is poorly defined. The tunnel angle averages about 33° in the first volution and about 38° in the second.

The septa are plane except in the polar regions, where very weak fluting may be developed. Septal pores have not been noted. The number of septa ranges from 7 to 9 in the first volution, ranges from 11 to 15 in the second, and is about 18 in the third.

The spiral wall has an average thickness of 0.011 mm in the first volution, 0.016 mm in the second, and 0.018 mm in the third. It consists of a very thin tectum and keriotheca. Measurements of a single specimen (fig. 2, *e*, *g*) show the tectum in the second whorl to be 0.0063 mm thick, and the keriotheca to be 0.0095 mm thick, with the individual alveolus about 0.0042 mm thick. Eight alveoli in this specimen occupy 0.063 mm.

*Discussion.*—*Oketaella earglei*, n. sp., is somewhat larger, has one less volution, has a somewhat thicker wall, has a larger proloculus, and less well developed chomata than *O. oscurensis* Thompson, Verville, and Lokke, 1956.

*Oketaella earglei* has less well-developed chomata, a somewhat larger proloculus, and differs in shape from *O. lenensis* Thompson, Verville, and Lokke, 1956. *O. lenensis* has an inflated subfusiform shape; that of *O. earglei* is more spherical. *Oketaella earglei* has about the same size, shape, and form ratio as *O. inflata* Thompson and Lamerson, 1957 (*in* Thompson, 1957), but *O. earglei* has a larger proloculus, thicker spiral wall, and poorly developed chomata.

The poorly defined chomata of *O. earglei* are typical of that species. In all other described species the chomata are well developed. This species is named for D. Hoye Eargle, U.S. Geological Survey, in recognition of his contributions to Pennsylvanian stratigraphy in Brown and Coleman Counties, Tex.

The holotype and illustrated paratypes have been deposited at the U.S. National Museum.

*Age and distribution.*—*Oketaella earglei* n. sp. has been found in the lower part of the Canyon Group and is of Late Pennsylvanian age. The holotype (fig. 2, *a*) and all figured specimens (fig. 2, *a–g*) are from the Adams Branch Limestone Member of the Graford Formation and were collected about 7 feet below the base of the Cedarton Shale Member at USGS loc. f10109. The locality is in Brown County, on the west side of U.S. Highway 377, between the community of Winchell and the highway bridge across the Colorado River. The

EXPLANATION OF FIGURE 2

*Oketaella earglei* Myers, n. sp. All figured specimens are from the Adams Branch Limestone Member of the Graford Formation, USGS loc. f10109. Magnification of *a–f*, ×120; *g*, ×250.

*a*. Axial section of the holotype. USNM 642560.
*b*. Equatorial section of a paratype, with a subquadrate cross section of the proloculus. USNM 642561.
*c*. Equatorial section of a paratype. USNM 642562.
*d*. Axial section of a paratype showing the aperture of the proloculus and the initial chamber. USNM 642563.
*e*. Axial section of a paratype with the alveolar structure of the wall preserved in the outer whorl. USNM 642564.
*f*. Imperfectly oriented axial section of a paratype. USNM 642565.
*g*. Enlarged portion of *e* showing keriotheca and pendulous shaped alveoli in the outer whorl.

TABLE 1.—*Measurements of* Oketaella earglei *Myers, n. sp.*

[All specimens from USGS loc. f10109]

| Specimen | Volution | Form ratio | Height of whorl (mm) | Wall thickness (mm) | Tunnel angle (degrees) | Septal count | Diameter of proloculus (mm) | Radius vector (mm) | Half length (mm) |
|---|---|---|---|---|---|---|---|---|---|
| 1 | 1 | 1.0 | 0.050 | 0.012 | 42 | | 0.122 | 0.122 | 0.124 |
| | 2 | 1.4 | .070 | .020 | | | | .220 | .316 |
| 3 | 1 | 1.2 | .049 | .012 | 30 | | .134 | .189 | .220 |
| | 2 | 1.7 | .073 | .015 | 44 | | | .231 | .390 |
| | 3 | | .183 | .012 | | | | .440 | |
| 5 | 1 | 1.2 | .031 | .012 | 30 | | .134 | .110 | .134 |
| | 2 | 1.6 | .055 | .024 | 50 | | | .183 | .293 |
| | 3 | 1.5? | .079 | .018 | | | | .280 | .426? |
| 6 | 1 | 1.2 | .024 | .112 | 23 | | .125 | .063 | .075 |
| | 2 | 2.5 | .037 | .024 | 30 | | | .100 | .250 |
| | 3 | 1.5 | .073 | .024 | | | | .250 | .375 |
| 7 | 1 | 1.2 | .037 | .012 | | | .116 | .110 | .134 |
| | 2 | 1.2 | .048 | | | | | .183 | .224 |
| | 3 | 1.2 | .110 | .012 | | | | .305 | .365 |
| 8 | 1 | .83 | .024 | .012 | 34 | | .134 | .110 | .091 |
| | 2 | .86 | .048 | .020 | | | | .183 | .158 |
| | 3 | .96 | .091 | .024 | | | | .290 | .280 |
| 10 | 1 | 1.4 | .036 | .012 | 24 | | .158 | .122 | .170 |
| | 2 | 1.5 | .061 | .024 | 33 | | | .200 | .293 |
| | 3 | 1.4 | .073 | .024 | | | | .316 | .427 |
| 11 | 1 | 1.3 | .025 | .015 | 32 | | .134 | .097 | .122 |
| | 2 | 1.5 | .030 | .024 | | | | .144 | .220 |
| 12 | 1 | 1.9 | .024 | .012 | 25 | | .096 | .085 | .158 |
| | 2 | 2.0 | .053 | .012 | | | | .144 | .292 |
| | 3 | | .085 | .024 | | | | .260 | |
| 12a | 1 | 1.0 | .018 | .012 | | | .185 | .144 | .144 |
| | 2 | 1.4 | .030 | .012 | | | | .185 | .268 |
| 13 | 1 | 1.3 | .061 | .012 | 32 | | .120 | .122 | .158 |
| | 2 | 1.2 | .103 | .018 | | | | .244 | .300 |
| 14 | 1 | 1.1 | .024 | .012 | 24 | | .110 | .097 | .110 |
| | 2 | 1.3 | .037 | .018 | 52 | | | .146 | .195 |
| | 3 | 1.3 | .073 | .024 | | | | .250 | .330 |
| 15 | 1 | 1.0 | .049 | .012 | 22 | | .079 | .097 | .097 |
| | 2 | 1.1 | .061 | .012 | | | | .180 | .195 |
| 16 | 1 | 1.2 | .031 | .012 | 69 | | .134 | .134 | .158 |
| | 2 | 1.2 | .049 | .018 | | | | .210 | .260 |
| 17 | 1 | 1.5 | .061 | .010 | 44 | | .095 | .116 | .171 |
| | 2 | 1.5 | .061 | .012 | 37 | | | .195 | .293 |
| 18 | 1 | 1.0 | 0.037 | 0.012 | 28 | | 0.134 | 0.122 | 0.122 |
| | 2 | 1.2 | .049 | .018 | 31 | | | .183 | .219 |
| | 3 | 1.1 | .061 | .018 | | | | .290 | .320 |
| 19 | 1 | 1.5 | .024 | .012 | 22 | | .122 | .097 | .144 |
| | 2 | 1.6 | .027 | .018 | | | | .134 | .215 |
| 20 | 1 | 1.0 | .024 | .012 | 56 | | .110 | .097 | .097 |
| | 2 | 1.1 | .042 | .016 | | | | .155 | .170 |
| 22 | 1 | 2.0 | .037 | .012 | 27 | | .145 | .110 | .215 |
| | 2 | 2.0 | .049 | .018 | | | | .183 | .365 |
| 23 | 1 | 1.4 | .031 | .012 | 27 | | .110 | .085 | .122 |
| | 2 | 1.1 | .043 | .012 | | | | .153 | .170 |
| 24 | 1 | 1.3 | .037 | .112 | 39 | | .134 | .110 | .146 |
| | 2 | 1.5 | .049 | .018 | | | | .170 | .256 |
| 25 | 1 | 1.3 | .024 | .012 | 34 | | .122 | .097 | .122 |
| | 2 | 1.2 | .073 | .012 | | | | .183 | .219 |
| 26a | 1 | | .062 | .010 | | 9 | | .158 | |
| | 2 | | .068 | .012 | | 15 | | .244 | |
| 26 | 1 | 1.3 | .037 | .006 | 30 | | .097 | .085 | .110 |
| | 2 | 1.3 | .049 | .012 | | | | .146 | .195 |
| 28 | 1 | 1.1 | .030 | .012 | 36 | | .122 | .110 | .122 |
| | 2 | 1.1 | .050 | .012 | 44 | | | .182 | .194 |
| | 3 | 1.2 | .122 | .015 | | | | .315 | .390 |
| 29 | 1 | .9 | .024 | .006 | 25 | | .085 | .085 | .073 |
| | 2 | 1.1 | .037 | .012 | 21 | | | .134 | .152 |
| | 3 | 1.6 | .073 | .015 | | | | .220 | .353 |
| 34 | 1 | .8 | .030 | .012 | 35 | | .122 | .103 | .085 |
| | 2 | 1.1 | .049 | .012 | | | | .170 | .194 |
| | 3 | 1.3 | .062 | .012 | | | | .250 | .315 |
| 34a | 1 | | .037 | .012 | | 7 | .122 | .134 | |
| | 2 | | .062 | .015 | | 13 | | .207 | |
| 36 | 1 | | .062 | .012 | | 8 | [1].110 | .134 | |
| | 2 | | .062 | .012 | | 11 | .136 | .220 | |
| 38 | 1 | | | | | 8 | | | |
| | 2 | | | | | 14 | | | |
| | 3 | | | | | 8 | | | |

[1] Elliptical proloculus (long diameter, 0.36; short diameter, 0.110).

collections were made in a roadcut from the upper 6 inches of a bluish-gray limestone that is overlain by 7 feet of brownish-white massive limestone that is at the top of the Adams Branch Limestone Member. The Adams Branch is underlain by the Brownwood Shale Member, and is overlain by the Cedarton Shale Member. Together, the three members comprise the Graford Formation, which lies at the base of the Canyon Group. Other specimens of *Oketaella earglei* have been noted in the upper part of the Adams Branch elsewhere in and near Brown County, in north-central Texas.

## REFERENCES


Jewett, J. M., 1941, Classification of the Marmaton Group Pennsylvanian, in Kansas: Kansas State Geol. Survey Bull 38, pt. 11, p. 285–344, pl. 1–9.

Myers, D. A., 1960, Stratigraphic distribution of some Pennsylvanian Fusulinidae from Brown and Coleman Counties, Texas: U.S. Geol. Survey Prof. Paper 315–C, p. 37–53, pl. 15–24, fig. 9–10, 1 table.

Thompson, M. L., 1942, Pennsylvanian System in New Mexico: New Mexico Bur. Mines and Mineral Resources Bull. 17, 92 p., 8 fig.

——— 1951, New genera of fusulinid Foraminifera: Cushman Found. Foram. Research, Contr., v. 2, p. 115–119, pl. 13–14.

——— 1954, American Wolfcampian fusulinids: Kansas Univ. Paleont. Contr., Protozoa, art. 5, p. 1–226, pl. 1–52, fig. 1–14.

——— 1957, Northern midcontinent Missourian fusulinids: Jour. Paleontology, v. 31, p. 289–328, pl. 21–30, fig. 1–2.

Thompson, M. L., Verville, G. J., and Lokke, D. H., 1956, Fusulinids of the Desmoinesian-Missourian contact: Jour. Paleontology, v. 30, p. 793–810, pl. 89–93, 1 fig.

# GRAPTOLITE-BEARING SILURIAN ROCKS OF THE HOULTON-SMYRNA MILLS AREA, AROOSTOOK COUNTY, MAINE

By LOUIS PAVLIDES and WILLIAM B. N. BERRY, Beltsville, Md., Berkeley, Calif.

*Abstract.*—One of the most complete Silurian graptolite sequences in the United States, spanning early Llandovery to early Ludlow time, occurs in the Houlton-Smyrna Mills area of northeastern Maine. Graptolites of similar Early Silurian age occur close to, and both above and below, the conformable and gradational contact that separates the dominantly clastic rocks of the Smyrna Mills Formation of Silurian age from the underlying limy rocks of the ribbon rock member of the Meduxmekeag Formation of Middle Ordovician to Early Silurian age. The Taconic orogeny, therefore, did not affect this belt of rocks, which regionally makes up the Aroostook-Matapedia anticlinorium in the northern Appalachians.

One of the most complete Silurian graptolite sequences presently known in the United States occurs in the Houlton–Smyrna Mills area, in southeastern Aroostook County, Maine (fig. 1). The general geology of most of this area has been summarized elsewhere (Pavlides and others, 1964; Pavlides and Canney, 1964), and only a short review will be given in this report.

Glacial drift covers the region, and bedrock is exposed in small irregular outcrops that in many places are polished pavements. The terrane of the Houlton–Smyrna Mills area consists of closely folded Paleozoic rocks locally intruded by postkinematic granitic plutons. Steep to vertical bedding and cleavage characterize the region, the sedimentary rocks being closely folded along east- and northeast-trending fold axes with steep to vertical axial planes. Near Smyrna Mills, fold axes in a belt several miles wide have been warped convexly to the north, a result of the emplacement of the Cochrane Lake pluton and of the Hunt Ridge pluton and its associated bordering injected zone (fig. 1) after the regional folding of the Acadian orogeny (Pavlides and others, 1964).

The postkinematic granitic plutons have been intruded into terrane that is in the chlorite grade of regional metamorphism and have imprinted a local thermal metamorphism on this terrane; consequently, they are enclosed by hornfels aureoles. Where limy rocks of the Meduxnekeag Formation are thermally metamorphosed, as around the Nickerson Lake and Cochrane Lake plutons and along the north side of the Hunt Ridge pluton, various types of calc-silicate hornfels were developed. In thermally metamorphosed rocks of the Smyrna Mills Formation which were orginally quartzose and pelitic, biotite, and biotite-cordierite and biotite-garnet hornfels were formed, as around the Pleasant Lake pluton and parts of the Hunt Ridge and Cochrane Lake plutons. Where ferruginous manganese deposits can be traced into parts of the thermal aureoles, as on the east side of the Hunt Ridge pluton, magnetite has formed in these deposits. The hornfels terrane around the Cochrane Lake, Hunt Ridge, and Pleasant Lake plutons in the Smyrna Mills quadrangle generally has appreciable magnetic anomalies associated with it (Dempsey, 1962), and some of these may be caused by magnetite-bearing ironstone within thermally metamorphosed manganese deposits. Tremolite-bearing hornfels is also present locally and was developed from calcareous quartzose and pelitic rocks.

Despite the thermal metamorphism that these rocks have undergone, graptolites are locally preserved within them. At locality 12, southwest of Oakfield, they occur in biotite hornfels, and at locality 13, southeast of Oakfield, in tremolitic biotite hornfels; graptolites at locality 13, in sulfide-bearing rocks, are pyritized. The graptolites establish the Silurian age of the rocks.

## STRATIGRAPHY

### Silurian(?) and older rocks

Phyllite, quartzite, and volcanic rocks of the Grand Pitch Formation of Cambrian(?) age and volcanic rocks of the Dunn Brook Formation of Ordovician or Silurian age, or both, occur in the Lunksoos Lake–Weeksboro anticline (Pavlides and others, 1964). The southeast limb of this fold, which extends across the northwest

U.S. GEOL. SURVEY PROF. PAPER 550-B, PAGES B51-B61

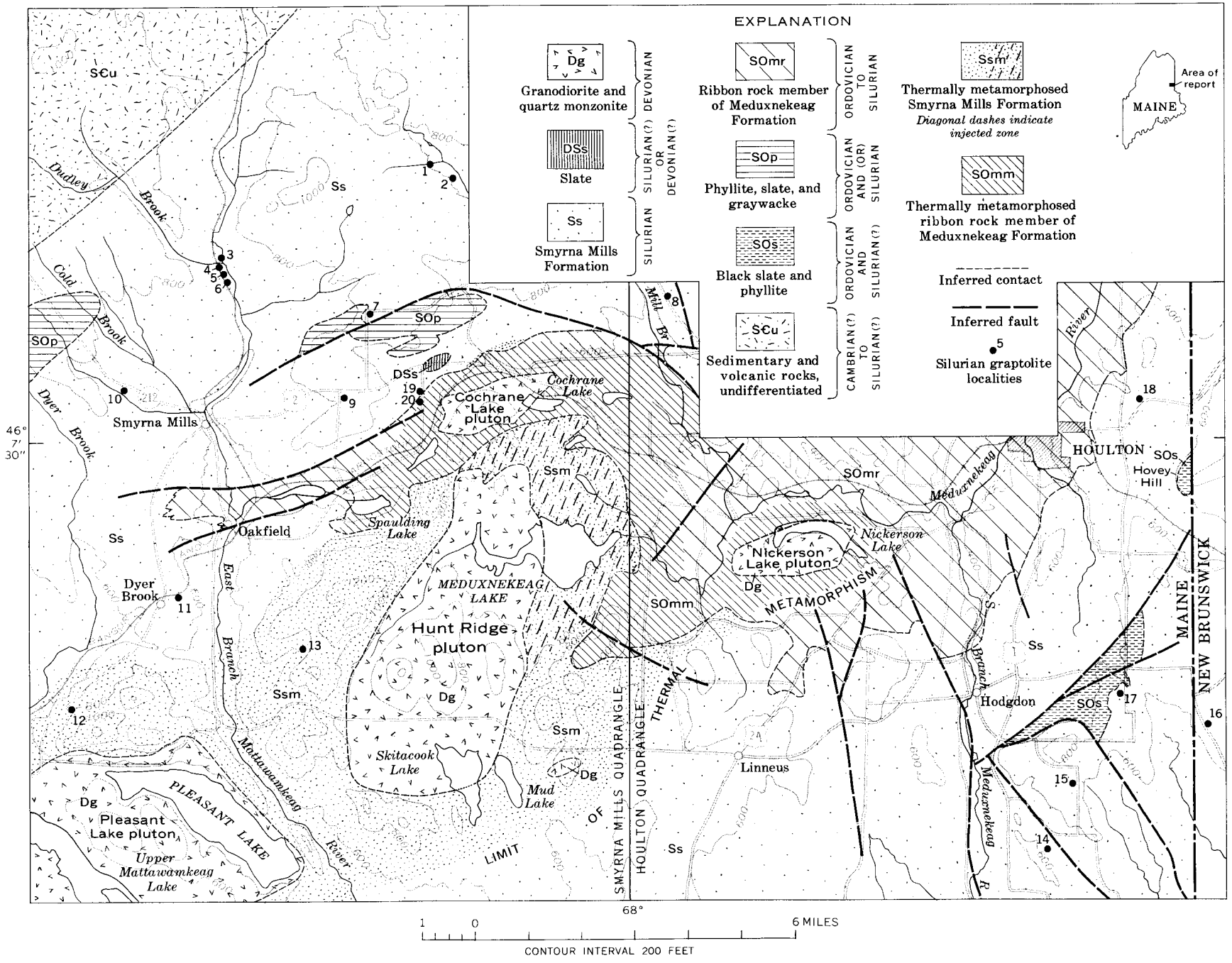


FIGURE 1.—Preliminary generalized geologic map of the Houlton–Smyrna Mills area, Aroostook County, Maine.

part of the report area, is shown on figure 1 as a unit of undifferentiated rocks of Cambrian(?) to Silurian(?) age. The Ordovician rocks in the eastern part of the area, at Hovey Hill and east of Hodgdon, are mostly green phyllite and black carbonaceous slate. Some of the green phyllite associated with these rocks may be, in part, of Silurian age. Rocks that may be of Ordovician age, of Silurian age, or both, occur northeast and northwest of Smyrna Mills. Northeast of Smyrna Mills these rocks are chiefly green phyllite, and northwest of Smyrna Mills they are chiefly graywacke and slate interlayered with each other in varying proportions. Calcareous slate that contains brachiopods of Silurian or Devonian age (A. J. Boucot, oral commun., 1963) occurs in a small area 5 miles northeast of Smyrna Mills. Cyclically layered slate similar to slate that occurs elsewhere in Maine in the Seboomook Formation of Devonian age (Boucot, 1961) crops out south of locality 8 of figure 1. Because of the apparent conformity of this slate and the enclosing Silurian rocks, and because of the possibility that cyclically layered slate may also have been deposited in the Silurian, this slate unit is provisionally considered to be of Silurian age in this report and is not shown as a separate unit.

### Ordovician and Silurian rocks

*Ribbon rock member of the Meduxnekeag Formation.*—The limy ribbon rock member has heretofore been considered of Middle and Late(?) Ordovician age (Pavlides and others, 1961 and 1964; Pavlides and Canney, 1964; Pavlides, 1962 and 1965; and Boucot and others, 1964). With the recent discovery of Early Silurian graptolites in the upper few hundred feet, the ribbon rock member is now known to range from the Middle Ordovician upward through graptolite zone 19 of the early Llandovery, in the Lower Silurian (see table 3). In and near the Houlton–Smyrna Mills area the member forms the core rock over much of the length of the Aroostook-Matapedia anticlinorium, which trends north and northeast, north of the Smyrna Mills area (Pavlides and others, 1964, fig. 1). The east flank of the core rocks of the Aroostook-Matapedia anticlinorium has recently been defined in western New Brunswick (Pavlides, unpublished data). This anticlinorium extends across New Brunswick and along the southern side of the Gaspé Peninsula, Quebec, and as now known it is cored largely by the ribbon rock member of the Meduxnekeag Formation or by similar rocks of coeval ages. Along the Gaspé Peninsula, the rocks believed to be the lithologic and temporal equivalents of the ribbon rock member of the Meduxnekeag Formation include the limestones of the Matapedia Group (Beland, 1958, 1960) the Pabos Formation (Kindle, 1935), and the Whitehead Formation (Schuchert and Cooper, 1930).

Within the Houlton–Smyrna Mills area, the ribbon rock member of the Meduxnekeag Formation consists chiefly of thin- to medium-bedded calcic and ankeritic limestones interlayered with one another and with slate. The contact between the limy rocks of the ribbon rock member of the Meduxnekeag Formation and the overlying clastic rocks of the Smyrna Mills Formation has recently been exposed about 4 miles east of Smyrna Mills in a new roadcut along which two fossil localities have been found (loc. 19 and 20, fig. 1). The rocks on opposite sides of the contact are conformable; the contact is gradational, being characterized by an increase in slate and siltstone interbeds upwards from the gray-blue platy limestone beds of the ribbon rock member into the overlying Smyrna Mills Formation. This gradational passage occurs in a transition zone about 300 feet thick. The base of the Smyrna Mills Formation is placed at the lowest level where no gray-blue limestone beds appear in the section.

### Silurian rocks

*Smyrna Mills Formation.*—The Smyrna Mills Formation is here named after the town of Smyrna Mills (fig. 1). The Smyrna Mills Formation crops out at numerous places within the town, and a good section is exposed at the type locality along the North Branch of the Mattawamkeag River from the town of Smyrna Mills northward to the mouth of Dudley Brook.

A wide variety of sedimentary rocks makes up the Smyrna Mills Formation, but in greatly differing abundance (table 1). Slate, siltstone, quartzite, and quartz graywacke in this unit include both calcareous and noncalcareous types. The calcareous rocks, where weathered, generally are characterized by a buff or pale-orange coating or thin rind. Muscovite, in flakes lying along bedding surfaces in a generally random orientation, is also a characteristic constituent of these rocks.

The slate and the silty and sandy clastic rocks generally are interbedded throughout the Smyrna Mills. At some places the proportion of slate nearly equals that of the coarser grained clastic rocks. Elsewhere the slate either forms thin partings between the clastic rocks, or it forms the bulk of the rock mass, with the coarser clastic beds occurring as sparce thin interbeds or being totally absent. Thickness of layering ranges from a quarter of an inch to several feet. Massive rocks without any visible layering are also present. Bedding in the slate consists mostly of irregularly spaced laminations.

Lithic graywacke, conglomerate, carbonaceous slate (commonly pyritic), maroon and red slate, siltstone, and manganiferous ironstone of both the hematitic and siliceous carbonate types (Pavlides, 1962, p. 50–64),

TABLE 1.—*Approximate lithologic composition of the Smyrna Mills Formation*

| Lithology | Abundance (percent) |
|---|---|
| Gray-green and green micaceous siltstone, quartzite, and quartz graywacke | 60–70 |
| Gray-green and green slate | 25–35 |
| Conglomerate, lithic graywacke, and black carbonaceous slate | 2–3 |
| Manganiferous ironstone and red and maroon siltstone and slate | 2–3 |

occur as relatively thin and small lenticular layers. The manganiferous beds make up the manganese deposits of the southern district of Aroostook County, Maine, in the Houlton quadrangle (White, 1943, p. 137–142; Miller, 1947, p. 16–18; Pavlides, 1955, p. 6–9; and Eilertsen, 1958). The lenticular and nonpersistent nature of these deposits and of the other distinctive rock types prevents their use as marker beds for defining more closely the structural relationships and for refining stratigraphic subdivisions. For example, the manganese deposits in the Houlton quadrangle occur at various stratigraphic levels in the Smyrna Mills Formation. One such level occurs in a belt about 1,500 feet wide within about 300 feet of the contact with the stratigraphically lower Meduxnekeag Formation. It consists of small, widely separated, lenticular manganese deposits of both the hematitic and siliceous carbonate types. This belt extends from about the longitude of Houlton westward into the thermal aureole of the Hunt Ridge pluton.

Manganese deposits also occur at different stratigraphic levels at various places south of this belt. Small deposits are present in the fault blocks southeast of Hodgdon that contain graptolite localities 14 (early Ludlow age) and 15 (middle or late Llandovery age). A few are present in the fault block containing graptolite localities 16 and 17 (late Wenlock age), east of Hodgdon. In contrast to the numerous manganese deposits found in the Silurian rocks of the Houlton quadrangle, only a few are known from the Smyrna Mills quadrangle. One of them is northeast of Smyrna Mills at locality 7 (fig. 1), where a siliceous carbonate layer half a foot thick occurs near calcareous micaceous quartzite that contains graptolites of early Ludlow age. Another manganese deposit in the Smyrna Mills quadrangle occurs north of Smyrna Mills between graptolite localities 4 and 5, which are in a geologic section in which stratigraphic superposition of graptolite associations indicative of different ages can be demonstrated. Vertically dipping beds characterize the section. At locality 4 a 1-foot-thick bed of carbonaceous and pyritic slate contains graptolites of late Wenlock age. Structurally and stratigraphically above this bed (to the southwest) is a 50-foot interval of rusty-weathered green slate that is overlain by a 25-foot-thick manganese deposit. This deposit consists chiefly of manganiferous red and maroon hematitic slate that encloses three manganiferous banded hematite layers, each of which is about 1 foot thick. Above the manganese deposit is rusty-weathered green slate, about 50 feet thick, which in turn is overlain by about 320 feet of weathered siltstone. About 300 feet from the base of this unit, graptolites of early Ludlow age (locality 5, fig. 1) are present. The manganese deposit falls somewhere near the Wenlock-Ludlow boundary but cannot be assigned to either series as it occurs between localities 4 and 5 in an interval that lacks fossils.

Rocks of the Smyrna Mills Formation exposed near the Cochrane Lake pluton, north of the Meduxnekeag Formation in the Smyrna Mills quadrangle, contrast with those in the southern part of the Houlton quadrangle in that those north of the Meduxnekeag (1) locally contain coarse-grained lithic graywacke near the base of the section and (2) do not contain a belt of manganiferous deposits in their lower part. Manganese deposits, in general, are rare in the Smyrna Mills quadrangle; but the presence of maroon siltstone and slate there may represent zones where chemical sedimentation took place but was not of a nature to produce sedimentary manganese deposits. A rather marked facies contrast is characteristic of rocks of the Smyrna Mills Formation in the Smyrna Mills and Houlton quadrangles, although the graptolites suggest that the different lithologies of the Smyrna Mills Formation were deposited about contemporaneously in both areas.

Because of the close folding and the lack of stratigraphic sections free of structural complications, it is not possible to obtain measured thicknesses of the Smyrna Mills Formation. However, on the basis of selected cross sections constructed at various places, it is estimated that the formation is at least 6,000 feet thick.

The Smyrna Mills Formation spans early Llandovery through early Ludlow time of the Silurian.

## GRAPTOLITE FAUNAS

The list of graptolites recognized in collections from each of the 20 localities in figure 1, and the age interpretation for each collection are given in table 2. Because stratigraphic units have not been delineated within the Smyrna Mills Formation, the stratigraphic (superpositional) order of the collections has not been established within this formation with the exception of the collections at localities 4 through 6, north of Smyrna Mills, and at locality 14, southeast of Hodgdon. Most of the graptolites studied are poorly preserved and fragmentary, but a few collections did yield ex-

ceptionally well preserved specimens which reveal a high degree of morphological detail. Only those localities yielding either well-preserved rhabdosomes or those considered particularly critical in terms of age significance will be discussed in this report. Collections from localities not specifically mentioned include mostly poorly preserved, fragmentary specimens of which only general identification is possible and from which only a broad age determination may be made.

Silurian graptolites in North America and their known stratigraphic ranges are similar to those in the typical Silurian sequences in Britain. The ages assigned to the collections listed in table 2 have been determined by comparison of the graptolites with the ranges and the diagnostic associations of species that typify the British Silurian graptolite zones. Most of the collections include two or more species whose occurrence together compares closely with associations that typify some of the Silurian graptolite zones recognized in the British Isles by Elles and Wood (1918). Comparison has also been made with the species composition of the German Silurian graptolite zones as outlined by Münch (1952). The German and British zonal successions are similar, and the ranges of species in each are also closely comparable in most cases.

The series and graptolite zone subdivisions of the British Silurian section, and correlation of the classical American Silurian units with them, are shown in table 3. Jones (1925) introduced the 3 stages and 13 substages of the Llandovery as litholigic units. (The substages were termed groups in his work.) Williams (1951) studied the brachiopod faunas and their evolutionary development in the rocks of the Llandovery district and demonstrated (1951, p. 130) that "each substage has a characteristic brachiopod assemblage." The Llandovery substages ($A_1$ to $A_4$, $B_1$ to $B_3$, and $C_1$ to $C_6$) as currently used are founded upon brachiopod evolutionary development following Williams' study. The North American Silurian faunas are closely comparable with the British faunas, in both diagnostic joint occurrences and in stratigraphic ranges of species; only the Niagaran of the American Silurian subdivisions is based upon a diagnostic fauna which can be recognized outside the typical area. Therefore, the American Silurian faunas have been correlated directly with the British Silurian faunas, and the British systemic subdivisions of the Silurian have been extended into North America. The correlation of the graptolite zones with the series and stages based upon shelly fossils is not precise, but enough graptolites do occur in shelly-fossil sequences, and enough shelly fossils in graptolitic successions, to provide a reasonably good correlation between the units based upon each type of fossil assemblage.

### Llandovery age

The oldest Silurian graptolites in the report area occur just east of Smyrna Mills (loc. 9A, table 2) in a thin impure vertically dipping phyllitic limestone zone within the Smyrna Mills Formation. Specimens of a small climacograptid from here have markedly alternate thecae and are closely similar to *Climacograptus minutus* as discussed by Elles and Wood (1906, p. 211–212, pl. 27, figs. 12 a–c). *C. minutus* occurs in British zones 17 and 18 (Elles and Wood, 1918, table A). In the German sequence it ranges from the basal part of the Silurian into beds correlative with British zone 18. The oldest Silurian rocks in the Houlton-Smyrna Mills area thus are early Llandovery in age. The age and calcareous aspect of the rocks at locality 9A suggest that the rocks are in a transition zone, with lenticular or intertonguing relationships, between the Smyrna Mills Formation and the upper part of the ribbon rock member of the Meduxnekeag Formation. Collection B at locality 9 (table 2) is from vertically dipping rusty-weathered quartzite about 15 feet north of collection A and includes some monograptids with lobate thecae and some with slender rhabdosomes and plain, tubular thecae. The oldest joint occurrence of these kinds of monograptids in Britain is in zone 19; they also appear together in beds of comparable age in Germany. These kinds of monograptids range into beds of Wenlock age in both successions.

Graptolites indicative of British zone 19 (middle Llandovery) age in the ribbon rock member of the Meduxnekeag Formation occur 350 feet beneath its contact with the Smyrna Mills Formation at locality 20, east of Smyrna Mills (fig. 1). A relatively well preserved specimen of *Monograptus triangulatus* and a few specimens of *M. revolutus* are present in the collection. Collection 19 (table 2) is from the lower part of the Smyrna Mills Formation, 100 feet above its contact with the ribbon rock member of the Meduxnekeag Formation and 450 feet stratigraphically above collection 20. This collection also contains a few relatively well preserved specimens of *Monograptus revolutus* and one of *M. triangulatus*. The association of species in the collection from locality 19 is suggestive of a probably British-zone-19 age. The stratigraphic relationships (described earlier) and the ages of the rocks indicated by the collections from localities 19 and 20 demonstrate that the transition from the limy rocks of the ribbon rock member of the Meduxnekeag Formation upwards into the clastic rocks of the Smyrna Mills Formation took place during the span of time represented by British graptolite zone 19.

TABLE 2.—*Silurian graptolites of the Houlton and Smyrna Mills quadrangles, Maine*

| Age | Llandovery | | | | | | | Lla. to Wen. | Wenlock | | | | | | Wen. to Lud. | Early Ludlow | | | | | | | | | | Lud. |
|---|---|---|---|---|---|---|---|---|---|---|---|---|---|---|---|---|---|---|---|---|---|---|---|---|---|---|
| Locality No. (fig. 1) | 9 | | 19 | 20 | 15 | 11 | 8 | 10 | 3 | 4 | 17 | 16 | | | 13 | 18 | 14 | | | | 5 | 6 | 7 | 2 | 1 | 12 |
| | A | B | | | | | | | | | | A | B | C | | | A | B | C | D | | | | | | |
| Graptolites \ U.S. Geological Survey No. | SD-7392 | SD-7393 | SD-7452 | SD-7451 | SD-3196 | SD-7395 | SD-7396 | SD-7397 | SD-7398 | SD-7399 | SD-3192 | SD-7401 | SD-7402 | SD-7403 | SD-7404 | SD-7405 | SD-7406 | SD-7407 | SD-7408 | SD-7409 | SD-7419 | SD-7420 | SD-7421 | SD-7422 | SD-7423 | SD-7424 |
| *Climacograptus minutus* Carruthers | × | | | | | | | | | | | | | | | | | | | | | | | | | |
| *C. scalaris* cf. var. *normalis* Lapworth | | | × | × | | | | | | | | | | | | | | | | | | | | | | |
| *C.* sp. | | | | × | | × | | | | | | | | | | | | | | | | | | | | |
| *Cyrtograptus lundgreni* Tullberg | | | | | | | | | | ? | | | | | | | | | | | | | | | | |
| *C.* sp. | | | | | | | | | × | | | × | | | | | | | | | | | | | | |
| *Desmograptus* sp. | | | ? | | | | | | | | | | | | | | | | | | | × | | | | |
| *Monograptus argutus* Lapworth | | | | | | | | | | | | | | | | | | | | | | | | | | |
| *M.* cf. *M. atavus* Jones | | | × | | | | | | | | | | | | | | | | | | | | | | | |
| *M. bohemicus* (Barrande) | | | | | | | | | | | | | | | | | | | | | | × | × | | | × |
| *M. clintonensis* (Hall) | | | | | | ? | ? | | | | | | | | | | | | | | | | | | | |
| *M. colonus* cf. var. *compactus* Wood | | | | | | | | | | | | | | | | | | | | | | | | | × | × |
| *M.* cf. *M. crinitus* Wood | | | | | | | | | | | | | | | | | | | | | | | × | | | |
| *M.* cf. *M. discus* Tornquist | | | | | | × | | | | | | | | | | | | | | | | | | | | |
| *M. dubius* (Suess) | | | | | | | | | | | | | | | | | | | | | × | × | | × | | ? |
| *M.* cf. *M. dubius* (Suess) | | | | | | | | | | | | | | | × | × | | | | | | | | | | |
| *M. flemingii* (Salter) | | | | | | | | | × | × | ? | | | | | | | | | | | | | | | |
| *M.* cf. *M. griestoniensis* (Nicol) | | | | | | × | | | | | | | | | | | | | | | | | | | | |
| *M. incommodus* Tornquist | | | ? | | | | | | | | | | | | | | | | | | | | | | | |
| *M.* aff. *M. micropoma* (Jaekel) | | | | | | | | | | | | | | | | | | | | | | | | × | | |
| *M. nilssoni* (Barrande) | | | | | | | | | | | | | | | | | | | | | ? | ? | × | | | |
| *M.* cf. *M. praedubius* Boucek | | | | | | | | | | | | | | | × | | | | | | | | | | | |
| *M. priodon* (Bronn) | | | | | | ? | ? | | | | | | | | | | | | | | | | | | | |
| *M. revolutus* Kurck | | | × | × | | | | | | | | | | | | | | | | | | | | | | |
| *M. revolutus* cf. var. *austerus* Tornquist | | | | × | | | | | | | | | | | | | | | | | | | | | | |
| *M. roemeri* (Barrande) | | | | | | | | | | | | | | | | | | | | | ? | ? | | | | |
| *M. scanicus* Tullberg | | | | | | | | | | | | | | | | | | | | | | | × | ? | × | |
| *M. spiralis* (Geinitz) | | | | | | ? | | | | | | | | | | | | | | | | | | | | |
| *M. spiralis* var. *contortus* (Perner) | | | | | | × | | | | | | | | | | | | | | | | | | | | |
| *M. testis* var. *inornatus* Elles | | | | | | | | | | ? | | | | | | | | | | | | | | | | |
| *M. triangulatus* (Harkness) | | | × | × | | | | | | | | | | | | | | | | | | | | | | |
| *M. tumescens* cf. var. *minor* (McCoy) | | | | | | | | | | | | | | | | | | | | × | | | | | | |
| *M. uncinatus* Tullberg | | | | | | | | | | | | | | | | | | | | | | | | × | | |
| *M. varians* Wood | | | | | | | | | | | | | | | | ? | | | | | | | | ? | | |
| *M. vicinus* Perner | | | | | | | | | | | | | | | | × | | | | | | | × | | | |
| *M.* n. sp. (of the *M. communis* type) | | | | | | × | | | | | | | | | | | | | | | | | | | | |
| *M.* n. sp. (thecae of the *M. vomerinus* type but thecal apertures are spinose) | | | | | | | | | | | | | | | | | | | | | | | × | | | |
| *M.* n. sp. (hooked thecae) | | | | | | × | | | | | | | | | | | | | | | | | | | | |

| | 9 | 19 | 20 | 15 | 11 | 8 | 10 | 3 | 4 | 17 | 16 | 13 | 18 | 14 | 5 | 6 | 7 | 2 | 1 | 12 |
|---|---|---|---|---|---|---|---|---|---|---|---|---|---|---|---|---|---|---|---|---|
| *M.* sp. (of the *M. chimaera* type) | | | | | | | | | | | | | | | | | | | × | |
| *M.* sp. (of the *M. colonus* type) | | | | | | | | | | | | | | | ? | | ? | | | |
| *M.* sp. (of the *M. dubius* type) | | | | | | | | × | × | ? | × | ? | × | × | × | | | | | × | × | | × | × |
| *M.* sp. (of the *M. flemingii* type) | | | | | | | | | | | | ? | × | | | | | | | | | | | |
| *M.* sp. (of the *M. tumescens* type) | | | | | | | | | | | | | | | × | | | | ? | × | | | × | |
| *M.* sp. (of the *M. uncinatus* type) | | | | | | | | | | | | | | | × | | | | × | × | | | | |
| *M.* sp. (of the *M. vomerinus* type) | | | | | | | | | ? | | | | | | | | | | | | | | | |
| *M.* sp. (of the *M. vulgaris* type) | | | | | | | | | | | | | | | × | | | | × | | | | | |
| *M.* sp. (with hooked thecae) | | | | | | | × | × | | | ? | | | | | | | | | | | | | |
| *M.* sp. (with lobate thecae) | | × | | | × | | | | | | | | | | | | | | | | | | | |
| *M.* sp. (with simple tubular thecae and long slender rhabdosomes) | | | | | | × | × | × | | | | | | | × | × | × | × | | | | | | |
| *M.* sp. (with simple tubular thecae) | | × | | | | | | | | | | × | × | | | | | | | | | | | |
| *Retiolites geinitzianus* var. *angustidens* (Elles and Wood) | | | | | | × | | | | | | | | | | | | | | | | | | |
| Retiolitid | | | | | | | | | | | | | | ? | | | | | | | | | | |
| *Rhaphidograptus* sp. (Elles and Wood) | | | | ? | | | | | | | | | | | | | | | | | | | | |

Llandovery:
- 9. A. Early Llandovery.
  B. Llandovery to Wenlock.
- 19. Middle Llandovery.
- 20. Do.
- 15. Middle or late Llandovery.
- 11. Late Llandovery, in the interval of British zone 22 (*Monograptus turriculatus*) to British zone 24 (*M. griestoniensis*).
- 8. Probably late Llandovery.

Llandovery to Wenlock:
- 10. Late Llandovery to Wenlock.

Wenlock:
- 3. Late Wenlock.
- 4. Do.
- 17. Possibly late Wenlock.
- 16. A–C. Possibly latter part of Wenlock.

Wenlock to Ludlow:
- 13. Wenlock to early Ludlow.

Early Ludlow:
- 18. Early Ludlow, *Monograptus nilssoni* and *M. scanicus* zone.
- 14. A–D. Early Ludlow.
- 5. Early Ludlow, *Monograptus nilssoni* and *M. scanicus* zone.
- 6. Do.
- 7. Do.
- 2. Do.
- 1. Do.

Ludlow:
- 12. Ludlow.

TABLE 3.—*Correlation of the British (type) and American sections [1] for the Silurian with respect to graptolite zonation*

| | British section | | | | Graptolite zones | American section | | |
|---|---|---|---|---|---|---|---|---|
| | | Series | | | | Group or formation | Provincial series | |
| Silurian | Upper | Ludlovian | Upper | | | Rondout and Cobleskill | Cayuga | Upper |
| | | | Lower | | 36 | | | |
| | | | | | 35 | Bertie | | |
| | | | | | 34 | | | |
| | | | | | 33 | Salina Group | | |
| | | | | | 32 | | | |
| | | Wenlockian | | | 31 | Lockport | Niagara | Middle |
| | | | | | 30 | Rochester | | |
| | | | | | 29 | | | |
| | | | | | 28 | | | |
| | | | | | 27 | | | |
| | | | | | 26 | | | |
| | Lower | Llandoverian | Upper (C) | $C_6$ | 25 | Clinton Group | | |
| | | | | $C_5$ | 24 | | | |
| | | | | $C_4$ | 23 | | | |
| | | | | $C_3$ | 22 | Albion Group | | Lower |
| | | | | $C_2$ | | | | |
| | | | | $C_1$ | 21 | | | |
| | | | Middle (B) | $B_3$ | 20 | | | |
| | | | | $B_2$ | | | | |
| | | | | $B_1$ | 19 | | | |
| | | | Lower (A) | $A_4$ | | | | |
| | | | | | 18 | | | |
| | | | | $A_3$ | 17 | | | |
| | | | | $A_2$ | | | | |
| | | | | $A_1$ | 16 | | | |

[1] Stages and series taken from Pavlides and others (1964) and Boucot and others (1964).

The first Silurian graptolite obtained from the ribbon rock member of the Meduxnekeag Formation in Maine was collected by Mr. David Roy of the Massachusetts Institute of Technology in 1964 from an exposure on the south bank of the Aroostook River south of Washburn, Maine, near the boundary between Washburn and Wade Townships. The graptolite was referred to W. B. N. Berry for identification. It is *Monograptus* cf. *M. cyphus*, a form suggestive of a British-zone-18 (early Llandovery) age. Roy's find of a clearly identifiable monograptid from the ribbon rock member of the Meduxnekeag Formation makes the suggested Ordovician age for a small group of poorly preserved graptoloids (Boucot and others, 1964, p. 26) from a roadcut exposure almost on strike with, and a few hundred feet southward from, the locality from which Roy's specimen came, seem quite unlikely. The fragmental specimens referred to by Boucot and others have not been reexamined, but their stratigraphic position with respect to the rocks bearing *Monograptus*

cf. *M. cyphus*, indicates that they are also most probably Early Silurian in age. Thus the upper part of the ribbon rock member of the Meduxnekeag Formation exposed in Maine has been demonstrated to be of early to middle Llandovery age by the graptolite finds near Washburn and at locality 20 of figure 1.

Of the other collections bearing combinations of species suggestive of a Llandovery age, only the collection from locality 11, southwest of Oakfield (fig. 1), yielded well-preserved, readily identifiable specimens that occur in both slate and siltstone. Many of the specimens from here (see table 2) have been partly or wholly replaced by pyrite, so that their morphologic features are easily studied. The commonest element in this collection is a slender monograptid, with markedly sigmoidally curved thecae, which is similar in rhabdosome size and thecal characteristics to the forms figured by Elles and Wood (1911, text figs. 280 a, b; pl. 41; figs. 6 a, b) as *Monograptus* cf. *M. griestoniensis*. *Monograptus spiralis* var. *contortus* and monograptids of the *M. priodon* and *M. communis* groups are other common elements of the fauna from locality 11. Specimens which are similar to *M. discus* but slightly thinner than typical material, and specimens of *Retiolites geinitzianus* var. *angustidens*, are less abundant but distinctive members of the fauna from this locality. The species associated at locality 11 clearly indicate a late Llandovery age about equivalent to that of the British zone of *Monograptus griestoniensis* (zone 24) or perhaps a zone or two slightly older.

The other collections with an association of species which are suggestive of a Llandovery age (table 2) are composed of poorly preserved, fragmentary rhabdosomes in which only the general rhabdosome form and thecal type are discernible. Monograptids of the *M. priodon* group, or at least forms with straight, stout rhabdosome form and hooked thecae, and slender forms with simple, tubular thecae, are typical members of these collections. The occurrence of such forms together suggests that they belong in the latter part of the Llandovery.

### Wenlock age

The British and continental Wenlock graptolite zones are based primarily upon particular single species of *Cyrtograptus*. Identification of these zones therefore depends on the finding of relatively well preserved specimens of *Cyrtograptus*. Inasmuch as the cyrtograptids found in Maine are not well preserved and cound not be certainly identified, individual Wenlock zones could not be recognized here. The Wenlock may be divided into an upper part on the basis of the occurrence together of monograptids of the *Monograptus flemingii* and *M. testis* groups, and into a lower part containing early members of the *M. vomerinus* and *M. dubius* groups, along with the last representatives of the *M. priodon* group and with *M. riccartonensis*.

Rocks at localities 3 and 4, north of Smyrna Mills, contain an assemblage which is indicative of late Wenlock age. Cyrtograptids occur with *Monograptus flemingii* at both locality 3 and locality 4. A poorly preserved coiled monograptid similar to *M. testis* var. *inornatus* is also present at locality 4. The proximal portions of the cyrtograptids at locality 4 compare closely with those of *Cyrtograptus lundgreni*, which is among the youngest of the cyrtograptids and is the typical species of the youngest zone in the British Wenlock. Collections at localities 3 and 4 may be from the same bed, although on opposite limbs of a small fold. They may be age correlatives of the British latest Wenlock zone 31, that of *C. lundgreni*. Locality 5, approximately 425 feet stratigraphically above locality 4, includes a group of species (table 2) indicative of an early Ludlow age.

Monograptids with the general rhabdosome and thecal form of *Monograptus flemingii*, and others belonging to the *M. dubius* group, are present at localities 16 (black slate) and 17 (siltstone), east of Hodgdon. This association is considered to be of possible or probable late Wenlock age. No clearly early Wenlock collections have been found in the area, and none of the late Wenlock collections may be confidently assigned a zonal position.

### Ludlow age

Collections of early Ludlow age are the most numerous in this region and contain some of the best-preserved specimens. Siltstone at localities 2 and 6, northeast and north, respectively, of Smyrna Mills, and calcareous siltstone at locality 7, also northeast of Smyrna Mills, yielded the most diverse and best-preserved faunas (table 2). Collections from locality 14 (table 2) are from a stratigraphic sequence in siltstone southeast of Hodgdon, with collection A at the base; B, 6 inches above A; C, 8 inches above B; and D, 15 inches above C. The forms identified in each of these collections (A–D) are suggestive of an early Ludlow age.

The graptolites of Ludlow age from the Smyrna Mills Formation are similar in morphological detail to those described by Berry (1964) from the upper member of the Perham Formation in the Presque Isle quadrangle, Maine. In addition to most of the species recognized in the Perham, the collections of early Ludlow age in the Smyrna Mills Formation contain *Monograptus uncinatus* and a form that appears to have close affinities with *M. micropoma*. A new species with markedly sigmoidally curved thecae similar to those of *M. vomerinus*, but which differs in pos-

797-218 O—66——5

sessing spinose apertural margins, is also present. The rocks of the Smyrna Mills Formation that contain graptolites of early Ludlow age are considered (as is the upper part of the Perham Formation in the Presque Isle quadrangle) correlative with both the *Monograptus nilssoni* and *Monograptus scanicus* zones (zones 33 and 34) of the British Silurian. The two zones have not, at present, been recognized as separate units in northern Maine, and they are not, as yet, clearly separable in England (Berry, 1964). Jaeger (1964; written commun., 1965) indicated that the two may be distinguished in a number of areas in continental Europe and North Africa. The zonal designation used for the age of these Maine collections is *Monograptus nilssoni* and *Monograptus scanicus* zone, with the understanding that such a zone is the correlative of zones 33 and 34 of the British Silurian of Elles and Wood (1918) and of equivalent zones in continental Europe.

No collection indicative of an age younger than early Ludlow was found in the present study, although the association obtained at locality 12 (table 2), northwest of Pleasant Lake, may be slightly younger than the other Ludlow age collections. Monograptids of most of the kinds present in it do range into the middle Ludlow in Britain and on the Continent.

The graptolite-bearing rocks of Silurian age in the Houlton–Smyrna Mills area thus span most of Silurian time, from the early Llandovery into the Ludlow. In this interval, apparently only the early part of the Wenlock is not represented in the collections.

## GENERAL CONSIDERATIONS

The gradational nature of the contact between the upper part of the ribbon rock member of the Meduxnekeag Formation and the overlying Smyrna Mills Formation, and the temporal equivalence of the graptolites on both sides of this contact (locs. 19 and 20, table 2), demonstrate the absence of a Taconic unconformity in the Houlton and Smyrna Mills area. The structurally conformable nature of the contact between the ribbon rock member of the Meduxnekeag Formation and the Silurian rocks of the Presque Isle area was earlier recognized by Pavlides (Boucot and others, 1964, p. 91). The general area now occupied by the Aroostook-Matapedia anticlinorium, therefore, was a basin of uninterrupted sedimentation from about Middle Ordovician through early Ludlow (Late Silurian) times. Elsewhere in the northern Appalachians, on opposite sides of this Aroostook-Matapedia belt of rocks, the Taconic or related orogenies did indeed profoundly affect the region; marked angular unconformities separate pre- and post-Taconic rocks to the west in Maine, in southeast New Brunswick, and in the Gaspé Peninsula of Quebec. The change in the nature of the sedimentation from limy (ribbon rock member of the Meduxnekeag Formation) to clastic (Smyrna Mills Formation and the lower part of the Perham Formation) in the Aroostook-Matapedia belt may reflect the effects of the Taconic orogeny in nearby areas during early Llandovery time. This also indicates that the Taconic orogeny extended into Early Silurian time rather than being restricted to the latter part of the Ordovician in this part of Maine.

Although the Smyrna Mills Formation is not closely subdivided on the basis of its lithologic aspect, rocks containing Llandovery- and Wenlock-age graptolites, in general, have more slate and locally contain conglomerate and lithic graywacke near their base. The Ludlow-age rocks are mostly thin- to medium-bedded calcareous and micaceous quartzite and quartz graywacke.

Manganese deposition in the area was not restricted to one or a few specific time intervals within the Silurian; deposits have been found in all parts of the section and with graptolites indicate of all three Silurian series. No deposits of manganese occur in the ribbon rock member of the Meduxnekeag Formation; however, those in the Smyrna Mills Formation seem to be somewhat more numerous in the rocks of Llandovery and Wenlock age than in those of Ludlow age. Environments favorable to manganese deposition thus appear to have occurred at different times during the Silurian at different places within the area of the two quadrangles, and may have recurred at any given place one or more times during the entire span of the Silurian.

Parts of the Smyrna Mills Formation are the temporal equivalents of the Frenchville and Perham Formations in the Presque Isle quadrangle (Boucot and others, 1964, p. 33–40) of north-central Aroostook County, Maine, about 45 miles north of the Houlton–Smyrna Mills area. No Silurian fossils older than late Llandovery been found in those formations in the Presque Isle area, whereas early Llandovery graptolites occur near Smyrna Mills. The rocks of late Llandovery age in the Frenchville Formation in the Presque Isle quadrangle are, in general, more coarse grained than those of the same age in the Houlton–Smyrna Mills area. The lithologic aspect of the Wenlock-age rocks is generally similar in both areas, but the Ludlow rocks are coarser grained and more quartzose in the Houlton–Smyrna Mills area than they are to the northwest in the Presque Isle quadrangle and nearby areas. Naylor and Boucot (1965) have pointed out this difference in the Ludlow rocks by referring the Houlton and Smyrna Mills area to a belt of "graywacke and slate" which is parallel to and southeast of a belt of "calcareous shale or slate" which includes the Presque Isle area.

The Maple Mountain Formation in the Howe Brook quadrangle, Maine, 20 miles to the north of Medux-nekeag Lake (Pavlides, 1964, p. B5), is similar in lithologic aspect to part of the Smyrna Mills Formation in the Houlton–Smyrna Mills area. It has yielded Silurian fossils from two localities and, hence, it is at least in part coeval with the Smyrna Mills Formation in the Houlton–Smyrna Mills area.

## REFERENCES


Beland, Jacques, 1958, Preliminary report on the Oak Bay area: Quebec Dept. Mines Prelim. Rept. 375, 12 p.

——— 1960, Preliminary report on Rimouski-Matapedia area: Quebec Dept. Mines Prelim. Rept. 430, 18 p.

Berry, W. B. N., 1964, Early Ludlow graptolites from the Presque Isle quadrangle, Maine: Jour. Paleontology, v. 38, p. 587–599.

Boucot, A. J., 1961, Stratigraphy of the Moose River synclinorium: U.S. Geol. Survey Bull. 1111–E, p. 153–188.

Boucot, A. J., Field, Michael, Fletcher, Raymond, Forbes, W. N., Naylor, R. G., and Pavlides, Louis, 1964, Reconnaissance geology of the Presque Isle quadrangle, Maine: Maine Geol. Survey Quad. Mapping Ser., no. 2, 123 p.

Dempsey, W. J., 1962, Aeromagnetic map of the Smyrna Mills quadrangle, Aroostook County, Maine: U.S. Geol. Survey Geophys. Inv. Map GP–294.

Eilertsen, N. A., 1958, Investigation of manganese areas, Hammond Plantation and Hodgdon Township[s], southern district, Aroostook County, Maine: U.S. Bur. Mines Rept. Inv. 5392, 38 p.

Elles, G. L., and Wood, E. M. R., 1901–18, Monograph of British graptolites: Paleontographical Soc., London, 539 p., 52 pls.

Jaeger, H., 1964, Der gegenwärtige Stand der stratigraphischen Erforschung des Thüringer Silurs: Abhandl. d. Deutschen Akad. d. Wissenschaften zu Berlin, Kl. Bergb., Huttenw. u. Montangeol. Jahrb. 1964, no. 2, p. 27–51.

Jones, O. T., 1925, The geology of the Llandovery district; pt. I. The southern area: Geol. Soc. London Quart. Jour., v. 81 p. 344–388.

Kindle, C. H., 1935, Stratigraphy of southeastern Quebec: Geol. Soc. America Proc., 1934, p. 354.

Miller, R. J., 1947, Manganese deposits of Aroostook County, Maine: Maine Geol. Survey Bull. 4, 77 p.

Münch, A., 1952, Die Graptolithen aus dem anstehenden Gotlandium Deutschlands und der Tschechoslowakei: Geologica, v. 7, Schrift, d. Geol. Institut. d. Univ. Berlin, Greifswald, Halle, Rostock, 157 p., 62 pls.

Naylor, R. S., and Boucot, A. J., 1965, Origin and distribution of rocks of Ludlow age (Late Silurian) in the northern Appalachians: Am. Jour. Sci., v. 263, p. 153–169.

Pavlides, Louis, 1955, Description of deposits *and* Character of ore, *in* Eilertsen, N. A., Investigation of the Littleton Ridge manganese deposit and vicinity, southern district, Aroostook County, Maine: U.S. Bur. Mines Rept. Inv. 5104, p. 6–9.

——— 1962, Geology and manganese deposits of the Maple and Hovey Mountains area, Aroostook County, Maine: U.S. Geol. Survey Prof. Paper 362, 116 p. [1963]

——— 1964, The Hovey Group of northeastern Maine: U.S. Geol. Survey Bull. 1194–B, p. B1–B6.

——— 1965, Geology of the Bridgewater quadrangle, Maine: U.S. Geol. Survey Bull. 1206, 72 p.

Pavlides, Louis, and Canney, F. C., 1964, Geological and geochemical reconnaissance, southern part of Smyrna Mills quadrangle, Maine: Art. 140 *in* U.S Geol. Survey Prof. Paper 475–D, p. D96–D99.

Pavlides, Louis, Mencher, Ely, Naylor, R. S., and Boucot, A. J., 1964, Outline of the stratigraphic and tectonic features of northeastern Maine *in* Geological Survey Research 1964: U.S. Geol. Survey Prof. Paper 501–C, p. C28–C38.

Pavlides, Louis, Neuman, R. B., and Berry, W. B. N., 1961, Age of the "ribbon rock" of Aroostook County, Maine: Art. 30 *in* U.S. Geol. Survey Prof. Paper 424–B, p. B65–B67.

Schuchert, Charles, and Cooper, G. A., 1930, Upper Ordovician and Lower Devonian stratigraphy and paleontology of Perce, Quebec: Am. Jour. Sci., ser. 5, v. 20, p. 161–176, 265–392.

White, W. S., 1943, Occurrence of manganese in eastern Aroostook County, Maine: U.S. Geol. Survey Bull. 940–E, p. 125–161.

Williams, Alwyn, 1951, Llandovery brachiopods from Wales with special reference to the Llandovery district: Geol. Soc. London Quart. Jour., v. 107, p. 85–136.

# STRATIGRAPHIC SIGNIFICANCE OF TERTIARY FOSSILS FROM THE ORCA GROUP IN THE PRINCE WILLIAM SOUND REGION, ALASKA

By GEORGE PLAFKER and F. S. MacNEIL, Menlo Park, Calif.

*Abstract.*—The Orca Group, a thick complexly deformed and sparsely fossiliferous sequence of predominantly eugeosynclinal clastic and volcanic rocks, underlies an area of roughly 4,000 square miles in the southern and eastern parts of the Prince William Sound region. New collections of marine megafossils from the lower, predominantly volcanic unit of the Orca Group and pollen from the predominantly sedimentary upper part of the Orca indicate that the Orca Group is of early Tertiary age, most probably middle to late Eocene, rather than of Mesozoic age as previously inferred. The Orca Group was deposited during the early Tertiary in a geosyncline situated along the present northern and western margin of the Gulf of Alaska. A major period of orogeny that probably culminated in late Eocene or early Oligocene time resulted in complex deformation of the Orca Group, in emplacement of granitic batholiths, and in economically important copper, gold, and antimony mineralization.

The Orca and Valdez Groups (originally termed Orca and Valdes Series) are the two broad stratigraphic units into which the bedded rocks of the Prince William Sound region were originally subdivided (Schrader, 1900, p. 404-410; Schrader and Spencer, 1901, p. 34-39). Geologists who subsequently mapped in the region have found Schrader's subdivisions useful even though local lithologic similarities between the two groups, structural complexity, and a virtual absence of diagnostic fossils have precluded precise definition of what constitutes the two groups or the stratigraphic and structural relationships of the included beds. The approximate areal distribution of the two units as compiled by Moffit (1954, pl. 8), with minor modifications based on reconnaissance observations by Plafker, in 1964, is shown on figure 1. Numerous granitic intrusive bodies that cut both the Valdez and Orca Groups, and unconsolidated Quaternary deposits that locally mantle the indurated rocks, are not differentiated on the map.

The Valdez Group has been assigned a Mesozoic age largely on the basis of three collections of *Inoceramus* found within its area of outcrop. Diagnostic fossils have not previously been obtained from the Orca Group. Generally the Orca Group has been considered to be younger than the Valdez, mainly because it is somewhat less metamorphosed than the Valdez Group and supposedly overlies the Valdez with angular unconformity. Moffit (1954, p. 275) states that the two groups are everywhere in fault contact, and he questions the validity of the assumed age relationship between the two groups. He concludes that "the fossil evidence regarding the age of the sedimentary rocks of the Prince William Sound region, although scanty and applied to an extensive area, suggests correlation rather than separation of the groups and casts doubt on the adequacy of the reasons offered for suggesting that they are two distinct groups." On the basis of the evidence from fossils available to him, Moffit favored a Mesozoic (probably Late Cretaceous) age for both groups.

Other workers (Payne, 1955; Miller and others, 1959, p. 14, 21) have inferred that at least the lower part of the Orca Group is part of a narrow belt of "greenstone graywacke and slate" that borders the Gulf of Alaska from Kodiak Island on the west to Baranof Island in southeastern Alaska. The sequence was tentatively assigned a pre-Late Cretaceous, and probable Early Jurassic to Early Cretaceous age on the basis of fossil evidence in southeastern Alaska, and on correlations with dated sequences of lithologically similar rocks elsewhere.

Studies of new fossil collections obtained from the Orca Group in 1964, and restudy of the available invertebrate megafossils previously collected from the Valdez Group, demonstrate that the Orca Group is definitely younger than the Valdez Group, and that it is of early Tertiary, rather than of Mesozoic age.

## OUTLINE OF THE MAJOR STRATIGRAPHIC UNITS IN PRINCE WILLIAM SOUND

### Valdez Group

The Valdez Group crops out along the northern and western shores of Prince William Sound and also under-

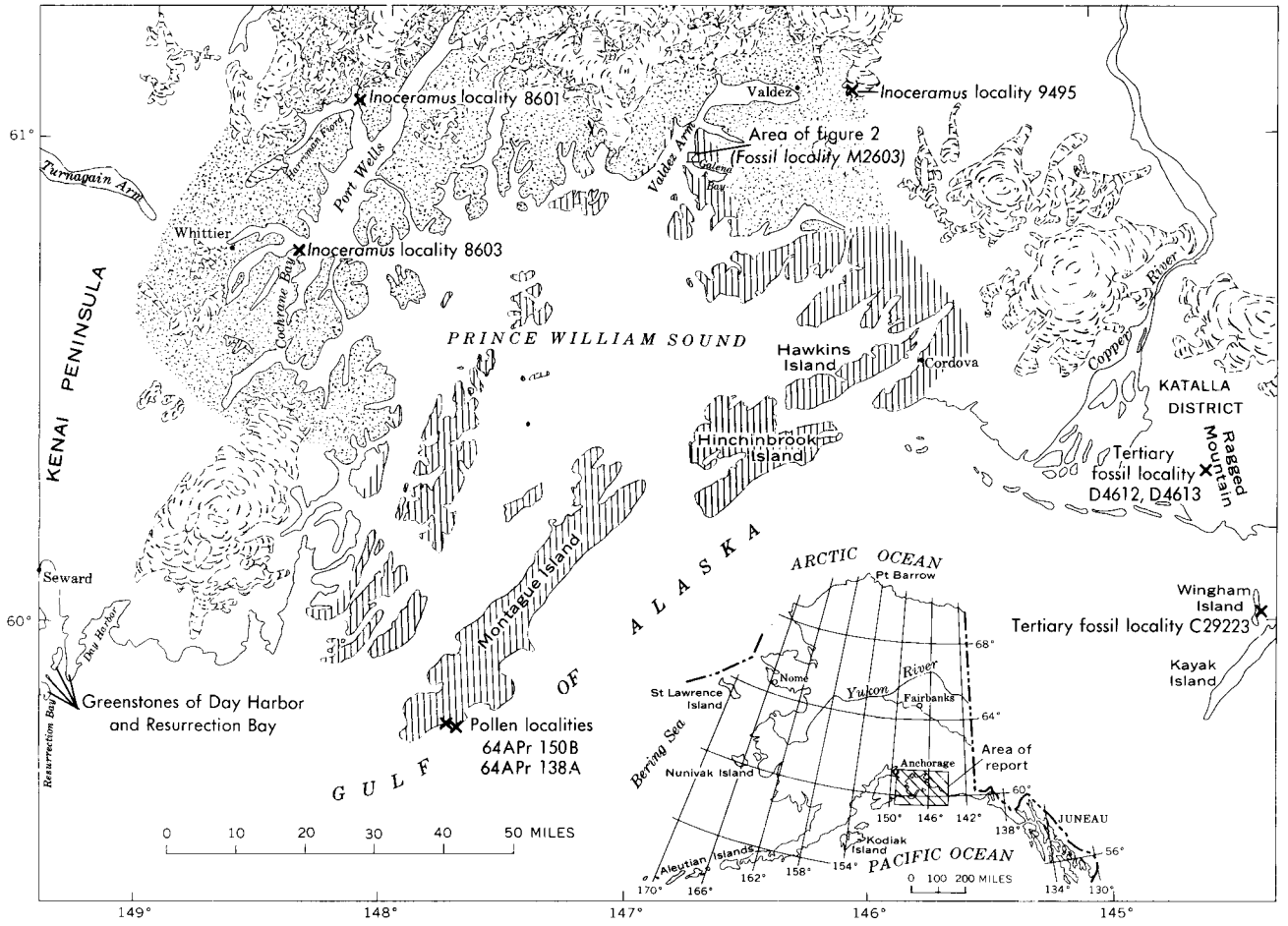


FIGURE 1.—Index map of the Prince William Sound region, showing the approximate outcrop areas of the Orca Group (ruled pattern) and Valdez Group (stippled pattern), and localities referred to in the text.

lies much of the adjacent Chugach Mountains and the Kenai Mountains on the Kenai Peninsula. It is composed of a thick sequence of lithologically monotonous eugeosynclinal sediments that have been closely folded and mildly metamorphosed to hard graywacke and slate or argillite with minor amounts of pebble and cobble conglomerate. The graywacke and argillaceous rocks commonly exhibit rhythmically alternating, finely laminated graded beds. These rocks are interbedded with, or intruded by, small lenticular bodies of mafic fine-grained igneous rocks that are extensively altered to greenstone. The entire sequence is intruded by numerous dikes and stocks of biotite- and biotite-hornblende granite, and it is locally metamorphosed to schistose graywacke and phyllite.

The thickness of the Valdez is unknown because the base is nowhere exposed and the beds are duplicated and interrupted by complex folding and faulting. The sequence is exposed across strike for a distance of 50 miles to the north of Prince William Sound, suggesting that it is probably tens of thousands of feet thick.

The only diagnostic invertebrate fossils thus far obtained from the Valdez Group were collected in 1913 by B. L. Johnson (1914, p. 208–209), in the Port Wells area [USGS 8601 and 8603 (float)] and from float in a moraine of the Valdez Glacier near Valdez (USGS 9495) at localities shown on figure 1. The fossils are poorly preserved specimens of *Inoceramus* that according to D. L. Jones (oral commun., April 2, 1965), of the U.S. Geological Survey, indicate a definite Jurassic or Cretaceous age but that cannot be more closely dated. On the basis of comparison with species from Wyoming and Utah they were formerly assigned a Late Cretaceous age by Imlay and Reeside (1954, p. 227–228).

The Valdez Group is remarkably similar in lithologic characteristics to, and is probably synchronous with, rocks exposed along the Chugach Mountains geosyncline (Payne, 1955), which extends from the central part of Kodiak Island through the Kenai and Chugach Mountains to southeastern Alaska. Diagnostic fossils collected from the probably equivalent slate-graywacke sequence to the east of the Copper

River (Yakutat Group) include *Buchia* identified by D. L. Jones as *B. mosquensis* and *B. piochii*? of Late Jurassic age and *B.* cf. *B. okensis* and *B. subokensis*? of Berriasian (earliest Cretaceous) age (Miller, 1961). A single specimen of a foraminifer from the Yakutat Group was identified by Ruth Todd, of the U.S. Geological Survey, as *Nodosaria affinis* Reuss, which in the southern United States is indicative of a Late Cretaceous or Paleocene age (Brabb and Miller, 1962). From the foregoing evidence it is concluded that the Valdez Group and its probable lithologic equivalents are of Jurassic to Cretaceous age.

### Orca Group

The Orca Group occurs mainly on the eastern shores of Prince William Sound and on the islands in the central and southern part of the sound (fig.1). It is distinguished from the Valdez Group mainly by a more diverse lithology with abundant volcanic rocks and by a somewhat lesser degree of metamorphism.

The lower part of the Orca consists largely of dark graywacke and argillite which intertongue with abundant volcanic and conglomeratic rocks. The volcanic rocks are flows, flow breccias, and intrusive sills and dikes, all of basaltic composition. They have been intensly altered and are grouped for convenience of description under the term "greenstone." Most of the flows are characterized by strikingly well developed pillow structures suggestive of submarine extrusion. The conglomeratic rocks are poorly sorted, ranging from pebble and cobble conglomerate to conglomeratic argillite that contain sparsely distributed lithic clasts throughout a hard matrix of dark-gray argillite. In the absence of volcanic rocks, the more intensely altered graywacke and argillite of the lower unit are difficult to distinguish from the lithologically similar rocks of the Valdez Group. For this reason, and because of the prevailing structural complexity, the location and nature of the contacts between the two groups are largely conjectural. Detailed geologic studies will be required before these contacts can be mapped with confidence, especially in the southwestern part of the Prince William Sound region where the lower, volcanic part of the Orca Group is interbedded with thick units of sedimentary rocks that are extensively intruded and partially metamorphosed so that they strongly resemble the graywacke and slate of the Valdez Group.

The upper part of the Orca Group consists mainly of sandstone and argillite or hard siltstone with minor amounts of volcanic and conglomeratic rocks. The sandstones are predominantly of the graywacke type but also include abundant light-colored arkosic types and minor carbonaceous, tuffaceous(?), and calcareous sandstones. Dark-gray to black dense, hard siltstone which locally has been converted to argillite is interbedded with the sandstone. The graywacke and siltstone commonly form rhythmically alternating graded beds. The upper sequence includes some thin beds of light-gray-weathering limestone and reddish-brown shale or siltstone.

The structure of the Orca Group is exceedingly complex, and the sequence undoubtedly includes numerous unrecognized unconformities and faults. Folds range from open to tightly appressed and locally are overturned both to the north and to the south. They are of small amplitude and lateral extent and are complicated by intricate drag folding and minor thrust faults. Neither the base nor the top of the sequence has definitely been recognized. The complex structure and apparent absence of key beds preclude a reliable estimate of the thickness of the Orca Group. The prevailing steep dips, which occur over an extensive outcrop area, suggest that it totals tens of thousands of feet.

Fossils previously collected from the Orca Group include numerous nondiagnostic wormlike marine organisms, *Terebellina palachei* Ulrich, a few unidentifiable clams, borings and tracks of possible marine organisms, and abundant carbonized plant remains.

## NEW PALEONTOLOGIC DATA

### Megafossils

During the course of field investigations into the geologic effects of the Alaska earthquake of March 27, 1964, Plafker, W. H. Bastian, D. S. McCulloch, and L. R. Mayo collected diagnostic fossils from the Orca Group at the head of a small cove about a mile north of the entrance to Galena Bay (figs. 1 and 2).

The fossils occur within calcarious concretions in the matrix of a conglomeratic argillite in the lower part of the Orca. The conglomeratic bed is 50 to 100 feet thick and is interstratified with greenstone pillow lava, graywacke, and argillite. Bedding is defined by sandstone bands 1 to 4 inches thick near the north end of the exposure with dips ranging from 25° N. 65° W. to 28° N. 45° W. The contacts are not exposed, although the structural relationships with the overlying interbedded flows and sediments indicate approximate structural conformity or possible slight angular unconformity with the overlying and underlying greenstone flows (fig. 2).

The conglomeratic argillite bed consists predominantly of hard dark-gray massive argillite that contains sporadically distributed angular to subangular unsorted clastic debris (fig. 3). The coarse fraction includes blocks 8 feet in maximum dimension; more commonly the clasts are less than 6 inches in diameter. They con-

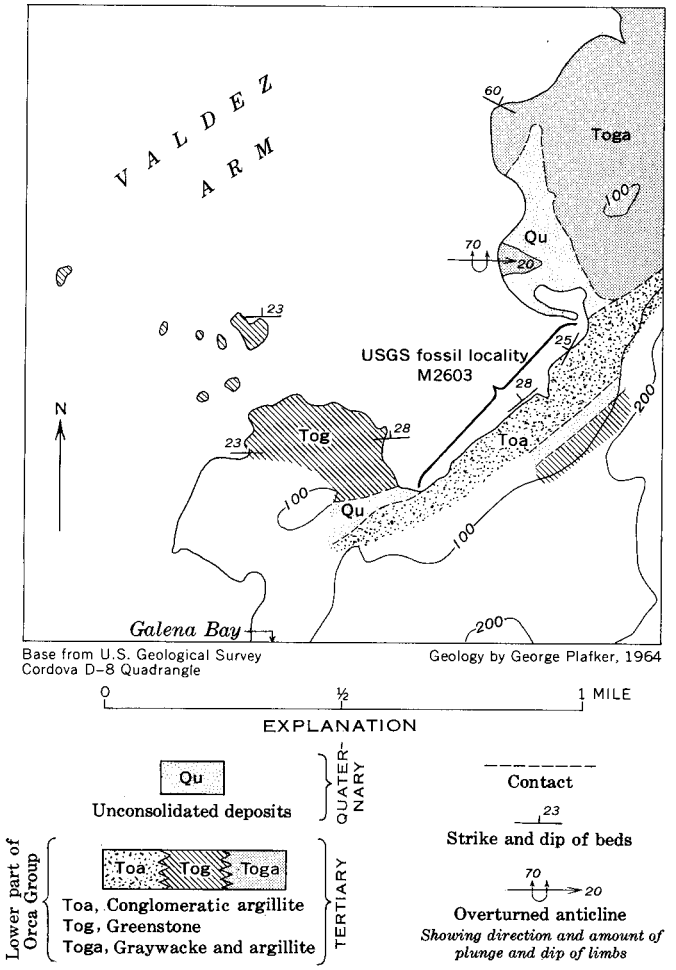


FIGURE 2.—Sketch map showing the location and geologic setting of USGS fossil locality M2603, near the entrance to Galena Bay.

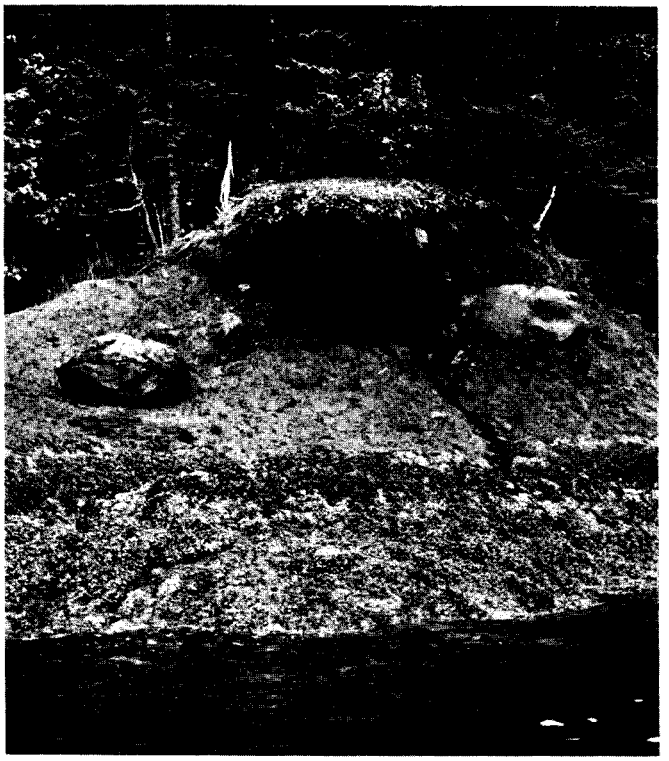

FIGURE 3.—Conglomeratic argillite at fossil locality M2603, near the entrance to Galena Bay. Cobbles and boulders of graywacke, argillite, slate, and greenstone are irregularly distributed throughout a matrix of hard black argillite. Graywacke boulder in left center of view is 3 feet long. Fossiliferous calcareous concretions occur within the argillite matrix. Horizontal bands near water are formed by zoned algae and barnacles, not bedding.

sist either of angular cobbles and boulders of greenstone that are lithologically indistinguishable from the enclosing flows, or of graywacke, argillite, and slate detritus similar to the predomimant lithologic types of the Valdez Group that crops out immediately to the north. The concretions, which consist of dense smooth calcareous argillite containing finely disseminated grains of iron sulfide, are irregularly distributed throughout the matrix of the conglomerate. They are in the shape of spheres or oblate spheroids up to 5 inches in maximum dimension. An estimated 10 percent of the concretions contain fragmental or entire fossil crabs; a few mollusks and a single fragment of worm-bored wood were also found. The concretions appear to be diagenetic, having formed prior to induration by precipitation of calcium carbonate and iron sulfide around decaying organisms and other nuclei buried in the mud matrix of the conglomerate. Thus the contained fossils probably are reliable indicators of the age of the conglomeratic argillite bed.

Examples of the fossils, which were prepared and identified by MacNeil, are illustrated in figure 4. The most abundant fossil is the crab *Branchioplax washingtoniana* Rathbun; many well-preserved specimens with the slender appendages still intact were obtained. According to Rathbun (1926, p. 42), only one known species can be referred to this genus. The type is from the Oligocene of Oregon and Washington. It has also been reported by Rathbun (1926, p. 44) from the Cowlitz Formation in Washington (late Eocene), but H. B Stenzel (written commun. to D. J. Miller, June 1946) states that the material from the Cowlitz is too poor for positive identification and that the species is not present in any Eocene collections that he has identified from Oregon. Two specimens of another crab, *Raninoides vaderensis* Rathbun, are also present. The species is described by Rathbun from upper Eocene beds of Washington and reported from supposed middle Eocene beds of Oregon. After acid preparation one of the concretions yielded several excellent molds of the clam *Acila decisa* (Conrad), a species originally described from an unknown locality in California. Three synonyms of the species are well documented stratigraphically, one of them *A. lajollaensis* Hanna, having been

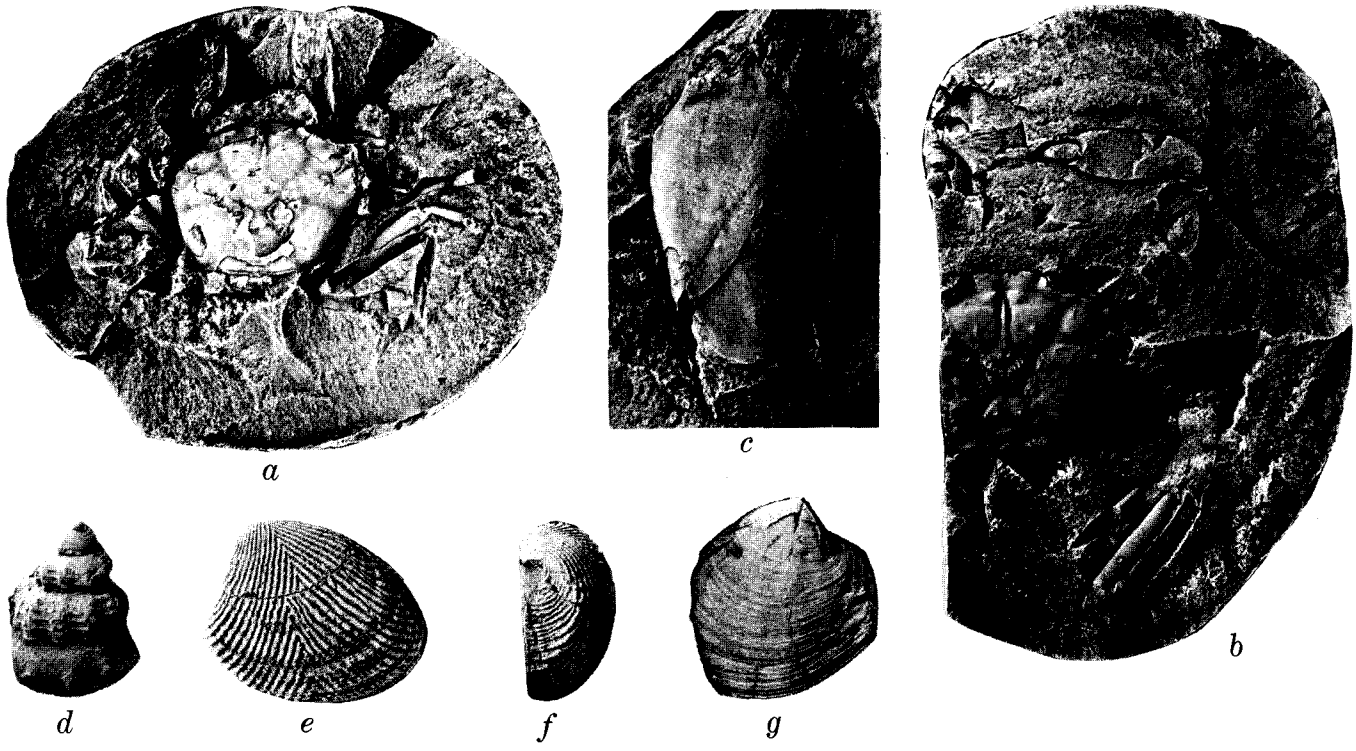


*a* and *b*, *Branchioplax washingtoniana* Rathbun (× 1)
*a*, Ventral side of partly testaceous specimen, USNM 649414.
*b*, Ventral side of acid-treated specimen, showing interior details on internal mold, USNM 649415.
*c*, *Raninoides vaderensis* Rathbun (× 1)
Dorsal view of carapace, USNM 649416.
*d*, ?Cancellarid (× 2)
Decorticated spire (rubber cast), USNM 644861.
*e* and *f*, *Acila decisa* (Conrad) (× 2) USNM 644862
*e*, Right valve (rubber cast).
*f*, Escutcheonal view of same specimen.
*g*, *Periploma* cf. *P. eodiscus* Vokes (× 1½)
Left valve (rubber cast), USNM 644863.

FIGURE 4.—Specimens from USGS locality M2063, on a small cove on the east side of Valdez Arm, about 1 mile north of the entrance to Galena Bay, Prince William Sound, Alaska. Orca Group. Eocene.

accepted by Schenck (1936, p. 55) as the neotype for the species. All its known occurrences in California, Oregon, and Washington are in middle and upper Eocene beds, and it is generally recognized as a good guide fossil to the Eocene. An excellent mold of one specimen of the clam *Periploma* cf. *P. eodiscus* Vokes was also obtained with acid preparation. It has the same shape as Vokes' species and shows details of the sculpture, but unfortunately Vokes' specimen does not. *P. eodiscus* was described from the Domengine Formation (middle Eocene) of California.

### Pollen

Six samples of indurated siltstone and limestone collected during the 1964 field season from the upper, predominantly sedimentary, part of the Orca Group were analyzed for pollen by the palynological laboratory of the Stanford University School of Earth Sciences, through the courtesy of W. R. Evitt. Identifiable pollen was found in two of the samples (field numbers 64APr 150B and 64APr 138A) of carbonaceous siltstone from Neck Point on the southeast end of Montague Island. The residues from the remaining samples contain much organic material, but no identifiable fossils. Evitt's report (written commun., Nov. 10, 1964) on the pollen is as follows:

> The alder (Alnus) pollen in sample 64APr 150B (PL–1875) is rare and rather poorly preserved, but identification of this pollen type is made easy by its very distinctive characters which are robust enough to have withstood the processes that rendered the rest of the pollen and spores unidentifiable. Pollen of this type has not been reported from pre-Tertiary material to my knowledge. It is abundant in many Tertiary samples from Alaska.
>
> The single triporate grain recovered from sample 64APr 138A (PL–1873) is less distinctive. It probably indicates a Tertiary age, but could possibly be from the highest Cretaceous (Maestrichtian). Only one grain was observed and this is insufficient evidence for a firm age determination.

### Age of the Orca Group

The crab *Raninoides vaderensis* Rathbun and the pelecypods *Acila decisa* (Conrad) and *Periploma*

cf. *P. eodiscus* Vokes indicate a probable middle to late Eocene age for the lower volcanic unit of the Orca Group. *Branchioplax washingtoniana* Rathbun has a longer range and could indicate either an Eocene or Oligocene age. The upper age limit of the Orca Group is not known because specifically diagnostic fossils have not been obtained from it nor is it known to be overlain by younger dated Tertiary rocks. On the basis of the limited data now available, the Orca Group is assigned an early Tertiary rather than a Mesozoic age. Because the megafossils were collected from close to the base of the Orca, the lower age limit of the sequence is probably middle to late Eocene. The upper age limit is unknown, and the group may include rocks younger than Eocene.

## CORRELATIONS

Bedded volcanic and sedimentary rocks occur elsewhere along the margin of the Gulf of Alaska, in the Katalla district to the east of Prince William Sound, and along the seaward coast of the Kenai Peninsula and the Kodiak Island group to the southwest of the Sound. The age relationships of these rocks are imperfectly known because of a paucity of diagnostic fossils and structural complexities that mask their relationships with dated older and younger formations. Payne (1955), and more recently Miller and others (1959, p. 21), considered these rocks and the Orca Group to be part of a "Mesozoic greenstone-graywacke-slate sequence" bordering the Gulf of Alaska from Kodiak Island on the west to Baranof Island in southeastern Alaska. However, the limited available evidence from fossils and the lithologic characteristics of these rocks strongly suggest that at least a part of this sequence is of early Tertiary rather than of Mesozoic age.

In the Katalla district the lower, predominantly volcanic unit of the Orca Group may be represented by a sequence of bedded greenstone and associated sedimentary rocks that form the backbone of Ragged Mountain and much of Wingham Island (fig. 1). These rocks, which are complexly deformed and slightly metamorphosed, have generally been considered to be Mesozoic or older (Martin, 1908, p. 26-27; Miller, 1951, p. 11-13). However, the only known fossils from them are diatoms and silicoflagellates from impure limestone on Ragged Mountain (localities D4612 and D4613) that according to K. E. Lohman, of the U.S. Geological Survey, strongly suggest a late Eocene age, and specimens of *Turitella* from a float limestone cobble on Wingham Island (locality C29223) believed to be of probable middle Eocene age (Miller, 1961, explanatory notes). Possible lithologic equivalents of the upper, predominantly sedimentary part of the Orca Group in the Katalla district include complexly deformed predominantly marine siltstone and sandstone of the Stillwater and Tokun Formations of middle to late Eocene age, and the undifferentiated sandstone-siltstone sequences of probable early Tertiary age. Concretions containing small crabs of the same genera as those from the Orca Group, *Raninoides* and *Branchioplax*, are virtually the only fossils found in the type area of the Stillwater Formation. The crab *Branchioplax washingtoniana* Rathbun, the most abundant fossil species collected from the Orca Group, is also the characteristic fossil of the upper Tokun in the Katalla district. Thus, the available fossils from the Katalla district suggests that part or all of the lower Tertiary sequence, including the volcanic unit of Ragged Mountain and Wingham Island, may be synchronous with the Orca Group in the Prince William Sound area.

A thick sequence of unfossiliferous ellipsoidal greenstone flows and associated mildly metamorphosed sedimentary and tuffaceous rocks, almost identical in lithologic characteristics with the lower part of the Orca Group, underlies the peninsula between Day Harbor and Resurrection Bay on the southern coast of the Kenai Peninsula. The lithologic similarities were noted by U. S. Grant (*in* Martin and others, 1915, p. 223–225) who suggested that the volcanic rocks and associated tuffs may correlate with the Orca Group of Prince William Sound. No age-diagnostic fossils have been obtained from the sequence.

Along the southeast coast of the Kodiak group of islands there occurs a belt as much as 10 miles wide of ellipsoidal and amygdaloidal lavas interbedded with, and overlain by, a thick sequence of isoclinally folded clastic sedimentary rocks, commonly with graded bedding. The volcanic unit previously was assigned a probable Triassic or late Paleozoic age by Capps (1937, p. 137) on the basis of a tenuous correlation with a lithologically similar but significantly more metamorphosed sequence of pre-Upper Triassic rocks on the west side of the Kenai Peninsula near Seldovia and Port Graham. The associated isoclinally folded sedimentary sequence was considered to be of Eocene age on the basis of two fossil plants collected from the Trinity Islands, which, according to R. W. Brown, indicate an Eocene or younger age, and on the questionable correlations with the Kenai Formation of the Kenai Peninsula (Capps, 1937, p. 153). More recent detailed geologic mapping by G. W. Moore, of the U.S. Geological Survey, and by petroleum-company geologists has shown that the greenstone-graywacke-siltstone sequence is less metamorphosed and probably younger than the adjacent rocks to the northwest from which *Inoceramus* of Mesozoic age have been collected (Imlay and Reeside, 1954, p. 227–228). It is also more

deformed, and probably older, than overlying predominantly clastic continental rocks containing a fossil flora that according to J. A. Wolfe, of the U.S. Geological Survey, is of Oligocene age. A single pelecypod collected in 1963 by Moore from the upper part of the unit is a new species, and possibly a new genus of Vesicomyidae. This family ranges throughout the Cenozoic, but its only representatives thus far recognized in Alaska are from rocks of late Oligocene age in the Katalla district. The fragmentary fossil collections and the relative degree of deformation and metamorphism as compared with the dated rocks that supposedly underlie and overlie the greenstone-graywacke-siltstone sequence of Kodiak Island, suggest that it could be of early Tertiary age, although neither its upper nor lower age limits can be precisely determined.

## PALEOGEOGRAPHIC SPECULATIONS

The new age data for the Orca Group and the reappraisal of available data on lithologically similar rocks along the Gulf of Alaska suggest that the margin of the Gulf of Alaska at the beginning of Tertiary time was the site of a eugeosyncline that lay parallel to, and south of, the Chugach Mountains geosyncline. This linear basin of deposition was at least 500 miles long, extending westward from the Katalla district into the Prince William Sound region, where it bent abruptly southwestward to the Kodiak group of islands. The northern margin extended beneath the present Chugach-Kenai-Kodiak Mountains, and the western margin lay seaward from the present coast.

Early in the history of the geosyncline a thick sequence of mafic volcanic rocks was erupted onto the rapidly subsiding basin floor from numerous centers that are now represented by lenticular piles of ellipsoidal flows. Contemporaneous regional deformation, uplift, and erosion of the Chugach Mountains geosyncline that extended through the Chugach and Kenai Mountains and the central part of the Kodiak group of islands supplied muddy sands and argillaceous and conglomeratic sediments that intertongue with the volcanic rocks. In the later history of the geosyncline, volcanic activity diminished, and the basin was filled with predominantly rhythmically bedded clastic detritus beneath which the preexisting volcanic highlands were buried.

The Orca rocks and their equivalents were later complexly folded, faulted, and probably extensively intruded by granitic rocks. At least part of the widespread gold, copper, and antimony deposits in the Orca Group, and possibly some of those in the Valdez Group, were associated with the intrusions.

The time of this major episode of tectonic deformation cannot be ascertained in the Prince William Sound area by stratigraphic methods because rocks younger than the Orca are absent. Radiometric dating of the granitic intrusive rocks that cut the Orca may provide an upper age limit for the orogeny; samples of the intrusive have been submitted for potassium-argon age determinations. Elsewhere along the margin of the Gulf of Alaska, the available evidence suggests that the episode of deformation may have culminated in the time interval from late Eocene to early Oligocene. The occurrence of shallow marine or brackish-water strata of late Eocene to early Oligocene age, local unconformities in upper Eocene strata (Plafker and Miller, 1957), and marked differences in the degree of induration and deformation between the early Teritary and younger strata support such an age for the deformation.

## REFERENCES


Brabb, E. E., and Miller, D. J., 1962, Reconnaissance traverse across the eastern Chugach Mountains, Alaska: U.S. Geol. Survey Misc. Geol. Inv. Map I–341.

Capps, S. R., 1937, Kodiak and adjacent islands, Alaska: U.S. Geol. Survey Bull. 880–C, p. 111–184.

Imlay, R. W., and Reeside, J. B., 1954, Correlation of Cretaceous formations of Greenland and Alaska: Geol. Soc. America Bull., v. 65, p. 223–246.

Johnson, B. L., 1914, Port Wells gold-lode district: U.S. Geol. Survey Bull. 592–G, p. 195–236.

Martin, G. C., 1908, Geology and mineral resources of the Controller Bay region, Alaska: U.S. Geol. Survey Bull. 335, 141 p.

Martin, G. C., Johnson, B. L., and Grant, U. S., 1915, Geology and mineral resources of the Kenai Peninsula, Alaska: U.S. Geol. Survey Bull. 587, 243 p.

Miller, D. J., 1951, Preliminary report on the geology and oil possibilities of the Katalla district, Alaska: U.S. Geol. Survey open-file rept., 66 p.

——— 1961, Geology of the Katalla district, Gulf of Alaska Tertiary province, Alaska: U.S. Geol. Survey open-file rept.

Miller, D. J., Payne, T. G., and Gryc, George, 1959, Geology of possible petroleum provinces in Alaska: U.S. Geol. Survey Bull. 1094, 131 p.

Moffit, F. H., 1954, Geology of the Prince William Sound region, Alaska: U.S. Geol. Survey *Bull. 989–E*, p. 225–310, illus. incl. geol. map.

Payne, T. G., 1955, Mesozoic and Cenozoic tectonic elements of Alaska: U.S. Geol. Survey Misc. Inv. Map I–84.

Plafker, George, and Miller, D. J., 1957, Reconnaissance geology of the Malaspina district, Alaska: U.S. Geol. Survey Oil and Gas Inv. Map OM–189.

Rathbun, M. J., 1926, The fossil stalk-eyed Crustacea of the Pacific slope of North America: U.S. Nat. Mus. Bull. 138, 155 p., 39 pls.

Schenck, H. G., 1936, Nuculid bivalves of the genus *Acila:* Geol. Soc. America Spec. Paper 4, 149 p., 18 pls.

Schrader, F. C., 1900, A reconnaissance of a part of Prince William Sound and the Copper River district, Alaska, in 1898: U.S. Geol. Survey 20th Ann. Rept., pt.7, p. 341–428.

Schrader, F. C., and Spencer, A. C., 1901, The geology and mineral resources of a portion of the Copper River district, Alaska: U.S. Geol. Survey Spec. Pub., 94 p.

# STRATIGRAPHIC RELATIONS OF UPPER CRETACEOUS ROCKS, LAMONT-BAIROIL AREA, SOUTH-CENTRAL WYOMING

By MITCHELL W. REYNOLDS, Denver, Colo.

*Abstract.*—Unconformities in Upper Cretaceous rocks of south-central Wyoming mark areas of uplift and erosion, and account for the thinning and absence of the Mesaverde Formation near Lamont and Bairoil. An unconformity at the base of the Teapot Sandstone Member of the Mesaverde bevels the underlying part of the Mesaverde from south to north. Local tectonic activity in post-Teapot and early Lewis time resulted in additional uplift and in truncation of the Mesaverde Formation across the area by marine planation. Maximum truncation of strata occurs on the west and north flanks of Lost Soldier anticline, where the Mesaverde is absent; and on the south flank of the Sweetwater arch, where the Mesaverde is absent and the Lewis Shale lies on progressively lower portions of the Cody Shale.

Production of oil and gas from rocks of Late Cretaceous age in Wyoming provides incentive for local and regional geologic studies to synthesize the Late Cretaceous depositional and tectonic history. Local areas of anomalous stratigraphic relations exist, and conflicting interpretations of these relations have been made. Such areas may provide important clues for interpretation of the geologic past.

The Lamont-Bairoil area of south-central Wyoming appears to be one of the critical locales, not only because of an anomalous section of rocks of Late Cretaceous age, but also because of conflicting interpretations that have been published on the area during the past 40 years. Early workers generally agreed that the stratigraphic section in the Lamont-Bairoil area is anomalous because of drastic thinning of the Mesaverde Formation and the Cody and Lewis Shales.

Fath and Moulton (1924) first mapped the Lamont-Bairoil area in detail and observed that the Mesaverde Formation thins from 1,900 to 200 feet in a distance of 12 miles. They account for the thinning as follows: "This thinning could be explained by assuming a local deformation centering somewhere to the west which shallowed the sea or perhaps even caused a slight elevation above the water level during Mesaverde time." (Fath and Moulton, 1924, p. 27.)

After mapping the area in 1960, Guyton (1960) concluded that the thinning of the Mesaverde Formation on the flanks of the Lost Soldier anticline may have resulted from thinning or nondeposition on a local structural high (p. 54). He also described (p. 15) a large-scale intertonguing of the Cody and Mesaverde. Weimer and Guyton (1961, p. 139) proposed a somewhat different interpretation of the geology. Studies by Weimer, a reinterpretation of Guyton's 1960 work, and a reevaluation of regional stratigraphic and faunal data, led them to conclude that the thinning of the Mesaverde was not the result of local structural growth of the Lost Soldier anticline, but was rather the result of regional thinning and facies change from the Mesaverde into the Cody Shale (Weimer and Guyton, 1961, p. 139).

In 1962 Zapp and Cobban published a preliminary report describing the results of a regional study of intertonguing relations of marine and nonmarine rocks of Late Cretaceous age in Wyoming (Zapp and Cobban, 1962). They presented evidence that time-equivalent strata separated by more than 4,000 feet of beds in nearby areas are virtually in contact in the Lamont-Bairoil area. Zapp and Cobban (1962, p. D52) attributed the relation to depositional thinning and truncation associated with extreme local tectonic differentiation.

The present investigation was undertaken to evaluate and document the role of uplift and erosion, depositional thinning, facies change, intertonguing, or a combination of these factors as cause of the thinning and disappearance of the Mesaverde Formation in the Lamont-Bairoil area. Detailed geologic mapping on a scale of 1:24,000 has been done in critical parts of four 7½-minute quadrangles centering around Lamont and Bairoil, with reconnaissance mapping extending southward along Separation Rim and the Shamrock Hills (fig. 1). Detailed stratigraphic sections of the Mesaverde Formation and adjacent strata were measured at

U.S. GEOL. SURVEY PROF. PAPER 550-B, PAGES B69-B76

closely spaced intervals north of Lamont, south of Bairoil, and at Separation Rim; the Upper Cretaceous section described by Barlow (1959) on the west flank of the Rawlins uplift was examined carefully (figs. 1, 2, sec. A). Descriptions of sections measured by Chuman (1954) were examined but were found to be lacking in sufficient detail to be used in this investigation.

The writer had access to unpublished field notes of A. D. Zapp and to previously unreported faunal data of the U.S. Geological Survey from this and nearby areas. J. R. Gill, of the U.S. Geological Survey, contributed additional material on regional stratigraphic relations. W. A. Cobban, also of the U.S. Geological Survey, identified collections of fossils from this and previous investigations.

## NOMENCLATURE

Stratigraphic nomenclature used in this report is modified from Fath and Moulton (1924, p. 10, 11). The name Cody Shale is used in place of the Niobrara and Steele Shales, inasmuch as the Niobrara cannot be identified consistently throughout the mapped area. Thus the name Cody Shale is applied to all strata lying between the Frontier Formation below and the Mesaverde Formation or Lewis Shale above. The terms Mesaverde and Lewis are used in the sense of Fath and Moulton (1924, p. 10, 26–28) for littoral, brackish, and nonmarine beds and for marine beds, respectively, overlying the Cody Shale and underlying the Lance Formation of this report. Use of the terms Mesaverde and Lewis in this way is now known (Weimer, 1959, p. 10–12; Scott and Cobban, 1959, p. 129–130) to be incorrect in south-central Wyoming, because strata bearing the names in Wyoming are not correlative with those of the type area of the formations in southwestern Colorado.

The name Lance Formation, as used in this report, is applied to all strata of very shallow marine and dominantly nonmarine origin overlying the Lewis Shale and underlying the Fort Union Formation. At Rawlins these strata correspond to the "Laramie" Formation of Dobbin and Reeside (1929, p. 20–23), who recognized that the "Laramie" is equivalent to the Lance Formation as mapped to the north. Most subsequent reports or maps (Love and others, 1955; Barlow, 1959, p. 111) apply the name Lance to the same strata. The Lance Formation of this report corresponds to the upper member of the Mesaverde and the Lance Formation of Weimer and Guyton (1961, p. 142, 145).

## MESAVERDE FORMATION

The Mesaverde Formation in the Lamont-Bairoil area contains rocks of littoral, brackish, and nonmarine facies. Typical exposures of the formations are north of Lamont, on the Tully Ranch in the SW¼ sec. 34, T. 27 N., R. 89 W., and in the NW¼ sec. 3, T. 26 N., R. 89 W. (see photographs in Fath and Moulton, 1924, pl. VI–A); and south of Bairoil, in secs. 25 and 26, T. 26 N., R. 90 W., across the Lost Soldier Rim. The basal contact of the formation in these sections is drawn, following Fath and Moulton (1924, p. 27), just below the lowest white cliff- or ledge-forming sandstone. Thin interbedded marine sandstone and shale, gradational into the Mesaverde, are thus included in the underlying Cody Shale. Thick grayish-orange sandstone beds of shallow marine origin which lie below the gradational interval around Lost Soldier anticline and along the east flank of the Camp Creek syncline, are also included in the Cody Shale.

In the Lamont-Bairoil area, white sandstone beds of shallow-water marine origin, containing rare *Ophiomorpha*, occur (1) at the base of the Mesaverde, and (2) about 100 feet above the base. The beds are separated by nonmarine and brackish-water carbonaceous shale in the vicinity of Bairoil. Southward, west of Rawlins and at Separation Rim (fig. 2 and table 1, sec. A and B), the sandstones are pale grayish orange and the intervening strata are marine and brackish-water beds. Overlying this lower sequence of littoral sandstones and interbedded brackish and nonmarine beds throughout the area is a thick sequence of interbedded sandstone, siltstone, and claystone. Ironstone concretions are abundant in some beds. This upper sequence is characterized by extreme lateral lithologic variation, by intertonguing, and by pale grayish-orange, light brownish-gray, and dusky-red coloration. Plant fragments are common and some siltstones are locally lignitic. Near Lamont and Bairoil (fig. 2 and table 1, secs. C, D, and E) the upper sequence is thin and is entirely nonmarine, whereas at Separation Rim and to the south, it is thicker, and near the center contains several thick sandstone beds, probably of shallow marine origin, interbedded with plant-bearing siltstone and olive shale (fig. 2, sec. B).

A sandstone which weathers light gray to white and which contains silt and light-brown lignitic siltstone in its upper part is found at the top of the Mesaverde Formation at Lost Soldier Rim and Tully Ranch (fig. 1, locs. C and E; fig. 2, secs. C and E). This sandstone forms a ridge or hogback at the top of each section. The lithology and stratigraphic position of the sandstone suggest that it is the Teapot Sandstone Member of the Mesaverde (Fath and Moulton, 1924, p. 27) and that it is also equivalent to the Pine Ridge Sandstone Member of the Mesaverde in the Hanna and Laramie basins (Dobbin and others, 1929, p. 140). It is correlative with the Teapot Sandstone Member as mapped in the southeastern Wind River basin

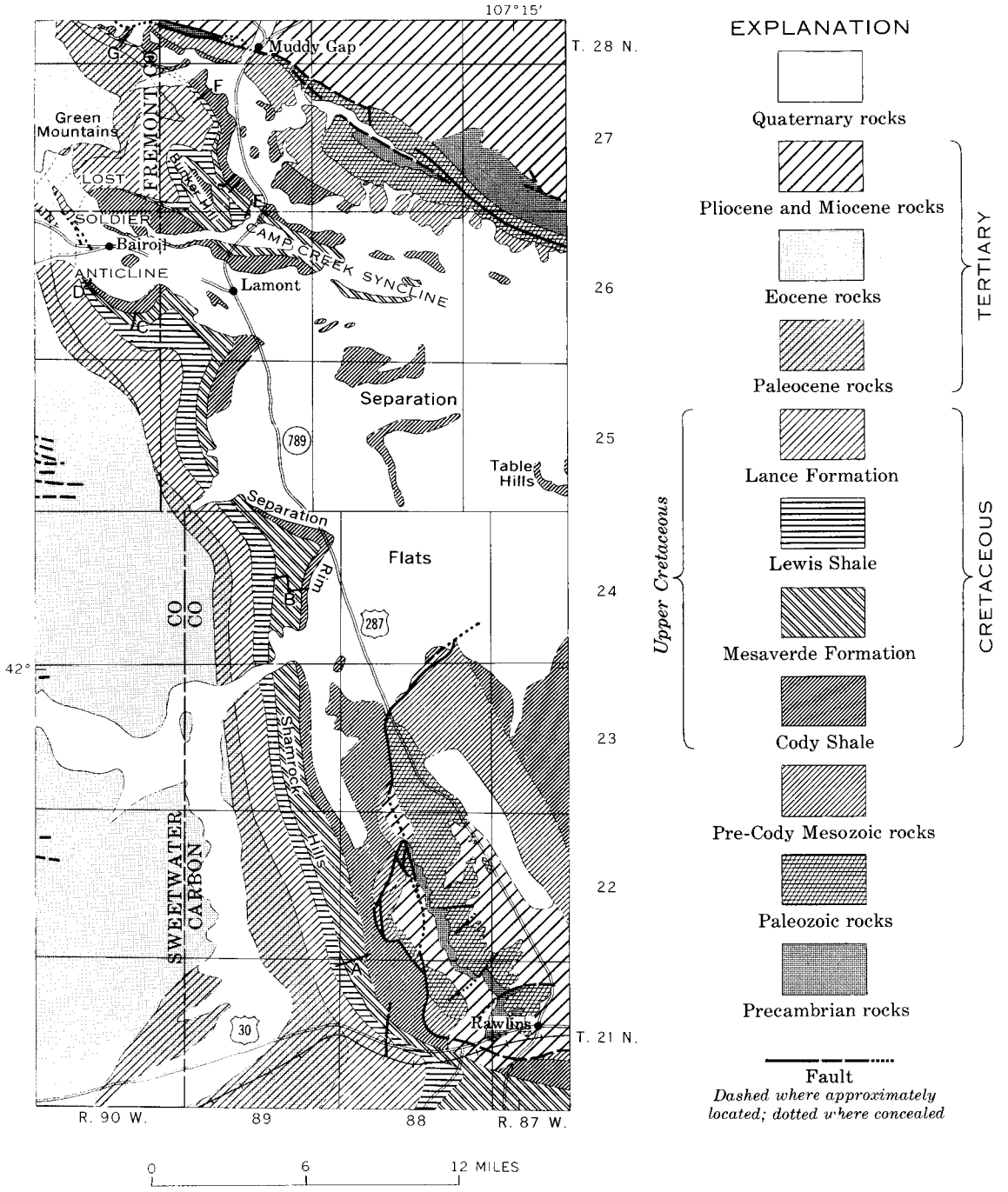


Figure 1.—Geologic map of the Rawlins–Muddy Gap area, south-central Wyoming, showing the location of Lamont and Bairoil and measured sections (A-G) referred to in text. Geology modified from Love and others (1955).

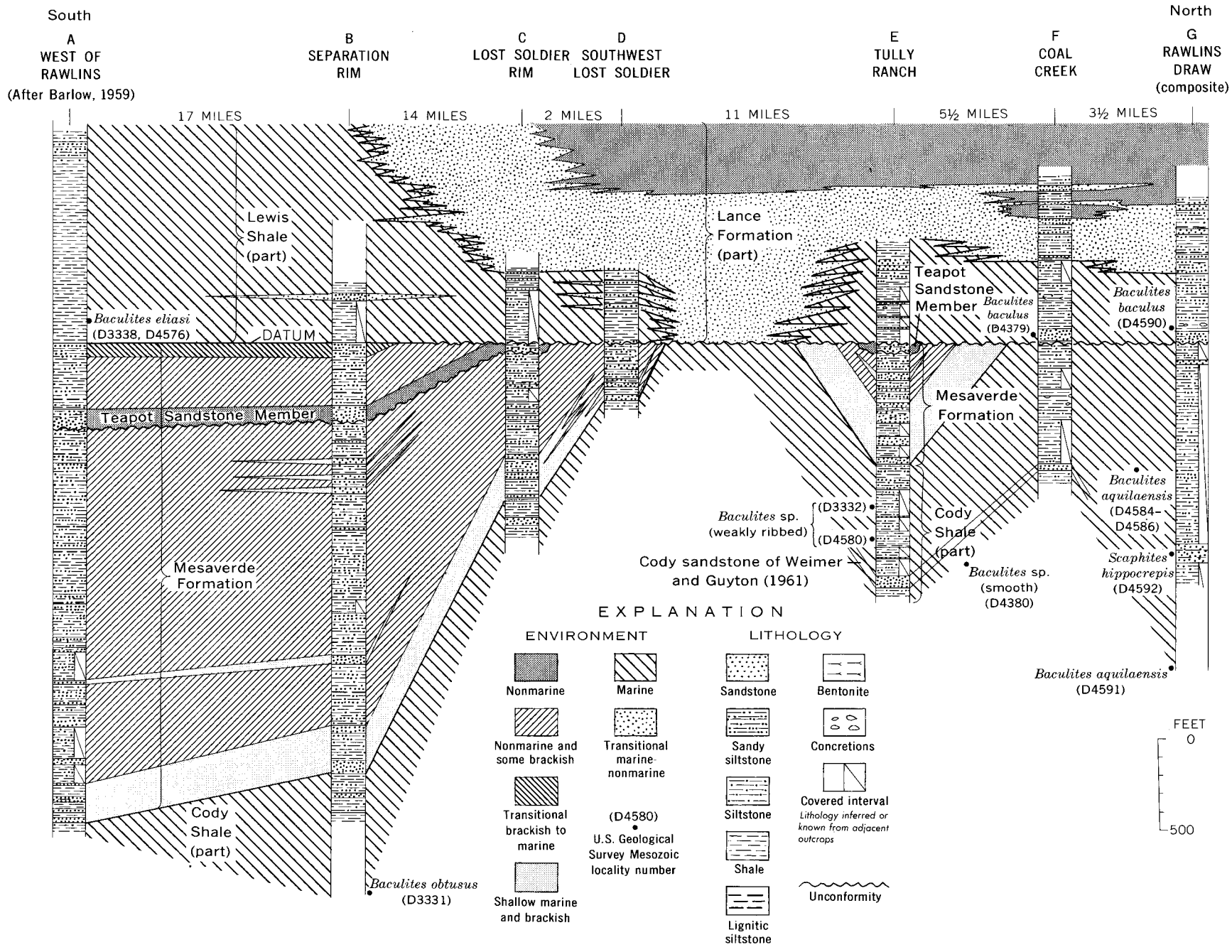


FIGURE 2.—Correlation of stratigraphic sections of the Mesaverde Formation and adjacent strata in the Lamont-Bairoil area, showing (a) thinning of the Mesaverde from south to north, (b) truncation of the Mesaverde across the Lost Soldier anticline and on the south flank of the Sweetwater arch southwest of Muddy Gap, and (c) facies change of the Lewis Shale to the Lance Formation across the Lost Soldier anticline. Contacts between the Lewis and Lance and between transitional marine and nonmarine Lance are diagrammatic. See figure 1 for locations of stratigraphic sections.

TABLE 1.—*Location of sections shown on figure 2*

| No. | Name | Section | Township N. | Range W. |
|---|---|---|---|---|
| A | West of Rawlins | 6 | 21 | 88 |
| B | Separation Rim | 14 and 15 | 25 | 90 |
| C | Lost Soldier Rim | NW¼ 25, E½ 26 | 26 | 90 |
| D | Southwest Lost Soldier | NW¼ 22 | 26 | 89 |
| E | Tully Ranch | SW¼ 34, NW¼ 3 | 27, 26 | 89 |
| F | Coal Creek | NW¼ 8 | 27 | 89 |
| G | Rawlins Draw (composite) | SE¼ 26, NW¼ 36 | 28 | 90 |

(Barwin, 1961, p. 176). Abundant plant debris, casts, and carbonized remains of plant roots crossing laminae in siltstone and braided bedding in the fine-grained and very fine grained sandstone indicate a nonmarine origin for the Teapot in the Lamont-Bairoil area.

The Teapot is critical for determining relationships of strata within the Mesaverde Formation. At the Lost Soldier Rim and Tully Ranch sections (fig. 2, secs. C and E), the member is about 60 feet thick and lies about 600 and 800 feet, respectively, above the base of the Mesaverde. The Teapot is overlain by marine shale of the Lewis Shale at the Tully Ranch section, and it dips beneath an alluvium-covered valley. presumably cut in Lewis Shale, at Lost Soldier Rim. At Separation Rim (fig. 2, sec. B) the Teapot is 65 feet thick, lying about 2,000 feet above the base of the Mesaverde; about 360 feet of nonmarine, brackish- or shallow-water marine beds, in ascending order, overlie the Teapot and underlie the Lewis Shale. The Teapot Sandstone Member can be traced southward from Separation Rim to near Rawlins (fig. 2, sec. A) where it is the 110-foot light-gray and brownish-gray sandstone, described by Barlow (1959, p. 112), 2,164 feet above the base of the Mesaverde Formation. Nearly 400 feet of nonmarine and brackish-water sedimentary rocks separate the Teapot from the Lewis Shale at this locality. These rocks seem to be the eastern equivalent of the Almond Formation of the Rock Springs uplift to the west.

Faunal control is lacking in the Mesaverde Formation below the Teapot Sandstone Member. Thicknesses and stratigraphic relations show, however, that the Teapot rests unconformably on the underlying rocks of the Mesaverde, progressively truncating the underlying rocks from south to north. The truncation is gradual from west of Rawlins to Separation Rim but increases greatly from Separation Rim to Tully Ranch; the rate of downcutting between Separation Rim and Tully Ranch is about 90 feet per mile. Lenses of fine-pebble conglomerate found in the Teapot Sandstone Member in the NE¼NW¼ sec. 3, and SW¼NW¼ sec. 4, T. 26 N., R. 89 W., suggest a not-far-distant source and imply possible uplift and erosion. North of sec. 16, T. 27 N., R. 89 W., the Lewis Shale lies unconformably on the Cody Shale, and the northward extent of pre-Teapot truncation cannot be determined.

Much of the thinning of the Mesaverde Formation in the Lamont-Bairoil area seems to have resulted from pre-Teapot erosion; part of it may have been due to depositional thinning. Speculation might be made regarding the seemingly thick Mesaverde section below the Teapot to the south, and about the contrast of the nearly conformable relations there with the strong disconformity near Bairoil. Sedimentation was probably uniform during deposition of most of the lower part of the Mesaverde, so that the thickness was similar over the entire area. Regional uplift, and possibly emergence, terminated deposition and initiated large-scale erosion of the Mesaverde (J. R. Gill, oral commun., 1965) prior to deposition of the Teapot Sandstone Member. Differential upwarp north of Separation Rim and on the southern flank of the Sweetwater arch, which adjoins the area of figure 1 on the north, accompanied the broad regional arching. The Teapot was then deposited across the region, with stronger discordance in areas of local upwarp than in areas of regional arching. Inasmuch as less of the lower part of the Mesaverde was eroded at Rawlins than farther northward, its present thickness there can probably be considered close to normal, rather than abnormally thick (Weimer, 1961, p. 25, 27). Deposition of nonmarine deposits and of later shallow-marine deposits continued on the margins of the Lewis sea in at least the southern part of the area following deposition of the Teapot Sandstone Member. Post-Teapot deposition (equivalent to the Almond of the Rock Springs uplift) may have continued in the northern area, but evidence of it was subsequently removed by erosion during early Lewis time.

## LEWIS SHALE

Marine shale and littoral sandstone compose the Lewis Shale in the Lamont-Bairoil area. The thickness and lithology of the formation vary northward from Rawlins to Muddy Gap (see sections on fig. 2), with the more striking changes taking place across the Lost Soldier anticline. The pronounced change in thickness results primarily from lateral northward gradation from sandy shale to alternating beds of marine sandstone and shale, and then to accumulations of brackish-water deposits intercalated with littoral sandstone in the vicinity of Bairoil. Northeast of Bairoil facies changes occur in the reverse sequence. Some thinning on the southwest and northeast flanks of Lost Soldier anticline

results from depositional onlap over the fold when it was structurally positive in early Lewis time.

At Rawlins the Lewis is about 1,900 feet thick (Barlow, 1959, p. 111) and is predominantly dark-gray marine shale with sandy shale and sandstone in the upper third of the formation. Thin sandstone of shallow-marine origin occurs lower in the Lewis at Separation Rim. Littoral sandstone is common throughout the formation on the southwest flank of Lost Soldier anticline (fig. 2, sec. D). There, local strong convergence of the sandstone beds is evident from surface mapping and from study of aerial photographs. No unconformity is evident within the Lewis or Lance, and the thinning is attributed to depositional thinning and to onlap upon the fold. Northeast of Bairoil, marine shale with sporadic marine sandstone beds and limestone concretions compose the Lewis; northwestward from sec. 8, T. 27 N., R. 89 W., more thin marine sandstone and siltstone occur in the formation. The thickness of the Lewis varies northward from 0 feet in sec. 35, T. 27 N., R. 90 W., near Bairoil, to as much as 525 feet on the northeast limb of the Camp Creek syncline.

In the area shown on figure 1 the basal contact of the Lewis Shale is marked by the change from nonmarine rocks of the Mesaverde to marine shale or thin marine sandstone of the basal part of the Lewis. Where the Mesaverde Formation is absent, the Lewis Shale unconformably overlies the Cody Shale. The contact is marked by a thin dark-gray marine shale along part of its extent, or by glauconitic and calcareous marine sandstone. The sandstone locally contains phosphate nodules and fish teeth, and in sec. 8, T. 27 N., R. 89 W. (fig. 2, stratigraphic section F) contains the ammonite *Baculites baculus*.

The contact between the marine Lewis and overlying nonmarine Lance is one of both vertical and lateral transition, characterized by thick accumulations of brackish-water and shallow-water marine deposits. The transition interval is best developed on the west and north flanks of the Lost Soldier anticline, where the entire Lewis Shale is represented by littoral sandstone, brackish-water shale, and coal that unconformably overlie the Cody Shale (fig. 2, between secs. D and E). From Bunker Hill anticline, where the transition interval is thick and overlies marine shale of the Lewis, the interval thins northwestward by gradation into nonmarine beds. Weimer and Guyton (1961, p. 142–146, figs. 4 and 5) designated the thick transitional beds between the Cody Shale and the Lance Formation as the upper member of the Mesaverde Formation and recognized that these beds are lateral equivalents of the Lewis Shale to the south. They also recognized that the absence of the Lewis in parts of the area was due to a facies change from marine shale into coal-bearing sandstone and shale of the Lance.

## RELATIONS OF LEWIS SHALE TO UNDERLYING FORMATIONS

Stratigraphic relations at the base of the Lewis Shale are critical for determining the means of thinning of the Mesaverde Formation. Through much of the area, beds of the Lewis are nearly parallel to beds of the Mesaverde or Cody, or truncate them at very low angles. On the west and southwest flanks of Bunker Hill, where the Teapot Sandstone Member is absent, the basal contact of the Lewis cuts sharply across nonmarine beds of the lower part of the Mesaverde. Individual sandstone beds in the Mesaverde, mapped on the east flank of the Camp creek syncline (fig. 2, between secs. E and F), appear to thin somewhat in a northward direction, but show no lateral facies change to marine siltstone or shale. Progressively lower sandstone beds disappear, presumably by truncation, in a strike valley cut in Lewis Shale. North of the NW¼ sec. 16, T. 27 N., R. 89 W., to sec. 28, T. 28 N., R. 90 W., the Mesaverde is absent and the Lewis Shale rests unconformably on the Cody Shale (fig. 2, stratigraphic sections F and G).

In secs. 22 and 26, T. 26 N., R. 90 W., south of Bairoil, nonmarine beds of the Mesaverde Formation clearly abut against the basal contact of the Lewis Shale as shown in figure 2, sections C and D.

The entire Mesaverde Formation is truncated by erosion centered in the Lost Soldier area and southwest of Muddy Gap on the southern flank of Sweetwater arch. No fossil soil indicative of subaerial exposure and erosion in early Lewis time is present upon truncated beds of the Mesaverde or Cody. At the section near Rawlins, and at Separation Rim, the presence of brackish-water sediments beneath the Lewis with apparent conformity suggests a gradual encroachment of the sea during the Lewis transgression. The evidence seems to indicate that the lower part of the Mesaverde and the upper part of the Cody were eroded by submarine plantation in the Lewis sea. Local uplift may have occurred prior to, and during, the advance of the Lewis sea which ultimately covered the area. Fossils characteristic of the *Baculites eliasi* zone occur near the base of the Lewis near Rawlins (fig. 2, sec. A) and in the vicinity of Seminoe Dam (W. A. Cobban, written commun., 1963), whereas the younger *B. baculus* zone occurs at the base of the Lewis at Coal Creek and northwestward (fig. 2, secs. F and G). The stratigraphic interval represented by the two ammonite zones in this area is not known, but the Lewis strata are thought to lap depositionally upon an area

which was positive and from which Mesaverde and Cody strata were removed in early Lewis time.

The truncated edge of the Mesaverde trends northeast through sec. 16, T. 26 N., R. 90 W., sec. 35, T. 27 N., R. 90 W., and sec. 16, T. 27 N., R. 89 W. Detailed subsurface studies are not as yet complete, but preliminary work indicates that in T. 27 N., R. 91 W., shallow-water marine and brackish-water deposits of the basal part of the Lance Formation lie directly on the Cody Shale; the Mesaverde is absent and the Lewis is represented by the basal transition beds of the Lance. In the Chicago Corp. Republic Natural Gas 1 Government Sultemeir well, located north of Bairoil in the SW¼SE¼ sec. 28, T. 27 N., R. 90 W., sandstone beds in the depth interval 1,730 to 2,180 feet are not Mesaverde (Weimer and Guyton, 1961, p. 144), but are beds developed in the upper part of the Cody. The same beds can be seen on the outcrop about 1 mile southeast of the well (SW¼ sec. 34, T. 27 N., R. 90 W.) and in the SE¼ sec. 35 and the S½ sec. 36, T. 27 N., R. 90 W. The overlying beds, in the interval from 1,405 to 1,730 feet, are the upper part of the Cody Shale. Transitional shallow-marine beds included in the Lance overlie the Cody Shale. The Mesaverde Formation is absent in the well.

## PALEONTOLOGIC EVIDENCE

Fossil collections support the conclusion drawn from detailed mapping, that the Mesaverde Formation is absent in parts of the Lamont-Bairoil area as a result of truncation. Stratigraphic positions of diagnostic fossil collections are shown in figure 2. At Separation Rim (fig. 2, sec. B) a collection of the ammonite *Baculites obtusus* from the Cody Shale is separated from the Lewis Shale by about 3,000 feet of strata that include 1,700 feet of nonmarine sediments of the Mesaverde. North-northwest of Lamont, near section E (fig. 2), the next older ammonite, *Baculites* sp. (weakly ribbed) (for sequence of ammonite zones see Zapp and Cobban, 1962, p. D54), is separated from fossiliferous beds of the Lewis Shale by 1,000 feet of beds that include a 350-foot-thick remnant of nonmarine Mesaverde. In the NW¼ sec. 8, T. 27 N., R. 89 W., (fig. 2, stratigraphic section F), a sandstone bed containing *Baculites baculus* overlies marine shale of the Cody. A smooth baculite, which forms the next older zone below the weakly ribbed species of baculite, was found below the Cody sandstone of Weimer and Guyton (1961, p. 139) south of the *B. baculus* locality (between secs. E and F, fig. 2). In the vicinity of Rawlins Draw (sec. G), the ammonites *B. aquilaensis* and *Scaphites aquisgranensis*, which occur in the zone of *Scaphites hippocrepis*, were found in the Cody from about 700 to 1,800 feet and at 1,100 feet, respectively, below the base of the Lewis Shale. *B. baculus* occurs in the lower part of the Lewis at this locality. Eighteen ammonite zones that normally occur between the *S. hippocrepis* and *B. baculus* zones were not found at Rawlins Draw. In addition to confirming the presence of an unconformity below which the Mesaverde Formation is absent, the fossil collections thus indicate that progressively older strata of the Cody are in contact with the Lewis Shale (fig. 2, sec. F and G).

An estimate of the thickness of Cody Shale that is absent in the Rawlins Draw area as a result of erosion can be made by comparison with nearby sections. The estimate involves two assumptions—that the rate of sedimentation during Cody time was approximately the same over the region, and that the stratigraphic interval through which fossils characteristic of the *S. hippocrepis* zone were collected at Rawlins Draw represents nearly the entire range zone of that ammonite. There the range zone occupies an interval about 700 to 1,800 feet below the top of the Cody. Fath and Moulton (1924, p. 25) measured a total thickness of 4,745 feet of Cody Shale in secs. 5 and 6, T. 26 N., R. 88 W., north of the Camp Creek syncline, and collected *S. hippocrepis* 2,650 feet below the top of the Cody. If the thickness of their section is considered as a nearly normal one, then 850 to 1,950 feet of strata have been removed from the Rawlins Draw area; the thickness of strata inferred to have been removed depends on the location of the horizon within the *S. hippocrepis* zone from which their collection was taken. Very likely their collection came from a horizon equivalent to one about 1,100 feet below the top of the Cody at Rawlins Draw; if so, about 1,550 feet of beds has been eroded. J. R. Gill and W. A. Cobban (oral commun., 1965) collected fossils of the *S. hippocrepis* zone about 2,260 feet below the top of the Cody at Ervay basin (sec. 23, T. 34 N., R. 89 W.), 36 miles north of Rawlins Draw. Comparison of the Rawlins Draw and Ervay basin data suggests that an estimated 1,160 to 1,560 feet of Cody Shale is absent at Rawlins Draw.

The original thickness of the Mesaverde Formation in the Lamont-Bairoil area is unknown but can be extrapolated from adjacent areas. West of Rawlins 2,650 feet of Mesaverde is present (Barlow, 1959, p. 112); comparison with the section at Seminoe Dam suggests that 600 feet of the lower part of the Mesaverde strata may be absent beneath the Teapot at Rawlins (J. R. Gill, oral commun., 1965). Thus a total thickness of about 3,200 feet is possible for the Mesaverde originally present in the Lamont area.

At least 4,400 feet and possibly as much as 5,200 feet of strata is absent at Rawlins Draw northwest of Lamont. As much as 2,500 feet of the missing strata may have been removed by pre-Teapot erosion. Zapp

797-218 O—66——6

and Cobban (1962, p. D52) also concluded, after comparing the Lamont and Seminoe Lake areas, that more than 4,000 feet is absent north of Lamont.

## REFERENCES


Barlow, J. A., Jr., 1959, Cretaceous section, west flank of Rawlins uplift, *in* Rocky Mountain Assoc. Geologists Guidebook 11th Ann. Field Conf., Washakie, Sand Wash, and Piceance Basins, 1959: p. 110–113.

Barwin, J. R., 1961, Stratigraphy of the Mesaverde Formation in the southern part of the Wind River Basin, Wyoming, *in* Wyoming Geol. Assoc. Guidebook 16th Ann. Field Conf., Green River, Washakie, Wind River, and Powder River Basins, 1961: p. 171–179.

Chuman, R. W., 1954, The stratigraphy of the Mesaverde Formation and Lewis Shale north of Rawlins, Wyoming: Nebraska Univ. M.S. thesis, 74 p.

Dobbin, C. E., Hoots, H. W., Dane, C. H., and Hancock, E. T., 1929, Geology of the Rock Creek oil field and adjacent areas, Carbon and Albany Counties, Wyoming: U.S. Geol. Survey Bull. 806–D, p. 131–153.

Dobbin, C. E., and Reeside, J. B., Jr., 1929, The contact of the Fox Hills and Lance Formations: U.S. Geol. Survey Prof. Paper 158–B, p. 9–25.

Fath, A. E., and Moulton, G. F., 1924, Oil and gas fields of the Lost Soldier-Ferris district, Wyoming: U.S. Geol. Survey Bull. 756, 57 p.

Guyton, J. W., 1960, Geology of the Lost Soldier area, Sweetwater, Fremont, and Carbon Counties, Wyoming: Wyoming Univ. M.A. thesis, 70 p.

Love, J. D., Weitz, J. L., and Hose, R. K., 1955, Geologic map of Wyoming: U.S. Geol. Survey.

Scott, G. R., and Cobban, W. A., 1959, So-called Hygiene Group of northeastern Colorado, *in* Rocky Mountain Assoc. Geologists Guidebook 11th Ann. Field Conf., Washakie, Sand Wash, and Piceance Basins, 1959: p. 124–131.

Weimer, R. L., 1959, Upper Cretaceous stratigraphy, Colorado, *in* Rocky Mountain Assoc. Geologists Guidebook 11th Ann. Field Conf., Washakie, Sand Wash, and Piceance Basins, 1959: p. 9–16.

——— 1961, Uppermost Cretaceous rocks in central and southern Wyoming and northwest Colorado, *in* Wyoming Geol. Assoc. Guidebook 16th Ann. Field Conf., Green River, Washakie, Wind River, and Powder River Basins, 1961: p. 17–28.

Weimer, R. L., and Guyton, J. W., 1961, Geology of the Muddy Gap-Lamont area, Wyoming, *in* Wyoming Geol. Assoc. Guidebook 16th Ann. Field Conf., Green River, Washakie, Wind River, and Powder River Basins, 1961: p. 139–147.

Zapp, A. D., and Cobban, W. A., 1962, Some Late Cretaceous strand lines in southern Wyoming: Art. 134 *in* U.S. Geol. Survey Prof. Paper 450–D, p. D52–D55.

# THE MILNOR CHANNEL, AN ICE-MARGINAL COURSE OF THE SHEYENNE RIVER, NORTH DAKOTA

By CLAUD H. BAKER, JR., Grand Forks, N. Dak.

*Work done in cooperation with the North Dakota State Water Commission*

*Abstract.*—Earlier geologists regarded the ridges of sand and gravel above the highest beach of glacial Lake Agassiz in southeastern North Dakota as evidence for a glacial lake that predated Lake Agassiz. They referred to the lake as Lake Milnor and to the ridges as the Milnor beaches. Recent studies indicate, however, that the ridges are part of a much larger deposit of sand and gravel that (1) extends from the Sheyenne River in Ransom County, N. Dak., to the vicinity of Lake Traverse in Roberts County, S. Dak., and that (2) probably was formed in an ice-marginal drainage channel instead of in a lake. It is proposed that the Milnor beaches be renamed the Milnor channel deposits.

Low discontinuous ridges of sand and gravel, lying above the highest (Herman) shoreline of glacial Lake Agassiz in Sargent County in southeastern North Dakota, were identified as beach ridges by earlier workers (Upham, 1896, p. 310; Leverett, 1932, p. 121). The ridges were thought to have formed along the shores of Lake Milnor, named after the town of Milnor, N. Dak., near which the ridges are the most prominent. Lake Milnor was believed to be a narrow ice-marginal lake, ancestral to Lake Agassiz. Colton and others (1963) mapped Lake Agassiz deposits extending to the line of the Milnor beaches, but did not show the Milnor beaches or associated deposits.

The Milnor beaches are part of a long sinuous deposit of sand and gravel in and beside a long topographic depression or channel that extends from the southernmost bend of the Sheyenne River in Ransom County, N. Dak., to the vicinity of Lake Traverse in Roberts County, S. Dak. (figs. 1 and 2). The width of the channel ranges from 1 to 3 miles. The southwest side of the channel generally is marked by a conspicuous steep slope; the northeast side is less distinct. The channel is poorly drained, and throughout much of its length the bottom is occupied by a chain of lakes and swamps.

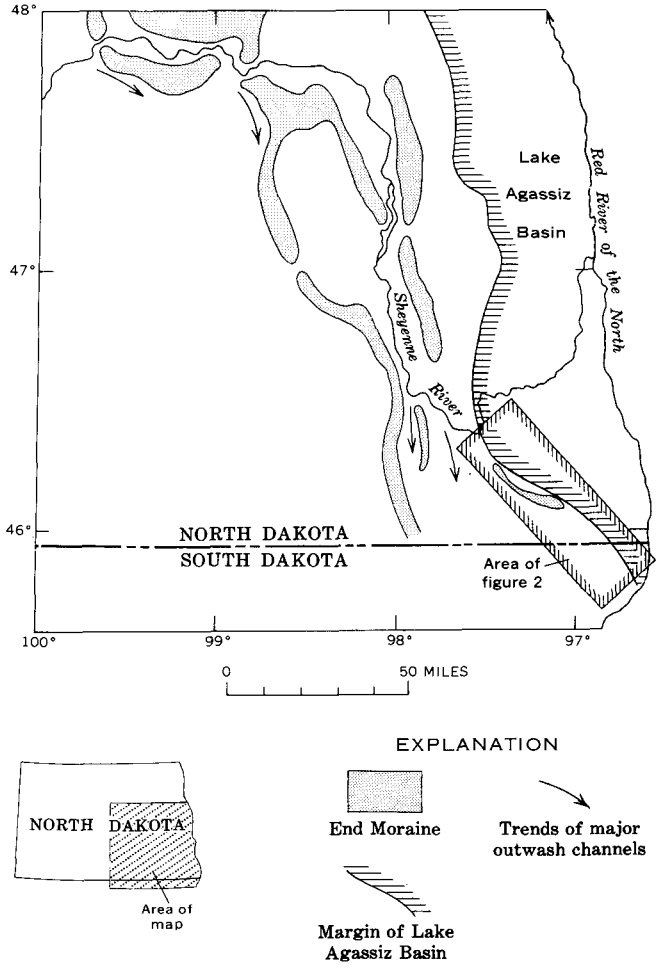


FIGURE 1.—Map of parts of North Dakota and South Dakota, showing relation of the Sheyenne River and end moraines to Lake Agassiz Basin (after Colton and others, 1963).

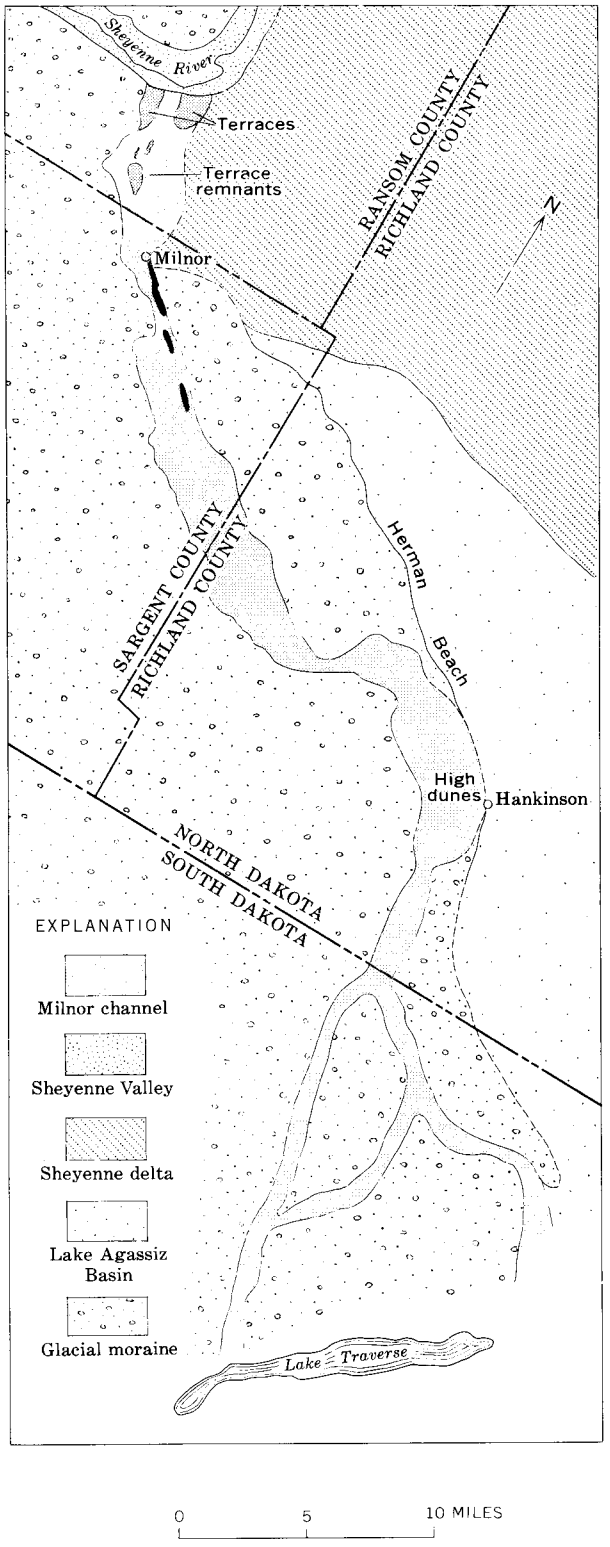


FIGURE 2.—Map of the Milnor channel. Location is shown on figure 1. Ridges shown as black areas near Milnor, formerly termed "Milnor beaches," are described as channel deposits in this report.

At its north end the channel terminates at the present Sheyenne River valley (fig. 2), and its floor stands about 40 feet above the floor of the Sheyenne Valley. At this end the channel has the form of an inner valley, about 25 feet deep and 1,000 feet wide, intrenched between terraces of sand and gravel that are about 3 miles long, that stand about 35 feet below the adjacent terrain, and that represent a former valley floor nearly 3 miles wide. Elongate hills of sand and gravel, the tops of which are about level with the terraces, extend south for another 3 miles. These hills appear to be erosional remnants of a more extensive terrace.

From the Sheyenne Valley to Milnor the channel deposits are bordered on the east by the Sheyenne delta, an extensive body of sand and gravel that was deposited in Lake Agassiz. The deltaic deposits are lithologically similar to the channel deposits, and the contact between the deltaic and channel deposits cannot be distinguished. Near Hankinson (fig. 2) the northeast edge of the channel deposits abuts against the Herman beach, which is marked by high sand dunes. In this area the course of the channel cannot be traced with certainty. Glacial till separates the channel deposits from Lake Agassiz deposits between Milnor and Lake Traverse, except in the area of high dunes near Hankinson. The southwest side of the channel is bordered by glacial till throughout its length.

The Milnor beaches are discontinuous low elongate ridges of sand and gravel. Although the ridges are most prominent near Milnor they are also present farther south. The ridges are on the channel floor, near the edges of the channel, most commonly on the northeast side. The steep slope on the southwest side of the channel also has been mapped as "Milnor beach" (Leverett, 1932, fig. 17).

The character of the Milnor beaches themselves and of the extensive deposits associated with them suggests a fluvial rather than a lacustrine origin, and the terms "Milnor beaches" and "Lake Milnor" therefore seem to be misnomers. Evidence cited in the following paragraphs suggests that the deposits probably were formed in an ice-marginal drainage channel. The evidence includes the general shape and areal relations of the deposits, the grain size of the sediments, and the existence of terraces and terrace remnants north of Milnor. Also, the presence of till deposits (largely ground moraine) on the northeast side of the channel, separating the channel from the basin of former Lake Agassiz, is more consistent with a fluvial origin of the channel than with a lacustrine origin.

The long sinuous form of the sand and gravel deposits is more suggestive of a stream channel than of a lakebed.

The deposits not only extend from the valley of the Sheyenne River to a well-defined valley at Lake Traverse, but they generally occupy a topographic depression.

The sediments making up both the "beach" ridges and the associated deposits are relatively coarse grained. The ridges themselves, as well as the terraces and terrace remnants north of Milnor, are composed largely of fine to medium gravel, and nearly all the associated deposits in the channel floor are coarser than medium sand. Moreover, there is no silt or clay in the channel. Lake sediments are characteristically fine grained, and lake floors generally are marked by deposits of silt and clay. Futhermore, gravel beaches are generally indicative of strong wave action, and large waves are not common to narrow lakes. The features termed beach ridges could have been formed in a stream channel where tributary streams entered the channel directly from the ice. Sediment delivered to a stream in this way might well be sorted by the main current, and the coarser fraction deposited as a bar near the mouth of each tributary. (The steep slope on the southwest side of the channel is attributed to current erosion, irrespective of the origin of the ridges themselves.) The terraces and terrace remnants north of Milnor have no parallel in lacustrine deposits. In composition and general form they resemble stream terraces and, therefore, suggest a fluvial environment.

The areas of glacial till that separate the channel deposits from the Herman beach of Lake Agassiz have considerable relief and show no evidence of ever having been covered by the water of Lake Agassiz. The presence of this till suggests that the Milnor beaches could not have been formed in a body of water that was an early stage of Lake Agassiz, for the growing lake should have inundated the till and smoothed it off. The presence of this unaltered till favors the hypothesis that the deposits were formed in an ice-marginal channel prior to the origin of Lake Agassiz, and that Lake Agassiz never had a higher stage than that marked by the Herman beach.

The regional slope of the land surface is to the northeast, and the Sheyenne River, which heads in east-central North Dakota, flows eastward through two major end moraines before it veers southward along the west side of a third moraine (fig. 1). The river breaches this third moraine northwest of Milnor and flows southeastward to the northwest end of the channel associated with the Milnor beaches. There it bends north, and from this bend its course is generally northeastward, down the regional slope, to its junction with the Red River of the North.

Each major end moraine intersected by the Sheyenne River is bordered along its outer (southwestern) edge by an outwash channel (Colton and others, 1963). Although most of these channels no longer contain perennial streams, some of them in Eddy, Barnes, and Ransom Counties appear to be former ice-marginal courses of the river. Apparently the Sheyenne River was an ice-marginal stream for much of its history during the glaciation. The deposit of sand and gravel near Milnor, with the channel, ridges, and terraces, is believed to be an ice-marginal channel fill that marks a pre-Lake Agassiz course of the Sheyenne River. The general shape of the entire deposit, its location with respect to the Sheyenne River, the coarseness of the sediments, the existence of terraces and terrace remnants near its north end, and the presence of glacial till on its northeast side all lend support to this interpretation. Accordingly, it is proposed that the names "Lake Milnor" and "Milnor beaches" be replaced by the terms Milnor channel and Milnor channel deposits.

## REFERENCES

Colton, R. B., Lemke, R. W., and Lindvall, R. M., 1963, Preliminary glacial map of North Dakota: U.S. Geol. Survey Misc. Geol. Inv. Map I-331.

Leverett, Frank, 1932, Quaternary geology of Minnesota and parts of adjacent states: U.S. Geol. Survey Prof. Paper 161, 149 p.

Upham, Warren, 1896, The glacial Lake Agassiz: U.S. Geol. Survey Mon. 25, 658 p.

# STRUCTURAL CONTROL OF WIND GAPS AND WATER GAPS AND OF STREAM CAPTURE IN THE STROUDSBURG AREA, PENNSYLVANIA AND NEW JERSEY

By JACK B. EPSTEIN, Beltsville, Md.

*Abstract.*—Wind gaps and water gaps in the Stroudsburg area, in eastern Pennsylvania and northern New Jersey, are located where resistant rocks dip steeply and have a narrow width of outcrop, where folds die out over short distances, or where folding was more intense locally than nearby. All gaps trend about perpendicular to the strike of the ridges, and parallel to major cross-joint sets. These observations favor the hypothesis of structural control of the location of stream gaps, rather than that of regional superposition of the streams upon the resistant rocks. A second type of structural control, in which more resistant beds were exposed in Wind Gap than in Delaware Water Gap, may explain the capture of Wind Gap River by tributaries of the Delaware River.

## WIND GAPS AND WATER GAPS

Numerous and extensive investigations of wind and water gaps in the Appalachians have contributed to the controversies regarding Appalachian geomorphic evolution. Many geologists believe that after the Appalachian orogeny the drainage divide between streams that flowed southeastward into the Atlantic and those that flowed toward the continental interior was located either in the crystalline highlands southeast of the present Great Valley or in the Valley and Ridge province. The divide has since shifted westward to its present position in the Appalachian Plateau. The location of the original divide, the means by which the divide migrated, and the process or processes by which the numerous wind and water gaps were formed are problems that need to be considered in any hypothesis which attempts to explain the drainage development of the Appalachians.

Johnson (1931) believed that the original drainage lines were obliterated during a Cretaceous marine transgression and that the present drainage pattern is mainly the result of superposition from a coastal-plain cover. The location of a gap was purely by chance and is not systematically related to any weakness in the ridge, although there may have been local adjustment to structure.

Meyerhoff and Olmstead (1936) believed that the present drainage descended from the pattern which had been established in Permian time and which had been controlled by structure and topography produced during the Appalachian orogeny. Hence gaps are found along transverse structures or in the northwest limbs of overturned folds.

Thompson (1949) argued that the original divide, which lay on crystalline rocks along the Blue Ridge-Reading Prong axis, was unstable because the southeastward-flowing streams had shorter courses than those that flowed northwestward. As a result, the divide shifted northwestward by normal stream erosion (headward piracy), and the gaps in Kittatinny and Blue Mountains are located at points of rock weakness.

Strahler (1945), who favored Johnson's hypothesis, stressed that the main test substantiating superposition was to show lack of coincidence of gaps and sites of structural weakness (specifically, transverse faults).

Structural characteristics and features other than transverse faults, however, may influence the resistance to erosion of hard-rock ridges. These include, among others: (1) changes in outcrop width, owing to changes of dip; (2) abrupt changes in strike, owing to dying out of folds; (3) local weakness of otherwise resistant rocks as a result of the overturning of beds and accompanying shearing; (4) closely spaced joints and strong folding resulting from intense local stress; (5) cross folds and attendant fracturing; (6) thinning of resistant units, which reflects the original processes of sedimentation; (7) thinning or elimination of resistant strata by strike faulting; and (8) change in facies.

Detailed structural data from gaps in the Stroudsburg area, presented by previous investigators, generally have been scanty. Detailed mapping of Blue and Kittatinny Mountains and of ridges to the north has shown that there is a correlation of gaps with one or more of the following conditions: (1) steep dips of beds and narrow outcrop widths of resistant units,

U.S. GEOL. SURVEY PROF. PAPER 550-B, PAGES B80-B86

(2) dying out of folds within short distances, and (3) more intense folding locally than nearby. The parallelism of the gaps is controlled by prominent southeast-trending cross-joint sets present throughout the area. A plot of nearly four hundred joints shows a strong maximum with a strike of N. 14° W. and a dip about vertical.

### Gaps in Blue and Kittatinny Mountains

Blue and Kittatinny Mountains, parts of a single ridge supported by the Shawangunk Conglomerate, are cut by several gaps: Delaware Water Gap, Totts Gap, Fox Gap, and Wind Gap. Figure 1 shows the locations of the gaps and other major physiographic features. Figure 2 shows the distribution of geologic formations and the structural geology of the area, and demonstrates the correlation of gap location with the three structural conditions mentioned above.

*Delaware Water Gap.*—Many early observers of Delaware Water Gap believed that it was the result of a violent cataclysm. Interesting excerpts of these early discussions are reported by Miller and others (1939, p. 139–142). Rogers (1858, v. 1, p. 283, v. 2, p. 896) noted that the ridge crest is offset 700 feet at the gap. He attributed the displacement to a transverse fault, as did Ashley (1935, p. 1406) and Willard (1938, p. 23). Chance (1882, p. 338), Johnson and others (1933, p. 26), Miller and others (1939, p. 144), and Strahler (1945, p. 58–59) believed that the ridge is offset by a slight flexure. Thompson (1949, p. 56, 59) found many small faults which he suggested might be offshoots of a major transverse fault, and attempted to show that the gap is structurally controlled.

During the present study no cross fault could be found at Delaware Water Gap. The Shawangunk Conglomerate consists of three units that match at river level and have contacts that are not displaced (fig. 3). The bedding dips 35° to 45° to the northwest on both sides of the stream at the bottom of the gap. At the top of the ridge on the New Jersey side, at Mt. Tammany, the dip is about 50°, whereas on the Pennsylvania side the dip decreases upward toward Mt. Minsi, being less than 25° at a place halfway up the mountain. Clearly, there is a small flexure at the gap; the beds on the New Jersey side dip more steeply than those in Pennsylvania, and the ridge crest in New Jersey lies about 700 feet northwest of the axis of the crest on the Pennsylvania side. The flexure can be seen by looking west from the New Jersey bank. Consideration of the structural geometry (fig. 4) reveals that there was an abrupt change in strike of the beds that formerly occupied the site of the gap. As a consequence the brittle Shawangunk must have been weakened by extensive fracturing in the flexure zone. Structural control is therefore thought to have determined location of the gap.

A series of folds in the Bloomsburg Redbeds along the course of Delaware River north of the gap dies out to the southwest, within a short distance (fig. 2). Probably the rocks are more highly sheared here, and resistance to erosion is less, than in the areas between gaps where similar folds were not observed.

Perhaps equally important in controlling the location of Delaware Water Gap is the fact that the outcrop width of the Shawangunk Conglomerate is narrower at the gap site than to the northeast where the formation

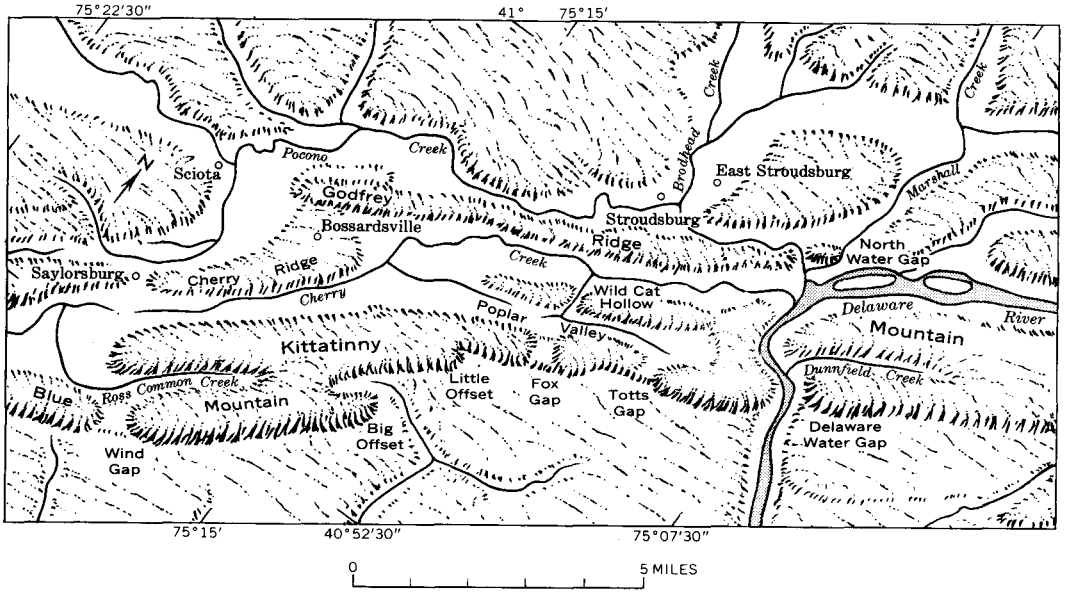


FIGURE 1.—Physiographic diagram of the Stroudsburg area, Pennsylvania and New Jersey.

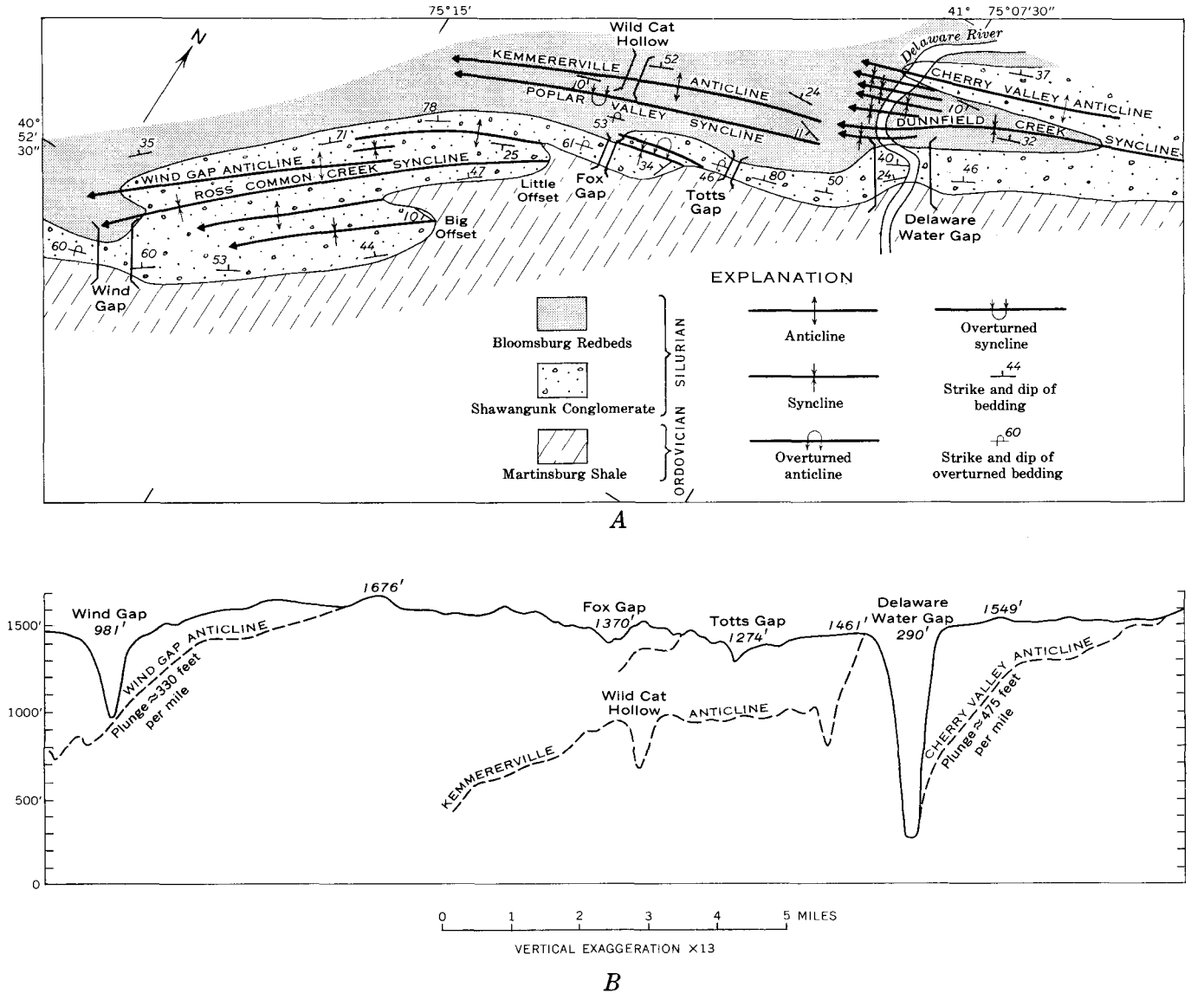


FIGURE 2.—*A*, Geologic map of the Stroudsburg area, Pennsylvania and New Jersey. *B*, projected longitudinal topographic profile, showing relation of geologic structure to location of gaps in Blue and Kittatinny Mountains (fig. 1). Profile viewed from the southeast. Dashed lines indicate topography behind main ridge and correspond approximately to crests of major anticlines. Several small folds north of Wind Gap, similar to those in Delaware Water Gap, are not shown; their extent is not well known because outcrops are poor. Topography from Wind Gap quadrangle, Pennsylvania–New Jersey (15 min.), and Portland quadrangle, New Jersey (7½ min.).

is repeated in the southwest-plunging Cherry Valley anticline. The river now flows on the Shawangunk where it crosses the anticline, but undoubtedly it flowed on the weaker Bloomsburg Redbeds earlier in its history before cutting down into the Shawangunk. This is an example of local superposition.

*Totts Gap.*—The beds at Totts Gap are more strongly overturned than elsewhere along the ridge crest in the area of study, and it seems likely that the rocks here were weakened more than in adjacent areas. Moreover, the Shawangunk Conglomerate has a narrow outcrop width at Totts Gap. Thompson (1949, p. 58) observed that between Totts Gap and Delaware Water Gap the ridge crest is lower where joints are more closely spaced than elsewhere, and that at Totts Gap, the lowest point along this stretch, the joints are most closely spaced. Whether this reflects greater stress, or whether it is due to chance exposure of different beds in the Shawangunk that possess different structural characteristics, is difficult to determine.

*Fox Gap.*—Fox Gap is located where two southwest-plunging folds die out over a short distance, much as they do at Delaware Water Gap. Also, the beds are strongly overturned, and the outcrop width is narrow.


FIGURE 3.—Aerial photograph and geologic map of Delaware Water Gap. The Bloomsburg Redbeds, Sb, of Silurian age are underlain by three members of the Shawangunk Conglomerate: Ssu, upper conglomerate and quartzite member; Ssm, middle black argillite, quartzite, and conglomerate member; and Ssl, lower quartzite and conglomerate member. The Martinsburg Shale, Om, of Ordovician age underlies the Shawangunk.

*Wind Gap.*—Geologic Structures in Wind Gap duplicate those in the Delaware Water Gap area. Two major folds plunge out north of the gap. The Shawangunk Conglomerate is not repeated to the northwest because the Wind Gap anticline plunges to the southwest. There is a 15° difference in strike in beds in the ridge crest on either side of the gap, indicative of a flexure similar to that at Delaware Water Gap. In addition, several small folds in the Bloomsburg Redbeds are similar to those in the Bloomsburg at Delaware Water Gap. These folds were not included in figure 2*A* because outcrops are too few to permit tracing of their trends. Thinning of the outcrop width of the Shawangunk at the gap is evident on figure 2*A*. This is indicative of near-vertical dips which can be seen in cuts along the highway where it passes through the gap.

### Gaps in Godfrey Ridge

Godfrey Ridge lies about 2½ miles north of Kittatinny Mountain and is supported by complexly folded Upper Silurian and Lower Devonian limestone, shale, sandstone, and conglomerate. Silty shale and sandstone of the Esopus Shale and Oriskany Formation support the higher parts of the ridge (fig. 5). Small folds are numerous and die out rapidly. Sags in the ridge crest are numerous, but it is difficult to relate structural features to them. The two largest gaps in Godfrey Ridge, the gap of Brodhead Creek and North Water Gap, are located about 2½ miles north-northwest of Delaware Water Gap.

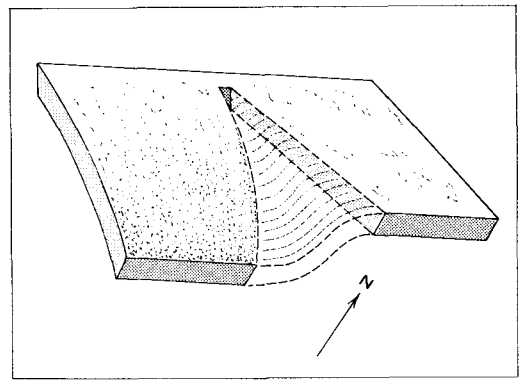

FIGURE 4.—Diagram showing reconstructed flexure at Delaware Water Gap. Dashed lines show form of bed before gap was cut. Presence of the flexure accounts for the topographic offset of the ridge and suggests extensive fracturing of the Shawangunk Conglomerate at the gap site in the flexure zone.

*Gap of Brodhead Creek.*—Brodhead Creek cuts through Godfrey Ridge at an altitude of about 300 feet. No rock crops out in the creek bottom, but bedrock is exposed in the creek bed about 1 mile upstream. Therefore, bedrock cannot be far below creek level in the gap. Folding at the gap is so complex that Willard (1938, p. 23) believed that the gap is the site of a north-south tear fault. Evidence of faulting could not be found, however. Rather, there are four overturned folds in the southwestern part of the ridge near Brod-

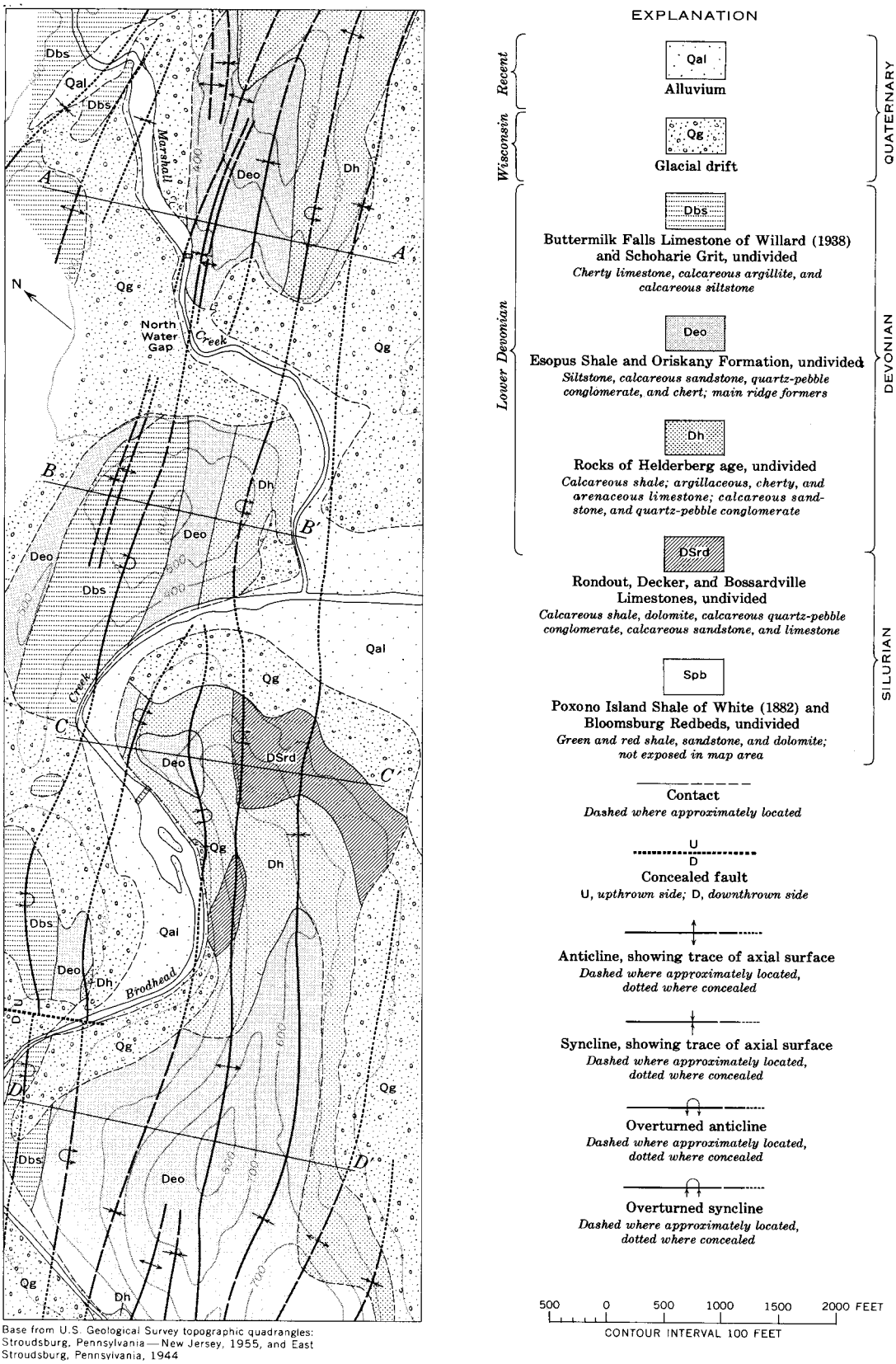


Base from U.S. Geological Survey topographic quadrangles: Stroudsburg, Pennsylvania—New Jersey, 1955, and East Stroudsburg, Pennsylvania, 1944

FIGURE 5.—Geologic map and sections of the area near North Water Gap and the gap of Brodhead Creek. Geology by J. B. Epstein, assisted by A. G. Epstein, 1962–63.

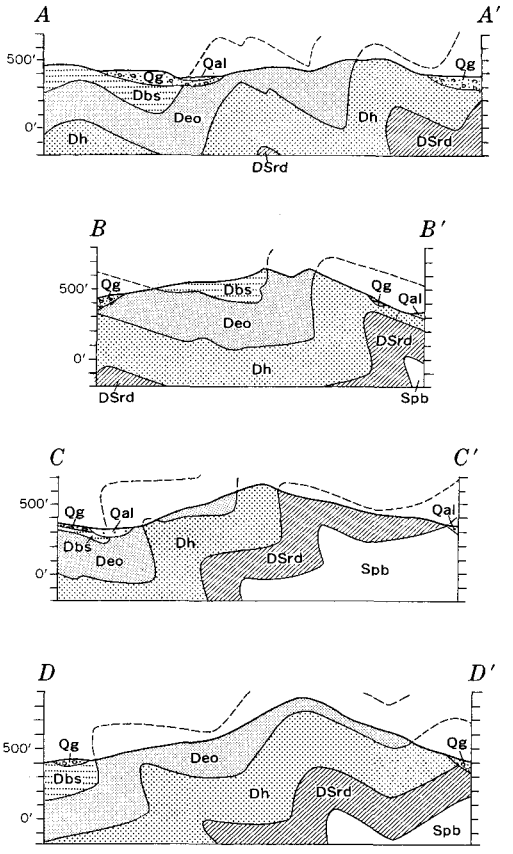


LINES OF SECTIONS ARE SHOWN ON FACING PAGE

head Creek, two of which die out and are absent in the northeastern part. The abrupt dying out of folds is well illustrated by sections *B–B′* and *C–C′* in figure 5. Change in strike of the beds that formerly occupied the site of the gap is inferred, as it is at Delaware Water Gap.

*North Water Gap.*—North Water Gap is located where Marshall Creek cuts through Godfrey Ridge, about half a mile northeast of the gap of Brodhead Creek. It is almost as deep as the latter, but no bedrock is exposed in the creek floor. Glacial debris which may be of great thickness [1] is found along the course of the creek in the gap. Clearly, North Water Gap was much deeper in preglacial times.

The structure at North Water Gap is similar to the structure at the gap of Brodhead Creek. Two folds trending toward the gap from the northeast die out within the valley and do not reappear in the ridge to the southwest (compare sections *A–A′* and *B–B′* in fig. 5). The two gaps are therefore located at sites where folds plunge out abruptly, and implication of structural control is clear. Moreover, because of near-vertical dips, the Oriskany and Esopus, which together make up the main ridge support, have a narrow outcrop width.

[1] Bedrock was penetrated at a depth of 296 feet in a water well near the west bank of the Delaware River at an altitude of about 300 feet and approximately 2,000 feet southeast of the mouth of the gap, as reported by a local resident.

## STREAM CAPTURE

Structural relations in the Stroudsburg area are believed to have controlled not only the locations but also the history of the gaps. For example, Wind Gap was cut by a stream that was later captured north of Blue Mountain by tributaries of either the Lehigh River to the west or of the Delaware River to the east (Wright, 1896; Ver Steeg, 1930; Willard, 1939; Mackin, 1941). Mackin showed that the drainage changes in the Wind Gap area were exceedingly complex and implied that evidence of the original captor of the Wind Gap River may be gone. Nevertheless it seems likely on the basis of structural considerations that the tributaries of the Delaware were more agressive than those of the Lehigh, and that one captured the headwaters of Wind Gap River. Why was Wind Gap River, rather than the Delaware River tributary, beheaded? Mackin speculated that the present Delaware may have captured a stream which flowed through Culvers Gap in Kittatinny Mountain, 23 miles to the northeast, and greatly increased its own advantage at that time by this addition to its volume. Study of figure 2*B* suggests an alternative explanation.

The Wind Gap River was captured just after it had cut down to an altitude of about 980 feet, the present altitude of the floor of the gap. At that level the stream had reached the resistant Shawangunk Conglomerate in the Wind Gap anticline at about 980 feet, just northwest of the present gap, and its downcutting was retarded. The Delaware River, if it was at a similar altitude at that time, as seems likely, was still cutting down through weaker Bloomsburg Redbeds in the Cherry Valley anticline where the top of the Shawangunk is several hundred feet lower. The lower altitude of the top of the Shawangunk at Delaware Water Gap is explained by the difference in plunge of the folds: the Cherry Valley anticline plunges about 475 feet per mile while the Wind Gap anticline plunges about 330 feet per mile. Later, after the Delaware had captured the headwaters of Wind Gap River and cut through the Bloomsburg, it was superimposed on the Shawangunk in the Cherry Valley anticline and slipped down the plunge of the fold in a curving course. The curve was accentuated when it migrated downstream and reached the steeply dipping Shawangunk quartzites and conglomerates just west of the gap.

## SUMMARY

Each of six major gaps in the Stroudsburg area is located in an area possessing some combination of the following structural features: (1) dying out of folds over a short distance, and associated abrupt changes in strike of bedding; (2) steep dip and narrow width of outcrop of resistant strata; and (3) folding that was more intense locally than in the surrounding rocks. None of these structural features is present along the ridges where there are no gaps. The presence of the gaps in the Stroudsburg area, at places where structural control seemingly was effective, does not favor the concept of regional superposition. Rather, it favors those hypotheses which maintain that gaps are located in zones of structural weakness where erosion was most effective during the course of stream competition along the ancestral drainage divide. Comparison of the structural settings of Wind Gap and Delaware Water Gap suggests that differences in the underlying rocks are an important factor in the development of gaps. The presence of resistant beds at a markedly higher altitude at Wind Gap favored the abandoning of Wind Gap as a result of stream piracy. At Delaware Water Gap, on the other hand, the resistant beds are several hundred feet lower. The Delaware River continued cutting down through the overlying softer rocks after Wind Gap had been abandoned by its stream.


## REFERENCES


Ashley, G. H., 1935, Studies in Appalachian Mountain sculpture: Geol. Soc. America Bull., v. 46, p. 1395–1436.

Chance, H. M., 1882, Special survey of the Delaware Water Gap, *in* White, I. C., The Geology of Pike and Monroe Counties: Pennsylvania Geol. Survey, 2d ser., Rept. G6, 407 p.

Johnson, D. W., 1931, Stream sculpture on the Atlantic slope, a study in the evolution of Appalachian rivers: New York, Columbia Univ. Press, 142 p.

Johnson, D. W., Bascom, Florence, and Sharp, H. S., 1933, Geomorphology of the central Appalachians: Internat. Geol. Cong., 16th, United States, 1932, Guidebook 7, Excursion A–7, 50 p.

Mackin, J. H., 1941, Drainage changes near Wind Gap, Pennsylvania—a study in map interpretation: Jour. Geomorphology, v. 4, p. 24–52.

Meyerhoff, H. A., and Olmstead, E. W., 1936, The origins of Appalachian drainage: Am. Jour. Sci., 5th ser., v. 32, p. 21–42.

Miller, B. L., Fraser, D. M., and Miller, R. L., 1939, Northampton County, Pennsylvania, geology and geography: Pennsylvania Geol. Survey, 4th ser., Bull. C48, 496 p.

Rogers, H. D., 1858, The geology of Pennsylvania, a government survey: Philadelphia, v. 1, 586 p.; v. 2, 1045 p.

Strahler, A. N., 1945, Hypothesis of stream development in the folded Appalachians of Pennsylvania: Geol. Soc. America Bull., v. 56, p. 45–88.

Thompson, H. D., 1949, Drainage evolution in the Appalachians of Pennsylvania: New York Acad. Sci. Annals, v. 52, art. 2, p. 31–62.

Ver Steeg, Karl, 1930, Wind gaps and water gaps of the northern Appalachians: New York Acad. Sci. Annals, v. 32,p. 87–220.

White, I. C., 1882, The geology of Pike and Monroe Counties: Pennsylvania Geol. Survey (2d), Rept. G6, 407 p.

Willard, Bradford, 1938, A Paleozoic section at Delaware Water Gap: Pennsylvania Geol. Survey, 4th ser., Bull. G11, 35 p.

——— 1939, Stratigraphy and structure of the Kittatinny (Blue) Mountain gaps, *in* Miller, B. L., Fraser, D. M., and Miller, R. L., Northampton County, Pennsylvania, geology and geography: Pennsylvania Geol. Survey, 4th ser., Bull. C48, p. 145–158.

Wright, F. B., 1896, The origin of the Wind Gap: Am. Geologist, v. 18, p. 120–123.

# SANDBLASTED BLOCKS ON A HILL IN THE COASTAL PLAIN OF NEW JERSEY

By JAMES P. MINARD, Washington, D.C.

*Abstract.*—Sandblasted blocks from an indurated layer in the Beacon Hill Gravel are present on a hill in the north-central part of the Atlantic Coastal Plain in New Jersey. The blocks have pitted ends and fluted, faceted, and polished surfaces, thought to have been cut during the Wisconsin Glaciation when strong winds from a continental ice sheet blew over a sandy surface devoid of vegetation. The climate probably was similar to that now prevailing in northern Greenland.

Wind-faceted, fluted, and polished blocks as much as 9 feet long are present near the top of one of the highest hills in the Coastal Plain province in New Jersey. Ventifacts are present in New Jersey in much of the Coastal Plain province and in parts of the Piedmont province, but most of them range in size from pebbles to small boulders. These small ventifacts are largely on sandy lowlands and, where numerous, are in association with sand dunes such as those just west of Hammonton (Minard and others, 1955, p. 13), about 45 miles southwest of the Roosevelt quadrangle (fig. 1). The sandblasted blocks described in this paper are different in that they are large, occur near a hilltop, are more fluted and grooved, are not associated with ancient or modern sand dunes, and are not erratics but were derived locally from an indurated layer in the Beacon Hill Gravel of Pliocene(?) age which caps the highest hills in the area. The blocks probably were sandblasted during the Wisconsin Glaciation when the environment was characterized by a cold climate, little or no vegetation, strong winds, and available sand. During Wisconsin time the ice advanced farther south in this region than during any other glaciation, and the ice front was only about 20 miles north of the hill on which the blocks are present.

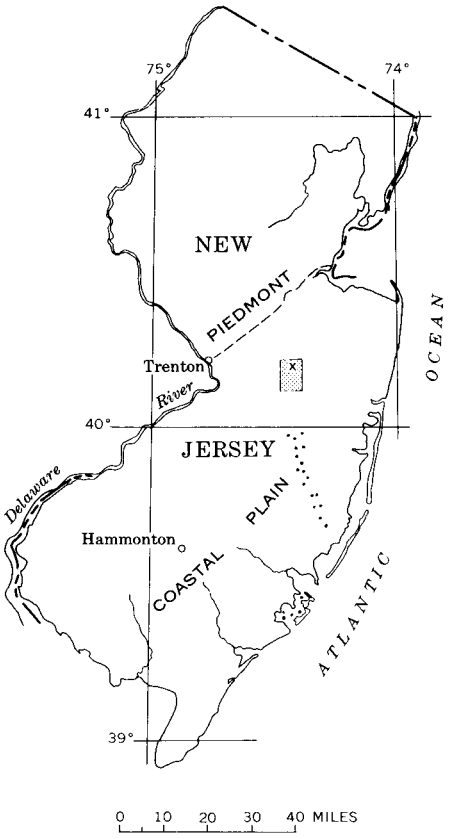


FIGURE 1.—Index map showing location of the Roosevelt quadrangle (shaded), the hill (×) on which the wind-eroded boulders are present, and other features and places mentioned in the text. Curved band of dots south of the Roosevelt quadrangle represents hills capped by the Beacon Hill Gravel.

## BEACON HILL GRAVEL

The Beacon Hill Gravel consists mostly of dusky-yellow and very light-gray,[1] siliceous, medium- to coarse-grained sand and gravel, but locally it is firmly cemented by iron oxide into hard layers (fig. 2) and is moderate brown. The pebbles, which are as much as 3 inches across, and granules are composed of chert, quartz, sandstone, and quartzite. The sand is mostly quartz but contains considerable chert. Detrital heavy minerals are mostly zircon and dark opaque minerals,

[1] Colors used are taken from E. N. Goddard and others (1948).

FIGURE 2.—Pit in which the wind-eroded blocks are present. The entire exposure is Beacon Hill Gravel. Sand and gravel cemented by iron oxide form the dark indurated layer, which is 3 to 4 feet thick. The sandblasted blocks were derived from this layer or a similar one.

particularly ilmenite and related minerals. The formation is characterized by crudely to well stratified horizontal beds of sand and gravel and by some cross-stratified sand. In the Roosevelt quadrangle it caps the highest hills, which form a discontinuous, curved, linear pattern that trends south and southwest as shown on the geologic map of the quadrangle (Minard, 1964). South of the Roosevelt quadrangle the gravel caps another linear series of hills trending south to southeast (fig. 1). These hilltop deposits, which are at progressively lower elevations toward the south, appear to be continuations of the deposits in the Roosevelt quadrangle.

The base of the formation ranges in altitude from about 340 feet in the northern part of the Roosevelt quadrangle (in the pit where the blocks are present) to about 310 feet in the west-central part. The basal contact is irregular and locally channel shaped, and the basal 1 foot of material contains coarser gravel than that in the overlying part. All the characteristics of the gravel suggest that it now consists of erosional remnants of deposits of a stream which formerly flowed southward. Because of both the indurated layers and the porosity of the gravel and sand, the Beacon Hill is more resistant to erosion than the underlying formations, which are quartz sand of Miocene age beneath the steep upper slopes and quartz and glauconite sands of Cretaceous and Tertiary age beneath the gentle lower slopes (Minard, 1964). As the surrounding land surface was lowered the Beacon Hill remained to cap the hills.

A maximum age of Pliocene is indicated for the Beacon Hill Gravel by the stratigraphic position of the deposit on the Cohansey Sand, which is of Miocene(?) and Pliocene(?) age and overlies the Kirkwood Formation of middle Miocene age. Hollick (*in* Ries and others, 1904, p. 138–139) correlated flora in the Cohansey with certain European upper Miocene flora which he believed to be comparable to Pliocene flora of America. Therefore, if the Cohansey is upper Miocene or Pliocene in age, the Beacon Hill, which unconformably overlies the Cohansey, probably is at least as young as Pliocene. The present hilltop position of the Beacon Hill and the presence of adjacent broad, deep valleys, particularly to the northwest, indicate extensive erosion and reduction of the land surface since deposition of the gravel. The time required for such erosion, plus the presence in the valleys of fluvial deposits of at least two glacial or interglacial stages, suggests that the Beacon Hill Gravel is not younger than early Pleistocene.

## LOCATION AND DESCRIPTION OF THE BLOCKS

The blocks were found in a large excavation in the Beacon Hill Gravel near the top of a hill 1½ miles east-northeast of Perrineville, N.J., in the northern part of the Roosevelt 7½-minute quadrangle (fig. 1). The highest part of the hill, which is the northernmost of several summits of nearly equal altitude, is more than 360 feet above sea level and has a relief of more than 200 feet in a distance of ¾ mile. The blocks were found only on this hill, although the Beacon Hill Gravel also caps several of the nearby hills.

The floor of the excavation is strewn by many large blocks of iron-oxide-cemented gravel, some as much as 9 feet long. Some of the blocks have faceted and fluted surfaces (fig. 3), whereas others are merely burnished. Sharp hairline ridges form the intersections of wind-faceted and polished surfaces (fig. 4). The surface features of the blocks are strikingly similar to those reported from other regions, such as those by Segerstrom (1962, fig. 93.2, p. C92), Thornbury (1954, fig. 12.2, p. 300), and Denny (1941, p. 257), and to surface features I saw in the Western Desert of Egypt in 1961. Pebbles of quartz and chert have been scoured part way through, and their surfaces are flush with the softer matrix. Grooves and flutes in the sides and upper surfaces of the blocks are typically ½ to 1½ inches wide and deep, and pits in the ends reach similar depths. The pits are mostly the result of the impact of particles driven perpendicularly against the ends of the blocks. Near the edges of the ends of the blocks, the pits grade into the grooves which tend to become shallow farther along the sides of the blocks, probably

FIGURE 3.—Wind-eroded block whose surface has been extensively grooved and fluted by wind-blown sand. The block measures about 3 × 4 × 9 feet. The grooves tend to radiate from the windward (right) end.

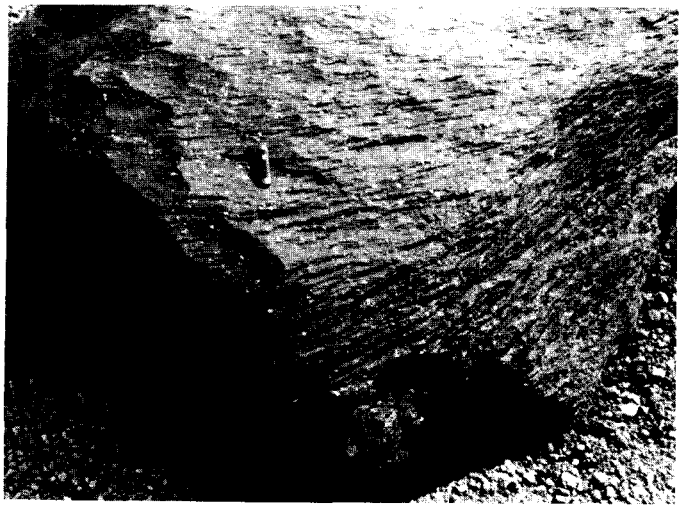

FIGURE 4.—Near end of the block shown in figure 3. In addition to flutes and grooves, faceted and polished surfaces separated by sharp ridges are evident.

because of a decrease in the abrading force of the grains due to an oblique angle of impact.

Mather and others (1942, p. 1168–1169), during studies of Pleistocene geology of western Cape Cod, concluded that conspicuous development of grooves in wind-eroded boulders reflects the coarse texture of the rock but is independent of rock structure. Study of the sandblasted blocks in New Jersey suggests, however, that grooving was in part dependent on rock structure, being facilitated where the direction of sandblasting was somewhat parallel to weaker lines in the blocks (that is, to crude alinements of softer chert pebbles and to softer matrix between pebble layers). The ridges are commonly along zones of quartz pebbles in the rock, whereas most of the grooves have been carved along crude alinements of softer chert pebbles and matrix. The pits in the ends of the blocks are largely in the matrix, and the pinnacles are held up by pebbles (as noted by Sharp, 1949, p. 178), some of which, particularly the chert pebbles, are etched.

The sandblasted blocks are unusual in several ways. Other ventifacts in the coastal plain region of New Jersey are small and were transported to or near their present location prior to being shaped by the wind. The blocks in the Roosevelt quadrangle are large, may have been partly sandblasted while still in place as part of the indurated layer, and are presently located within a few feet of their original position. There are other indurated layers in other coastal-plain formations but of the few seen, none seemed to have been exposed or in a position favorable to being sandblasted during Pleistocene time.

## ORIGIN OF BLOCKS AND AGE OF SANDBLASTING

The lack of evidence of wind erosion on the surfaces of the indurated layer that have been exposed by recent pit operations (fig. 2) suggests that the present exposures of the layer were covered at the time that sandblasting occurred. Moreover, none of the sandblasted blocks was found in its natural position; all appear to have been bulldozed aside and left on the floor of the pit (which is 10 to 15 feet below the parent ledge) as sand and gravel were removed around them. Some blocks around the edge of the pit appear to rest in lag positions on the original hill slope. The blocks probably were wind eroded either while resting on a flat or sloping surface as lag material, or while still an integral but exposed part of the ledge, or both.

The climate of the region during the existence of this former surface must have been very different from that of the present, for no such erosive processes are taking place today in the area. The hills are now covered by vegetation, and there is no modern aeolian erosion or deposition. The latest time when such conditions existed probably was during the last Pleistocene glaciation when vegetation was sparse because of intense cold, and strong winds blew from the nearby continental ice mass. The fact that it was cold is shown by involutions which I have seen in near-surface materials at many places in New Jersey, both to the west and south of the Roosevelt quadrangle; these involutions are evidence of the former presence of perennially frozen ground. Similar features were reported from New Jersey by Wolfe (1953, plates 2A

and 3A). The presence of the terminal moraine of the Wisconsin Glaciation a short distance to the north also indicates a former cold climate. The lack of vegetation at that time is suggested by the existence of ancient stabilized sand dunes in many areas on the coastal plain in New Jersey, particularly on the outcrops of the Cohansey Sand. Hack (1955, p. 17–21) describes sand dunes in the Brandywine area of Maryland and postulates that the sand was deposited when the climate differed from that of today—possibly during the Pleistocene when vegetation was sparse. Mather and others (1942, p. 1173) favor a cold semiarid climate during late Wisconsin time for the formation of ventifacts on Cape Cod.

Wind erosion in such cold places as Antarctica and northern Greenland is presently very effective. William E. Davies, U.S. Geological Survey (oral commun., 1965), reports an abundance of sandblasted boulders on the sand and gravel plains in front of the ice in northern Greenland. These boulders were eroded by sand-laden winds, of a fairly constant direction, blowing off the icecap. Because of the frost features, the stabilized sand dunes, and the proximity of the Wisconsin terminal moraine, the climate on the coastal plain of New Jersey during the latest Pleistocene glaciation is thought to have been similar to that of northern Greenland today. If so, conditions conducive to wind erosion of an intensity sufficient to sandblast the blocks would have been present.

## SUMMARY AND CONCLUSIONS

Sandblasted blocks on the coastal plain in New Jersey are evidence of the former occurrence of climatic conditions under which winds transported sand and silt with sufficient force to flute, facet, and polish exposed rock. The blocks probably were eroded during the Wisconsin glacial age when the climate was cold, the landscape was partly or largely bare of vegetation, and the abundant sand was easily moved by strong winds. Evidence for a cold climate includes the widespread frost involutions in near-surface materials in adjacent areas, and the presence of the Wisconsin terminal moraine 20 miles to the north. Evidence for a land surface devoid of vegetation is the presence of many sand dunes in the coastal-plain region. The surface features of the blocks are similar to those on rocks in other regions, that are thought to have been eroded by wind-transported sand during glacial times or in an arid climate.

## REFERENCES

Denny, C. S., 1941, Quaternary geology of the San Acacia area, New Mexico: Jour. Geology, v. 49, no. 3, p. 225–260.

Goddard, E. N., chm., and others, 1948, Rock-color chart: Washington, Natl. Research Council (repub. by Geol. Soc. America, 1951).

Hack, J. T., 1955, Geology of the Brandywine area and origin of the upland of southern Maryland: U.S. Geol. Survey Prof. Paper 267–A, p. 1–43.

Mather, K.F., Goldthwait, R. P., and Thiesmeyer, L. E., 1942, Pleistocene geology of western Cape Cod, Massachusetts: Geol. Soc. America Bull., v. 53, p. 1127–1174.

Minard, J. P., 1964, Geology of the Roosevelt quadrangle, New Jersey: U.S. Geol. Survey Geol. Quad. Map GQ–340.

Minard, J. P., Holman, W. W., and Jumikis, A. R., 1955, Engineering soil survey of New Jersey, report 18, Atlantic County: New Brunswick, N.J., Rutgers Univ. Press, Eng. Research Bull. 32, 58 p.

Ries, Heinrich, Kümmel, H. B., and Knapp, G. N., 1904, The clays and clay industry of New Jersey: New Jersey Geol. Survey Final Rept. of the State Geologist, v. 6.

Segerstrom, Kenneth, 1962, Deflated marine terraces as a source of dune chains, Atacama Province, Chile: Art. 93 *in* U.S. Geol. Survey Prof. Paper 450–C, p. C91–C93.

Sharp, R. P., 1949, Pleistocene ventifacts east of the Big Horn Mountains, Wyoming: Jour. Geology, v. 57, no. 2, p. 175–195.

Thornbury, W. D., 1954, Principles of geomorphology: New York, John Wiley and Sons, Inc., 618 p.

Wolfe, P. E., 1953, Periglacial frost thaw basins in New Jersey: Jour. Geology, v. 61, no. 2. p. 133–141.

# PRE-WISCONSIN GLACIAL DEPOSITS IN NORTHERN KENTUCKY

By LOUIS L. RAY, Washington, D.C.

*Abstract.*—Three tills of pre-Wisconsin age are present in Kentucky. The oldest, the Nebraskan, is most widespread and most deeply weathered, and occurs on remnants of a preglacial upland. Till of Kansan age is less widespread and less deeply weathered, overlies the Nebraskan till on the upland near Cincinnati, and is present elsewhere at subsummit positions in valleys cut in the glaciated upland during Aftonian time. The youngest till, the Illinoian, is least weathered, and is present at a few places within the Ohio Valley, entrenched during Yarmouth time, and on the adjacent hills southeast of Cincinnati.

## PREVIOUS INTERPRETATIONS

To understand the present interpretation of the glacial history of northern Kentucky, a brief review of the previous interpretations is helpful, for in many ways the changes in ideas parallel the conceptual growth of glacial geology.

As early as 1847, Christy (1848) described the southern boundry of the area of erratic pebbles of "primary" rock that could be traced from northwest Pennsylvania across Ohio to Cincinnati, on to Madison, Ind., and then generally westward to the Mississippi River. He intimated that between Cincinnati and Madison (fig. 1) similar erratics probably were present across the Ohio Valley in northern Kentucky. South of the area of erratics, Christy reported quartz pebbles that might be mistaken for "Diluvium." Absence of stratification led him to conclude that they had not been deposited by icebergs but that deposition resulted from "the force of the currents of the receding water at the period of the second and last grand (continental) elevation" (Christy, 1848, p. 8).

Twenty-five years later, glacial drift had been recognized in northern Kentucky. Warder (1872, p. 390) suggested that the so-called Split Rock conglomerate within the Ohio Valley southwest of Cincinnati was possibly a terminal moraine—a suggestion made again by Durrell (1956). Sutton (1877, p. 226) believed that the conglomerate was not of the same age as a similar conglomerate on the nearby hills, for "the deposits of the one period must have been made prior to the formation of the present Ohio Valley: the other after the river had cut down its channel to nearly its present depth." Thus, glacial drift of two ages, separated in time of deposition by a major interval of valley cutting, was suggested for northern Kentucky—a suggestion not accepted by Leverett (1929, p. 55).

In 1883, G. F. Wright postulated glacial damming of the Ohio River at Cincinnati, with development of a backwater lake of such proportions that the site of Pittsburgh, Pa., was inundated by some 300 feet of water—a postulate in which White (1884) concurred. When Wright's comprehensive report on the glacial boundary in the region from Illinois to Pennsylvania was published (1890), the concept of glacial damming of the Ohio was challenged by T. G. Chamberlin in his introduction to the report.

Wright made no attempt to separate the moraines and associated fresh drift to the north from the weathered attenuated drift south of the moraines. Where attenuated drift on the uplands of northern Kentucky contained only scattered quartz pebbles, he was uncertain of its relationship to glacial ice. Presumably this was the material that Christy (1848) thought might be mistaken for "Diluvium" and that today is interpreted to be deeply weathered drift, or silttil (Leighton and Ray, 1965). Chamberlin (*in* Wright, 1890, p. 15) paved the way for later workers by suggesting that the attenuated drift was not only older than the moraines and the associated fresh drift to the north, but that it might represent more than one drift deposit.

By the end of the century the glacial boundary in northern Kentucky had been mapped by Leverett (1899). Although he toyed with the possibility of a pre-Illinoian drift, the deposits were mapped as being of Illinoian age (Leverett, 1929), and as such they are shown on the Glacial Map of North America (Flint and others, 1945). Leverett's boundary, with modifications, is that used today (fig. 1).

On the "Glacial Map of the United States East of the Rocky Mountains" (Flint and others, 1959), drift of Illinoian age in Kentucky was restricted to a narrow

U.S. GEOL. SURVEY PROF. PAPER 550-B, PAGES B91–B94



797-218 O—66——7

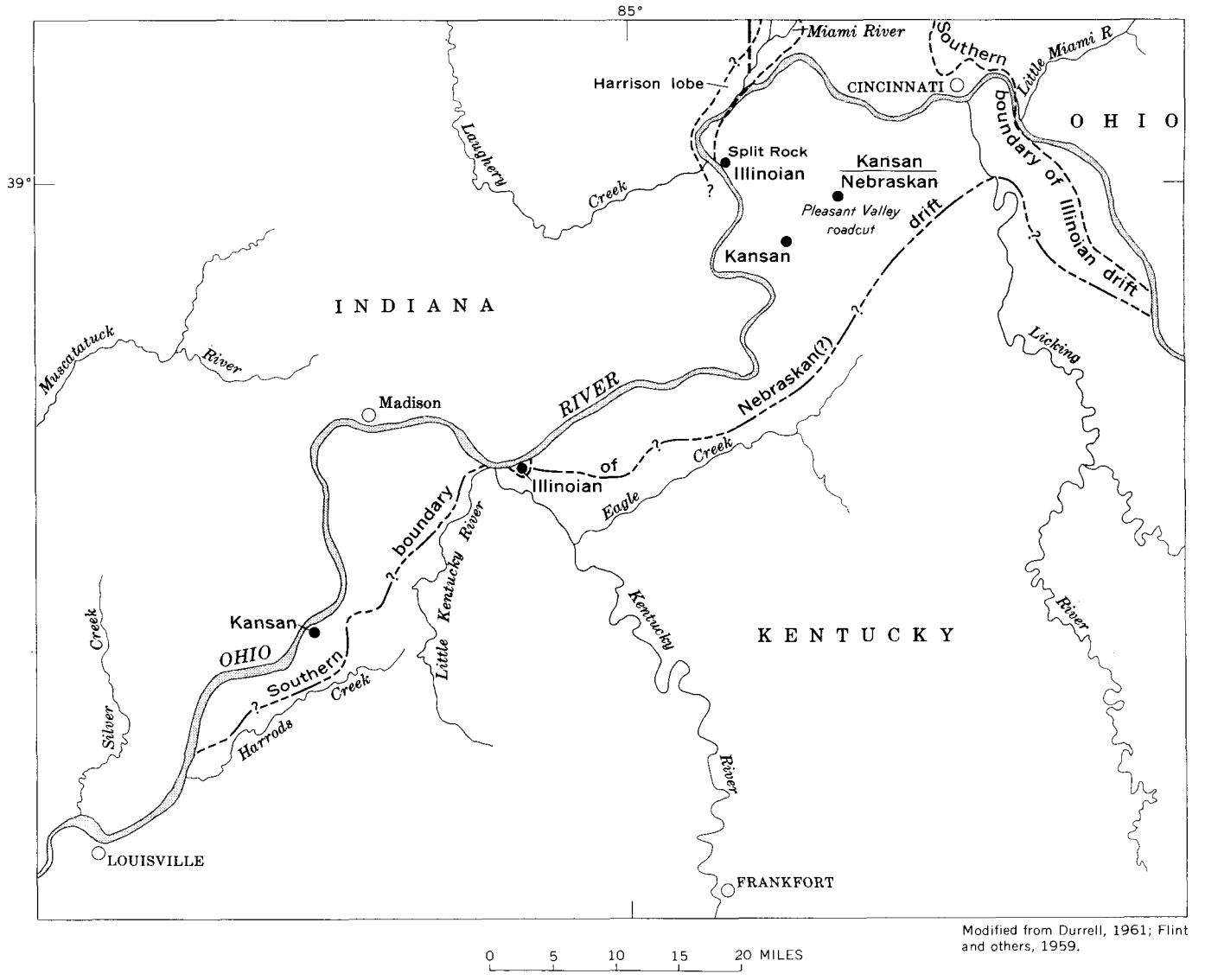


FIGURE 1.—Map of northern Kentucky, southeastern Indiana, and southwestern Ohio, showing critical exposures of pre-Wisconsin till (dots).

belt on the hills above Cincinnati. Elsewhere, drift formerly mapped as Illinoian was assigned a Kansan age except for a small area downstream from Cincinnati where Durrell (1956) proposed that a tongue of ice of Illinoian age, the Harrison lobe, extended from the Miami Valley into and down the Ohio Valley to the conglomerate at Split Rock, Ky. There are, however, other masses of Illinoian till within the Ohio Valley, downstream to a point immediately above the mouth of the Kentucky River (fig. 1), where the till of Illinoian age has a characteristic morainal topography (Leverett, 1929, p. 53). Thus, until recently, only two pre-Wisconsin drifts were recognized in Kentucky—that of Kansan age on the uplands and that of Illinoian age within the Ohio Valley and to a limited extent upstream from Cincinnati, on hills adjacent to the valley.

## PRESENT INTERPRETATION

Recent studies in northern Kentucky reveal three, rather than two, pre-Wisconsin drifts that were widely separated in time of deposition and whose distribution is related to the geomorphic development of the region. The youngest drift, of Illinoian age, is confined to the present Ohio River valley and the adjacent hills upstream from Cincinnati (fig. 1). The two older drifts, of Nebraskan and Kansan ages, are recognized on the partly dissected upland south and southwest of Cincinnati (Leighton and Ray, 1965). Farther west, weathered and altered drift (silttil) of Nebraskan age is present on ridge crests, and drift of Kansan age is present at subsummit positions in stream valleys tributary to the Ohio and on a bedrock bench along the wall of the Ohio Valley (Ray, 1957).

The best exposure in which the two oldest tills crop out on the upland of northern Kentucky is southwest of Cincinnati in a cut along Pleasant Valley Road (fig. 1). Here, the older till is assigned a Nebraskan age, and the overlying till, from which it is separated by a well-developed profile of weathering and a remnant of humic soil, is assigned a Kansan age (Leighton and Ray, 1965). The Nebraskan till rests on proglacial outwash and was deeply weathered in place during Aftonian time, with the production of a gumbotil profile of weathering as a result of poor drainage conditions on the upland. The overlying Kansan till was also deeply weathered in place, with the production of a similar gumbotil profile of weathering. Later, however, as streams cut headward into the upland in Yarmouth time, drainage conditions improved and a second-cycle profile of weathering changed the upper part of the gumbotil to silttil.

In order to explain the distribution and weathering profiles of these two ancient tills on the upland and elsewhere in northern Kentucky, it is necessary to relate them to the regional geomorphic history.

Prior to the invasion of the ice sheet of Nebraskan age there were two distinct physiographic units in northern Kentucky adjacent to the present Ohio Valley. Between the Cincinnati, Ohio, and Madison, Ind., areas was a relatively flat upland of low relief, known in Indiana as the Dearborn Upland (Malott, 1922). Drainage on this surface appears to have been to the north to the Mahomet-Teays drainage system. Between Madison and the Louisville, Ky., area, preglacial erosion, presumably Pliocene, appears to have stripped the gently dipping strata of shale and limestone to produce a westward-sloping surface on both sides of the Ohio Valley, known in Indiana as the Muscatatuck Regional Slope (Malott, 1922). The first ice sheet, the Nebraskan, is believed to have moved across both the upland and the westward-sloping surface to the outer boundary of the drift, as mapped by Leverett (1899, 1929; see also Jillson, 1929). Ice-front drainage in Kentucky at this time may have been largely along an ancient high-level Eagle Creek-Harrods Creek system (fig. 1) to the preglacial Ohio Valley in the Louisville area (Leverett, 1929, p. 29). Present observations of depth and character of weathering of till on the dissected uplands indicate that the maximum glacial invasion of Kentucky was by the ice of Nebraskan age, and not by that of Kansan age (Flint and others, 1959).

Preglacial drainage, disrupted by the Nebraskan glaciation, became integrated into an ancestral Ohio River that crossed the upland and the regional slope and continued on to the ancient preglacial valley in the Louisville area. (For a summary of theories concerning evolution of the Ohio Valley, see Wayne, 1952.) With disappearance of the ice of Nebraskan age in the Cincinnati area, the new integrated river was established in a channel around and to the north of the city in the well-known valley that passes by Hamilton, Ohio (Fenneman, 1916; Durrell, 1961).

During Aftonian interglacial time the river, with its enlarged drainage basin, became entrenched below the upland surface (Brand, 1934; Durrell, 1961) and the regional slope. Short tributaries cut headward from the main valley, and marginal dissection of the glaciated upland and the regional slope began. The glaciated upland south and southwest of Cincinnati remained relatively undissected, however, because of its distance from the major drainage channel. Poor drainage on the upland surface is recorded by the gumbotil profile of weathering in the upper part of the till of Nebraskan age (Leighton and Ray, 1965).

The second glacial invasion of northern Kentucky, the Kansan, while less extensive, crossed the Ohio River north of Cincinnati and in part overlapped the earlier glacial deposits of Nebraskan age on the upland. To the west, where ice of Kansan age crossed the entrenched Ohio River it was not sufficiently vigorous to move on to the dissected upland, and till was deposited at subsummit positions in valleys below the older drift-mantled upland. Melt-water drainage channels of this time were complex and have not been determined. It is possible, however, that the Eagle Creek and perhaps the Harrods Creek channels were used temporarily, that ephemeral channels crossed the upland south of Cincinnati, and that for perhaps the first time the channel now occupied by the Ohio River at Cincinnati was outlined and used temporarily before the older channel to the north was again freed of ice.

The succeeding Yarmouth interglacial time was one of deep incision by the river and its tributaries, and of deep weathering of the glacial deposits. It was the time when the so-called Deep Stage of the major bedrock valleys was developed. Dissection of the upland was extended by headward erosion of tributary streams, producing a mature topography along the Ohio. Headward expansion of the tributaries improved drainage conditions on the uplands so that the gumbotil developed on Kansan till south and southwest of Cincinnati was modified by a second-cycle silttil profile of weathering (Leighton and Ray, 1965). Where only Nebraskan till was present on the uplands, thick silttils also developed. Prior to the advance of the Illinoian glacier the maximum entrenchment (Deep Stage) of the Ohio and dissection of the uplands had been completed in the glaciated area.

During the third glaciation of Kentucky, the Illinoian, the entrenched channel of the Ohio River to the north of Cincinnati was in large part ice covered and rendered inoperable. At this time, according to Durrell (1961), the present channel of the Ohio between the mouths of the Little Miami and Miami Rivers was developed, so that the uplands of Kentucky were separated from those of Ohio. No ice of Illinioan age moved across the broad upland of northern Kentucky. Upstream from and southeast of Cincinnati, however, ice crossed the valley of the entrenched Ohio River and moved on to the adjacent dissected highlands (fig. 1). Between Cincinnati and the mouth of the Kentucky River, ice of Illinoian age was confined to the river valley, where its presence is indicated by several isolated masses of till that rise along the bedrock valley wall above the level of the valley train of Wisconsin age.

## CONCLUSIONS

Present studies indicate that tills of three glacial ages are present in northern Kentucky. Deeply weathered till of Nebraskan age, the most widespread, is present on the uplands from the vicinity of Cincinnati to the vicinity of Louisville. Less widespread till of Kansan age, also deeply weathered, overlies the Nebraskan till on the uplands south and southwest of Cincinnati; elsewhere it is present at subsummit positions in valleys tributary to the Ohio or on a bedrock bench along the river valley. Less-weathered till of Illinoian age is present at only a few places within the deeply entrenched Ohio Valley and on the adjacent hills above Cincinnati.

## REFERENCES


Brand, L. S., 1934, Some notes on the Pleistocene history of the Cincinnati region: Ohio Jour. Sci., v. 34, p. 67–85.

Christy, David, 1848, Letter on geology (to M. de Verneuil); Erratic rocks of North America: Rossville, Ohio, 11 p.

Durrell, R. H., 1956, Illinoian boundary in southwestern Ohio and northern Kentucky [abs.]: Geol. Soc. America Bull., v. 67, p. 1751.

——— 1961, The Pleistocene geology of the Cincinnati area, *in* Geol. Soc. America, Guidebook for field trips, Cincinnati meeting, 1961: p. 47–57.

Fenneman, N. M., 1916, Geology of Cincinnati and vicinity: Ohio Geol. Survey Bull. 19, 207 p.

Flint, R. F., and others, 1945, Glacial map of North America, scale 1:4,555,000: Geol. Soc. America Spec. Paper 60, 2 sheets.

——— 1959, Glacial map of the United States east of the Rocky Mountains, scale 1:1,750,000: Geol. Soc. America, 2 sheets.

Jillson, W. R., 1929, Geologic map of Kentucky, scale 1:500,000: Kentucky Geol. Survey, ser. 6.

Leighton, M. M., and Ray, L. L., 1965, Glacial deposits of Nebraskan and Kansan age in northern Kentucky, *in* Geological Survey Research 1965: U.S. Geol. Survey Prof. Paper 525–B, p. B126–B131.

Leverett, Frank, 1899, The Illinois glacial lobe: U.S. Geol. Survey Mon. 38, 817 p.

——— 1929, Pleistocene of northern Kentucky: Kentucky Geol. Survey, ser. 6, v. 31, p. 1–80.

Malott, C. A., 1922, The physiography of Indiana, *in* Handbook of Indiana geology: Indiana Dept. Conservation, Div. Geology Pub. 21, p. 59–256.

Ray, L. L., 1957, Two significant new exposures of Pleistocene deposits along the Ohio River valley in Kentucky: Jour. Geology, v. 65, p. 542–545.

Sutton, George, 1877, Glacial or ice deposits in Boone Co., Ky., of two distinct and widely distant periods: Am. Assoc. Adv. Sci. Proc. 25, p. 225–231.

Warder, R. B., 1872, Geology of Dearborn, Ohio, and Switzerland counties [Ind.]: Indiana Geol. Survey, Ann. Rept. 3–4, p. 387–434.

Wayne, W. J., 1952, Pleistocene evolution of the Ohio and Wabash valleys [Ind.]: Jour. Geology, v. 60, p. 575–585.

White, I. C., 1884, Effects of the glacial dam at Cincinnati along the upper basin of the Ohio: Western Reserve Hist. Soc. Tract 60, v. 2, p. 273–278.

Wright, G. F., 1883, Recent investigations concerning the southern boundary of the glaciated area of Ohio: Am. Jour. Sci., ser. 3, v. 26, p. 44–56.

———1890, The glacial boundary in western Pennsylvania, Ohio, Kentucky, Indiana, and Illinois, with an introduction by T. C. Chamberlin: U.S. Geol. Survey, Bull. 58, 112 p.

# DISTRIBUTION AND GEOLOGIC STRUCTURE OF TRIASSIC ROCKS IN THE BAY OF FUNDY AND THE NORTHEASTERN PART OF THE GULF OF MAINE [1]

By A. RICHARD TAGG and ELAZAR UCHUPI, Woods Hole, Mass.

*Work done in cooperation with the Woods Hole Oceanographic Institution, Woods Hole, Mass.*

*Abstract.*—Results of a seismic survey made of the Bay of Fundy and the northeastern part of the Gulf of Maine, using a continuous seismic profiler with sparker sound source, indicate that the Acadian Triassic basin extends westward beyond the Bay of Fundy for a distance of 120 kilometers. Reflecting horizons which may represent bedding planes have dips of about 5° to 10° and generally dip away from basement highs. No evidence of a marginal fault was found along the northwest side of the basin.

The U.S. Geological Survey in cooperation with the Woods Hole Oceanographic Institution initiated a program in 1962 to investigate the topography, sediments, stratigraphy, and geologic structure off the east coast of the United States. The present report deals with the structure of the Bay of Fundy and part of the Gulf of Maine.

The Bay of Fundy is a trough 170 kilometers long and 50 to 70 km wide, trending northeast between Nova Scotia and New Brunswick in eastern Canada. To the southwest it opens into the Gulf of Maine, and to the northeast it divides and ends in Chignecto Bay and Minas Basin (fig. 1). The Bay of Fundy is located along the axis of a broad syncline—known as the Acadian Triassic basin—which plunges gently toward the Gulf of Maine (Powers, 1916).

Triassic rocks are exposed along the entire length of the Bay of Fundy on the Nova Scotia side. The New Brunswick shore, on the other hand, consists mainly of Paleozoic rocks with only isolated patches of Triassic rocks. North Mountain, a series of islands and peninsulas along the shore of Nova Scotia, is a long ridge underlain by a thick sequence of Triassic lava flows tilted gently toward the Bay of Fundy (fig. 2*A*). A large number of gaps on the ridge are located on north-trending right-lateral faults along which North Mountain has been displaced (Goldthwait, 1924, p. 18). North Mountain is separated from the mainland by Annapolis Valley, a partially submerged lowland carved out of the relatively soft Triassic sedimentary strata. The shore of the Bay of Fundy on the New Brunswick side consists, for the most part, of relatively short valleys separated by headlands having cliffs 20 to 30 meters high. Grand Manan Island, which rises 100 m above sea level, occupies part of the mouth of the bay.

The floor of the Bay of Fundy from Grand Manan Island to Chignecto Bay and Minas Basin is, for the most part, a smooth plain sloping southwestward, at about 0°04′ (about 1 m per km), toward the Gulf to Maine (fig. 2*A*). The bottom is very irregular in the vicinity of Grand Manan Island. Three basins ranging in depth from 119 to 211 m below sea level lie to the north, west, and east of Grand Manan Island. To the southwest of the island are the Murr Ledges, a broad area of innumerable small rocky reefs some of which rise above sea level. A ridge, which includes Grand Manan Banks, extends more than 100 km southwest from the Murr Ledges, and splits near lat 44° N. One segment trends south and the other southwest.

## METHODS OF STUDY

A series of continuous seismic profiles was made in order to locate the seaward boundary of Triassic rocks in the Triassic Acadian basin. The lines of profile were extended as near as possible to areas of known outcrops of Triassic rocks in order to facilitate inference of the presence of Triassic rocks on the floor of the bay. In the profiles the rocks believed to be Triassic dip appreciably, whereas strata thought to be younger are practically horizontal, making it possible to distinguish the Triassic rocks from non-Triassic rocks.

[1] Contribution No. 1653 of the Woods Hole Oceanographic Institution.

U.S. GEOL. SURVEY PROF. PAPER 550-B, PAGES B95-B98

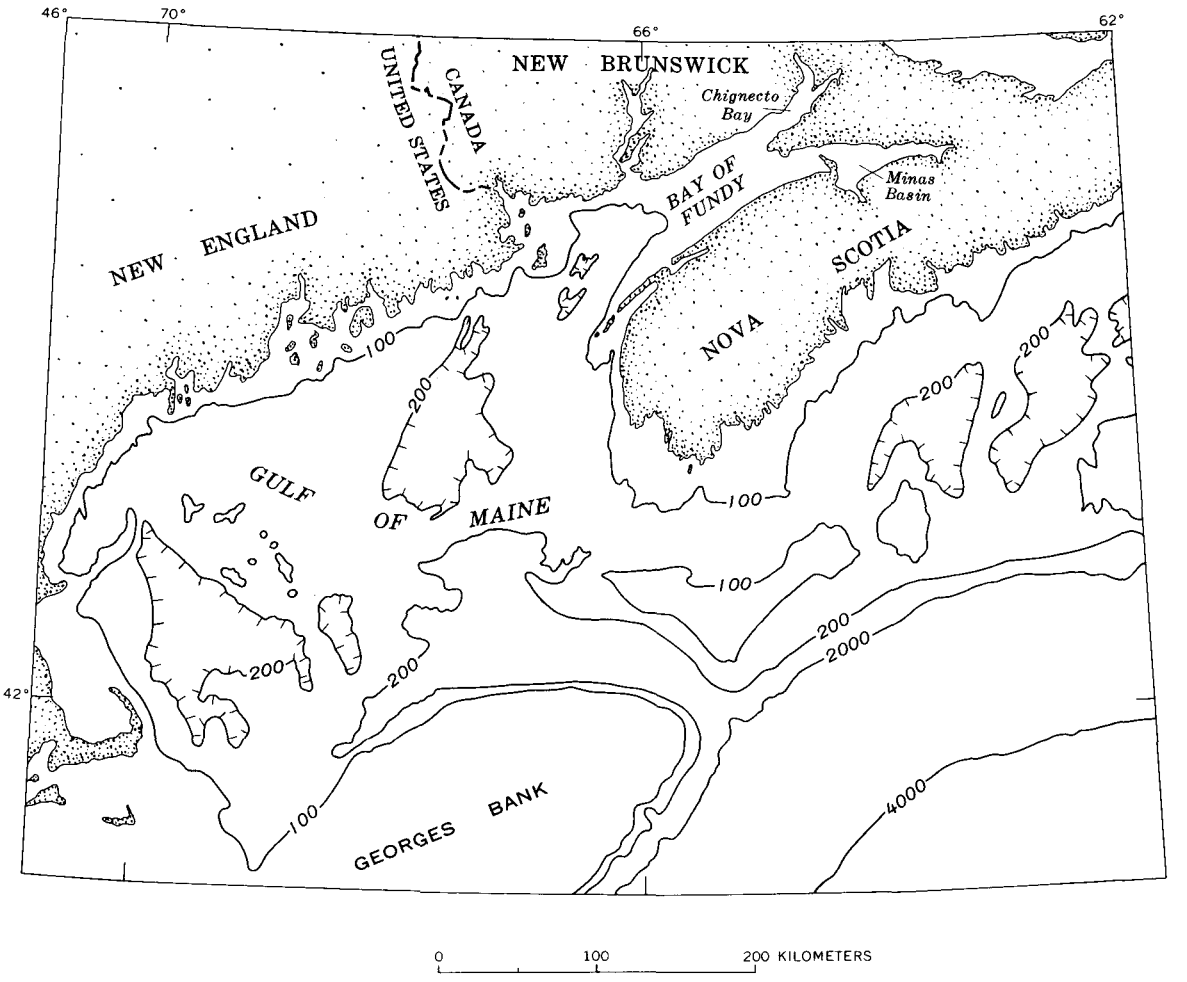


FIGURE 1.—Map showing location of the Bay of Fundy and the Gulf of Maine. Contours in meters below mean sea level.

The source of sound energy used during this investigation was a 10,500-joule sparker. Reflections from the bottom and from discontinuities below the bottom were received by a five-element hydrophone array towed behind the ship and recorded on a graphic recorder and tape recorder aboard the ship. The tapes were later replayed at different frequency intervals to improve the recordings obtained in the field. The various reflecting surfaces were traced on plastic overlays and reduced visually to a convenient size from which the profiles in figure 3 were made.

## DISTRIBUTION AND STRUCTURE OF THE TRIASSIC ROCKS

The interpretation of data obtained during this survey is summarized on figure 2*B*, and a few selected profiles are shown on figure 3. Seismic profiles taken across the Bay of Fundy are believed to show that the Triassic strata dip gently toward the axis of the bay (profile 5, fig. 3). Parallel to the axis these beds generally dip toward the Gulf of Maine, although there are reversals that may reflect irregularities in the Paleozoic basement. This is illustrated also in other profiles (not shown in fig. 3) where the Triassic rocks lap onto Paleozoic basement highs. Southwest of Grand Manan Island, Triassic beds, capped by thin veneers of Quaternary sediments, are localized within three narrow troughs separated by Paleozoic basement highs. The northernmost of the troughs is located between the Murr Ledges and the mainland, the central one between the Murr Ledges and the Grand Manan Banks, and the third south of the Grand Manan Banks (fig. 2*B*). The Triassic strata within the three basins generally dip away from the basement highs. In all the seismic sections, the Triassic strata are truncated by an irregular erosion surface and capped by Quaternary deposits of various thicknesses. Glacial action during the Pleistocene was probably responsible for the erosional surface atop the Triassic beds. Later,

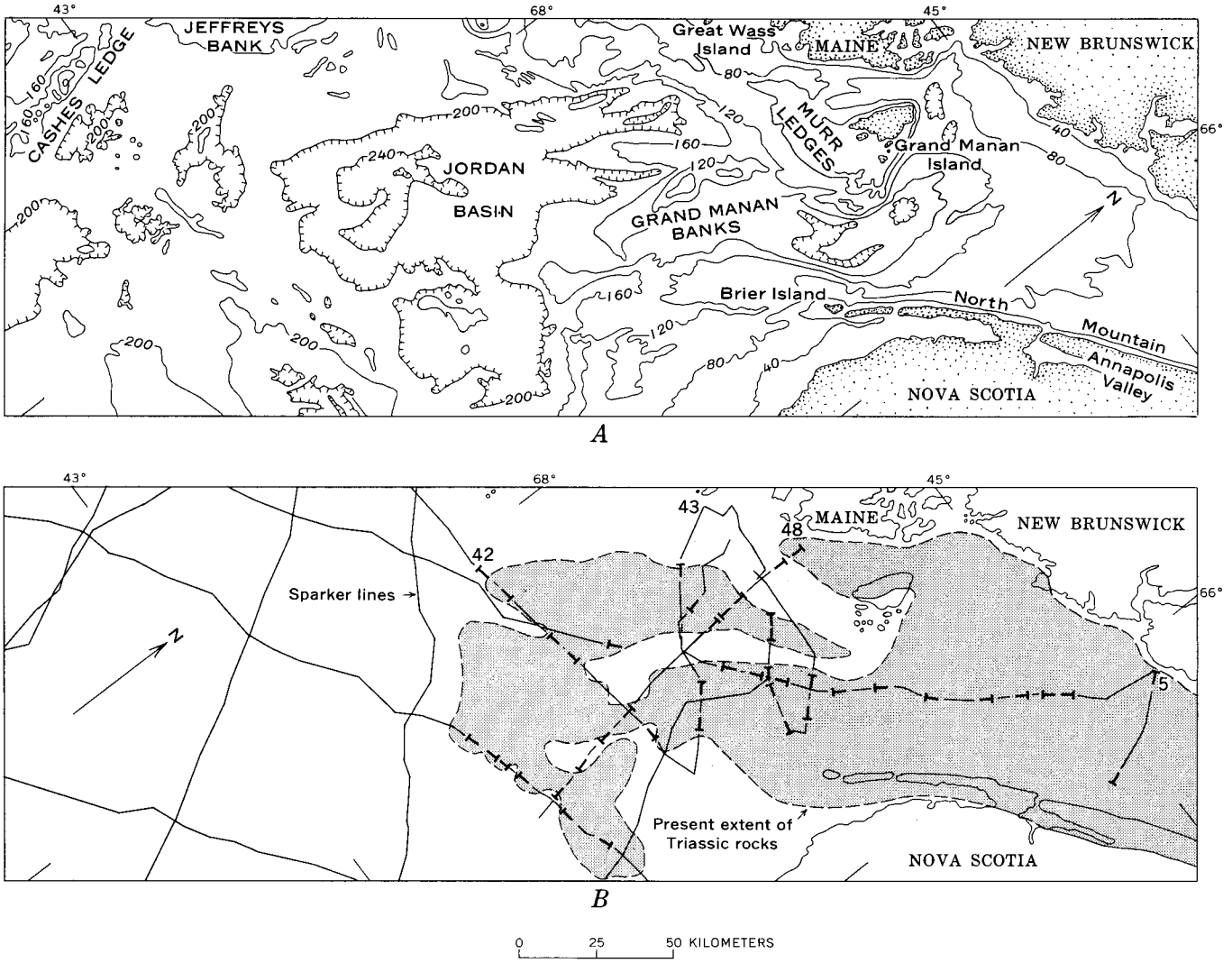


FIGURE 2.—*A*. Bathymetry of the Bay of Fundy and part of the Gulf of Maine. Contours are in meters below mean sea level. *B*. Map showing the western extension (stippled) of Triassic rocks in the Acadian Triassic basin. Offshore boundaries are based on data from continuous seismic profiles, and land boundaries are based on known locations of Triassic rocks. Apparent dip (the dip of the stratum in the direction of the profile) is indicated by symbol T (long limb extends in direction of dip) on selected sparker lines. Map shows boundaries of the main mass of Triassic rocks, but not details of inliers within the mass.

with retreat of the ice and rise in sea level, the erosional surface was mantled by sediments reworked from nearby topographic highs.

The western margin of the Triassic rocks seems to be near long 68° W. and does not extend to Cashes Ledge as suggested by Drake and others (1954) or to Jeffreys Bank as suggested by Johnson (1925). Deposits reported by Drake and others (1954) from immediately north and east of Cashes Ledge, and having a compressive velocity of 12,000–13,000 feet per second (4.0 km per sec), may be part of the Paleozoic basement or may be Cretaceous in age. Deposits having such velocities were also reported by Hoskins and Knott (1961) from Cape Cod Bay, and because of similarities between the Cape Cod Bay sediments and the known Cretaceous strata off Gay Head, Martha's Vineyard, Hoskins and Knott suggested that the deposits in Cape Cod Bay are probably Cretaceous in age. The rocks north and east of Cashes Ledge may also be of the same age. At any rate, rocks of Triassic age do not extend in an unbroken body west of long 68° W.

Johnson (1925) and Koons (1941, 1942) suggested that the Acadian Triassic basin is bounded on the New Brunswick side by a marginal fault which Johnson named the Fundian fault. Seismic profiles which cross the probable location of this suggested fault, such as profiles 42 and 43, do not show indications of faulting. Since the reflecting horizons within the area of Triassic rocks generally dip away from basement highs and have dips of rarely more than 10°, it is suggested that the

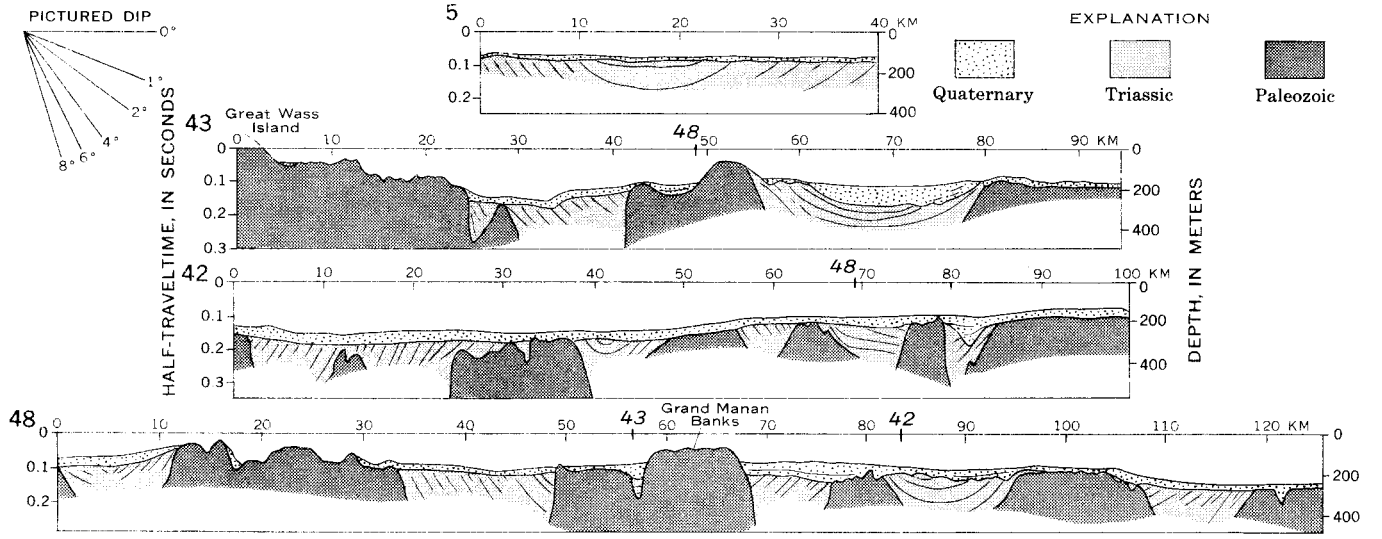


FIGURE 3.—Continuous seismic profiles across parts of the Bay of Fundy and the Gulf of Maine. Location of these profiles (Nos. 5, 43, 42, and 48) is shown on figure 2*B*. Profile intersections are shown on the horizontal scale by ticks and by the italic numbers of the intersecting profiles. Thicknesses on the vertical scale are shown in terms of traveltime and in meters; thicknesses in meters are based on the calibration velocity of the recorder used (1,463 m/sec). Lines within the areas of Triassic rocks are reflecting horizons derived from the seismic profiles. Profiles have a vertical exaggeration of ×22, which causes the pictured dips to be more than the actual dips; actual dips of the reflecting horizons are less than 10°.

contact between the Paleozoic basement and the Triassic strata to a depth of at least 1,000 m below sea level is depositional. The writers suggest, therefore, that the linearity of the Maine–New Brunswick coast, suggested by Johnson (1925) as evidence for the existence of the Fundian fault, is due to the removal of the weak and gently dipping Triassic sediments from the underlying Paleozoic basement. The conspicuous scarp south of Great Wass Island (profile 43), cited by both Johnson and Koons as evidence of the fault, cannot be traced west of the island (Shepard, 1930, 1942). Profile 43, which extends within a few kilometers of Great Wass Island, shows that the scarp is developed on the Paleozoic basement and that the nearest Triassic strata are 20 km away. Moreover, the gentle slope of the scarp (it does not exceed 2°) is not typical of fault-line scarps. If the scarp was formed by marine erosion from a marginal fault, it has retreated 20 km since faulting took place. However, there is no evidence for such a retreat because the area south of the scarp is occupied by irregular topography instead of by a smooth erosional platform.

## SUMMARY

Rocks of Triassic age occupy the floor of the Bay of Fundy and extend beyond its mouth for a distance of about 120 km into the Gulf of Maine. West of the bay the Triassic basin consists of three narrow troughs. Seismic profiles show no evidence for a marginal fault on the southeast or northwest. The low slopes (commonly less than 2°) of surfaces which were detected by the seismic method, including surfaces between the inferred rock units, suggest depositional contacts. During the Pleistocene Epoch, the Triassic rocks appear to have been deeply eroded by glacial action. Following the retreat of the ice and a rise in sea level, the low areas were buried by reworked sediments from nearby topographic highs.

## REFERENCES

Drake, C. L., Worzel, J. L., and Beckman, W. C., 1954, Geophysical investigations in the emerged and submerged Atlantic coastal plain; pt. 9, Gulf of Maine: Geol. Soc. America Bull., v. 65, p. 957–970.

Goldthwait, J. W., 1924, Physiography of Nova Scotia: Geol. Survey of Canada Mem. 140, 179 p.

Hoskins, Hartley, and Knott, S. T., 1961, Geophysical investigation of Cape Cod Bay, Massachusetts, using the continuous seismic profiler: Jour. Geology, v. 69, p. 330–340.

Johnson, D. W., 1925, The New England–Acadian shore line: New York, John Wiley and Sons, 608 p.

Koons, E. D., 1941, The origin of the Bay of Fundy and associated submarine scarps: Jour. Geomorphology, v. 4, p. 237–249.

——— 1942, The origin of the Bay of Fundy; a discussion: Jour. Geomorphology, v. 5, p. 143–150.

Powers, Sidney, 1916, The Acadian Triassic: Jour. Geology, v. 24, p. 1–26 and 105–268.

Shepard, F. P., 1930, Fundian faults or fundian glaciers: Geol. Soc. America Bull., v. 41, p. 659–674.

——— 1942, Origin of the Bay of Fundy; a reply: Jour. Geomorphology, v. 5, p. 137–142.

# MEASUREMENT OF THE VELOCITY OF HIGH-AMPLITUDE SHOCK WAVES IN ROCK MATERIALS BY MEANS OF STRAIN GAGES

By MICHAEL H. CARR, Menlo Park, Calif.

*Abstract.*—Shock waves, ranging in amplitude from 10 to 150 kilobars, were generated in rock materials with C–4 explosives. To measure the speed of a shock wave, SR–4 strain gages were placed at different positions along the path of the shock wave. The signals emitted by the gages on arrival of the shock wave were recorded on an oscilloscope so that the time interval between successive gage signals could be calculated. From this time interval the shock speeds were determined. In some instances an elastic wave arrived at the gages before the shock wave so that the elastic-wave velocity was measured instead of the shock-wave velocity. The measured speeds in specimens of the Coconino Sandstone ranged from 2.9 to 4.2 km/sec, in a sandstone from the Moenkopi Formation from 2.5 to 2.9 km/sec, in a basalt from 5.5 to 6.0 km/sec, and in Yule marble from 2.3 to 5.2 km/sec.

Knowledge of how a material behaves when it is subjected to high shock stresses is essential for understanding the formation of craters by explosives or high-velocity impact. The energy of the explosive or projectile is initially converted to shock-wave energy. The subsequent partitioning of the energy between heating, comminution, throwout, and other processes is strongly dependent on the properties of shock waves in the materials involved. In general, to adequately describe shock behavior in a material, two properties of the shock wave must be measured; those normally chosen are the particle velocity and the shock-wave velocity. From these two parameters, and from the properties of the material in the unshocked state, the various thermodynamic properties of the shocked state can be determined. Of particular interest are pressure and specific volumn. These can be dervied from the measured velocities by the following equations:

$$u_s = V_0\sqrt{\frac{P_1-P_0}{V_0-V_1}} \text{ and } u_p = \sqrt{(P_1-P_0)(V_0-V_1)},$$

where $u_s$=shock-wave velocity, $u_p$=particle velocity, $V_0$=initial volume, $V_1$=volume at shock pressure, $P_0$=initial pressure, and $P_1$=shock pressure.

Methods of measuring the shock velocities that have been used previously, such as pin contactor and photographic techniques, although very accurate, are both time consuming and expensive. A more convenient method for use with rock materials was therefore designed. Some loss of precision was thought acceptable in view of the considerations that inhomogeneities are normally found in rock material and that with the more convenient method a large number of runs could be made. In the new method, SR–4 strain gages are used to measure times of arrival of shock waves at different points along the path of the shock wave.

## EXPERIMENTAL METHOD

The shock-wave velocity was measured directly by placing strain gages at different positions in the path of the shock wave and measuring the time of arrival of the shock wave at the gages. The shock wave was generated by a rod of C–4 explosive 1 inch in diameter placed in contact with an aluminum rod 1 inch in diameter. The specimen, also in the form of a rod, was placed in contact with the aluminum so that the shock wave passed through the aluminum into the specimen (fig. 1). Two SR–4 strain gages, type C–7, were placed on the specimen approximately 1 cm apart at known distances from the aluminum–specimen interface. The gages consist of a paper carrier to which is bonded a fine wire arranged in the form of a grid. A change in the dimensions of the grid results in a change in the resistance of the wire. A potential was applied across the gages, and the signals generated by the gages on arrival of the shock wave were displayed on separate channels of an oscilloscope and recorded photographically. The oscilloscope was triggered by a signal induced in a wire embedded in the explosive. The distance between the two gages and the time interval between their successive signals permit the apparent shock-wave velocity to be calculated. To obtain the true shock-wave velocity the

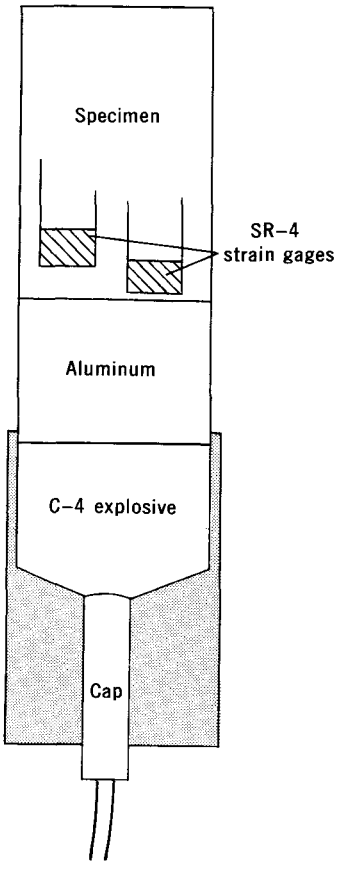


FIGURE 1.—Experimental configuration for measuring shock-wave velocities.

measured speed was corrected for nonplanarity of the shock wave. For this correction it was assumed that the detonation wave in the explosive started on the cap and moved radially away from it. Then the distance traveled by the shock wave between successive gage signals in a direction perpendicular to the shock wave could be computed. Using this corrected distance the true shock-wave velocity was calculated. The corrected distance differed significantly from the measured distance only in those cases where the gages were closer than 2.5 cm to the explosive.

The particle velocity in the specimen was derived indirectly using an impedance-match solution (Rice and others, 1958) across the aluminum–specimen interface. Two requirements of this solution are that the shock-wave parameters in the aluminum are known and that a single shock wave is generated in the specimen. The relation between particle velocity and shock-wave velocity for aluminum is well known (Rice and others, 1958); thus, only the shock-wave velocity in the aluminum needed to be measured. This was done in a way similar to that described above for the specimen. In many successive shots using the same explosive geometry, the arrival times of shock waves in aluminum as a function of distance from the aluminum–explosive interface were recorded (fig. 2). This function was differentiated to find the shock speed, a correction made for nonplanarity of the shock wave, and the shock pressure determined at different distances from the explosive. The pressures ranged from 240 kilobars adjacent to the explosive to 40 kb at 6 cm from the explosive. The impedance-match solution was then applied in those cases where only one shock wave was generated in the specimen. In most rocks the low-amplitude shock wave is unstable and breaks down into several shock waves so that the particle velocity cannot be computed using the impedance-match solution and the shock wave cannot be fully described.

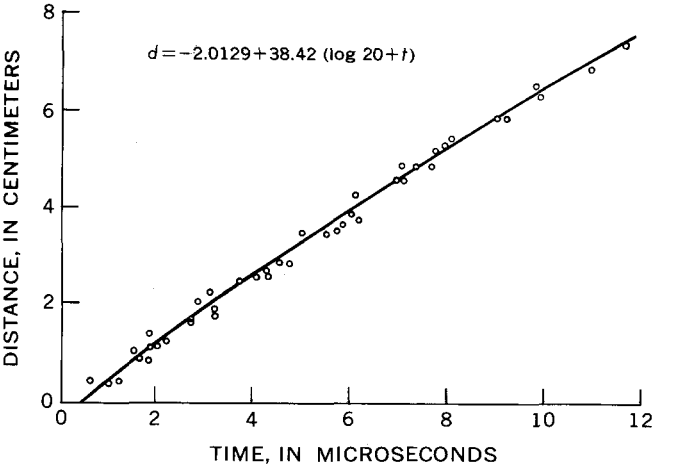


FIGURE 2.—Graph of time of arrival ($t$) of shock waves in aluminum as a function of distance from the explosive ($d$). The time ($t$) is measured from the time that the oscilloscope was triggered from a wire embedded in the explosive. Deviation from the computed line is due primarily to variation in the trigger time.

The time interval between successive gage signals depends on the distance between the gages and the speed of the shock wave, but was 2 to 3 microseconds in most cases. The arrival time of shock waves at the strain gages could be measured to within 0.04 μsec. The error in the distance measurements was negligible. For a shock-wave velocity of 5 km/sec the errors in time measurements lead to an error of ±0.2 km/sec in the measured velocity.

## RESULTS

### Coconino Sandstone

The results for samples of Coconino Sandstone from Meteor Crater, Ariz., are listed in table 1, and the Hugoniot curve, a plot of shock pressure against density behind the shock front, for the sandstone is shown in figure 3. Comparison of the Hugoniot curve determined by the strain-gage technique with that de-

TABLE 1.—*Experimental shock data for Coconino Sandstone, Moenkopi Formation, a basalt from Vacaville, Calif., and Yule marble*[1]

| Aluminum | Specimen | | | | |
|---|---|---|---|---|---|
| Shock pressure (kb) | Shock pressure (kb) | Shock-wave velocity (km/sec) | Particle velocity (km/sec) | Elastic-wave velocity (km/sec) | $\rho_0/\rho$[2] |
| **Coconino Sandstone** | | | | | |
| 240 | 134 | 3.9 | 1.7 | | 0.56 |
| 240 | 130 | 3.7 | 1.7 | | .55 |
| 235 | 138 | 4.2 | 1.6 | | .60 |
| 232 | 128 | 3.8 | 1.7 | | .56 |
| 212 | 109 | 3.6 | 1.5 | | .58 |
| 212 | 120 | 3.9 | 1.5 | | .61 |
| 185 | 100 | 3.6 | 1.4 | | .61 |
| 172 | 98 | 3.7 | 1.3 | | .65 |
| 137 | 75 | 3.3 | 1.1 | | .68 |
| 125 | 72 | 3.6 | 1.0 | | .73 |
| 110 | 58 | 3.1 | .9 | | .71 |
| 80 | 45 | 3.5 | .6 | | .81 |
| 42 | 22 | 2.9 | .4 | | .88 |
| 25 | 15 | 3.1 | .2 | | .92 |
| 20 | 11 | 3.2 | .2 | | .94 |
| **Sandstone from the Moenkopi Formation** | | | | | |
| 235 | | 2.9 | | 3.2 | |
| 218 | | 2.8 | | 2.9 | |
| 173 | | 2.8 | | 3.1 | |
| 140 | | 2.7 | | 3.1 | |
| 138 | | 2.6 | | 2.8 | |
| 88 | | 2.6 | | 3.0 | |
| 83 | | 2.7 | | 3.2 | |
| 76 | | 2.5 | | 3.0 | |
| 70 | | 2.7 | | 3.3 | |
| 70 | | 2.5 | | 3.0 | |
| 65 | | 2.7 | | 3.3 | |
| **Basalt** | | | | | |
| 159 | | | | 6.0 | |
| 120 | | | | 5.5 | |
| 119 | | | | 5.6 | |
| 100 | | | | 5.8 | |
| 88 | | | | 5.5 | |
| 75 | | | | 5.8 | |
| 70 | | | | 5.6 | |
| 62 | | | | 5.8 | |
| 50 | | | | 5.7 | |
| **Yule marble** | | | | | |
| 120 | | 4.2 | | | |
| 118 | | 3.8 | | | |
| 118 | | 5.1 | | | |
| 95 | | 2.9 | | | |
| 82 | | 5.2 | | | |
| 70 | | 4.5 | | | |
| 70 | | 2.3 | | | |
| 60 | | 5.2 | | | |
| 50 | | 3.6 | | | |

[1] All three shock-wave parameters (shock pressure, shock-wave velocity, and particle velocity) could be measured only for the Coconino Sandstone, in which only a single shock wave was generated and detected.

[2] $\rho_0$ is the original density of the specimen, $\rho$ is the density behind the shock front.

termined by the more accurate inclined-mirror technique (Gregson and others, 1963) suggests that the strain-gage measurements are in error for pressures

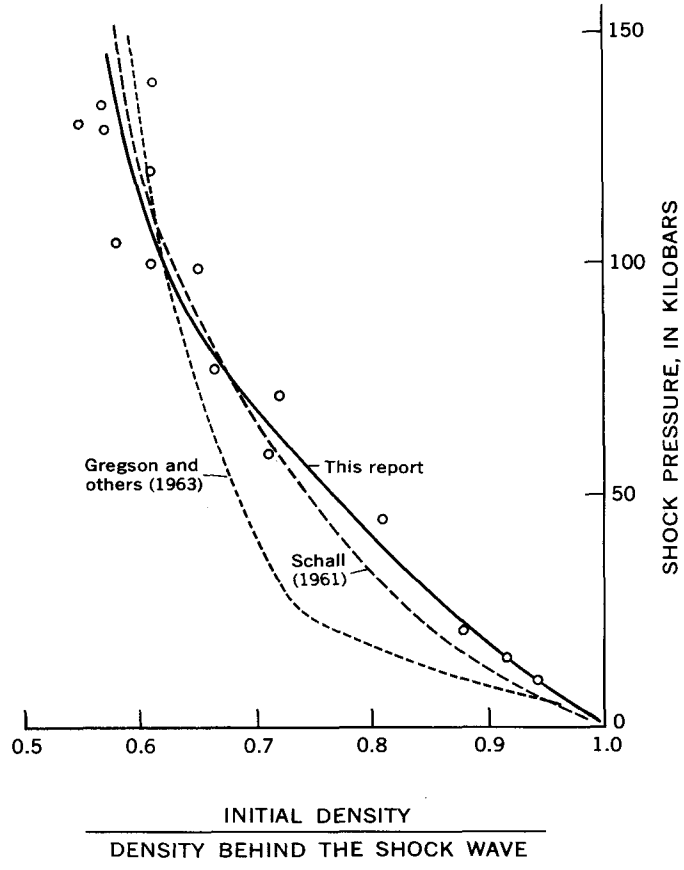


FIGURE 3.—Comparison of experimental shock data for the Coconino Sandstone with data of Gregson and others (1963) and Schall (1961).

less than 80 kb. For a given pressure the density is too low. Such an error could result if, in the low-pressure region, the elastic wave was detected and not the shock wave. For pressures greater than 80 kb there is good agreement between the different curves, suggesting that in this region the shock wave, not the elastic wave, was being detected; that is, the shock wave had overdriven the elastic wave.

At shock pressures greater than approximately 80 kb, the densities behind the shock front are higher than those achieved by compression of single-crystal quartz (Wackerle, 1962) and those calculated by extrapolation of the quartz isothermal-compression data of Bridgman (1948). Compression of porous materials results in a higher temperature for a given pressure than compression of nonporous material. At a particular shock pressure, therefore, the temperature in the sandstone will be higher than at the same pressure in pure quartz. This should result in a lower density at a given pressure for sandstone than for quartz, whereas the reverse is actually observed. McQueen and others (1963) have interpreted Wackerle's data to indicate that stishovite forms at 144 kb and 523°K. Gregson and others (1963)

have also suggested that the observed high densities in sandstones could be explained by the formation of stishovite. A similar interpretation may be made here to explain the anomalously high densities (see table 1). High densities would result if stishovite formed at approximately 80 kb but at a temperature higher than in pure quartz compression.

### Moenkopi Formation

The signals from gages mounted on samples of Moenkopi sandstones from Meteor Crater, Ariz., differed from those on Coconino Sandstone or aluminum. On the latter the gage signals were horizontal and then fell steeply after the arrival of the shock wave. For Moenkopi sandstone, gages farthest from the aluminum-sandstone interface yielded an initially horizontal signal followed by a signal having a shallow slope, after which the signal dropped off steeply (fig. 4). Signals

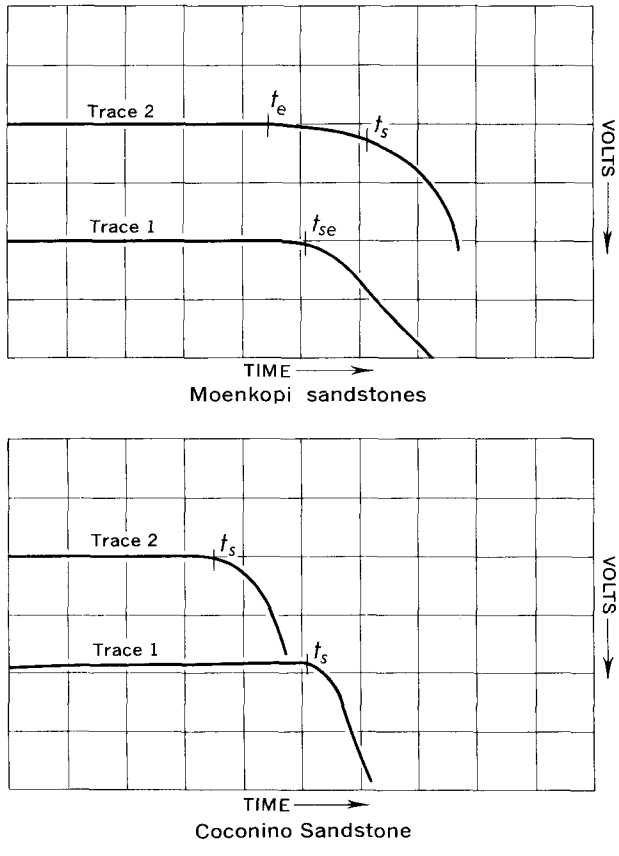


FIGURE 4.—Comparison of signals from gages on Moenkopi and Coconino sandstones. Traces 1 are from gages approximately 1 mm from the specimen–aluminum interface, traces 2 are from gages approximately 1.2 cm from the interface. $t_s$ denotes the arrival time of the shock wave, $t_e$ denotes the arrival time of the elastic wave, $t_{se}$ denotes the simultaneous arrival time of both waves. Horizontal scale 0.4 μsec/division, vertical scale 0.005 volts/division.

near the interface resembled those from the Coconino Sandstone.

The distinctive signals from Moenkopi sandstones are thought to result from superposition of two signals, one from a faster traveling elastic wave that arrives before the shock wave and the other from a low-amplitude, slower velocity shock wave (see table 1). The first observed signal on the gage farthest from the interface is taken to indicate the time of arrival of the elastic wave. This signal generally has a slope of 0.002 volts/μsec. The point at which the slope subsequently steepens is taken as the arrival time of the shock wave. The two waves cannot be distinguished in the signal from the gage nearest the aluminum-sandstone interface. This gage is only 1 mm from the interface, so the two waves have not traveled far enough to be appreciably separated in time.

If this interpretation is valid, then the elastic wave has a velocity of $3.11 \pm 0.15$ km/sec and for distances up to 6 cm from the explosive the shock speeds range from 2.5 to 3.1 km/sec. Because the shock wave has not overdriven the elastic wave, the impedance-match solution cannot be applied and the Hugoniot curve cannot be determined. The low speeds of the shock wave suggest that the shock pressures were in the 20–50 kb region. Furthermore, the fact that the elastic wave gave a detectable signal from the strain gages suggests that the elastic wave in a Moenkopi sandstone has a considerably higher amplitude than that in the Coconino Sandstone (approximately 5 kb, according to Gregson and others, 1963). An estimate of the amplitude of the elastic wave is 25 kb.

### Basalt

An attempt was made to measure the shock-wave velocities in a basalt from Vacaville, Calif. The measured speeds were found to be independent of the distance of the specimen from the explosive, suggesting that only signals from the elastic wave were detected. The speed of the elastic wave is $5.76 \pm 0.23$ km/sec over the pressure studied. Gregson and others (1963) gave 50 kb for the amplitude of the elastic wave in basalt and showed that the shock wave will overtake the elastic wave only for pressures in excess of 200 kb.

### Yule marble

Low-amplitude shock waves in carbonate rocks characteristically are multiple-step functions (Gregson and others, 1963). Table 1 shows that a wide range of speeds (2.3–5.2 km/sec) was determined for a sample of Yule marble from Gunnison County, Colo. The highest values probably represent the elastic-wave

speed, whereas the lower speeds are for the ensuing shock waves. The signals generally had shallower slopes than those from any of the other materials tested. This suggests that the pressure does not rise instantaneously at the various shock fronts but that the pressure-rise times are in the order of tenths of microseconds, far slower than in the other materials. Because of these long rise times and the short distance through which the shock wave travels in the marble before measurements are made, the wave structure behind the elastic wave is probably not one of discrete steps but rather one of regions of different shock stresses grading into one another. Thus, it is not possible to assign the measured speeds to specific shock waves.

## CONCLUSION

The response time of the SR–4 strain gages is sufficiently short (0.04 μsec) to enable shock speeds to be measured within small distances, and speeds up to 7 km/sec have been measured within a distance of 1 cm. To fully determine shock-wave characteristics in a material, two parameters of the shock wave must be measured. This necessitates using an impedance-match solution to describe the shock waves of strain gages alone are used. This solution was used successfully for Coconino Sandstone and metals but could not be used on most rock materials because of the multiple structure of the shock waves and because shock-wave signals were obscured by elastic-wave signals. The strain-gage technique, if combined with another technique such as pin contactors (Minshall, 1955), high-speed photography (Gregson and others, 1963), or X-ray methods (Schall, 1961), could provide a complete solution. Even without additional techniques, however, the strain-gage technique gives a reasonably accurate estimate of the shock energy imposed on a material and the peak shock pressure in pressure regions where the shock wave has overdriven the elastic wave.

## REFERENCES

Bridgman, P. W., 1948, The compression of 39 substances to 100,000 kg/cm²: Am. Acad. Arts Sci. Proc., v. 76, p. 55–70.

Gregson, V. G., Ahrens, T. J., and Peterson, C. F., 1963, Dynamic properties of rocks: Menlo Park, Calif., Stanford Research Institute, 72 p.

McQueen, R. G., Fritz, J. N., and Marsh, S. P., 1963, On the equation of state of stishovite: Jour. Geophys. Research, v. 68, p. 2319–2322.

Minshall, S., 1955, Properties of elastic and plastic waves determined by pin contractors and crystals: Jour. Appl. Physics, v. 26, p. 463–469.

Rice, M. H., McQueen, R. G., and Walsh, J. M., 1958, Compression of solids by strong shock waves, *in* Sietz, Frederick, and Turnbull, David, eds., Solid state physics, v. 6: New York, Academic Press, p. 1–63.

Schall, Rubi, 1961, High speed measurement of shock compressibility in the 1-mb range, *in* Proceedings of the International Congress on High-Speed Photography: New York, Academic Press, p. 184–187.

Wackerle, Jerry, 1962, Shock wave compression of quartz: Jour. Appl. Physics, v. 33, p. 3224–3232.

# SEISMIC SURVEYING WITH FIRECRACKERS— A MODIFICATION OF THE SLEDGEHAMMER METHOD

By J. H. CRINER, Nashville, Tenn.

*Work done in cooperation with the Tennessee Division of Water Resources*

*Abstract.*—Firecracker explosions proved a successful substitute for blows of a sledgehammer, after the sledgehammer method of seismic surveying failed as a means of determining the depth to bedrock beneath the floor of Trace Creek valley in Humphreys County, Tenn. Further modification of the method by use of a single geophone to record the arrival of shock waves from a linear series of successive explosions resulted in a substantial economy of time and effort.

Seismic refraction is a widely used method for determining depths to relatively shallow interfaces such as the water table or surfaces of contact between rock materials of different densities. The method commonly involves (1) producing a shock by dropping a heavy weight or by exploding a small charge of dynamite at points on the land surface where the depth to one or more interfaces is to be determined, and (2) measuring the time required for the first shock wave to reach stations at different distances from the shock point. The principles of the seismic-refraction method and the procedures for computing shock-wave velocities and depths to the interfaces are described in textbooks of geophysics; Todd (1955, p. 5–6; 1959, p. 225–228) summarizes the method and its use in ground-water studies.

This paper describes a modification of the methods ordinarily followed in seismic-refraction studies. An M–80 salute (a type of firecracker containing 1 gram of black powder) is used to produce the shock. Moreover, instead of using a linear series of geophones (seismometers) to detect the arrival of refracted waves generated by a shock at a single point, one geophone is used to detect the arrival of refracted waves generated by a linear series of successive shocks. These modifications are the result of experimentation during the course of a seismic survey in the Trace Creek basin, Humphreys County, Tenn.

The Trace Creek basin consists of a central valley bordered by low hills. The floor of the valley is underlain, in descending order, by a layer of unconsolidated fine to coarse rock debris, a layer of dense fine-grained rock material, and bedrock which is principally cherty limestone. The bordering hills are bedrock mantled by a thin and discontinuous layer of soil and rock debris. The average depth to the bedrock surface beneath the floor of the central valley is about 30 feet. In places, however, there are bedrock troughs, some of which are more than 100 feet deep and as much as 300 feet wide. The troughs seem to be steep walled and to extend across the valley in line with the north- to northwestward-trending tributaries of Trace Creek. The bedrock troughs and the valleys of the tributaries with which they are alined are thought to owe their existence to erosion along the best-developed fractures in the regional joint pattern.

## USE OF FIRECRACKERS

Because part of the surface water in Trace Creek and part of the ground water in the zone of saturation beneath the valley floor are believed to drain from the basin through open fractures associated with some of the bedrock troughs, a seismic survey was planned to determine the precise location and extent of the troughs and the probable lithology and water-transmitting capacity of the rock material filling them. Accordingly, portable seismic surveying equipment consisting of a sledgehammer, a timer, and two geophones was procured and several lines were surveyed. Although the plotted data produced curves of "textbook quality," data from test holes bored with an auger at selected points along the lines of survey showed that the data did not represent shock waves refracted from the bedrock surface. Instead, some data represented refractions from the

water table, and other refractions from interfaces within the material that mantles the bedrock. Failure to obtain shock-wave refraction from the bedrock surface probably was due to the failure of sledgehammer blows to produce shock waves of sufficient energy to travel through the full thickness of the mantling material and then be refracted back to a reasonably distant geophone. Furthermore, because of noise in the study area caused by highway, railroad, and air traffic and by wind and overhead electric power lines, the instrument had to be operated at low sensitivity settings and thus did not attain its potential effectiveness.

Anchor-bolt projectile guns, with and without projectiles, and other devices were used to produce shock waves of higher energy and to direct the waves downward, but these also proved unsuccessful. Use of dynamite caps was not considered because of the dangers involved in their use, and the resultant restrictive licensing requirement. After all these sources of energy proved inadequate, M–80 salutes were tested successfully.

The experimentation with firecrackers included determination of (1) the kind of switch or triggering device most suitable for starting the seismic timer at the exact moment of a detonation, (2) the size of charge needed for various distances from the geophones, (3) the other equipment and changes in procedure that would facilitate making a survey by this method, and (4) the precautions needed to ensure safe use of the method. These studies also demonstrated the overall utility and economy in the use of firecrackers for seismic surveying at shallow depths.

A dynamite-cap exploder that starts the timer and simultaneously detonates the firecracker by means of a squib (a small, low-power electrical cap manufactured by a chemical explosives company) was used to synchronize starting of the seismic timer with the explosion. An effort to use the timer-starting switch which is provided with the sledgehammer (by removing it and attaching it to a 50–lb steel plate that is placed over a firecracker about to be exploded) proved unsuccessful.

Preparation of an M–80 salute for use in seismic surveying requires removal of the fuse and insertion of a squib which has electrical leads. Squibs with 4-foot electrical leads may be purchased as a stock item. As the hole resulting from removal of the fuse is too small for the squib, a wooden punch (or pencil) is used to enlarge the hole until it admits the squib. Glue and tape are used to seal in the powder, to secure the squib in place, and to prevent absorption of moisture from the ground. The firecrackers are placed in holes punched in the ground with a crowbar, and the holes are backfilled to reduce upward loss of energy and as a safety precaution against blowout. Experiment shows that a single M–80 salute is not sufficient for distances of more than 700 feet from the geophone; when greater distances are involved, one or more salutes are taped to the one fitted with a squib. Figure 1 illustrates the components and assembly of firecracker charges for seismic surveying.

## SURVEYING WITH A SINGLE GEOPHONE

The procedure in making the first complete survey with firecrackers was the same as that followed when the sledgehammer was used, except that the two geophones were more widely separated and the distances between shock points were greater. The geophones were connected to the timer by means of an 800-foot and a 15-foot length of coaxial cable. Although the first survey was successful, it was felt that too much time was expended in laying the rather heavy and bulky coaxial cable (50 pounds) and in walking the length of that cable at least three times for each firecracker-detonation series. Furthermore, too much time was required to extend a line of survey and to assemble the equipment for overnight storage or for removal to the site of another survey. Accordingly, consideration was given to modification of the method followed in making the first successful survey by using one geophone and lightweight cable.

In surveying the second line, only one geophone was used and it was connected to the seismic timer by means of a 15-foot length of coaxial cable. The outside end of a 1,000-foot spool of twin-conductor cable (weight, 5 pounds) was connected to the exploder, which was situated near the timer. Cable was unrolled on a hand reel until the reel reached the nearest firecracker site, and there the other end of the cable (exposed at the center of one side of the reel) was attached, by means of clips, to the squib leads. After the firecracker was exploded and the traveltime of the resulting shock waves had been recorded the spool was carried to the next nearest firecracker site, where again the end of the cable was clipped to the squib leads. By proceeding in this fashion, only as much cable was unrolled as was needed to obtain sufficient data for computation of the depth to bedrock. Generally, the maximum depth from which refracted shock waves were recordable was about one-third of the horizontal distance between the geophone and the most distant firecracker-detonation site.

Figure 2 illustrates the modified method of seismic surveying and includes a sample plot of the data from which depths to the two indicated interfaces could be computed. Bedrock-depth or interface determinations may be spaced as closely as desired by resetting the geophone at appropriate distances from the original position and repeating the procedure outlined above. Each plotted point on the graph (upper diagram, fig. 2) repre-

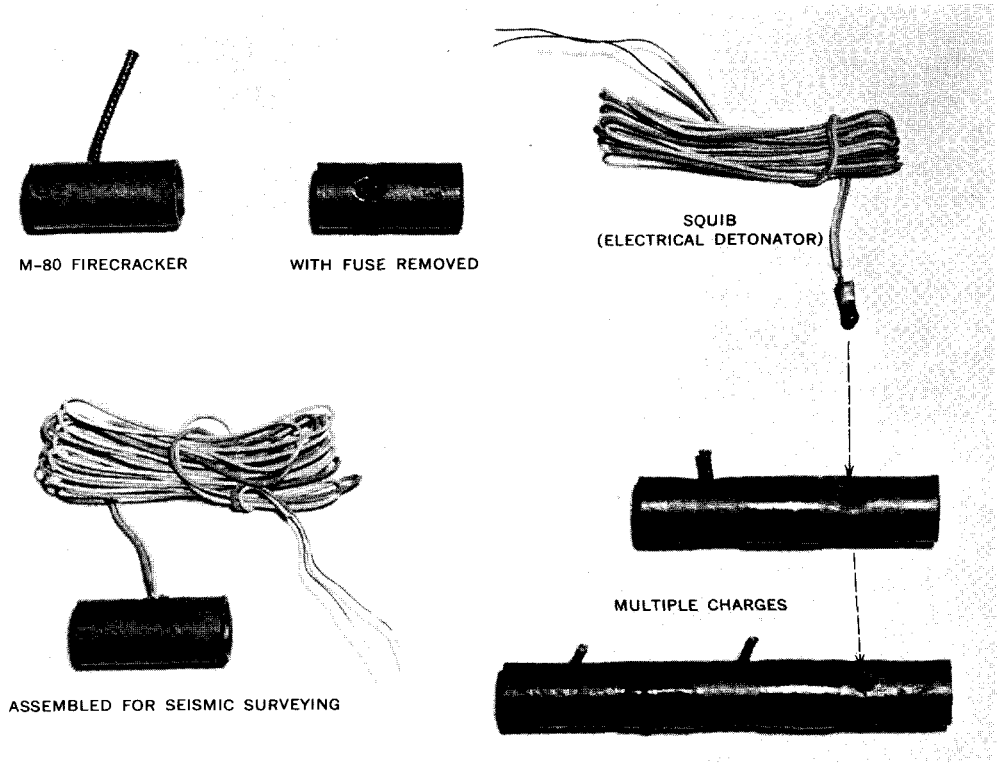


FIGURE 1.—Components of the firecracker charges, illustrating the preparation of single and multiple charges.

sents one shot in the ground, and the velocity curves ($v_1$, $v_2$, and $v_3$) are drawn through the best alined sets of points. The intersections of the velocity curves represent interfaces in the subsurface, and determine the $x_1$ and $x_2$ distances at which the depths to interfaces are computed. The manuals for the several instruments available differ slightly in procedural methods and computations, but all can be adapted to use firecrackers and the procedure described in this paper.

Modification of the method that was followed in making the first successful survey with firecrackers reduced the weight and bulk of the necessary equipment to less than half and afforded a saving in time of more than 25 percent. Further experimentation probably would lead to additional refinement of the method and even greater advantages. For example, it is possible that both the dynamite-cap exploder and squib could be dispensed with by using a loop of fine-gage wire to connect the firecracker to the starter outlet of the timer. The firecracker then would be detonated by igniting its fuse, and the explosion would break the circuit and thereby start the timer at the precise moment of the start of the shock wave. If buried deeper than

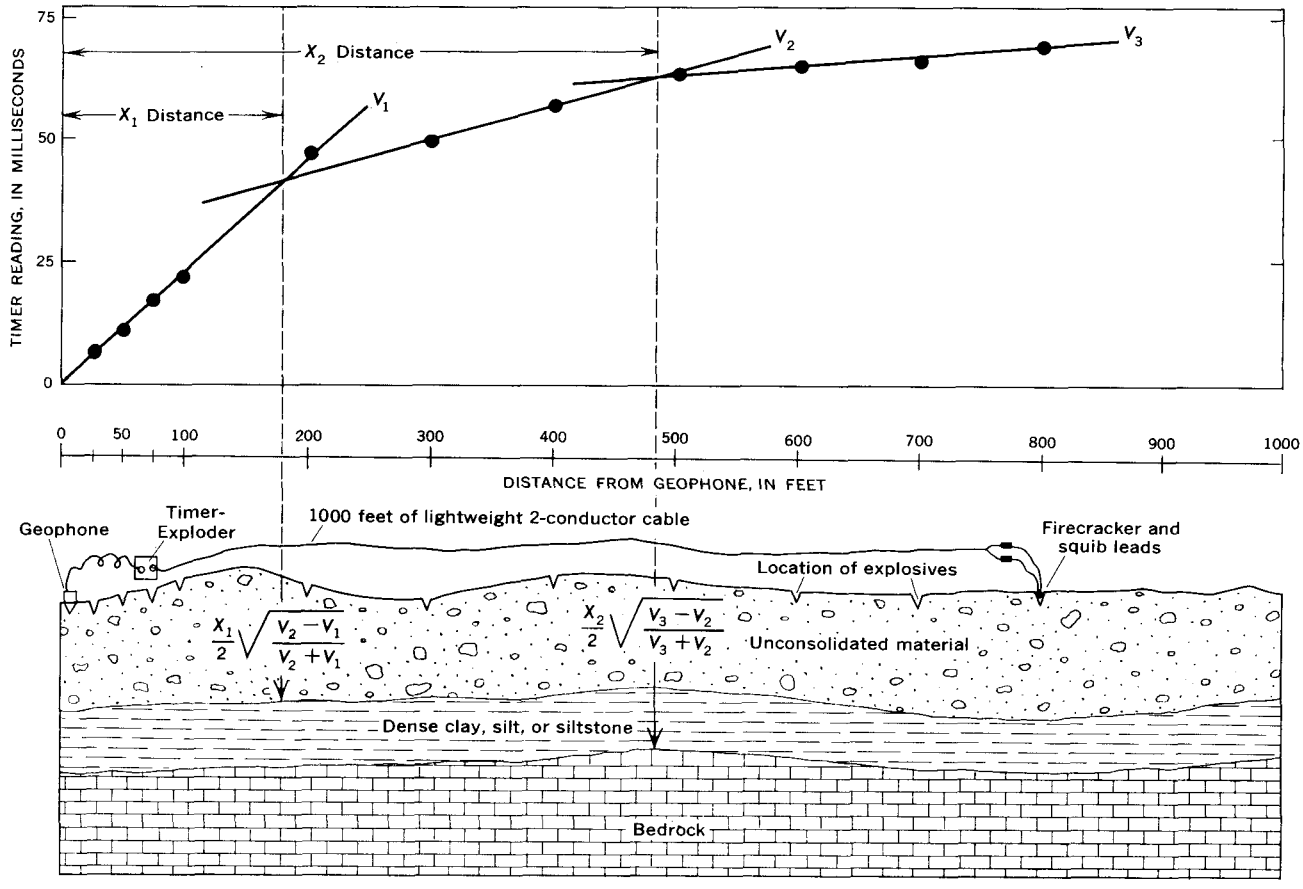


FIGURE 2.—Modified seismic-survey method using firecrackers and one geophone. Upper diagram, representative traveltime plot. Lower diagram, cross section showing disposition of survey equipment, explosive locations, and formulas used for computing depths to the indicated interfaces.

2 inches in the ground, the firecrackers obviously would need to be equipped with extra-long fuses.

Use of firecrackers for producing shock waves is safe and inexpensive. As the M–80 salutes cost (1965 prices) about $3.00 per hundred and the squibs about $25.00 per hundred, the cost of materials for each detonation was $0.28. Since completion of the survey in the Trace Creek basin, the manufacturer of the squib offered a similar electrical cap that probably would function equally as well and would cost only $3.00 per hundred thus reducing the cost of materials per detonation to $0.06.

## REFERENCES

Todd, D. K., 1955, Investigating ground water by applied geophysics: Am. Soc. Civil Engineers Trans., v. 81, separate 625, 13 p.

——— 1959, Ground water hydrology: New York, John Wiley & Sons, Inc., 336 p.

# RELATION BETWEEN BOUGUER GRAVITY ANOMALIES AND REGIONAL TOPOGRAPHY IN NEVADA AND THE EASTERN SNAKE RIVER PLAIN, IDAHO

By DON R. MABEY, Denver, Colo.

*Abstract.*—An analysis of the relation between Bouguer gravity-anomaly values and regional elevation for 57 gravity stations in Nevada indicates that the Bouguer anomaly value for stations not effected by low-density Cenozoic rocks is approximately equal to 3 mgals plus −0.032 mgal per ft multiplied by the average elevation within 64 km of the station. The analysis of local anomalies is facilitated by the removal of a regional variation, computed by this method, from the measured anomalies. A similar treatment appears applicable to data from the eastern Snake River Plain if 35 mgals is added to the computed anomaly value.

The correlation between gravity anomalies and regional topography was recognized by early workers in this field. Putnam (1894) and Gilbert (1900), studying the early pendulum gravity data in the United States, followed earlier work by Faye and applied a correction to the free-air anomaly for a slab of material with a thickness equal to the difference between the elevation of the pendulum station and the average elevation surrounding the station. This is equivalent to adding to the simple Bouguer anomaly the effect of a slab of material extending from sea level to the average elevation around the station. Putnam determined averaged elevations over circular areas 100 miles in radius and Gilbert over areas 30 miles in radius. They found that this correction produced anomalies that averaged near zero. Subsequently, several methods of computing isostatic reductions, based on regional topography, were developed, and the use of corrections based on simple average elevation was largely abandoned. (For discussion of the historical development of the idea of isostasy see Heiskanen and Vening Meinesz, 1958, p. 124–146.) Woollard (1959) presented a graph of worldwide data showing the correlation of Bouguer gravity values and surface elevation. This graph clearly shows an inverse dependence of the Bouguer anomalies on elevation, but the scatter is large.

The inverse correlation between regional topography and Bouguer gravity anomalies in part of the Basin and Range province has been described by the writer (Mabey, 1960) previously. A quantitative analysis of the correlation in the Nevada portion of this area has proved useful in the separation of local gravity anomalies from regional anomalies. The general techniques used for gravity studies in Nevada were found to be applicable to similar studies in the eastern Snake River Plain, Idaho.

## NEVADA

From about 10,000 gravity stations in Nevada, 57 were selected as being representative of the stations on pre-Tertiary bedrock. These stations are not greatly affected either by local anomalies produced by low-density fill underlying the basins, or by large terrain effects. The elevation of each station is known, and the average elevation of circular areas of four sizes around each station (within a radius of 16, 32, 64, and 128 kilometers, respectively) was determined. Observed gravity relative to the gravity at the airport base station at Ely, Nev., is known to within 0.5 milligals. Free-air and Bouguer corrections were computed by standard methods, assuming a density of 2.67 grams per cubic centimeter in the Bouguer reduction.

By the methods of least squares the linear relationships between (1) the Bouguer anomaly values and (2) the station elevation and elevations averaged over the four different-sized areas were determined. The results are summarized in table 1. As the area used in determining the average elevation is increased, the slope (milligals per foot) of the linear relationship becomes more negative, and the intercept at sea level increases. For an area with a radius of 128 km the slope is approximately equal to the negative Bouguer correction coefficient corresponding to a density of 2.67 g per $cm^3$; the intercept is near zero for a radius of 64 km. The standard deviation is lowest for a radius of 64 km but only slightly higher for 32 km.

U.S. GEOL. SURVEY PROF. PAPER 550-B, PAGES B108-B110

A plot of Bouguer anomaly values and elevations averaged over areas 64 km in radius is shown on figure 1. With one exception, Bouguer anomaly values for all the stations are within 15 mgals of the line determined to be the best linear fit for the data. The exceptional station is in an extensive area of high-density bedrock.

TABLE 1.—*Summary of linear relation between Bouguer anomaly values and the average elevation of areas of different radius in Nevada*

| Radius (km) | Slope (mgals per ft) | Intercept (mgals) | Standard deviation (mgals) | Range in elevation (feet) |
|---|---|---|---|---|
| 0 | −0.022 | −54 | 16.1 | 1,400–7,500 |
| 16 | −.024 | −37 | 12.6 | 2,100–7,500 |
| 32 | −.026 | −29 | 9.9 | 2,100–7,300 |
| 64 | −.032 | +3 | 8.2 | 2,600–6,800 |
| 128 | −.034 | +16 | 13.4 | 3,000–6,600 |

The Bouguer anomaly value for locations in Nevada not effected by basin fill or other local anomalous masses can generally be predicted within 15 mgals by multiplying the average elevation relative to sea level of an area 64 km in radius around a station by −0.032 mgals per foot and adding 3 mgals, which is the intercept at sea level indicated in figure 1. Relative values over areas of several hundred square miles can usually be predicted within 5 mgals. In several areas in Nevada, study of the relation between Bouguer anomaly and regional elevation has proved to be an effective technique of isolating negative gravity anomalies associated with Cenozoic basins from the regional anomalies related to regional topography. The data from Nevada confirm the conclusion by Pakiser (1963, p. 5753) that: "For a region in isostatic equilibrium, no information on broad variations in crustal thickness can be obtained from gravity that cannot be inferred directly from regional variations in altitude above sea level."

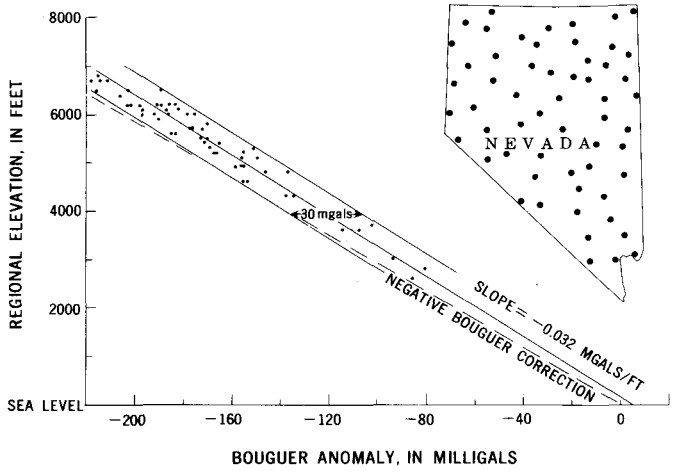


FIGURE 1.—Bouguer gravity anomaly and average elevation of areas 64 km in radius surrounding representative stations in Nevada. Map shows station locations. Linear relation was determined by method of least squares.

As an independent check of the application of this technique for estimating regional gravity anomalies, data from 12 U.S. Coast and Geodetic Survey pendulum stations in Nevada and adjoining parts of Utah and California were analyzed. The regional elevation was computed and a correction equal to the regional elevation multiplied by 0.032 mgals per foot minus 3 mgals was applied to the Bouguer anomaly. The results are summarized in table 2 and compared with the Pratt-Hayford isostatic anomalies. The data from these 12 stations indicate that the gravity values in this part of the Basin and Range province can be predicted as accurately by computing average elevation as by computing a Pratt-Hayford isostatic correction. Average elevations can be computed quickly and easily—isostatic corrections require much greater effort, unless the complete data for terrain corrections using Hayford zones A–O are available.

TABLE 2.—*Average Bouguer anomaly corrected for regional topography and average isostatic anomalies for 12 U.S. Coast and Geodetic Survey pendulum stations in Nevada and adjacent parts of Utah and California*

[Pratt-Hayford anomalies from Duerksen (1949)]

| | Bouguer anomaly corrected for regional topography (mgals) | Pratt-Hayford anomaly (mgals) for depth of compensation of— | | | |
|---|---|---|---|---|---|
| | | 56.9 km | 96 km | 113.7 km | 96 km [1] |
| Average anomaly (without sign) | 8.5 | 8.3 | 15.7 | 19.6 | 12.5 |
| Average anomaly (with sign) | 0 | −4.7 | −14.3 | −18.6 | −9.7 |

[1] Corrected for indirect effect.

## EASTERN SNAKE RIVER PLAIN, IDAHO

Gravity surveys of the Snake River Plain (Hill and others, 1961; Hill, 1963; LaFehr and Pakiser, 1962; and Bonini, 1963) have defined an extensive gravity high over the plain upon which are imposed local anomalies. The extensive high is obviously related to the low topography of the plain and probably reflects isostatic compensation here. Before the local gravity anomalies that are superimposed on the regional anomaly can be analyzed, they must be separated from the more extensive anomaly. Hill (1963), in an analysis of the data from the western part of the plain, assumed a regional anomaly based on the extrapolation of regional gradients on the sides of the plain. In the eastern part of the Snake River Plain an attempt has been made to remove the portion of the anomaly obviously associated with topography by computing average elevations and

applying a correction for the average elevation to the Bouguer anomaly values.

From low values of about −230 mgals over the high topography to the north, the Bouguer anomaly values rise over the Snake River Plain to a maximum of −70 mgals in the western part and about −130 mgals in the eastern part. South of the plain the values decrease, but not as markedly as to the north. A profile trending north-northwest across the plain near Pocatello, Idaho, illustrates the general character of the anomaly in the eastern Snake River Plain (fig. 2).

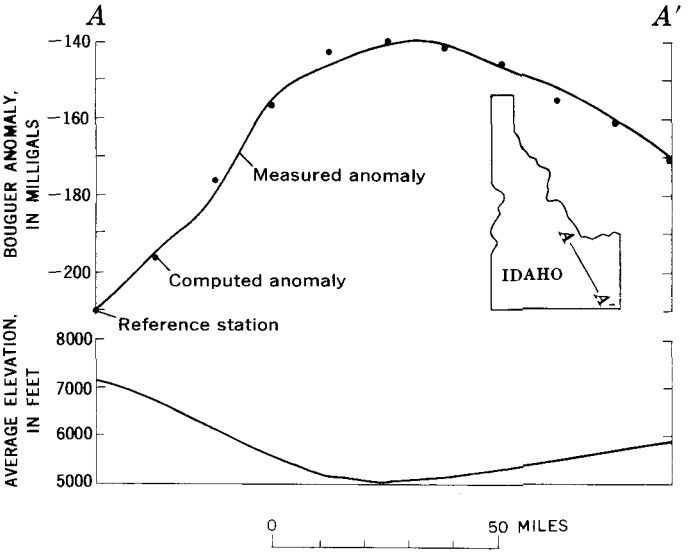


FIGURE 2.—Bouguer gravity profile $A$–$A'$ across the eastern Snake River Plain. Elevations are averaged over areas 64 km in radius. Computed anomaly values were obtained by adding the Bouguer anomaly at the reference station to the product of the negative Bouguer correction coefficient (−0.034 mgal per ft for $\rho = 2.67$ g per cm$^3$) times the difference between the average elevation around the point and the average elevation around the reference station.

In an effort to determine how much of the anomaly over the plain was directly related to the regional topography, average elevations were computed for circular areas 64 km in radius. The northwest end of the profile was taken as the reference station, and the difference between the average elevation of this point and of points at 20-km intervals along the profile was determined. This elevation difference multiplied by the negative Bouguer correction coefficient (−0.034 mgal per ft) was added to the anomaly value of the reference station. The good agreement between this computed anomaly and the measured anomaly indicates that the anomaly making up the regional high over this part of the Snake River Plain is closely related to the regional topography. Local residual anomalies computed by removing this regional anomaly probably reflect near-surface mass anomalies. However, a significant part of the regional anomaly may also reflect extensive mass anomalies that may extend to near the surface but which are systematic with topography.

Along the profile in figure 2 all the Bouguer anomaly values are about 35 mgals higher than would be computed by multiplying the average elevation by the negative Bouguer correction coefficient. However, the relative Bouguer anomaly correlates well with the relative average elevation along the profile. The generally high Bouguer anomaly values in eastern Idaho relative to the values in Nevada at similar regional elevations illustrate the necessity of investigating the relation between average elevation and gravity anomalies on a region-by-region basis rather than attempting to determine a universal relationship that can be applied to all areas.

## REFERENCES

Bonini, W. E., 1963, Gravity anomalies in Idaho: Idaho Bur. Mines and Geology Pamph. 132.

Duerksen, J. A., 1949, Pendulum gravity data in the United States: U.S. Coast and Geod. Survey Spec. Pub. 244, 218 p.

Gilbert, G. K., 1900, Notes on the gravity determinations reported by Mr. G. R. Putman: Philos. Soc. Washington Bull., v. 13, p. 31–75.

Heiskanen, W. A., and Vening Meinesz, F. A., 1958, The earth and its gravity field: New York, McGraw Hill, 470 p.

Hill, D. P., 1963, Gravity and crustal structure in the western Snake River Plain, Idaho: Jour. Geophys. Research, v. 68, no. 20, p. 5807–5819.

Hill, D. P., Baldwin, H. L., Jr., and Pakiser, L. C., 1961, Gravity, volcanism, and crustal deformation in the Snake River Plain, Idaho: Art. 105 *in* U.S. Geol. Survey Prof. Paper 424–B, p. B248–B250.

LaFehr, T. R., and Pakiser, L. C., 1962, Gravity, volcanism, and crustal deformation in the eastern Snake River Plain, Idaho: Art. 141 *in* U.S. Geol. Survey Prof. Paper 450–D, p. D76–D78.

Mabey, D. R., 1960, Regional gravity survey of part of the Basin and Range province: Art. 130 *in* U.S. Geol. Survey Prof. Paper 400–B, p. B283–B285.

Pakiser, L. C., 1963, Structure of the crust and upper mantle in the western United States: Jour. Geophys. Research, v. 68, no. 20, p. 5747–5756.

Putman, G. R., 1894, Relative determinations of gravity with half-second pendulums, and other pendulum investigations, *in* Report of the Superintendent of the U.S. Coast and Geodetic Survey showing the progress of the work during the fiscal year ending with June 1894: U.S. Coast and Geod. Survey, pt. II, App. 1, p. 9–50.

Woollard, G. P., 1959, Crustal structure from gravity and seismic measurements: Jour. Geophys. Research, v. 64, no. 10, p. 1521–1544

# PRELIMINARY REPORT ON REGIONAL AEROMAGNETIC ANOMALIES IN NORTHWESTERN MONTANA

By M. R. MUDGE, G. D. ROBINSON, and G. P. EATON, Denver, Colo.

*Abstract.*—Two large north-northwesterly trending magnetic anomalies occur on four widely spaced aeromagnetic traverses in northwestern Montana. One anomaly extends at least 60 miles along the western flanks of the Sawtooth and the Lewis and Clark Ranges. It is broad and has a gently sloping profile and a maximum amplitude of 700 gammas. A distinct gravity anomaly coincides with this magnetic anomaly. Thirty miles to the east, another magnetic anomaly extends for at least 40 miles along the western border of the High Plains. This anomaly is narrow, has a steep profile with a maximum amplitude of 1,600 gammas, and is not associated with a distinct gravity anomaly.

Reconnaissance aeromagnetic flights were made in 1964 over a part of northwestern Montana (fig. 1). Profiles made from 4 flights spaced approximately 20 miles apart and flown at constant barometric elevation of 8,500 feet indicate two large linear anomalies in the eastern segments of the flight lines (figs. 2 and 3). Both anomalies are conspicuous in the three northern flight lines, but only the western anomaly can be identified with assurance on the southern line. Owing to heavy cloud cover which hampered navigation and location during the survey along the southern line, the accuracy and significance of the data along this line are uncertain. The two anomalies are described briefly below and are interpreted in a preliminary fashion.

The magnetic data are supplemented by regional gravity data made available through the courtesy of the 1381st Geodetic Survey Squadron, Air Photographic and Charting Service, U.S. Air Force. The western high magnetic anomaly coincides with a high gravity anomaly. In addition, a large northerly trending low gravity anomaly is present near the west end of the profiles shown on figures 2 and 3 (west of the western high magnetic anomaly). This gravity anomaly is not accompanied by a magnetic anomaly. It appears to project southward toward a large quartz monzonite stock exposed east of Missoula and may be related to a buried northern extension of the stock.

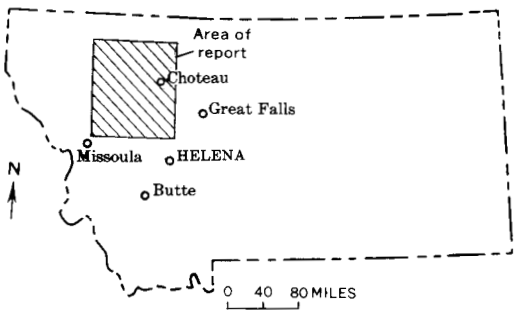


FIGURE 1.—Index map of Montana.

## WESTERN MAGNETIC ANOMALY

The western anomaly (figs. 2 and 3) is a broad asymmetrical positive magnetic anomaly with a maximum residual value of 700 gammas. The anomaly trends about N. 10° W. for 60 miles along the Lewis and Clark Range. The region of this anomaly is underlain mainly by fine-grained sedimentary rocks of the Missoula Group (Belt Series) of late Precambrian age, in thrust plates that dip gently westward (fig. 2).

Estimates of the depth of the rocks causing the anomalies along the three northern lines suggest that the source of the western anomaly lies 7,500 to 10,000 feet below the surface. The method and gradients of total magnetic intensity of Vacquier and others (1951, figs. A64, A65, A71, and A73) were used in calculating the depths of the source rocks. These estimates of depth may be in error by as much as 4,000 feet.

The coincidence of the positive regional gravity (fig. 3) anomaly with the western magnetic anomaly indicates the presence, at depth, of an elongate body of relatively dense rock with high magnetic susceptibility, possibly gabbro or a related rock. Gabbroic rocks occur in small isolated stocks a few miles south of flight line 1 (fig. 2) and are common elsewhere in the region, suggesting that gabbro may be present at depth

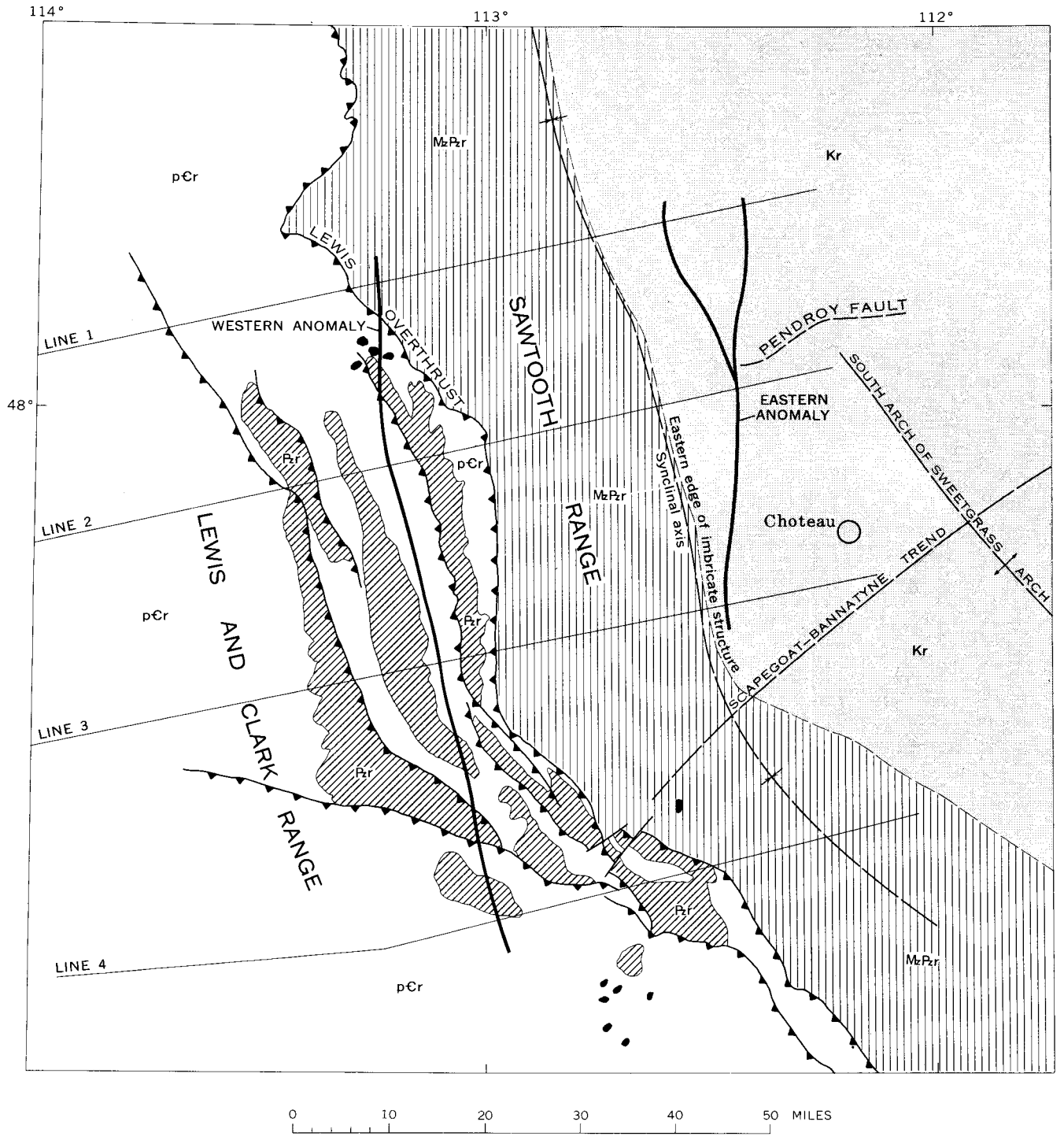


FIGURE 2.—Generalized geologic map of part of northwestern Montana, modified from Ross and others (1955) and Clapp (1932), showing the location of flight lines 1–4 of the aeromagnetic survey. p€r, Precambrian rocks; Pzr, Paleozoic rocks in thrust sheets; MzPzr, Mesozoic and Paleozoic rocks with imbricate structure and many isoclinal folds in eastern part; Kr, Upper Cretaceous rocks with large broad open folds; small black areas are stocks (mostly of quartz monzonite and gabbro). Major thrust faults shown with sawteeth on upper plate. The Scapegoat-Bannatyne trend (Alpha, 1955, p. 131) is a linear series of structural highs that involve the Precambrian crystalline basement. Heavy lines are drawn along the geometric center of the two magnetic anomalies.

here. The areal extent of the magnetic and gravity anomalies suggests a body of batholithic dimensions.

Superimposed on the profile of the western anomaly are small-scale irregularities that coincide with exposed mafic sills in the Belt rocks. Most of these sills are believed to be of late Precambrian age. However, the irregularities on the eastern flank of the western anomaly on line 3 are related to a pile of mafic sills of Late Cretaceous age.

## EASTERN MAGNETIC ANOMALY

The eastern magnetic anomaly has a double-peaked maximum of about 1,400 gammas on flight line 1, a single maximum of more than 1,600 gammas on line 2, and a broad high of diminished amplitude on line 3. Line 4 ends at or near the crest of what may be a southerly extension of this anomaly. The anomaly is at least 40 miles long and underlies the area west and northwest of Choteau, Mont. (fig. 1 and 2).

The top of the rocks producing the eastern anomaly is estimated to lie at the following depths: line 1—8,000 feet (± 4,000 feet); line 2— 9,300 feet (± 5,000 feet), and line 3—22,000 feet (± 8,000 feet).

The general regional stratigraphy and structure and data from wells suggest that the base of the Paleozoic section beneath the crest of the eastern anomaly on flight lines 1, 2, and 3 is at depths of approximately 9,200, 7,600, and 9,000 feet, respectively, and that stratified rocks of the upper Precambrian Belt Series are thin or absent. These figures, which for lines 1 and 2 are in fair agreement with the crude estimates based on the magnetic data, suggest that the top of the eastern anomaly source lies near the base of the Paleozoic section. The discrepancy in depth between geologic and gravity data on line 3 may indicate that the magnetic mass is at greater depth, possibly in the lower Precambrian metamorphic rocks. Both the depth and shape of the anomaly rule out the possibility that it is caused by near-surface or exposed beds of titaniferous magnetite in the widespread Upper Cretaceous Virgelle Sandstone (Wimmler, 1946).

The eastern, larger amplitude, magnetic anomaly is steeper and more symmetrical than the western anomaly. It has only a small residual gravity anomaly of 2 to 3 milligals associated with it, indicating that the rock mass responsible for the magnetic anomaly has little density contrast with its surroundings. This anomaly, therefore, is not caused by a large ultramafic mass that contrasts sharply in density with lower Paleozoic limestones and shales or that contrasts moderately with the andesite, trachyandesite, and diabase that underlie the Paleozoic rocks in the area (Alpha, 1955, p. 134). The gravity field beneath the crest of the eastern anomaly rises to the east in response to

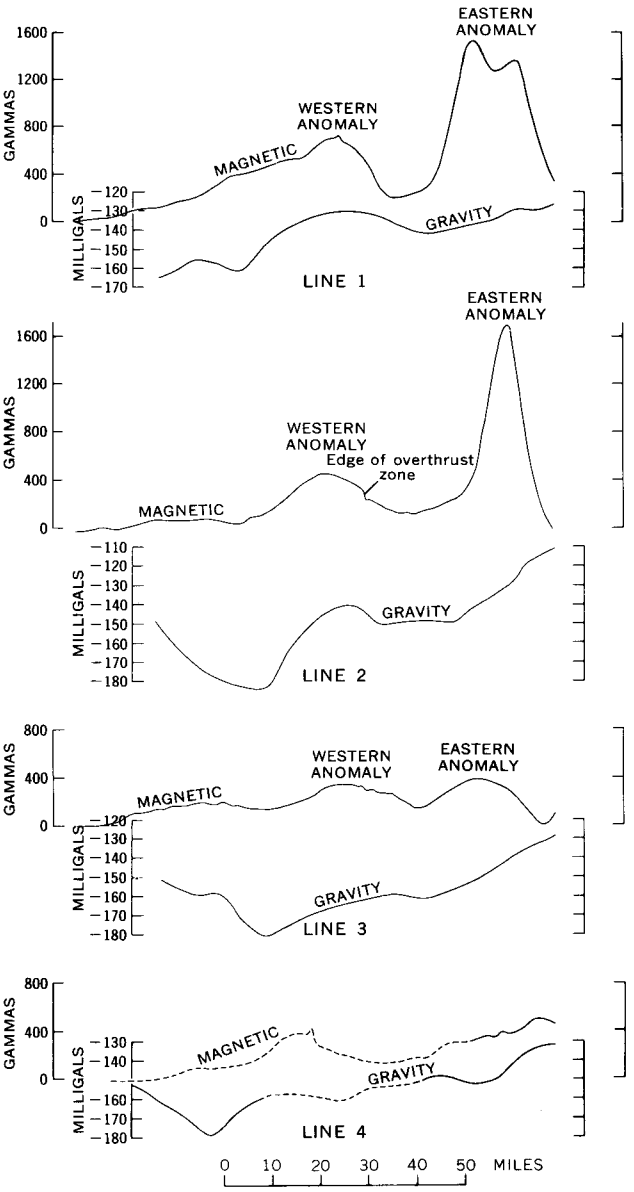


FIGURE 3.—Magnetic and gravity profiles along flight lines shown on figure 2. A correction for the earth's main field has been applied to the magnetic data. Dashed lines along line 4 reflect the uncertainty of the data along this traverse.

the Precambrian basement surface, which also rises along the south arch of the Sweetgrass arch (Dobbin and Erdmann, 1955). The basement surface also appears to be elevated to the southeast, where Precambrian crystalline rocks have been reported within 3,600 feet of the surface along the Scapegoat-Bannatyne trend (Alpha, 1955, p. 133–134). Thus the eastern magnetic anomaly seemingly lies along the flank of an uplifted part of the basement and because of its large amplitude cannot be assumed to reflect the basement surface. It may mark the buried eastern limit of the Belt Series. Many thousands of feet of Belt Series rocks crop out in the mountains a few miles west of

the trace of the anomaly, but none are known in wells that penetrate the crystalline basement a few miles to the east.

Probably the eastern magnetic anomaly is caused by a steep-sided subtabular mass of iron-rich rock of moderate density and regional extent. Rocks which meet the compositional requirements are not common, and more specific interpretation must await more detailed work. The eastern magnetic anomaly may be related to regionally metamorphosed iron formation. Such layered iron deposits are widespread in the Precambrian crystalline rocks in southwestern Montana (Geach, 1963, p. 78 and fig. 23). Unusually thick, extensive and steep-dipping iron formation, involved in tight folds or in fault blocks may be present at or near the base of the Paleozoic section and may produce the eastern anomaly.

Less likely sources for the anomaly are large nearly vertical dikes or sills. Such intrusive rocks may be of pre-Belt Series age, truncated erosionally at the base of the Paleozoic section, or alternatively of Late Cretaceous to middle Tertiary age, cutting the crystalline basement and perhaps rising into the lower part of the sedimentary column. The iron could be present in the plutonic rock, or in massive replacement deposits in adjacent country rock. There is some indirect evidence to support this latter possibility, inasmuch as replacement-type iron deposits near large intrusive bodies in Paleozoic carbonate rocks are numerous in the region to the southeast (Geach, 1963, p. 79–80 and fig. 23). Even the largest such deposits, however, as for example, those in the Running Wolf district about 50 miles southeast of Great Falls, are too small by several orders of magnitude (Roby, 1949) to offer direct analogues.

## REFERENCES

Alpha, A. G., 1955, The Genou trend of north-central Montana: Am. Assoc. Petroleum Geologists Rocky Mtn. Sec., Geological record, p. 131–138.

Clapp, C. H., 1932, Geology of a portion of the Rocky Mountains of northwestern Montana: Montana Bur. Mines and Geology Mem. 4, 30 p.

Dobbin, C. E., and Erdmann, C. E., 1955, Structure contour map of the Montana Plains: U.S. Geol. Survey Oil and Gas Inv. Map OM–178–A.

Geach, R. D., 1963, Iron, *in* U.S. Geological Survey, Mineral and water resources of Montana: U.S. Cong., 88th, 1st sess., Senate Comm. on Interior and Insular Affairs Rept., p. 77–80.

Roby, R. N., 1949, Investigations of Running Wolf iron deposits, Judith Basin County, Montana: U.S. Bur. Mines Rept. Inv. 4454, 7 p.

Ross, C. P., Andrews, D. A., and Witkind, I. J., 1955, Geologic map of Montana: U.S. Geol. Survey, 2 sheets.

Vacquier, Victor, Steenland, N. C., Henderson, R. G., and Zietz, Isidore, 1951, Interpretation of aeromagnetic maps: Geol. Soc. America Mem. 47, 151 p.

Wimmler, N. L., 1946, Exploration of Choteau titaniferous magnetite deposit, Teton County, Montana: U.S. Bur. Mines Rept. Inv. 3981, 12 p.

# GRANULITE AND PERIDOTITE INCLUSIONS FROM PRINDLE VOLCANO, YUKON-TANANA UPLAND, ALASKA

By HELEN L. FOSTER, ROBERT B. FORBES,[1] and DONAL M. RAGAN,[1]
Menlo Park, Calif.; College, Alaska

*Abstract.*—Lava of Prindle Volcano, an isolated alkali-olivine basalt cone in the Tanacross C–2 quadrangle, Yukon-Tanana Upland, Alaska, contains abundant peridotite and granulite inclusions. Prindle Volcano reinforces the evidence for the existence of a belt of eruptive centers of similar peridotite-bearing alkali-olivine basalt along the western margin of North America from Mexico to Alaska.

Prindle Volcano is a small inactive basaltic cone located on the southeast flank of the ridge which forms the interstream divide between the East Fork and the Dennison Fork of the Forty Mile River, Tanacross C–2 quadrangle, Yukon-Tanana Upland, Alaska (fig. 1). The base of the cone is about 3,300 feet above sea level. Peaks along the adjacent ridge rise to elevations exceeding 4,500 feet.

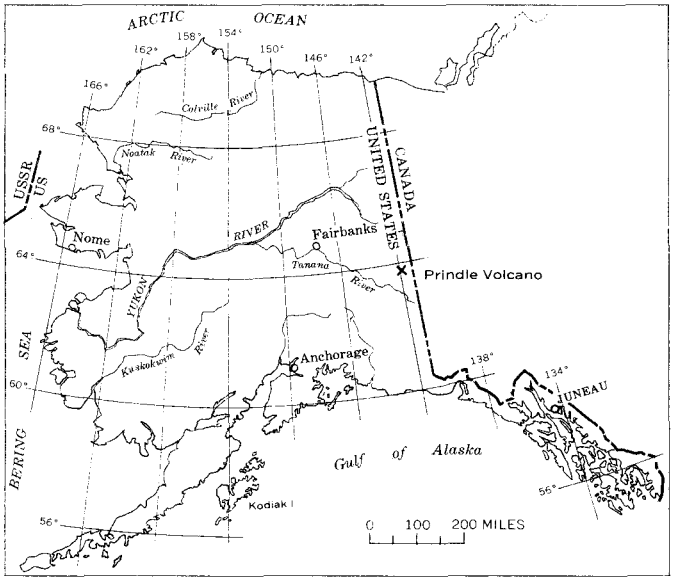


FIGURE 1.—Index map of Alaska, showing location of Prindle Volcano.

The volcano was first photographed and described by L. M. Prindle in 1905 (Mertie, 1931, p. 13, 39–40). It was again visited by geologists of the U.S. Geological Survey during the summers of 1963 and 1964. The cone is of particular interest because of its apparent youthfulness, its relative isolation from other occurrences of alkali-olivine basalt, and abundant ultramafic and granulite inclusions in the cone and adjacent flow.

The cone is approximately 3,000 to 3,500 feet in diameter at its base, and contains a crater about 300 feet deep, which is breached on the south (fig. 2). The highest elevation, 4,100 feet, is found on the northwest rim of the crater. A lava flow extends downslope from the breached crater to the southeast for approximately 4 miles, where it turns southwest and continues for 3 more miles along the west side of the valley of the East Fork.

The slopes of the cone are covered by grass, low bushes, and small spruce trees. Muskeg, containing

FIGURE 2.—Aerial view of Prindle Volcano. Ridge in background is composed of Birch Creek Schist. View north, 1963.

[1] Geophysical Institute and Geology Department, University of Alaska.

frost-wedge polygons and small ponds, mantles the crater floor, and permafrost is present at a depth of 2 feet. The lava flow in the valley is covered with trees.

The cone shows little evidence of dissection and frost action, which suggests that the eruptive activity occurred during Quaternary time.

## GEOLOGIC SETTING

The subvolcanic basement is composed of biotite and hornblende gneisses and schists, including augen gneiss with large feldspar porphyroblasts (Pelly Gneiss of Mertie, 1937, p. 203). The gneisses and schists have been intruded by fine- to medium-grained biotite-muscovite granite, porphyritic rocks, and pegmatite. Fine-grained biotite-muscovite granite underlies basalt at the southeastern base of the cone, and outcrops of similar granite occur on the ridge northwest of the cone. Porphyritic granitic rock crops out 1½ miles southeast of the volcano. The gneisses and schists that compose the ridges surrounding the cone are cut by granitic and pegmatitic dikes. Although mineral assemblages ranging from greenschist to amphibolite facies have been recognized in crystalline schists collected by the senior author during reconnaissance geologic mapping of areas adjacent to Prindle Volcano in the Tanacross quadrangle, granulite facies assemblages have not been detected.

The probable absence of exposed granulite facies terrane in the surrounding area is reinforced by petrographic data given by Mertie (1937, p. 48–52), which include amphibolite but not granulite facies mineral assemblages.

The gneisses and schists were mapped as Birch Creek Schist by Mertie (1937, p. 47 and pl. 1) and were considered by him to be of early Precambrian age (Mertie, 1937, p. 55). New regional stratigraphic and structural evidence has suggested that some units currently mapped as Birch Creek Schist may be younger (Forbes, 1960, p. 2085). The Birch Creek Schist is, at least in part, polymetamorphic (Forbes, 1960, p. 2085), and the dates of the events are still in question.

The granitic rocks exposed near the base of Prindle Volcano are similar in lithology and occurrence to those of Mesozoic age (Mertie, 1937, p. 210; Wasserburg and others, 1963, p. 258–259) cropping out elsewhere in the Yukon-Tanana Upland.

## HOST BASALT

The cone and lava flow are composed of vesicular alkali-olivine basalt, made up of (1) clinopyroxene, (2) olivine, (3) opaque minerals, and (4) a fine-grained to microcrystalline groundmass believed to contain occult nepheline and potassium feldspar. Plagioclase feldspar is conspicuously rare or absent. Two bulk chemical analyses, one of the scoriaceous phase (PVF–1–1–63) and the other of the flow phase (PVF–2–9–63) of the basalt, are shown in table 1, together with their respective norms.

TABLE 1.—*Bulk chemical analyses and molecular norms of basalt from the cone of Prindle Volcano*

[Analyst: M. Chiba, Japan Analytical Chemistry Institute, Tokyo, 1964]

| | PVF 1–1–63 (scoriaceous phase) | PVF 2–9–63 (flow phase) |
|---|---|---|
| **Chemical analyses (weight percent)** | | |
| $SiO_2$ | 42. 87 | 42. 84 |
| $Al_2O_3$ | 11. 17 | 10. 45 |
| $Fe_2O_3$ | 7. 98 | 4. 64 |
| FeO | 4. 78 | 8. 14 |
| CaO | 9. 56 | 9. 96 |
| MgO | 13. 82 | 14. 36 |
| $Na_2O$ | 3. 71 | 3. 78 |
| $K_2O$ | 1. 88 | 1. 83 |
| $H_2O+$ | . 39 | . 15 |
| $H_2O-$ | . 45 | . 27 |
| $TiO_2$ | 2. 71 | 2. 67 |
| $P_2O_5$ | . 96 | 1. 03 |
| MnO | . 16 | . 17 |
| $Cr_2O_3$ | . 06 | . 07 |
| Total | 100. 50 | 100. 36 |
| **Molecular norms** | | |
| Or | 10. 95 | 10. 59 |
| Ab | 9. 03 | 3. 89 |
| An | 8. 16 | 6. 01 |
| Ne | 14. 29 | 17. 61 |
| Di | 25. 95 | 28. 63 |
| Ol | 18. 49 | 22. 74 |
| Mt | 5. 74 | 4. 75 |
| Il | 3. 72 | 3. 64 |
| Ap | 1. 98 | 2. 10 |
| Ht | 1. 65 | . 00 |
| | 99. 96 | 99. 96 |

The comparative analyses are similar, but the flow phase is less oxidized than the scoriaceous phase, as shown by the difference in the $Fe_2O_3$:FeO ratio. The flow phase of this basalt contains 17.61 percent normative nepheline, and because of the presence of both nepheline and olivine in the norm, it is clearly an alkali-olivine basalt, as defined by Yoder and Tilley (1962, p. 352), or a basanitoid as defined by Macdonald and Katsura (1964, p. 86). Although nepheline is present in the norm, it has not been detected in the groundmass of the basalt.

## PERIDOTITE INCLUSIONS

The basalt of Prindle Volcano is rich in phenocrystal and xenocrystal olivine as well as inclusion aggregates. Xenocrystal material also includes orthopyroxene, clinopyroxene, spinel, and plagioclase. The xenocrysts

have apparently been derived by attrition from an unusually rich suite of ultramafic and feldspathic inclusions.

The ultramafic inclusions range in size from xenocrysts to rounded polycrystalline masses up to 5 inches in diameter. Most of the ultramafic inclusions are relatively unaltered, but some specimens contain secondary iddingsite along olivine grain boundaries, and orthopyroxene grains occasionally display marginal clinopyroxene reaction zones in contact with the host basalt.

Peripheral alteration zones are more commonly developed in the feldspathic (granulite) inclusions, as characterized by the partial fusion of quartz and plagioclase grains, and albite exsolution in potassium and plagioclase feldspar.

Although Ross and others (1954, p. 696–703), Forbes and Kuno (1965), and others have discussed the dominance of the assemblage diopside-enstatite (bronzite)-olivine-spinel in worldwide peridotite inclusion suites, several other volumetrically important peridotite mineral assemblages occur in the Prindle inclusion suite. Assemblages recognized to date include:

olivine-orthopyroxene-clinopyroxene-spinel
olivine-orthopyroxene-spinel
olivine-clinopyroxene-spinel
clinopyroxene-spinel
orthopyroxene-spinel

The textures and the fabrics of the inclusions are typical of those found in other peridotites. Variations in the textures of the different inclusion types are chiefly related to the proportion of two types of olivine grains. Coarse grains (up to 2 mm) with ragged boundaries and abundant deformation banding are often markedly inequidimensional; fabrics defined by these grains show no evidence of preferred form orientation. These large grains are surrounded by smaller (less than 1 mm), equidimensional grains which display little or no evidence of straining. Characteristically, these small second-generation grains have straight grain boundaries that meet at angles of approximately 120°. These same textures and structures have been found in other inclusions (Talbot and others, 1963, p. 164) and in intrusive dunite masses (Ragan, 1963, p. 563), and they indicate solid-state deformation and recrystallization, at least in the later history of the rock.

The fabric of the smaller olivine grains in several samples was determined. Crystallographic orientations of 50 grains of approximately uniform size were measured. Partial diagrams, using measurements from widely spaced traverses, were constructed; these diagrams showed the same basic patterns thus demonstrating the statistical homogeneity of the fabric on the scale of a single thin section. Crystallographic Z forms a point maximum; X forms a broad girdle approximately to the Z maximum, and Y, though with greater scatter, also shows participation with the girdle. Identical patterns of preferred orientation have also been found in other peridotite inclusions (Talbot and others, 1963, p. 167) and in intrusive bodies (Battey, 1960, p. 720).

## GRANULITE INCLUSIONS

Many of the fragments in the suite of inclusions are not peridotite, but crystalline schists of the granulite facies. Gneissose structure is common in these fragments as defined by the preferred orientation of pyroxene and the alternating compositional layers of pyroxene and plagioclase; the texture is typically crystalloblastic. The assemblages are characterized by hypersthene and (or) clinopyroxene and plagioclase.

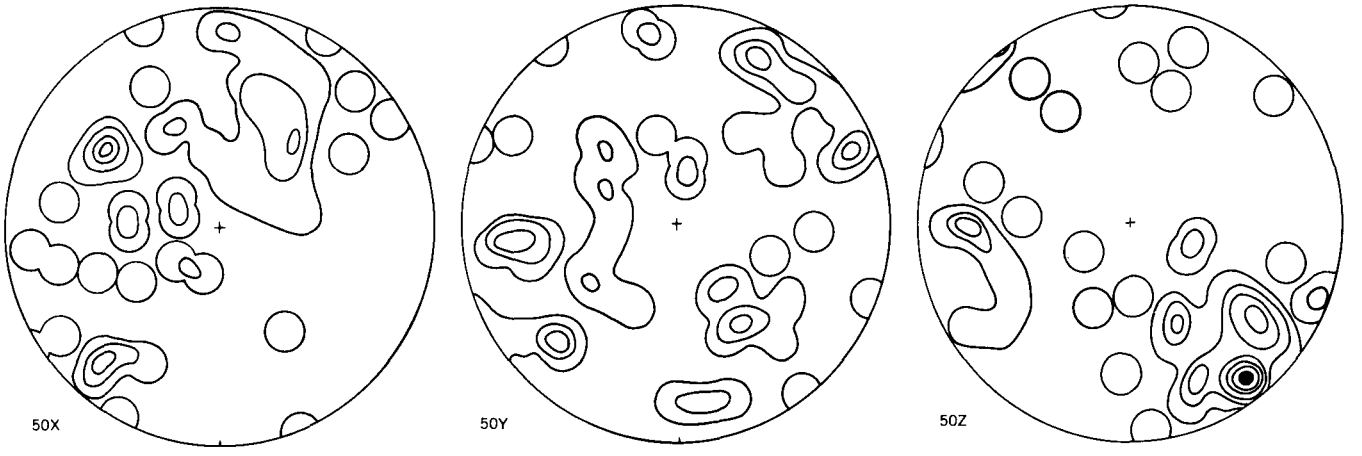


FIGURE 3.—Partial orientation diagrams of crystallographic X, Y, and Z for 50 olivine grains from inclusions in basalt from Prindle Volcano. Contours are spaced at 2-percent intervals, that is, 2, 4, 6 percent, and so forth, per 1 percent of area. (Equal area net, lower hemisphere.)

Mineral assemblages recognized to date include the following:

plagioclase-clinopyroxene-carbonate
plagioclase-clinopyroxene-carbonate-quartz
hypersthene-andesine-quartz
plagioclase-clinopyroxene-hypersthene-quartz
plagioclase-clinopyroxene-hypersthene
plagioclase-hypersthene-quartz

Accessory minerals include apatite, zircon, magnetite, and rutile. Minor sanidine has been detected in some of the above assemblages, but the role of sanidine as a stable coexistent phase remains in doubt, as secondary annealing from contact metamorphism may have recrystallized earlier potassium feldspar under conditions of the sanidinite facies. However, the uniform distribution of sanidine grains throughout the inclusions, seems to argue against a contact metamorphic origin.

Micas and amphiboles (hydrous phase) are absent. The occurrence of carbonate and quartz in some assemblages, without wollastonite, probably indicates that $CO_2$ pressures were higher than those associated with the stability field of wollastonite. These findings are in harmony with the views of Fyfe and others (1958, p. 234) who have noted that "wollastonite and grossularite characteristically are absent from these facies [granulite facies]." The presence of quartz + carbonate without wollastonite in the assemblage plagioclase-clinopyroxene-carbonate-quartz further supports the granulite facies origin of the feldspathic inclusions.

## CONCLUSIONS

The occurrence of peridotite inclusions in the alkali-olivine basalt of Prindle Volcano reinforces the evidence for the existence of a regional belt of such occurrences along the western margin of the North American continent from Mexico to northwestern Alaska, and thence to the Pribilof and Kanaga Islands. Recently Forbes and Kuno (1965), in summarizing the regional petrology of inclusion-bearing alkali-olivine basalts, noted that over 200 of these occurrences are now known. The host basalts are characteristically alkali-olivine basalts with nepheline and (or) leucite in the norm, and a strong similarity exists between the bulk chemical compositions of the host basalts in both the continental and oceanic occurrences. The relative position of Prindle Volcano to other peridotite-inclusion localities is shown in figure 4.

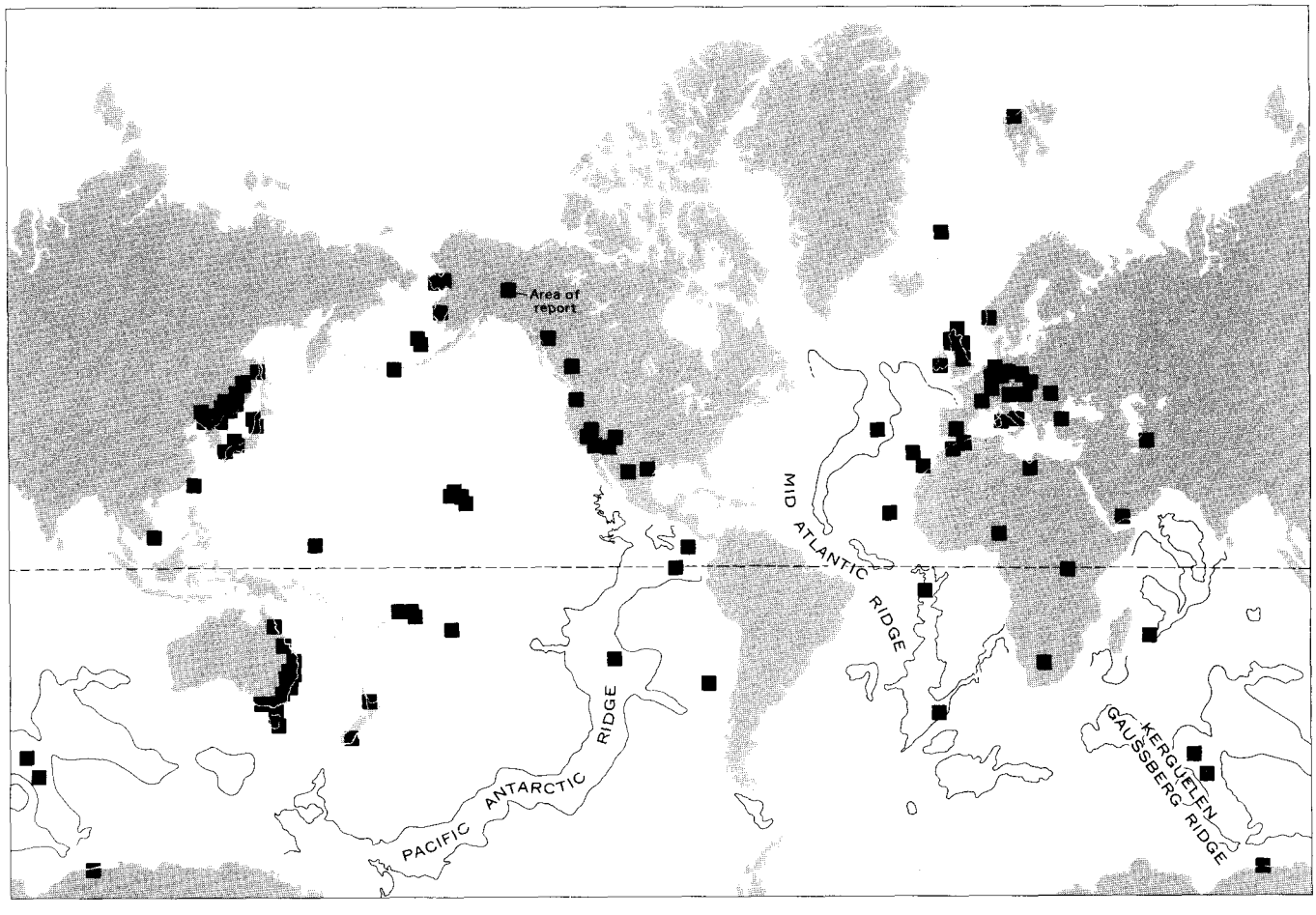


FIGURE 4.—Localities throughout the world where peridotite inclusions in basalt, including those from Prindle Volcano (area of report), are known. (After Forbes and Kuno, 1965.)

The coexistence of inclusions of hypersthene and hypersthene-diopside granulite, and peridotite, in the Prindle basalt is of great interest, as localities containing both inclusion types are rare. Eclogite fragments, such as those described from the basalt breccia pipes in eastern Australia (Lovering and Richards, 1964) may also exist in such occurrences; however, they have not been found in the Prindle basalt. It is possible that the granulite fragments were derived from the deep crust, as granulite-facies terrane is not known to occur in the surface exposures of the Birch Creek Schist in interior Alaska; however granulite-facies rocks have been reported from a fault block along the south margin of the Denali fault near the head of the Gulkana Glacier, about 130 miles southwest of Prindle Volcano (Hawkins and Ragan, 1965; Ragan and Hawkins, 1965).

Chemical and mineralogical studies of these inclusions and their constituent mineral phases are continuing, and it is hoped that the necessary evidence will be found to distinguish between a mantle versus a crustal origin for the inclusions.

## REFERENCES


Battey, M. H., 1960, The relationship between preferred orientation of olivine in dunite and the tectonic environment: Am. Jour. Sci., v. 258, no. 10, p. 716–727.

Forbes, R. B., 1960, Preliminary investigations of the petrology and structure of the Birch Creek Schist in the Fairbanks and Circle districts, Alaska [abs.]: Geol. Soc. America Bull., v. 71, no. 12, pt. 2, p. 2085.

Forbes, R. B., and Kuno, Hisashi, 1965, Regional petrology of peridotite inclusions and basaltic host rocks: Internat. Geol. Cong., 22d, New Delhi, 1964, Upper Mantle Symposium, 19 p.

Fyfe, W. S., Turner, F. J., and Verhoogen, John, 1958, Metamorphic reactions and metamorphic facies: Geol. Soc. America Mem. 73, 259 p.

Hawkins, J. W., Jr., and Ragan, D. M., 1965, Relict charnockitic rocks, granulite-facies gneisses, and migmatites in a polymetamorphic complex, Gulkana Glacier region, eastern Alaska Range; pt. 2, Petrology [abs.]: Geol. Soc. America Spec. Paper 82, p. 259.

Lovering, J. F., and Richards, J. R., 1964, Potassium-argon age study of possible lower-crust and upper-mantle inclusions in deep-seated intrusions: Jour. Geophys. Research, v. 69, no. 22, p. 4895–4901.

Macdonald, G. A., and Katsura, T., 1964, Chemical composition of Hawaiian lavas: Jour. Petrology, v. 5, no. 1, p. 83–133.

Mertie, J. B., Jr., 1931, A geologic reconnaissance of the Dennison Fork district, Alaska: U.S. Geol. Survey Bull. 827, 44 p.

——— 1937, The Yukon-Tanana region, Alaska: U.S. Geol. Survey Bull. 872, 276 p.

Ragan, D.M., 1963, Emplacement of the Twin Sisters dunite, Washington: Am. Jour. Sci., v. 261, no. 6, p. 549–565.

Ragan, D. M., and Hawkins, J. W., Jr., 1965, Relict charnockitic rocks, granulite-facies gneisses, and migmatites in a polymetamorphic complex, Gulkana Glacier region, eastern Alaska Range; pt. 1, Structure [abs.]: Geol. Soc. America Spec. Paper 82, p. 272.

Ross, C. S., Foster, M. D., and Myers, A. T., 1954, Origin of dunites and of olivine-rich inclusions in basaltic rocks: Am. Mineralogist, v. 39, no. 9–10, p. 693–737.

Talbot, J. L., Hobbs, B. E., Wilshire, H. G., and Sweatman, T.R., 1963, Xenoliths and xenocrysts from the lavas of the Kerguelen Archipelago: Am. Mineralogist, v. 48, no. 1–2, p. 159–179.

Wasserburg, G. J., Eberlein, G. D., and Lanphere, M. A., 1963, Age of the Birch Creek Schist and some batholitic intrusions in Alaska: Geol. Soc. America Spec. Paper 73, p. 258–259.

Yoder, H. S., and Tilley, C. E., 1962, Origin of basalt magmas; and experimental study of natural and synthetic rock systems: Jour. Petrology, v. 3, no. 3, p. 342–532.

# OCCURRENCE AND IDENTIFICATION OF JORDISITE AT AMBROSIA LAKE, NEW MEXICO

By HARRY C. GRANGER and BLANCHE L. INGRAM, Denver, Colo., Washington, D.C.

*Abstract.*—Certain black-stained zones in sandstone associated with primary uranium ore bodies at Ambrosia Lake, N. Mex., contain as much as several tenths of a percent molybdenum. Chemical and X-ray studies of impure separates of the black material indicate that it contains appreciable amounts of the amorphous molybdenum disulfide, jordisite.

Molybdenum is a common minor constituent of the primary uranium ores of the Ambrosia Lake district, New Mexico, and, locally, black-stained zones in sandstone associated with the uranium ore bodies contain as much as several tenths of a percent molybdenum. This paper reports results of preliminary parts of the investigation consisting of separation and chemical analyses of the molybdenum-rich material. The results tentatively confirm that the mineral is jordisite (Granger and others, 1961; Granger, 1963), and we will refer to it as jordisite throughout this paper.

## OCCURRENCE

At Ambrosia Lake, jordisite occurs on sand grains as an extremely fine-grained dark mineral coating that thoroughly stains the rock. Many of the jordisite-stained zones are jet black but some are brown or brownish black, perhaps because of closely associated dispersed organic material.

Much of the jordisite occurs in medium-grained to coarse-grained sandstone that sparkles brilliantly as light is reflected from pyramidal crystal faces on authigenic quartz overgrowths. Jordisite is nearly as common, however, in finer grained sandstone without quartz overgrowths and, in some places, impregnates mudstone.

Much of the jordisite is distributed zonally around unoxidized parts of the primary uranium ore bodies, or prefault ore (Granger and others, 1961; Granger, 1963). The distribution is spotty and erratic, but jordisite-rich zones are commonly within 5 feet either above or below a uranium ore layer or within a few tens of feet beyond the lateral termination of an ore layer. In some places, however, jordisite-rich bodies are partly to completely enclosed by primary uranium ore.

Jordisite in zones outside but near the uranium ore layers in sandstone occurs in two ways: (1) in irregular deposits as streaks and in feathery patterns along cross-laminae, and (2) as deposits with sharp, rounded boundaries in which the rock is more completely and uniformly stained. Both types of deposits tend to be elongate subparallel to the stratification. At some places the second type is also completely or partly enclosed by uranium ore. In addition, much of the primary uranium ore, whether it encloses distinct jordisite deposits or not, contains anomalous amounts of molybdenum, probably in the form of jordisite disseminated within it.

In some places the jordisite-rich rock also contains anomalous amounts of selenium, probably largely in the form of ferroselite ($FeSe_2$) which has been recognized in several mines in the Ambrosia Lake district.

Table 1 gives the sample localities and shows the correlation among sample numbers.

## SEPARATION OF THE JORDISITE

### Procedure

Because it occurs as a stain or in colloid-size particles we were unable to obtain a clean concentrate of jordisite. However, by leaching the sample with hydrofluoric acid, as described by Neuerburg (1961), but not evaporating the residue to complete dryness, undue oxidation of jordisite was prevented. The residue was recovered by centrifuging and decanting; it was then dried and screened. Most of the pyrite and zircon still present in the powder were removed by additional centrifuging in bromoform. The resulting impure concentrates are samples 1a, 2, 3, and 4. Sample 1b was obtained by an additional heavy-liquid separation

TABLE 1.—*Sample localities and correlation of sample numbers*

| Sample No. | | | | Locality | Occurrence |
|---|---|---|---|---|---|
| This report | Field | Denver | Washington | | |
| 1a | 26 G 58b | 268940 | 161733 | Marquez mine, sec. 23, T. 13 N., R. 9 W., at mine coord. S 2605–W 2175, ≈6,705 ft elev. | Molybdenum-rich rock between 3.3 and 4.5 ft above a primary uranium ore layer. |
| 1b | 26 G 58b | 268940 | 161734 | do | Do. |
| 2 | 26 G 58c | 268941 | 161735 | do | Molybdenum-rich rock between 2.2 and 3.0 ft above a primary uranium ore layer. |
| 3 | 37 G 61a | 294458 | 161736 | Sandstone mine, sec. 34, T. 14 N., R. 9 W., at U.S. Atomic Energy Comm. coord. 314,040 N.–547,500 E., ≈6,140 ft elev. | Middle of a molybdenum-rich body within a primary uranium ore layer. |
| 4 | 37 G 61b | 294459 | 161737 | do | Margin of a molybdenum-rich body within a primary uranium ore layer. |

(methylene iodide) of molybdenum-bearing material still remaining in the pyrite-rich fraction of sample 1.

### Efficiency of the separatory procedure

During the HF treatments the initial solutions turned blue, and during subsequent evaporations on the steam bath a blue stain was commonly noted on the walls of the polyethylene beakers indicating that some molybdenum was continually being oxidized and lost. Each time the residue was evaporated to near dryness, a faint $SO_2$ odor was also detected. It, therefore, seemed pointless to analyze each sample quantitatively and weigh the separates to determine losses incurred by the separatory procedure.

The 0.45-g separate from sample 3 was the only separate weighed. On the basis of the analyses in tables 2 and 4, only about 20 percent of the Mo and 70 percent of the Se were recovered. Similar losses were probably incurred during preparation of the other separates.

### Characteristics of the jordisite separates

The jordisite concentrates have the general appearance of lamp black. Viewed under the microscope (× 800 magnification) the separates consist of opaque aggregates too fine grained to be identified.

A variety of materials can be seen in the separates when viewed under an electron microscope. The largest discrete particles have a fragile, transluscent appearance and generally have a maximum dimension of less than 10 microns. Denser, opaque-appearing particles are mostly less than 1.0$\mu$ across. The finest particles seen are in the order of 0.001$\mu$ in diameter.

X-ray diffraction patterns of the jordisite separates show that pyrite was not entirely removed by the heavy-liquid separation. Patterns of separates 3 and 4 have a broad, low peak at about $2\theta = 14.4°$, $d = 6.15$ A, which is the position of a major molybdenite peak; it was entirely missing in the other patterns. Separate 1b yielded a barely perceptible peak at $2\theta = 36.0°$, $d = 2.49$ A, which is the position of the major ferroselite peak on diffractometer patterns.

Heating to red heat in a closed tube produced a gray selenium ring, a yellow sulfur ring, a pink selenium stain, and a broader white crystalline band that may have been caused by some sulfate sublimate. The residue remained black and seemingly unchanged in appearance.

## ANALYTICAL PROCEDURE

The most effective way found to decompose the samples was to sinter them with $Na_2O_2$ at 460°C (Rafter, 1950; Grimaldi and others, 1957) in zirconium crucibles. Selenium and sulfur were oxidized without loss, organic matter was easily removed by oxidation, and contamination from the zirconium crucibles was negligible.

### Silica, molybdenum, iron, and sulfur

Approximately 50 mg of sintered sample was dissolved with HCl. $SiO_2$ was determined gravimetrically after double-dehydration of this solution and volatilization of the $SiO_2$ with HF and excess $H_2SO_4$. The filtrate from the separation of $SiO_2$ was diluted to a definite volume and aliquots were used to determine $MoO_3$, $Fe_2O_3$, and S. Molybdenum was precipitated with alpha benzoinoxime and ignited to $MoO_3$ at 525°C. Iron was determined spectrophotometrically using O-phenanthroline. Sulfur was precipitated as $BaSO_4$ from a 7 percent HCl solution and the $BaSO_4$ was ignited and weighed. Preliminary studies showed that precipitation was quantitative and that negligible $BaMoO_4$ contamination would occur in 7–10 percent HCl solutions.

### Aluminum

Aluminum was determined spectrophotometrically with alizarin red S. A10-mg sample was sintered and leached with $H_2O$. The insoluble portion, containing practically all thei ron, was filtered off. After acidifying the filtrate, an $NH_4OH$ precipitation to methyl red end point was made to precipitate the Al.

### Selenium

Selenium was determined volumetrically. For total selenium, a 10-mg sample was sintered and dissolved in HCl; then elemental selenium was precipitated with $SO_2$. It was filtered and dissolved in HBr-$Br_2$ solution. The titration involves adding an excess of $Na_2S_2O_3$

solution, then an excess of $I_2$ solution, and finally reaching an exact end point with $Na_2S_2O_3$. Starch is used as the indicator (Trelease and Beath, 1949).

For the determination of elemental selenium in the separate, a 10-mg sample was digested with 10-percent KCN solution to dissolve it. Selenium was then determined in this solution as above. The solubility of $FeS_2$ and $MoS_2$ in 10-percent KCN solution was tested. They were insoluble. It was concluded that the selenides would also be insoluble. Since spectrographic analysis showed very small amounts of other elements likely to combine with Se, the KCN-soluble Se represents elemental Se in these separates.

### Thallium

Thallium was determined spectrophotometrically with dithizone. A 50-mg sample was sintered and leached with $H_2O$. The insoluble portion containing the thallium was filtered off and dissolved in 1 + 1 HBr. Prior to dithizone determination, the solution was treated with HF and more HBr, and thallium was extracted into isopropyl ether to separate it from iron and the small amounts of lead present.

## RESULTS OF ANALYSES

Data in tables 2, 3, and 4 show that the separation resulted in a marked concentration of Se, Cu, Mo, Cr, Co, Fe, Pb, Tl, and Ag, in approximately that order. S and organic C also probably were concentrated. Cu, Cr, Co, Pb, Tl, and Ag are minor constituents, and are generally not discussed.

Table 4 shows the major constituents of the jordisite separate. Silica and alumina still constitute a significant part of the separate despite the separation techniques used. Silica is probably in the form of amorphous silica precipitated during the separation process. Langmyhr and Graff (1959) point out that silica can be dissolved with excess HF and the solution may be partially evaporated without any detectable loss of silicon. Silicon in not volatilized until a constant-boiling ternary mixture of hydrofluoric acid, fluosilicic acid, and water is formed. This mixture is formed only after most of the HF is evaporated; consequently, silicon is not volatilized until close to the point of dryness.

Since the HF solutions were not evaporated to dryness during the separation process because of possible excessive oxidation of jordisite, silicon was not volatilized completely and perhaps was precipitated. The aluminum chloride treatment used in the separation technique would very likely precipitate any silicon in solution at the time.

TABLE 2.—*Analyses, in percent, of rock samples from which jordisite was separated* [1]

[Symbols: M, major constituent (> 10 percent); 0, looked for but not detected; ND, not determined. Analysts (U.S. Geological Survey, Denver, Colo.): spectrographic data, J. C. Hamilton, R. G. Havens; uranium, E. Fennelly, D. L. Ferguson; selenium, G. T. Burrow; arsenic, D. L. Ferguson, Claude Huffman; organic carbon, I. C. Frost]

| Element | 1 | 2 | 3 | 4 |
|---|---|---|---|---|
| Si | M | M | M | M |
| Al | 3 | 3 | 7 | 7 |
| Fe | .3 | .3 | .7 | .7 |
| Mg | .15 | .3 | .15 | .3 |
| Ca | .7 | 1.5 | 1.5 | 1.5 |
| Na | 1.5 | 1.5 | 1.5 | 1.5 |
| K | 1.5 | 1.5 | 3 | 3 |
| Ti | .07 | .07 | .07 | .07 |
| Mn | .015 | .015 | .03 | .03 |
| As | (.018) | (.037) | 0 | 0 |
| Ba | .03 | .07 | .07 | .07 |
| Be | 0 | 0 | .0003 | .0007 |
| Co | .0015 | .0007 | <.003 | <.003 |
| C (organic) | (<.3) | (<.3) | .09 | .15 |
| Cr | .0003 | .0003 | .0003 | .0003 |
| Cu | .0007 | .0007 | .0015 | .0015 |
| Ga | .0003 | .0003 | .0015 | .003 |
| Mo | .7 | .7 | .7 | .7 |
| Ni | .0007 | .0003 | .0003 | .0003 |
| Pb | .0015 | .0015 | .007 | .007 |
| Se | (.135) | (.076) | (.070) | (.038) |
| Sn | <.005 | <.005 | .003 | .003 |
| Sr | .007 | .015 | .015 | .015 |
| Tl | 0 | 0 | .015 | .007 |
| U | (.004) | (.004) | (.30) | (.33) |
| V | .07 | .07 | .07 | .3 |
| Y | 0 | 0 | .003 | .003 |
| Yb | ND | ND | <.003 | <.003 |
| Zr | .007 | .003 | .007 | .015 |

Looked for but not detected: P, Ag, Au, B, Bi, Cd, Ce, Dy, Er, Eu, Gd, Ge, Hf, Hg, Ho, In, Ir, La, Li, Lu, Nb, Nd, Os, Pd, Pr, Pt, Re, Rh, Ru, Sb, Sc, Sm, Ta, Tb, Te, Th, Tm, W, Zn. Other elements were not looked for.

Results are reported in percent to the nearest number in the series 7, 3, 1.5, 0.7, 0.3, and so forth, which represent approximate midpoints of group data on a geometric scale. The assigned group for semiquantitative results will include the quantitative value about 60 percent of the time.

[1] Semiquantitative spectrographic analyses except for data in parentheses, which are chemical analyses.

We made the following tentative assumptions, largely on the basis of the results of analyses of the separates (tables 3 and 4):

1. Molybdenum occurs entirely as $MoS_2$ (jordisite).
2. Iron is distributed largely between ferroselite and pyrite.
3. Sulfur is distributed largely between jordisite and pyrite, although some sulfide sulfur may have been oxidized to native sulfur during the separations.
4. Selenium was originally in the form of ferroselite but, in a manner similar to sulfur, elemental selenium was produced by oxidation of some of the ferroselite during the separations.
5. The form of the small amounts of Cu, Ti, Ca, and Tl is not known, but cannot significantly change the preceding assumptions.
6. $SiO_2$ and $Al_2O_3$ are not chemically combined with the other constituents.

TABLE 3.—*Spectrographic analyses, in percent, of jordisite separates*

[Symbols: M, major constituent (>10 percent); 0, looked for but not detected. Analyst: J. T. Harris, U.S. Geological Survey, Washington, D.C.]

| Element | 1a | 1b | 2 | 3 | 4 |
|---|---|---|---|---|---|
| Si | M | 7 | 5 | 5 | 7 |
| Al | .5 | .5 | .7 | .7 | .3 |
| Fe | 3 | 7 | 10 | 7 | 7 |
| Mg | <.00018 | <.00018 | <.00018 | .03 | .05 |
| Ca | .07 | .05 | .05 | .1 | .015 |
| Ti | .05 | .1 | .1 | .07 | .03 |
| Mn | .02 | .03 | .03 | .02 | .015 |
| Ag | .00015 | .0002 | .01 | .0007 | .0007 |
| B | .007 | .003 | .0015 | .003 | 0 |
| Ba | .005 | .002 | .002 | .01 | .002 |
| Ce | .03 | .05 | .02 | .05 | 0 |
| Co | .015 | .02 | .015 | .02 | .015 |
| Cr | .003 | .01 | .002 | .002 | .001 |
| Cu | .07 | .15 | .15 | .15 | .07 |
| Mo | M | M | M | M | M |
| Pb | .003 | .007 | .05 | .07 | .015 |
| Sn | .0003 | .003 | .0003 | .007 | 0 |
| Tl | .005 | .01 | .01 | .1 | .07 |
| V | .007 | .01 | .007 | .03 | .01 |
| Yb | .00015 | .0007 | .0005 | .0005 | .0005 |
| Zr | .002 | .01 | .007 | .007 | .003 |

Looked for but not detected: Na, K, P, As, Au, Be, Bi, Cd, Ga, Ge, Hf, Hg, In, La, Li, Nb, Ni, Pd, Pt, Re, Sb, Sc, Sr, Ta, Te, Th, U, W, Y, Zn, Pr, Nd, Sm, Eu. Other elements were not looked for.

Results are reported in percent to the nearest number in the series 1, 0.7, 0.5, 0.3, 0.2, 0.15, and 0.1, and so forth, which represent appoximate midpoints of group data on a geometric scale. The assigned group for semiquantitative results will include the quantitative values about 30 percent of the time.

TABLE 4.—*Chemical analyses, in percent, of jordisite separates*

[Symbol: ND, not determined. Analyst: Blanche Ingram, U.S. Geological Survey, Washington, D.C.]

| | 1a | 1b | 2 | 3 | 4 |
|---|---|---|---|---|---|
| $SiO_2$ | 32.1 | 8.9 | 8.1 | 4.8 | 20.5 |
| $Al_2O_3$ | 1.2 | .83 | 1.1 | 1.1 | 1.2 |
| Fe (total) | 2.7 | 6.3 | 6.4 | 5.2 | 5.8 |
| Mo | 16.8 | 27.3 | 22.8 | 22.4 | 15.9 |
| S (total) | 12.6 | 23.4 | 21.8 | 20.2 | 15.2 |
| Se (total) | 6.8 | 11.9 | 10.2 | 7.9 | 4.8 |
| Se (elemental) | 2.8 | 3.9 | 6.4 | 4.8 | 2.9 |
| Tl | ND | ND | ND | .08 | .05 |

7. All the remaining material constitutes organic matter, water, and, possibly, small amounts of insoluble fluorides produced during the separation and not completely eliminated by the aluminum chloride washings.

If these assumptions are correct, distribution of Mo, Fe, and nonelemental Se stoichiometrically among $MoS_2$ $FeS_2$, and $FeSe_2$ should utilize nearly all the sulfur in the sample. The results of these calculations are shown in table 5. A sulfur deficiency of 0.2 percent in separate 1a is probably well within analytical error and suggests that little or no elemental sulfur was produced. Among the remaining separates the maximum sulfur excess is only 1.2 percent and it is believed that this tends to substantiate the preceding assumptions. Pyrite can contain a few percent Se (Coleman, 1959) and molybdenite commonly contains 100–200 parts per million Se (Michael Fleischer, written commun., 1965), so that it is likely that some of the selenium calculated (table 5) to be present as $FeSe_2$ or Se is actually present in the pyrite or jordisite.

TABLE 5.—*Calculated composition, in percent, of the jordisite separates*

| | 1a | 1b | 2 | 3 | 4 |
|---|---|---|---|---|---|
| $MoS_2$ (jordisite) | 28.0 | 45.5 | 38.0 | 37.4 | 20.9 |
| $FeS_2$ (pyrite) | 2.9 | 7.5 | 11.0 | 8.9 | 11.0 |
| $FeSe_2$ (ferroselite) | 5.4 | 10.8 | 5.1 | 4.2 | 2.6 |
| S, elemental | [1](.2) | 1.2 | .7 | .4 | .9 |
| Se, elemental | 2.8 | 3.9 | 6.4 | 4.8 | 2.9 |
| $SiO_2$ | 32.1 | 8.9 | 8.1 | 4.8 | 20.5 |
| $Al_2O_3$ | 1.2 | .8 | 1.1 | 1.1 | 1.2 |
| Other impurities, including organic matter, $H_2O$, and small amounts of Cu, Ti, Ca, and Tl compounds | 27.6 | 21.4 | 29.6 | 38.4 | 40.0 |
| Total | 100 | 100 | 100 | 100 | 100 |

[1] Calculated deficiency after allowance for jordisite and pyrite.

## CONCLUSIONS

Because of the impure nature of the separates, the presence of jordisite was not fully substantiated. However, the most probable composition of the separate, based on chemical analyses, allows for the presence of molybdenum as a disulfide. X-ray patterns of the separates indicate that all major constituents other than pyrite are amorphous or very poorly crystallized. Since the molybdenum evidently occurs in an amorphous disulfide compound, it is tentatively concluded that it exists in the form of jordisite similar to the jordisite described by Meixner (1950) and Staples (1951).

## REFERENCES

Coleman, R. G., 1959, New occurrences of ferroselite ($FeSe_2$): Geochim. et Cosmochim. Acta, v. 16, p. 296–301.

Granger, H. C., 1963, Mineralogy, *in* Geology and technology of the Grants [New Mexico] uranium region, *prepared by* Society of Economic Geologists, V. D. Kelley [chm.], Uranium conference: New Mexico Bur. Mines and Mineral Resources Mem. 15, p. 21–37.

Granger, H. C., Santos, E. S., Dean, B. G., and Moore, F. B., 1961, Sandstone-type uranium deposits at Ambrosia Lake, New Mexico—an interim report: Econ. Geology, v. 56, no. 7, p. 1179–1210.

Grimaldi, F. S., Jenkins, L. B., and Fletcher, M. H., 1957, Selective precipitation of thorium iodate from a tartaric acid-hydrogen peroxide medium—application to rapid spectrophotometric determination of thorium in silicate rocks and in ores: Anal. Chem., v. 29, p. 848–851.

Langmyhr, F. J., and Graff, P. R., 1959, Studies in the spectrophotometric determination of silicon decomposed by hydrofluoric acid; I. Loss of silicon by decomposition with

hydrofluoric acid: Analytica Chimica Acta, v. 21, p. 334–339.

Meixner, Heinz, 1950, Über Jordisit (amorphes Molybdänsulfid) von Bleiberg in Kärnten [Concerning Jordisite (amorphous molybdenum sulfide) from Bleiberg, Corinthia]: Carinthia II, v. 139–40, p. 39–51.

Rafter, T. A., 1950, Sodium-peroxide decomposition of minerals in platinum vessels: Analyst, v. 75, p. 485.

Staples, L. W., 1951, Ilsemannite and jordisite: Am. Mineralogist, v. 36, nos. 7 and 8, p. 609–614.

Trelease, Sam F., and Beath, Orville A., 1949, Selenium, 1st ed.: Published by authors, at Champlain Printers, Burlington, Vt., p. 260.

# LOEWEITE, VANTHOFFITE, BLOEDITE, AND LEONITE FROM SOUTHEASTERN NEW MEXICO

By BETH M. MADSEN, Menlo Park, Calif.

*Abstract*—Optical data, chemical analyses, and X-ray powder data are given for four uncommon sulfate minerals: loewite, vanthoffite, bloedite, and leonite. The minerals occur in a marine evaporite, the Salado Formation of Permian age. This is the first report of loewite in the United States.

Potash deposits in the Permian evaporite sequence in New Mexico contain a sodium magnesium sulfate mineral, loeweite ($6Na_2SO_4 \cdot 7MgSO_4 \cdot 15H_2O$) not previously reported in the United States. Bloedite ($Na_2SO_4 \cdot MgSO_4 \cdot 4H_2O$ and vanthoffite ($3Na_2SO_4 \cdot MgSO_4$) from southeastern New Mexico had been tentatively identified by Schaller and Henderson (1932). Data on leonite ($K_2SO_4 \cdot MgSO_4 \cdot 4H_2O$), the potassium analog of bloedite, are included in this report because this mineral is closely associated with the others.

The potash deposits are in southeastern New Mexico about 20 miles east of the town of Carlsbad. They occur in the middle of the Salado Formation of Late Permian age, a marine evaporite composed dominantly of halite rock (Jones, 1954). The samples studied were obtained from diamond-drill cores and from exposures in potash mines.

The halite rock in which the double sulfate minerals occur is medium to coarse grained and ranges from colorless to gray green to brown to brick red. Loeweite, vanthoffite, bloedite, and leonite are constituents of the ore zones and are found together and with kainite, sylvite, kieserite, langbeinite, thenardite, aphthitalite, polyhalite, anhydrite, magnesite, dolomite, clay minerals, hematite, and halite.

## PHYSICAL AND OPTICAL PROPERTIES

In hand specimen loeweite, vanthoffite, bloedite, and leonite are indistinguishable from each other. They are similar in color, grading from colorless to gray to pale yellow. For all four minerals, the hardness lies between 2.5 and 4, the fracture is conchoidal, and the taste is very slightly bitter. All are transparent with a vitreous luster. Vanthoffite, bloedite, and leonite have no cleavage, whereas loeweite has a good cleavage{001}.

The optical and specific-gravity data are summarized in table 1. Optic angles were measured on a four-axes universal stage using small upper hemispheres in order to obtain sharp interference figures. Grains were selected whose optic plane could be rotated into the vertical plane of the microscope; $2V$ was measured directly by rotation from one optic plane to the other, and $V$ by rotation from the acute bisectrix to the optic axis. Values for $2V$ were corrected for the refractive index of the hemisphere and for the $\beta$-index of the mineral being measured, giving an accuracy of $\pm 2°$.

The indices of refraction were also determined on a four-axis universal stage using white light and the Becke-line colors method of Emmons and Gates (1948). To obtain final values of $\pm 0.001$, indices were bracketed with liquids 0.002 apart and verified with mixed intermediate liquids which were checked with a refractometer.

The specific gravities of the minerals were determined by the suspension method using bromoform-acetone mixtures whose densities were checked with a Westphal balance.

TABLE 1.—*Optical and specific gravity data for loeweite, vanthoffite, bloedite, and leonite*

| | Loeweite | Vanthoffite | Bloedite | Leonite |
|---|---|---|---|---|
| Indices of refraction: | | | | |
| $\alpha$ | 1.473 (±.001) | 1.486 (±.001) | 1.483 (±.001) | 1.480 (±.001) |
| $\beta$ | | 1.488 (±.001) | 1.486 (±.001) | 1.483 (±.001) |
| $\gamma$ | 1.490 (±.001) | 1.489 (±.001) | 1.487 (±.001) | 1.486 (±.001) |
| Optic sign | + | − | − | + |
| Optic angle | 0° | 83° (±2°) | 71° (±2°) | 90° (±2°) |
| Specific gravity (meas.) | 2.38 (±.01) | 2.69 (±.01) | 2.24 (±.01) | 2.20 (±.01) |

For chemical analyses, each mineral was separated from halite by handpicking. A split of each analyzed sample was used for thermogravimetric analysis, optics study, and X-ray study. Table 2 summarizes the re-

sults of the chemical analyses, and table 3 shows the results of semiquantitative spectrographic analyses. In table 4 the analyses were computed to 100 percent after calculating the Cl as NaCl and subtracting it. The recalculated chemical analyses are in good agreement with the theoretical compositions of the minerals. The formula for loeweite, $6Na_2SO_4 \cdot 7MgSO_4 \cdot 15H_2O$, derived from the analysis, agrees with the formula favored by Schneider and Zemann (1959) for structural reasons.

TABLE 2.—*Chemical analyses of loeweite, vanthoffite, bloedite, and leonite*

[Analyst: Robert Meyrowitz]

| Constituent | Loeweite | Vanthoffite | Bloedite | Leonite |
|---|---|---|---|---|
| $Na_2O$ | 18. 9 | 34. 0 | 19. 9 | 0. 6 |
| MgO | 14. 6 | 7. 3 | 12. 0 | 10. 9 |
| $K_2O$ | (a) | (a) | (a) | 25. 2 |
| $SO_3$ | 52. 2 | 57. 6 | 46. 1 | 42. 6 |
| Cl[b] | . 066 | . 82 | 1. 8 | . 92 |
| Br[b] | <. 005 | <. 005 | . 007 | . 007 |
| I[b] | <. 012 | <. 012 | <. 012 | <. 012 |
| $H_2O$ | 14. 2 | . 1 | 20. 9 | 19. 2 |
| $H_2O_{insoluble}$ | <. 1 | <. 1 | . 2 | . 1 |
| Subtotal | 100. 1 | 99. 9 | 100. 9 | 99. 5 |
| O—Cl | <. 0 | —. 2 | —. 4 | —. 2 |
| Total | 100. 1 | 99. 7 | 100. 5 | 99. 3 |

[a] See table 3.
[b] Determined by Marian Schnepfe: Cl, by Mohr microtitration; Br, by spectrophotometric method; and I, by oxidation.

TABLE 3.—*Semiquantitative spectrographic analyses*[1]

[Analyst: H. W. Worthing]

| Element | Loeweite | Vanthoffite | Bloedite | Leonite |
|---|---|---|---|---|
| Si | 0. 007 | 0. 0007 | 0. 003 | 0. 07 |
| Al | . 0007 | . 015 | . 03 | . 03 |
| Fe | . 003 | . 003 | . 007 | . 007 |
| Mg | 7 | 7 | 7 | 7 |
| Ca | . 015 | . 03 | . 015 | . 015 |
| Na | M | M | M | 1. 5 |
| K | . 07 | . 015 | . 03 | M |
| Mn | . 007 | . 007 | . 003 | . 0015 |
| Ba | . 0003 | . 003 | . 015 | . 0007 |
| Cr | 0 | . 0003 | . 0003 | . 0003 |
| Cu | . 00003 | . 00007 | . 00003 | . 0003 |
| Sr | 0 | . 0007 | . 0015 | . 0003 |

Looked for but not found: Ti, P, Ag, Au, B, Be, Bi, Cd, Ce, Co, Cs, Dy, Er, Eu, Ga, Gd, Ge, Hf, Hg, Ho, In, La, Li, Lu, Mo, Nb, Nd, Ni, Os, Pb, Pd, Pr, Pt, Rb, Re, Rh, Ru, Sb, Sc, Sn, Sm, Ta, Tb, Te, Th, Tl, Tm, U, W, Y, Yb, Zn, and Zr.

[1] Figures are reported to the nearest number in the series 7, 3, 1.5, 0.7, 0.3, 0.15, and so forth in percent. M, major constituent greater than 10 percent; 0, looked for but not found.

In table 5 the measured optical data are compared with the optical data calculated by the Gladstone and Dale method $[(n-1)/d = K]$. The specific refractive energy values ($K$) are from Larsen and Berman (1934, p. 30–32) and Jaffe (1956).

TABLE 4.—*Recalculated chemical analyses of loeweite, vanthoffite, bloedite, and leonite*

| Constituent | Weight percent[1] | Recalculated to 100 percent | Molecular proportions | Molecular ratios |
|---|---|---|---|---|
| **Loeweite ($6Na_2SO_4 \cdot 7MgSO_4 \cdot 15H_2O$)** | | | | |
| $Na_2O$ | 18. 8 | 18. 8 | 0. 30 | 1. 0 |
| MgO | 14. 6 | 14. 6 | . 36 | 1. 2 |
| $SO_3$ | 52. 2 | 52. 3 | . 65 | 2. 17 |
| $H_2O$ | 14. 3 | 14. 3 | . 79 | 2. 63 |
| **Vanthoffite ($3Na_2SO_4 \cdot MgSO_4$)** | | | | |
| $Na_2O$ | 33. 3 | 33. 9 | 0. 55 | 3. 05 |
| MgO | 7. 3 | 7. 4 | . 18 | 1. 0 |
| $SO_3$ | 57. 6 | 58. 7 | . 73 | 4. 05 |
| **Bloedite ($Na_2SO_4 \cdot MgSO_4 \cdot 4H_2O$)** | | | | |
| $Na_2O$ | 18. 3 | 18. 8 | 0. 30 | 1. 0 |
| MgO | 12. 0 | 12. 3 | . 305 | 1. 02 |
| $SO_3$ | 46. 1 | 47. 4 | . 59 | 1. 97 |
| $H_2O$ | 20. 9 | 21. 5 | 1. 19 | 3. 97 |
| **Leonite ($K_2SO_4 \cdot MgSO_4 \cdot 4H_2O$)** | | | | |
| $K_2O$ | [2] 25. 2 | 25. 5 | 0. 27 | 1. 00 |
| MgO | 10. 6 | 11. 2 | . 28 | 1. 04 |
| $SO_3$ | 42. 6 | 43. 6 | . 54 | 2. 00 |
| $H_2O$ | 19. 2 | 19. 7 | 1. 09 | 4. 04 |

[1] Analyses of Robert Meyrowitz (table 2) with Cl calculated as NaCl and removed.
[2] The Cl in excess of the NaCl was calculated as KCl and removed.

TABLE 5.—*Comparison of measured index of refraction with that calculated from rule of Gladstone and Dale for loeweite, vanthoffite, bloedite, and leonite*

| Mineral | Specific gravity (meas.) | $K$ | $dK+1$ | Mean index (meas.) |
|---|---|---|---|---|
| Loeweite | 2. 38 | 0. 2038 | 1. 485 | 1. 484 |
| Vanthoffite | 2. 69 | . 1790 | 1. 482 | 1. 488 |
| Bloedite | 2. 24 | . 2147 | 1. 483 | 1. 485 |
| Leonite | 2. 20 | . 2148 | 1. 473 | 1. 483 |

## THERMOGRAVIMETRIC ANALYSIS

Thermogravimetric analyses of loeweite, bloedite, and leonite were made by Charles A. Kinser, of the U.S. Geological Survey, and are shown as figure 1. A 200-milligram sample was used for each analysis with a heating rate of 4°C/minute from room temperature to 450°C. The curve for bloedite shows a total weight loss of water, of 21 percent, whereas the chemically determined $H_2O$ content is 21.5 percent. This curve also shows that loss occurs partly at about 120°C and partly at about 200°C, each loss equivalent to two molecules of water. This suggests that two molecules of water are bound in a different way from the

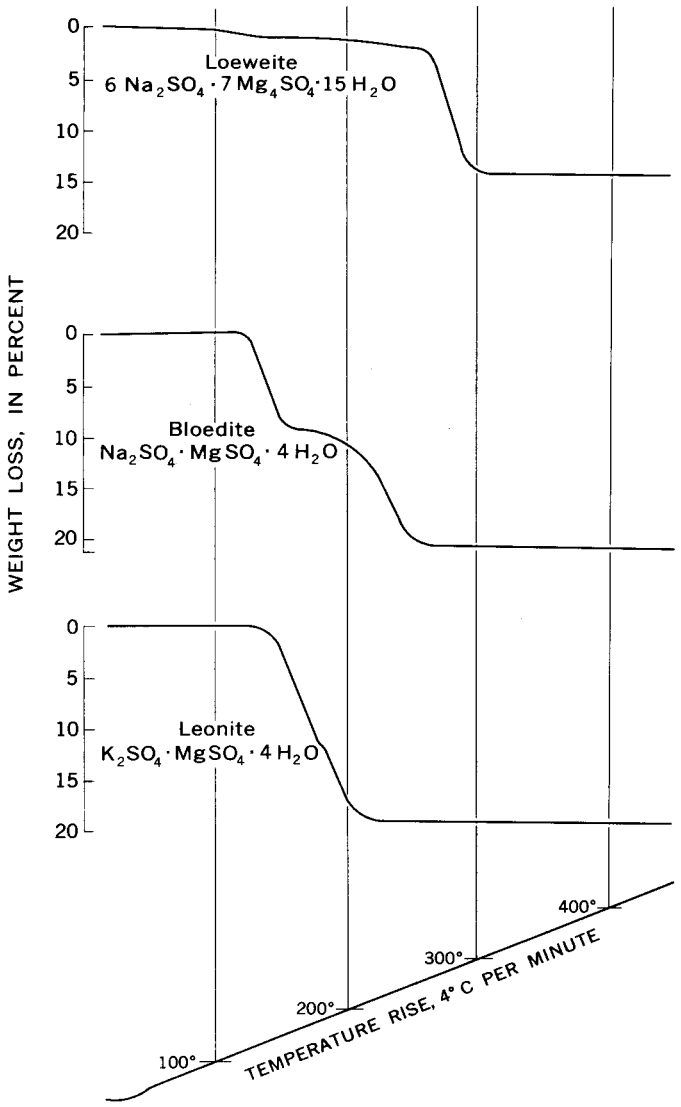


FIGURE 1.—Thermogravimetric analyses of loeweite, bloedite, and leonite.

other two. The heating of loeweite caused a 14.6-percent weight loss of water; the determined $H_2O$ content is 14.3 percent. The total weight loss of water for leonite was 19.2 percent as compared with a determined water content of 19.7 percent. There is a slight inflection on the leonite curve at 190°C, but water loss at this point does not represent an even number of molecules.

## X-RAY DATA

X-ray powder diffraction data for loeweite, vanthoffite, bloedite, and leonite are given in tables 6 through 10; figure 2 shows tracings of the diffraction patterns. The samples were run with a recording geiger counter diffractometer using Cu/Ni radiation, scan speed ¼° per minute, and silicon as the internal standard.

TABLE 6.—*X-ray powder diffraction data for loeweite*

| *I* | *d* (A) (meas.)[1] | *d* (A) (calc.)[2] | *hkl* | *I* | *d* (A) (meas.)[1] | *d* (A) (calc.)[2] | *hkl* |
|---|---|---|---|---|---|---|---|
| | | 16. 33 | 100 | | | 3. 36 | 004 |
| | | 13. 42 | 001 | | | 3. 29 | 104 |
| 83 | 10. 33 | 10. 37 | 101 | 88 | 3. 27 | 3. 27 | 322 |
| 24 | 9. 41 | 9. 43 | 110 | | | 3. 27 | 500 |
| | | 8. 16 | 200 | 37 | 3. 25 | 3. 24 | 223 |
| | | 7. 71 | 111 | | | 3. 18 | 313 |
| 37 | 6. 96 | 6. 97 | 201 | 100 | 3. 17 | 3. 17 | 501 |
| | | 6. 71 | 002 | | | 3. 16 | 114 |
| 20 | 6. 20 | 6. 21 | 102 | 19 | 3. 15 | 3. 15 | 412 |
| | | 6. 17 | 210 | | | 3. 14 | 330 |
| 42 | 5. 61 | 5. 61 | 211 | 5 | 3. 11 | 3. 10 | 204 |
| | | 5. 47 | 112 | | | 3. 09 | 420 |
| 48 | 5. 44 | 5. 44 | 300 | | | 3. 06 | 331 |
| 7 | 5. 18 | 5. 18 | 202 | | | 3. 02 | 403 |
| | | 5. 04 | 301 | 12 | 3. 01 | 3. 01 | 421 |
| | | 4. 71 | 220 | | | 2. 95 | 214 |
| 17 | 4. 54 | 4. 54 | 212 | 61 | 2. 94 | 2. 94 | 502 |
| | | 4. 53 | 310 | | | 2. 93 | 510 |
| 12 | 4. 47 | 4. 47 | 003 | | | 2. 87 | 323 |
| | | 4. 45 | 221 | 36 | 2. 86 | 2. 86 | 511 |
| | | 4. 32 | 103 | | | 2. 86 | 304 |
| 97 | 4. 29 | 4. 29 | 311 | | | 2. 85 | 332 |
| | | 4. 23 | 302 | 42 | 2. 80 | 2. 80 | 422 |
| | | 4. 08 | 400 | 46 | 2. 79 | 2. 79 | 413 |
| 98 | 4. 04 | 4. 04 | 113 | | | 2. 73 | 224 |
| | | 3. 92 | 203 | 50 | 2. 72 | 2. 72 | 600 |
| 1 | 3. 90 | 3. 91 | 401 | 96 | 2. 70 | 2. 70 | 314 |
| | | 3. 86 | 222 | | | 2. 69 | 512 |
| 55 | 3. 75 | 3. 75 | 312 | | | 2. 68 | 005 |
| | | 3. 75 | 320 | | | 2. 68 | 430 |
| | | 3. 62 | 213 | | | 2. 67 | 601 |
| 17 | 3. 61 | 3. 61 | 321 | | | 2. 65 | 105 |
| 10 | 3. 56 | 3. 56 | 410 | | | 2. 64 | 503 |
| | | 3. 49 | 402 | 37 | 2. 63 | 2. 63 | 431 |
| 90 | 3. 46 | 3. 46 | 303 | 34 | 2. 61 | 2. 61 | 520 |
| | | 3. 44 | 411 | | | | |

[1] X-ray diffractometer data: Cu/Ni radiation; silicon powder used as internal standard; scanned at ¼° per minute from 70 to 6° 2$\theta$.
[2] All calculated spacing ≥2.61 permitted by the space group are listed. Indices and *d* spacings were calculated from least-square refinement of X-ray powder data by Daniel E. Appleman (table 10) using digital computer program (Evans and others, 1963).

TABLE 7.—*X-ray powder diffraction data for vanthoffite*

| *I* | *d* (A) (meas.)[1] | *I* | *d* (A) (meas.)[1] | *I* | *d* (A) (meas.)[1] | *I* | *d* (A) (meas.)[1] |
|---|---|---|---|---|---|---|---|
| 6 | 8. 95 | 74 | 2. 90 | 5 | 2. 24 | 8 | 1. 88 |
| 15 | 5. 81 | 32 | 2. 85 | 2 | 2. 23 | 10 | 1. 87 |
| 8 | 4. 60 | 33 | 2. 84 | 8 | 2. 19 | 4 | 1. 87 |
| 28 | 4. 24 | 61 | 2. 83 | 41 | 2. 17 | 3 | 1. 85 |
| 7 | 4. 10 | 35 | 2. 82 | 32 | 2. 17 | 7 | 1. 84 |
| 28 | 4. 03 | 4 | 2. 69 | 14 | 2. 16 | 19 | 1. 82 |
| 13 | 3. 94 | 24 | 2. 59 | 4 | 2. 15 | 23 | 1. 82 |
| 28 | 3. 92 | 24 | 2. 58 | 3 | 2. 12 | 7 | 1. 78 |
| 7 | 3. 75 | 5 | 2. 55 | 4 | 2. 04 | 3 | 1. 76 |
| 6 | 3. 49 | 8 | 2. 46 | 3 | 2. 04 | 2 | 1. 72 |
| 10 | 3. 48 | 24 | 2. 46 | 4 | 2. 01 | 7 | 1. 71 |
| 95 | 3. 44 | 12 | 2. 45 | 7 | 2. 00 | 2 | 1. 69 |
| 94 | 3. 43 | 4 | 2. 38 | 5 | 2. 00 | 3 | 1. 67 |
| 3 | 3. 34 | 7 | 2. 36 | 4 | 1. 98 | 4 | 1. 65 |
| 4 | 3. 31 | 4 | 2. 32 | 3 | 1. 97 | 5 | 1. 60 |
| 60 | 3. 12 | 13 | 2. 31 | 5 | 1. 96 | 22 | 1. 58 |
| 19 | 3. 06 | 8 | 2. 30 | 11 | 1. 95 | 11 | 1. 58 |
| 78 | 2. 99 | 5 | 2. 29 | 9 | 1. 95 | 4 | 1. 57 |
| 100 | 2. 91 | 5 | 2. 25 | 8 | 1. 94 | 4 | 1. 57 |

[1] X-ray diffraction data: Cu/Ni radiation; silicon powder used as internal standard; scanned 1/4° per minute from 60 to 6° 2$\theta$.

TABLE 8.—*X-ray powder diffraction data for bloedite*

| *I* | *d* (A) (meas.)[1] | *I* | *d* (A) (meas.)[1] |
|---|---|---|---|
| 1 | 5. 48 | 11 | 2. 27 |
| 100 | 4. 56 | 4 | 2. 19 |
| 2 | 4. 47 | 7 | 2. 17 |
| 59 | 4. 29 | 6 | 2. 14 |
| 9 | 4. 13 | 7 | 2. 11 |
| 7 | 3. 98 | 15 | 2. 03 |
| 5 | 3. 85 | 9 | 1. 96 |
| 18 | 3. 80 | 11 | 1. 93 |
| 17 | 3. 33 | 8 | 1. 86 |
| 61 | 3. 29 | 7 | 1. 79 |
| 73 | 3. 25 | 8 | 1. 79 |
| 33 | 2. 97 | 6 | 1. 68 |
| 31 | 2. 73 | 9 | 1. 67 |
| 9 | 2. 68 | 2 | 1. 60 |
| 27 | 2. 65 | 4 | 1. 57 |
| 12 | 2. 58 | 5 | 1. 55 |
| 2 | 2. 45 | 6 | 1. 52 |
| 8 | 2. 31 | 5 | 1. 50 |
| 8 | 2. 30 | | |

[1] X-ray diffractometer data: Cu/Ni radiation; silicon powder used as internal standard; scanned ¼° per minute from 64 to 14° 2$\theta$.

TABLE 9.—*X-ray powder diffraction data for leonite*

| *I* | *d* (A) (meas.)[1] | *d* (A) (calc.)[2] | *hkl* | *I* | *d* (A) (meas.)[1] | *d* (A) (calc.)[2] | *hkl* |
|---|---|---|---|---|---|---|---|
| | | 9. 83 | 001 | | | 2. 74 | 401 |
| | | 7. 39 | 110 | | | 2. 70 | 023 |
| 6 | 6. 07 | 6. 08 | −111 | 15 | 2. 63 | 2. 63 | −132 |
| 22 | 5. 88 | 5. 86 | 200 | | | 2. 63 | −402 |
| | | 5. 75 | 111 | | | 2. 57 | 132 |
| 9 | 5. 27 | 5. 25 | −201 | | | 2. 54 | −313 |
| 14 | 4. 93 | 4. 92 | 002 | 6 | 2. 53 | 2. 53 | −223 |
| | | 4. 84 | 201 | 6 | 2. 50 | 2. 50 | 420 |
| 13 | 4. 77 | 4. 76 | 020 | | | 2. 47 | −421 |
| | | 4. 29 | 021 | 8 | 2. 46 | 2. 46 | 330 |
| 14 | 4. 20 | 4. 21 | −112 | | | 2. 46 | 004 |
| 13 | 3. 99 | 3. 99 | 112 | | | 2. 42 | −331 |
| | | 3. 95 | −202 | | | 2. 42 | 402 |
| 6 | 3. 70 | 3. 70 | 220 | | | 2. 38 | 223 |
| | | 3. 62 | 310 | 47 | 2. 38 | 2. 38 | 040 |
| | | 3. 61 | 202 | | | 2. 38 | 421 |
| 20 | 3. 52 | 3. 53 | −221 | | | 2. 37 | −114 |
| 41 | 3. 49 | 3. 49 | −311 | | | 2. 36 | 331 |
| 100 | 3. 42 | 3. 42 | 022 | | | 2. 35 | −204 |
| | | 3. 40 | 221 | | | 2. 33 | 313 |
| 36 | 3. 31 | 3. 30 | 311 | | | 2. 31 | 041 |
| | | 3. 28 | 003 | | | 2. 30 | −422 |
| | | 3. 06 | 130 | 3 | 2. 29 | 2. 29 | 114 |
| | | 3. 06 | −113 | | | 2. 29 | −403 |
| 48 | 3. 04 | 3. 04 | −222 | | | 2. 28 | 510 |
| | | 3. 04 | −312 | | | 2. 27 | −133 |
| | | 2. 98 | −203 | | | 2. 26 | −511 |
| | | 2. 95 | −131 | | | 2. 26 | −332 |
| | | 2. 93 | 113 | 9 | 2. 21 | 2. 21 | 133 |
| | | 2. 93 | 400 | | | 2. 21 | 240 |
| | | 2. 91 | 131 | | | 2. 20 | 204 |
| | | 2. 88 | −401 | | | 2. 18 | 024 |
| 27 | 2. 88 | 2. 88 | 222 | | | 2. 18 | 511 |
| | | 2. 80 | 312 | 24 | 2. 17 | 2. 17 | −241 |
| 18 | 2. 75 | 2. 76 | 203 | | | | |

[1] X-ray diffractometer data: Cu/Ni radiation; silicon powder used as internal standard; scanned at ¼° per minute from 60° to 10° 2$\theta$.

[2] All calculated spacings ≧2.17 permitted by the space group are listed. Indices and *d*-spacings were calculated from least-square refinement of X-ray powder data by Daniel E. Appleman (table 10) using digital computer program (Evans and others, 1963).

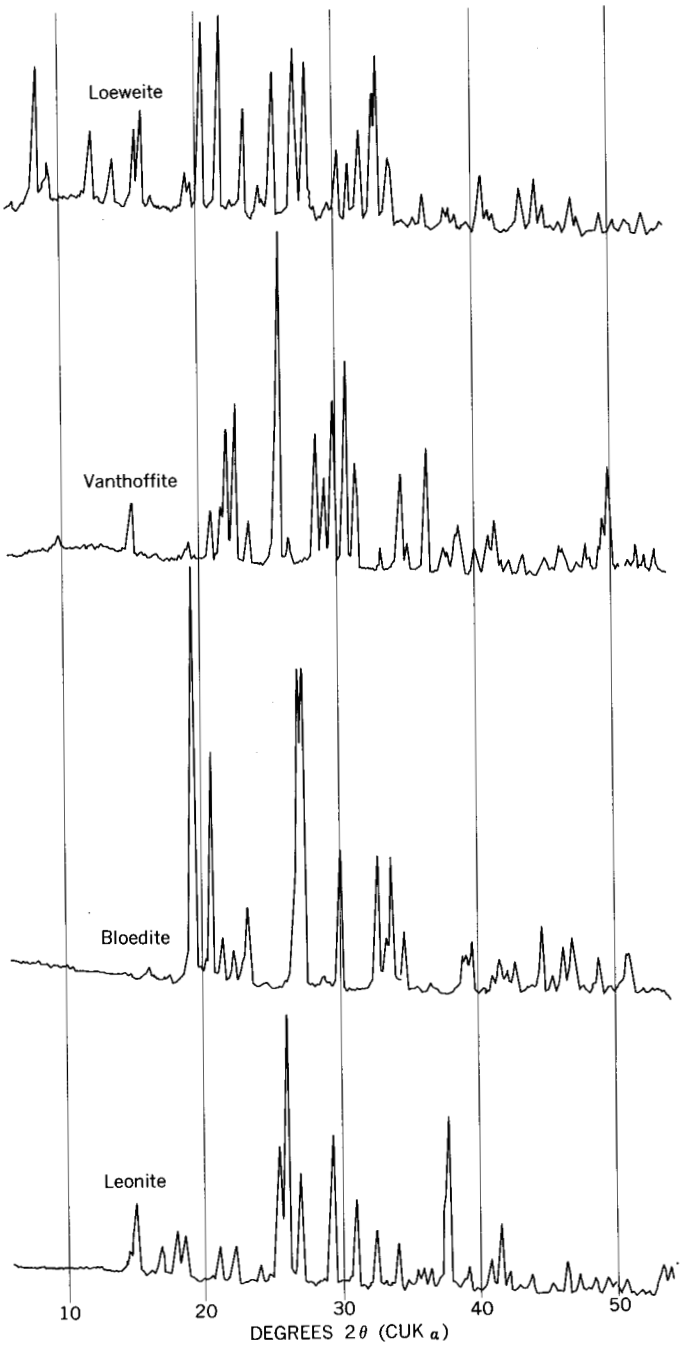


FIGURE 2.—X-ray diffraction patterns of loeweite, vanthoffite, bloedite, and leonite; nickel-filtered Cu$K_\alpha$ radiation, scanning speed 2° per minute, scale factor 8, multiplier 1, time constant 4 seconds.

The unit-cell dimensions were derived by least-square analysis of the X-ray data for loeweite and leonite and are given in table 10. The refinement was carried out on the Burroughs-220 computer by D. E. Appleman using a program written by Evans and

TABLE 10.—*Unit-cell data for loeweite and leonite*

| | Loeweite | Leonite |
|---|---|---|
| Composition | $6Na_2SO_4 \cdot 7MgSO_4 \cdot 15H_2O$ | $K_2SO_4 \cdot MgSO_4 \cdot 4H_2O$ |
| Cell values: [1] | | |
| *a* (A) | 18. 85 | 11. 78 |
| *b* (A) | | 9. 52 |
| *c* (A) | 13. 42 | 9. 88 |
| B | | 95°17.1′ |
| *a*:*b*:*c* | | 1. 237:1:038 |
| Cell volume [1] ($A^3$) | 4204 | 1103 |
| Crystal system | Hexagonal | Monoclinic |
| Space group | [2] *C* 1/3*i* | [3] *C* 2/*m* |
| Specific gravity (calc.) | 2. 36 | 2. 21 |
| Specific gravity (meas.) | 2. 38 | 2. 20 |

[1] Derived by Daniel E. Appleman using a digital computer program for least-squares refinement of unit-cell parameters (Evans and others, 1963).
[2] Schneider and Zemann (1959).
[3] Schneider (1960).

others (1963). An attempt to index the bloedite pattern from the unit-cell dimensions given by Lauro (1940) proved unsuccessful. The pattern for vanthoffite did not index with unit-cell dimensions published by Fischer and Hellner (1964).

## REFERENCES


Emmons, R. C., and Gates, R. M., 1948, The use of Becke colors in refractive index determination: Am. Mineralogist, v. 33, p. 612–618.

Evans, H. T., Jr., Appleman, D. E., and Handwerker, D. S., 1963, The least squares refinement of crystal unit cells with powder diffraction data by an automatic computer indexing method: Am. Cryst. Assoc., Ann. Mtg., 1963, Cambridge, Mass., Abs.

Fischer, V. W., and Hellner, Erwin, 1964, Über die Struktur des Vanthoffits: Acta Cryst., v. 17, p. 1613.

Jaffe, H. W., 1956, Application of the rule of Gladstone and Dale to minerals: Am. Mineralogist, v. 41, p. 757–777.

Jones, C. L., 1954, The occurrence and distribution of potassium minerals in southeastern New Mexico, *in* New Mexico Geol. Soc. Guidebook of southeastern New Mexico, 5th Field Conf., p. 107–112.

Larsen, E. S., Jr., and Berman, Harry, 1934, The microscopic determination of the nonopaque minerals 2d ed.: U.S. Geol. Survey Bull. 848, 266 p.

Lauro, Carlo, 1940, Ricerche Röntgenografiche sulla Bloedite: Periodico Di Mineralogia, v. 11, no. 1, p. 89–100.

Schaller, W. T., and Henderson, E. P., 1932, Mineralogy of drill cores from the potash field of New Mexico and Texas: U.S. Geol. Survey Bull. 833, 124 p., 38 pls.

Schneider, Walter, 1960, Neubestimmung der Kristallstruktur des Leonits, $K_2Mg(SO_4)_2.4H_2O$: Die Naturwissenschaften, no. 12, p. 278.

Schneider, Walter, and Zemman, Josef., 1959, Die Kristallographischen Konstanten von loweit: Beitr. Mineralog. Petrog., v. 6, p. 201–202.

# RARE-EARTH THORIUM CARBONATE VEINS OF THE ROAD GULCH AREA, NORTHERN WET MOUNTAINS, COLORADO

By MORTIMER H. STAATZ and NANCY M. CONKLIN, Denver, Colo.

*Abstract.*—Carbonate veins containing four rare-earth-bearing minerals—monazite, bastnaesite, thorite, and fergusonite—occur along a northeast-trending shear zone that extends for a distance of 1,560 feet. This shear zone lies 1.4 miles west of the large alkalic intrusive complex centered around McClure Mountain. The veins differ from most of the thorium-bearing veins southeast of the alkalic complex in having principally a gangue of of carbonate rather than quartz, and in having a content of rare earths exceeding that of thorium. The chemical and physical character of these veins indicate that they should be classed as carbonatites.

The Wet Mountains area of central Colorado is well known for its numerous thorium-bearing veins that are found northeast, east, west, and south of a large intrusive alkalic complex. This alkalic complex, which occupies an area of about 20 square miles, is centered on McClure Mountain (Parker and Hildebrand, 1963, p. E8). Two smaller bodies of alkalic rocks occur a few miles to the southwest and southeast of the large alkalic complex. The thorium-bearing veins are most abundant southeast of the alkalic rock areas, where more than 1,000 such veins have been noted (M.R. Brock, oral commun., 1964). Some of these veins have been described by Christman and others (1953), Singewald and Brock (1956), and Christman and others (1959). The principal thorium mineral of the veins is thorite, which generally occurs in zones of feldspathized rock permeated with limonite and earthy hematite that commonly contain quartz, barite, and specularite. Rare earths are present but are less abundant than thorium.

In contrast to these siliceous veins several carbonate veins are present which are richer in rare earths than in thorium (Christman and others, 1953, p. 25; Christman and others, 1959, p. 530). These veins lie along a discontinuous northeast-trending shear zone on the west side of the alkalic complex centered on McClure Mountain.

The shear zone that contains the rare-earth-bearing carbonate veins cuts across the mountains about 0.3 mile northwest of Road Gulch. The shear zone is in the E½ sec. 4, T. 20 S., R. 73 W., 6th principal meridian and 5.8 miles N. 43° E. of the town of Hillside. The Dreamer's Hope claim covers most of the shear zone shown in figure 1*B*, and some of the old Homestake claims covered most of the shear zone shown in figure 1*C*. Veins have been found along the shear zone for a distance of 1,560 feet (fig. 1*A*). At the northeast end of the zone a fairly continuous vein is exposed for 445 feet in 5 pits, a shaft, and an outcrop (fig. 1*B*). To the southwest for 415 feet along an east-facing slope, outcrops are covered, but farther southwest on a ridge and along the side of a small valley, either 1 or several discontinuous veins are exposed in 3 pits (fig. 1*C*). Thirty feet southwest of the southwesternmost of these three pits neither shear zone nor vein is visible in a well-exposed diorite body, but on the southwest side of the diorite body, 410 feet from the last exposure of the vein, another vein is exposed in a small pit on the same trend (fig.1*A*). This vein appears to be on a continuation of the same shear zone.

## GEOLOGY

The veins, where exposed, range in width from 0.3 to 8 feet, but are generally about 1 to 2 feet thick. Characteristically, they pinch and swell abruptly; in one 10-foot-long pit the vein decreases in thickness from 1.3 to 0.3 feet. Because of widely separated exposures and pinching and swelling, it is problematical whether the shear zone is occupied by several long veins or by a number of shorter ones. Although the veins all strike northeastward, the strike varies locally by as much as 30° (fig. 1*B*); the veins dip steeply southeastward or are vertical.

Several rock types occur in the vicinity of the veins. The oldest is a well-foliated hornblende gneiss, which consists of about two-thirds andesine and one-third

U.S. GEOL. SURVEY PROF. PAPER 550-B, PAGES B130-B134

hornblende. It was mapped in only one area (fig. 1*C*), where it has been largely replaced by later granite, as indicated by small streaks and patches of the hornblende gneiss in the granite. Diorite, which occurs in a body approximately 85 feet wide, is similar in composition to the gneiss, but is not foliated. It is also older than the granite, as it is embayed by several apophyses of the granite (fig. 1*C*). A gneissic biotite granite, which in part is a migmatite and in some areas contains schlieren of older rocks and a few small albite-quartz-perthite pegmatites, is by far the most common rock. Both the hornblende gneiss and the granite have a foliation that dips steeply and is variable in strike; they are both cut by the shear zone.

A pink fine-grained granite, which has a fetid odor when freshly broken, appears to be related at least structurally to the shear zone. It commonly bounds one or both sides, or lies a short distance away from the shear zone and is discordant with the older rocks mentioned above (fig. 1*B* and *C*). Possibly this rock is of metasomatic origin related to the formation of the veins. The pink fine-grained granite has an average grain size of about 0.4 mm. It consists of 40 to 55 percent orthoclase, 30 to 35 percent quartz, 10 to 20 percent plagioclase, and from less than 1 percent to 5 percent of various accessory minerals. Accessory minerals vary both in amount and species, but biotite, sericite, magnetite, hematite, chlorite, and apatite have been noted. The fine-grained granite occurs in irregular-shaped bodies with a general northeastward strike. Pink feldspar-rich rocks having a fetid odor are related to thorium mineralization in the central Wet Mountains (Christman and others, 1959, p. 509–510) and in the southern Caballo Mountains, N. Mex. (Staatz and others, 1965). Most of these rocks differ from those described in the present report, however, in having only a small amount of quartz.

## MINERALOGY AND COMPOSITION OF THE VEINS

The rare-earth veins are medium to coarse grained and in places are banded. On a weathered surface they are generally brown to red, but where freshly broken they commonly are white, red, brown, or black. All the minerals in these veins were identified from their X-ray patterns. Carbonate minerals make up the bulk of the veins. The principal one is dolomite, but small amounts of calcite, scattered masses of siderite, and a little rhodochrosite are also present. Quartz is almost as plentiful as dolomite and locally may exceed it. Barite in varying amounts occurs throughout most of the veins. Iron oxide minerals are abundant and occur as scattered crystals, aggregates of crystals, and as thin films around other minerals, especially the carbonates. Hematite is perhaps the most common of the iron oxide minerals and occurs both in the earthy and in the specular form; limonite, at least some of which is goethite, is present in most places; and magnetite in small scattered crystals occurs in minor amounts.

The above-mentioned minerals make up the bulk of all the veins. In addition, small amounts of several to many of the following minerals are found in various parts of the veins: thorite, monazite, bastnaesite, fergusonite, rutile, zircon, pyrite, fluorite, apatite, psilomelane, orthoclase, albite, illite, muscovite, biotite, chlorite, hornblende, and crocidolite. Some of these like illite, crocidolite, or apatite, are locally distributed, whereas others, like pyrite or rutile, are widespread.

Thorium or rare earths, or both, occur in thorite, monazite, bastnaesite, and fergusonite. Commonly 2 or 3 of these minerals occur in the same sample, although bastnaesite and monazite have not been found together. Possibly this is due to monazite forming in preference to bastnaesite, if sufficient phosphorus is available. Mineralogic examination indicated that the thorium and rare-earth minerals vary erratically in distribution and abundance along the veins.

Quantitative spectrographic analyses of samples from the veins and prospect dumps are given in table 1 (p. B134). The location of the samples—six of which represent the entire vein width—are given in figure 1. Elements determined are Th, Ce, La, Nd, Y, Yb, U, Nb, Ba, and Sr. Rare earths of the yttrium group, here represented by Y and Yb, are totaled as are those of the cerium group, represented by Ce, La, and Nd. Such a grouping is used because rare-earth minerals commonly contain mostly one group or the other. These two groups when plotted against each other or against other analyzed elements surprisingly show no correlation. Moreover, no correlations can be drawn between any two elements exclusive of rare earths. This lack of correlation suggests that the minerals containing these elements are randomly distributed and vary erratically and independently in the veins. Additional analyses for $ThO_2$ and rare earths of the Dreamer's Hope and Homestake claims are given by Christman and others (1953, p. 22; 1959, p. 530).

All the veins are radioactive; and a comparison of the thorium and uranium content indicates that all appreciable radioactivity is due to thorium. The thorium content, which ranges from less than 0.05 percent to 0.23 percent is small, however, compared to the total rare-earth content (ΣRE), which ranges from somewhat greater than 0.05 percent to 4.4 percent (table 1). The RE : Th ratio for those samples, where a measurable amount of thorium was found, ranges from 5 to 25. These samples are quite different from those reported from veins in the McKinley Mountain area on the

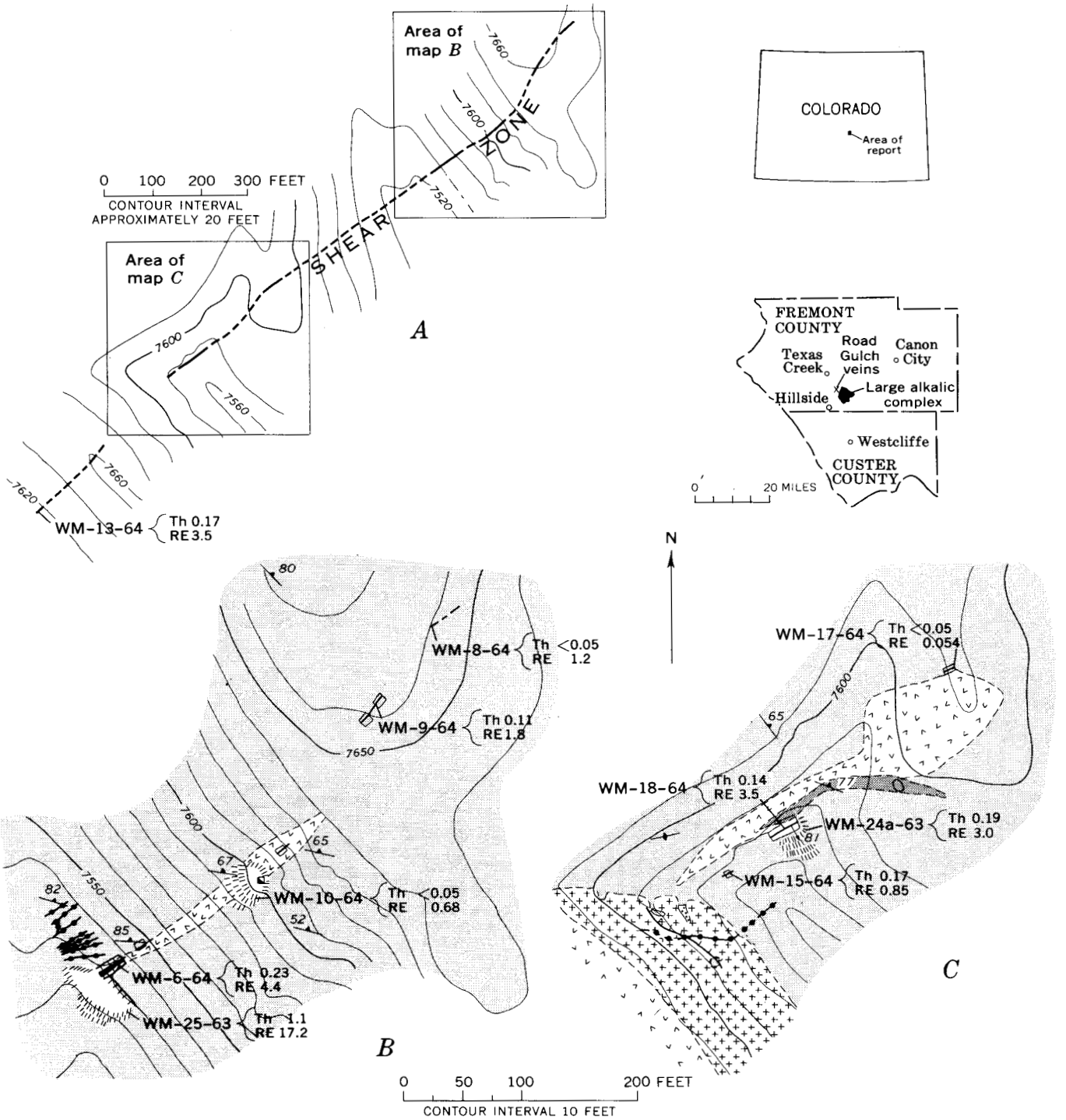


FIGURE 1.—Index map (*A*) showing shear zone that contains the rare-earth carbonate veins north of Road Gulch, and geologic maps of the northeastern (*B*) and central (*C*) parts of the shear zone, showing the outcrops of the veins, and the sample localities. Geology and topography by M. H. Staatz; datum level assumed.

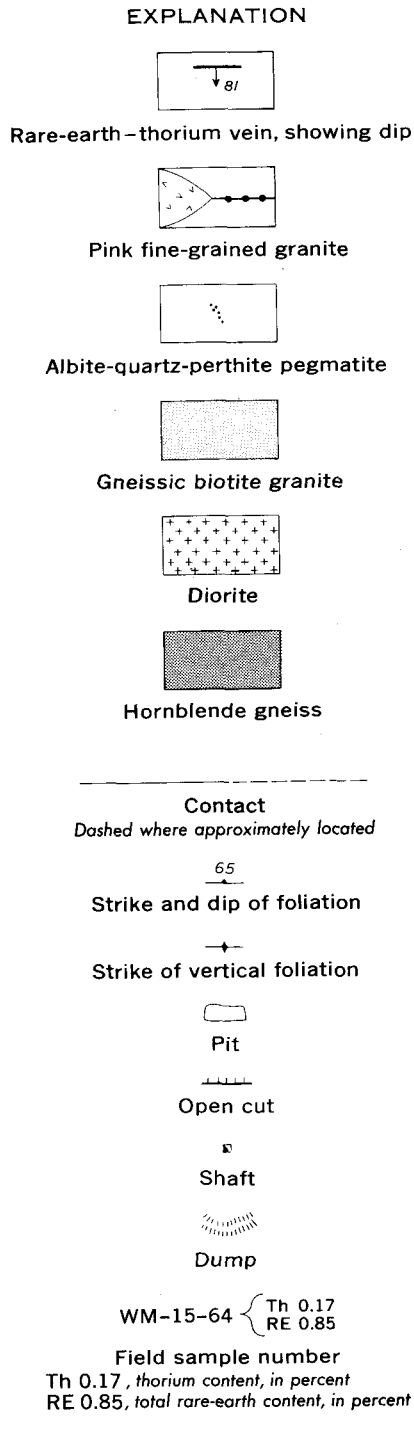


EXPLANATION FOR FIGURE 1.

southwest side of the complex (Christman and others, 1959, tables 5 and 6), where in only 1 sample out of 14 did the rare-earth content exceed the thorium content. Moreover, the RE : Th ratio of this one sample was much lower than that of the Road Gulch veins, being only 1.48.

The high barium content is due to the presence of barite. The mineral containing stromtium is not known, although it may be a carbonate. The amount of strontium in a sample is completely independent of the amount of barium. Niobium in the vein is probably chiefly in fergusonite, the only niobium mineral identified. The niobium content of the veins is not high enough to be of economic interest.

The chemical composition of the Road Gulch veins, characterized by high carbonate content, and abnormally large concentrations of the rare earths, barium, strontium, and niobium, suggests that these rocks are carbonatites. Carbonatites are commonly in or related to alkalic igneous rocks, and these veins lie only 1.4 miles west of one of the largest alkalic intrusive complexes in North America.

## REFERENCES

Christman, R. A., Brock, M. R., Pearson, R. C., and Singewald, Q. D., 1959, Geology and thorium deposits of the Wet Mountains, Colorado—a progress report: U.S. Geol. Survey Bull. 1072–H, p. 491–535.

Christman, R. A., Heyman, A. M., Dellwig, L. F., and Gott, G. B., 1953, Thorium investigations, 1950–52, Wet Mountains, Colorado: U.S. Geol. Survey Circ. 290, 40 p.

Parker, R. L., and Hildebrand, F. A., 1963, Preliminary report on alkalic intrusive rocks in the northern Wet Mountains, Colorado: Art. 181 *in* U.S. Geol. Survey Prof. Paper 450–E, p. E8–E10.

Singewald, Q. D., and Brock, M. R., 1956, Thorium deposits in the Wet Mountains, Colorado *in* Page, L. R., Stocking, H. E., and Smith, H. B., compilers, Contributions to the geology of uranium and thorium by the United States Geological Survey and Atomic Energy Commission for the United Nations International Conference on Peaceful Uses of Atomic Energy, Geneva, Switzerland, 1955: U.S. Geol. Survey Prof. Paper 300, p. 581–585.

Staatz, M. H., Adams, J. W., and Cronklin, N. M., 1965, Thorium-bearing microcline-rich rocks in the southern Caballo Mountains, Sierra County, New Mexico: U.S. Geol. Survey Prof. Paper 525–D, p. D48–D51.

TABLE 1.—*Quantitative spectrographic analyses of veins along the shear zone north of Road Gulch, northern Wet Mountains, Colo.*

[Location of samples shown on figure 1. Analysts: Samples WM-24a-63 and WM-25-63, R. G. Havens; all others, N. M. Conklin. Abbreviations: ND, not determined; NC, not calculated]

| Field No. | Laboratory No. | Type of sample | Composition (weight percent) | | | | | | | | | | ΣRE[1]/Th |
|---|---|---|---|---|---|---|---|---|---|---|---|---|---|
| | | | La | Ce | Nd | Y | Yb | ΣRE[1] | Th | U | Ba | Sr | Nb | |
| WM-24a-63 | D113183 | Selected material from dump. | 1.2 | 1.3 | 0.48 | 0.034 | 0.0013 | 3.0 | 0.19 | ND | 8.4 | 0.23 | 0.012 | 15.9 |
| WM-25-63 | D113184 | do | 5.0 | 8.8 | 3.2 | .20 | .0047 | 19.2 | 1.1 | ND | 13.0 | .18 | <.01 | 15.6 |
| WM-6-64 | D114638 | 1.9-ft chip sample across entire vein. | 1.6 | 2.1 | .64 | .063 | .0039 | 4.4 | .23 | <0.05 | 6.3 | .38 | <.005 | 19.2 |
| WM-8-64 | D114639 | Grab sample of dump material. | .37 | .58 | .20 | .013 | .00074 | 1.2 | <.05 | <.05 | 1.1 | .14 | .017 | NC |
| WM-9-64 | D114640 | 2.5-ft chip sample across entire vein. | .60 | .91 | .28 | .016 | .00088 | 1.8 | .11 | <.05 | 3.1 | .050 | .0059 | 16.4 |
| WM-10-64 | D114641 | Grab sample of dump material from shaft. | .22 | .29 | .10 | .065 | .0040 | .68 | <.05 | <.05 | .37 | .055 | .0094 | NC |
| WM-13-64 | D114642 | 6.0-ft chip sample across northern 6 ft of an 8-ft vein. | .36 | .64 | .26 | .021 | .00096 | 1.3 | .17 | <.05 | 7.7 | .11 | .014 | 7.5 |
| WM-15-64 | D114643 | 1.7-ft chip sample across entire vein. | .18 | .44 | .16 | .064 | .0036 | .85 | .17 | <.05 | 1.0 | .43 | .0057 | 5.0 |
| WM-17-64 | D114644 | 1.3-ft channel sample across entire vein. | .045 | <.1 | <.07 | .0087 | .00074 | .054 | <.05 | <.05 | .28 | .072 | .011 | NC |
| WM-18-64 | D114645 | 1.8-ft channel sample across entire vein 6 ft below surface. | 1.2 | 1.7 | .56 | .063 | .0030 | 3.5 | .14 | <.05 | 3.8 | .21 | .0093 | 25.2 |

[1] Total of rare earths analyzed.

# FIELD DETERMINATION OF NANOGRAM QUANTITIES OF MERCURY IN SOILS AND ROCKS

By MARGARET HINKLE, KAM WO LEONG, and F. N. WARD, Denver, Colo.

*Abstract.*—A method for determining nanogram quantities of mercury in geological materials is based on the catalytic effect of mercury on the reaction of ferrocyanide with nitrosobenzene to produce a violet-colored compound whose intensity is proportional to the mercury present. The mercury is released by heating a sample of soil or crushed rock to about 650°C. As little as 30 nanograms of mercury (30 parts per billion in a 1-gram sample) can be detected. The reliability of the method is adequate to permit its use in geochemical surveys that utilize mercury as a pathfinder element.

During the past several years, there has been considerable interest in the use of mercury as a pathfinder element for concealed hypogene deposits (Ginzburg, 1960, p. 13; Hawkes and Webb, 1962, p. 73). To measure the small amounts of mercury occurring in the halos around such deposits, very sensitive spectrographic (Sergeev, 1961) and vapor-absorption procedures (Hawkes and Williston, 1962; Vaughn and McCarthy, 1964) have been developed. Both types of measurement, however, require elaborate and expensive instrumentation, and this has tended to reduce the potential usefulness of mercury surveys in geochemical prospecting. Accordingly, a simple chemical procedure was developed to offset the limitations imposed by the costly instrumentation. Although the method has not been completely tested and evaluated, the preliminary results are encouraging, especially in view of the great interest in mercury as a pathfinder element.

This procedure is based on the catalytic effect of mercury on the reaction of ferrocyanide with nitrosobenzene to produce a violet-colored compound whose intensity is related to the mercury concentration (Asperger and Murati, 1954). The color can be measured spectrophotometrically (that is, with an instrument) or by visual comparison with standard solutions of known mercury content.

The method described here permits the determination of as little as 30 nanograms ($3\times10^{-8}$ grams) of mercury, which is 30 parts per billion in a 1-gram sample. Larger samples can be used to achieve the determination of smaller content, but this is generally unnecessary because the background amount of mercury in most rocks is of the same order of magnitude (Turekian and Wedepohl, 1961).

## EQUIPMENT

In addition to such regular laboratory equipment as pipets and volumetric flasks, the following equipment is also needed to carry out the mercury analysis:

Aluminum heating block with magnetic stirrer; combination is commercially available.
Magnets, ½-inch, Teflon-covered.
Pyrex test tubes, 16×150 mm.
Pyrex test tubes, 18×75 mm, prepared by cutting off top end of 18×150 mm tube, and fitting with female standard taper 1/20.
Rack, test-tube.
Tube, delivery, 21 cm long, bent at right angles and fitted with male standard taper 1/20.
Tube furnace, electric (alternatively, a propane torch can be used as a heat source).
Water bath, constant-temperature.

## REAGENTS

All reagents needed for this analytic technique are prepared with demineralized water as follows:

Acetate buffer: Dissolve 164 g anhydrous sodium acetate or 272 g trihydrate in 1 liter water. Add glacial acetic acid until pH is 3.25, as measured with a pH meter.
Bromine-buffer reagent: Mix 10 ml acetate buffer, 5 ml bromine water saturated at room temperature, and 85 ml water.
Ferrocyanide solution: Dissolve 0.422 g $K_4Fe(CN)_6$ in water and dilute to 1 liter.
Nitrosobenzene solution: Dissolve 8 mg nitrosobenzene in 90 ml water at 70°C (nitrosobenzene melts at 68°C); cool solution and add 10 ml acetate buffer.
Mercury standard: Dissolve 0.1354 g reagent-grade mercuric chloride in 100 ml 1*N* sulfuric acid. This standard contains 1,000 micrograms mercury per ml. Prepare 100 μg per ml and 10 μg per ml standards by dilution with 1*N* $H_2SO_4$. These standards are stable for about 3 months at ordinary temperatures. A fresh working standard of 1 μg per ml should be

U.S. GEOL. SURVEY PROF. PAPER 550-B, PAGES B135-B137

prepared every day by diluting the 10 μg per ml standard with water.

Preparation of standard solutions: Pipet aliquots of working standard (1 μg Hg per ml) into a series of test tubes as follows: none to first tube, 30 lambda to second, 50 lambda to third, 100 to fourth, 200 to fifth, 400 to sixth, and 800 lambda to seventh tube. Add 5 ml bromine buffer-reagent to each tube and continue with step 4 of procedure.

## PROCEDURE

The procedure for analysis includes the following steps:

1. Place 0.1 to 0.5 g of minus-40 mesh soil or rock sample into an 18 × 75 mm test tube, fit delivery tube, and insert end of tube containing sample into tube furnace maintained at about 650°C.
2. Heat sample for 2 min and collect evolved vapors in 4 ml bromine-buffer reagent contained in 16 × 150 mm test tube.
3. Remove sample tube from hot furnace, disconnect delivery tube, and rinse with 1 ml bromine-buffer reagent. Add rinse to collecting reagent.
4. Place magnetic stirring bar in test tube containing collected vapors, insert tube in aluminum heating block fitted over magnetic stirrer, and heat test tube at 95°C until bromine distillation is complete and solution colorless. Heat for an additional 2 min. Cool solution to 25°C and remove magnet.
5. Add 1 ml potassium ferrocyanide and 2 ml nitrosobenzene solutions to the contents of the test tube, mix, and place test tube in water bath at 50°C for 45 min.
6. Remove tubes from water bath, cool rapidly, and compare with standard solutions by viewing axially. Alternatively, use a spectrophotometer to measure absorbance at 528 millimicrons and ascertain mercury content by reference to a previously established standard curve.
7. The parts per billion of mercury are obtained from the following equation:

$$\text{ppb Hg} = \frac{\text{nanograms Hg}}{\text{grams sample}}$$

## EXPERIMENTS AND DISCUSSION

A possible mechanism suggested by Asperger and others (1953) for the catalytic reaction is as follows:

$$Fe(CN)_6^{-4} \overset{H_2O}{\rightleftarrows} [Fe(CN)_5(H_2O)]^{-3} + CN^{-1}$$

$$[Fe(CN)_5(H_2O)]^{-3} + C_6H_5NO \overset{Hg^{+2}}{\rightarrow} [Fe(CN)_5(C_6H_5NO)]^{-3} + H_2O$$

$$CN^{-1} + H_2O \rightleftarrows HCN + OH^{-1}$$

Other reactions such as the oxidation of the ferrocyanide or nitrosobenzene compete with the catalytic reaction, whose rate is temperature dependent. A temperature of 50°C and a heating period of 45–60 minutes are optimum for the catalysis effect. At 60°C the reaction proceeded too rapidly, and all standard solutions of a given series turned a uniform dark pink within 20 minutes. At a temperature of less than 50°C the catalytic reaction was too slow, and air oxidation of ferrocyanide occurred.

Under uniform conditions of time and temperature the amount of the colored compound formed is proportional to the mercury content. The absorbance of the colored compound, however, is directly proportional to the mercury concentration only with amounts of mercury up to about 100 nanograms in the final solution. Between 100 nanograms and about 400 nanograms the absorbance is not linear but nevertheless is sufficiently reproducible to permit valid measurements.

With mercury amounts greater than 400 nanograms the absorbance curve flattens; that is, the absorbances increase more slowly with mercury concentration, and differences in absorbance become difficult to measure except by changing the geometry of the system or by increasing the sensitivity of the detector. Use of spectrophotometric equipment allows changes in detector sensitivity, but the system geometry is more easily changed and in the range of 400 to 800 nanograms visual, rather than instrumental, comparisons are made by viewing the colored product axially. This mode takes advantage of the longer light path—5 cm—of the final solution in a test tube.

The color of the complex formed is stable for at least 30 minutes at room temperature and for as long as 90 minutes if the solutions are kept at refrigerator temperatures. The color fades rapidly if exposed to sunlight, as reported by Asperger and Murati (1954).

Distillation of mercury from the soil or rock sample effects a separation from most elements which interfere with the subsequent estimation. During heating, any sulfides present evolve small amounts of hydrogen sulfide and any organic matter decomposes. The hydrogen sulfide, as well as other decomposition products, decolorizes the bromine water and leads to losses of mercury because of the failure of the collecting solution to retain the mercury vapors. The use of small samples and the addition of iron filings to the sample mixture help to prevent the evolution of large volumes of hydrogen sulfide and thereby lessen the danger of loss during distillation.

The evolved mercury vapor was collected in different solutions such as bromide or bromide-buffer mixtures. The best combination proved to be a mixture of saturated bromine water and buffer prepared as described above. Under the experimental conditions given in the procedure, no further pH adjustment is necessary and the excess bromine is eliminated by heating the test tube in a heating block and stirring vigorously.

Various techniques were tried to improve the distillation and recovery of mercury, such as the use of nitrogen

to flush out the system, and the generation of gases in situ by heating decomposable compounds such as oxalic acid. The most consistent results were obtained by simply heating the crushed sample to about 650°C for 2 minutes in a 75-mm test tube fitted with a standard taper 14/20 to a delivery tube bent at a right angle to the test tube.

## RESULTS

The repeatability of the proposed procedure was tested by making 5 separate determinations on different soils and rocks all containing less than 1 part per million mercury. The range of the repeat determinations, the relative standard deviation, and the confidence limits at the 95-percent level are shown in table 1.

TABLE 1.—*Repeatability of mercury determinations*

| Sample No. | Material | Mercury found (ppb) | | | Relative standard deviation (percent) |
|---|---|---|---|---|---|
| | | High | Low | Mean and confidence limits at 95-percent level | |
| 1 | Flaky shale | 50 | 30 | 38±10. 0 | 21. 2 |
| 2 | Granite, fresh | 100 | 70 | 80±15. 2 | 15. 3 |
| 3 | Breccia (latite phonolite). | 100 | 80 | 84±11. 2 | 10. 6 |
| 4 | do | 110 | 90 | 100±12. 4 | 10. 0 |
| 5 | Granite, altered | 130 | 110 | 125±11. 1 | 8. 4 |
| 6 | Shale | 170 | 160 | 165± 9. 1 | 3. 5 |
| 7 | Limestone | 950 | 860 | 907±36. 3 | 3. 5 |

As a test of the validity of the catalytic method the results obtained thereby on different kinds of rocks and soils were compared with those obtained by the vapor absorption method (Vaughn and McCarthy, 1964). The comparison is given in table 2.

The slightly dissimilar results obtained by the two methods are due in part to differences in manner of standardization. Possible lack of homogeneity of the samples is also a factor that is difficult to evaluate. Nevertheless, the results obtained by both methods are nearly interchangeable and thus it appears that the catalytic procedure is useful when the mercury content of soils and rocks is used as a parameter in geochemical exploration.

TABLE 2.—*Determinations of mercury by catalytic and vapor-absorption methods*

| Sample No. | Material | Mercury content (ppb) | |
|---|---|---|---|
| | | Catalytic method | Vapor-absorption method |
| 1 | Granite, fresh | 20 | 40 |
| 2 | Breccia (latite phonolite) | 70 | 110 |
| 3 | Granite, altered | 200 | 290 |
| 4 | Breccia (latite phonolite) | 200 | 470 |
| 5 | Limestone | 2, 000 | 5, 090 |
| 6 | Flaky shale | 80 | 50 |
| 7 | Alluvium | 100 | 150 |
| 8 | Weathered shale | 80 | 200 |
| 9 | do | 180 | 300 |
| 10 | Shale | 100 | 300 |
| 11 | Weathered shale | 520 | 800 |
| 12 | Shale | 200 | 450 |

## REFERENCES


Asperger, S., and Murati, I., 1954, Determination of mercury in the atmosphere: Anal. Chemistry, v. 26, p. 543–545.

Asperger, S., Murati, I., and Cupahin, O., 1953, Kinetics of the reaction of potassium ferrocyanide and nitrosobenzene: the catalytic action of mercuric ions and ultraviolet light: Jour. Chem. Soc., p. 1041–1046.

Ginzburg, I. I., 1960, Principles of geochemical prospecting: New York, Pergamon Press, 311 p.

Hawkes, H. E., and Webb, J. S., 1962, Geochemistry in mineral exploration: New York, Harper and Row, 415 p.

Hawkes, H. E., and Williston, S. H., 1962, Mercury vapor as a guide to lead-zinc-silver deposits: Mining Cong. Jour., v. 48, no. 12, p. 30–32.

Sergeev, E. A., 1961, Methods of mercurometric investigations: Internat. Geol. Rev., v. 3, no. 2, p. 93–99.

Turekian, K. K., and Wedepohl, K. H., 1961, Distribution of the elements in some major units of the earth's crust: Geol. Soc. America Bull., v. 72, p. 175–192.

Vaughn, W. W., and McCarthy, J. H., Jr., 1964, An instrumental technique for the determination of submicrogram concentrations of mercury in soils, rocks, and gas, *in* Geological Survey Research 1964: U.S. Geol. Survey Prof. Paper 501–D, p. D123–D127.

# TELLURIUM AND MERCURY IN JASPEROID SAMPLES

By T. G. LOVERING, H. W. LAKIN, and J. H. McCARTHY, Denver, Colo.

*Abstract.*—Ninety-three samples of jasperoid from 22 areas, including 14 mining districts, were analyzed for tellurium and mercury by new methods capable of detecting 0.1 ppm of tellurium (by precipitation of gold in HCl) and 0.01 ppm of mercury (by atomic absorption). These samples had been analyzed spectrographically for minor elements and classified on the basis of their field relations, composition, and other characteristics as either "favorable type" (commonly associated with metalliferous ore), or "unfavorable type" (not commonly associated with ore).

Tellurium content of these samples ranges from 200 to $<0.1$ ppm, mercury content from 90 to 0.02 ppm. Statistically significant associations were found between Te and As, Bi, Ag, Sb, Pb, Cu, Hg, and Ba; and between Hg and Ag, Pb, Cu, Te, Zn, Sb, As, Bi, and Mo, in order of decreasing strength of association. Tellurium content of $>1$ ppm and mercury content of $>5$ ppm are found to be characteristic of jasperoid of the favorable type.

Ninety-three samples of jasperoid and chert from 22 areas, including 14 mining districts and mineralized areas, were analyzed for tellurium and mercury (table 1). Information was gathered on (1) the variation of mercury and tellurium in jasperoid and chert, and (2) the suites of minor elements most significantly associated with mercury and tellurium in jasperoid. The objective was to test the significance of these two elements as criteria for recognizing metalliferous ore-associated jasperoid bodies. New sensitive methods of analysis capable of detecting as little at 0.1 part per million of tellurium and 0.01 ppm of mercury were used. Tellurium was found in 52 samples in amounts ranging from the limit of detection up to a maximum concentration of 200 ppm. Mercury was found in all 93 samples in concentrations ranging from 0.02 ppm up to 90 ppm. Jasperoid samples from the following districts and mineralized areas are included in the group of samples analyzed: Kokomo, Gilman, Leadville, Pando, and Uncompahgre in Colorado; Santa Rita in New Mexico; Tri-State (Oklahoma-Kansas-Missouri); Tintic, Mercur-Ophir, Bingham, San Francisco, and Vernon in Utah; Metaline in Washington; and Shirley Basin in Wyoming.

## METHODS OF CHEMICAL ANALYSIS

Tellurium was determined in the jasperoid by a method based on the induced precipitation of elemental gold from a $6N$ HCl solution containing gold chloride, cupric chloride, and hypophosphorous acid; the amount of the gold reduced is proportional to the amount of tellurium present (Lakin and Thompson, 1963). The jasperoid was fused with sodium carbonate to effect solution. The elemental gold precipitate was collected on filter paper and compared visually with standards prepared in the same way. The precision of analysis is $\pm 25$ percent.

The analytical method used for the determination of mercury is based on the principle of atomic absorption. Mercury is vaporized by rapidly heating the sample to about 600°C with radiofrequency energy. The mercury vapor is selectively trapped by amalgamation with gold while interfering gasses are expelled from the system. The trapped mercury is volatilized by heating the gold, and the resulting vapor is carried by an air stream into an absorption chamber. Mercury vapor absorbs ultraviolet light in the chamber, producing a signal which is converted to digital form and calibrated to mercury concentration. The instrument is described in detail by Vaughn and McCarthy (1964). The precision of analysis in the range is about $\pm 20$ percent.

## DATA ANALYSIS

The samples included in this study were part of the suite used to establish criteria for the recognition of jasperoid associated with sulfide ore (Lovering and Hamilton, 1962), and our classification as "favorable" or "unfavorable" is the same as the classification used in that paper for "productive" or "barren," respectively. This change in terminology has been made because the term "productive" is commonly interpreted as meaning not merely associated with ore, but actually minable as ore.

The samples included in the original study cited above were first separated into two groups on the basis

TABLE 1.—*Tellurium and mercury content of 93 samples of jasperoid and chert*

[F, favorable jasperoid; U, unfavorable jasperoid; C, chert]

| Sample No. | Locality | Classification | Te (ppm) | Hg (ppm) |
|---|---|---|---|---|
| I–2 | Specimen Mountain, Colo. | U | <0.1 | 0.7 |
| 5 | Taylor Park, Colo | C | <.1 | .15 |
| 1273 | Caddo Gap, Ark | C | <.1 | .6 |
| 13 | Argyle quadrangle, South Dakota. | C | <.1 | .8 |
| 15 | Iron Mountain, N. Mex. | C | <.1 | 1.5 |
| 18 | Death Valley, Calif. | C | <.1 | 1.0 |
| 19 | Shirley Basin, Wyo | F | <.1 | 2.0 |
| 20A | Gunnison River Canyon, Colo. | F | <.1 | .55 |
| 20B | do | U | <.1 | .45 |
| II–1 | Metaline district, Washington. | F | <.1 | .65 |
| III–3 | Kokomo district, Colorado. | F | <.1 | 8 |
| 4A | do | F | <.1 | 8 |
| 4B | do | F | <.1 | 12 |
| IV–2 | Gilman district, Colorado. | U | <.1 | 2.0 |
| 3 | do | U | <.1 | .50 |
| 4 | do | F | <.1 | 1.0 |
| 5A | do | U | <.1 | 1.2 |
| 6 | do | U | <.1 | 1.2 |
| 8 | do | C | <.1 | 1.7 |
| V–1 | Leadville district, Colorado. | F | <.1 | 10 |
| 2 | do | F | <.1 | 8 |
| 4 | do | F | <.1 | 6 |
| 5 | do | F | <.1 | 6 |
| 6 | do | F | <.1 | 10 |
| VI–3 | Pando area, Colorado | U | <.1 | 3.5 |
| 5 | do | U | <.1 | 1.0 |
| 8 | do | U | <.1 | .8 |
| VII–1A | Tintic district, Utah | F | <.1 | 25 |
| 1B | do | F | <.1 | 20 |
| 2 | do | F | 5 | 90 |
| 3 | do | U | <0.1 | 4 |
| 5 | do | F | 4 | 30 |
| 6 | do | F | <.1 | 7 |
| 6A | do | F | 40 | 40 |
| 7 | do | F | 15 | 10 |
| 8 | do | F | 20 | 35 |
| 9 | do | F | 40 | 8 |
| 10 | do | F | 5 | 8 |
| 11 | do | F | 10 | 30 |
| 11A | do | F | 12 | 17 |
| 11B | do | F | 40 | 35 |
| 12 | do | F | 80 | 1.2 |
| 12B | do | F | 200 | 30 |
| 13 | do | F | 200 | 15 |
| 14 | do | F | 15 | 2.5 |
| 14A | do | F | 15 | 30 |

TABLE 1.—*Tellurium and mercury content of 93 samples of jasperoid and chert*—Continued

[F, favorable jasperoid; U, unfavorable jasperoid; C, chert]

| Sample No. | Locality | Classification | Te (ppm) | Hg (ppm) |
|---|---|---|---|---|
| VII–15 | Tintic district, Utah | U | <0.1 | 1.2 |
| 15A | do | U | <.1 | 10 |
| 16 | do | U | .4 | 1.0 |
| 16A | do | U | 1.5 | 1.0 |
| 16B | do | U | .3 | 1.7 |
| 17B | do | U | .6 | 1.0 |
| VIII–1 | Tri-State district (Oklahoma-Kansas-Missouri). | C | .15 | 1.0 |
| 2 | do | F | <.1 | 7 |
| IX–1A | Mercur-Ophir districts, Utah. | F | 12 | 2.0 |
| 1B | do | U | .1 | .8 |
| 1C | do | U | 4 | 8 |
| 2A | do | F | 12 | 10 |
| 2B | do | U | .5 | 3.5 |
| 3A | do | U | .1 | 1.2 |
| 3C | do | U | .1 | 15 |
| 4 | do | U | 4 | 5 |
| 5 | do | F | 60 | 2.5 |
| 6 | do | F | 20 | 25 |
| 7 | do | U | .2 | 2.5 |
| 8 | do | U | 2.5 | 1.2 |
| 9 | do | U | .4 | .3 |
| 10 | do | F | 12 | 1.5 |
| 12 | do | U | <.1 | 1.2 |
| 13 | do | F | <.1 | .1 |
| 14 | do | F | 15 | .7 |
| 15 | do | F | 2.5 | 5.5 |
| X–1A | Uncompahgre district, Colo. | F | 15 | 6.5 |
| 1B | do | F | 15 | 17 |
| 1C | do | F | 1 | 3.5 |
| XII–2 | Bingham district, Utah. | F | 2.5 | 1.5 |
| 3 | do | U | <.1 | 5.0 |
| 4 | do | F | 20 | 2.0 |
| 5 | do | F | 200 | 2.0 |
| 6 | do | F | 80 | .8 |
| XIV–1 | Santa Rita district, N. Mex. | F | <.1 | .15 |
| 2 | do | U | <.1 | .25 |
| 4 | do | F | 20 | .9 |
| XV–1 | Tasmania, Australia | U | .5 | .00 |
| 2 | do | U | <.1 | .02 |
| 3 | do | U | 2 | .35 |
| XVI–1 | San Francisco district, Utah. | U | 1 | .15 |
| 2 | do | U | .15 | .3 |
| 3 | do | U | .3 | .07 |
| 7 | do | U | <.1 | .05 |
| 8 | do | U | <.1 | 1.2 |
| 10 | do | U | .1 | .09 |
| XVII–1 | Vernon area, Utah | U | .1 | .25 |

of their known field association or lack of association with ore bodies. The frequency of occurrence of various attributes in samples from each group was then compared statistically, and point scores were awarded to the attributes, depending on the statistical significance of the observed differences in their distributions. The total scores for all such attributes were then calculated for each sample and the final classification as productive (favorable) or barren (unfavorable) was made on the basis of this total score. The reader is referred to the earlier paper (Lovering and Hamilton, 1962) for further details on the derivation and application of the classification system used in this study.

A few samples of syngenetic or diagenetic chert are included in the group analyzed for mercury and tellurium. All these yielded scores placing them in the unfavorable category, so they were grouped with the unfavorable jasperoid samples for statistical tests. Table 1 shows the sample number, locality, classification, and the tellurium and the mercury content of each sample.

These 93 samples had previously been analyzed spectrographically by the 3-step method for 40 elements, 12 of which are present in detectable concentrations in more than 20 percent of the samples. Figures were reported in percent to the nearest number in the series, 7, 3, 1.5, 0.7, 0.3, 0.15, and so forth. The assigned group included the quantitative value about 60 percent of the time.

Two sets of tables were prepared in the present study, showing tellurium and mercury analyses, respectively, arranged in order of decreasing concentration, plus the corresponding analyses for each of the other 13 elements. Ranks were then assigned to the reported concentrations of each element, and the strength of association between tellurium and mercury and each of the other elements was tested using Spearman's rank correlation coefficient corrected for tied ranks (Siegel, 1956, p. 202–213).

There are 48 favorable and 45 unfavorable samples in the entire suite. The classified analyses for tellurium and mercury were first examined to determine the concentration level ($C$) of the element above which most of the samples are of the favorable type, and below which most of the samples are of the unfavorable type. The frequency data for the two elements were then entered in $2\times2$ contingency tables of the form shown below and the dichotomy tested for significance by chi square (Siegel, 1956, p. 104–111).

| | $>C$ | $<C$ |
|---|---|---|
| Favorable | | |
| Unfavorable | | |

## INTERPRETATION AND CONCLUSIONS

Rank correlation coefficients between mercury and tellurium and the other elements are tabulated below, together with their significance levels calculated from Student's $t$ distribution (Siegel, 1956, p. 212).

| | | | | | |
|---|---|---|---|---|---|
| Significant at 0.001 | Te vs. As | +0.62 | Significant at 0.001 | Hg vs. Ag | +0.66 |
| | Te vs. Bi | +.62 | | Te vs. Pb | +.66 |
| | Te vs. Ag | +.55 | | Te vs. Cu | +.48 |
| | Te vs. Sb | +.49 | | Te vs. Te | +.41 |
| | Te vs. Pb | +.46 | | Te vs. Zn | +.38 |
| | Te vs. Cu | +.44 | | Te vs. Sb | +.37 |
| | Te vs. Hg | +.41 | | Te vs. As | +.35 |
| | Te vs. Ba | +.35 | Significant at 0.01 | Te vs. Bi | +0.31 |
| Not significant | Te vs. Zr | +0.26 | | Te vs. Mo | +.27 |
| | Te vs. Sr | +.24 | | Te vs. Ba | +0.22 |
| | Te vs. Zn | +.17 | Not significant | Te vs. Ni | +.20 |
| | Te vs. Mo | +.15 | | Te vs. Sr | +.18 |
| | Te vs. Ni | −.07 | | Te vs. Zr | −.04 |

The significance level indicates the proportion of values as great as, or greater than, the observed value, which could occur by chance if the population distributions of the two elements were completely independent. For example, the statement that the correlation of +0.66 between mercury and silver is significant at the 0.001 level means that this strong an association between these elements in the jasperoid samples could occur by chance less than once in a thousand times, if in fact there were no association between mercury and silver in the jasperoids represented by the samples.

The two elements, tellurium and mercury, show notable differences in their associations in spite of the fact that they are both volatile, mobile elements. Both elements correlate relatively strongly with silver, moderately with copper, and not significantly with nickel, strontium, or zirconium. Tellurium associates relatively strongly with arsenic, bismuth, silver, and antimony; moderately with lead, copper, mercury, and barium; and shows no significant association with either zinc or molybdenum. Mercury, on the other hand, associates most strongly with silver and lead; moderately with copper, tellurium, zinc, antimony, and arsenic; weakly with bismuth and molybdenum; and not significantly with barium, nickel, strontium, or zirconium.

Examination of the data showed that a majority of the favorable samples contain tellurium in concentrations $\geqq 1$ ppm, and mercury in concentrations $\geqq 5$ ppm; most of the barren samples contain less than these amounts. The resulting contingency tables are shown below.

| | Te≧1 ppm | Te<1 ppm | Hg≧5 ppm | Hg<5 ppm |
|---|---|---|---|---|
| Favorable | 30 | 18 | 30 | 18 |
| Unfavorable | 7 | 38 | 6 | 39 |

The values of chi squared obtained from these 2 distributions are greater than 15 and thus significant at the 0.001 level. Therefore, the presence of tellurium in concentrations of 1 ppm or more, or the presence of mercury in concentrations of 5 ppm or more, is a criterion for the recognition of favorable jasperoid.

The data in table 1 show that there are differences in the mercury and the tellurium content of favorable jasperoid from district to district. Ten districts from which favorable jasperoid was collected are represented by more than 1 sample; the samples from 5 of these show less than 1 ppm of tellurium, and samples from 4 such districts contain less than 5 ppm of mercury. The 5 districts represented by samples containing more than 1 ppm of tellurium (Tintic, Mercur-Ophir, Uncompaghre, Bingham, and Santa Rita) yielded a total of 35 favorable and 19 unfavorable samples, and 4 of the unfavorable samples assayed $>1$ ppm of tellurium. The 6 districts represented by samples containing more than 5 ppm of mercury (Kokomo, Leadville, Tintic, Tri-State, Mercur-Ophir, Uncompahgre, and Bingham) yielded a total of 42 favorable and 18 unfavorable jasperoid samples; 30 of the favorable samples and 5 of the unfavorable samples assayed $>5$ ppm of mercury.

Although these distributions suggest that the presence of tellurium or mercury in jasperoid samples in the amounts specified is a valid criterion for the recognition of favorable jasperoid, their absence in these amounts is not, by itself, indicative of unfavorable jasperoid. Mercury and tellurium are two more elements whose concentration in jasperoid samples can be used in conjunction with the other criteria listed by Lovering and Hamilton (1962, p. C11) for the classification of jasperoid samples as favorable or unfavorable.

## REFERENCES

Lakin, H. W., and Thompson, C. E., 1963, Tellurium—a new sensitive test: Science, v. 141, No. 3575, p. 42–43.

Lovering, T. G., and Hamilton, J. C., 1962, Criteria for the recognition of jasperoid associated with sulfide ore: Art. 63 *in* U.S. Geol. Survey Prof. Paper 450–C, p. C9–C11.

Siegel, Sidney, 1956, Nonparametric statistics for the behavioral sciences: New York, McGraw-Hill Book Co., 312 p.

Vaughn, W. W., and McCarthy, J. H., Jr., 1964, An instrumental technique for the determination of submicrogram concentrations of mercury in soils, rocks, and gas, *in* Geological Survey Research 1964: U.S. Geol. Survey Prof. Paper 501–D, p. D123–D127.

# URANIUM-LEAD AND POTASSIUM-ARGON AGES OF PARTS OF THE AMARGOSA THRUST COMPLEX, DEATH VALLEY, CALIFORNIA

By T. W. STERN, M. F. NEWELL, and C. B. HUNT,[1]
Washington, D.C., Baltimore, Md.

*Abstract.*—Zircon from Precambrian augen gneiss in the lower plate of the Amargosa thrust has a $Pb^{207}/Pb^{206}$ age of 1,820 million years. Feldspar from Tertiary quartz monzonite and monzonite porphyry intrusives has yielded a K-Ar age of 12 to 14 m.y. Biotite in the Precambrian augen gneiss has a K-Ar age of 11 to 14 m.y. and reflects the reheating associated with the emplacement of younger intrusions and the volcanic rocks. Pb-$\alpha$ ages of zircon in the igneous rocks are also Tertiary but have a large probable error compared to the calculated age, due to the uncertainty involved in measuring lead below 10 parts per million by spectrochemical means.

The determined ages agree well with the stratigraphic and structural relationships determined by field geologic mapping. However, the ages are inconclusive as a means of establishing whether the igneous rocks were derived by melting of the Precambrian rocks and as to what extent the volcanic rocks were derived by differentiation of intrusions that breached their roofs.

Precambrian gneiss, in part containing augen of potash feldspar and of biotite, forms the lower plate of the Amargosa thrust fault at the east foot of the Panamint Range. Granitic intrusions have invaded the thrust fault by spreading laterally along it and doming the upper plate. Volcanic rocks younger than the intrusions and in part fed by dikes cutting the granitic intrusions form a complex referred to as the Amargosa chaos that was itself involved in later movements of the upper plate of the thrust. On the basis of field studies of these structural and igneous relationships, Hunt (in press) suggested that the thrust faulting, metamorphism, emplacement of the granite, and volcanism in this part of Death Valley (figs. 1 and 2) may be related as follows:

1. Part of the metamorphism of the Precambrian rocks under the Amargosa thrust fault may have been caused by the thrusting and (or) by the emplacement of granitic masses along the thrust.

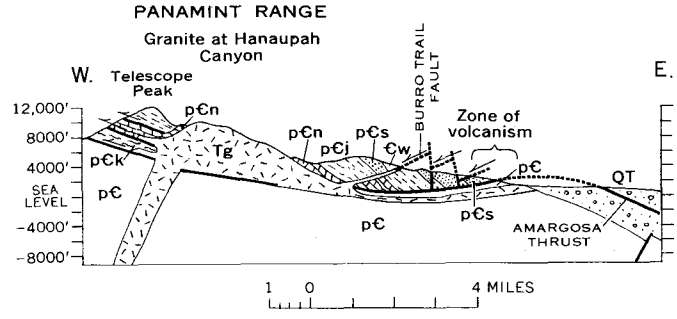


FIGURE 1.—Diagrammatic cross section of the Panamint Range (from Hunt, in press). Along the Amargosa thrust late Precambrian and Paleozoic sedimentary formations have been thrust westward onto older Precambrian metamorphic rocks (p€). Tertiary granitic intrusions (Tg) have spread laterally along the thrust, doming the upper plate. Volcanic rocks occur along the exposed belt of the thrust (see fig. 2). p€k, Kingston Peak(?) Formation; p€n, Noonday Dolomite; p€j, Johnnie Formation; p€s, Stirling Quartzite; €w, Wood Canyon Formation; QT, Tertiary and Quaternary valley fill in Death Valley.

2. The granitic masses, although injected into their present position, may have been derived from advanced metamorphism and melting of Precambrian rocks along the thrust.
3. The volcanic rock may have been derived by differentiation of the injected granitic masses when their roofs were breached.

Some support for the hypothesis was added by R. L. Erickson (*in* Hunt, in press), who discovered that the Precambrian rocks contain colorless rounded zircon, that the volcanic rocks and porphyries contain euhedral pink zircon, and that the granitic masses contain both kinds (fig. 3). To test the hypothesis further, 200-pound samples of the pertinent rocks were collected for radiometric age study. Five of the samples, shown on figure 2 and described in table 1, were found to contain enough zircon for analysis by U-Pb and (or) Pb-$\alpha$ methods.

[1] The Johns Hopkins University.

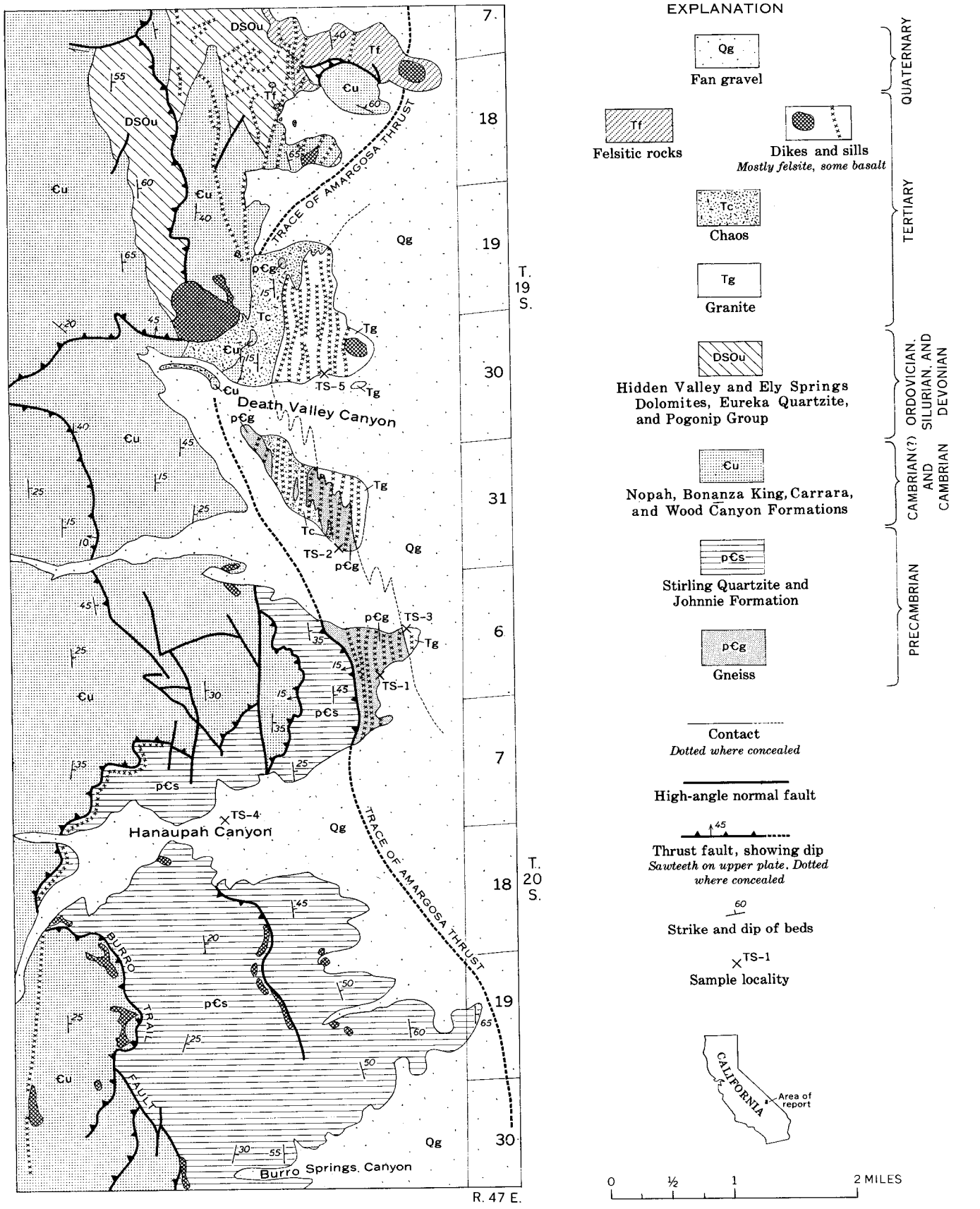


FIGURE 2.—Map of the Amargosa thrust complex at the east foot of the Panamint Range, showing location of samples collected for radiometric dating. (After Hunt, in press.)

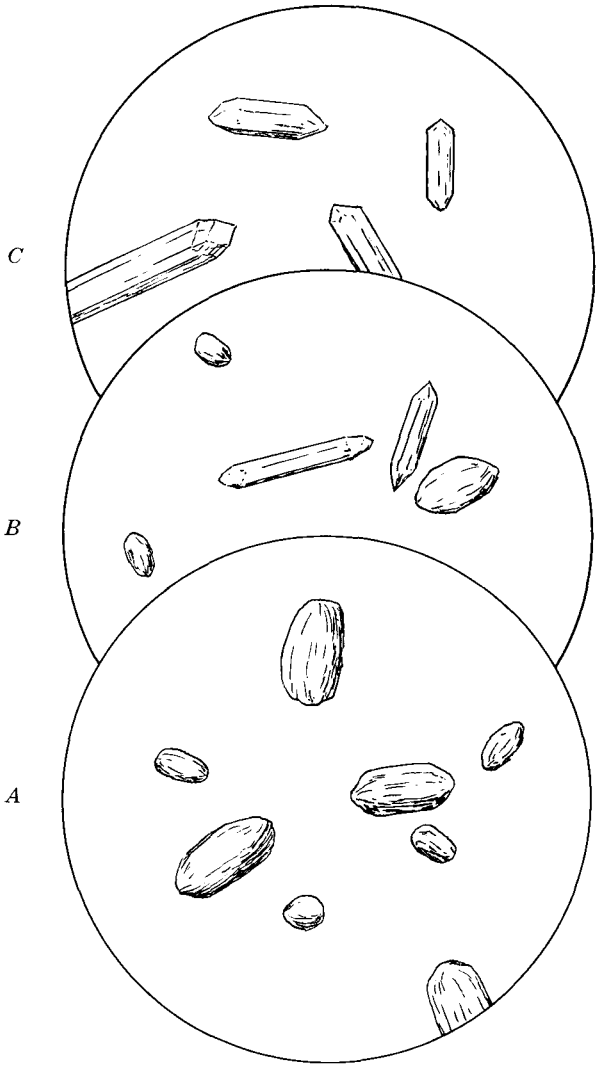


FIGURE 3.—Zircon from the Amargosa thrust complex, Death Valley, Calif. Precambrian augen gneiss contains colorless round zircon (*A*). The granitic rock in the complex contains similar round zircon and sharply terminated, euhedral pink zircon (*B*). Felsitic dikes cutting the granite contain only pink, euhedral zircon (*C*). Width of fields, 1.35 mm. (From Hunt, in press.)

*Acknowledgments.*—We were aided by a visiting committee consisting of James Gilluly, G. D. Robinson, and A. C. Waters. They helped collect the 200-pound samples and freely gave advice, for which we are very grateful. The K-Ar age determinations on five of the samples were made by H. H. Thomas and Paul Elmore, and the spectrographic lead determinations were made by Harold Westley.

## AGE DETERMINATIONS

Results of U-Pb and Th-Pb age determinations on zircon are given in tables 2 and 3. K-Ar age determinations are shown in table 4, and Pb-$\alpha$ ages are given in table 5.

TABLE 1.—*Description of samples*

| *Sample* | *Description* |
|---|---|
| TS–1 | Augen gneiss, Amargosa thrust complex, lower plate, at 1,120 ft elevation, 3,200 ft. WNW of SW cor. sec. 6, T. 20 S., R. 47 E., Bennett's Well quadrangle, Inyo County, Calif. Considered as possible parent material for TS–5. |
| TS–2 | Augen gneiss, Amargosa thrust complex, lower plate, at 1,480 ft elevation, south end of hill 1969, 1 mi WNW of NW cor. sec. 6, T. 20 S., R. 47 E., Bennett's Well quadrangle, Inyo County, Calif. Considered as possible parent material for TS–5. |
| TS–3 | Felsitic dike at 1,080 ft elevation, 3,200 ft SW of NW cor. sec. 6, T. 20 S., R. 47 E. Related to the volcanic rocks and thought to be derived from TS-5 type of intrusion. |
| TS–4 | Monzonite porphyry at Hanaupah Canyon. Collected as boulders at canyon mouth. Thought to be derived from TS–5 type of intrusion. |
| TS–5 | Quartz monzonite phase of Tertiary granite in Amargosa thrust complex. South base of hill 1673, 6,000 ft WNW of SW cor. sec. 30, T. 19 S., R. 47 E. at mouth of Death Valley Canyon on north side of canyon. Believed to be derived from TS–1 and TS–2 types of rock and possibly parent material for TS–3 and TS–4 types. |

TABLE 2.—*Zircon ages by the* U-Pb *and* Th-Pb *methods*

| Sample | Rock | Age (m.y.) | | | |
|---|---|---|---|---|---|
| | | $Pb^{206}/U^{238}$ | $Pb^{207}/U^{235}$ | $Pb^{207}/Pb^{206}$ | $Pb^{208}/Th^{232}$ |
| TS–1 | Augen gneiss. | 1, 525 | 1, 640 | 1, 800 | 1, 665 |
| TS–2 | do | 1, 495 | 1, 520 | 1, 555 | 1, 110 |

Constants: $U^{238}$: $\lambda = 1.54 \times 10^{-10}$ year $^{-1}$.
$U^{235}$: $\lambda = 9.72 \times 10^{-10}$ year $^{-1}$.
$Th^{232}$: $\lambda = 4.88 \times 10^{-11}$ year $^{-1}$; $U^{238}/U^{235} = 137.7$.

TABLE 3.—*Analytical data for* U-Pb *and* Th-Pb *age determinations*

| Sample | Concentration (ppm) | | | Atom percent | | | |
|---|---|---|---|---|---|---|---|
| | Pb | U | Th | $Pb^{204}$ | $Pb^{206}$ | $Pb^{207}$ | $Pb^{208}$ |
| TS–1 | 160 | 557 | 142 | 0. 065 | 81. 14 | 9. 68 | 9. 11 |
| TS–2 | 169 | 610 | 135 | . 111 | 82. 51 | 9. 40 | 7. 98 |

Concentrations are believed to be correct to within 2 percent of the reported value. Replicate analyses of a standard shelf solution of common lead were reproducible to within 0.5 percent for $Pb^{206}/Pb^{204}$, 0.2 percent for $Pb^{206}/Pb^{207}$, and 0.4 percent for $Pb^{206}/Pb^{208}$. The $Pb^{206}/Pb^{204}$ for the above analyses would not be expected to be as precise as the standard shelf solution.

When as in these determinations the $Pb^{206}/U^{238}$ and $Pb^{207}/U^{235}$ ages do not agree within about 5 percent the sample is considered to be discordant. This lack of agreement can be caused by a loss or gain of lead and (or) uranium or by analytical errors and uncertainty in decay constants. The amount of discordance in these samples is too large to be ascribed solely to analytical errors and uncertainties in the decay constants, and therefore it seems that the zircon did not remain a

TABLE 4.—K-Ar *age determinations*

[Analyses by H. H. Thomas and Paul Elmore, U.S. Geological Survey]

| Sample | Mineral and rock | $K_2O$ (percent) | $K^{40}$ (ppm) | Radiogenic $Ar^{40}$ (ppm) | Radiogenic $Ar^{40}$ (percent) | $Ar^{40}/K^{40}$ | Age (m.y.) |
|---|---|---|---|---|---|---|---|
| TS-1 | Biotite in augen gneiss. | 4.32 | 4.38 | 0.00355 | 41 | 0.000811 | 14 |
| TS-2 | Biotite in augen gneiss. | 6.29 | 6.37 | .00403 | 49 | .000633 | 11 |
| TS-4 | K-feldspar in monzonite porphyry. | 5.93 | 6.01 | .60439 | 44 | .000730 | 12 |
| TS-5 | K-feldspar in quartz monzonite. | 3.70 | 3.75 | .00314 | 17 | .000837 | 14 |

Constants: $K^{40}\lambda_\epsilon = 0.585 \times 10^{-10}$/yr,
$\lambda_\beta = 4.72 \times 10^{-10}$/yr, and
$K^{40} = 1.22 \times 10^{-4}$ g/g K.
Overall analytical error is approximately 10 percent of the age result.

TABLE 5.—Pb-$\alpha$ *age determination on zircon*

| Sample | Rock | $\alpha$/mg-hr | Pb (ppm) [1] | Age (m.y.) [2] |
|---|---|---|---|---|
| TS-3 | Dike | 260 | 5.0 | 50±10 |
| TS-4 | Monzonite porphyry | 269 | 2.0 | 20±10 |
| TS-5 | Quartz monzonite | 219 | 2.4 | 30±10 |

[1] Average of duplicate determinations by Harold Westley.
[2] Ages (rounded to nearest 10 m.y.) calculated from the equation $t = C\ \mathrm{Pb}/\alpha$, where $t$ is the calculated age; $C$ is a constant based on the U/Th ratio and has a value of 2,485; Pb is the lead content in parts per million; and $\alpha$ is the alpha counts per milligram per hour.

closed system in respect to its content of uranium and lead.

Several different models for the interpretation of discordant U-Pb ages have been proposed. On a U-Pb parent-daughter diagram (fig. 4), the curve drawn through the points where the $Pb^{206}/U^{238}$ and $Pb^{207}/U^{235}$ ages are equal is known as concordia. Wetherill (1956, p. 320) suggested a graphical method in which a chord is drawn through the point defined by the measured isotopic ratios of a mineral. This chord intersects concordia in two places. The lower intersection, assuming several qualifying assumptions, represents the time of lead loss or of uranium gain. The upper intersection gives the original age of the mineral. When, as in the present study, several widely spaced points can be used to define a common chord the accuracy with which the intercepts can be located is substantially increased.

Lanphere and others (1963, p. 293) have made U–Pb age determinations on zircon separated from Precambrian augen gneiss from the upper Pleasant Canyon area, about 10 miles south of Hanaupah Canyon where the samples described in this paper were collected. The augen gneiss in the upper Pleasant Canyon and Hanaupah Canyon areas is older than the Pahrump Series, and presumably they are of the same age. They form the lower plate of the Amargosa thrust. Using K–Ar age data, Lanphere and others (1963, p. 292) assumed a possible episodic lead-loss event at 143 million years and drew a chord from this point through their zircon samples TP–20 and CP–93R, to obtain an intersection with concordia at 1,790 m.y. Our zircon sample TS–1 has suffered less lead loss or less uranium addition than either of the zircon samples analyzed by Lanphere and others. The chord passing through TP–20, CP–93R, and TS–1 intersects concordia at 1,820 m.y. and about 240 m.y.

Another model helpful in the interpretation of discordant ages was advanced by Tilton (1960, p. 2933); it is based on the hypothesis that lead is continuously lost from the mineral by diffusion throughout geologic time. A continuous diffusion curve fits our sample TS–1 and Lanphere's TP–20 and CP–93R. The primary age calculated from a continuous diffusion model is 1,850 m.y.

The second zircon sample, TS–2, from the augen gneiss does not fall on the same chord as TS–1 and the samples studied by Lanphere and others. Even though this rock appears more highly metamorphosed, its zircon is more nearly concordant at approximately 1,570 m.y. If TS–2 had been the first and only zircon from the Death Valley area analyzed, one might have erroneously concluded that since it is practically concordant it gives the age of the gneiss. It is therefore important to analyze a number of zircon samples from any one rock type to establish a reliable estimate of ages of emplacement and deformation in metamorphic areas.

Samples of biotite from the augen gneiss samples have K–Ar ages of 14 and 11 m.y. (table 4). Presumably these low ages result from the loss of argon during metamorphism.

The zircon samples concentrated from the Tertiary monzonite porphyry, quartz monzonite, and the dike were all low in lead content, and isotope dilution analyses could not be made. Pb–$\alpha$ ages (table 5) were completed but have high probable errors compared to the calculated age of the rocks. This is due to the uncertainty in spectrochemical analysis of samples containing less than 10 parts per million of lead. The calculated Pb–$\alpha$ ages of these rocks are Tertiary. The K–Ar ages of 12 and 14 m.y. determined on potassium feldspar from the monzonite porphyry and quartz monzonite (table 4) are believed more reliable than the Pb–$\alpha$ ages on the zircon from the same rocks.

## INTERPRETATION

The ages of the zircon in the augen gneiss, determined by the U–Pb and Th–Pb methods (tables 2 and 3), support the field evidence that these rocks in the lower plate of the Amargosa thrust fault are of Precambrian

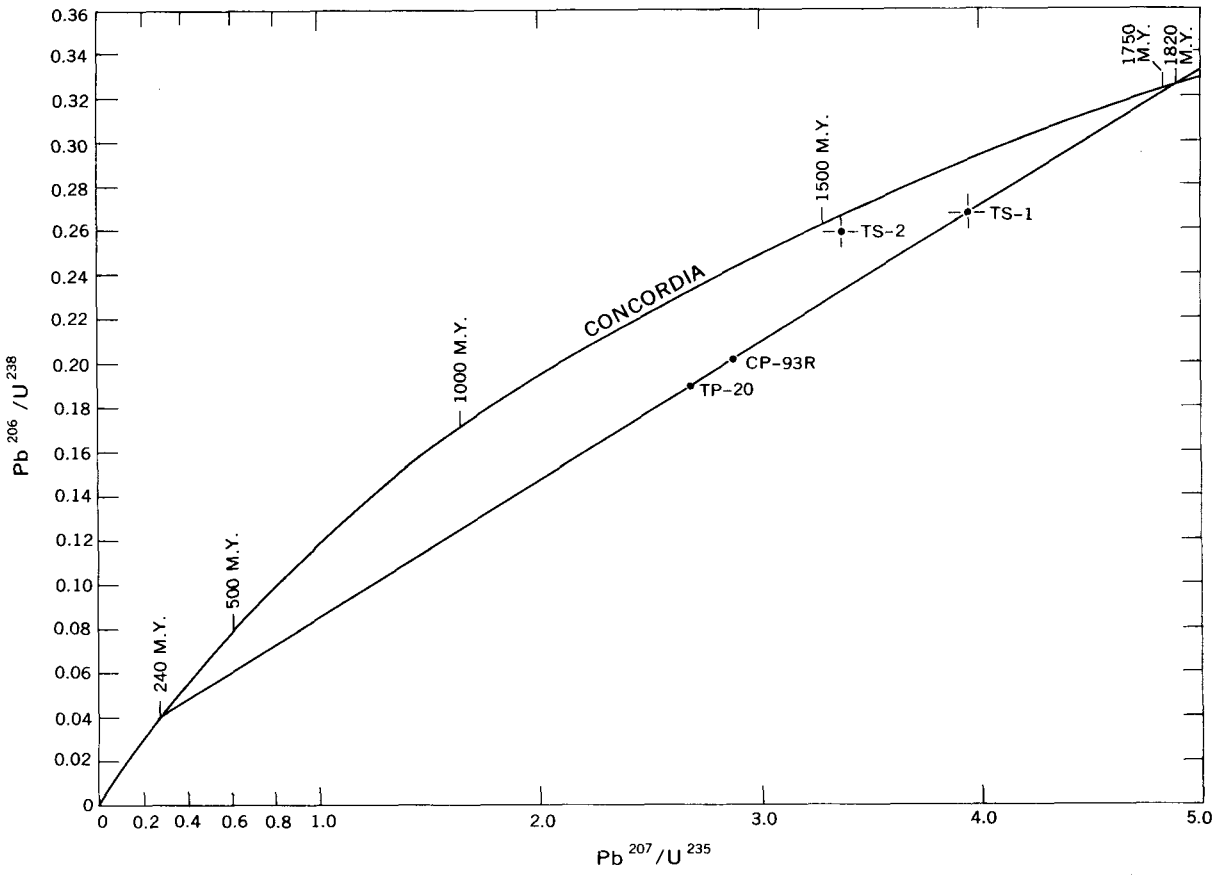


FIGURE 4.—Daughter-parent (concordia) diagram for zircon samples. The chord defines the loci of samples 1,820 m.y. old that lost varying proportions of lead episodically about 240 m.y. ago. ●, Lanphere and others (1963); +, this report.

age. The episodic lead-loss model age is about 1,820 m.y.

The relative sequence of the Tertiary rock types as indicated by the Pb–$\alpha$ ages is inconsistent with the field evidence because the dike (TS–3) is part of the swarm that cuts the quartz monzonite (TS–5) and should therefore be younger. Unfortunately it is difficult to evaluate the accuracy of lead determinations in the range of lead content from 2 to 5 parts per million. Problems of foreign lead contamination and analytical spectrochemical techniques are serious. It is, therefore, not possible to make meaningful comparisons between Pb–$\alpha$ and K–Ar ages for samples containing only a few parts per million of lead. Moreover, part of the zircon in the quartz monzonite may consist of relict Precambrian crystals similar to those found in augen gneiss (TS–1 and TS–2) (fig. 3*A* and *B*), and the indicated Pb–$\alpha$ age therefore would be too great. If the true age of the rock is about 15 m.y., as indicated by the K–Ar dates (table 4), 0.5 percent of relict zircon would double the age and give the 30-m.y. figure that was obtained. Figure 3 *B* shows that the rock contains a considerable proportion of colorless rounded zircon like that in the augen gneiss. According to this interpretation the youngest Pb–$\alpha$ ages (20 m.y.) would be the most reliable and should give the closest agreement with the comparable K–Ar ages (11–14 m.y.). Such a relationship is evident in the data in tables 4 and 5. Although this explanation of the variability of the Pb–$\alpha$ ages no doubt applies in some degree it would be premature to conclude that contamination by "old age" zircon is the only factor involved.

Similarly, all attempts to measure the ultimate age of the augen gneiss by the K–Ar method are impaired by the complete loss of argon from the biotite crystals, presumably as a thermal effect of the igneous activity. Such complete degassing does not appear to have happened in comparable environments elsewhere, as for example in the La Sal Mountains, Utah (Stern and others, 1965, p. 1503). However, in the La Sal Mountains study, hornblende, a more stable mineral than biotite, was dated. The intrusions were hypabyssal porphyries, and the contact metamorphic effects are slight (Hunt and others, 1953, p. 165) like the porphyry represented by TS–4. Consequently, these intrusions did not produce the pronounced thermal effects typical

of the quartz monzonite (TS–5) that cuts the Amargosa thrust complex.

The measured K–Ar ages of biotite in the augen gneiss are about the same as those for potassium-feldspar in the igneous rocks and fall in the range from 11 to 14 m.y. (table 4). This evidence accords with the indicated Tertiary age (30 m.y. by K–Ar determination on muscovite) of a supposedly Precambrian vein in the Funeral Mountains (Wasserburg and others, 1959, p. 702) and could be interpreted to support the suggestion that some of the metamorphic minerals in the Precambrian rocks are attributable to Tertiary igneous and structural activity. It is equally likely, however, that the minerals, notably the biotite, are in fact Precambrian and that they lost their argon as a result of thermal expansion in the course of the later igneous activity. If this happened, the isotopic ages would indicate only the latest activity. In other words, the age determinations are consistent with Hunt's earlier interpretation of a continuum, but they are equally consistent with the more conventional interpretation that the metamorphic and igneous rocks are unrelated.

## REFERENCES

Hunt, C. B., in press, Stratigraphy and structure, Death Valley, California: U.S. Geol. Survey Prof. Paper 494–A.

Hunt, C. B., Averill, Paul, and Miller, R. L., 1953, Geology and geography of the Henry Mountains region, Utah: U.S. Geol. Survey Prof. Paper 228, 234 p.

Lanphere, M. A., Wasserburg, G. J. F., Albee, A. L., and Tilton, G. R., 1963, Redistribution of strontium and rubidium isotopes during metamorphism, World Beater Complex, Panamint Range, California, *in* Craig, H., Miller, S. L., and Wasserburg, G. J., eds., Isotopic and cosmic chemistry: Amsterdam, North-Holland Publishing Co., 553 p.

Stern, T. W., Newell, M. F., Kistler, R. W., and Shawe, D. R., 1965, Zircon uranium-lead and thorium-lead ages and mineral potassium-argon ages of La Sal Mountain rocks, Utah: Jour. Geophys. Research, v. 70, p. 1503–1507.

Tilton, G. R., 1960, Volume diffusion as a mechanism for discordant lead ages: Jour. Geophys. Research v. 65, p. 2933–2945.

Wasserburg, G. J., Wetherill, G. W., and Wright, L. A., 1959, Ages in the Precambrian terrane of Death Valley, California: Jour. Geology, v. 67, p. 702–708.

Wetherill, G. W., 1956, Discordant uranium-lead ages, I.: Am. Geophys. Union Trans., v. 37, p. 320–326.

# LAVA COILS OF SOME RECENT HISTORIC FLOWS, HAWAII

By DALLAS L. PECK, Hawaiian Volcano Observatory

*Abstract.*—Coiled strips of lava occur on the surface of Alae lava lake, formed by the August 1963 eruption of Kilauea Volcano, and in the feeder channels of the 1954, October 1963, and March 1965 Kilauean flows. They were observed in the process of formation on Makaopuhi lava lake during the March 1965 eruption. The coils that occur along shear zones display a consistent sense of coiling along each zone and indicate the relative direction of movement—coils that spiral inward in a clockwise direction record right-handed shear, and in a counterclockwise direction, left-handed shear. The shears and coils on Alae lava lake show that during a late stage of the eruption, lava flowed outward from the vents beneath the crust in a stream that shifted from one side to the other of the major axis of the lake.

Voluted strips of lava, called lava coils in this report, were found on the surface of Alae lava lake (fig. 1) when it was first examined by J. G. Moore, Shigeo Aramaki, and the author 4 days after the August 1963 eruption of Kilauea Volcano. The coils range from 2 inches to 4 feet in diameter and from 2 to 12 inches in height, and resemble coils of rope (fig. 2). Typically each consists

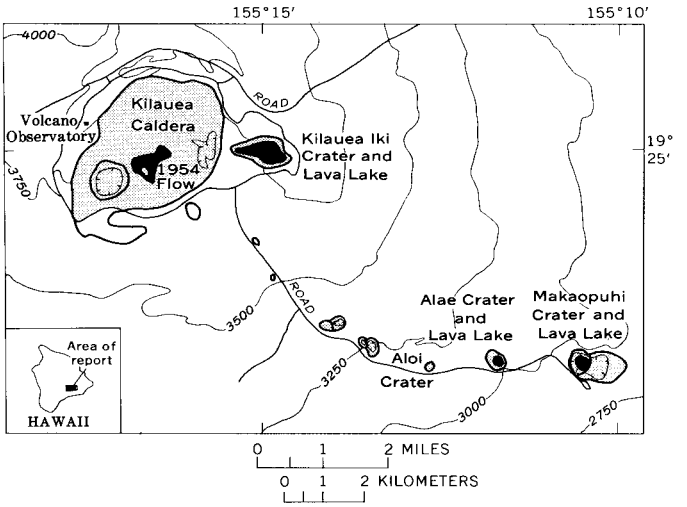


FIGURE 1.—Index map of the summit and the upper east rift zone of Kilauea Volcano, Hawaii. Boundaries of craters and Kilauea Caldera are shown by heavy lines. Lava lakes and 1954 flow shown as solid areas.

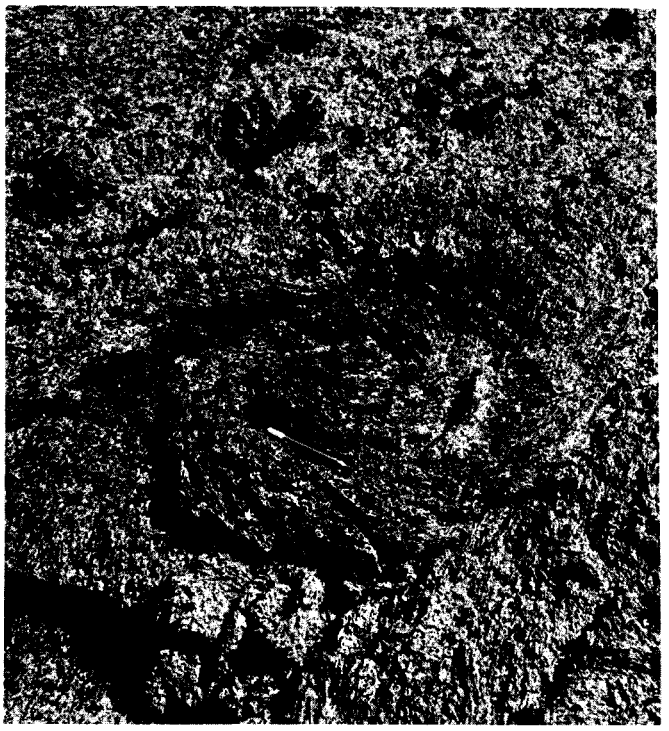

FIGURE 2.—Lava coil on the surface of Alae lava lake, Hawaii. Pencil in center of photograph gives scale.

of a single coiled strip attached to the surface of the lava at the outer whorl, but unattached forms and forms composed of a double strip or a doubly coiled strip (shaped like the letter "S") are also found. The coils occur as two distinct types. One consists of small (less than 1 foot in diameter) roughly equant coils that range from coplanar forms to forms with the center higher or lower than the rim. Together with irregular clots and strips of lava, these occur along shear zones (fig. 3) formed between a relatively static block of crust and an adjacent moving block of crust above a flowing jet of lava. The other type consists of larger coplanar coils (such as the one shown in fig. 2) that do not occur along recognizable shear zones; observations during the March 1965 eruption, however,

U.S. GEOL. SURVEY PROF. PAPER 550-B, PAGES B148-B151

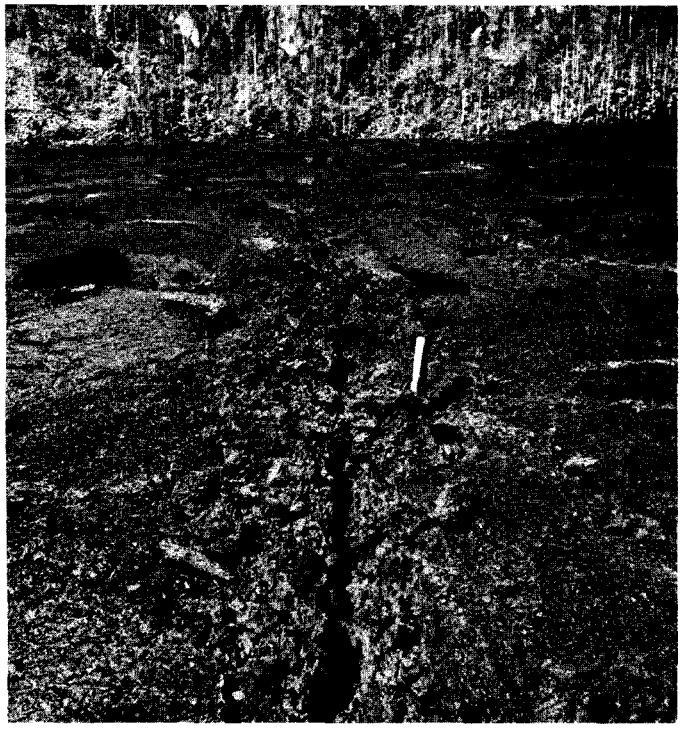

FIGURE 3.—Shear zone on the surface of Alae lava lake. Irregular clots of lava along the shear zone include lava coils. Geologic pick in center of photograph gives scale.

indicate that shears are present when these coils are formed but such shears are not preserved.

Both clockwise and counterclockwise coils[1] are found; with few exceptions all are coiled in the same sense along any one shear zone. Where the relative displacement along shears on the lava lake can be determined by drag of the filamented lava surface (Wentworth and Macdonald, 1953, p. 35) the coils show a consistent relationship to the direction of shearing—clockwise coils occurring along right-handed shears, and counterclockwise coils along left-handed shears. A similar relationship between coiling and direction of shearing is well displayed in the May 1954 flow in Kilauea Caldera (fig. 1), examined at the suggestion of J. P. Eaton and G. A. Macdonald. Each feeder channel of the flow is bounded by shears produced by drag along the edge of the flowing lava (Macdonald and Eaton, 1957, p. 55–64). In the southeast lobe (fig. 4) abundant lava coils consistently spiral in a counterclockwise direction along the northeast side of the channel and in a clockwise direction along the southwest side. Shears and coils are best displayed along the narrow parts of the channel where the flow of lava was concentrated in a well-defined stream; where the channel widens, the shears splay out and disappear and coils are much less abundant.

[1] Taken arbitrarily as the direction of spiraling inward from the outer whorl.

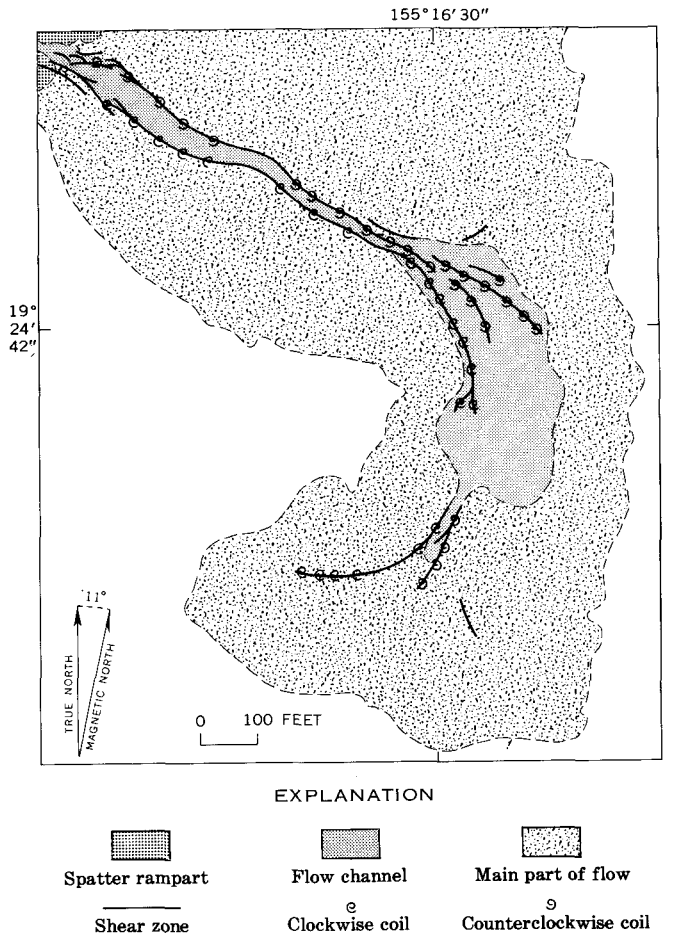


FIGURE 4.—Sketch map of the feeder channel of the southeast lobe of the 1954 lava flow, Kilauea Caldera, Hawaii. Dashed lines, boundary of 1954 flow (sketched from aerial photographs), flow channel, and rampart.

Coils were observed forming during the March 5–15, 1965, eruption of Kilauea Volcano. This eruption poured 9 million cubic yards of lava into a 325-foot-deep lava lake in the west pit of Makaopuhi Crater and an additional 29 million cubic yards onto the surface of the east rift zone along a stretch of 8 miles to the east.

On March 11, lava from the vents on the west side of Makaopuhi Crater poured into the lake through covered tubes and flowed across the lake just below the surface in a broad well-defined jet. The jet was bounded by shears, marked at the surface by thin glowing cracks. Between $12^h05^m$ and $13^h05^m$,[2] three flat coils each 10 to 20 feet across were seen from the observation platform at the rim of the crater (700 feet above the lake) to form at right-handed offsets in the shears (fig. 5) near the center of the lake. Each coil started as a wrinkle in the plastic crust only 1 to 2 inches thick; the wrinkle revolved at rates as great as 1 revolution per 5 minutes because of drag between the

[2] All times given are hours and minutes, Hawaiian standard time.

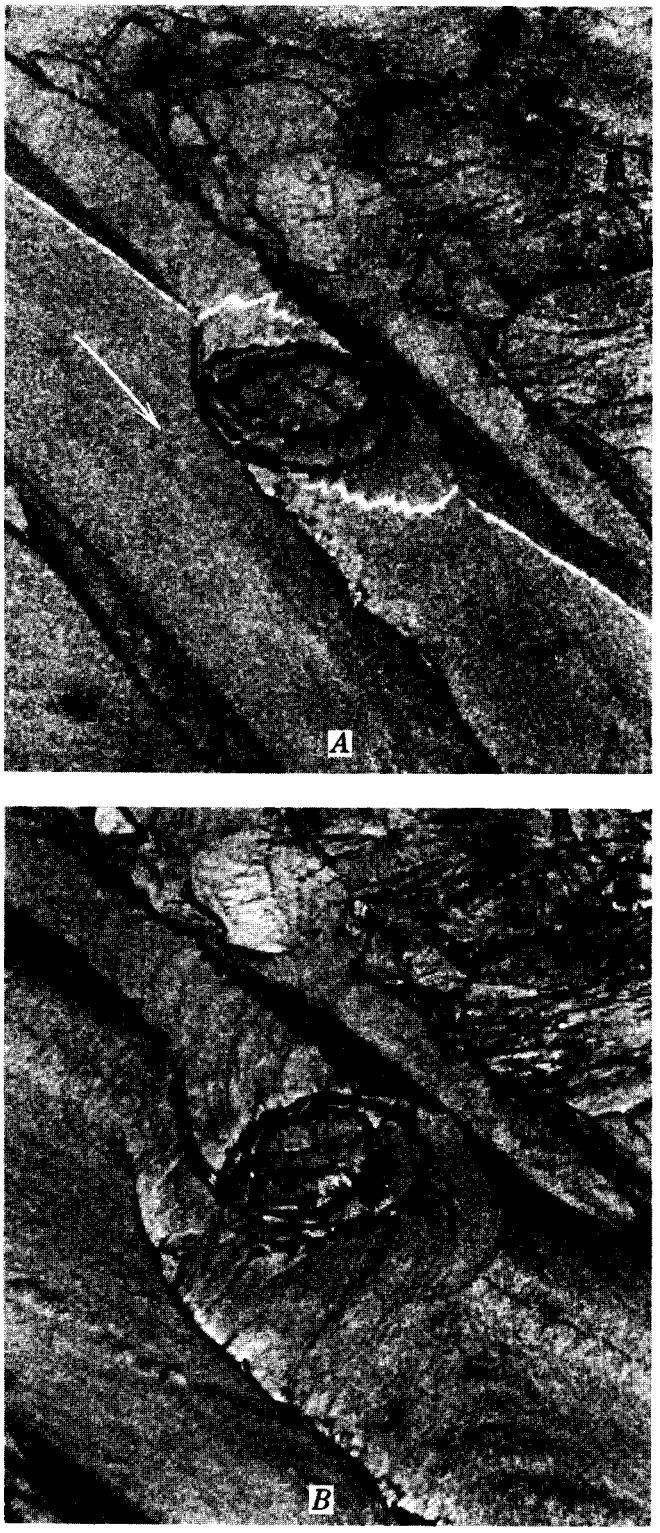


FIGURE 5.—Lava coils on the surface of Makaopuhi lava lake. *A*, Coil forming at $12^h49^m$ March 11, 1965. A shear, marked by glowing red cracks when the photograph was taken, shows as jagged white lines in the photograph. Lava on the near side of the shear is flowing to the right (arrow); that on the far side is static. The coil is estimated to be about 10 feet in diameter. *B*, Coil at $13^h04^m$ March 11, 1965. The coil stopped rotating at $12^h58^m$.

jet and the adjacent static lava. While it revolved, the adjacent crust was pushed into wrinkles which were drawn out to form additional whorls. Rotation, and growth, stopped after 15 to 30 minutes.

On March 15, smaller coils were observed from a distance of 50 to 100 feet forming in more viscous crust 3 to 4 inches thick near the edge of the lava lake. The coils, which were roughly equant forms 6 to 12 inches across, formed along a deeply furrowed shear zone at the edge of a large moving slab of crust; the slab, which was several hundred feet across, was being rafted toward the edge of the lake at a rate of 1 foot per minute by an underlying flowing jet of lava. Small pieces and strips of crust attached to either side of the shear were rotated because of frictional drag from the other side; as these rotated, a strip of plastic crust was coiled around them. The coiling of a strip of crust is illustrated by the sketches in figure 6, which were kindly provided by R. S. Fiske, of the U.S. Geological Survey. All the coils on Makaopuhi lava lake were destroyed at the end of the eruption by repeated foundering of the crust during the drainback of 3 million cubic yards of lava into the vent.

On Alae lava lake (fig. 1) the distribution of shear zones and coils provides a clue to the pattern of subcrustal flow in the lake during a late stage of the eruption (fig. 7). The eruption began at about $18^h00^m$ on August 21, 1963. During the first few hours, fountains on the floor and north wall of Alae Crater poured more than 100,000 cubic yards of lava an hour into the growing lava lake (Peck and others, 1964). The lava flowed outward from the vents beneath the crust of the lake, rafting pieces of the crust across the lake and piling them at the far end to form a jumbled levee of folded and faulted slabs. After $06^h00^m$ on August 22, however, the level of the lake began to fall slowly, although fountaining continued at a diminished rate. During the evening of August 22d, activity at the remaining fountains on the floor of the crater became weaker, and the area of active circulation in the lake decreased. The surface above circulating lava was broken by glowing cracks outlining lobate areas of dark crust; the outer cracks were the site of crustal foundering and overflow, and these darkened as the hours passed, beginning at the far end of the lake. By $00^h03^m$ on August 23d the lake was dark except for a few scattered spots, and by $08^h10^m$ the eruption was over.

The distribution of shear zones, lava coils, and the pressure ridges and linear squeeze ups that mark the sites of the glowing cracks, indicates that early in the evening of August 22d the major flow of lava from the fountains was in a stream beneath the crust lying northeast of the long axis of the lake. Between

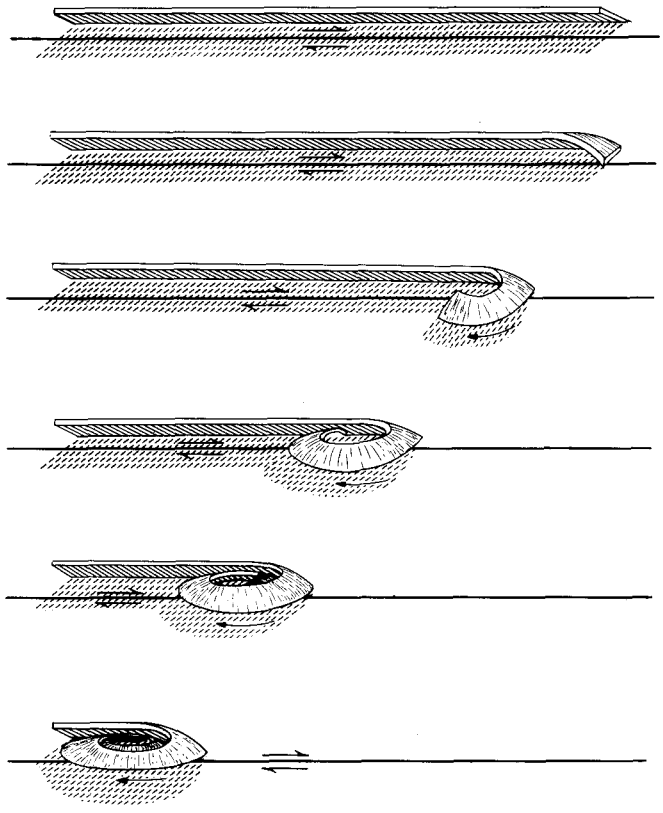

FIGURE 6.—Sketches of the progressive coiling of a strip of crust along a shear (from R. S. Fiske, U.S. Geological Survey).

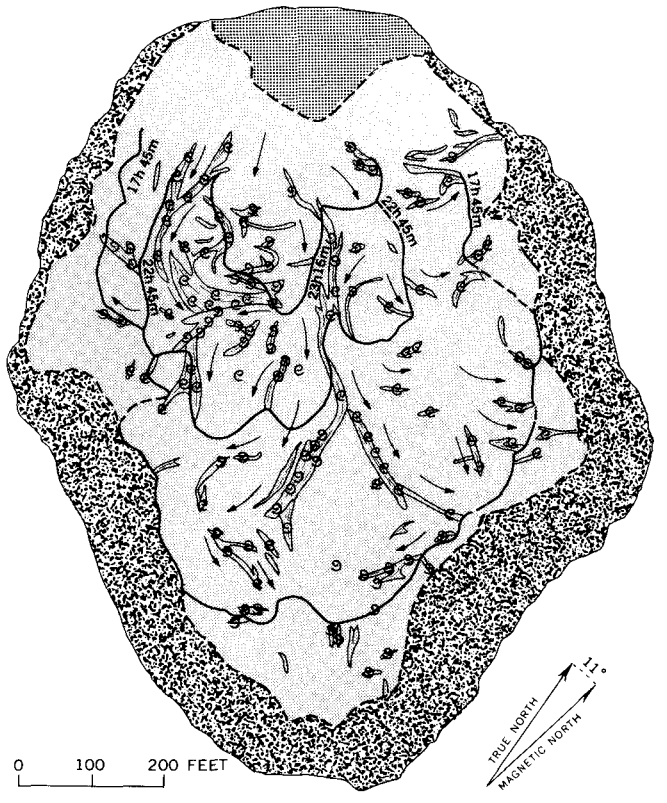


EXPLANATION

Spatter rampart

Levee and moat

Interior part of lake

Shear zone

e
Clockwise coil

9
Counterclockwise coil

17h45m
Outer margin of active lava circulation, dashed where approximately located, at 17h45m, 22h45m, and 23h16m on August 22, 1963, during a late stage of the eruption. Margins are loci of pressure ridges and linear squeeze ups

Inferred direction of subcrustal lava flowage

FIGURE 7.—Sketch map of shear zones and lava coils on Alae lava lake and the inferred directions of subcrustal lava flowage.

$17^h45^m$ and $22^h45^m$ the stream shifted to a position southwest of the major axis. In each instance the flow of lava was deflected at the southeast end of the lake, probably by a buttress of static viscous lava. Subsidiary currents split off from the stream toward the margins of the lake, diminishing in vigor with greater distance from the vents. Lava plunged down at the edge of active circulation, as shown by the foundering of pieces of crust during the eruption, and presumably flowed back toward the vents along the bottom of the lake.

Lava coils have also been found at Kilauea in the feeder channels of the easternmost flow of the October 1963 eruption and of the March 1965 flow on the east side of Napau Crater. B. N. Temperley, of the Geological Survey of South Africa, independently discovered coils in feeder streams of recent lava of the Chyulu basaltic volcano in Kenya (J. G. M. McCall, oral commun., May 1964). He ascribes the formation of the coils to the upward exudation of lava through ephemeral shear cracks in the chilled surface of the early crust, and concludes that the coiling was caused by drag of a vortex in the stream immediately below the crust (B. N. Temperley, written commun., 1965).

## REFERENCES

Macdonald, G. A., and Eaton, J. P., 1957, Hawaiian volcanoes during 1954: U.S. Geol. Survey Bull. 1061–B, p. 17–72.

Peck, D. L., Moore, J. G., and Kojima, George, 1964, Temperatures in the crust and melt of Alae lava lake, Hawaii, after the August 1963 eruption of Kilauea Volcano—a preliminary report, *in* Geological Survey Research 1964: U.S. Geol. Survey Prof. Paper 501–D, p. D1–D7.

Wentworth, C. K., and Macdonald, G. A., 1953, Structures and forms of basaltic rocks in Hawaii: U.S. Geol. Survey Bull. 994, 98 p.

# PHOSPHATE DEPOSITS IN THE BASAL BEDS OF THE MAQUOKETA SHALE NEAR DUBUQUE, IOWA

By C. ERVIN BROWN, Washington, D.C.

*Abstract.*—Basal beds of the Maquoketa Shale of Late Ordovician age contain phosphatic fossils, nodules, and pellets. Rapid rock and semiquantitative spectrographic analyses of samples from these beds in the vicinity of Dubuque, Iowa, show as much as 17.7 percent $P_2O_5$ through a thickness of 3.1 feet. Dolomitic beds 20 to 40 feet above the base of the Maquoketa also contain about 17 percent $P_2O_5$. The most abundant minor elements in the phosphorite beds are strontium, barium, cerium, copper, and lanthanum. Even though sparsely scattered crystals of sphalerite, galena, and barite are found in these or nearby beds, zinc was not detected, and lead and barium contents are very small. Although the phosphate deposits are thin, their geographic location in the midcontinent farming region favors their use as fertilizer raw material.

The basal beds of the Maquoketa Shale of Late Ordovician age have long been known to contain phosphatic material along much of the outcrop belt extending from northwestern Illinois to southern Minnesota (fig. 1). During the course of geologic mapping of the Dubuque South and Dubuque North quadrangles, Iowa, (Brown and Whitlow, 1960, and Whitlow and Brown, 1963a), it was noted that the phosphatic zone is thicker and appears to be richer there than elsewhere in the region. The area was revisited in 1964, a few sections were measured, and 14 samples were collected (fig. 2) for analysis in order to evaluate the possibility that the phosphatic zone may be economically valuable for fertilizer raw material.

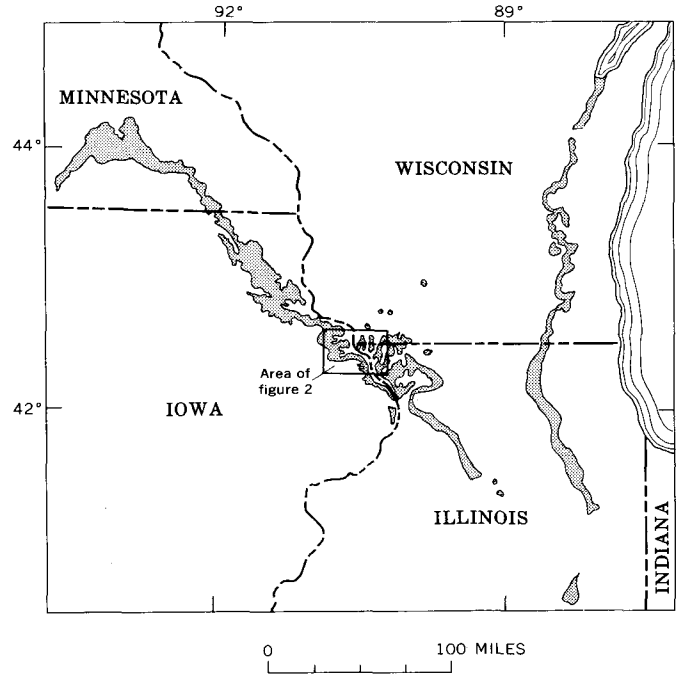


FIGURE 1.—Index map showing outcrop belts of the Maquoketa Shale (shaded), and area of study. Modified from the geologic map of the United States (Stose and Ljungstedt, 1932).

## STRATIGRAPHY

The Maquoketa Shale consists of shale with interbedded thin argillaceous dolomite and limestone. Because the rocks are thin bedded and weakly indurated, natural outcrops are rare and occur only in recently slumped creek banks and in the steep headward stretches of streams. Where the bedrock is Maquoketa Shale the topography is smooth and gently rolling, in contrast to the bluff-lined valleys formed in the overlying Silurian dolomites and the underlying Galena Dolomite.

The stratigraphy of the Maquoketa Shale in Iowa was described by Ladd (1929), and the subsurface distribution in Iowa by Agnew (1955). Gutstadt (1958) made regional correlations with other Upper Ordovician rocks in the midcontinent region. Brown and Whitlow (1960) described the stratigraphy of the Maquoketa Shale in the vicinity of Dubuque, Iowa, and that description is applicable to the area involved in this report.

The Maquoketa Shale of Late Ordovician age overlies the Dubuque Shaly Member of the Galena Dolomite of Middle Ordovician age. The Dubuque Member is uniformly bedded grayish-yellow dolomite in beds less

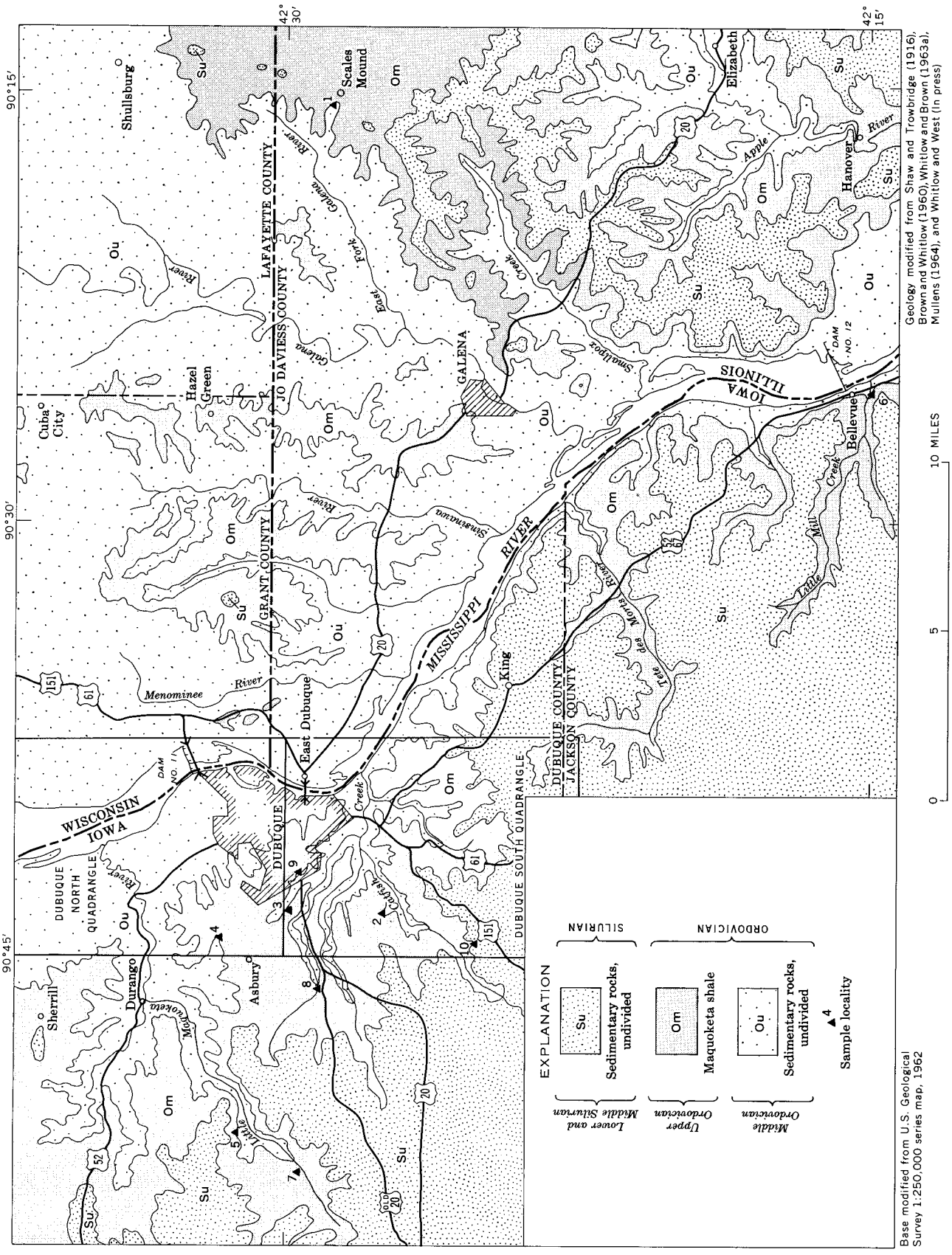


FIGURE 2.—Generalized geologic map showing the outcrop belt of the Maquoketa Shale and sample localities near Dubuque, Iowa.

than 1 foot thick in the upper 20 feet. The dolomite beds are interlayered with thin dolomitic shaly layers as much as 2 inches thick.

The Maquoketa in the vicinity of Dubuque has three identifiable rock units—a lower unit, the brown shaly unit; a middle unit, the Brainard Member; and a thin upper unit, the Neda Member, which at most places is eroded away.

The contact of the Maquoketa with the underlying Galena, although apparently conformable in the area discussed in this report, is believed to be disconformable regionally. The contact between the Maquoketa Shale and overlying Lower Silurian rocks is an ancient erosion surface (Whitlow and Brown, 1963b) which has about 135 feet of relief in the Dubuque South quadrangle, so that here the remaining thickness of the Maquoketa ranges from about 250 feet to 115 feet.

The phosphatic material in the vicinity of Dubuque is in the brown shaly unit, which ranges in thickness from 35 to 50 feet in the Dubuque South quadrangle and averages about 40 feet. Beds in the basal few feet are grayish brown, earthy, silty, and locally have thin clay interlayers. These beds contain small phosphatized fossils and numerous phosphatic nodules and pellets. Layers composed of light-colored silt and dark minute phosphatic pellets have the color of ground black pepper. Locally, as at sample locality 2 (fig. 2), a few feet of brown dolomite containing similar phosphatic material occurs directly above the friable silty bed.

Although the basal phosphatic beds are persistent, regionally the lithology of the overlying shale is markedly variable. For example, in the vicinity of Dubuque the lower unit is mainly brown fissile shale, but at Scales Mound, Ill. (loc. 1, near east edge of fig. 2) the shale in the lower part of the formation is olive gray and silty, and at Bellevue, Iowa (loc. 6, near south edge of fig. 2), the lower unit consists of only about 10 feet of brown shale.

The thin basal zone of small fossils was recognized as early as 1854 by Daniels (1854) who called it the *Nucula* shale after the common pelecypod found in it and described the zone as a "fossil Lilliput." Ladd (1929) called these beds the "depauperate zone" and described it as a zone of universal smallness. He identified 44 species, most of which are less than ¼-inch across. Agnew (1955) recognized the fossiliferous phosphatic material at the base of the Maquoketa in cuttings from many wells throughout Iowa, and Gutstadt (1958) found phosphatic depauperate fossils and pellets in well cuttings from the middle of the Maquoketa in central Illinois. He believes that on a regional scale this zone is not confined to the basal beds, but also occurs elsewhere in the section.

Immediately below the depauperate zone and cemented to the top of the Dubuque Shaly Member of the Galena Dolomite is an irregular phosphatic crust as much as 2 inches thick that contains phosphatized normal-sized fossils and pyrite, which in most outcrops is oxidized to limonite. At most places this crust appears to be a partial replacement of dolomite. The analyzed specimen, B–64–10 (table 2) from locality 9 is a weathered piece of this material.

In the upper part of the brown shaly unit a zone 10 to 20 feet thick contains argillaceous brownish-yellow dolomite beds that are interlayered with the shale. Both the dolomite and shale have a strong bituminous odor when broken. The dolomite beds locally contain numerous 3- to 5-inch straight conical cephalopods, and some also contain abundant minute phosphatic pellets and depauperate fossils. Samples B–64–3 from locality 8 and B–64–12 from locality 7 (fig. 2) are chip samples from these beds.

Near Dubuque the Brainard Member of the Maquoketa is mainly greenish-gray soft dolomitic shale that is sticky and plastic when wet. The upper part of the Brainard contains thin fossiliferous limestone beds and is overlain by the Neda Member, which is red, ferruginous shale having layers containing abundant flattened 2-mm-long limonite oolites. Sample B–64–20 from locality 10 (fig. 2) is a specimen from one of the oolitic layers. The Neda also contains phosphatic nodules as much as 1 inch across, which are concentrated locally as a basal conglomerate in the overlying Lower Silurian rocks (Whitlow and Brown, 1963b). The Neda has a maximum thickness of 5 feet in the Dubuque area and is only rarely preserved at high places on the ancient erosion surface of the Maquoketa.

## SAMPLING

Samples from the basal beds of the Maquoketa were collected from freshly cleaned vertical sections at roadcuts and natural outcrops. The samples were taken from channels about 3 inches wide and 1 inch deep. Chip samples were collected continuously through indurated dolomitic beds that are about 20 feet above the bottom of the Maquoketa.

The lithology, thickness, and $P_2O_5$ content of the sampled beds at 8 of the 10 sample localities (fig. 2) are given in table 1.

## ANALYTICAL DATA

Major- and minor-element content of the samples are given in table 2. The samples were analyzed in laboratories of the U.S. Geological Survey, using X-ray fluorescence supplemented by methods described by Shapiro and Brannock (1962). The minor-element content was determined by semiquantitative spectro-

TABLE 1.—*Location, lithologic description, and $P_2O_5$ content of beds in the Maquoketa Shale in the vicinity of Dubuque, Iowa*

| Locality No. (fig. 2) | Location description | Lithology | Thickness (feet) | Sample No. | $P_2O_5$ content (percent) |
|---|---|---|---|---|---|
| 1 | Railroad cut along Illinois Central Railroad, ½ mile west of Scales Mound, Jo Daviess County, Ill. | Shale, soft, greenish-gray, silty; interbedded with a few 1- to 2-inch gray finely crystalline dolomite layers. | 20+ | | |
| | | Phosphate rock, pale-grayish-brown, dolomitic, silty and friable. Composed of small phosphatic fossils, nodules, and 1- to 2-mm pellets mixed with silt and clay. 2-inch dolomitic layers at base. | 1.0 | B–64–9 | 11.1 |
| | | Shale, olive-gray, silty, thin-bedded | 2.8 | | |
| | | Phosphate rock, pale-yellowish-brown, dolomitic, silty, and friable; directly overlies Galena Dolomite. | .5 | B–64–7 | 12.9 |
| 2 | Creek bank, NE¼SE¼ sec. 4, T. 88 N., R. 2 E., Dubuque County, Iowa. | Shale, dark-yellowish-brown, fissile | 2+ | | |
| | | Dolomite, dark-yellowish-brown, fine-grained; contains numerous 1-mm phosphatic pellets throughout and has scattered phosphatic nodules and fossils mainly in lower few inches. | 1.3 | B–64–14 | 17.5 |
| | | Phosphate rock, silty, friable; consists of minute phosphatic pellets, fossils, and nodules with silt and clay; lower 1 inch is a rind of phosphatic material and pyrite cemented to the upper surface of the Galena Dolomite. | 1.8 | B–64–13 | 17.8 |
| 3 | New roadcut, NW¼NE¼ sec. 27, T. 89 N., R. 2 E., Dubuque County, Iowa. | Shale, soft, brownish-gray, dolomitic; contains scarce phosphatic fossils and nodules. | 5 | | |
| | | Phosphate rock, silty, friable; contains numerous 1-mm discoidal phosphatic pellets and nodules and fossils less than ½ inch long; 0.3-foot bed of yellowish-gray clay in middle; thin phosphatic rind with limonite on top of Galena Dolomite. | 2.1 | B–64–15 | 14.7 |
| 4 | Creek bank, NW¼NW¼ sec.16, T. 89 N., R. 2 E., Dubuque County, Iowa. | Shale, grayish-brown fissile; weathers to light brownish gray; upper part is silty and dolomitic and contains phosphatic material. | 6 | | |
| | | Phosphate rock; alternating grayish-brown silty layers with phosphatic material and yellowish clay-rich layers; phosphatic depauperate fossils and nodules abundant in layer near top and 0.5-foot layer in middle of zone; phosphatic crust 0.1 foot thick on top surface of Galena Dolomite. | 2.2 | B–64–16 | 13.5 |
| 5 | Twin Springs quarry, SW¼ sec. 16, T. 89 N., R. 1 E., Dubuque County, Iowa (upper few feet of quarry face). | Shale, grayish-brown, fissile | 4+ | | |
| | | Siltstone, phosphatic, grayish-brown, friable; thin crust of phosphatic material on top surface of Galena Dolomite. | 1.1 | B–64–11 | 7.9 |
| 6 | South bank of Little Mill Creek about 200 yards west of mill in Bellevue, Jackson County, Iowa. | Shale, soft, grayish-green | 20+ | | |
| | | Shale, brownish-gray, fissile | 8 | | |
| | | Covered interval; probably shale as above | 3+ | | |
| | | Shale, grayish-brown | .7 | | |
| | | Phosphate rock, grayish-brown, hard, dolomitic, pyritic, numerous jumbled minute dusky-brown flattened pellets; depauperate fossils and pellets as much as ¼ inch long. Matrix is yellowish-brown dolomite; forms 4 thin irregular beds at water level (Galena Dolomite forms creek bed). | 1.5 | B–64–17 | 12.9 |
| 7 | Roadcut at Graf, Dubuque County, Iowa. | Dolomite, argillaceous, grayish-orange; 6- to 8-inch beds, contains numerous 3- to 6-inch orthoceracone cephalopods; dolomite alternates with 6-inch grayish-brown shale layers. | 10+ | | |
| | | Dolomite, silty, phosphatic; contains numerous discoidal 1-mm pellets and depauperate fossils. | 2 | B–64–12 | 12.6 |
| | | Shale, grayish-brown, fissile; probably no more than 5 feet above top of Galena Dolomite. | 10 | | |
| 8 | Creek bank north of old U.S. Route 20 in SW¼ sec. 29, T. 89 N., R. 2 E., Dubuque County, Iowa. | Shale, dolomitic, yellowish-brown, silty, phosphatic | 6 | B–64–1 | 6.1 |
| | | Dolomite, yellowish-brown, silty; in beds 0.5 to 1 foot thick; numerous orthoceracone cephalopods. | 5 | B–64–3 | 16.9 |
| | | Dolomite, yellowish-brown, silty, phosphatic | 3.7 | | |
| | | Shale, grayish-brown, fissile; bottom is probably about 5 feet above top of Galena Dolomite. | 10 | B–64–6 | 3.6 |

graphic analysis. Fluorine was determined in only eight of the samples. The organic content was determined in a specimen of fissile brown shale, B–64–6, and in the silty brown dolomite, B–64–1, both of which have a strong bituminous odor when broken.

The average $P_2O_5$ content of channel samples (locs. 1–6, table 1) from the basal silty phosphatic material in the Maquoketa Shale is 13 percent. The highest grade samples are from locality 2, where 3.1 feet of rock contains 17.7 percent $P_2O_5$. This thickness in-

TABLE 2.—*Analyses of phosphatic rock from the Maquoketa Shale in the vicinity of Dubuque, Iowa*

[Rapid rock analysis by Paul Elmore, Sam Botts, Lowell Artis, and John Glenn. Minor elements by semiquantitative spectrographic analysis, J. L. Harris, analyst. ND, not determined]

| Constituent | Locality (fig. 2) and sample Nos. | | | | | | | | | | | | | |
|---|---|---|---|---|---|---|---|---|---|---|---|---|---|---|
| | 1 | | 2 | | 3 | 4 | 5 | 6 | 7 | 8 | | | 9 | 10 |
| | B-64-9 | B-64-7 | B-64-13 | B-64-14 | B-64-15 | B-64-16 | B-64-11 | B-64-17 | B-64-12 | B-64-1 | B-64-3 | B-64-6 | B-64-10[1] | B-64-20[2] |
| **Major constituents (in weight percent)** | | | | | | | | | | | | | | |
| $SiO_2$ | 9.5 | 14.7 | 20.1 | 5.7 | 19.2 | 18.0 | 23.8 | 8.0 | 11.9 | 23.8 | 13.6 | 44.2 | 8.2 | 36.5 |
| $Al_2O_3$ | 3.7 | 4.6 | 4.6 | .85 | 5.7 | 5.0 | 6.2 | 2.7 | 2.6 | 3.2 | 1.9 | 10.4 | 2.1 | 9.7 |
| $Fe_2O_3$ | 6.0 | 4.0 | 2.8 | .89 | 4.5 | 3.7 | 5.7 | 4.8 | 1.8 | 1.3 | 1.2 | 2.1 | 7.7 | 23.2 |
| FeO | .88 | .68 | .32 | .28 | .12 | .26 | .34 | .96 | .44 | .32 | .24 | .64 | .24 | 60 |
| MgO | 8.1 | 8.0 | 5.9 | 10.7 | 6.2 | 7.2 | 8.2 | 9.4 | 9.8 | 11.0 | 10.3 | 5.4 | .50 | 4.1 |
| CaO | 29.1 | 29.4 | 30.1 | 35.8 | 28.5 | 29.1 | 22.3 | 30.7 | 32.1 | 24.1 | 30.1 | 12.1 | 42.2 | 7.2 |
| $Na_2O$ | .32 | .23 | .40 | .23 | .30 | .22 | .22 | .20 | .20 | .16 | .21 | .27 | .32 | .23 |
| $K_2O$ | 1.3 | 1.6 | 1.9 | .34 | 2.2 | 2.0 | 2.6 | 1.0 | 1.0 | 1.2 | .81 | 4.2 | .79 | 3.2 |
| $H_2O^-$ | 1.8 | .42 | .66 | .35 | .64 | .72 | 1.2 | .25 | .40 | .45 | .40 | .58 | .62 | .68 |
| $H_2O^+$ | 2.0 | 2.0 | 1.8 | .85 | 2.6 | 2.3 | 2.8 | 1.4 | 2.0 | 2.4 | 1.4 | 1.8 | 2.4 | 5.1 |
| $TiO_2$ | .18 | .22 | .24 | .05 | .31 | .26 | .29 | .14 | .18 | .18 | .11 | .54 | .14 | .57 |
| $P_2O_5$ | 11.1 | 12.9 | 17.8 | 17.5 | 14.7 | 13.5 | 7.9 | 12.9 | 12.6 | 6.1 | 16.9 | 3.6 | 30.0 | 2.2 |
| MnO | .04 | .04 | .06 | .07 | .04 | .04 | .04 | .06 | .06 | .06 | .05 | .03 | .02 | .07 |
| $CO_2$ | 17.5 | 17.5 | 12.5 | 24.8 | 12.9 | 15.5 | 17.8 | 21.0 | 21.8 | 23.5 | 22.3 | 10.4 | 1.6 | 6.8 |
| S | 2.8 | 1.6 | .35 | .12 | .12 | .14 | .12 | 3.7 | .40 | .18 | .48 | .60 | .16 | .00 |
| F | 1.8 | 1.3 | 1.6 | ND | 1.4 | 1.0 | .65 | 1.2 | ND | ND | ND | ND | 2.6 | ND |
| $SO_3$ | 3.9 | .37 | ------- | ------- | ------- | ------- | ------- | .38 | .50 | ------- | ------- | ------- | ------- | ------- |
| Organic matter | ND | ND | ND | ND | ND | ND | ND | ND | ND | 2.0 | ND | 3.6 | ND | ND |
| Total | 100 | 100 | 100 | 98.6 | 99 | 99 | 100 | 100 | 98 | 100 | 100 | 100 | 100 | 100 |
| **Minor elements (in weight percent)[3]** | | | | | | | | | | | | | | |
| Ag | 0 | 0 | 0.0001 | 0 | 0.0001 | 0 | 0.0001 | 0 | 0 | 0 | 0 | 0 | 0.0001 | 0 |
| B | 0 | .001 | .002 | 0 | .002 | .001 | .001 | 0 | 0 | .001 | .0007 | .007 | 0 | .005 |
| Ba | .02 | .02 | .03 | .015 | .03 | .03 | .07 | .015 | .015 | .015 | .015 | .03 | .02 | .02 |
| Be | 0 | .0001 | .0001 | .0001 | .0001 | .0001 | .0001 | .0001 | 0 | .0001 | .0001 | .0002 | .0001 | .0003 |
| Ce | .02 | .03 | .02 | .02 | .02 | .02 | .02 | .02 | .01 | 0 | .02 | 0 | .03 | .01 |
| Co | .0015 | .0015 | 0 | 0 | 0 | 0 | 0 | .0015 | 0 | 0 | 0 | .001 | .0015 | .0015 |
| Cr | .005 | .005 | .007 | .002 | .007 | .007 | .007 | .003 | .002 | .003 | .003 | .007 | .003 | .003 |
| Cu | .01 | .005 | .007 | .005 | .007 | .01 | .005 | .01 | .002 | .003 | .003 | .005 | .015 | .0007 |
| Ga | .0005 | .0007 | .0007 | 0 | .001 | .0007 | .001 | .0003 | .0003 | .0002 | .0003 | .0015 | .0002 | .0015 |
| La | .015 | .015 | .015 | .015 | .015 | .015 | .01 | .015 | .01 | 0 | .01 | 0 | .02 | 0 |
| Mo | .0005 | .0005 | .0003 | 0 | .0003 | .0005 | .0007 | .0007 | 0 | 0 | 0 | .0003 | .001 | .0005 |
| Nb | 0 | 0 | 0 | 0 | 0 | 0 | 0 | 0 | 0 | 0 | 0 | 0 | 0 | .001 |
| Ni | .007 | .007 | .015 | .002 | .005 | .005 | .003 | .005 | .002 | .003 | .002 | .003 | .007 | .003 |
| Pb | .007 | .003 | .02 | .003 | .005 | .005 | .005 | .005 | .003 | .002 | .002 | .005 | .015 | .002 |
| Sc | .001 | .001 | .001 | .0007 | .001 | .001 | .001 | .001 | .0007 | .0007 | .0007 | .001 | .0007 | .0007 |
| Sn | 0 | 0 | .003 | 0 | 0 | 0 | 0 | 0 | 0 | 0 | 0 | 0 | 0 | 0 |
| Sr | .05 | .05 | .05 | .05 | .05 | .05 | .02 | .05 | .07 | .02 | .05 | .02 | .07 | .015 |
| V | .002 | .003 | .003 | .001 | .003 | .003 | .005 | .002 | .0015 | .0015 | .0015 | .007 | .002 | .01 |
| Y | .007 | .007 | .01 | .01 | .007 | .007 | .007 | .007 | .007 | .005 | .01 | .005 | .01 | .005 |
| Yb | .0005 | .0005 | .007 | .001 | .0007 | .0007 | .0007 | .0005 | .0005 | .0003 | .0007 | .0003 | .001 | .0005 |
| Zr | .003 | .003 | .007 | .0005 | .007 | .007 | .005 | .003 | .002 | .002 | .003 | .01 | .003 | .02 |

[1] Specimen of 2-inch phosphatic crust on top of Galena Dolomite, from SE¼NE¼ sec. 27, T. 89 N., R. 2 E., Dubuque County, Iowa.

[2] Specimen of red shale containing limonite oolites and phosphatic nodules from Neda Member of Maquoketa Shale, SW¼ sec. 21, T. 88 N., R. 2 E., Dubuque County, Iowa.

[3] Results are reported in percent to the nearest number in the series 1, 0.7, 0.5, 0.3, 0.2, 0.15, and 0.1, and so forth, which represent approximate midpoints of group data on a geometric scale. The assigned group for semiquantitative results will include the quantitative value about 30 percent of the time. Elements looked for, but not detected: As, Au, Bi, Cd, Ge, Hf, Hg, In, Li, Pd, Pt, Re, Sb, Ta, Te, Th, Tl, U, W, Zn, Pr, Nd, Sm, Eu, Gd, Tb, Dy, Ho, Er, Tm, Lu.

cludes 1.3 feet of phosphorite with a dolomite matrix and 1.8 feet with a silt and clay matrix. Chip sample B–64–3, of dolomite at locality 8, contains 16.9 percent $P_2O_5$ through a thickness of 8.7 feet. It is planned to resample this section and other exposures of these dolomitic beds, as this high $P_2O_5$ content in dolomite was not expected.

Except for included clay and quartz silt, sample B–64–10 is representative of the phosphatic material. The recalculated analysis of this sample for total CaO, $P_2O_5$, F, and $CO_2$ is:

| *Constituent* | *Content (percent)* |
|---|---|
| CaO | 55.2 |
| $P_2O_5$ | 39.3 |
| F | 3.4 |
| $CO_2$ | 2.1 |
| Total | 100.0 |

The phosphatic material, cryptocrystalline and ap-

parently isotropic, has the approximate composition of carbonate fluorapatite.

Rocks with a silt and clay matrix have a high $SiO_2$ and $Al_2O_3$ content. A carbonate matrix is shown by the high $CO_2$ content. Pyrite is present in most of the samples of the silty depauperate zone as is shown in the analyses by the high iron and sulfur content; where oxidized to limonite as in sample B–64–15, the iron content is high but the sulfur is low. The phosphatic dolomite, such as sample B–64–14, does not contain pyrite and consequently is relatively low in iron.

The content of minor elements does not vary appreciably between samples. Strontium, barium, cerium, copper, and lanthanum are most abundant; other members of the cerium and lanthanum rare earths were not detected. The small amount of lead, and the absence of zinc, seems paradoxical because this area is in a lead-zinc mining district, and sphalerite, and galena crystals are very sparsely scattered in these and adjacent beds. Barite, sphalerite, smithsonite, and galena are commonly in vugs in the underlying beds of the Dubuque Shaly Member of the Galena Dolomite.

## SUMMARY AND CONCLUSIONS

The basal few feet of the Maquoketa Shale consists mostly of phosphorite with a silty and clayey matrix that contains some pyrite. The maximum known thickness of the soft silty phosphorite close to Dubuque is 2.2 feet at sample localities 3 and 4, and the average thickness within a 4-mile radius of Dubuque is estimated to be 2 feet. These beds are known to be continuous regionally.

Dolomitic beds that occur immediately above the silty phosphorite at locality 2, but that normally are more than 20 feet higher in the section, appear to contain as much phosphatic material as the basal silty zone. These beds are as much as 10 feet thick and contain less pyrite than the lower phosphatic zone. Their areal extent is unknown; however, they are continuous but variable in thickness in the Dubuque South quadrangle.

The basal silty phosphatic zone in the Maquoketa is favorably situated for strip mining because it lies directly above the flat-lying Galena Dolomite, which would make an excellent floor, and the gentle slopes (7 to 15 percent grade) developed on the Maquoketa would allow considerable width of stripping before the overburden became too thick. The bedrock is covered with a deposit of loess, loam, residual clay, and in Iowa, glacial till. This deposit generally ranges in thickness from about 5 to 20 feet. Locally on the uplands as much as 50 feet of surficial deposits remain. The tough sticky residual clay and glacial till might cause difficulty in stripping, but on the other hand, the thick loess and loam would enable easy resoiling in order to reclaim the land for farming.

Because the basal silty phosphorite is earthy and friable, separation of the phosphatic fossils, pellets, and nodules from the silt and clay could possibly be accomplished simply by washing and screening. Phosphatic material in the stratigraphically higher dolomitic beds would be more difficult to separate from the matrix.

The quantity of material near the outcrop in the basal silty phosphorite in the Dubuque South and Dubuque North quadrangles can be estimated as follows: The outcrop length at the bottom contact of the Maquoketa Shale is about 160 miles. The estimated thickness of the rock near Dubuque is 2 feet. Assuming a stripping width of 100 feet and a density of 110 pounds per cubic foot, the raw phosphatic rock per acre would be about 4,790 tons. A 1-mile strip 100 feet wide would contain more than 58,000 tons of phosphate rock, and a 100-foot strip along the 160-mile outcrop length would contain 9 million tons. Possibly as much as a third of the 160-mile outcrop length in the two quadrangles is within populated areas or beneath excessively thick overburden. Therefore a more realistic tonnage estimate would be about 6 million tons of material averaging 15 percent $P_2O_5$. Data for the stratigraphically higher and locally thicker dolomitic beds are too scanty to justify estimation of phosphate resources.

Although the deposits are thin, and high in iron content, they are continuous over a large area, and their geographic location is extremely favorable for the fertilizer industry. Dubuque is centrally located in the midcontinent farming region and is served by 5 U.S. highways, 4 major railroads, and barges on the Mississippi River. In addition, a superphosphate plant using phosphate rock shipped more than 1,000 miles by barge is operating there, and a plant manufacturing sulfuric acid, a necessity for the fertilizer industry, is at the south edge of Dubuque.

## REFERENCES

Agnew, A. F., 1955, Facies of Middle and Upper Ordovician strata in Iowa: Am. Assoc. Petroleum Geologists Bull., v. 39, no. 9, p. 1703–1752.

Brown, C. E., and Whitlow, J. W., 1960, Geology of the Dubuque South quadrangle, Iowa-Illinois: U.S. Geol. Survey Bull. 1123–A, p. 1–93.

Daniels, Edward, 1854, First annual report on the geological survey of the State of Wisconsin: Wisconsin Geol. Survey, 84 p.

Grant, U.S., and Burchard, E. F., 1907, Description of the Lancaster and Mineral Point quadrangles [Wisconsin-Iowa-Illinois]: U.S. Geol. Survey Geol. Atlas, Folio 145, 14 p.

Gutstadt, A. M., 1958, Upper Ordovician stratigraphy in eastern interior region: Am. Assoc. Petroleum Geologists Bull. v. 42, no. 3, p. 513–547.

Ladd, H. S., 1929, The stratigraphy and paleontology of the Maquoketa shale of Iowa: Iowa Geol. Survey Ann. Rept., v. 34, p. 305–448.

Mullens, T. E., 1964, Geology of the Cuba City, New Diggings, and Shullsburg quadrangles, Wisconsin and Illinois: U.S. Geol. Survey Bull. 1123–H, p. 437–531.

Shapiro, Leonard, and Brannock, W. W., 1962, Rapid analysis of silicate, carbonate, and phosphate rocks: U.S. Geol. Survey Bull, 1144–A, p. A1–A56.

Shaw, E. S., and Trowbridge, A. C., 1916, Galena-Elizabeth quadrangles [Illinois-Iowa]: U.S. Geol. Survey Geol. Atlas, Folio 200, 13 p.

Stose, G. W., and Ljungstedt, O. A., 1932, Geologic map of the United States: U.S. Geol. Survey.

Whitlow, J. W., and Brown, C. E., 1963a, Geology of the Dubuque North quadrangle, Iowa-Wisconsin-Illinois: U.S. Geol. Survey Bull. 1123–C, p. 139–168.

——— 1963b, The Ordovician-Silurian contact in Dubuque County, Iowa: Art. 62, *in* U.S. Geol. Survey Prof. Paper 475–C, p. C11–C13.

Whitlow, J. W., and West, W. S., in press, Geology of the Kieler quadrangle, Wisconsin and Illinois: U.S. Geol. Survey Geol. Quad. Map GQ–487.

# TRONA IN THE WILKINS PEAK MEMBER OF THE GREEN RIVER FORMATION, SOUTHWESTERN WYOMING

By WILLIAM C. CULBERTSON, Denver, Colo.

*Abstract.*—About 67 billion tons of trona is contained in 24 beds more than 3 feet thick in the Wilkins Peak Member of the Eocene Green River Formation. These beds lie at depths of 400 to 3,500 feet in a 1,400-square-mile area in the Green River basin. Another 36 billion tons of mixed trona and halite is contained in 14 beds more than 3 feet thick in the southern part of this area.

Trona ($Na_2CO_3 \cdot NaHCO_3 \cdot 2H_2O$), a mineral formed in saline lakes, can be readily processed to form the important industrial commodity soda ash (sodium carbonate). The largest known deposit of trona in the world underlies an area of about 1,400 square miles in the southern part of the Green River basin in southwestern Wyoming (fig. 1). The trona occurs as beds in the Wilkins Peak Member of the Green River Formation of Eocene age and lies at depths ranging from about 400 to 3,500 feet.

Although dissolved sodium carbonate had been known in water wells at the town of Green River as early as 1896, the immense deposit of bedded trona to the west was not found until many years later. Exploration for trona began in the early 1940's after the U.S. Geological Survey recognized a 10-foot bed of nearly pure trona in the core of an oil and gas test hole. By 1963 many new trona beds had been found and their lateral extent had been approximately determined as the result of the drilling of about 100 core holes in the Green River basin (Bradley, 1964, p. 41). The first trona mine, the Westvaco mine (fig. 1), began large-scale production of soda ash in 1953; the second mine, Stauffer Chemical Co.'s Big Island mine, began production in 1962. By late 1964 the two mines had developed a combined capacity for producing more than 1 million tons of refined soda ash per year, and the proposed site of a third mine was announced.

*Acknowledgments.*—My thanks are due to the Diamond Alkali Co., Stauffer Chemical Co., Kern County Land Co., and Texota Oil Co., and to J. M. Perkins, consulting engineer, for permission to examine the cores of their trona test holes, or to use their descriptions of the cores. Much of the basic data for this report was derived from reports of Deardorff (1963) and Brown (1950).

## STRATIGRAPHY

The Wilkins Peak Member of the Green River Formation consists of thin persistent beds of oil shale, dolomitic marlstone, claystone, trona, limestone, and tuff (Culbertson, 1961). In the eastern part of the area, the Wilkins Peak also contains persistent units of mudstone and crossbedded siltstone and sandstone. These units thin and become finer grained northward and westward, until they disappear or grade into claystone or clayey marlstone.

In the Green River basin, lacustrine sediments assigned to the Wilkins Peak consist of a lens of saline sediments—the saline facies—that interfingers with nonsaline sediments—the fresher water facies (Bradley, 1964, p. 40, 41). The saline facies (fig. 2 and table 1) is characterized by abundant crystals of shortite, or their molds, and contains lesser amounts of other saline minerals such as northupite, pirssonite, gaylussite, and searlesite. The saline facies contains more than 40 beds of trona, or of trona and halite, that range in maximum thickness from a few inches to about 40 feet. Of these beds, 25 exceed 3 feet in maximum thickness (exclusive of interbeds) and 100 square miles in areal extent (fig. 2). At least 5 beds are less than 3 feet in maximum thickness, but are 100 to 400 square miles in areal extent. In addition, there are 10 or more beds up to 4 feet in thickness and less than 100 square miles in areal extent.

Most of the beds of the Wilkins Peak Member that are exposed along the eastern side of the basin belong to the fresher water facies (fig. 2). The beds that belong to the saline facies contain only molds of shortite, or calcite pseudomorphs after shortite. The calcite pseudomorphs presumably resulted from the exposure

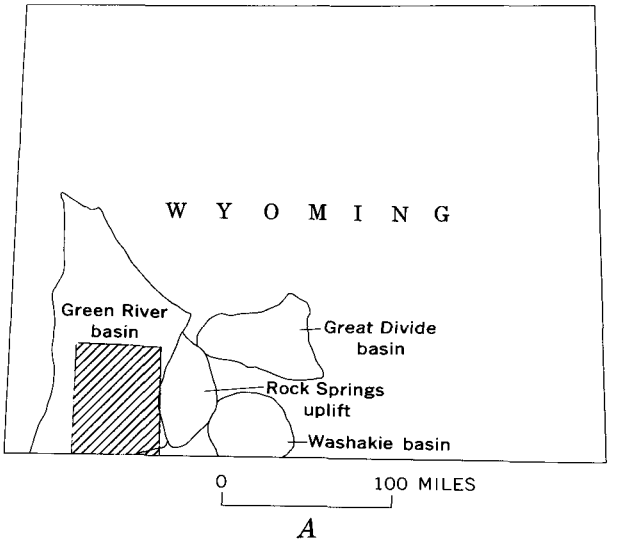


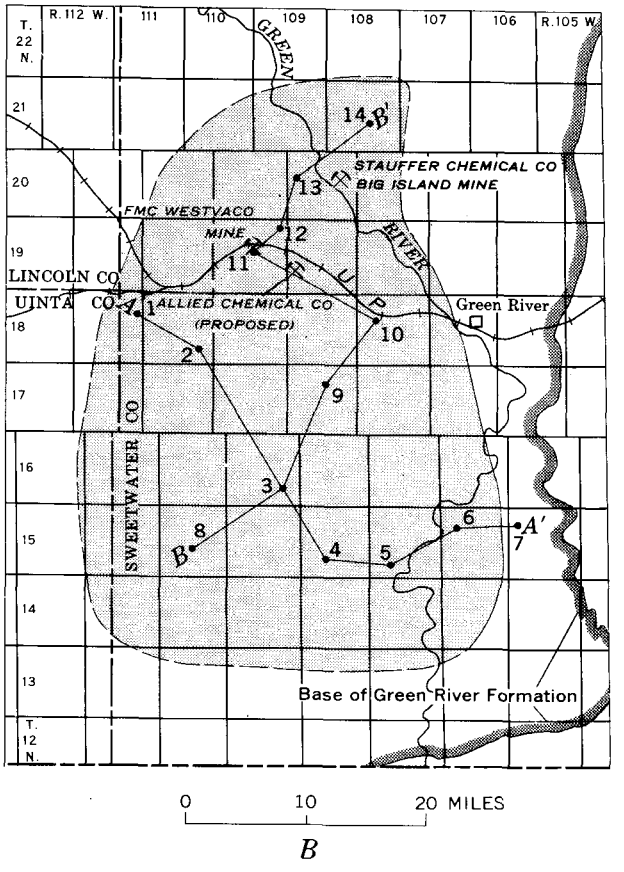


Figure 1.—Index maps showing (*A*) location of area of report (cross ruled), and (*B*) location of columnar sections *A–A′* and *B–B′* (fig. 2) and area of trona deposition (shaded).

of shortite to percolating water, because Fahey (1962, p. 23) states that water differentially decomposes shortite into sodium carbonate, which goes into solution,

TABLE 1.—*Source of data and location of stratigraphic columns shown on figure 2*

| No. of column (fig. 2) | Source of data (drill hole unless given otherwise) | Location of column | | | Depth to bed 17 (feet) |
|---|---|---|---|---|---|
| | | Sec. | Township (north) | Range (west) | |
| 1 | Diamond Alkali Co., No. 1. | 12 | 18 | 112 | 1, 739 |
| 2 | Stauffer Chemical Co., Granger No. 2. | 26 | 18 | 111 | 1, 880 |
| 3 | Diamond Alkali Co., Finley No. 2. | 26 | 16 | 110 | 1, 862 |
| 4 | Perkins No. 2 | 32 | 15 | 109 | 2, 260 |
| 5 | Perkins No. 1 | 32 | 15 | 108 | 1, 541 |
| 6 | Texota Oil Co., Post No. 1. | 18 | 15 | 107 | 996 |
| 7 | Measured section on Sage Creek. | 7, 8, 9 | 15 | 106 | ------ |
| 8 | Phillips Petroleum Co., Cedar Mountain No. 1. | 28 | 15 | 111 | 2, 638 |
| 9 | Diamond Alkali Co., Sturm No. 1. | 10 | 17 | 109 | 1, 493 |
| 10 | Diamond Alkali Co., No. 3. | 17 | 18 | 108 | 1, 320 |
| 11 | Marston Shaft No. 1 and Union Pacific No. 2. | 15 | 19 | 110 | 1, 490 |
| 12 | Westvaco No. 10 | 1 | 19 | 110 | 1, 524 |
| 13 | Stauffer Chemical Co., Big Island No. 1. | 18 | 20 | 109 | 1, 546 |
| 14 | Stauffer Chemical Co., Big Island No. 12. | 22 | 21 | 108 | ------ |

and into calcium carbonate, which forms calcite pseudomorphs. Decomposed shortite is probably the source of the sodium carbonate in water found in shallow wells at the town of Green River (Schultz, 1910, p. 583–589), and in wells in T. 23 N., R. 106 W. Solution of trona probably is not a factor because the affected wells are updip from the area of known trona deposition.

The stratigraphic position and correlation of the 25 trona beds shown on figure 2 are based on the study of many cores, logs of test holes, and outcropping rocks. The trona beds are correlated locally by comparing thickness of beds and intervals between beds, but the correlation of beds across long distances involves the recognition of facies changes and necessitates the use of marker beds. The most useful markers are oil-shale beds because they are more persistent than the trona beds and extend from the saline facies of the Wilkins Peak Member into the fresher water facies. The Wilkins Peak Member contains about 63 beds of oil shale that range in thickness from a few inches to about 4 feet and that yield from 10 to 40 gallons of oil per ton on destructive distillation. Other usable markers are the 9 sandstone-mudstone units and the many thin (1 to 18 inches) beds of tuff, several of which are persistent across many hundreds or thousands of square miles (fig. 2).

Gamma-ray, neutron, and sonic logs of test holes are useful in drill-hole correlation, especially where a hole

is not cored. Thick beds of trona, or trona and halite, generally are distinguishable from the other sedimentary rocks in the gamma-ray–neutron logs by their extremely low gamma-ray radioactivity and low neutron radioactivity, but trona could not be differentiated from halite. In sonic logs, trona beds are characterized by low-interval-transit time. The beds of trona, or trona and halite shown in column 8, figure 2, were identified by their gamma-ray-neutron-log characteristics, and by comparison with core descriptions of nearby holes. Oil-shale beds of the Wilkins Peak are usually recognizable in neutron logs by low radioactivity, and in sonic logs by their higher interval transit time.

Figure 2 shows the position of the contact between the Laney Shale and Wilkins Peak Members of the Green River Formation, which is placed at the base of the continuous sequence of the varved brown fish-bearing oil shale in the lower part of the Laney (Culbertson, 1962). In the eastern part of the area the upper part of the Wilkins Peak consists of interbedded marlstone, claystone, oil shale, and limestone in beds 1 to 5 feet thick that in many places contain saline minerals. Westward the upper part of the Wilkins Peak Member becomes sandy and lacks saline minerals, but the lower oil-shale sequence of the Laney can be recognized with a fair degree of certainty in the cuttings and in electrical and gamma-ray logs of wells. This sandy sequence of the Wilkins Peak is here considered to be the approximate lacustrine equivalent of rocks assigned to the upper tongue of the Wasatch Formation along the western edge of the basin by Oriel (1961, p. 151). The lower oil-shale sequence of the Laney is considered to be equivalent to his "upper tongue of the Green River Formation."

## LOCATION, EXTENT, AND RESOURCES OF TRONA

The 25 thickest beds of trona, or of trona and halite, range in areal extent from 100 to 1,000 square miles (table 2). The areal extent of beds 1 to 17 generally increases from oldest to youngest. Beds 1 to 12 are virtually restricted to the southern half of the area, but beds 14 to 17 extend over much of the southern two-thirds of the area. Beds 1 to 12 and 14 are roughly circular lenses whose centers lie within a small area just east and south of locality 3 (figs. 1 and 2). Beds 15, 16, and 17 are also roughly circular in area and are centered at points 4 to 6 miles north of locality 3.

Beds 13 and 18 are much smaller, irregularly shaped lenses. Bed 13 is elongate in a northerly direction and lies east of locality 3. Bed 18 consists of two lenses, one lying mainly east of locality 3 and the other northeast of locality 2.

TABLE 2.—*Estimated resources of trona, and intermixed trona and halite, by bed, in southwestern Wyoming*

| Bed No. | Total area of bed (sq mi) | Resources of trona [1] | | | Resources of intermixed trona and halite [2] | | |
|---|---|---|---|---|---|---|---|
| | | Average thickness (ft) | Area (sq mi) | Short tons (billions) | Average thickness (ft) | Area (sq mi) | Short tons (billions) |
| 1 | 420 | 8.8 | 385 | 6.3 | | | |
| 2 | 450 | 10.9 | 375 | 7.5 | 15 | 10 | 0.3 |
| 3 | 440 | 4.8 | 275 | 2.4 | 7 | 10 | 0.1 |
| 4 | 500 | 6.6 | 450 | 5.5 | | | |
| 5 | 630 | 7.2 | 485 | 6.4 | 10 | 35 | 0.7 |
| 6 | 580 | 5.4 | 340 | 3.4 | 5.9 | 80 | 0.8 |
| 7 | 560 | 3.9 | 290 | 2.1 | 5.0 | 10 | 0.1 |
| 8 | 490 | 3.8 | 175 | 1.2 | | | |
| 9 | 660 | 4.7 | 175 | 1.5 | 9.4 | 250 | 4.3 |
| 10 | 510 | 3.9 | 55 | 0.4 | 6.3 | 255 | 3.0 |
| 11 | 640 | 4.6 | 90 | 0.8 | 8.7 | 410 | 6.6 |
| 12 | 600 | 6.1 | 190 | 2.2 | 7.7 | 335 | 4.7 |
| 13 | 240 | 4.7 | 50 | 0.4 | | | |
| 14 | 700 | 7.2 | 420 | 5.6 | 8.7 | 200 | 3.2 |
| 15 | 900 | 6.2 | 505 | 5.8 | 9.7 | 235 | 4.2 |
| 16 | 880 | 3.9 | 145 | 1.0 | 7.6 | 255 | 3.6 |
| 17 | 1,000 | 7.7 | 640 | 9.1 | 8.8 | 210 | 3.4 |
| 18 | 270 | | | | 5.0 | 65 | 0.6 |
| 19 | 200 | 6.3 | 85 | 1.0 | | | |
| 20 | 280 | 5.7 | 145 | 1.5 | | | |
| 21 | 190 | 4.0 | 20 | 0.1 | | | |
| 22 | 300 | 4.5 | 35 | 0.3 | | | |
| 23 | 220 | 3.5 | 20 | 0.1 | | | |
| 24 | 100 | 10.1 | 70 | 1.2 | | | |
| 25 | 110 | 7.9 | 85 | 1.2 | | | |
| Total | | | | 67.0 | | | 35.6 |

[1] Excludes trona that contains recognizable halite or that is less than 3 feet thick.
[2] Excludes trona and halite less than 3 feet thick.

After deposition of beds 1 to 18, the center of trona deposition shifted first northward, and then eastward, although a small amount of trona was deposited in the southeast in beds 22 and 23 (figs. 1 and 2). Beds 19, 20, and 21 are smaller lenses, elongate northerly, whose centers lie in the west half of T. 19 N., R. 110 W. Bed 22 occurs as 2 small lenses, the larger of which is centered just northwest of locality 12 and the smaller about 3 miles northeast of locality 4. Bed 23 is an elongate north-trending lens lying east of localities 3 and 11. Beds 24 and 25 are the smallest in areal extent, and each consists of two lenses. The thicker lens of each bed is centered at or near the operations of the Stauffer Chemical Co. (fig. 1), which is mining bed 24 at a depth of about 800 feet. The other lens of each bed is centered northeast of locality 10.

The trona in these beds is translucent to opaque and ranges from yellowish brown to pearly white to colorless. In general, it occurs as layers separated from each other either by persistent layers or thin contorted stringers of oil shale or marlstone. The amount of impurities in the trona is somewhat conjectural, because detailed analyses are not available for most of the beds.

Where the beds are free of halite the amount of impurities is estimated to be between 3 and 25 percent. One of the purest beds is No. 17; at the Westvaco mine it contains 4 to 6 percent impurities, which consist of dolomite crystals, detrital particles of quartz and clay, and a small amount of organic material (Fahey, 1962, p. 43 and 44).

Fifteen beds contain halite (NaCl) at one or more places in the area south of locality 9. The halite occurs either intermixed with trona or interbedded with trona (Deardorff, 1963). At most places halite constitutes only a few percent of the bed, but locally it exceeds 80 percent. No halite has been reported from beds 1, 4, 8, and 19 to 25, but beds 9, 10, 11, 12, 16, and 18 are predominantly mixed trona and halite.

The estimates of the amount of trona and of intermixed trona and halite in southwest Wyoming (table 2) are based on much of the core data obtained in the last 25 years. Many of the data used in these estimates represent cores of widely spaced boreholes, so no attempt

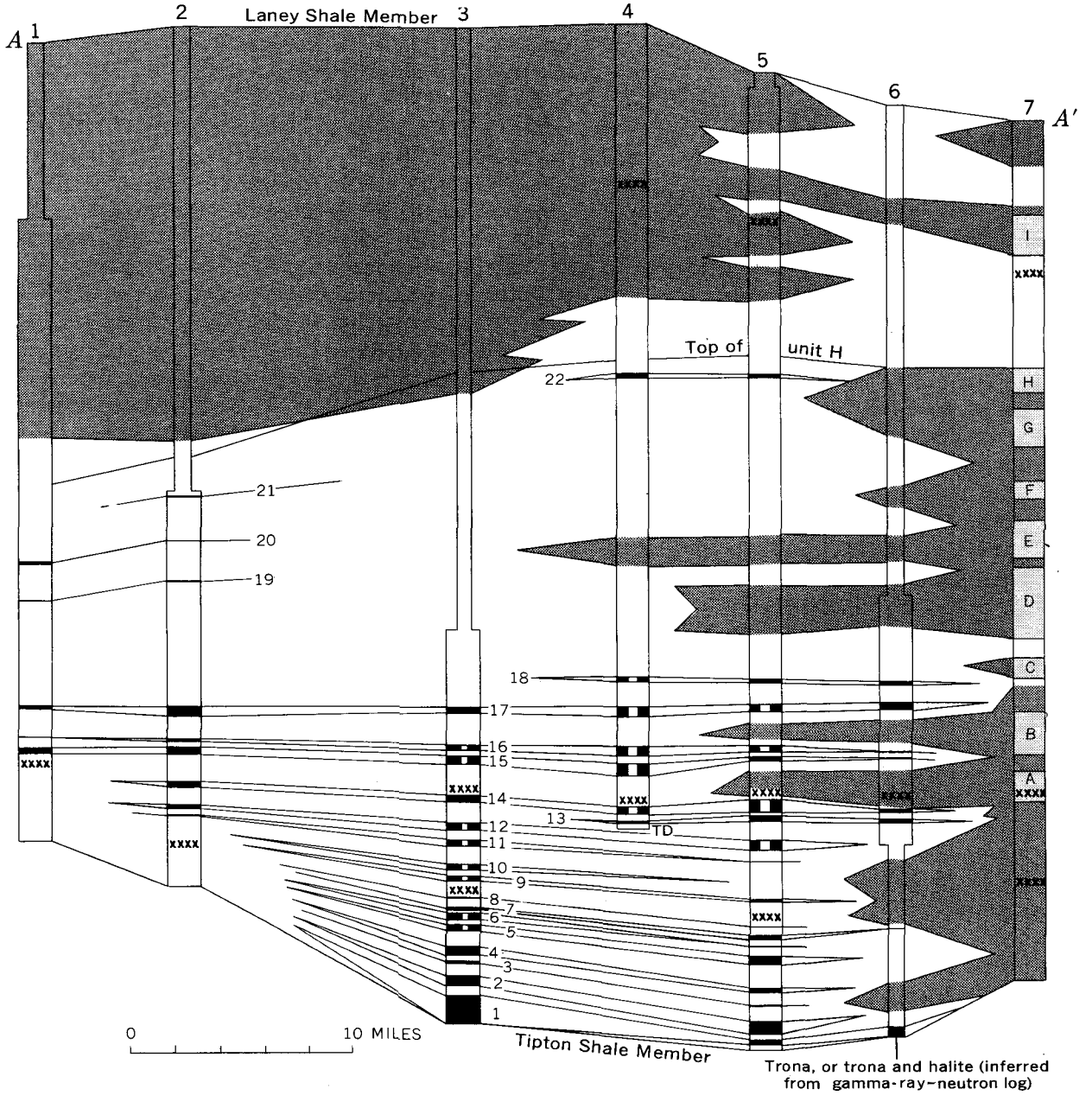


FIGURE 2.—Columnar sections of Wilkins Peak Member of Gr their position with respect to 9 sandstone-mudstone u of column is cored hole, or exposure in shaft or outcr 13) not included by Deardorff (1963) or Love (1964, fig. 1 of sections shown on figure 1. TD, total depth of hole

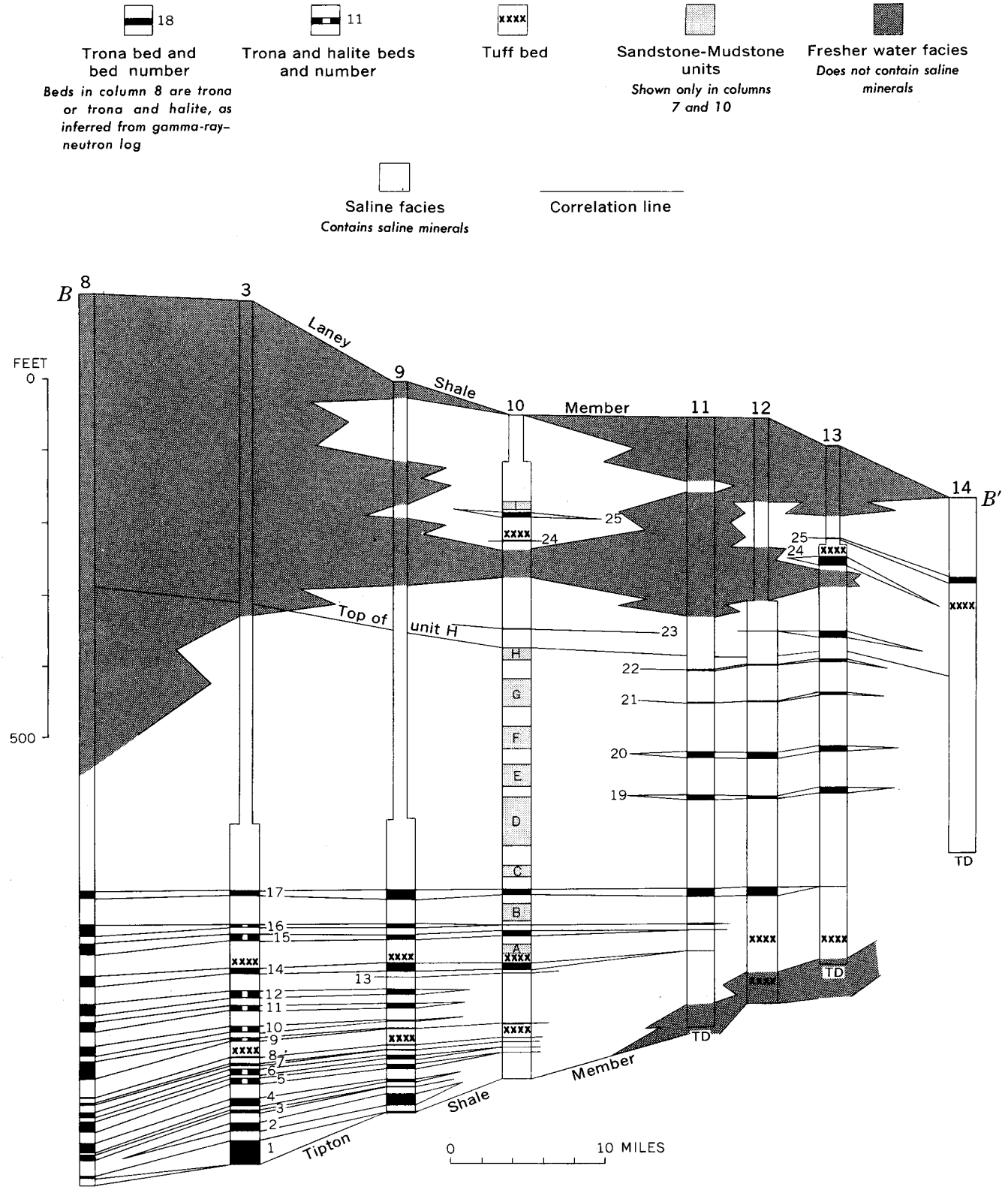


iver Formation, showing 25 beds of trona, or trona and halite, and
ıd 3 tuff beds described previously (Culbertson, 1961). Wide portion
ırrow portion is rotary drilled hole. Beds 1 to 17 include one bed (No.
ıd exclude one bed (between 8 and 9) that these authors include. Lines
ertical scale is same for both parts of illustration.

was made to calculate measured or indicated reserves. The data are believed sufficiently close, however, to provide a basis for reasonable approximation of the total or ultimate resources. The largest probable source of error in these estimates is the location of the boundary of each deposit. The scarcity of drilling in the south and west, particularly, necessitated extrapolating data several miles beyond known points of information. In calculating resources of trona, all beds, or parts of beds, containing less than 3 feet of trona were excluded as being too thin for economic development in the foreseeable future. Oil-shale or marlstone partings were excluded in computing the total thickness of trona in each bed. Trona containing recognizable halite was excluded from the estimate of trona resources because halite is generally considered to be a contaminant of trona. However, in southwest Wyoming, the amount of mixed trona and halite is large and generally occurs in thicker beds than those containing only trona. Because future technological advances may make this mineral mixture valuable, its resources were calculated separately.

The total resources of halite-free trona are estimated to be 67 billion tons (table 2). Of this amount, 75 percent is contained in beds 1, 2, 4, 5, 6, 14, 15, and 17. All of these exceed 10 feet in maximum thickness, and bed 1 is reported to be as much as 40 feet thick (Love, 1964, p. 24). Four other beds—Nos. 19, 20, 24, and 25—also locally exceed 10 feet in thickness, but do not underlie such large areas as the older beds.

The resources of mixed trona and halite more than 3 feet thick are estimated to be about 36 billion tons (table 2). These resources are contained in 14 beds in the southern part of the area, of which 10 beds exceed 10 feet in maximum thickness.

## REFERENCES

Bradley, W. H., 1964, Geology of Green River Formation and associated Eocene rocks in southwestern Wyoming and adjacent parts of Colorado and Utah: U.S. Geol. Survey Prof. Paper 496–A, 86 p.

Brown, P. L., 1950, Occurrence and origin of the known trona deposits in Sweetwater and Uinta Counties, Wyoming: Wyoming Univ. Master's thesis, 82 p.

Culbertson, W. C., 1961, Stratigraphy of the Wilkins Peak Member of the Green River Formation, Firehole Basin quadrangle, Wyoming: Art. 348 *in* U.S. Geol. Survey Prof. Paper 424–D, p. D170–D173.

———1962, Laney Shale Member and Tower Sandstone Lentil of the Green River Formation, Green River area, Wyoming: Art. 78 *in* U.S. Geol. Survey Prof. Paper 450–C, p. C54–C57.

Deardorff, D. L., 1963, Eocene salt in the Green River Basin, Wyoming, *in* Symposium on salt: Northern Ohio Geol. Soc., p. 176–195.

Fahey, J. J., 1962, Saline minerals of the Green River Formation: U.S. Geol. Survey Prof. Paper 405, 50 p.

Love, J. D., 1964, Uraniferous phosphatic lake beds of Eocene age in intermontane basins of Wyoming and Utah: U.S. Geol. Survey Prof. Paper 474–E, 66 p.

Oriel, S. S., 1961, Tongues of the Wasatch and Green River Formations, Fort Hill area, Wyoming: Art. 63 *in* U.S. Geol. Survey Prof. Paper 424–B, p. B151–B152.

Schultz, A. R., 1910, Deposits of sodium salts in Wyoming *in* Contributions to economic geology 1909: U.S. Geol. Survey Bull. 430, p. 570–589.

# HYDROTHERMAL ALTERATION NEAR THE KENNECOTT COPPER MINES, WRANGELL MOUNTAINS AREA, ALASKA—A PRELIMINARY REPORT

By E. M. MacKEVETT, JR., and A. S. RADTKE, Menlo Park, Calif.

*Abstract.*—Hydrothermal alteration near the Kennecott mines in Alaska consists of an early dolomitic phase and a later jarosite–illite–potassium feldspar phase that has been recognized only recently. The dolomitic alteration is widespread throughout the lower part of the Chitistone Limestone, the host for the Kennecott copper deposits. The jarosite–illite–potassium feldspar alteration is less extensive and is largely confined to the vicinity of known ore deposits; it is characterized by light-brown zones of jarosite, illite, potassium feldspar, and montmorillonite that are best developed near the contact between the Nikolai Greenstone and the Chitistone Limestone, especially in the area between the Erie and Jumbo mines.

Zones of hydrothermal alteration that may be useful in prospecting and exploration and may lead to a fuller understanding of the genesis of the copper lodes occur near the Kennecott copper deposits in the southern Wrangell Mountains, Alaska. Continuing studies may provide additional data on the extent and types of the hydrothermal alteration, its spatial and temporal relations to the ore, and also may lead to the discovery of other localities where the rocks have been hydrothermally altered.

The Kennecott mines include the Bonanza, Jumbo, Erie, and Mother Lode properties in the McCarthy C–5 and C–6 quadrangles about 240 miles east of Anchorage and about 60 miles west of the Canadian border (fig. 1). Smaller mines and prospects with a geologic setting similar to the Kennecott deposits are located near the confluence of Glacier Creek and the Chitistone River, near Donoho Peak, and east of McCarthy Creek (fig. 1). The Kennecott mines are renowned for the large size and high grade of their chalcocite-rich ore bodies. They have been most thoroughly described by Bateman and McLaughlin (1920) and less extensively by other geologists, notably Moffit (1938, p. 118–125) and Lasky (1928). The chalcocite ore bodies form irregular massive replacements, veins, and stockworks in the lower part of the Late Triassic Chitistone Limestone, commonly near its conformable contact with the subjacent Nikolai Greenstone of late Middle or early Late Triassic age or both. Several small copper deposits that commonly contain chalcopyrite, bornite, chalcocite, and pyrite also occur in the Nikolai Greenstone in the general region, but they have not been amenable to mining. The areal geology near the Kennecott deposits has been mapped by Moffit (1938, pl. 1) and in more detail by MacKevett (1963, 1965, and unpub. data).

The Nikolai Greenstone, Chitistone Limestone, and younger Late Triassic and Jurassic sedimentary rocks from an extensive northwest-trending belt along the southern flank of the Wrangell Mountains. Locally these rocks are overlain unconformably by marine Cretaceous sedimentary rocks, and in places are overlapped by the Wrangell Lava of Tertiary and Quaternary age. Fine-grained Tertiary intrusive rocks, which have porphyritic and altered phases and may have some relation to the ore formation, crop out chiefly within a zone as much as 2 miles wide south of, and subparallel to, the belt of Mesozoic rocks. The ore deposits of the Kennecott mines are also close to a plexus of faults (MacKevett, 1963, and unpub. data) that has shattered and brecciated the Chitistone Limestone.

One of the features considered by previous workers to be characteristic of the Kennecott lodes is the paucity or absence of wallrock alteration (Bateman and McLaughlin, 1920, p. 34). Bateman and McLaughlin (1920, p. 34, 35) believe that the local masses of coarse calcite and the widespread dolomite in the lower part of the Chitistone Limestone formed through hydrothermal activity; however, they believe that these minerals predate ore deposition and are unrelated to it.

Hydrothermal alteration near the Kennecott mines consists of an extensive dolomitic phase and a subsequent, more restricted, jarosite–illite–potassium feldspar phase that was recognized during the summer of

U.S. GEOL. SURVEY PROF. PAPER 550–B, PAGES B165–B168

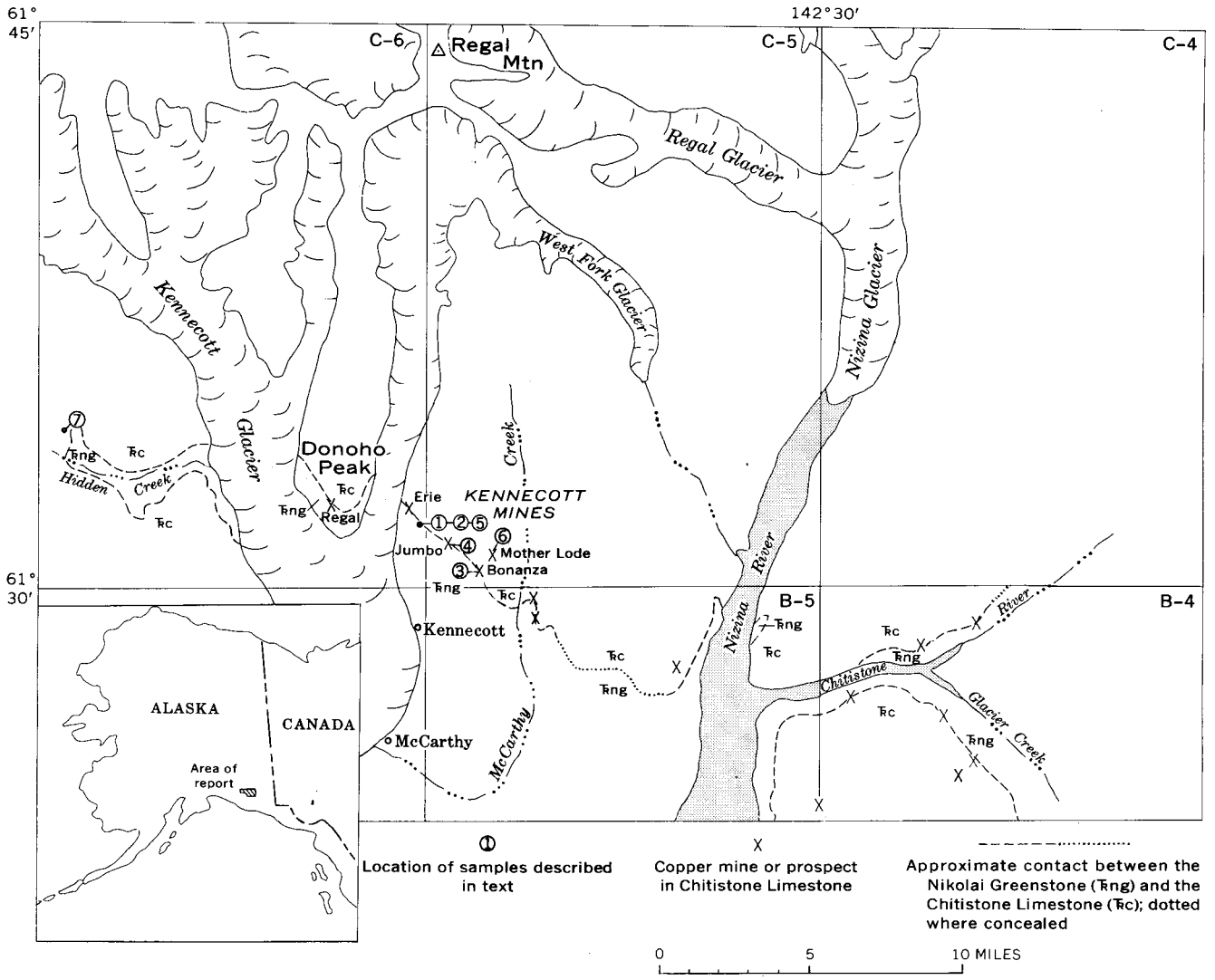


FIGURE 1.—Index map showing sample locations, the Kennecott mines, and nearby mines and prospects in the Chitistone Limestone, southeastern Alaska.

1963. Dolomite is common throughout the lowermost few hundred feet of the Chitistone Limestone, where it has been found at numerous localities, including many far beyond the known limits of ore deposition in the McCarthy C–5 and adjacent quadrangles (fig. 1). Most of the ore at the Kennecott mines is in the dolomitic parts of the Chitistone Limestone (Bateman and McLaughlin, 1920, p. 24); however, much of the dolomite is unaccompanied by ore. The dolomite forms irregular, commonly sparry, masses that crosscut bedding and transect and replace limestone. Minerals characteristic of the jarosite–illite–potassium feldspar alteration stage locally coat dolomite or occupy fractures in dolomite. Semiquantitative spectrographic analyses of dolomitized and unaltered Chitistone Limestone from near the mines are shown in table 1 (Nos. 1 and 2) and indicate that the introduction of magnesium is one of the significant chemical changes accompanying the dolomitization. The common association of dolomitization with certain types of ore deposits has been noted by Hewett (1928). The dolomitization in the Chitistone Limestone probably represents a preliminary and widespread alteration stage that preceded the ore-forming sequence, somewhat analogous to the early dolomitization described by Lovering and others (1949) and by Proctor (1964) for the East Tintic and North Tintic districts respectively in Utah.

The jarosite–illite–potassium feldspar alteration is characterized by the introduction of potassium and removal of many other elements. Alteration zones of this type are distributed intermittently near the greenstone-limestone contact between the Jumbo and Erie mines, at the Regal mine (fig. 1), and elsewhere. Discrete alteration zones are as much as 400 feet long and 10 feet thick and are conformable with the greenstone and overlying limestone. These zones are suscep-

TABLE 1.—*Semiquantitative spectrographic analyses of altered and unaltered rocks from near the Kennecott mines*

[Analysts: I. H. Barlow, Chris Heropoulus, and H. W. Worthing. M, major constituent, greater than 10 percent; leaders (dashes), element not detected]

| Element | 1 Dolomitized Chitistone Limestone | 2 Chitistone Limestone | 3 Altered Chitistone Limestone | 4 Typical Nikolai Greenstone | 5 Leached Nikolai Greenstone | 6 Jarosite–illite–potassium feldspar altered material |
|---|---|---|---|---|---|---|
| Si | 0.1 | 1 | 0.15 | M | M | M |
| Al | .05 | .15 | .1 | 10 | 10 | 7 |
| Fe | .07 | .2 | .15 | M | 10 | 7 |
| Mg | M | 1 | .07 | 7 | 1.5 | 1 |
| Ca | M | M | M | 5 | .7 | 1 |
| Na | .07 | .04 | ------- | 1.5 | .3 | 2 |
| K | ------- | ------- | ------- | .07 | 7 | 5 |
| Ti | .005 | .02 | .002 | 1.7 | 1 | 1 |
| Mn | .007 | .005 | .03 | .15 | .02 | .01 |
| Ag | ------- | ------- | ------- | ------- | ------- | ------- |
| As | ------- | ------- | 1.5 | ------- | ------- | ------- |
| B | ------- | ------- | ------- | .001 | .03 | .005 |
| Ba | .002 | .0007 | .0015 | .01 | .02 | .02 |
| Co | .0005 | ------- | ------- | .005 | .003 | .0015 |
| Cr | .0003 | .003 | .0005 | .03 | .03 | .02 |
| Cu | .001 | .0005 | .0007 | .02 | .015 | .01 |
| Ga | ------- | ------- | ------- | .003 | .005 | .003 |
| Nb | ------- | ------- | ------- | .001 | .002 | .0015 |
| Ni | ------- | .001 | .0002 | .02 | .01 | .003 |
| Sc | ------- | ------- | ------- | .007 | .007 | .005 |
| Sn | ------- | ------- | ------- | ------- | ------- | ------- |
| Sr | .02 | .1 | .03 | .03 | .07 | .07 |
| V | .0015 | .0015 | .002 | .07 | .07 | .07 |
| Y | ------- | .001 | ------- | .005 | .003 | .003 |
| Yb | ------- | ------- | ------- | .0005 | .0005 | .0005 |
| Zr | ------- | ------- | ------- | .015 | .01 | .01 |

Results reported in percent to the nearest number in the series 1, 0.7, 0.5, 0.3, 0.2, 0.15, 0.1, and so forth, which represent approximate midpoints of group data on a geometric scale. Assigned group for semiquantitative results will include the quantitative value about 30 percent of the time.

Other elements looked for but not found in any specimen: Au, Be, Bi, Cd, Ce, Ge, Hf, Hg, In, La, Li, Mo, Pb, Pd, Pt, Re, Sb, Ta, Te, Th, Tl, U, W, Zn.

Sample descriptions and locations:

1. Average of two samples, one from the ridge south of the Bonanza mine and the other from cliffs east of the Nizina River near the southeast corner of the McCarthy C–5 quadrangle.
2. Average of two samples from southeast part of McCarthy C–5 quadrangle near the junction of the Nizina River and the West Fork.
3. Altered Chitistone Limestone from dump of the Bonanza mine.
4. Average of 9 samples of Nikolai Greenstone collected at intervals of about 300 feet across the greenstone section on the ridge southwest of the Jumbo mine.
5. Leached and altered Nikolai Greenstone at upper contact of greenstone between the Erie and Jumbo mines, locality 2 on figure 1.
6. Material representative of the zones of jarosite–illite–potassium feldspar alteration between the Erie and Jumbo mines, locality 1 on figure 1.

tible to erosion and form narrow topographic benches. The altered zones consist of very fine grained light-brown cohesive masses that probably mainly resulted from the intense alteration of the Nikolai Greenstone, a process that obliterated the primary minerals, structures, and textures of the greenstone. A sample from the Nikolai (fig. 1, No. 1), representative of the jarosite–illite–potassium feldspar alteration zones, consists, in order of decreasing abundance, of jarosite, quartz, montmorillonite, illite, and potassium feldspar.[1] A semiquantitative spectrographic analysis of this sample (table 1, No. 6) reflects an introduction of potassium when compared with unaltered Nikolai Greenstone (table 1, No. 4), but it does not show appreciable amounts of copper or other heavy metals.

At the Regal mine (fig. 1) however, the uppermost 1 to 2 feet of the Nikolai Greenstone has been leached and altered and contains malachite and probably also jarosite and illite. This material has not been studied in detail. That the jarosite and potassium feldspar-bearing clayey zones were derived from intense alteration of the Nikolai Greenstone is suggested, in part, by similarities in trace-element content of the zones, the underlying leached greenstone, and typical Nikolai Greenstone that has not been hydrothermally altered (table 1, Nos. 4, 5, and 6). The age relationships of the minerals in the jarosite-rich alteration zones could not be determined, and possibly the mineral assemblage represents more than one alteration stage.

Jarosite–illite–potassium feldspar alteration also affected the uppermost 1 to 2 feet of the Nikolai Greenstone subjacent to the cohesive altered zones. This hydrothermally altered greenstone is dark brown, and its amygdules have been strongly leached, resulting in voids that are partly filled with hydrothermal minerals that also permeate contiguous parts of the rock. The introduced minerals consist of potassium feldspar, jarosite, goethite, illite, and traces of montmorillonite. A semiquantitative spectrographic analysis (table 1, No. 5) of this leached and altered Nikolai Greenstone is notable for its high potassium and low iron, magnesium, calcium, and sodium content when compared to analyses representative of typical Nikolai Greenstone (table 1, No. 4). The potassium probably was introduced by hydrothermal solutions from an extraneous source, as potassium is only a minor constituent of nearby rocks.

Of 53 samples of typical Nikolai Greenstone from the McCarthy C–5 quadrangle that were analyzed by semiquantitative spectrographic methods (MacKevett, unpub. data) only 13 contain potassium in detectable amounts (greater than about 0.5 percent), and the maximum value of these is 1.5 percent. The $K_2O$ content of 5 Nikolai Greenstone samples from the C–5 quadrangle as determined by chemical analyses ranges from 0.32 to 0.81 percent (MacKevett, unpub. data).

The Nikolai Greenstone is an amygdaloidal basalt that, besides its dominant primary minerals, contains abundant chlorite and subordinate amounts of calcite,

[1] Alteration products described in this report were identified by X-ray diffraction methods.

quartz, and epidote that fill the amygdules and occur rarely as alteration products scattered throughout the rock. These minerals probably formed from deuteric alteration. However, the Nikolai Greenstone has not been pervasively altered like most greenstones elsewhere, and its primary minerals and textures generally are preserved. Possibly some of the chlorite formed during a later stage of hydrothermal alteration that was superposed on the deuterically altered lava marginal to zones of jarosite–illite–potassium feldspar alteration.

Fracture surfaces in the Chitistone Limestone above the jarosite–illite–potassium feldspar altered zones (fig. 1, No. 5) are thinly coated with kaolinite but apparently lack jarosite or illite, an indication that the greenstone was more receptive to this type of alteration than the limestone.

Samples from the Kennecott mines, however, provide some evidence for hydrothermal alteration that may be related to the potassium-enrichment stage. Medium-gray limestone found on the dump of the Bonanza mine is speckled with canary-yellow blotches that consist of clusters of very minute crystals of orpiment and traces of jarosite. Sample 3 (fig. 1 and table 1) is typical of this limestone. A sample of partly recrystallized limestone (fig. 1, No. 4) from basal Chitistone Limestone at the Jumbo mine is cut by calcite veinlets that contain chalcocite and azurite along with trace amounts of orpiment and jarosite. Minerals identified in samples of limestone from the dump at the Mother Lode mine (fig. 1, No. 6) include calcite, dolomite, kaolinite, and traces of jarosite as components of yellow clayey veinlets, and kaolinite and quartz as local surface coatings.

Hydrothermally altered zones north of Hidden Creek (fig. 1, No. 7) may represent a phase of the jarosite–illite–potassium feldspar alteration. This locality is far from known ore bodies in the Chitistone Limestone, although a few small copper deposits occur in the Nikolai Greenstone near Hidden Creek. The alteration occurs in and near a dike, 6 to 10 feet thick, emplaced along a thrust fault that separates the Chitistone Limestone and the Nikolai Greenstone. Irregular zones of coarse sparry calcite, as much as 50 feet long and 10 feet thick, are sporadically distributed along the fault, and the dike and the contiguous wallrock have been hydrothermally altered. The zones of coarse sparry calcite also contain minor quantities of kaolinite and trace amounts of jarosite. The altered greenstone in the footwall contains calcite, chlorite, quartz, illite, and traces of epidote. Illite is the only mineral that is atypical of the greenstone. Alteration products in the dike are calcite, dolomite, kaolinite, quartz, and minor amounts of jarosite and montmorillonite.

Brownish zones that in general resemble zones of jarosite–illite–potassium feldspar alteration have been noted near the Chitistone Limestone–Nikolai Greenstone contact at several other places, particularly along the canyon walls of Hidden Creek and in the cliffs north of the Chitistone River (fig. 1).

The origin of the Kennecott ore bodies is uncertain. Details of the relationships between ore formation, dolomitization, and jarosite–illite–potassium feldspar alteration are not known. Spatial and probably genetic relationships between these processes are indicated, however, by the localization of the Kennecott type lodes in and near dolomitized phases of the limestone and by the fact that the potassium-rich alteration zones are best developed in an area near the major known ore bodies.

## REFERENCES

Bateman, A. M., and McLaughlin, D. H., 1920, Geology of the ore deposits of Kennecott, Alaska: Econ. Geology, v. 15, no. 1, p. 1–80.

Hewett, D. F., 1928, Dolomitization and ore deposition: Econ. Geology, v. 23, no. 8, p. 821–863.

Lasky, S. G., 1928, Transverse faults at Kennecott and their relations to the main fault system: Am. Inst. Mining Metall. Engineers Tech. Pub. 152, 17 p.

Lovering, T. S., and others, 1949, Rock alteration as a guide to ore—East Tintic district, Utah: Econ. Geology Mon. 1, 64 p.

MacKevett, E. M., Jr., 1963, Preliminary geologic map of the McCarthy C–5 quadrangle, Alaska: U.S. Geol. Survey Misc. Geol. Inv. Map I–406.

——— 1965, Preliminary geologic map of the McCarthy C–6 quadrangle, Alaska: U.S. Geol. Survey Misc. Geol. Inv. Map I–444.

Moffit, F. H., 1938, Geology of the Chitina Valley and adjacent area, Alaska: U.S. Geol. Survey Bull. 894, 137 p. [1939]

Proctor, P. D., 1964, Fringe zone alteration in carbonate rocks, North Tintic district, Utah: Econ. Geology, v. 59, no. 8, p. 1564–1587.

# ZONAL DISTRIBUTION OF ELEMENTS IN SOME URANIUM-VANADIUM ROLL AND TABULAR ORE BODIES ON THE COLORADO PLATEAU

By DANIEL R. SHAWE, Denver, Colo.

*Work done in cooperation with the U.S. Atomic Energy Commission*

*Abstract.*—Uranium, vanadium, and selenium are zonally distributed within and near some uranium-vanadium roll and tabular ore bodies in sandstone on the Colorado Plateau. The zones are concentric with the curved boundaries of the rolls, and parallel to the boundaries of tabular bodies. The zones are compatible with a theory that ore and other introduced elements were precipitated at an interface between two solutions with different properties, now represented by the ore boundary.

The form of Colorado Plateau uranium-vanadium roll and tabular ore bodies, particularly the roll type, and variations in shape of the ore bodies related to variations in sandstone host-rock lithology, indicate ore deposition at an interface between two solutions with different properties. If the interface theory is correct, different elements may be arranged in zones related to the postulated interface position, reflecting chemical and physical gradients that existed across the interface.

New chemical data on the eU, U, V, Cu, Pb, Zn, As, and Se content of roll ore bodies in mines in Colorado and Utah, and comparison of the U, V, and Se data with previously published data for roll and tabular ore bodies in the same and other mines in Colorado, Utah, and New Mexico, show that these elements are, in fact, systematically and similarly zoned in both types of ore bodies.

Data on some other elements indicate similarities in their distribution, too, but these data are not presented in this paper.

## PHYSICAL CHARACTERISTICS OF DEPOSITS

### Roll ore bodies

Roll ore bodies are long and narrow, and lie with their axes parallel to sandstone stratification and direction of greatest permeability of the sandstone. They have crescent-shaped or more complex cross sections whose edges cross the bedding of the host rock. Rolls are common in uranium-vanadium deposits in the Morrison Formation (Upper Jurassic). Their general form was first made clear by Fischer (1942, p. 367, 379–380), and some details of roll ore bodies have been published more recently (Shawe, 1956; Shawe and Granger, 1965). Commonly the "inner" or concave surface of a crescent-shaped roll appears to be a sharp boundary between ore-grade and less mineralized sandstone, whereas the "outer" or convex surface is diffuse, showing a gradual decrease of ore-mineral concentrations into less mineralized sandstone. The sharply defined inner side of a roll is believed to represent approximately the position of the solution interface. Uranium and vanadium ore and other minerals commonly occur in visible "bands" or zones concentric with the curved boundaries of the rolls. Roll ore bodies may form the lateral edges of tabular ore bodies, and in such deposits are merely the sharply curved lateral terminations of the tabular bodies which are otherwise nearly concordant with bedding of the host rock. Many tabular ore bodies are not modified by roll-like forms.

### Tabular ore bodies

Tabular ore bodies are roughly lenticular in cross section, nearly concordant to sandstone stratification, and commonly are elongate in plan with their long axes parallel to the direction of greatest permeability of the sandstone. They are the most common type of uranium ore body on the Colorado Plateau. Epigenetic minerals occur in layers near and parallel to some tabular layers of uranium and vanadium ore minerals

(for example, Fischer, 1960, p. 19; Granger and others, 1961, p. 1200).

## MINES SAMPLED

Deposits for which chemical data have not been published previously are the three roll ore bodies at the Virgin No. 3 mine in Colorado, and one roll body each in the Allor No. 12 and Little Pittsburg No. 5 mines in Utah. Data for the other deposits described below have been published in the indicated reports. The location of all the mines is shown in figure 1.

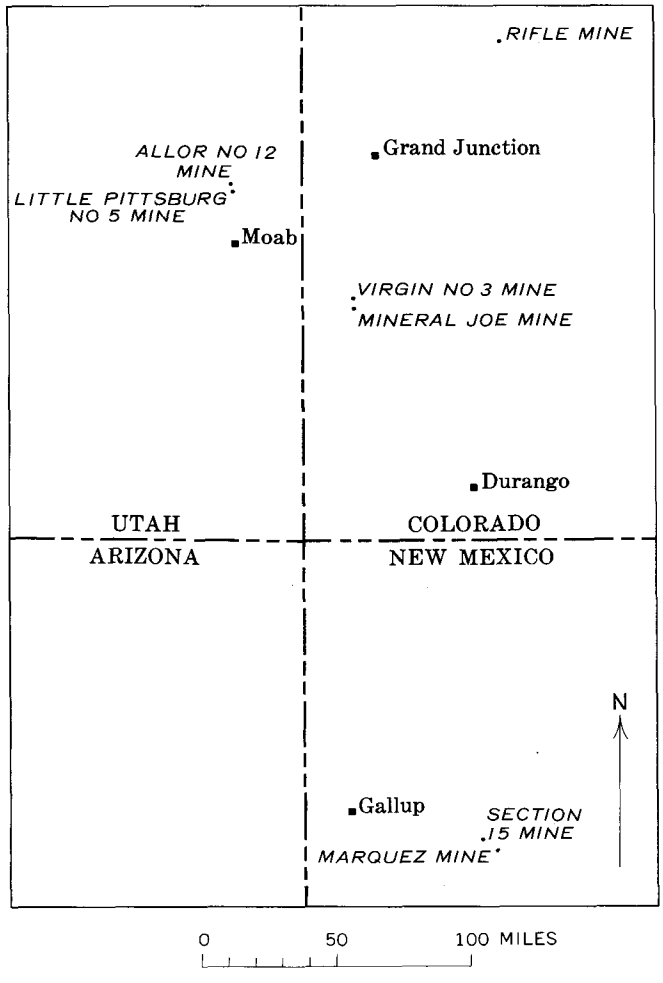


FIGURE 1.—Map of part of the Colorado Plateau, showing the location of sampled mines.

### Colorado

The Virgin No. 3 mine, in the Uravan district, Montrose County, is in the uppermost sandstone unit (ore-bearing sandstone) of the Salt Wash Member of the Morrison Formation. The deposit lies below the water table. It had recently been opened at the time it was sampled, and was considered to be relatively unoxidized (Garrels and others, 1959, p. 184). One roll was sampled in 1953 by the author and two rolls were sampled in 1954 by the author and Lyman C. Huff, of the U.S. Geological Survey. Analyses of the tabular ore layer were published previously by Garrels and others (1959, table 3).

The Mineral Joe mine, in the Paradox district, Montrose County, is in the upper part of the Salt Wash Member of the Morrison Formation. The roll ore body and host rock were slightly oxidized when sampled (Garrels and others, 1959, p. 177; 184).

The Rifle mine, in Garfield County, is in the Entrada Sandstone (Upper Jurassic) and the Navajo(?) Sandstone (Jurassic and Triassic(?)). The two tabular ore layers are thoroughly oxidized (Fischer, 1960).

### Utah

The Allor No. 12 and Little Pittsburg No. 5 mines are in the Yellow Cat area of the Thompson district, Grand County. Both mines are in sandstone units in the lower part of the Salt Wash Member. The Allor No. 12 deposit is below the water table and appeared to be relatively unoxidized when sampled, whereas the Little Pittsburg No. 5 deposit, which is close to the surface, is above the water table and is oxidized. The rolls in these mines were sampled in 1955 by N. L. Archbold, of the U.S. Geological Survey.

### New Mexico

The Section 15 and Marquez mines, in the Ambrosia Lake district, McKinley County, are in the upper part of the Westwater Canyon Member of the Morrison Formation (Granger and others, 1961; H. C. Granger, oral communication, 1965). One of the black tabular ore bodies at the Section 15 mine is unoxidized and below the water table; the other is nearly unoxidized but above the water table. The black tabular ore body at the Marquez mine is enclosed by oxidized sandstone and is below the water table.

## RESULTS

Diagrams of the five ore bodies sampled in the present study, the location of samples collected, and partial chemical analyses of the samples are shown in figures 2 and 3 (p. B172–B174). A diagrammatic comparison of the relative positions of the uranium, vanadium, and selenium zones in two of the rolls at the Virgin No. 3 mine (fig. 2*A*, *B*) and similar zones in roll and tabular ore bodies previously described is shown in figure 4 (p. B175).

The uranium-to-vanadium ratios of all samples summarized in figure 4 are arranged in spatial sequence from top to bottom across tabular ore layers, and from concave side inward through roll ore bodies. The samples from different suites of course are not equally spaced so that the comparisons are crude, yet figure 4

illustrates the similar, regular distribution of zones enriched in uranium, vanadium, and selenium. Selenium is most highly concentrated close to the sharp boundary between weakly mineralized rock and ore in all examples for which data are available. The partly oxidized tabular ore layer in the Section 15 mine, however, is unique in having high-selenium layers at both the top and the bottom edges of uranium ore. The edge of strongest vanadium mineralization generally lies at the sharp visible ore boundary, whereas the edge of strongest uranium mineralization lies farther within the ore body in most cases. The distribution of vanadium in the partly oxidized tabular layer in the Section 15 mine is also unique in that the vanadium-enriched zone is below rather than above the uranium-enriched zone. In general, uranium-to-vanadium ratios increase abruptly at the boundary between weakly mineralized rock and ore; in some ore bodies the relative increase in uranium occurs at the edge of the vanadium-rich layer and in others at the edge of the uranium-rich layer.

The consistent repetition of the pattern of distribution of the zones in these suites of samples collected from random cross sections of ore bodies shows that the zones truly have shell-like configurations parallel or concentric with the ore boundaries.

## CONCLUSIONS

Similarity in the zonal distribution of uranium, vanadium, and selenium near the edges of both rolls and tabular uranium-vanadium ore bodies suggests that both types were formed the same way, a conclusion already apparent where the two forms of ore bodies occur together and are physically continuous. The zonal distribution of elements also is compatible with a theory that ore and other elements were precipitated in the vicinity of an interface between two solutions, now marked by the sharp concave edge of roll ore bodies, or one (generally the upper?) edge of tabular ore layers. The zonation of the layers of different elements is believed to be related to the different responses of the elements to an interface that existed between two chemically and physically different solutions. Elements which are concentrated in the zones may have come from either or both of the solutions, and were moved to the interface because of differences in chemical (such as concentration, Eh, pH) and physical (such as temperature, density) potentials at the interface. Apparently oxidation of the ore deposits has not affected the gross distribution of uranium, vanadium, and selenium.

## REFERENCES

Fischer, R. P., 1942, Vanadium deposits of Colorado and Utah: U.S. Geol. Survey Bull. 936–P, p. 363–394.

——— 1960, Vanadium-uranium deposits of the Rifle Creek area, Garfield County, Colorado: U.S. Geol. Survey Bull. 1101, 52 p.

Garrels, R. M., Larsen, E. S., 3d, Pommer, A. M., and Coleman, R. G., 1959, Detailed chemical and mineralogical relations in two vanadium-uranium ores, pt. 15 *of* Garrels and Larsen, compilers, Geochemistry and mineralogy of the Colorado Plateau uranium ores: U.S. Geol. Survey Prof. Paper 320, p. 165–184.

Granger, H. C., Santos, E. S., Dean, B. G., and Moore, F. B., 1961, Sandstone-type uranium deposits at Ambrosia Lake, New Mexico—an iterim report: Econ. Geology, v. 56, p. 1179–1210.

Shawe, D. R., 1956, Significance of roll ore bodies in genesis of uranium-vanadium deposits on the Colorado Plateau, *in* Page, L. R., Stocking, H. E., and Smith, H. B., compilers, Contributions to the geology of uranium and thorium . . . : U.S. Geol. Survey Prof. Paper 300, p. 239–241.

Shawe, D. R., and Granger, H. C., 1965, Uranium ore rolls—an analysis: Econ. Geology, v. 60, p. 240–250.

797–218 O—66——12

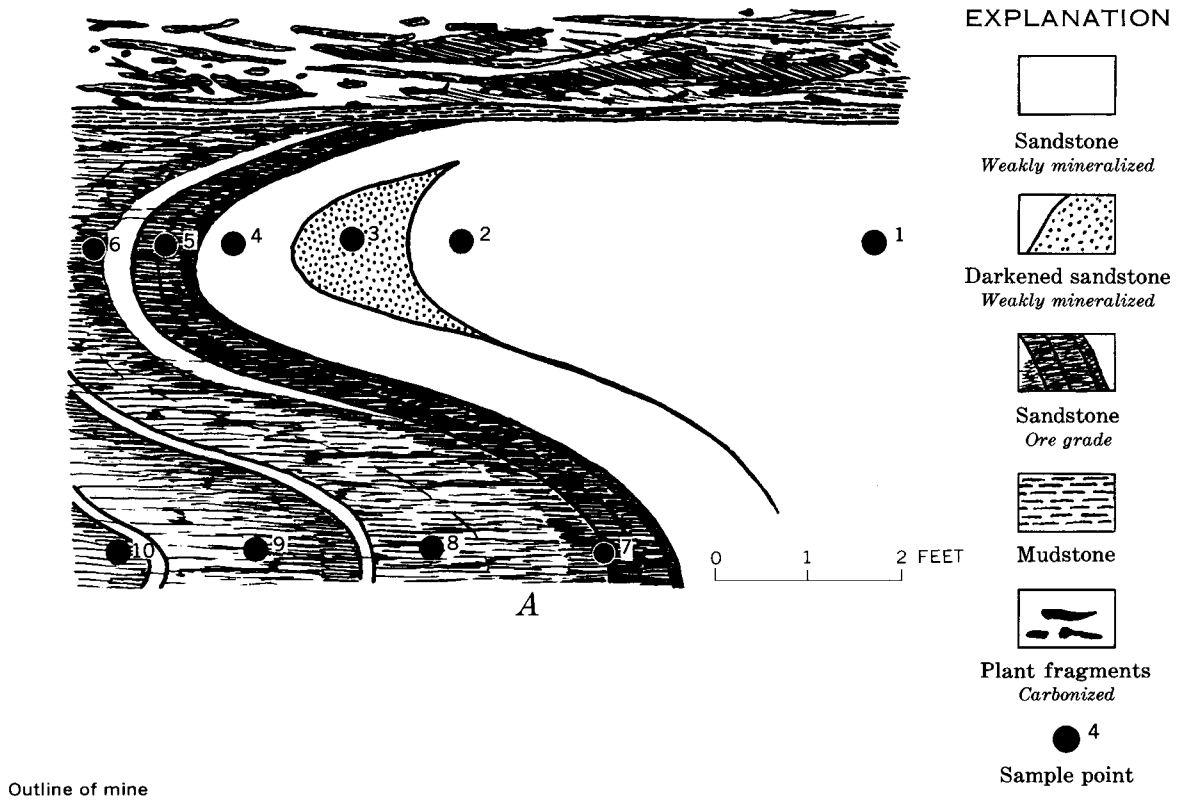


FIGURE 2.—Sections and chemical analyses of roll ore bodies in the Virgin No. 3 mine, Uravan distr

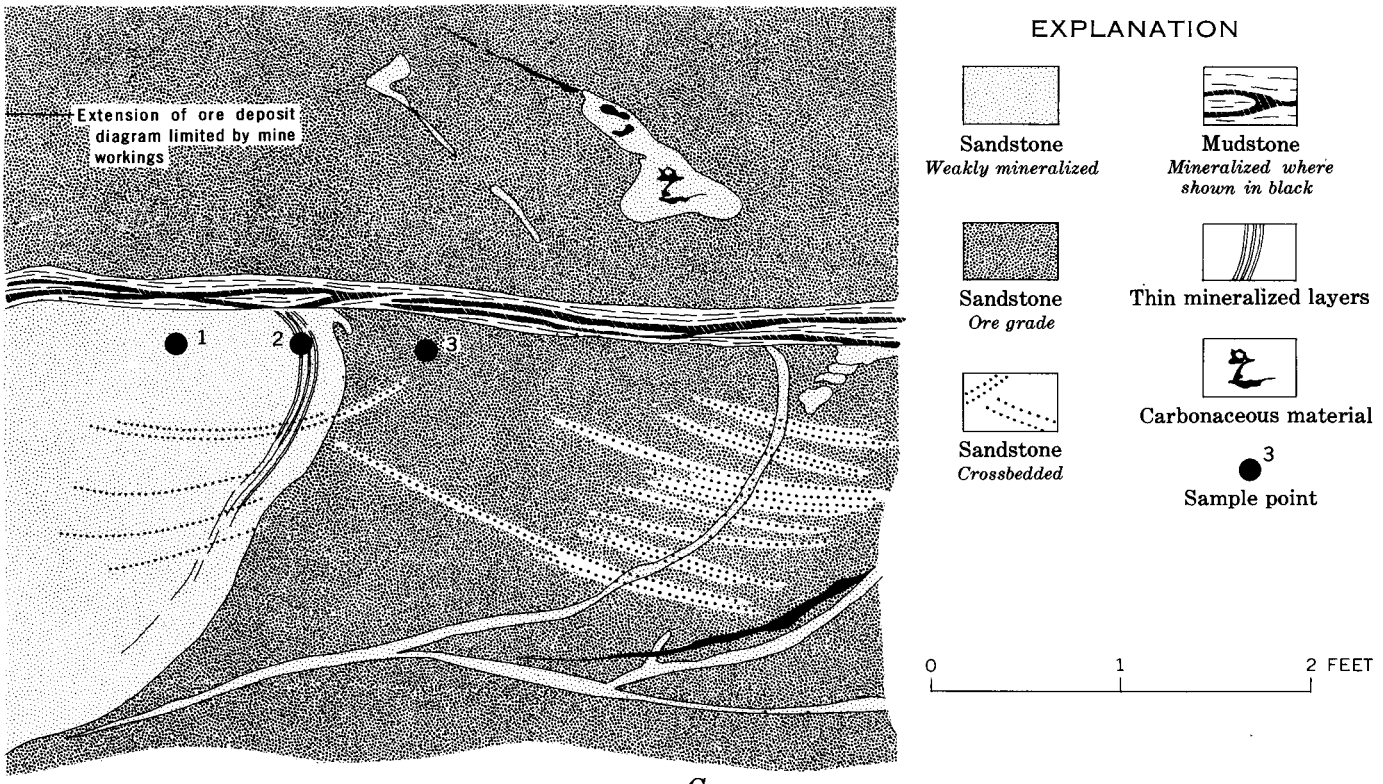


*C*

[Analysts: Sylvia Furman, H. H. Lipp, J. McClure, J. P. Schuch, and C. E. Thompson, U.S. Geological Survey]

| Sample No. | Laboratory No. | Percent | | | Parts per million | | | | |
|---|---|---|---|---|---|---|---|---|---|
| | | eU | U | V | Cu | Pb | Zn | As | Se |
| **A** | | | | | | | | | |
| 1 | 211102 | 0.004 | ------- | 0.3 | 20 | 20 | 20 | 20 | 10 |
| 2 | 211103 | .005 | 0.006 | .2 | 20 | 20 | <20 | 50 | 20 |
| 3 | 211104 | .003 | ------- | .3 | 20 | 20 | <20 | 40 | 20 |
| 4 | 211105 | .003 | ------- | .2 | 20 | 30 | <20 | 10 | 200 |
| 5 | 211106 | .065 | .068 | 1.5 | 20 | 20 | 20 | 40 | 70 |
| 6 | 211107 | .11 | .12 | 2.5 | 20 | 20 | <20 | 40 | 15 |
| 7 | 211108 | .073 | .12 | 2.5 | 20 | 20 | <20 | 60 | 7 |
| 8 | 211109 | .016 | .021 | 2.5 | 20 | <20 | <20 | 20 | 10 |
| 9 | 211110 | .041 | .051 | 2.5 | 20 | 20 | <20 | 40 | 10 |
| 10 | 211111 | .13 | .15 | 2.5 | 20 | 20 | <20 | 90 | 15 |
| **B** | | | | | | | | | |
| 1 | 211093 | 0.009 | 0.011 | 0.09 | 20 | 20 | 20 | 40 | 20 |
| 2 | 211094 | .008 | .009 | .09 | 20 | <20 | 20 | 10 | 10 |
| 3 | 211095 | .030 | .027 | .2 | 20 | <20 | 20 | 20 | 50 |
| 4 | 211096 | .22 | .34 | 1.2 | 20 | <20 | 20 | 100 | 150 |
| 5 | 211097 | .26 | .40 | 1.5 | 20 | <20 | 20 | 150 | 20 |
| 6 | 211098 | .39 | .61 | 1.2 | 20 | <20 | 20 | 150 | 1,500 |
| **C** | | | | | | | | | |
| 1 | 211099 | 0.008 | 0.012 | 0.09 | 20 | <20 | <20 | 10 | 40 |
| 2 | 211100 | .10 | .15 | .2 | 20 | <20 | <20 | 20 | 1,500 |
| 3 | 211101 | .17 | .17 | 6.0+ | 20 | 20 | 20 | 40 | 30 |

Montrose County, Colo. *A*, "S" roll ore body; *B*, ore roll with irregular edge; *C*, simple roll ore body.

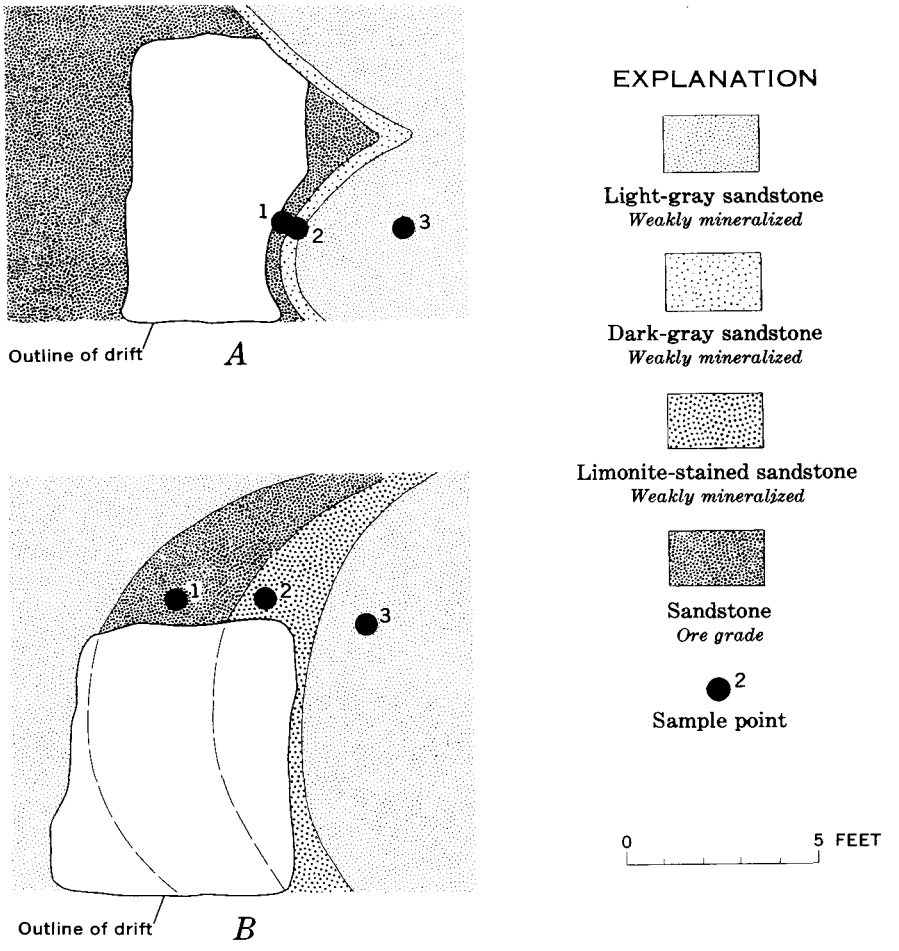


[Analysts: M. Finch, C. G. Angelo, H. H. Lipp, G. T. Burrow, J. P. Schuch, E. C. Mallory, Jr., and H. E. Crowe, U.S. Geological Survey]

| Sample No. | Laboratory No. | Percent | | | Parts per million | | | | |
|---|---|---|---|---|---|---|---|---|---|
| | | eU | U | V | Cu | Pb | Zn | As | Se |
| **A** | | | | | | | | | |
| 1 | 224015 | 0.014 | 0.013 | 0.61 | <10 | 10 | 20 | 40 | 7 |
| 2 | 224017 | .004 | .009 | .06 | <10 | <10 | <10 | 100 | 8 |
| 3 | 224014 | .002 | .002 | <0.06 | <10 | 20 | <10 | <10 | 200 |
| **B** | | | | | | | | | |
| 1 | 224016 | 0.011 | 0.005 | 0.82 | <10 | 10 | <10 | 60 | 1 |
| 2 | 224018 | <.001 | ------- | .06 | <10 | <10 | 10 | 20 | 9 |
| 3 | 224013 | .002 | .003 | <0.06 | 20 | <10 | <10 | 60 | 2 |

FIGURE 3.—Sections and chemical analyses of roll ore bodies in two mines in the Yellow Cat area, Thompson district, Grand County, Colo. *A*, unoxidized roll ore body in the Allor No. 12 mine; *B*, oxidized roll ore body in the Little Pittsburg No. 5 mine.

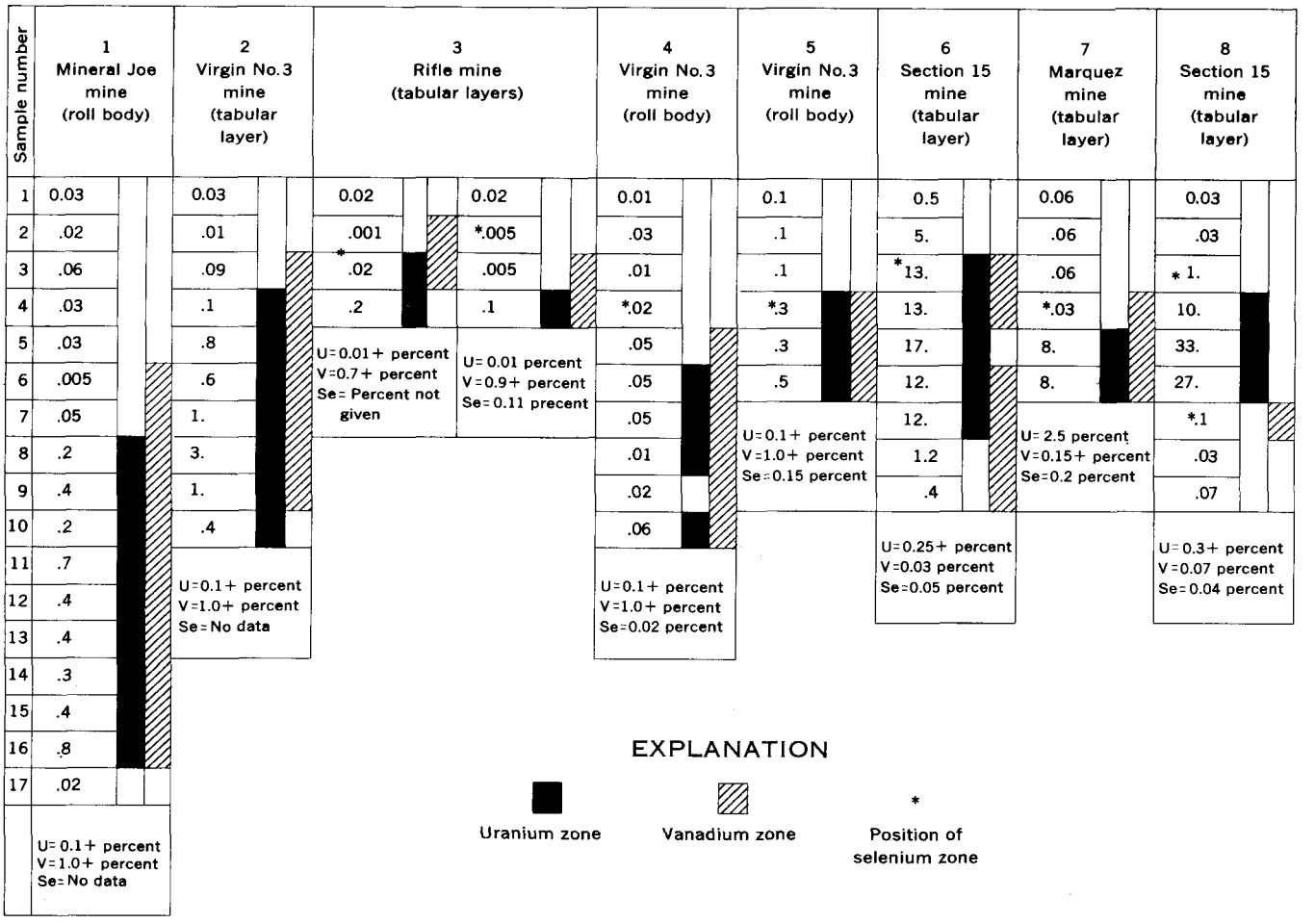


1, Calculated from Garrels and others (1959, table 1).
2, Calculated from Garrels and others (1959, table 3).
3, Calculated from Fischer (1960, fig. 7, samples 1 and 4).
4, Calculated from analyses accompanying figure 2*A* (this paper).
5, Calculated from analyses accompanying figure 2*B* (this paper).
6, Calculated from Granger and others (1961, fig. 5a).
7, Calculated from Granger and others (1961, fig. 5b).
8, Calculated from Granger and others (1961, fig. 5c).

FIGURE 4.—Diagram comparing uranium-vanadium ratios, and positions of higher grade uranium, vanadium, and selenium zones in some Colorado Plateau uranium-vanadium deposits. Cut-off grade for uranium, vanadium, and selenium content is listed at the bottom of each column of samples.

# URANIUM, THORIUM, AND RADIUM ANALYSES BY GAMMA-RAY SPECTROMETRY (0.184–0.352 MILLION ELECTRON VOLTS)

By C. M. BUNKER and C. A. BUSH, Denver, Colo.

*Abstract.*—A combination of graphical- and mathematical-interpretation techniques applied to gamma-ray spectrometer data provides a direct method for measuring uranium and an indirect method for measuring thorium and radium in whole-rock samples. Detection limits with a 200-channel spectrometer system including a 4- by 5-inch NaI crystal, a maximum data-accumulation time of 1,000 minutes, and 400- to 900-gram samples are 1.5 ppm for uranium and 1 ppm for thorium and equivalent radium.

Methods of uranium and thorium radioisotope analyses by gamma-ray spectrometry were investigated to seek an improvement on previously reported techniques by other investigators. These analyses are important geologically because they may aid age determinations, be used as an exploration method for locating hydrothermally altered rock which may contain nonradioactive ore minerals (Moxham and others, 1965), and provide radioelement data required for studies of heat flow. Also, thorium analysis by gamma-ray spectrometry of samples containing a few tens of parts per million is more rapid than by other analytical techniques.

Gamma-ray spectrometers have been used for the past 15 years to measure the radioelement content of samples. Qualitative measuring techniques were described by Hofstader and McIntyre (1950) and Kahn and Lyon (1953). Hurley (1956) described a method for uranium and thorium analyses by using the low-energy portion of the gamma-ray spectrum. At about the same time, Adams and others (1958) devised a method for measuring uranium, thorium, and potassium using gamma-ray energies higher than those used by Hurley. The method described here is similar in the use of low energies, 0.184–0.352 Mev (million electron volts), to those described by Hurley and by Mero (1960), but is different in the method of interpretation, in the additional analysis for parent uranium, and in the increased sensitivity which permits analysis of radioelements in low concentrations. The method provides analyses of uranium determined from the $U^{235}$ content, equivalent radium (as defined by Rosholt, 1959) determined from the Pb $^{214}$ content, and equivalent thorium based on the Pb $^{212}$ content.

The technique described here has several advantages over other types of measurements inasmuch as (1) sample preparation is limited to crushing and weighing, and chemical treatment is not needed, and (2) much of the interpretation of the data is graphical, and complex mathematical equations are not used. Also, relative to alpha-counting or mass-spectrometer techniques, much larger samples can be used to provide an analysis of a more representative sample.

The disadvantages are that (1) only one parent radioisotope, $U^{235}$, can be measured quantitatively, (2) the $U^{235}$ cannot be interpreted quantitatively when the thorium-uranium ratio exceeds about 10 because such higher ratios cause a masking of the $U^{235}$ energy by the $Pb^{212}$ energy line, and (3) large samples must be available when the radioisotope content is in the order of a few parts per million.

B. R. Doe and J. N. Rosholt furnished analytical data and the samples used for uranium, radium, and thorium calibration standards; their aid is gratefully acknowledged.

## INSTRUMENTATION AND OPERATIONAL PROCEDURES

Two detection systems and two suites of sample sizes were used to cross-check the relative sensitivity, reliability of results, and whether interpretation methods applied to data from one system are generally applicable to another. Both systems are basically the same, consisting of multichannel pulse-height analyzers and sodium iodide crystals to which are coupled photomultiplier tubes. The pulses from the photomultiplier tube–crystal detector are transmitted to the analyzers where they are sorted electronically and stored in a memory circuit. The spectra obtained from the samples are plotted on $X$–$Y$ records from

which the gamma-ray energies and intensities are interpreted.

The spectrometer system used for most of the analyses consists of a 400-channel pulse-height analyzer and a 5-inch diameter by 4-inch-thick NaI (Tl) crystal detector viewed with a 5-inch-diameter photomultiplier tube. The detector and sample are centered in a lead box lined with steel; internal dimensions are 32 inches per side and 38 inches high. The spectra are accumulated in 200 channels from which the background spectrum is subtracted prior to each sample analysis.

The other spectrometer system, used as an independent check on the general interpretation method, consists of a 256-channel pulse-height analyzer, and a 3-inch-diameter by 3-inch-thick NAI(Tl) crystal detector viewed with a 3-inch-diameter photomultiplier tube. The detector and the sample are centered in a radiation shield that is 18 inches in diameter and 48 inches in height and is surrounded, except for an 8-inch-diameter port at the top, by a 3-inch annulus of mercury contained in a steel tank. The shield is lined with cadmium and copper to reduce backscatter radiation. During this study, 128 channels were used to retain a negative spectrum of the background and another 128 channels were used to obtain a net spectrum from the sample being analyzed.

The data-accumulation time varied according to the radiation intensity of each sample and to some extent according to operational convenience. The accumulation time used on the 200-channel system ranged from 10 to 1,000 minutes (0.167 to 16.7 hours). The 1,000-minute analyses were required for samples containing less than 10 ppm uranium or thorium and were run overnight for expediency. Spectra from samples containing several hundred parts per million of these radioelements can be obtained in as little as 10 minutes. The 128-channel system was operated in constant increments of 30,000 seconds (8.33 hours) because of instrument limitations; this amount of time is generally sufficient to obtain interpretable spectra.

The 200-channel and 128-channel systems were adjusted to accept gamma-ray energies ranging from 0 to 0.5 Mev and 0 to 0.43 Mev, respectively. The gamma-ray energies used for determining uranium and thorium content occur within this range.

Rock samples are crushed to less than pea size, weighed, enclosed in thin-walled plastic containers with lids, and sealed with tape to prevent radon or thoron loss. The samples are not analyzed for 2 weeks after being sealed, to permit short-lived radiogenic daughters to reach equilibrium with the parent $Ra^{226}$. The transient equilibrium state permits an indirect analysis of long-lived parents by measuring the daughter products because the parent-daughter ratio between daughter and parent radioisotopes is virtually proportional and constant. Sample sizes differed depending on the crystal size used and on the amount of material available. Two-hundred-gram samples, 3 inches in diameter and about 1 inch deep, were used with the 3- by 3-inch detector; 400- to 900-gram samples 6 inches in diameter and about 1.5 inches deep were used with the 4- by 5-inch detector. The samples are placed directly on the detectors of both the 128- and 200-channel systems when spectra are obtained.

## INTERPRETATION METHOD

Spectra of uranium and daughter products, thorium and daughter products, and $Ra^{226}$ and daughter products (fig. 1) accumulated with the 200-channel system show the energies and radioisotopes used for analysis. Some energies are related to both the uranium and thorium series. In the uranium series, $Ra^{226}$ and one of its daughters, $Pb^{214}$, contribute the greatest number of energy peaks in the energy span used in this investigation. The energies emitted by these radioisotopes are 0.187 Mev from $Ra^{226}$, and 0.242, 0.259, 0.295, and 0.352 Mev from $Pb^{214}$. $U^{235}$ constitutes approximately 0.72 percent of the total uranium, and no significant variation in the ratio between $U^{235}$ and the more abundant $U^{238}$ has yet been measured. $U^{235}$ is measurable by its 0.184-Mev gamma-ray energy. In the thorium series, the most significant energy is 0.238 Mev from $Pb^{212}$. Another energy peak at 0.32 Mev related to thorium daughters was observable, but is less significant. When all the radioisotopes were present in a sample, several of the energy lines overlapped and appeared as a single peak because the inherent resolution of the detection system is insufficient to separate closely adjacent energies into separate and distinct peaks. As a result of testing several interpretation techniques, a method for minimizing the effects of interfering energies was developed.

The configuration of the spectra provided a direct method of determining that thorium was present in a sample. The spectra of samples containing only radium (fig. 1*A*) showed that the tops of the 0.242, 0.295, and 0.352 Mev peaks were always in a straight line with relatively constant slope. $Pb^{212}$ from the thorium series emits a 0.238 Mev energy which, when present, is the only other major contributor, along with $Pb^{214}$, to the 0.24 energy peak. The linear relation of the three energy peaks from $Ra^{226}$ and daughters provides a rapid interpretation technique for thorium analysis. A line drawn through the tops of the 0.295 and 0.352 Mev energy peaks is extended through the vertical center of the 0.24 Mev energy peak (fig. 2). When the line intersects the peak below the top, the presence

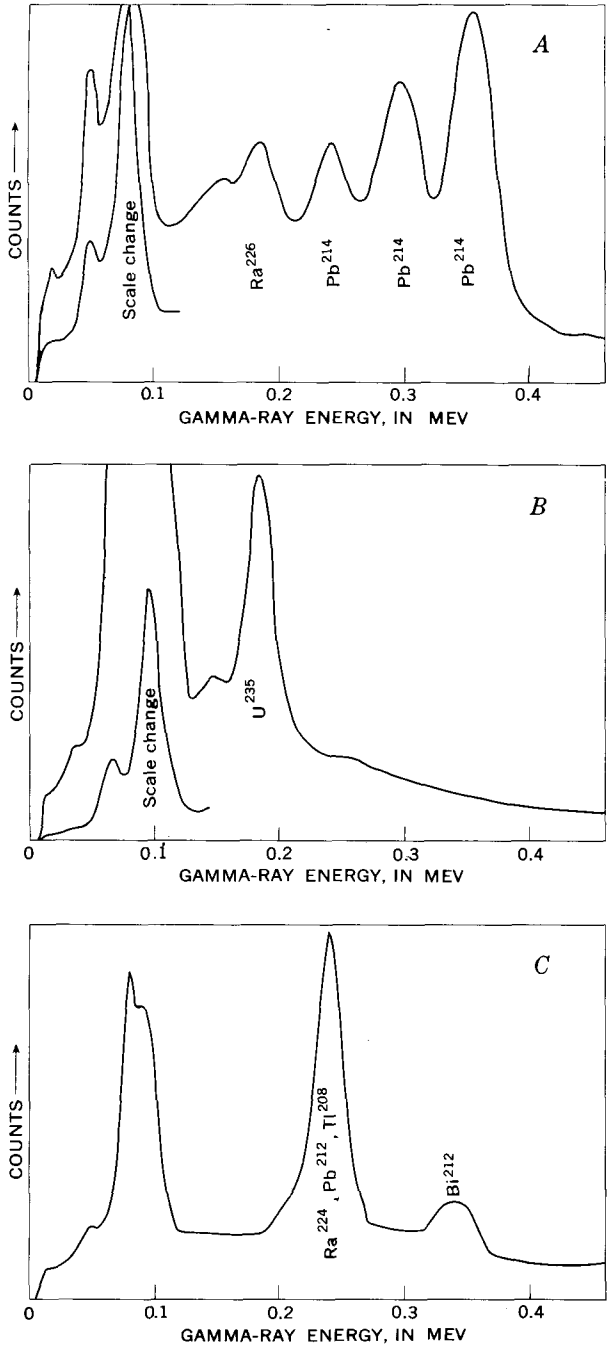


FIGURE 1.—Gamma-ray spectra of (*A*) $Ra^{225}$ and daughters, (*B*) $U^{235}$, and (*C*) $Th^{232}$ daughters, in energy range of 0 to 0.47 Mev.

of $Pb^{212}$ is indicated, and the peak amplitude is thereby directly related to the thorium content.

One of the major differences between the present and previous interpretation methods is that, previously, peak amplitudes have been measured from the *X*-axis baseline. This is a valid method when no energies greater than the one being interpreted are present in significant amounts. The presence and relative

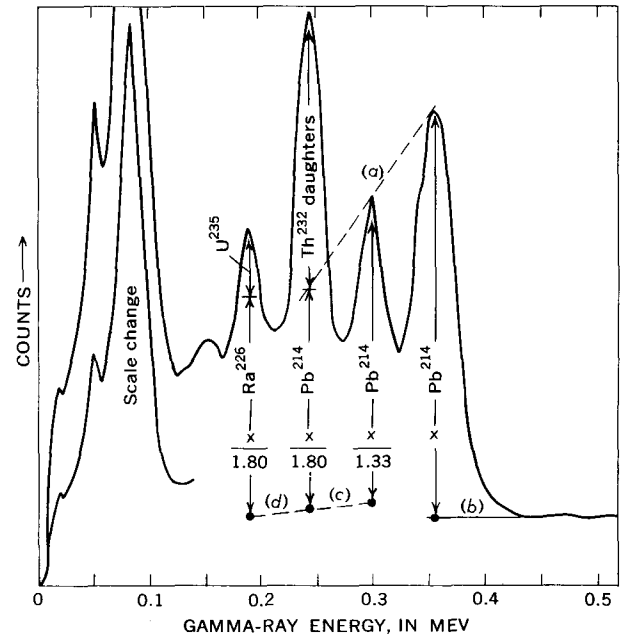


FIGURE 2.—Gamma-ray spectrum of mixed natural radioisotopes, and method of interpretation. Thorium-daughter content is determined by extending line (*a*) through $Pb^{214}$ peaks (0.295 and 0.352 Mev) and measuring excess amplitude in 0.24-Mev energy peak. Equivalent radium is measured by extending a tangent line (*b*) from the valley to $Pb^{214}$ peak (0.352 Mev) and measuring the amplitude (*x*). Baseline (*c*) is adjusted for sample weight by measuring down from top of $Pb^{214}$ peaks at 0.24 Mev and 0.30 Mev and applying factors determined from standards containing $Ra^{226}$ and daughters (table 1). Baseline (*d*) is an extension of baseline (*c*) to below 0.18-Mev peak and amplitude related to $Ra^{226}$ is determined; excess is $U^{235}$

amounts of radioisotopes emitting higher energies than the interpreted energy cause the baseline to shift upward by different amounts because of different amounts of beta radioactivity, Compton scattering, and internal scattering in the samples, thereby increasing the error in the measurement of the peak amplitude if the *X*-axis baseline is used consistently. The spectra from natural radioisotopes show a relatively flat valley from about 0.43 to 0.53 Mev (fig. 2); this valley is used as the nominal baseline from which most of the peak amplitudes are measured. As explained below, adjustments of the baseline were sometimes required for the effects of sample weight.

Equivalent radium is determined from the amplitude of the 0.352-Mev energy peak from $Pb^{214}$. That peak is adjacent to the valley used to establish the baseline and is least affected by the presence of other radioisotopes in the sample.

$Ra^{226}$ and its daughter, $Pb^{214}$, caused the most interference with other radioisotope analyses. A method described below for determining and removing the effect of the radium and $Pb^{214}$ energies from the total spectrum leaves other energy peaks isolated, and from these

remaining peaks other radioisotopes are interpreted quantitatively. Samples of different weights (200, 400, 500, and 600 g) and with different amounts of radium and daughters in transient equilibrium, but without other radioisotopes, were prepared as standards to determine differences in peak-amplitude ratios related to sample weight (table 1). The peak amplitudes

TABLE 1.—*Peak-amplitude ratios related to sample weight*

| Radioisotopes<br>Gamma-ray energies (Mev) | | $Pb^{214}/Pb^{214}+Ra^{226}$<br>0.352/0.18 | $Pb^{214}/Pb^{214}$<br>0.352/0.24 | $Pb^{214}/Pb^{214}$<br>0.352/0.295 |
|---|---|---|---|---|
| System | Sample weight (grams) | Amplitude ratios | | |
| 200-channel | 400 | 1.80 | 1.80 | 1.33 |
| | 500 | 1.63 | 1.70 | 1.28 |
| | 600 | 1.61 | 1.64 | 1.26 |
| 128-channel | 200 | 2.72 | 2.47 | 1.43 |

from the radium standards is measured from a horizontal line extended through the valley between 0.43 and 0.53 Mev. Because the 0.352-Mev energy peak is least affected by interfering energies from other natural radioisotopes in rock samples, the amplitude of this energy peak is used to establish the amplitude ratios.

When samples are the same weight as the radium standards, the data from the appropriate size standard are normally used to establish the baseline, which is generally a horizontal extension of the valley in the region of 0.43 to 0.53 Mev. Use of samples and standards of the same weight is not mandatory, but an adjustment of the baseline is required to eliminate the effect of different weights on some energy peaks.

The baseline is adjusted to correct for the effect of sample weight by (1) completing the process used to determine the presence of thorium, (2) measuring the amplitude of the 0.352-Mev energy peak, (3) determining the theoretical amplitudes of the 0.24-Mev and 0.295-Mev energy peaks based on their ratios to the 0.352-Mev peak in radium samples, and (4) plotting points directly below the 0.24- and 0.295-Mev energy peaks at distances representing the theoretically correct amplitude for each. Connecting these points and extending the line from the bases of the 0.24- and 0.295-Mev energies to a point below the 0.18-Mev peak gives an adjusted baseline (fig. 2). The method was checked by applying the data from one standard to the spectrum from another, and it was determined that the baseline changed from a horizontal line to a curve and that this change compensated for the effect of differences in sample thickness and weight.

Uranium analyses determined from the $U^{235}$ content are more difficult to make and are subject to greater error than the equivalent radium and thorium analyses because more adjustments of the spectrum are required. After the thorium contribution is determined and the baseline is adjusted, the effect of $Ra^{226}$ and $Pb^{214}$ on the 0.18-Mev energy peak is established by applying the amplitude ratio of the 0.352- and 0.187-Mev energy peaks. Any remaining amplitude is assumed to be caused by the presence of the 0.184-Mev energy from $U^{235}$ (fig. 2).

Because the amplitudes of the 0.24-Mev energy from $Pb^{212}$ and the 0.352 energy from $Pb^{214}$ were interpreted differently (no correction for baseline changes was applied) than the $U^{235}$ energy peak, the amplitudes were not corrected by using the radium standards to adjust the results for the effects of sample weight. Instead, another factor, determined empirically, was applied separately to the amplitudes of these two energy peaks to relate the results to a standard sample weight. A large sample was split into different weights ranging from 200 to 1,000 g and each was placed in a 6-inch diameter container used with the 200-channel spectrometer system. The 400-g size was arbitrarily chosen as the standard weight. The results (fig. 3) relate sample weight to the multiplication factor which had to be applied to the energy-peak amplitude measured from a sample of any weight to equate it to the standard weight.

After the peak amplitude at each energy level is determined by the above methods, each amplitude measured in counts is divided by the accumulation time and the sample weight to express the results, commonly

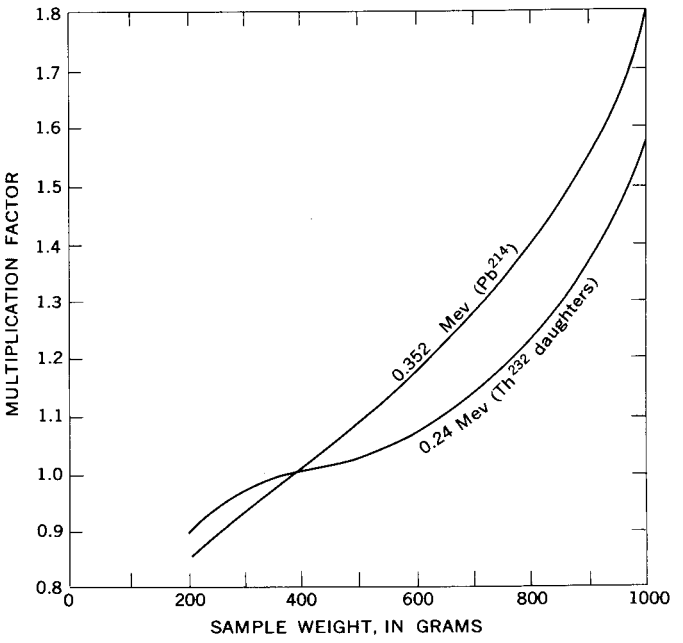


FIGURE 3.—Multiplication factor required to equate peak amplitude (counting rate) from different sample weights to standard 400-gram weight.

in counts per minute per gram of sample. These data are related to the uranium, radium, and thorium content, expressed in parts per million, of standard samples analyzed previously by other analytical techniques (table 2). The relation between the two types of data obtained with both spectrometer systems is shown on calibration plots (figs. 4, 5) prepared for interpreting the natural radioisotope content of previously unanalyzed samples.

TABLE 2.—*Comparison between gamma-ray spectrometer and chemical analyses*

| Sample No.[1] | Uranium (ppm) | | Ra-226 (ppm) | | Thorium (ppm) | | $U_\gamma/U_{chem}$ | $Ra_\gamma/Ra_{chem}$ | $Th_\gamma/Th_{chem}$ |
|---|---|---|---|---|---|---|---|---|---|
| | Chem. | γ | Chem. | γ | Chem. | γ | | | |
| **200-channel system** | | | | | | | | | |
| S5A | 6.00 | 6.3 | | 7.0 | 15.8 | 15.7 | 1.15 | | 0.99 |
| S5B | 5.76 | 5.4 | | 7.9 | 17.2 | 16.3 | .94 | | .95 |
| S5C | 6.34 | 5.8 | | 6.9 | 15.7 | 16.4 | .91 | | 1.04 |
| K-1 | 3.24 | 3.2 | | 3.8 | 8.6 | 8.4 | .99 | | .98 |
| K-2 | 3.45 | 3.0 | | 3.5 | 8.6 | 8.5 | .87 | | .99 |
| K-3 | 2.18 | 2.8 | | 3.2 | 8.1 | 8.2 | 1.28 | | 1.01 |
| K-4 | 1.92 | 2.0 | | 4.0 | 8.0 | 8.3 | 1.04 | | 1.04 |
| K-5 | 2.06 | 3.2 | | 4.0 | 7.6 | 8.4 | 1.55 | | 1.11 |
| Los Posos obsidian | 5.2 | 5.2 | | 7.9 | 18.3 | 18.1 | 1.00 | | .99 |
| 79148 | 1,500 | 1,700 | 650 | 650 | | | 1.13 | 1.00 | |
| 79156 | 14,200 | 16,300 | 5,800 | 7,900 | | | 1.15 | 1.36 | |
| 79167 | 14,300 | 13,800 | 11,400 | 12,000 | | | .96 | 1.05 | |
| 79170 | 15,500 | 17,000 | 9,000 | 8,800 | | | 1.10 | .98 | |
| 256358 | 11,200 | 9,700 | 570 | 490 | | | .87 | .86 | |
| 256360 | 330 | 290 | 830 | 830 | | | .88 | 1.00 | |
| 256361 | 36,800 | 36,000 | 10,900 | 10,300 | | 300 | .98 | .94 | |
| 256362 | 330 | 320 | 320 | 380 | | 25 | .97 | 1.18 | |
| 256364 | 1,000 | 950 | 2,500 | 2,700 | | | .95 | 1.09 | |
| 256365 | 1,100 | 1,200 | 960 | 960 | | | 1.09 | 1.00 | |
| 256366 | 1,100 | 1,040 | 1,500 | 1,180 | | | .95 | .79 | |
| 256367 | 2,300 | 3,300 | 4,500 | 5,500 | | | 1.43 | 1.22 | |
| 256369 | 490 | 530 | 370 | 350 | | 1.7 | 1.08 | .95 | |
| 256372 | 6,800 | 9,700 | 8,500 | 8,600 | | | 1.42 | 1.01 | |
| 256373 | 2,100 | 2,000 | 1,700 | 1,500 | | | .95 | .88 | |
| SB-364 | 188 | 190 | | 220 | 12.4 | 21 | 1.01 | | 1.69 |
| G-2 | 1.86 | | | 5.6 | 24.3 | 25.9 | | | 1.07 |
| 3633 | [2] 22.9 | 37 | | 33 | [2] 83.0 | 89 | 1.57 | | 1.08 |
| **128-channel system** | | | | | | | | | |
| G-1 | 3.7 | | | 12 | 52 | 61 | | | 1.17 |
| S5B | 5.76 | 6.6 | | 4.3 | 17.2 | 17.4 | 1.15 | | 1.01 |
| S5C | 6.34 | 5.8 | | 4.3 | 15.7 | 15.5 | .91 | | .99 |
| K-1 | 3.24 | 3.1 | | 1.6 | 8.6 | 7.8 | .96 | | .91 |
| 234601 | 6,100 | 5,800 | 2,400 | 2,500 | | | .95 | 1.04 | |
| 256365 | 1,100 | 1,050 | 960 | 1,020 | | | .96 | 1.06 | |
| 256366 | 1,100 | 1,070 | 1,500 | 1,440 | | | .97 | .96 | |
| 256464 | 580 | 590 | 310 | 330 | | | 1.02 | 1.06 | |
| 256465 | 650 | 700 | 340 | 380 | | | 1.08 | 1.12 | |
| 256466 | 800 | 910 | 500 | 410 | | | 1.14 | .82 | |
| 256467 | 1,400 | 1,750 | 2,000 | 2,100 | | | 1.25 | 1.05 | |
| 256468 | 4,800 | 4,600 | 2,800 | 2,600 | | | .96 | .93 | |

[1] 5- and 6-digit numbers are USGS laboratory numbers; others are field numbers.
[2] 3-run average.

## RESULTS

The calibration plots show that for thorium and radium the relation between counting rate (peak amplitude) and the quantities of those radioelements is a straight line with a slope of unity. This relation permits the periodic use of a few standards at intervals along the calibration line to determine changes in instrument response and to adjust the analyses accordingly. The uranium calibration also shows a linear relation between counting rate and radioelement content, but for some unknown reason, the slope is not unity. The interpretation method worked equally well with both spectrometer systems.

The accuracy of the method is indicated by the displacement of points from the calibration line and is

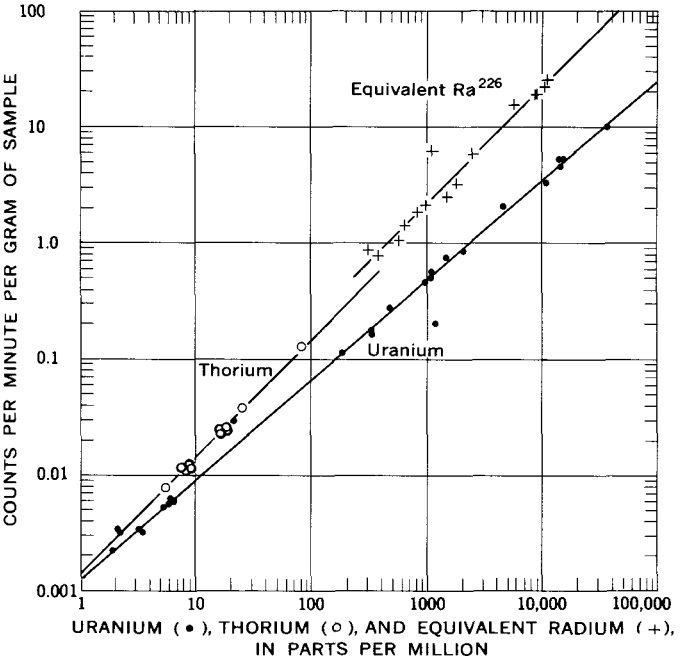


FIGURE 4.—Calibration plot relating radiation intensity to radioelement content. Data obtained with 200-channel system and 400-gram standards.

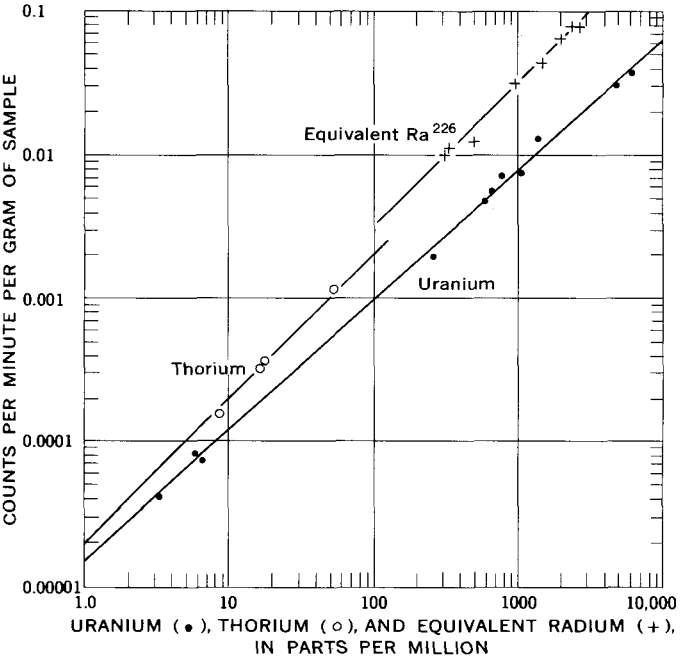


FIGURE 5.—Calibration plot relating radiation intensity to radioelement content. Data obtained with 128-channel system and 400-gram standards.

calculated by the ratios of the 200-channel spectrometer data and chemical analyses. The spectrometer technique, however, is not infallible. The error at one standard deviation was 5, 12, and 12.5 percent for thorium, uranium, and equivalent radium, respectively. Whether large errors are caused by erroneous chemical or spectrometer analyses could not be determined, but other interpretation methods are being investigated in an attempt to reduce the error.

The lower limit of detection is related directly to the interdependent factors of radiation intensity in each energy and data-accumulation time. The data-accumulation time was limited arbitrarily to 1,000 minutes (an overnight count) because an additional expenditure of time did not seem economical, considering that other analytical techniques for determining low concentrations of the radioelements may be more rapid and economical. Sufficient peak amplitude is required to identify the energy and to measure the counting rate regardless of whether the amplitude results from high intensity or from a long accumulation time. Another limiting factor is the large ratios between radioisotopes. A large thorium-uranium ratio affects both the uranium and radium interpretations. Most of the rocks and soils analyzed in this laboratory have thorium-uranium ratios of 4 or 5 to 1 and most of those samples caused no interpretation problems when interpretable amplitudes were present. One sample (G–2) with a ratio of 14:1 could not be analyzed for uranium content because the uranium energy peak was obscured by the adjacent $Pb^{212}$ (thorium) peak. Similarly, when the equivalent radium-thorium ratio exceeds 15:1, erroneous interpretations of thorium are made. Excluding the one example of an anomalously high thorium-uranium ratio, the detection limits of the radioelements in samples containing uranium, radium, and their daughters, and thorium are: uranium, 1.5 ppm; equivalent radium, 1 ppm; and thorium, 1 ppm. Although no samples containing radioelements at or below these limits were available for analysis, the energy peaks from available samples were used to estimate the minimum interpretable amplitude and the detection limits were determined on this basis. The detection limit would be lower if only one radioelement were present.

Repetitive 400-minute measurements during a 3-day period were made on a sample containing uranium, radium, and thorium to determine the repeatability of the detection system and the interpretation method. The peak amplitudes accumulated in 400 minutes are sufficient to reduce the standard deviation of the amplitudes to less than 1 percent in all peaks; therefore, all other differences are caused by the detection system or by interpretation. The results (table 3) show that the interpretation of the uranium content is the least repeatable; and because the error is much greater for the uranium than for the other radioisotopes the error difference could probably be attributed to interpretation rather than to the detection system.

TABLE 3.—*Ten repeated measurements of the counting rate on a 400-g sample, 400-minute accumulation time per analysis*

| Radioisotope<br>Gamma-ray energy (Mev) | $U^{235}$<br>0. 187 | $Pb^{212}$<br>0. 238 | $Pb^{214}$<br>0. 352 |
|---|---|---|---|
| | Counts per minute | | |
| 1 | 10. 8 | 52. 0 | 27. 8 |
| 2 | 11. 7 | 53. 1 | 28. 4 |
| 3 | 12. 0 | 53. 0 | 28. 3 |
| 4 | 11. 5 | 52. 5 | 27. 8 |
| 5 | 11. 6 | 52. 3 | 27. 8 |
| 6 | 12. 0 | 53. 3 | 28. 3 |
| 7 | 10. 3 | 51. 3 | 28. 0 |
| 8 | 12. 2 | 52. 5 | 28. 8 |
| 9 | 12. 0 | 53. 3 | 28. 2 |
| 10 | 12. 3 | 52. 8 | 27. 9 |
| Average | 11. 6 | 52. 6 | 28. 1 |
| Deviation: | | | |
| Counts | −1. 3, +0. 7 | −1. 3, +0. 7 | −0. 3, +0. 7 |
| Percent | −11. 2, +6. 0 | −2. 5, +1. 3 | −1. 1, +3. 9 |
| Mean | 11. 3 | 52. 3 | 28. 3 |
| Deviation: | | | |
| Counts | ±1. 0 | ±1. 0 | ±0. 5 |
| Percent | ±8. 8 | ±1. 9 | ±1. 8 |

Sensitivity, the ability to measure small changes in radioelement content, was estimated from the calibration plots. Although more analyses would be required than are presently available to definitely establish the value of the sensitivity, it appears to be about 10 percent of any determined value for all the radioelements.

## REFERENCES


Adams, J. A. S., Richardson, J. E., and Templeton, C. C., 1958, Determinations of thorium and uranium in sedimentary rocks by two independent methods: Geochim. et Cosmochim. Acta, v. 13, p. 270–279.

Hurley, P. M., 1956, Direct radiometric measurement by gamma-ray scintillation spectrometer, Part I and II: Geol. Soc. America Bull., v. 67, p. 395–412.

Hofstader, Robert, and McIntyre, J. A., 1950, Gamma-ray spectrometry with crystals of NaI(T1): Nucleonics, v. 7, no. 3, p. 32–37.

Kahn, B., and Lyon, W. S., 1953, Scintillation spectrometer in radiochenical analysis: Nucleonics, v. 11, no. 11, p. 61–63.

Mero, J. L., 1960, Uses of the gamma-ray spectrometer in mineral exploration: Geophysics, v. 25, no. 5, p. 1054–1076.

Moxham, R. M., Foote, R. S., and Bunker, C. M., 1965, Gamma-ray spectrometer studies of hydrothermally altered rock: Econ. Geol., v. 60, no. 4, p. 653–671.

Rosholt, J. N., 1959, Natural radioactive disequilibrium of the uranium series: U.S. Geol. Survey Bull. 1084–A, p. 1–30.

# PORTABLE CORE DRILL AND THIN-SECTION LABORATORY FOR FIELD USE

By G. BRENT DALRYMPLE and RICHARD R. DOELL, Menlo Park, Calif.

*Abstract.*—This report describes a portable thin-section laboratory with which 2 men can make 8 to 10 thin sections per hour in the field. Tests of the equipment show that it increases the efficiency of sampling for combined paleomagnetic and potassium-argon studies because the suitability of a sample for dating can be determined before any effort has been expended on collecting oriented samples for paleomagnetic study.

The efficiency of collecting samples for combined paleomagnetic and radiometric studies of geomagnetic polarity reversals and geomagnetic secular variation has been greatly improved by the development of a thin-section "laboratory" that is easily portable. With this equipment, thin sections of moderate quality can be prepared in the field at the rate of 8 to 10 per hour by two persons. We have used this equipment to determine the suitability of lava flows (mostly basalts and andesites) for whole-rock potassium-argon analysis. However, such a portable thin-section laboratory could be used in a wide variety of ways by other workers in the earth sciences.

The paleomagnetic studies mentioned above generally require the collection of 5 to 8 carefully oriented samples from each lava flow that is to be investigated. Even with efficient coring and orienting techniques (Doell and Cox, 1965, p. 22) this takes considerable time. The value of a collection of samples from any given lava flow is greatly enhanced if the flow can be dated by the potassium-argon technique. Thus, by knowing in advance which lava flows are suitable for dating (roughly a function of the degree of apparent alteration and absence of groundmass glass), the available field time can be more efficiently used. As an example, in 1961, paleomagnetic collections from more than 200 lava flows were made on the islands of Kauai and Hawaii. Subsequent examination of thin sections of these samples revealed that about 10 percent of the lava flows sampled are suitable for potassium-argon dating. In 1965, using the portable thin-section lab, more than 100 samples from 2 thick sequences of lava flows on the island of Oahu, in Hawaii, were collected, and thin sections were prepared and analyzed, all in a period of 2 days. On the basis of these preliminary examinations, paleomagnetic collections were made from more than 50 of the lava flows examined in these 2 sequences. Well over half of these 50 flows are suitable for potassium-argon age analysis, and most of the others are closely related stratigraphically to datable flows. The overall value to the paleomagnetic studies of this collection of samples from 50 lava flows should be roughly equal to, or even greater than, that of the earlier collection from 200 lava flows.

*Acknowledgments.*—We wish to thank Messrs. Major Lillard and Bernard Pflaum for construction and modification of the equipment described here.

## COLLECTION OF SAMPLES

Although rock chips removed with a geologist's hammer are suitable for making thin sections with the field equipment described here, we find that it is very desirable to obtain the samples with a small portable coring drill. There are two principal reasons for this: (1) the core drill makes is possible to sample any desired near-surface portion of an outcrop, and (2) fewer cutting operations are required in the preparation of the thin sections than if chips are used.

The coring drill is shown in figure 1. A small ¾-horsepower gasoline motor is fitted, through a gear-reduction transmission, to a commercial masonry core bit that has a 1-inch inside diameter and is diamond impregnated. The transmission and water-coolant feed-through assembly were designed and constructed by the Geological Survey for this purpose. Details of this assembly are shown in figure 2. The fuel tank is pressurized by a small pump in one of the handles to permit drilling in any position. Coolant water, which passes through a metering valve in the other handle, is obtained through a short piece of plastic

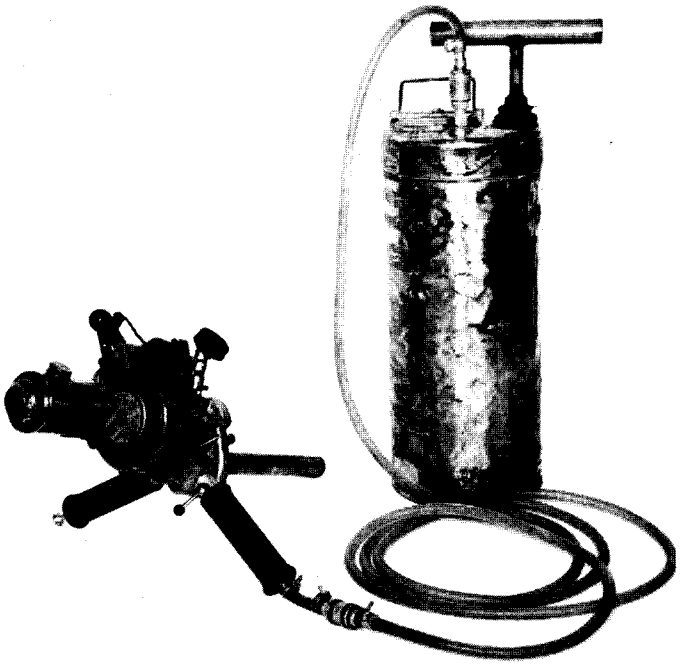

FIGURE 1.—Portable coring drill and pressurized water tank. During use the water tank is carried in a backpack.

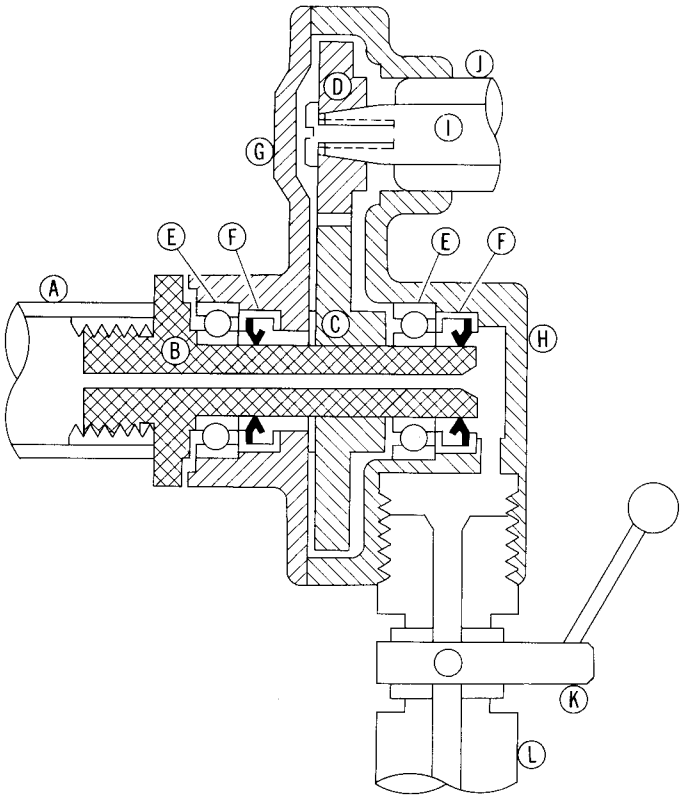


FIGURE 2.—Details of the special gear-reduction transmission unit. *A*, core drill; *B*, drill shaft; *C*, shaft gear; *D*, motor-drive gear; *E*, shaft bearings; *F*, shaft seals; *G*, transmission-case cover; *H*, transmission case; *I*, motor shaft; *J*, motor case; *K*, water-metering valve; *L*, right handle.

hose connected to a pressurized garden-type insecticide-spray tank. When in use, the tank is carried in a backpack. One tank of coolant water (2½ gallons) is sufficient for drilling about 50 cores from 1 to 1½ inches long. The cores are readily removed from the outcrop by wedging a screwdriver in the drill cut.

## PREPARATION OF THIN SECTIONS

Components of the portable thin-section "laboratory" are shown in figure 3. The gasoline-powered saw is a commercial product that employs an 8-inch diamond blade and uses the same type of motor as the drill described above.

Details of the specimen holder are shown in figure 4. The holder is fitted to the saw by means of clamps supplied by the manufacturer, and its orientation and position are adjusted by the use of shims and lateral positioning in the clamps. The operation of the equipment shown in figure 3 is described below, and a list of all equipment needed for making thin sections in the field is given in the summary at the end of this article.

First, the core is clamped in the opening through the left-hand side of the holder (fig. 4), and the uneven end of the core is cut off (fig. 5*A*). Rock chips, suitably trimmed to fit in the holder clamp, may also be used. The core or chip must be firmly clamped so that a smooth cut is obtained. The saw marks are quickly removed by hand polishing on a glass plate, using 400-grit silicon carbide lapping compound. The sample is then washed and placed on an aluminum hotplate, over a small single-burner camp stove, to be dried and heated. A glass slide is also heated on the hotplate, Lakeside 70C cement applied, and the sample cemented to the slide in the usual manner.

After the cement has been hardened by placing the slide on an aluminum cooling plate (to speed the cooling), the slide is fitted in the frame on the right-hand side of the sample holder (fig. 4), and the excess rock of the core is trimmed off. The surface tension of the coolant water holds the glass slide in the frame. Blowing through the small hole in the sample holder, behind the slide in the frame (fig. 3), helps to release the glass slide from the frame, but because this hole is not essential, it is not shown in figure 4. The holder should be positioned so that a slice of uniform thickness (about $\frac{1}{64}$ inch) is obtained. The sample is then repeatedly passed through the saw while slight pressure is applied on the saw blade as shown in figure 5*B*. This is continued until the rock slice begins to "fray" on the edges and becomes translucent; this is easily seen through the clear plastic of the sample holder. With a little experience and care a moderately uniform section near the required thickness can be quickly obtained. The final

FIGURE 3.—Equipment making up the portable thin-section laboratory. From left to right: microscope, slides, flashlight, refracting oil, Lakeside cement, glass plate, stove, cooling plate, forceps, lapping compound, squeeze bottle, and saw.

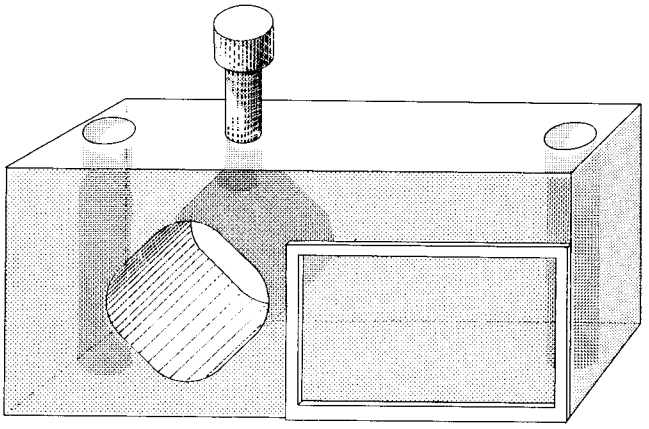

FIGURE 4.—Clear-plastic sample holder. Core is clamped in opening through left-hand side of holder for first cut. Glass slide with attached core fits in frame on right for trimming off of excess rock.

grinding is done by hand on the glass plate; a polarizing microscope is used for thickness control. Ordinarily, water is used as the cooling and lubricating medium in both the cutting and grinding operations, but for friable materials the use of kerosene will minimize "plucking" and produce more satisfactory results. If desired, a cover glass can be cemented to the rock slice with canada balsam. However, we prefer to use a drop of refracting oil instead because of the saving in time. It should be noted that some oils, for example, clove oil, will attack the Lakeside cement and ruin the slide if left on for more than a few minutes.

## THIN-SECTION ANALYSIS

The particular needs for thin-section analysis in the field will determine the type of microscope required. Our needs are adequately filled by a very inexpensive lightweight student microscope. We attached one piece of Polaroid sheet in a small metal holder (to function as an analyzer) to the zoom-type objective of the microscope, and fitted another piece of Polaroid sheet (the

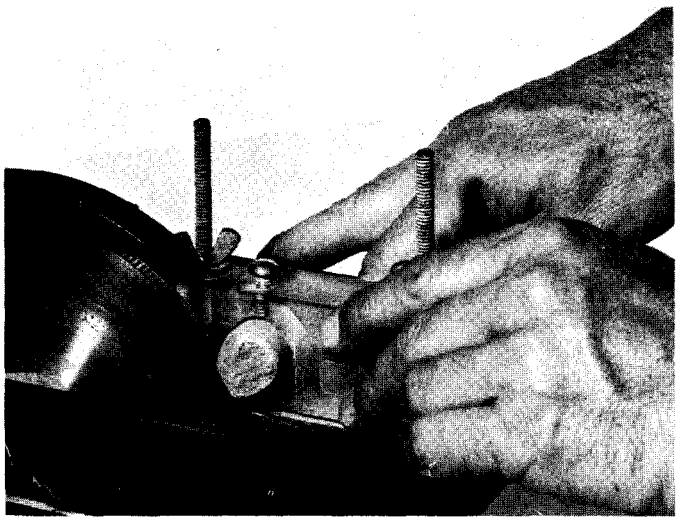

*A*

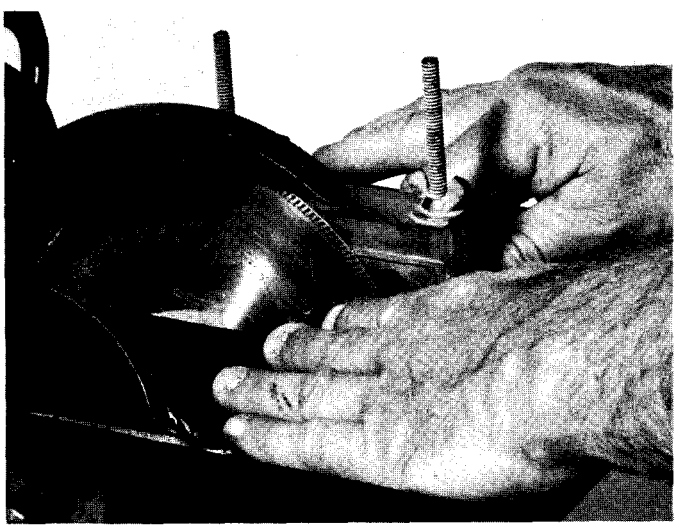

*B*

FIGURE 5.—Cutting operations: *A*, cutting off uneven end of core before grinding and cementing core to glass slide; *B*, preparing a very thin rock slice.

polarizer) in a small slide beneath the microscope stage in such a manner that the Polaroid sheet may easily be inserted and removed from the optical path. Light is provided by a 6-volt flashlight equipped with a plastic diffuser.


## SUMMARY

A list of the required equipment, subdivided into that needed for sample collection, thin-section preparation, and thin-section analysis, is as follows:

### Sample collection

Portable core drill fitted with a diamond core bit (1-inch ID).
2½-gallon pressurized water tank.
4-foot length of ¼-inch ID heavy-wall plastic tubing with fittings for attachment to drill and tank.
Screwdriver, Hammer } for core removal.

### Thin-section preparation

Portable diamond saw.
Glass plate, 6 in. × 6 in. × ¼ in.
Single-burner camp stove fitted with a ½-inch-thick aluminum hotplate.
Aluminum cooling plate, ½ inch thick.
Plastic squeeze bottle, ½-liter capacity.
Pair of small forceps for handling hot samples and slides.
Diamond scribe for marking slides.
Lakeside cement.
Glass slides.
Lapping compound.

### Thin-section analysis

Microscope.
Flashlight equipped with diffuser.
Refracting oil.

With a full tank of water and sufficient fuel for about 50 sample cores, the complete sampling equipment weighs 50 pounds. The equipment for the preparation of thin sections, ready for use, weighs about 25 pounds; and the microscope, flashlight, and oil that we use for thin-section analysis weigh a total of 6 pounds. Thus, the entire unit is easily backpacked by two persons. Our experience has shown that 2 persons can prepare 8 to 10 thin sections of moderate quality each hour with the use of this equipment.


## REFERENCE

Doell, R. R., and Cox, Allan, 1965, Measurement of the remanent magnetization of igneous rocks: U.S. Geol. Survey Bull. 1203–A, p. A1–A23.

# DETERMINATION OF CARBON DIOXIDE IN LIMESTONE AND DOLOMITE BY ACID-BASE TITRATION

By F. S. GRIMALDI, LEONARD SHAPIRO, and MARIAN SCHNEPFE, Washington, D.C.

*Abstract.*—Acid-base titration methods based on the dissolution of a sample in an excess of standard acid, followed by back titration with a standard base, have been developed for the rapid determination of carbon dioxide in limestone and dolomite. Difficulties arising from the solubility of some silicates are minimized by conducting the acid decomposition under mild conditions. In one procedure this is realized by overnight digestion of the sample with acid at room temperature; in another procedure the sample is boiled for a short time with a predetermined, limited amount of excess acid.

Many methods have been described for determining carbon dioxide in limestone and dolomite. Those depending on gas evolution followed by either a volumetric or a gravimetric finish have long been known (Fresenius and Cohn, 1904). These early methods, which with minor modifications are still the standard methods of today, yield very satisfactory results. However, two disadvantages affect these methods. The gas-evolution methods require that special apparatus be set up; this is a deterrent where only a few samples are to be analyzed occasionally. Furthermore, only one sample can be analyzed at a time, severely limiting the number of samples that can be analyzed per day on a routine basis.

The most obvious approach to the elimination of these disadvantages is the use of a simple acid-base titration method in which the sample is dissolved in a known excess of standard acid and then back-titrated with standard alkali. Undoubtedly this approach has been tried by many and found wanting. Certain mineral phases such as silicates of calcium and magnesium lead to erroneous results because of their partial solubility in acid and their failure to be reconstituted in a back titration. Thus, for the analytical procedure to succeed, conditions in the initial attack of the sample with acid should be mild enough to minimize attack of such silicates, yet powerful enough to decompose the carbonates. This paper presents several procedures that accomplish this end.

## METHODS

In one of the proposed methods, attack of the silicate phase is minimized by decomposing the carbonate overnight at room temperature with 0.5$N$ acid. This method is especially advantageous where a large number of samples is to be analyzed routinely. In another proposed procedure, the sample is boiled for a short time with an excess of 0.2$N$ acid. Two titrations are made. An initial titration provides the information on acid consumption necessary to allow a second sample to be decomposed with a very limited amount of excess acid, thus minimizing the solution of the silicates.

More often than not the two titrations yield the same result, especially for unmetamorphosed rocks. Obviously, in these instances one titration suffices and offers a time advantage where rapid results are needed. The applicability of the single-titration method can be determined easily on a few randomly selected samples from a given large lot. The dual-titration procedure is generally more dependable and is to be preferred where relatively few samples are to be analyzed. Either approach should prove satisfactory as a field method.

## PROCEDURES

### Reagents

Standard hydrochloric acid solution, 0.5$N$, for procedure A.
Standard hydrochloric acid solution, 0.2$N$, for procedure B.
Standard sodium hydroxide solution, 0.35$N$, for procedure A.
Standard sodium hydroxide solution, 0.2$N$, for procedure B.
Bromphenol blue indicator: prepare a 0.1 percent w/v aqueous solution from water-soluble bromphenol blue.
The hydrochloric acid solutions were standardized against pure sodium carbonate using bromphenol blue as indicator. The sodium hydroxide solutions were standardized against the acids, again using bromphenol blue as indicator.

### Procedure A. Decomposition at room temperature

To a 250-ml beaker containing 0.5 g of sample ground to pass 100 mesh, add 25 ml of 0.5$N$ HCl by pipet. Swirl the beaker

U.S. GEOL. SURVEY PROF. PAPER 550-B, PAGES B186-B188

to ensure thorough wetting of the sample. Cover the beaker and allow the mixture to stand overnight at room temperature. On the following day add 8 to 10 drops of bromphenol blue indicator and back-titrate the excess acid with 0.35*N* NaOH to the blue end point.

### Procedure B. Double titration, limited acid

To a 250-ml beaker containing 0.5 g of sample ground to pass 100 mesh, add 25 ml of water and 50 ml of 0.2*N* HCl with a buret. Bring the mixture to a boil, continue to the complete evolution of $CO_2$, and then boil an additional 2 minutes. Add 8 to 10 drops of bromphenol blue indicator and titrate with 0.2*N* NaOH to the blue end point. On the basis of the volume of NaOH used in this titration, a volume of 0.2*N* HCl calculated to lead to a back titration of 1 to 7 ml is added to a second 0.5-g portion of sample. The solution is boiled and back-titrated as before. The $CO_2$ content is calculated from this second titration.

Sample solutions containing considerable dark insoluble material which might obscure the visibility of the end point should be filtered before titrating with base. With samples containing appreciable amounts of ferrous iron, the detection of the end point is also improved by the addition of several grams of ammonium chloride to the solution before titration with base.

## RESULTS AND DISCUSSION

### Interference

Consideration of what problems might arise is tantamount to answering the question "what reaction can consume acid that is not reversed in titrating to a pH of 4, the bromphenol blue end point?" The common cations aluminum and ferric iron, which might dissolve to some extent and consume acid, will also consume an equivalent amount of alkali in the back titration and so should give no serious difficulties. This is true regardless of whether these cations were derived initially from oxides or from clays. Soluble alkali, alkaline earth, and magnesium silicates would interfere, inasmuch as a very high pH would be required to titrate silicic acid. Here, thymolphthalein (pH 10.5) would perhaps be a better indicator were it not for errors that would arise from the resulting partial titration of magnesium originally present as carbonate. The situation is not improved with phenolphthalein as an indicator. Phosphate should be expected to cause difficulty inasmuch as only a third of the phosphate will be back-titrated at pH 4.

Carbonates containing cations not precipitable at pH 4 (siderite, smithsonite, cerussite, strontianite, and others) should be readily handled by the procedures.

### Test of procedures

A series of limestones and dolomites from various localities was analyzed by both procedures. The samples varied in composition as follows: $SiO_2$ varied from a few percent to over 60 percent, $Al_2O_3$ from a few percent to over 13 percent, FeO from less than 1 percent to over 30 percent, $CO_2$ from several percent to 47 percent; the maximum CaO was 56 percent, and the maximum MgO 22 percent. A comparison of results obtained with procedures A and B and conventional methods is given in table 1. Table 2 presents data obtained with procedure B on a variety of carbonate rocks and on some other rocks containing silicate minerals, with different amounts of excess acid. The results obtained by conventional methods are also shown. The results shown for procedure A in table 1 are sufficiently accurate for most routine applications of the method.

TABLE 1.—*Content of carbon dioxide, in percent, in limestone and dolomite, as determined by three procedures*

| Sample | Procedure A | Procedure B | Conventional methods |
|---|---|---|---|
| NBS No. 88 | 47.2 | 47.2 | 47.3 |
| NBS No. 1a | 34.1 | 33.9 | 33.5 |
| 154517 | 28.5 | 28.0 | 27.9 |
| 31 | 45.7 | 45.4 | 45.4 |
| 21 | 25.9 | 25.5 | 25.4 |
| 23 | 37.1 | 36.8 | 36.6 |
| 30 | 34.3 | 34.0 | 34.0 |
| 2399 | 38.4 | 38.7 | 38.7 |
| 2400 | 39.0 | 39.2 | 39.3 |
| 2431 | 22.0 | 20.7 | 20.6 |
| 2432 | 25.1 | 25.1 | 25.2 |
| 1522 | 44.5 | 44.1 | 44.4 |
| 1524 | 42.5 | 42.5 | 42.3 |
| 1948 | 14.2 | 13.8 | 13.8 |
| 2028 [1] | 31.1 | 30.5 | 30.6 |

[1] Siderite sample.

TABLE 2.—*Content of carbon dioxide in a variety of rocks as determined by procedure B, and the effect of various amounts of excess acid.*

| Sample | Type | Locality | 0.2*N* HCl (ml) | 0.2*N* NaOH back titrated (ml) | $CO_2$ (percent) | |
|---|---|---|---|---|---|---|
| | | | | | Procedure B | Conventional methods |
| NBS No. 88. | Dolomite | | 61.14 | 7.35 | 47.3 | 47.25 |
| | | | 58.11 | 4.37 | [1] 47.3 | |
| | | | 56.82 | 3.14 | 47.3 | |
| | | | 52.99 | 1.36 | 47.2 | |
| NBS No. 1a. | Argillaceous limestone. | | 52.83 | 14.28 | 33.9 | 33.53 |
| | | | 41.31 | 2.77 | 33.9 | |
| | | | 41.20 | 2.65 | [2] 33.9 | |
| | | | 39.83 | 1.38 | 33.9 | |
| | | | 39.62 | 1.13 | 33.9 | |
| 154517 | Limestone | Iron Mountain, Utah. | 51.65 | 17.62 | 30.0 | 27.91 |
| | | | 48.55 | 14.65 | 29.9 | |
| | | | 45.45 | 12.47 | 29.1 | |
| | | | 42.35 | 10.00 | 28.5 | |
| | | | 39.25 | 7.28 | 28.0 | |
| | | | 36.16 | 4.41 | 28.0 | |
| | | | 34.14 | 2.25 | [1] 28.1 | |
| | | | 33.33 | 1.65 | 27.9 | |
| 31 | Dolomitic limestone. | Arizona | 103.45 | 51.52 | 45.7 | 45.4 |
| | | | 61.98 | 10.05 | 45.6 | |
| | | | 56.82 | 4.95 | 45.7 | |
| 21 | Limestone | Wyoming | 103.45 | 74.43 | 25.5 | 25.4 |
| | | | 51.65 | 22.77 | 25.4 | |
| | | | 30.99 | 2.20 | 25.3 | |
| 23 | Limestone | Utah | 51.65 | 9.80 | 36.8 | 36.6 |
| | | | 44.42 | 2.57 | 36.8 | |
| 30 | Limestone | New Mexico | 51.65 | 13.02 | 34.0 | 34.0 |
| | | | 41.32 | 2.78 | 33.9 | |

See footnotes at end of table.

TABLE 2.—*Content of carbon dioxide in a variety of rocks as determined by procedure B, and the effect of various amounts of excess acid*—Continued

| Sample | Type | Locality | 0.2*N* HCl (ml) | 0.2*N* NaOH back titrated (ml) | $CO_2$ (percent) | |
|---|---|---|---|---|---|---|
| | | | | | Procedure B | Conventional methods |
| 2399 | Dolomite and altered glass tuff. | Green River Formation, Wyoming. | 51.65 | 7.75 | [2] 38.7 | 38.7 |
| | | | 46.48 | 2.62 | 38.7 | |
| | | | 45.43 | 1.62 | [2] 38.6 | |
| 2400 | Dolomite and altered glass tuff. | Green River Formation, Wyoming. | 50.95 | 6.33 | 39.3 | 39.3 |
| | | | 46.65 | 2.03 | 39.3 | |
| 2431 | Biotitic limestone. | Bethany, Conn. | 52.83 | 26.41 | 23.1 | 20.6 |
| | | | 30.48 | 6.62 | 21.0 | |
| | | | 28.00 | 4.44 | 20.7 | |
| | | | 26.41 | 2.98 | 20.6 | |
| | | | 26.00 | 2.43 | 20.7 | |
| 2432 | Impure marble | Prospect, Conn. | 52.83 | 24.45 | 25.0 | 25.2 |
| | | | 51.65 | 23.20 | 25.0 | |
| | | | 36.16 | 7.92 | 24.9 | |
| 1522 | Dolomite | Willis quadrangle, Montana. | 52.83 | 2.67 | 44.1 | 44.43 |
| 1524 | Limestone | do | 52.83 | 4.54 | 42.5 | 42.27 |
| 1658 | Porphyry | West of Long Lake, Wash. | 4.23 | 2.83 | 1.2 | .95 |
| 1660 | Welded tuff | Washington | 52.83 | 49.90 | 2.5 | 1.63 |
| | | | 5.28 | 3.33 | 1.7 | |
| 1852 | Tuff(?) | Nevada | 52.83 | 49.78 | 2.7 | 2.51 |
| | | | 5.28 | 4.21 | 2.3 | |
| 1948 | Limestone | | 50.94 | 34.40 | 14.4 | 13.8 |
| | | | 21.13 | 5.60 | 13.7 | |
| | | | 22.08 | 6.06 | [1] 14.1 | |
| | | | 18.96 | 3.19 | [1] 13.9 | |
| 2028 | Siderite | | 51.73 | 15.91 | [2] 31.5 | 30.6 |
| | | | 41.14 | 9.28 | [2] 28.0 | |
| | | | 41.10 | 8.24 | [2 3] 28.9 | |
| | | | 41.10 | 6.75 | [1 2] 30.2 | |
| | | | 41.18 | 6.55 | [1 2] 30.5 | |
| 2266 | Metagabbro | Idaho | 9.25 | 4.82 | 3.9 | 3.82 |
| 159686 | Mudstone | Nevada | 52.83 | 42.49 | 9.1 | 8.43 |
| | | | 12.68 | 3.12 | 8.4 | |
| | | | 11.00 | 1.60 | 8.3 | |

[1] 10-min. boiling with acid.
[2] $NH_4Cl$ added before back titration with NaOH.
[3] 5-min. boiling with acid.

The following comments refer only to procedure B:

1. A boiling time of 2 minutes was generally adequate except in the case of siderite (sample 2028), which required 10 minutes. In the presence of ferrous iron, the indicator seems to adsorb strongly on the precipitates formed in the back titration, obscuring the end point. This difficulty is prevented by the addition of $NH_4Cl$ prior to the back titration. Whether the addition of $NH_4Cl$ alters the surface properties of the precipitates or prevents attainment of a localized pH high enough to precipitate ferrous hydroxide is not known, but its use is effective in eliminating the difficulties. This addition was advantageous in samples 2028 and 2399. Ammonium chloride does not otherwise affect the results.

2. Results based on boiling times of 2 and 10 minutes are not significantly different (for example, NBS No. 88, 154517, 1948, table 2).

3. Many samples present no difficulty regardless of the amount of excess acid used (for example, NBS No. 1a, NBS No. 88, 21, 23, 30, 31, and 2399, table 2). In other cases the use of a limited amount of excess acid was sufficient to overcome difficulties arising from decomposable silicates (for example, see 2431 and 154517 especially). Results with sample 154517 show the trend as excess acid is diminished stepwise. It is also evident from the results of the slowly decomposable dolomite in sample NBS No. 88 that as little as 1 ml excess of acid is sufficient to decompose this carbonate.

## REFERENCE

Fresenius, C. R., and Cohn, A. I., 1904, Quantitative chemical analysis, v. 1: New York, John Wiley and Sons, 780 p.

# DETERMINATION OF SILVER IN MINERALIZED ROCKS BY ATOMIC-ABSORPTION SPECTROPHOTOMETRY

By CLAUDE HUFFMAN, JR., J. D. MENSIK, and L. F. RADER, Denver, Colo.

*Abstract.*—A rapid and precise atomic-absorption spectrophotometric method for the determination of silver in mineralized rocks is described. The procedure consists of digesting the sample with nitric acid, centrifuging the diluted solution, and atomizing it into an atomic-absorption spectrophotometer for measurement of silver at a wavelength of 3,284 A. Silver ranging in concentration from 1 ppm to about 9,000 ppm (or about 0.03 to 250 oz troy/ton) can be determined without preliminary separations even in the presence of high concentrations of diverse elements.

The history of the development, technology, and use of atomic-absorption spectrophotometry in analytical chemistry has been reviewed comprehensively by Gilbert (1962) and Scribner and Margoshes (1964). Specific applications to the determination of various elements by atomic-absorption spectrophotometry are also extensively covered in the reviews. However, little has been published dealing with rock and mineral analysis by this method and especially as it may bear upon the determination of silver.

This study describes the determination of silver by atomic-absorption spectrophotometry in mineralized rocks containing from 1 part per million to about 9,000 ppm of silver. The method is rapid and precise. No chemical separations, fusions, or concentrations of the sample are required. The silver is simply dissolved in concentrated nitric acid following the procedure outlined below. About 60 determinations can be completed per man day. The method has a detection limit of 1 ppm of silver (about 0.03 oz troy per ton) in the sample. Lower levels of concentration might be determined by concentrating the silver, by enhancement of atomic absorption in the flame by organic solvents (Lockyer and others, 1961), or by preheating the compressed air prior to passing it through the burner of the atomic-absorption flame (Strasheim and others, 1962). A practical need for levels of concentration ranging below 1 ppm in the samples must be demonstrated because of possible low-level contamination problems, increased time for the treatment of the samples, and increased cost of the determinations.

## SAMPLES ANALYZED

The following three suites of samples were analyzed for silver and the results compared with those obtained by other methods: (1) Mineralized rocks from five locations in the Idaho Springs district, Colorado, that had been analyzed previously in this laboratory by the fire-assay method for gold and silver. (2) Miscellaneous mineralized rocks and ores submitted for fire assaying over the past several years by workers on various projects. These samples were from Clear Creek, Gilpin, and Boulder Counties, Colo., and are considered representative of the different varieties of materials that may be expected to occur with silver in the Front Range, Colo. (3) Minerals of various composition made available by H. W. Lakin, of the U.S. Geological Survey. These samples are not pure mineral separates but contain gangue rock and other associated minerals. Taken together these samples contain more than 20 elements in relatively large amounts (5 to >10 percent) and in different combinations that may be expected in natural occurrences.

## APPARATUS AND REAGENTS

The atomic-absorption spectrophotometer used in this study is commercially available as Perkin-Elmer model 303. The standard operating conditions given in the instruction manual for operating the instrument are suitable: oxidizing flame of air-acetylene (clear, nonluminescent); gage pressures, air 8.5 and acetylene 9 pounds per square inch. The wavelength used for detection of silver is 3,284 angstroms. The hollow-cathode silver lamp is operated at 12 milliamps.

Standard stock silver solution (1 milliliter = 500 ppm of Ag). Dissolve 0.1000 gram of silver metal with 10 ml of nitric acid and dilute to 200 ml volume with water. Prepare the following dilutions of the

U.S. GEOL. SURVEY PROF. PAPER 550-B, PAGES B189-B191

stock solution to contain 0.0200, 0.1000, 0.5000, 1.0000, 2.5000, and 5.0000 ppm of silver in 5-percent nitric acid.

## PROCEDURE

Transfer 1 g of rock powder to a 100-ml beaker. Moisten the sample with 2 ml of water, then add 10 ml of concentrated nitric acid, covering the beaker with a watchglass. After any vigorous reaction subsides, place the covered beaker on a hotplate and boil the solution gently so that some refluxing occurs for about 15 minutes. Swirl the beaker occasionally to mix the solution and alleviate bumping. Cool, add 25 ml of water, and heat on a steam bath for about 30 minutes. Transfer the solution and any insoluble material to a 50-ml volumetric flask, cool, dilute to volume, and mix. Decant about half of the solution into a 50-ml centrifuge tube and centrifuge it for about 5 minutes. Measure the absorbance of the clear solution by atomizing portions into the flame. Determine the silver content of the sample by using a standard calibration curve prepared as indicated below.

Measure the absorbance of standards containing 0.0200, 0.1000, 0.5000 and 1.0000 ppm of silver using the × 10 expansion scale of the atomic-absorption spectrophotometer. Standard solutions containing 1.0000, 2.5000 and 5.0000 ppm of silver are read on the less sensitive scales of the instrument. The absorbance readings versus concentrations of the standard solutions are used to plot calibration curves for the silver determination.

## RESULTS AND DISCUSSION

Comparative studies were made on all samples, using two different acid decomposition procedures preparatory to atomic-absorption measurement of the silver content. These results were then compared with those obtained by fire assay for the mineralized rocks and ores and by a colorimetric field test for the mineral samples.

The separate acid-decomposition procedures studied were (1) reflux boiling of the samples with nitric acid and (2) complete decomposition with nitric, perchloric, and hydrofluoric acids. The acid decompositions of the samples were made on 1 g of material in each case, but the fire-assay fusions were made on either 0.5 assay ton (14.583 g) or on 1.0 assay ton (29.166 g) of sample. The fire-assay method differs from the method here described in that it is based on a fusion decomposition followed by a gravimetric weighing and requires much larger weights of sample.

Table 1 gives the silver results on 5 samples fire assayed 3 times and determined also by atomic absorption on 1 solution prepared by acid boil and 2 solutions prepared by complete acid decomposition. The precision, regardless of acid treatment, and the agreement between the separate methods are good. Sample size does not seem to be a critical factor, and complete decomposition of the samples is of no advantage on these samples for the range of silver present.

TABLE 1.—*Comparison of atomic-absorption and fire-assay methods for determination of silver in mineralized rock, Idaho Springs, Colo.*

[Assay results obtained by W. D. Goss, O. M. Parker, and L. B. Riley; calculated from ounces per ton to parts per million by the factor 34.29]

| Sample No. | Silver (ppm) | | | | | |
|---|---|---|---|---|---|---|
| | Fire assay | | | Atomic absorption | | |
| | Run 1 | Run 2 | Run 3 | Nitric acid boil | Complete solution with acids | |
| | | | | | Solution 1 | Solution 2 |
| D114572 | 2 | 1 | <1 | 2 | 4 | 4 |
| D114571 | 2 | 3 | 2 | 3 | 5 | 5 |
| D114570 | ------ | 29 | 27 | 27 | 31 | 29 |
| D114568 | 28 | 30 | 29 | 30 | 32 | 30 |
| D114569 | 175 | 152 | 180 | 170 | 165 | 140 |

Table 2 shows comparison data similar to those of table 1 but for a greater variety of mineralized rocks representing the Colorado Front Range. The reproducibility of the atomic-absorption method is indicated by separate determinations (4th and 6th columns) each on a different solution. Also included in this table are results obtained by the colorimetric field method as described by Nakagawa and Lakin (1965). Again the agreement between methods and treatments is satisfactory for most geologic problems. Emphasis is directed to the acid-boil results (6th column, table 2) because this treatment is the most rapid and economical without sacrificing either reproducibility or reliability.

Testing of the atomic-absorption method for interferences from other ions or elements in solution was done by analyzing a variety of mineral ore samples. These data are given in table 3. The mineral name given to the bulk samples is that of the most abundant constituent. The second column lists the principal elements that could be considered as potential sources of chemical interference because of their extremely large concentrations with respect to the silver content. Other elements suggested by the mineral name seem most unlikely to cause interference. No interference in the determination of silver in these samples was noted even though no separations or other special treatments were made prior to atomizing the solutions into the flame.

Tests were made to check the solubility of silver in the presence of chloride and of iodide by boiling with nitric

TABLE 2.—*Comparison of silver determined by atomic absorption and other methods on mineralized rocks and ores from Clear Creek, Gilpin, and Boulder Counties, Colo.*

| Sample No. | Silver (ppm) | | | | | |
|---|---|---|---|---|---|---|
| | Fire assay [1] | Atomic absorption | | | | Geochemical colorimetric field test [2] |
| | | Complete solution with acids | | | Nitric acid boil | |
| | | Solution 1 | Solution 2 | Average | | |
| D91397 | 3 | 2 | 2 | 2 | 2 | 2 |
| D223179 | 3 | 6 | 7 | 7 | 5 | 3 |
| D227045 | 4 | 9 | 9 | 9 | 10 | 8 |
| D223180 | 9 | 7 | 7 | 7 | 5 | 10 |
| D234557 | 6 | 12 | 13 | 13 | 11 | 10 |
| D224702 | 31 | 32 | 32 | 32 | 30 | 40 |
| D222893 | 24 | 31 | 31 | 31 | 29 | 40 |
| D216092 | 38 | 53 | 30 | 42 | 52 | 60 |
| D229657 | 40 | 50 | 50 | 50 | 48 | 50 |
| D223188 | 51 | 55 | 55 | 55 | 55 | 60 |
| D223181 | 110 | 121 | 121 | 121 | 120 | 150 |
| D222897 | 146 | 133 | 156 | 145 | 156 | 150 |
| D209488 | 182 | 170 | 152 | 161 | 167 | 150 |
| D216090 | 182 | 232 | 195 | 214 | 236 | 140 |
| D223184 | 228 | 238 | 235 | 237 | 226 | 300 |
| D230155 | 726 | 738 | 730 | 734 | 752 | 750 |

[1] Assayed by D. L. Skinner in 1953, uncorrected for slag and cuppell losses (Bugbee, 1948, p. 101).
[2] Analysis by H. M. Nakagawa and H. W. Lakin (1965); weighted mean of 3 runs.

acid because silver is associated with the halide group in some occurrences. These tests were made by adding 2, 50, 100, and 200 milligrams of sodium chloride and 1.05, 2.15, and 5.0 mg of potassium iodide to 1.0-g portions of sample D223181 previously found to contain 121 ppm of silver (table 2). The tests were then carried through the procedure as described above. Results of all these tests showed complete recovery of silver.

TABLE 3.—*Comparison of atomic-absorption determination of silver with the geochemical colorimetric method on impure minerals of diverse composition.*[1]

| Nominal mineral | Principal elements of potential analytical interference | Silver (ppm) | | |
|---|---|---|---|---|
| | | Atomic absorption | | Geochemical colorimetric field test [2] |
| | | Complete solution with acids | Nitric acid boil | |
| Cervantite | Sb | 1 | 1 | 0.5 |
| Psilomelane | Mn | 1 | 1 | .5 |
| Descloizite | Pb, Zn, V, Cu | 1 | 1 | .7 |
| Allanite | Rare-earth elements. | 5 | 3 | 2 |
| Pyrite | Fe | 7 | 6 | 4 |
| Pentlandite | Ni | 3 | 3 | 4 |
| Pyrrhotite | Fe, Cu, Ni | 5 | 4 | 3.5 |
| Hemimorphite | Zn, Si (sol.), Cd | 4 | 4 | 3.5 |
| Arsenical gold ore. | As | 5 | 5 | 7.5 |
| Glauconite | K, Fe, Si (sol.) | 10 | 8 | 10 |
| Molybdenite | Mo, Ti | 24 | 16 | 10 |
| Hydrozincite | Zn | 14 | 14 | 30 |
| Arsenopyrite | As, Fe | 16 | 16 | 30 |
| Thorite | Th, P, rare-earth elements. | 8 | 9 | >8 |
| Niccolite | Ni, As | 34 | 32 | 50 |
| Chalcopyrite | Cu, Fe, Bi | 158 | 155 | 150 |
| Cerussite | Pb | 180 | 175 | 100 |
| Native antimony. | Sb | [3] 5 | 170 | 200 |
| Galena | Pb | 600 | 600 | 600 |
| Scheelite | W, Pb | 315 | 430 | 400 |
| Anglesite | Pb | 1,090 | 970 | 500 |
| Smaltite | As, Co | 1,550 | 1,530 | >1,600 |
| Tetrahedrite | Sb, Cu, Mn, Fe | 8,200 | 8,000 | 4,000 |

[1] Fire assay of these mineral samples could not be made because of insufficient material.
[2] Analyzed by Nakagawa and Lakin (1965).
[3] The silver reacted with other ions under this treatment and could not be recovered in this test.

## REFERENCES


Bugbee, E. E., 1948, A textbook of fire assaying, 3d ed.: New York, John Wiley and Sons, Inc. 314 p.

Gilbert, P. T., Jr., 1962, Absorption flame photometry: Anal. Chemistry, v. 34, no. 5, anal. reviews, p. 210R–220R.

Lockyer, R., Scott, J. E., and Slade, Susan, 1961, Enhancement of atomic absorption in the flame by organic solvents: Nature, v. 189, p. 830–831.

Nakagawa, H. M., and Lakin, H. W., 1965, A field method for the determination of silver in soils and rocks, *in* Geological Survey Research 1965: U.S. Geol. Survey Prof. Paper 525–C, p. C172–C175.

Scribner, B. F., and Margoshes, Marvin, 1964, Emission spectrometry: Anal. Chemistry, v. 36, no. 5, ann. reviews, p. 329R–343R.

Strasheim, A., Butler, L. R. P., and Maskew, E. C., 1962, The determination of certain impurities in gold by atomic absorption spectroscopy: Jour. South African Inst. Mining and Metallurgy, v. 62, pt. 2, p. 796–806.

# OBSERVED CONFIGURATION AND COMPUTED ROUGHNESS OF THE UNDERSIDE OF RIVER ICE, ST. CROIX RIVER, WISCONSIN

By KEVIN L. CAREY, Madison, Wis.

*Abstract*—Ripple- and dune-like features on the underside of the cover of river ice on the St. Croix River, Wis., change with time and closely resemble ripples and dunes found on alluvial streambeds. In 12 observations the wavelength and amplitude of the "ice-dunes" averaged about 0.65 foot and 0.07 foot, respectively. In all dune profiles the steeper slopes were on the downstream sides of the features. No suspended sediment or frazil (slush) ice was present in the flow. It is suggested that the features may owe their origin to fluid turbulence. The Manning roughness coefficient, calculated for the underside of the ice by a new method which uses the results of discharge measurements through the ice and supporting field data, is related to the observed characteristics of the underside of the ice.

Ripples and dunes were observed on the underside of the ice cover on the St. Croix River near Danbury, in northwestern Wisconsin, during a study of methods of computing discharge of ice-affected streams. Owing to the width of the stream in the area (200 to 240 feet) and the ice thickness (1 to 2 feet), the ice cover is sufficiently flexible to rise and fall with the common stage variations that occur throughout the winter. Bridging, or the presence of an air space between the underside of the ice and the flowing water, does not occur, and closed-conduit flow prevails during the period of ice cover. Because the relief on the bottom surface of the ice was formed while the ice was everywhere in contact with the water, rather than in contact with the atmosphere, the relief features are thought to be analogous in some way to those that occur on the beds of alluvial streams.

## METHODS OF STUDY

A straight reach of the river about half a mile long was used as the study area. A continuous water-stage recorder was located in a concrete house and well at the upstream end of the reach and a metal-pipe well was installed for reference at the downstream end. Fourteen discharge measurements were obtained at approximately 8-day intervals during the period of ice cover in the winter of 1964–65.

The procedure that was followed each day that hydraulic data were obtained involved (1) measuring the discharge at the upstream end of the reach, and (2) measuring the areas of two additional cross sections of the river, one at the middle of the reach and one at the downstream end. Areas of the middle and downstream cross sections were adjusted to compensate for any change in stage occurring between the time of the discharge measurement and the time of the measurement of the particular cross section. Mean gage heights applicable to the time of the discharge measurement were obtained at both ends of the reach. From these data the hydraulic parameters listed and discussed in a later section of this report were determined.

The underside of a block of the river ice was examined on each of the last 12 of the 14 days on which discharge measurements were made. This record of the condition of the underside of the ice was made to provide some explanation for changes in $n$ (Manning roughness coefficient) or $f$ (Darcy-Weisbach friction factor) with time.

For each observation, a block of ice measuring about 4 feet by 5 feet was cut out with a power-driven ice auger and an ice chisel. The freely floating block was turned upside down to expose the underside. The ice surface was sponged off to remove the loose water and the puddles from the low spots. A thin covering of flat black enamel spray paint was applied to darken the surface, so that it could be photographed with good contrast. To assure that variations with respect to time (rather than to location in the reach) were observed, the ice blocks were cut from midstream in the same general area. However, each block was cut sufficiently far from those previously examined to

insure a representative, undisturbed sample. Depth of the water under the ice in the observation area was about 3 feet. The average velocity of the flow under the ice in this area was about 2 feet per second. The bed is composed of coarse gravel (mean diameter about 1 inch) and very minor amounts of sand; gaging-station records indicate that it is quite stable.

## CONFIGURATION OF THE UNDERSIDE OF THE ICE

In 11 of the 12 observations of the underside of the ice blocks the form of the ice surface was rather similar; one block differed from all the rest. Configurations displayed on the underside of the 11 ice blocks (figs. 1–5, 7, 8) were closely analogous to the ripple and dune patterns found in the bed forms of an alluvial stream flowing over medium to fine sand. The configuration on 1 block (fig. 6) was not comparable with that of the other 11 blocks, and will be discussed later. For the 11 comparable ice blocks, the "ice dunes" were sharp crested, and both dunes and ripples were oriented roughly transversely to the flow. These features persisted laterally for lengths from as little as 0.5 foot to at least 4 feet and faded or merged into similar forms that were out of phase with their neighbors. Where the lateral persistence was poor the dune crests were commonly arcuate in plan (concave downstream). The wavelength, measured from crest to crest in a direction parallel to the flow, averaged 0.65 foot, but ranged from 0.5–0.6 foot on one block to 0.6–1.0 foot on another block. Amplitude, measured from trough to crest, averaged 0.07 foot, but ranged from 0.03–0.05 foot on one block to 0.06–0.14 foot on another block. All the dune profiles were not similar, and the greatest amplitudes did not occur on the blocks that had the greatest wavelengths. Though the upsteam slopes of the dunes averaged 8 to 1, one block had upstream dune slopes as gentle as 14 to 1 and another block had slopes as steep as 4 to 1. Similarly, the downstream dune slopes averaged 1.6 to 1, but one block had slopes as gentle as 2.9 to 1 and another block had slopes as steep as 0.8 to 1. Steep upstream dune slopes accompanied steep downstream dune slopes, and gentle upstream slopes accompanied gentle downstream slopes. Two observations noted "potholes" about 0.10 foot in diameter on the downstream slopes of the dunes. The axes of these cylindrical holes were vertical, and their bottoms were slightly deeper than the bottoms of the troughs.

During two of the observations, a second block of ice was cut about 30 feet from the riverbank and in the same cross section as the block from the midstream observation area. Dunes on each of these blocks cut near the bank had wavelengths that were 50 to 100 percent longer and amplitudes that were 40 to 70 percent greater than those on the midstream blocks. The depth below the ice in the area where these blocks were examined was about 1.3 feet; the average velocity in this part of the stream was about 1 foot per second. Thus depth and velocity were about half as large as the values found in midstream.

The configuration found in 1 of the observations (fig. 6) was not comparable with the 11 described above. The configuration on this particular block was quite irregular, and somewhat analogous to the bed forms that might be found in an alluvial stream flowing over a mixture of medium and coarse sand and fine gravel. Prominent features were three large, narrow, roughly wedge shaped dunes arranged in a line parallel to the flow. The crests of these dunes were about 2.2 feet apart. The remainder of the block was covered with a hummocky, irregular surface of dunes and ripples. Local relief, or amplitude, of this configuration was about 0.10 to 0.20 foot, with a total relief of about 0.25 foot.

The dissimilarity of this block is due to its composition. The top part of the ice sheet was made up of stratified nonhomogeneous ice containing a great number of small air bubbles, and the remainder was made up of clear ice having no entrained air. Presumably the bubbly ice formed when the floating pans of frazil (slush) ice coalesced, jammed, and became solidly frozen to form the initial ice cover of the winter. The bubbly ice also grew in thickness as the result of snowfalls. As the weight of a new snow cover depressed the ice, water overflowed through small openings in the ice near the banks. This water then saturated the bottom few inches of the snow cover, and the resulting slush layer eventually froze. Repeated instances of this process evidently caused the stratification observed in the bubbly ice. The clear-ice part of the ice cover is believed to be the result of progressive freezing of water at the bottom of the ice cover, with the heat having been removed by conduction upward through the ice cover. The configuration on the ice block last described was formed in nonhomogeneous ice (the clear layer being absent at this time), while the configuration on the underside of the other blocks was formed in clear ice.

Note that observation of this aberrant ice block was preceded and followed by observations of typical configurations formed in clear ice. It is therefore inferred that the clear-ice part of the cover can grow or diminish in thickness with time. This interpretation leads, in turn, to the belief that the configurations on the underside of the river ice are not solely erosional features, but are the result of both erosion and accretion, that is, melting and freezing. At the time of the observations, and presumably throughout the period of ice cover, the suspended load of the flow was virtually nil,

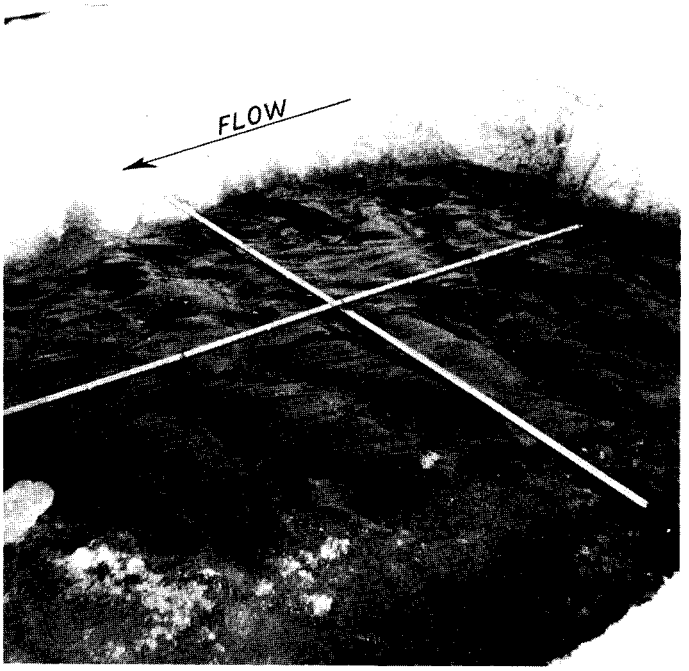


FIGURE 1.—Underside of ice block, January 5, 1965; wavelength 0.5 to 0.6 foot, amplitude 0.10 to 0.12 foot; $n_I = 0.0151$. Crossed rods, 4 feet long, give scale. Note the crenulations parallel to the flow direction.

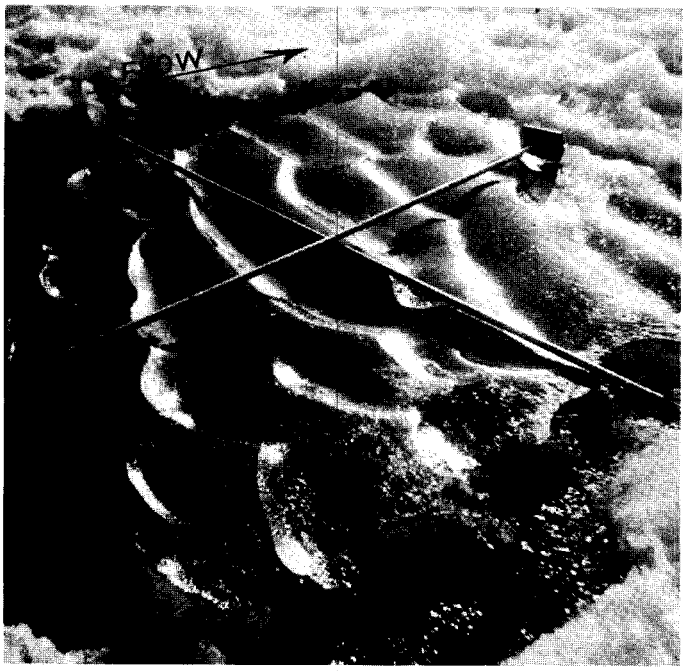

FIGURE 3.—Underside of ice block, January 26, 1965; wavelength 0.6 to 0.8 foot, amplitude 0.05 to 0.06 foot; $n_I = 0.0161$. Crossed rods, 4 feet long, give scale.

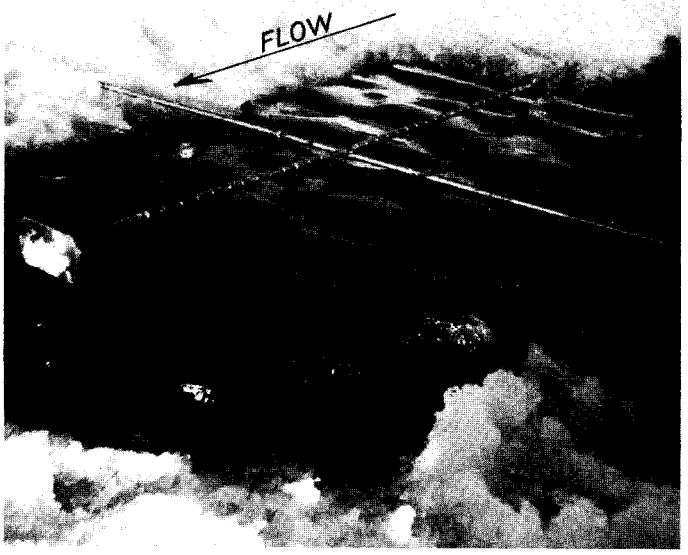


FIGURE 2.—Underside of ice block, January 18, 1965; wavelength 0.5 to 0.6 foot, amplitude 0.06 to 0.08 foot; $n_I = 0.0135$. Crossed rods, 4 feet long, give scale.

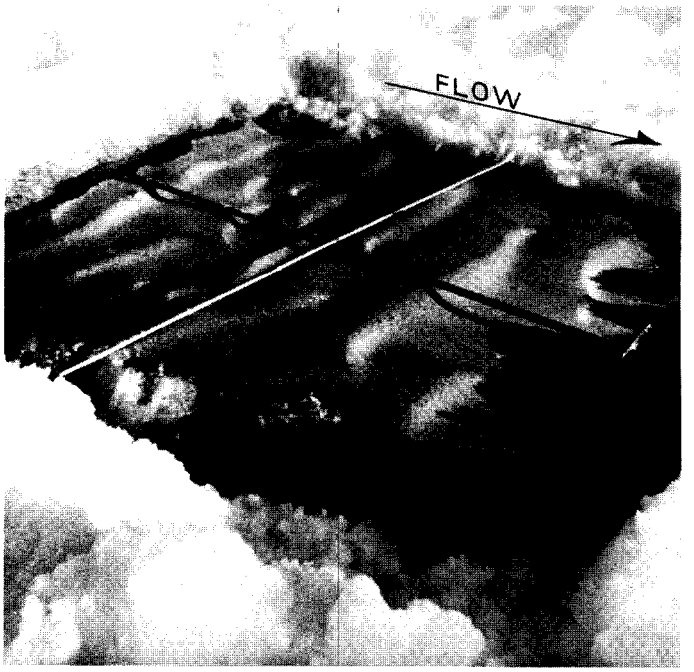


FIGURE 4.—Underside of ice block, February 3, 1965; wavelength 0.6 to 0.8 foot, amplitude 0.03 to 0.05 foot; $n_I = 0.0145$. Crossed rods, 4 feet long, give scale. Grainy, subdued appearance is due to blowing snow which frosted the wet ice surface.

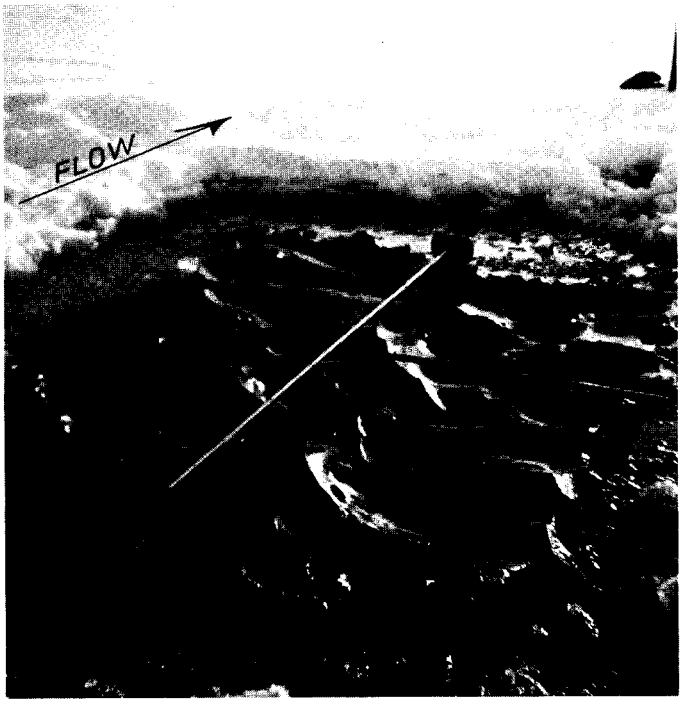


FIGURE 5.—Underside of ice block, February 18, 1965; wavelength 0.5 to 0.7 foot, amplitude 0.06 to 0.14 foot; $n_I=0.0229$. Crossed rods, 4 feet long, give scale.

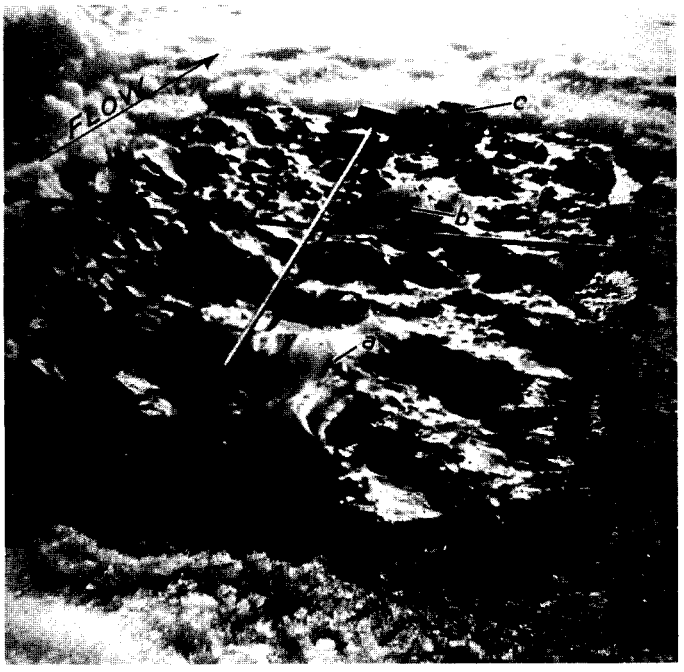


FIGURE 6.—Underside of ice block, February 24, 1965; wavelength (exclusive of large dunes) 0.5 to 0.6 foot, local relief (amplitude) 0.10 to 0.20 foot, total relief 0.25 foot; $n_I=0.0245$. Crossed rods, 4 feet long, give scale. Note the large, wedge-shaped dunes *a*, *b*, and *c*. This configuration is formed in bubbly, nonhomogeneous ice.

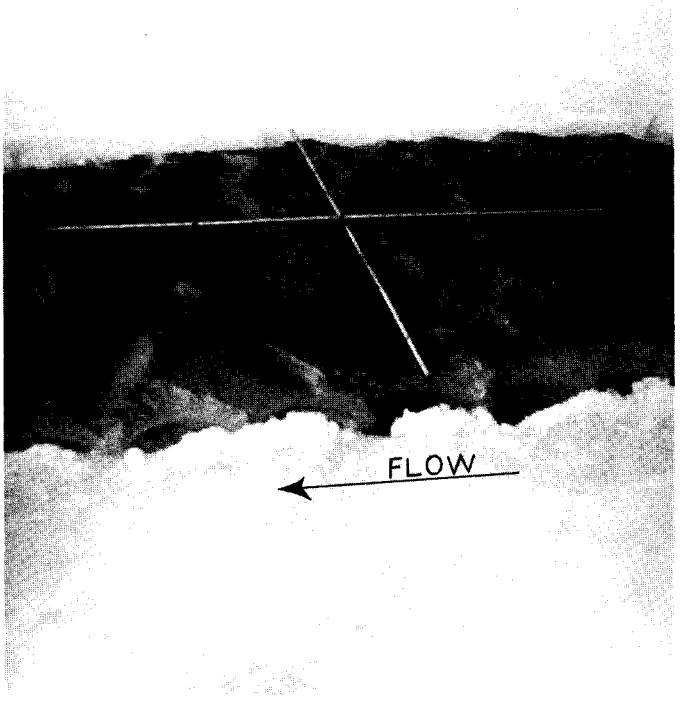


FIGURE 7.—Underside of ice block, March 6, 1965; wavelength 0.6 to 1.0 foot, amplitude 0.06 to 0.10 foot; $n_I=0.0281$. Crossed rods, 4 feet long, give scale.

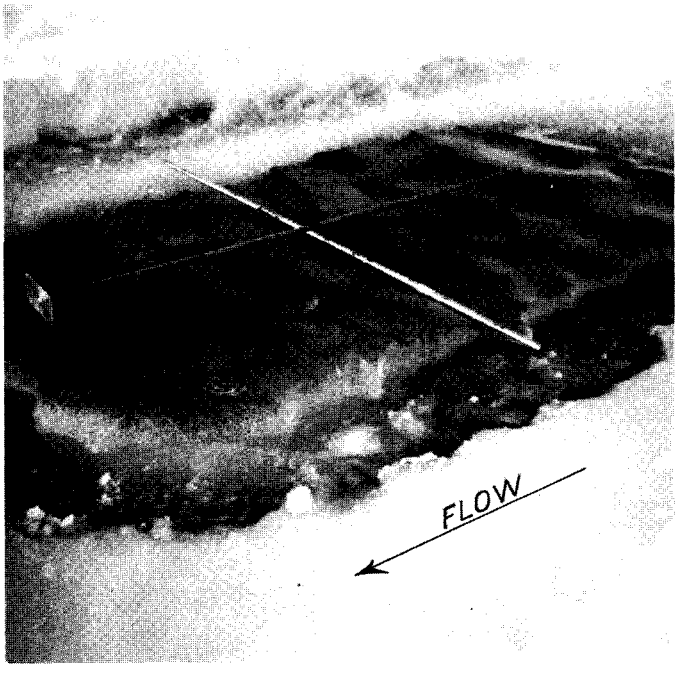


FIGURE 8.—Underside of ice block, March 20, 1965; wavelength 0.6 to 0.9 foot, amplitude 0.06 to 0.08 foot; $n_I=0.0244$. Crossed rods, 4 feet long, give scale.

and frazil ice was not present in the flowing water. For the present, only speculation on the cause of the development of the configurations is appropriate. However, the hypothesis favored by the writer is that variations in the intensity of fluid turbulence from point to point within the flow cause very slight variations in temperature from point to point on the ice–water interface, and that these temperature variations cause simultaneous melting and freezing at different points on the interface. Simultaneous freezing at one point and melting at another nearby point would certainly produce relief on the underside of the ice. Future work is planned to determine whether the "ice-dunes" migrate downstream; and, if they migrate, whether this movement is to be explained by simultaneous progressive freezing (accretion) on their downstream faces and melting (erosion) on their upstream faces. In addition, the wavelength and frequency of the fluid turbulence will be investigated, for comparison with the wavelength of the "ice-dunes."

## COMPUTATION OF THE MANNING ROUGHNESS COEFFICIENT FOR THE UNDERSIDE OF THE ICE

Previous investigators have attempted to calculate a Manning roughness coefficient for the underside of the ice cover, knowing the $n$ value for the streambed and the $n$ value for the combination of the streambed and the ice cover (Pavlovskiy, 1931; Lotter, 1932, 1933, 1941; Belokon, 1940; Sabaneev, 1948). Chow (1959) has presented a brief description of Pavlovskiy's method, and Nezhikhovskiy (1964) has discussed the limitations in development and defects in principle of all the pertinent existing formulas.

A new approach to the calculation of the roughness coefficient of the underside of the ice is presented here. The procedure uses the Kármán-Prandtl resistance equation for turbulent flow in rough pipes (Rouse, 1946) and it employs assumptions adapted from a flume-sidewall correction method first presented by Johnson (1942) and used by Vanoni and Brooks (1957). The Kármán-Prandtl resistance equation is a relation between the Darcy-Weisbach friction factor and the relative roughness of a conduit. Although the Darcy-Weisbach friction factor is soundly based on modern hydraulic principles, it is dependent on hydraulic parameters of flow in addition to boundary roughness. Because the Manning roughness coefficient is ideally dependent only on the boundary roughness, it provides a better comparison. Both the Darcy-Weisbach friction factor for the ice and the Manning roughness coefficient for the ice have been determined for each discharge measurement.

Terms used in the discussion below are as follows:

$A$=mean cross-sectional area for the reach,
$P$=mean wetted perimeter,
$R$=A/P=mean hydraulic radius, (1)
$V$=mean velocity through the reach,
$S_e$=slope of the energy gradient,
$g$=acceleration of gravity,
$f=8gRS_e/V^2$=Darcy-Weisbach friction factor, (2)
$n=1.486R^{2/3}S_e^{1/2}/V$=Manning roughness coefficient, (3)
$r_o$=Conduit radius in the Kármán-Prandtl equation, and
$k$=effective size of the roughness projections of the boundary surface of flow in the Kármán-Prandtl equation.

The quantities $S_e$ and $g$ apply to the entire flow, to the flow in the bed section, or to the flow in the ice-cover section. (The terms "bed section" and "ice-cover section" are explained in the first assumption below.) All the other terms and formulas may be used with the subscript $B$ for the bed section, the subscript $I$ for the ice-cover section, or without any subscript for the entire cross section.

The assumptions made for the calculations are:

(1) The cross section can be divided into two parts, one section exerting shear on the bed, and the other section exerting shear on the underside of the ice cover. The boundary between the bed section and the ice-cover section is considered as the locus of a surface of zero shear within the flow. As such, this boundary is not included in either wetted perimeter, $P_B$ or $P_I$.

(2) The mean velocity in the bed section, $V_B$, and the mean velocity in the ice-cover section, $V_I$, are each equal to the mean velocity of the entire cross section, $V$.

(3) The formulas for $R$, $f$, and $n$ can be applied to each section as if it were a channel by itself.

With regard to the first assumption, it may be argued that to postulate a surface of zero shear is unjustified for turbulent flow. Nothing is here advanced in favor of or against such an argument, except the statement that if a surface of zero shear does not exist, then a surface of minimum shear does exist, and that any shear on such a surface in sediment-free turbulent flow would be believed to be very small compared to the shear on either the bed or the underside of the ice. Concerning the second assumption, it is of course not known that $V_B=V_I=V$. However, this assumption is necessary to solve the problem, and it is believed to be a reasonable one. If future work establishes a relation between $V$ and $V_B$ or $V_I$, this assumption will be unnecessary. In view of the foregoing comments, this

analysis is approximate to the degree that the shear on the so-called surface of zero shear is greater than zero, and to the degree that $V_B$ or $V_I$ differs from $V$.

The quantities $A$, $P_B$, $P_I$, $R$, $V$, $S_e$, $g$, $f$, and $n$ are known, or are readily determined, for each discharge measurement. The unknowns of primary interest are the Darcy-Weisbach friction factor for the ice, $f_I$, and the Manning roughness coefficient for the ice, $n_I$.

The mathematical background for the method is as follows:

The Kármán-Prandtl resistance equation for turbulent flow in rough pipes is

$$\frac{1}{\sqrt{f}}=2\log_{10}\frac{r_o}{k}+1.74.$$

For a pipe, the actual radius of the cross section is twice the hydraulic radius; thus $r_o$ is replaced by $2R$ to give

$$\frac{1}{\sqrt{f}}=2\log_{10}\frac{2R}{k}+1.74. \quad (4)$$

It is now assumed that equation 4 may be applied to the bed section. Data from open-water discharge measurements (including slope values and additional cross sections in the reach) must be analyzed to calculate a value of $k_B$, the effective size of the roughness projections of the bed. This value is assumed constant throughout the winter period, on the basis of what has already been stated concerning the character of the bed. It should be evident that this approach is applicable only to streams which possess stable beds during the ice-covered period.

Replacing $f$ in equation 4 by its equivalent from equation 2, and applying the subscript $B$ to the terms, provides the relation

$$\frac{V_B}{\sqrt{8gR_BS_e}}=2\log_{10}\frac{2R_B}{k_B}+1.74. \quad (5)$$

In accordance with the foregoing discussion, all the terms in equation 5 except $R_B$ are known for each discharge measurement. Since equation 5 is a transcendental equation with the unknown appearing on both sides of the equal sign, a trial-and-error procedure is indicated for the determination of the numerical value of $R_B$.

Once $R_B$ has been evaluated, $A_B$ is found from equation 1. Since the geometry of the cross section requires that

$$A=A_B+A_I,$$

the value of $A_I$ is directly determined, and $R_I$ follows from equation 1.

With $R_B$ and $R_I$ both determined, the use of equations 2 and 3 leads to the values of $f_B$, $n_B$, $f_I$, and $n_I$.

The foregoing method for calculating the Darcy-Weisbach friction factors and the Manning roughness coefficients proved quite sensitive but simple to use. An average of four trial values of $R_B$ was needed to satisfy equation 5 in the analysis of each of the discharge measurements made during the study period.

The results of the analyses of the 14 discharge measurements, summarized in table 1, give values of $n_I$ that range from 0.0100 to 0.0281 and that are generally lower in the early part of the period of ice cover.

TABLE 1.—*Winter measurements of stream discharge and channel geometry, computed hydraulic parameters, and observations of configuration of the underside of the ice on the St. Croix River near Danbury, Wis.*

[Symbols are defined in text]

| Date | Discharge $Q$ (cfs) | Mean velocity $V$ (fps) | Cross-sectional area | | | Wetted perimeter | | | Hydraulic radius | | | Energy gradient $S_e\times10^4$ (ft/ft) | Darcy-Weisbach friction factor | | | Manning roughness coefficient | | | Dunelike features on underside of ice | |
|---|---|---|---|---|---|---|---|---|---|---|---|---|---|---|---|---|---|---|---|---|
| | | | $A$ (ft²) | $A_B$ (ft²) | $A_I$ (ft²) | $P$ (ft) | $P_B$ (ft) | $P_I$ (ft) | $R$ (ft) | $R_B$ (ft) | $R_I$ (ft) | | $f$ | $f_B$ | $f_I$ | $n$ | $n_B$ | $n_I$ | Wavelength (ft) | Amplitude (ft) |
| 1964 | | | | | | | | | | | | | | | | | | | | |
| Dec. 15 | 700 | 1.57 | 446 | 355 | 91 | 440 | 220 | 220 | 1.01 | 1.62 | 0.414 | 3.64 | 0.0386 | 0.0614 | 0.0157 | 0.0182 | 0.0249 | 0.0100 | | |
| Dec. 21 | 716 | 1.54 | 465 | 346 | 119 | 440 | 220 | 220 | 1.06 | 1.57 | .541 | 3.64 | .0418 | .0622 | .0214 | .0191 | .0249 | .0122 | | |
| Dec. 30 | 837 | 1.62 | 518 | 325 | 193 | 439 | 220 | 219 | 1.18 | 1.48 | .881 | 4.38 | .0509 | .0638 | .0381 | .0215 | .0250 | .0177 | 0.5–0.7 | 0.05–0.06 |
| 1965 | | | | | | | | | | | | | | | | | | | | |
| Jan. 5 | 722 | 1.56 | 463 | 315 | 148 | 440 | 220 | 220 | 1.05 | 1.43 | .673 | 4.26 | .0475 | .0647 | .0304 | .0204 | .0248 | .0151 | .5–.6 | .10–.12 |
| Jan. 18 | 754 | 1.60 | 471 | 337 | 134 | 440 | 220 | 220 | 1.07 | 1.53 | .609 | 4.08 | .0439 | .0628 | .0250 | .0196 | .0249 | .0135 | .5–.6 | .06–.08 |
| Jan. 26 | 703 | 1.52 | 464 | 306 | 158 | 439 | 220 | 219 | 1.06 | 1.39 | .721 | 4.19 | .0497 | .0655 | .0339 | .0208 | .0250 | .0161 | .6–.8 | .05–.06 |
| Feb. 3 | 699 | 1.57 | 445 | 309 | 136 | 439 | 220 | 219 | 1.01 | 1.40 | .621 | 4.45 | .0470 | .0653 | .0288 | .0201 | .0250 | .0145 | .6–.8 | .03–.05 |
| Feb. 11 | 666 | 1.47 | 453 | 267 | 186 | 439 | 220 | 219 | 1.03 | 1.21 | .849 | 4.82 | .0592 | .0698 | .0488 | .0227 | .0253 | .0199 | .5–.7 | .07–.09 |
| Feb. 18 | 664 | 1.41 | 472 | 254 | 218 | 439 | 220 | 219 | 1.07 | 1.16 | .995 | 4.74 | .0662 | .0713 | .0614 | .0241 | .0253 | .0229 | .5–.7 | .06–.14 |
| Feb. 24 | 746 | 1.42 | 525 | 269 | 256 | 439 | 220 | 219 | 1.20 | 1.22 | 1.17 | 4.45 | .0678 | .0694 | .0664 | .0248 | .0252 | .0245 | Irreg. | Irreg. |
| Mar. 6 | 855 | 1.45 | 588 | 270 | 318 | 440 | 220 | 220 | 1.34 | 1.22 | 1.44 | 4.63 | .0754 | .0691 | .0815 | .0266 | .0252 | .0281 | .6–1.0 | .06–.10 |
| Mar. 12 | 788 | 1.45 | 543 | 282 | 261 | 439 | 220 | 219 | 1.24 | 1.28 | 1.19 | 4.34 | .0656 | .0680 | .0633 | .0246 | .0251 | .0240 | .6–.8 | .05–.07 |
| Mar. 20 | 752 | 1.43 | 527 | 271 | 256 | 439 | 220 | 219 | 1.20 | 1.23 | 1.17 | 4.45 | .0676 | .0692 | .0658 | .0248 | .0252 | .0244 | .6–.9 | .06–.08 |
| Mar. 30 | 928 | 1.60 | 580 | 308 | 272 | 440 | 220 | 220 | 1.32 | 1.40 | 1.24 | 4.63 | .0614 | .0653 | .0576 | .0240 | .0250 | .0230 | .5–.8 | .05–.07 |

The value of $n_B$ was found to be nearly constant (average 0.0251), as would be expected from the assumption of a constant value of $k_B$ for the winter period. It is well to notice that for any particular measurement the sum of $R_B$ and $R_I$ is not equal to $R$. The relation $R=R_B+R_I$ can be shown to be incorrect simply from the geometry of the cross section, but Pavlovskiy's method as described by Chow makes the assumption that $R=R_B+R_I$. Chow however has stated (written commun., 1965) that it is his knowledge that Pavlovskiy's "* * * assumption is entirely hypothetical and imaginative * * *" and that "* * * $R_B$ and $R_I$ are considered (in Pavlovskiy's method) as parts of the total contribution due to $R$ and therefore are not defined according to separation by the locus of zero shear."

The computed values of the Darcy-Weisbach friction factors and the Manning roughness coefficients must be termed provisional, because an insufficient number of open-water discharge measurements has been made from which $k_B$ can be accurately evaluated. However, for the purposes of this paper, a reasonable value of $k_B$ $=0.23$ foot was assumed from the available data. Regardless of the value of $k_B$ used in the computations, the values of $n_I$ are still useful for comparing one observation with another even though they may be inaccurate in an absolute sense.

Each ice observation except the last one can be paired with the succeeding observation, giving 11 instances of change in the underside configuration. These 11 changes in the character of the ice can be compared with the corresponding changes in the computed Manning roughness coefficient for the entire ice cover in the reach. Analyzed in this way, the observed character of the underside of the ice throughout the period of ice cover shows a rather consistent relation with the computed values of $n_I$. In 8 of the 11 cases, the ice became rougher (or smoother) with corresponding increase (or decrease) in $n_I$. The lack of this correspondence in the three remaining cases is most logically explained by the supposition that at those times the character of the underside of the ice on the block observed did not closely represent the general character of the underside of the ice throughout the entire reach.

## REFERENCES


Belokon, P. N., 1940, Engineering hydraulics of the flow under an ice cover (Inzhenernaya gidravlika potoka pod ledianym pokrovom): Gosenergoizdat, Moscow and Leningrad. [In Russian]

Chow, V. T., 1959, Open-channel hydraulics: New York, McGraw-Hill, 680 p.

Johnson, J. W., 1942, The importance of side-wall friction in bed-load investigations: Civil Eng., v. 12, no. 6, p. 329–331.

Lotter, G. K., 1932, Influence of conditions of ice formation and thickness on the design of diversion canals (Vliyaniye uslovii ledoobrazovaniya i tolshchiny l'da na raschet derivatsionnykh kanalov): All-Union Sci. Research Inst. of Hydraulic Engineering Trans. (Izvestiia VNIIG), v. 7, p. 55–80, Leningrad. [In Russian]

——— 1933, Considerations in the hydraulic design of channels with different roughnesses of the walls (Soobrazheniya k gidravlicheskomu raschetu rusel s razlichnoi sherokhovatostiyu stenok): All-Union Sci. Research Inst. of Hydraulic Engineering Trans. (Izvestiia VNIIG), v. 9, p. 238–241, Leningrad. [In Russian]

——— 1941, Method by Academy Member N. N. Pavlovskiy for determination of roughness coefficients of ice-covered channels (Metod akademika N. N. Pavlovskogo dlya opredeleniya koeffitsienta sherokhovatosti rusel, pokrytykh l'dom): All-Union Sci. Research Inst. of Hydraulic Engineering Trans. (Izvestiia VNIIG), v. 29, Leningrad. [In Russian]

Nezhikhovskiy, R. A., 1964, Coefficients of roughness of bottom surface of slush-ice cover: State Hydrol. Inst. Trans. (Trudy GGI), v. 110, p. 54–82, Leningrad [in Russian]; *translated in* Soviet Hydrology, Selected Papers, Am. Geophys. Union, no. 2, 1964, p. 127–150.

Pavlovskiy, N. N., 1931, On a design formula for uniform motion in channels with nonhomogeneous walls (K voprosu o raschetnoi formule dlya ravnomernogo dvizheniya v vodotokahk s neodnorodnymi stenkami): All-Union Sci. Research Inst. of Hydraulic Engineering Trans. (Izvestiia VNIIG), v. 3, p. 157–164, Leningrad. [In Russian]

Rouse, Hunter, 1946, Elementary mechanics of fluids: New York, John Wiley & Sons, 376 p.

Sabaneev, A. A., 1948, On the computation of a uniform flow in a channel with nonuniform walls: Leningrad Polytech. Inst. Trans., no. 5. [In Russian]

Vanoni, V. A., and Brooks, N. H., 1957, Laboratory studies of the roughness and suspended load of alluvial streams: California Inst. Technology Sedimentation Lab. Rept. E–68, Pasadena, Calif.

# TIME-OF-TRAVEL MEASUREMENTS ON THE PASSAIC AND POMPTON RIVERS, NEW JERSEY

By GILBERT M. HORWITZ and PETER W. ANDERSON, Trenton, N.J.

*Work done in cooperation with the*
*New Jersey State Departments of Health, Conservation and Economic Development, and Agriculture, and the Passaic Valley Water Commission*

*Abstract.*—Time-of-travel measurements were made on a 30-mile stretch of the Passaic River at times of medium-low flow (exceeded 67 percent of the time) and at extreme-low flow (exceeded 99.4 percent of the time). Additional measurements were made on a 6.4-mile reach of the Pompton River. Rhodamine-B dye was used to simulate soluble contaminants in the measurements. The river was divided into subreaches in order to (1) reduce the concentration of dye required, (2) reduce the problems of detection associated with dispersion, and (3) minimize the effect of variation in streamflow by reducing the time spent on the measurement. The time of travel of the peak concentration of dye in the Passaic River was 5 days during medium-low and 13 days during extreme-low flow.

The U.S. Geological Survey conducted three time-of-travel measurements during 1964 in the Passaic River basin, New Jersey (fig. 1), as part of a cooperative program to define the water-quality and streamflow characteristics in the basin above Little Falls.

The objective of these measurements was to define the time required for a soluble contaminant to pass through finite lengths of the river system. Applications of this information include prediction of the capacity of the stream to cope with waste-water discharges, and downstream warning and planning in the event of accidental spills of harmful contaminants into the river. For such purposes the traveltime data are of considerable importance to water managers, health officials, and hydrologists.

The reach of the Passaic River chosen for study is 29.8 miles in length, extending from the Geological Survey's stream-gaging station near Chatham (site 1, fig. 1) to the Passaic Valley Water Commission's intake in Little Falls (site 7). The drainage area at the Chatham gage is 100 square miles, and at the Little Falls intake, 762 square miles. Two major tributary systems

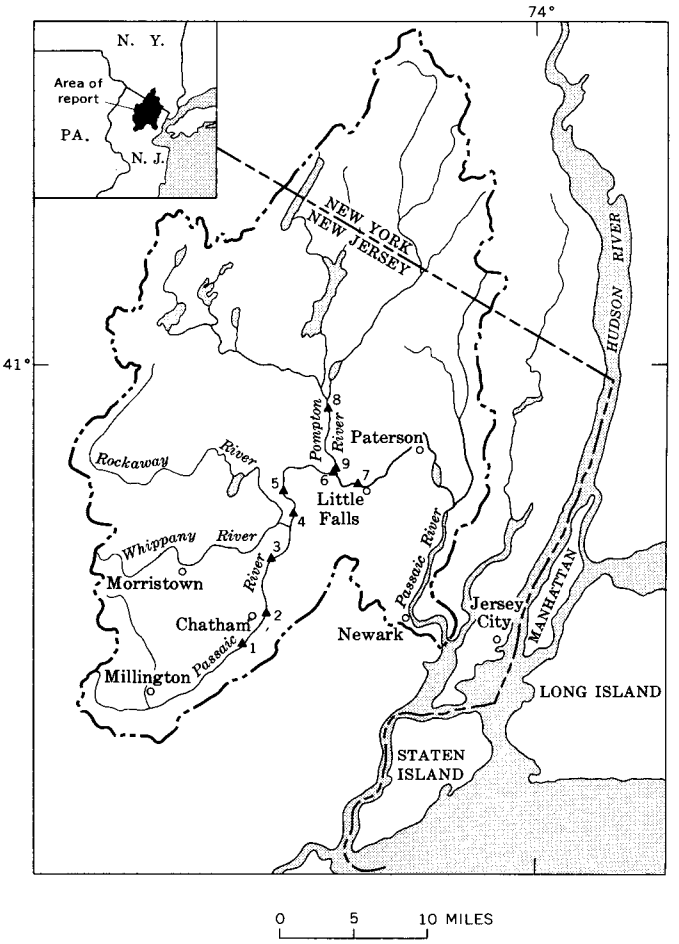


1, Chatham.
2, Florham Park.
3, Hanover.
4, Pine Brook.
5, Clinton.
6, Two Bridges.
7, Little Falls.
8, Pompton plains.
9, Two Bridges—Pompton River.

FIGURE 1.—Sampling sites for time-of-travel measurements in the Passaic River basin, New Jersey.

U.S. GEOL. SURVEY PROF. PAPER 550-B, PAGES B199–B203

flow into the Passaic River in the reach studied. The Rockaway-Whippany Rivers system drains 205 square miles and is confluent with the Passaic River above Pine Brook (site 4). The Pompton River system drains 381 square miles and flows into the Passaic River at Two Bridges (below site 6).

*Acknowledgments.*—The authors are exceedingly grateful to A. Bruce Pyle, of the New Jersey State Division of Fish and Game, for the loan of equipment, and to their coworkers Thomas J. Buchanan and James F. Wilson, for their advice and guidance in the study.

In addition to measurements on the Passaic River, measurements were made on the Pompton River between the stream-gaging station at Pompton Plains (site 8, fig. 1) and Two Bridges (site 9, fig. 1), a distance of about 6.4 miles. The drainage area at the gaging station is 355 square miles and at Two Bridges, 381 square miles.

## METHOD

Soluble contaminants were simulated in the measurements by using a fluorescent dye, Rhodamine B. Pritchard and Carpenter (1960) introduced this dye and its analytical measurement to hydrologic tracing. More recently Wright and Collings (1964) discussed its applications in dispersion studies, discharge measurements, and time-of-travel measurements. This dye has proven to be an excellent tracer in several Geological Survey measurements of the movement of soluble contaminants in stream channels (Buchanan, 1964; Wilson and Forrest, in press). Rhodamine B is readily detected with a fluorometer, an instrument which measures fluorescence. The dye is nontoxic to animal and plant life in the concentration used, relatively stable to light and bacterial action for several days, detectable in minute quantities (as low as 0.05 parts per billion), and inexpensive (Wright and Collings, 1964).

The 30-mile stretch of river was divided into 6 subreaches of various lengths (fig. 1), and time-of-travel measurements were made in each. Mileage intervals, drainage areas, and other pertinent information concerning the subreaches are presented in table 1. The principal advantages of using the subreach method are: the reduction of dye concentrations necessary, relative to those required for long reaches; lessening of the problems of detection associated with dispersion, especially during low streamflow conditions, because these lower velocities mean increased duration of flow and increased dilution, for a given reach; and minimizing of the likelihood of variations in streamflow by reduction of the time span of the measurement. A disadvantage is the loss of continuity of dispersion information. Previous studies (Buchanan, 1964; Wilson and Forest, in press) indicate that the cumulative longitudinal dispersion determined by dosing subreaches is not the same as that determined by following a single dose for the entire length of the reach. Peak concentration data are also different.

TABLE 1.—*Sampling sites and subreaches used in Passaic and Pompton Rivers time-of-travel measurements*

| Site No. (fig. 1) | Name | Distance below dosing site (miles) | Drainage area (sq mi) |
|---|---|---|---|
| **Passaic River sites** | | | |
| 1 | Chatham | 0 | 100 |
| 2 | Florham Park | 4.0 | |
| 3 | Hanover | 4.9 | 128 |
| 4 | Pine Brook | 5.7 | 349 |
| 5 | Clinton | 3.2 | |
| 6 | Two Bridges | 8.6 | 361 |
| 7 | Little Falls | 3.4 | 762 |
| | | 29.8 | |
| **Pompton River sites** | | | |
| 8 | Pompton Plains | 0 | 355 |
| 9 | Two Bridges | 6.4 | 381 |
| | | 6.4 | |

Doses of dye were injected at the upper end of each subreach. Water samples were collected at intervals, at sites downstream from the point of injection, and analyzed for dye content. Traveltime was then determined between the dosage and sampling sites for each reach. Gaging stations located at each end of the reach studied provided continuous records of streamflow during the measurements. Stream-discharge measurements were also made at each sampling site to ascertain with greater precision the interrelation between traveltime and discharge, and on each of the major tributaries to provide good definition of inflow.

## RESULTS

The first time-of-travel measurements were made on the Passaic River during the week of June 15, 1964; discharge rates were at magnitudes expected to be exceeded 67 percent of the time (based on long-term records at the Chatham gaging station). Each dye injection was traced through two successive subreaches during June to monitor longitudinal dispersion. Results of this measurement are tabulated in table 2.

A graphic illustration of a time-concentration curve is presented for the June measurement in figure 2. This curve shows the approximate concentration of dye at two sampling sites, the initial and peak traveltime, and the approximate passage time. Thus, the first trace of dye injected at Clinton arrived at Two Bridges 36.6 hours after its injection and at Little Falls, 17.2 hours after its arrival at Two Bridges. The peak concen-

TABLE 2.—*Results of Passaic River time-of-travel measurement, June 1964*

| Subreach | Discharge (cfs) [1] | Traveltime for— | | Estimated passage time of dye (hours) | Velocity of peak (miles per hour) |
|---|---|---|---|---|---|
| | | Leading edge of dye (hours) | Peak of dye concentration (hours) | | |
| Chatham to Florham Park | 59. 5 | 6. 3 | 9. 8 | 50. 1 | 0. 41 |
| Florham Park to Hanover | 55. 4 | 16. 0 | 19. 5 | 45. 0 | . 25 |
| Hanover to Pine Brook | 136 | 15. 3 | 18. 6 | 48. 8 | . 31 |
| Pine Brook to Clinton | 136 | 6. 7 | 9. 5 | 27. 2 | . 34 |
| Clinton to Two Bridges | 192 | 36. 6 | 43. 1 | 92. 3 | . 20 |
| Two Bridges to Little Falls | 320 | 12. 5 | 19. 0 | 69. 5 | . 18 |

[1] At lower end of subreach on June 17.

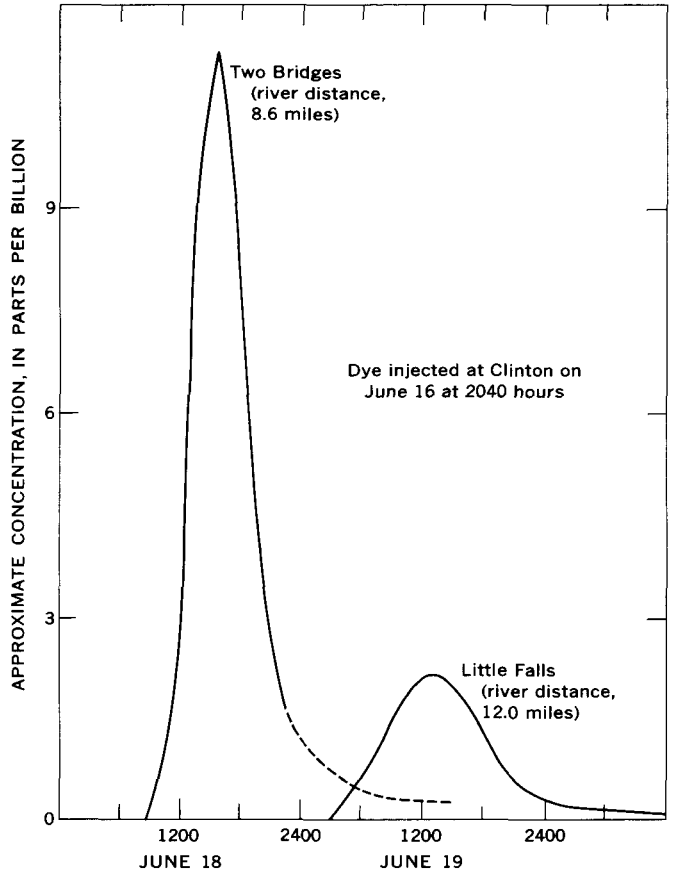


FIGURE 2.—Time-of-travel and longitudinal-dispersion characteristics of dye injected into the Passaic River at Clinton, N.J., and measured at Two Bridges and Little Falls, June 1964.

tration of dye lagged behind the initial time of arrival by 6.5 hours at Two Bridges and 10 hours at Little Falls. (Traveltimes in the second subreach are not consistent with those in table 2, as flow conditions had changed.) The dye cloud persisted in detectable concentration at Little Falls for more than 115 hours after its injection at Clinton.

The effects of longitudinal dispersion on the injected dye also are illustrated on this time-concentration curve. The leading edge of the dye cloud traveled at a faster rate—rapidly rising slope—than did the trailing edge. Also, there is an 80-percent reduction in dye concentration between Two Bridges and Little Falls, a distance of 12 miles. This reduction is not due entirely to dispersion; part of it is due to dilution of the dye by tributary inflow (note the decrease in area under the Little Falls curve), and part of it may be due to loss of dye on sediments and vegetation.

Vertical and lateral mixing of the dye was assumed to be essentially complete at the sampling sites. Cross-sectional sampling at the Clinton and Little Falls sampling sites indicated that while dye concentrations along the bank trailed those in the center, the magnitude of concentration and the shape of the concentration curve at midstream and along the bank were similar. Vertical mixing occurred shortly after injection, especially as depths in the reach studied rarely exceed 4 feet except in the Beatties Dam pool, just upstream from the Little Falls sampling location.

A second set of measurements on the Passaic River was completed during the week of September 20, 1964, under extreme-low flow conditions—at discharge rates which should be exceeded 99.4 percent of the time. Because of the low stream velocities, each injection of dye was traced through only one subreach during this measurement. In addition to the measurement of traveltimes in the Passaic River, a measurement of traveltimes in the Pompton River between Pompton Plains and Two Bridges was made in September. Results of these September measurements are tabulated in table 3.

Traveltimes for the two Passaic River time-of-travel measurements (tables 2 and 3) and streamflow measurements are plotted as a function of distance on figure 3. Since dye concentrations eventually went below detectable limits due to dilution, cutoff points for the trailing edge are arbitrary. This type of plot, for a range of discharge conditions, is of particular interest to the operator of a potable-water supply facility, such as the Passaic Valley Water Commission. Knowing the distance upstream to a toxic spill, a water-treatment plant operator can accurately estimate its initial time of arrival and the approximate time required for the solutes to pass the intake.

Variations in time of travel with discharge are illustrated on figure 4. Since this illustration is based only on the two measurements discussed herein, interpolation must be done with caution. A more reliable definition would require additional data. At a mean discharge

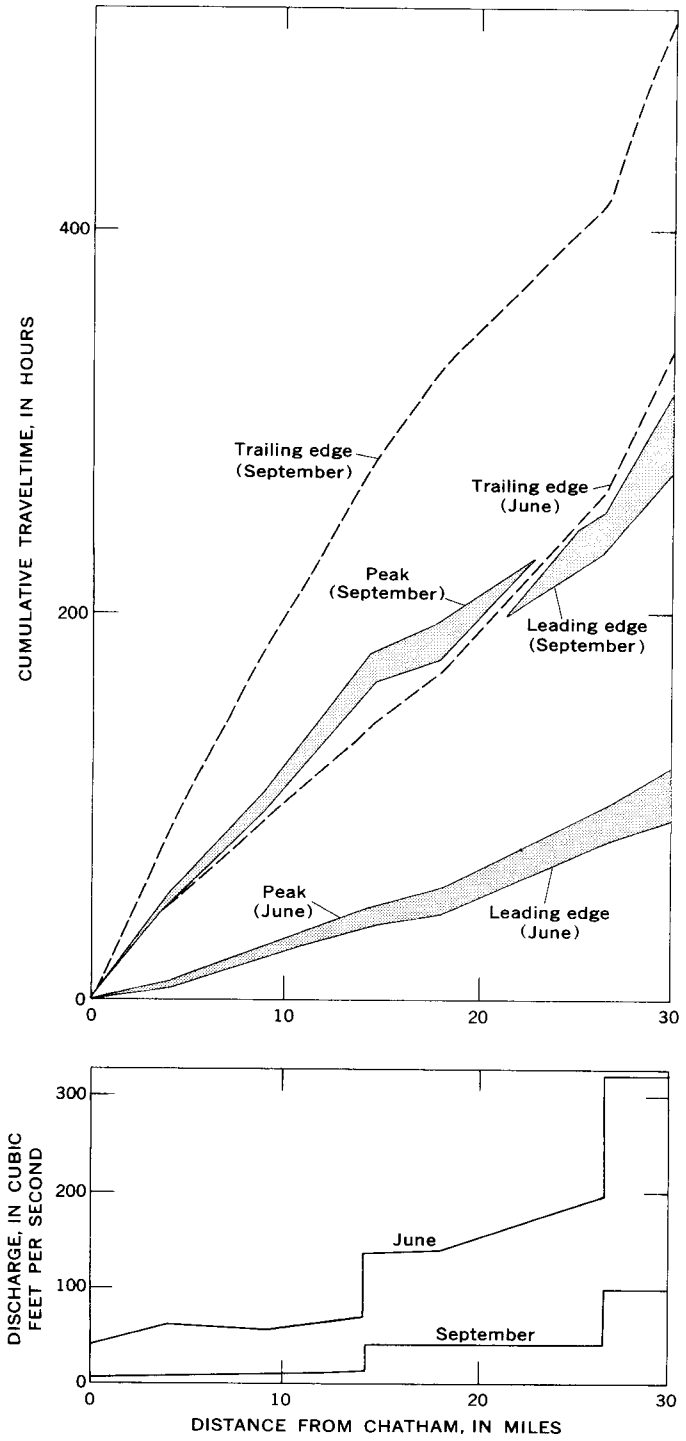


FIGURE 3.—Leading-edge, peak, and trailing-edge traveltime and discharge data, Passaic River, N.J., between Chatham and Little Falls.

of 50 cubic feet per second at the Chatham gage, estimated time of travel of the maximum concentration from the gaging station to Little Falls would be almost 4.5 days. At 10 cfs, the traveltime would be about 9 days. Similarly, if information were needed on the river between the confluence of the Rockaway-Whippany Rivers system near Pine Brook (fig. 1) and the Little Falls intake, an estimate of the traveltime could be obtained from this illustration (fig. 4); at a discharge of 50 cfs the expected traveltime would be about 2.7 days, while at 10 cfs, it would be about 4.3 days.

TABLE 3.—*Results of Passaic and Pompton Rivers time-of-travel measurements, September 1964*

| Subreach | Discharge (cfs)[1] | Traveltime for— | | Estimated passage time of dye (hours) | Velocity of peak (miles per hour) |
|---|---|---|---|---|---|
| | | Leading edge of dye (hours) | Peak of dye concentration (hours) | | |
| **Passaic River** | | | | | |
| Chatham to Florham Park | 5.58 | 48.6 | 52.8 | 86.8 | 0.08 |
| Florham Park to Hanover | 6.50 | 49.6 | 56.1 | 97.6 | .09 |
| Hanover to Pine Brook | 41.1 | 65.3 | 70.6 | 93.8 | .08 |
| Pine Brook to Clinton | 39.5 | 12.5 | 15.7 | 50.5 | .20 |
| Clinton to Two Bridges | 40.4 | 56.2 | 60.2 | 85.2 | .14 |
| Two Bridges to Little Falls | 103 | 40.3 | 58.3 | 94.8 | .06 |
| **Pompton River** | | | | | |
| Pompton Plains to Two Bridges | 37.1 | 37.6 | 50.1 | 94.6 | 0.13 |

[1] At lower end of subreach on September 22–23.

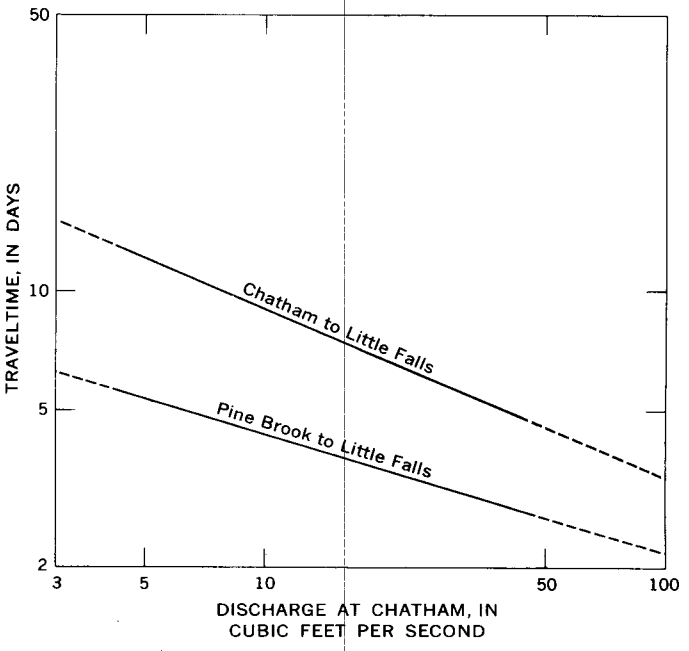


FIGURE 4.—Examples of graphs which show variations in traveltime of peak concentrations with discharge, Passaic River, N.J.

## SUMMARY

The primary purpose of conducting time-of-travel measurements in the Passaic River basin is to predict

accurately the time of travel of soluble contaminants for all streamflow conditions. Although data were collected only under an extreme-low flow condition (discharges expected to be exceeded 99.4 percent of the time) and under medium-low flow conditions (discharges expected to be exceeded 67 percent of the time), traveltimes for other discharges can be estimated by interpolation. Until additional tracer measurements can be made, these data provide the best available basis for estimates of traveltimes.

Total traveltime of the maximum comcentration of a soluble contaminant from Chatham to Little Falls, a distance of about 30 miles along the river, was determined to be about 5 days for discharges which are exceeded 64 percent of the time and about 13 days for flow rates exceeded 99.4 percent of the time. Velocities computed from traveltimes of the peak concentration averaged 0.27 mile per hour at the medium discharges and 0.11 mile per hour at the lower discharges.

Using the results of these studies, water managers, health officials, and hydrologists can predict the initial time of arrival of a contaminant, the magitude of the peak concentration, the average velocity of both the water and the contaminant, and the passage time of the contaminant. A water manager can estimate how long it would be necessary to discontinue the use of a particular water source to allow a contaminant to pass. Health officials can use these data in tracing the residence time and expected dispersion characteristics of soluble contaminants in streams. Hydrologists use the results of tracer studies to learn more about the effects of channel geometry and dams on dispersion, travel time, and discharge patterns in stream systems.

## REFERENCES

Buchanan, T. J., 1964, Time of travel of soluble contaminants in streams: Am. Soc. Civil Engineers Trans., v. 90, no. SA3, p. 1–12.

Pritchard, D. W., and Carpenter, J. H., 1960, Measurements of turbulent diffusion in estuarine and inshore waters: Internat. Assoc. Sci. Hydrology Bull. 20, p. 37–50.

Wilson, J. F., Jr., and Forrest, W. E., in press, Potomac River time-of-travel measurements, *in* Symposium on Diffusion in Oceans and Fresh Waters Proc., Lamont Geol. Observatory.

Wright, R. R., and Collings, M. R., 1964, Application of fluorescent tracing techniques to hydrologic studies: Am. Water Works Assoc. Jour., v. 56, no. 6, p. 748–754.

797–218 O—66——14

# BOTANICAL AND CHEMICAL CHARACTERISTICS DURING THE FALL OVERTURN OF A SMALL EUTROPHIC LAKE, PRETTY LAKE, INDIANA



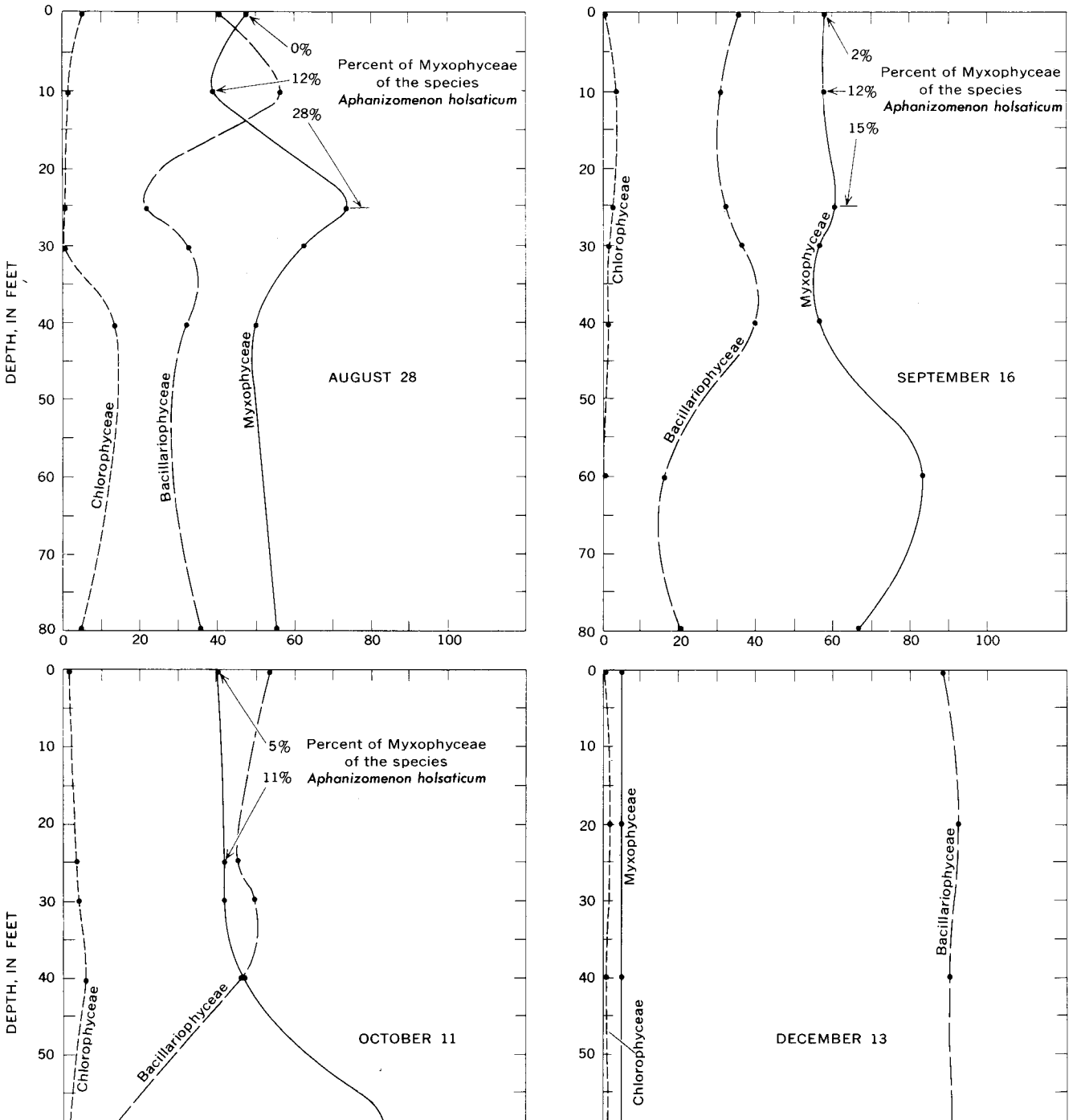

Chlorophyceae and of the Myxophyceae, few species of which are capable of growth in temperatures around 5°C. Some diatoms (Bacillariophyceae), grow very well in this temperature range, however, and they were predominant in the early winter population, as is illustrated by the data for December 13 (fig. 3). The dominant species were *Asterionella formosa* Hassall; *Fragilaria crotonensis* Kitton; *Cyclotella bodanica* Eulenstein; and *Melosira ambigua* (Grunow) Müeller.

Vertical mixing was a less important factor in the distribution of phytoplankton by December 13. In contrast to the relation that existed before the overturn, the decreasing trend in the number of cells to a depth of about 20 feet on December 13 (fig. 2) suggests that the light was effective only very near the surface. This would be expected when the elevation of the sun is at or near its annual low. The high concentration of phytoplankton below 60 feet is attributed largely to the settling out of the predominating diatoms (fig. 2, Dec. 13). Many of these cells were found to be dead.

## pH AND DISSOLVED-OXYGEN DISTRIBUTION

When the water is stratified, photosynthesis, respiration, and decomposition are the principal factors influencing pH and the concentration of dissolved oxygen in a lake. Part of the stratified lake water is isolated from the atmosphere, and its circulation is greatly reduced. The available oxygen in the isolated water is consumed by respiring organisms and by decomposing organic material that is in the sediment or is settling out from the epilimnion. In most instances the light intensity is too low to support photosynthesis. Oxygen consumption without replenishment continues, and the final decay product, hydrogen sulfide, becomes readily detectable in deep water samples. The corresponding pH is usually low. In the epilimnion, on the other hand, the supply of dissolved oxygen remains near saturation because of photosynthetic production, exchange of oxygen at the air-water interface, and circulation. The pH there is relatively high.

The distribution of dissolved oxygen and pH in Pretty Lake also reflected changes in the thermal pattern and in the phytoplankton populations. The profile for August 28 shows that a well-defined limit of dissolved oxygen existed at about 30 feet (fig. 4), which corresponded with the break in pH (fig. 5), with the base of the algal peak (fig. 2), and with the transitional temperature of the upper metalimnion (fig. 1). By

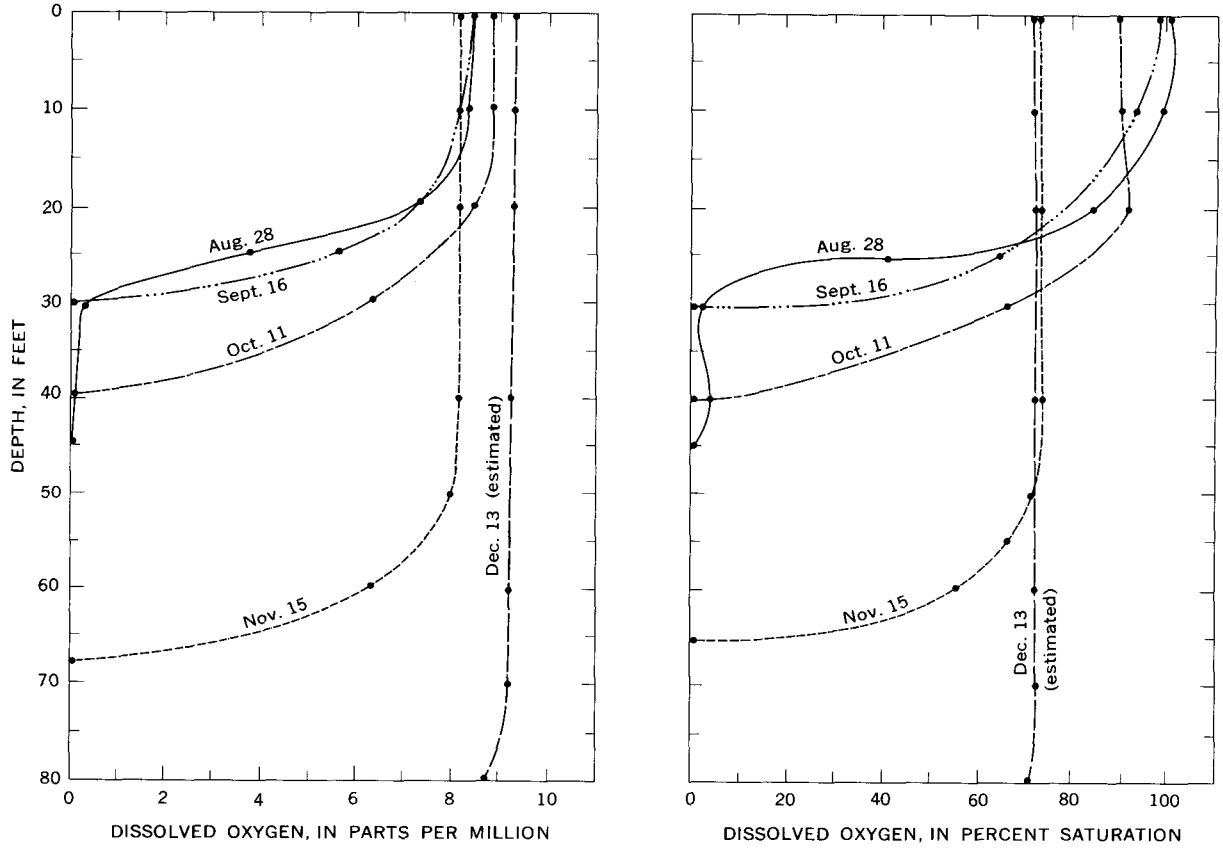


FIGURE 4.—Vertical profiles of dissolved oxygen at the center of Pretty Lake, fall 1963.

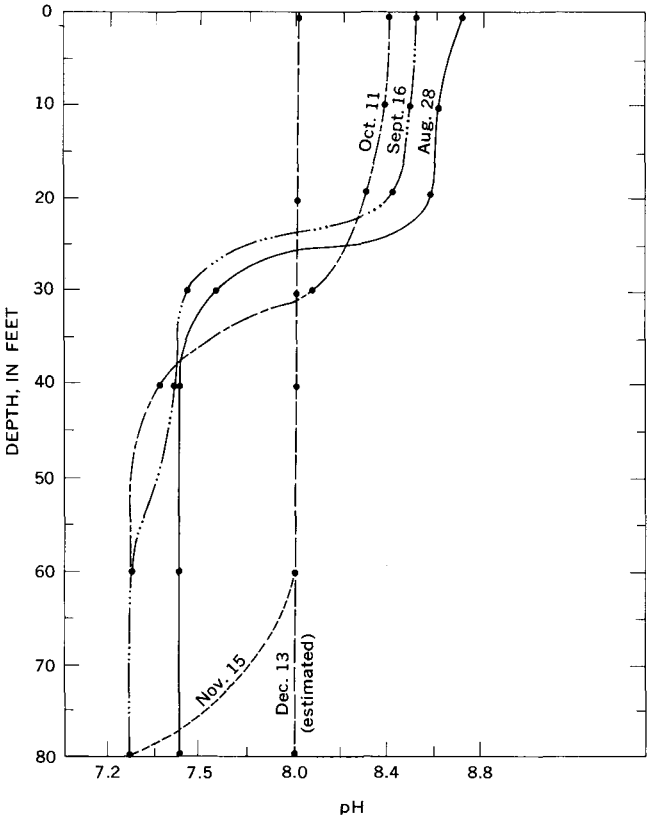


FIGURE 5.—Vertical profiles of pH at the center of Pretty Lake, fall 1963.

October 11, metalimnetic lowering had placed the lower limit of dissolved oxygen at a depth of 40 feet, which again corresponded with the break in pH but was slightly below the base of the algal peak. On November 15 the lower limit of measurable oxygen, at a depth of about 65 feet, appears to have coincided approximately with the breaks in pH and in temperature. The algal peak had diminished to a uniform concentration of cells from the surface to a depth of about 55 feet.

Only temperature and phytoplankton data are available for December 13. The water in the vertical was isothermal at that time, and it is assumed that pH and dissolved-oxygen concentration were uniform throughout the vertical during the period since the overturn.

The concentration of dissolved oxygen in the epilimnion decreased as its water was mixed with that of the oxygen-deficient hypolimnion. The percent-saturation curves for dissolved oxygen (fig. 4) show a decrease in the percent saturation in the upper waters between the periods of stratification and early circulation. The slight increase in dissolved oxygen at the surface, from about 8 parts per million before the overturn to about 9 ppm after the overturn (fig. 4, Dec. 13), probably resulted from the productivity of the enlarging diatom population (fig. 3 and table 1), and from the increased solubility of oxygen in the colder water.

TABLE 1.—*Percent concentration of dominant algal classes for all depths measured in the center of Pretty Lake, fall 1963*

| Classes of algae | Aug. 28 | Sept. 16 | Oct. 11 | Nov. 15 | Dec. 13 |
|---|---|---|---|---|---|
| Myxophyceae | 60 | 56 | 47 | 47 | 5 |
| Chlorophyceae | 2 | 2 | 3 | 7 | 1 |
| Bacillariophyceae (diatoms). | 32 | 32 | 45 | 40 | 90 |

## SUMMARY

The complete circulation that Pretty Lake underwent in the fall of 1963 is an example of an important process affecting water quality in many of the deep lakes and reservoirs in the middle latitudes. Despite this similarity in process, however, the lakes differ in important characteristics such as basin geometry, age, or other factors, and each body of water is unique. Details in the process of overturn therefore differ from one lake to another. Generally, a rich biota is directly related to oxygen depletion in the hypolimnion, which results in an oxygen profile such as the one presented for August 28 in figure 4. Such lakes are classified as eutrophic (rich in nutrients), and Pretty Lake appears to be an excellent example of this type of lake.

## REFERENCES

Drouet, Francis, 1959, Myxophycae, *in* Ward, H. B., and Whipple, G. C. (Edmondson, W. T., ed.) Fresh-water biology: New York, John Wiley & Sons, Inc., p. 95–114.

Ficke, J. F., 1965, Seasonal erasure of thermal stratification in Pretty Lake, Indiana, *in* Geological Survey Research 1965: U.S. Geol. Survey Prof. Paper 525–C, p. C199–C202.

Ruttner, Franz, 1963, Fundamentals of limnology, 3d ed.: Toronto, Univ., Toronto Press, 295 p.

# EFFECT OF GLACIAL GEOLOGY UPON THE TIME DISTRIBUTION OF STREAMFLOW IN EASTERN AND SOUTHERN CONNECTICUT

By M. P. THOMAS, Hartford, Conn.

*Abstract.*—In eastern and southern Connecticut the type and relative extent of glacial drift within a given area exert a predominant influence upon the runoff characteristics of streams draining the area. Flow-duration curves were studied for the period 1931–60, for streams in areas where the drift consists entirely of till, entirely of stratified drift, or partly of each; the average streamflow is 1.80 cubic feet per second per square mile. These curves show that the median annual minimum 7-day average flow (which in Connecticut is equivalent to the streamflow equaled or exceeded about 94 percent of the time) is 1.30 cfs per sq mi from a drainage area underlain exclusively by stratified drift, and only 0.013 cfs per sq mi from an area underlain exclusively by till, a ratio of 100 to 1.

Bedrock in Connecticut is covered nearly everywhere by unconsolidated deposits of glacial drift. Except in the Litchfield Hills in the northwestern part of the State, where the terrain is more rugged, and in the central lowland, which is underlain by glaciolacustrine deposits, the topography is rather uniform and is characterized by gently rolling hills. Despite the similarity of the topography throughout much of this region, however, the time distribution of streamflow differs markedly from place to place. The nature of the surficial deposits in a stream basin provides the dominant control on the runoff characteristics of that stream.

Although till is the predominant surficial glacial deposit in this region of gently rolling hills, the larger valleys and the lower ends of some tributary valleys are partly filled with stratified drift which rests on the till or directly on the underlying bedrock. The upper reaches of most streams, therefore, flow across rather uniform deposits of till while the larger streams, and the lower reaches of some tributaries, flow across stratified drift. The influence of these two types of deposits upon streamflow is thus in part topographic and in part lithologic.

The slopes of flow-duration curves (cumulative-frequency curves of discharge versus time) range from gentle to steep, depending on the flow characteristics of the streams. The gently sloping curves are representative of streams in terrains with relatively high infiltration and storage capacity. In these terrains a large part of the precipitation is held and then gradually released, providing a relatively high base flow. In Connecticut the curves with gentle slopes reflect the influence of ponds and lakes, and of deposits of relatively permeable stratified drift, which tend to equalize the flow during wet and dry periods. Steeply sloping flow-duration curves are characteristic of streams in relatively impervious terrains characterized by high surface runoff and low base flow. In Connecticut they commonly reflect the presence of relatively impermeable till at the land surface.

To evaluate quantitatively the influence of different proportions of till and stratified drift upon the shape and magnitude of flow-duration curves for streams in this type of terrain, all flow-duration curves for long-term gaging stations in these areas were adjusted for other factors known to affect their shape and magnitude.

The effect of seasonal and long-term variations in climate upon streamflow requires that all curves be adjusted to a common period of time. In order that the curves shall more nearly represent the long-term flow of each stream, this period should be as long as possible commensurate with the length of flow records in the area. The curves may then be considered probability curves and can be used to estimate the distribution of flows in the future, provided that there is little or no change in the environment. In Connecticut, the longer periods of record at gaging stations correspond closely to the water years 1931–60 (the period October 1930 to September 1960). This 30-year period was therefore selected as the basic period for reference, and all flow-duration curves were adjusted to it.

The climate of Connecticut is relatively homogeneous, but average streamflow varies up to 18 percent

above and below the statewide average. Flows throughout any common period were assumed to be affected in proportion to variations in this average flow. Each flow-duration curve was, therefore, adjusted throughout to a common average streamflow of 1.80 cubic feet per second per square mile, which is approximately the mean for the State. This adjustment compensates for areal differences in climate.

Since streamflow varies with the size of the basin from which it drains, the effect of drainage area upon flow duration was compensated for by converting the total flow of each stream to flow per square mile of drainage area.

Daily flows of the smaller streams in Connecticut are not usually influenced appreciably by the withdrawal and return of water by man. Flows of some of the larger streams are affected to some extent, but average flows for 30 days or more are seldom altered significantly. The low-flow portion of any flow-duration curve for one of these larger streams which was seriously affected by regulation was not used in the analysis.

The effect of geology on flow duration could be studied after these adjustments of the shape and magnitude of the flow-duration curves had been made to compensate for differences in climate with respect to both time and location, and for differences in the size of drainage basins. The relation between the steepness of a flow-duration curve and the types and proportions of stratified drift in the drainage basin was expressed as the percentage of the total drainage area underlain by deposits of stratified drift. Little is known of the thickness of the stratified drift, so, despite its importance, this factor could not be considered.

The proportions of the drainage basins underlain by stratified drift were measured on maps of surficial geology. Recent maps which cover a large part of the area at scales of 1:24,000 or 1:62,500 have been prepared by the U.S. Geological Survey in cooperation with the Connecticut Geologic and Natural History Survey and the Rhode Island Water Resources Coodinating Board. For a small portion of the area not covered by these maps, an earlier map by Flint (1930), at a scale of 1:125,000, was used. Since there are no similar maps available for the parts of those basins which lie in Massachusetts, the relative areas of stratified drift in Massachusetts, for streams rising there and passing through Connecticut, could not be detetmined.

Adjusted data resulting from analysis of records of streamflow from 23 selected gaging stations in Connecticut are shown in table 1. This table lists the station number and name of each gaging station where flow records have been obtained for many years, its total drainage area, and the area of stratified drift (including such deposits overlain by postglacial alluvium, other sediments, and swamps). Stratified drift is also expressed as a percentage of the total area of each basin. For 7 of these stations it was not possible to measure the area of stratified drift, as all or part of their basins are outside the State, and no maps of surficial geology are available. Flow data in table 1 include the average flow, and flows equaled or exceeded for various percentages of time for an average streamflow of 1.80 cfs per sq mi. Both are adjusted to the base period 1931–60.

For the 23 gaging stations in Connecticut listed in table 1, the proportion of the drainage area underlain by stratified drift ranges from 7 to about 45 percent. Sufficient data are available to define rather well the shapes of flow-duration curves for streams in such basins. Also listed at the bottom of table 1 are similar adjusted data for the Connetquot River near Oakdale, Long Island, N.Y. Records for this site were also used in the analysis because the Connetquot River basin is (1) completely underlain by stratified drift, (2) near the area being considered, and (3) characterized by topography similar to that in the parts of Connecticut studied. Use of this record makes it possible to infer the shapes of flow-duration curves for streams in basins underlain by more than 45 percent stratified drift, although these curves are not so reliably established as the curves for basins underlain by less than 45 percent stratified drift.

The effect of different amounts of stratified drift on flow duration is summarized in figure 1, which shows, by 10 percentiles of basin area underlain by stratified drift, the average flow-duration curves that would have applied to unregulated streams in the gently rolling terrain of Connecticut for the reference period 1931–60 if the average streamflow had been 1.80 cfs per sq mi. These curves were derived from data presented in table 1, for drainage areas that range from 11.6 to 1,545 square miles, but they probably apply to basins of a considerably wider range in area. They can also be used for areas having similar geology and topography throughout much of southern New England where the climate is similar to that of Connecticut.

For most gaging stations there is very good agreement between the data in table 1 and the average curves in figure 1, which is thought to indicate uniformity within each type of glacial drift. In table 1 the measured percentages of stratified drift for most sites are comparable with the effective percentages of stratified drift (the percentage required for the best fit of data to average curves). However, the flow-duration curves indicate that flow from a few basins does not conform as closely to the measured percentages

TABLE 1.—*Drainage area, area of stratified drift, average annual flow, and duration of daily flow at selected stream-gaging stations in Connecticut*

[Flow data are adjusted to the period Oct. 1, 1930 to Sept. 30, 1960]

| Station No. | Gaging station | Total drainage area (sq mi) | Stratified drift | | | Average annual flow (cfs per sq mi) | Flow (cfs per sq mi) which was equaled or exceeded for indicated percentage of time, adjusted to an average annual flow of 1.80 cfs per sq mi | | | | | | | | | | | | |
|---|---|---|---|---|---|---|---|---|---|---|---|---|---|---|---|---|---|---|---|
| | | | Measured area (sq mi) | Percentage of total area | | | 1 | 5 | 10 | 20 | 30 | 40 | 50 | 60 | 70 | 80 | 90 | 95 | 99 |
| | | | | Measured | Effective [1] | | | | | | | | | | | | | | |
| 1195 | Willimantic River near South Coventry | 121 | 23.3 | 19.2 | 25 | 1.76 | 9.4 | 5.1 | 3.8 | 2.65 | 2.05 | 1.6 | 1.2 | 0.95 | 0.70 | 0.47 | 0.29 | [2] 0.18 | [2] 0.08 |
| 1200 | Hop River near Columbia | 76.2 | 9.91 | 13.0 | 13.0 | 1.67 | 11 | 5.7 | 4.1 | 2.7 | 2.0 | 1.5 | 1.1 | .77 | .52 | .31 | .17 | .11 | .06 |
| 1210 | Mount Hope River near Warrenville | 27.8 | 1.94 | 7.0 | 11 | 1.87 | 12 | 5.9 | 4.1 | 2.7 | 1.95 | 1.45 | 1.1 | .75 | .50 | .29 | .14 | .09 | .04 |
| 1220 | Natchaug River at Willimantic | 169 | 29.6 | 17.5 | 17.5 | 1.80 | 11 | 5.6 | 4.0 | 2.7 | 2.0 | 1.5 | 1.15 | .82 | .58 | .36 | .19 | [2] .10 | [2] .03 |
| 1225 | Shetucket River near Willimantic | 401 | 72.2 | 18.0 | 18.0 | 1.76 | 10 | 5.4 | 3.9 | 2.65 | 2.0 | 1.55 | 1.2 | .87 | .60 | .40 | .25 | .17 | .10 |
| 1230 | Little River near Hanover | 29.1 | 5.26 | 18.1 | 22 | 1.92 | 10 | 5.3 | 3.9 | 2.65 | 2.0 | 1.55 | 1.15 | .86 | .63 | .46 | .33 | .25 | .16 |
| 1240 | Quinebaug River at Quinebaug | 157 | ------ | ------ | 29 | 1.75 | 9.0 | 5.0 | 3.7 | 2.6 | 2.0 | 1.6 | 1.25 | .95 | .70 | [2] .48 | [2] .29 | [2] .18 | [2] .07 |
| 1255 | Quinebaug River at Putnam | 331 | ------ | ------ | 26 | 1.77 | 8.9 | 5.5 | 3.8 | 2.65 | 2.0 | 1.6 | 1.25 | .94 | .69 | .49 | .30 | .21 | .11 |
| 1260 | Five Mile River at Killingly | 58.2 | 16.9 | 29.0 | 32 | 1.79 | 8.5 | 5.0 | 3.7 | 2.6 | 2.0 | 1.6 | 1.3 | 1.0 | .81 | [2] .63 | [2] .44 | [2] .30 | [2] .12 |
| 1265 | Moosup River at Moosup | 83.5 | 20.4 | 24.4 | 24.4 | 1.91 | 9.4 | 5.5 | 4.0 | 2.65 | 2.0 | 1.55 | 1.2 | .94 | .63 | [2] .38 | [2] .20 | [2] .12 | [2] .06 |
| 1270 | Quinebaug River at Jewett City | 711 | ------ | ------ | 30 | 1.80 | 8.3 | 5.1 | 3.8 | 2.6 | 2.0 | 1.6 | 1.25 | 1.0 | .78 | .55 | [2] .33 | [2] .19 | [2] .05 |
| 1275 | Yantic River at Yantic | 88.6 | 17.5 | 19.8 | 15 | 1.83 | 11 | 5.7 | 4.0 | 2.7 | 2.0 | 1.5 | 1.1 | .80 | .55 | .31 | .16 | .11 | .07 |
| 1845 | Scantic River near Broad Brook | [3] 85.8 | 38.4 | 44.8 | 44.8 | 1.50 | 7.1 | 4.7 | 3.5 | 2.55 | 2.0 | 1.7 | 1.35 | 1.15 | .92 | .74 | .57 | .46 | .31 |
| 1925 | Hockanum River near East Hartford | 74.5 | 29.6 | 41.6 | 41.6 | 1.58 | 7.4 | 4.5 | 3.5 | 2.55 | 2.0 | 1.7 | 1.4 | 1.15 | .98 | .79 | .56 | .40 | [2] .19 |
| 1935 | Salmon River near East Hampton | 105 | 16.5 | 15.7 | 15.7 | 1.76 | 11 | 5.5 | 4.0 | 2.7 | 2.0 | 1.55 | 1.15 | .80 | .50 | .30 | .18 | .13 | .07 |
| 1940 | Eightmile River at North Plain | 18.6 | 2.51 | 13.5 | 13.5 | 2.13 | 11.5 | 5.6 | 4.0 | 2.7 | 2.0 | 1.6 | 1.2 | .82 | .46 | .25 | .13 | .08 | .03 |
| 1950 | Menunketesuck River near Clinton | 11.6 | .88 | 7.5 | 10 | 1.97 | 11.5 | 5.8 | 4.1 | 2.75 | 2.0 | 1.5 | 1.1 | .72 | .41 | .23 | .12 | .07 | .02 |
| 1990 | Housatonic River at Falls Village | 632 | ------ | ------ | 24 | 1.75 | 9.2 | 5.3 | 3.9 | 2.65 | 2.0 | 1.55 | 1.15 | .90 | .69 | .51 | [2] .37 | [2] .30 | [2] .21 |
| 2000 | Tenmile River near Gaylordsville | 204 | ------ | ------ | 17 | 1.49 | 10.5 | 5.5 | 4.0 | 2.7 | 2.0 | 1.55 | 1.2 | .84 | .56 | .35 | .21 | .15 | .10 |
| 2005 | Housatonic River at Gaylordsville | 994 | ------ | ------ | 26 | 1.68 | 8.9 | 5.2 | 3.9 | 2.7 | 2.0 | 1.6 | 1.25 | .93 | .68 | .49 | .34 | [2] .28 | [2] .19 |
| 2015 | Still River near Lanesville | 68.5 | 18.8 | 27.4 | 27.4 | 1.83 | 9.2 | 5.1 | 3.7 | 2.6 | 2.0 | 1.55 | 1.2 | .92 | .70 | .54 | [2] .39 | [2] .32 | [2] .23 |
| 2030 | Shepaug River near Roxbury | 133 | 9.89 | 7.4 | 12 | 1.89 | 10.5 | 5.5 | 4.0 | 2.75 | 2.0 | 1.5 | 1.1 | .71 | .46 | .27 | .14 | .09 | .06 |
| 2055 | Housatonic River at Stevenson | 1,545 | ------ | ------ | 25 | 1.73 | 8.9 | 5.0 | 3.8 | 2.7 | 2.0 | 1.60 | 1.25 | .93 | .68 | .48 | .29 | [2] .17 | [2] .06 |
| 3065 | Connetquot River near Oakdale, Long Island, N.Y. | [4] 24 | 24 | 100 | 100 | 1.67 | 3.2 | 2.5 | 2.3 | 2.1 | 2.0 | 1.85 | 1.75 | 1.65 | 1.55 | 1.45 | 1.35 | 1.25 | 1.1 |

[1] Area adjusted to give good fit of data to average curves.
[2] Affected by regulation.
[3] All data adjusted so as to exclude area of relatively impervious glaciolacustrine deposits.
[4] Ground-water drainage area, composed wholly of stratified drift, is about 27 sq mi.

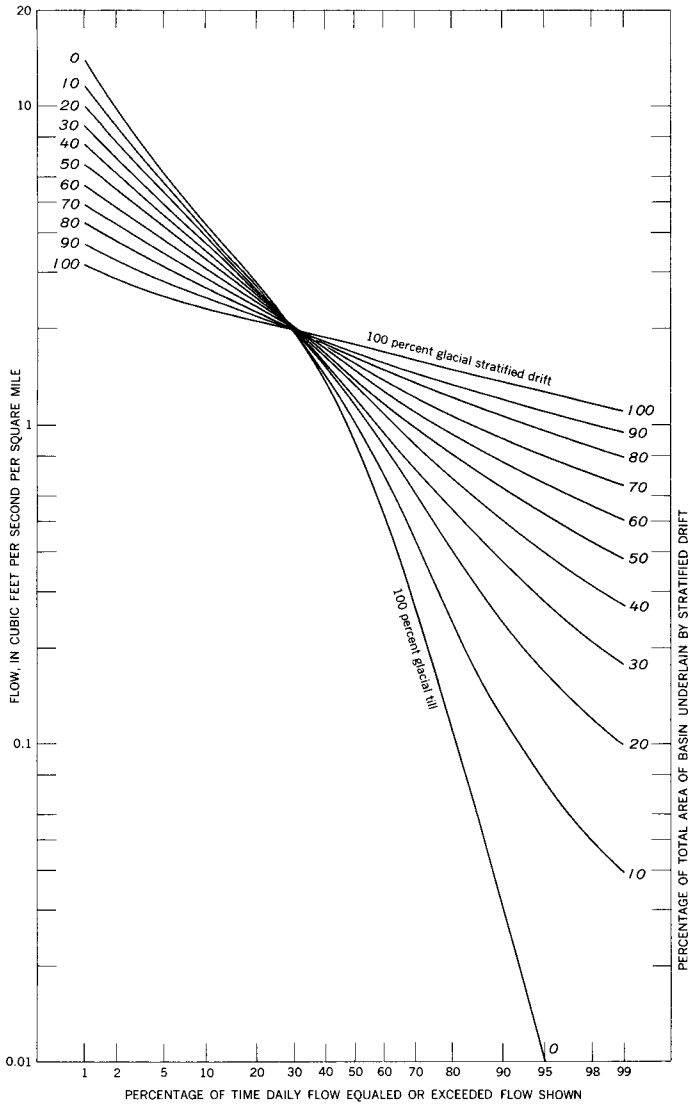


FIGURE 1.—Family of flow-duration curves which illustrate[8] the relation between variations in surficial geology and variations in the flow of streams. These curves apply to unregulated streams in gently rolling terrain in Connecticut that have an average flow of 1.80 cfs per sq mi. The curves are based on data from 24 gaging stations for the reference period October 1930 through September 1960.

of stratified drift as does the flow of the other streams. Flow-duration curves for stations 1195 and 1260 are affected by storage and regulation in large reservoirs within their basins; the net effect on flow duration appears to be similar to an increase in the percentage of stratified drift in the drainage area. The reason for the difference between the measured amount of stratified drift and the effective amount for stations 1210, 1230, and 1275 has not been determined.

Inspection of the curves in figure 1 reveals that the streamflow which is equaled or exceeded 30 percent of the time, in this type of terrain and at an average runoff of 1.80 cfs per sq mi, is always 2.0 cfs per sq mi. Evidently this rate is independent of the proportion of the drainage area covered by stratified drift. Flows which are equaled or exceeded less than 30 percent of the time are highest in basins underlain by till, and are progressively lower in basins with progressively greater amounts of stratified drift. On the other hand, flows equaled or exceeded more than 30 percent of the time are progressively higher in the basins which are underlain by progressively greater proportions of stratified drift. Other information can be read from these graphs. Thus, the curves indicate that for drainage areas underlain entirely by stratified drift, streamflows equaled or exceeded 94 and 90 percent of the time (which are approximately equivalent to the median annual 7-day minimum flow and 30-day minimum flow, respectively) are 1.30 and 1.37 cfs per sq mi, respectively. Corresponding streamflows from basins entirely of till are only 0.013 and 0.030 cfs per sq mi.

The curves shown in figure 1 are thought to be applicable to areas of gently rolling terrain composed of relatively uniform deposits of glacial till and stratified drift, where the climate is similar to that of Connecticut and where the average streamflow was 1.80 cfs per sq mi for the period October 1930 through September 1960. For the gaging stations in Connecticut which are listed in table 1, the average streamflow for this period ranged from 1.50 to 2.13 cfs per sq mi or from 83 to 118 percent of 1.80 cfs per sq mi. Any curve in figure 1 which is applied to an ungaged area should be adjusted to an approximated average streamflow that is based upon the known average flows for nearby streams or upon a map of the surrounding area on which isopleths have been drawn to indicate variations in average flow.

## REFERENCE

Flint, R. F., 1930, The glacial geology of Connecticut: Connecticut State Geol. and Nat. History Survey Bull. 47, 294 p., 1 map.

# PRELIMINARY EVALUATION OF THREE TRACERS USED IN HYDRAULIC EXPERIMENTS ON SAND MODELS

By J. M. CAHILL, Phoenix, Ariz.

*Abstract.*—In studies of movement of fluid through porous material, ion exchange and adsorption of dissolved particles on solids create an apparent delay in the movement of liquids tagged with tracers. In a laboratory study of the effect of tracers on this delay, the breakthrough and elution characteristics of the following three tracer solutions passing through a saturated column of loosely packed sand were compared: (1) radiophosphorus ($P^{32}$), (2) organic dye in a glycerine base, and (3) sodium chloride. Experimental data showed little difference between the effect of the three tracers on the movement of the fluid when the sand was chemically and physically compatible with the tracers.

Study of the movement of fluid through porous material requires the use of tracers to define the volume and velocity of the fluid. In sand models there are many different tracers that may be used for this purpose, the choice depending to a great extent on the nature of the problem to be studied. Only in rare instances is a tracer 100 percent effective in the analysis of experimental models, primarily because of the chemical and physical interactions between the fluids and solids in the system. These interactions lead to anomalies between the velocity determined from the true movement of the fluid and from the apparent movement. Sheppard (1962, p. 2) pointed out that tracers which are of the same composition as the fluid are required to portray exactly the behavior of a fluid in a particular environment. But if this stipulation were rigorously held, the tracer concept would be valueless, inasmuch as it is obviously impossible for the tracer to be identical with the fluid and at the same time distinct from it.

In hydraulic experiments on flow in sand models, the ideal tracer is one that travels with the fluid through the porous solid and is easely detectable. The chances of obtaining the ideal tracer are poor, because in most instances a part of the tracer is retained by the sand grains through a process of absorption and through ion exchange. Because a large surface area is available for the transfer of the tracer to the grains, adsorption and ion-exchange processes may cause significant loss of the tracer substance in a short distance (Ogata, 1964, p. G1). Thus, a correction term must be added on any mathematical expression describing the fluid movement.

Adsorption is the taking up of dissolved material on the surface of a solid in contact with the solution, and ion exchange is a reversible chemical reaction in which ions are exchanged betweeen a solid and a fluid mixture (Rose and Rose, 1956, p. 24, 597). These chemical processes are difficult to distinguish, however, without a study of surface chemistry; hence, in macroscopic studies of this nature these processes cannot be differentiated. In this report any mechanism involving the transfer of mass between the liquid and the solid is termed simply an "exchange" process.

The objective of this investigation was to evaluate the rates at which three selected fluid tracers pass through and can be flushed from silica sand. Radiophosphorus ($P^{32}$) and a green organic dye in a glycerine base are compared with a sodium chloride solution. Sodium chloride solutions are generally agreed to be effective tracers whenever the effects of the difference in the densities of the tracer-bearing and the preexisting fluids can be eliminated. Kaufman and Orlob (1956) utilized this same basis to compare various tracers, both radioactive and nonradioactive, and found that none of the other tracers tested was as effective as the common salt solution.

Dye in sand-model experiments is used primarily as a visual indicator of various flow phenomena, and radioactive phosphorus is used as a means of quantitatively defining the phenomena. Density effects associated with the use of salt can be readily eliminated by mixing glycerine and the clear water flowing through the model if the exchange (transfer of mass between the fluid and the solid) is small. In this experiment, inasmuch as the fluid was introduced from the bottom of the column,

U.S. GEOL. SURVEY PROF. PAPER 550-B, PAGES B213-B217

the slight differences in density between the two fluids could be ignored, and therefore glycerine was not added. Radiotracers are effective in obtaining quantitative data on the mass transport of fluids and on flow behavior because the tracers can be measured in extremely small quantities. Radiophosphorus, one of the common elements used in medical research, has two advantages as a radiotracer: it is readily available, and the radioactivity level of the tracer fluid (generally less than 1 millicurie per liter of liquid) is low. Radiophosphorus as a tracer was shown by Skibitzke (1960) to be a valuable tool in observing microscopic flow characteristics and fluid dispersion in granular material.

## EXPERIMENTAL EQUIPMENT AND PROCEDURE

The experiment was conducted with a vertical column of loosely packed saturated silica sand enclosed in a plastic tube, 2 inches in diameter and 24 inches long (fig. 1). Results of the mechanical analysis of the sand are given in figure 2. Fluid movement through the column was upward as indicated in figure 1*A*, and the effluent of displaced fluid was monitored as close as possible to the downstream end of the column. Positions of the head tanks were adjusted slightly for the different tracer runs so that the fluid flux was the same for all.

During use of the $P^{32}$ tracer the radioactivity of the effluent, which is a function of the concentration of $P^{32}$ in the effluent, was measured in a "well-type" counter containing a sodium iodide scintillation crystal. A pulse-height analyzer was used in conjunction with the well counter to minimize the backscattering of the bremsstrahlung or secondary-gamma radiation. The read-out of the radiation analyzer was recorded by a continuous graphic recorder as the effluent passed through a thin-walled brass tube in the well counter (fig. 1*B*). The concentration of sodium chloride tracer was measured by means of an electrical conductivity probe (fig. 1*C*). The instrumentation consisted of a wheatstone bridge in conjunction with a continuous graphic recorder to show the electrical conductivity of the fluid effluent. The concentration of green-dye tracer was measured by means of a photoelectric color den-

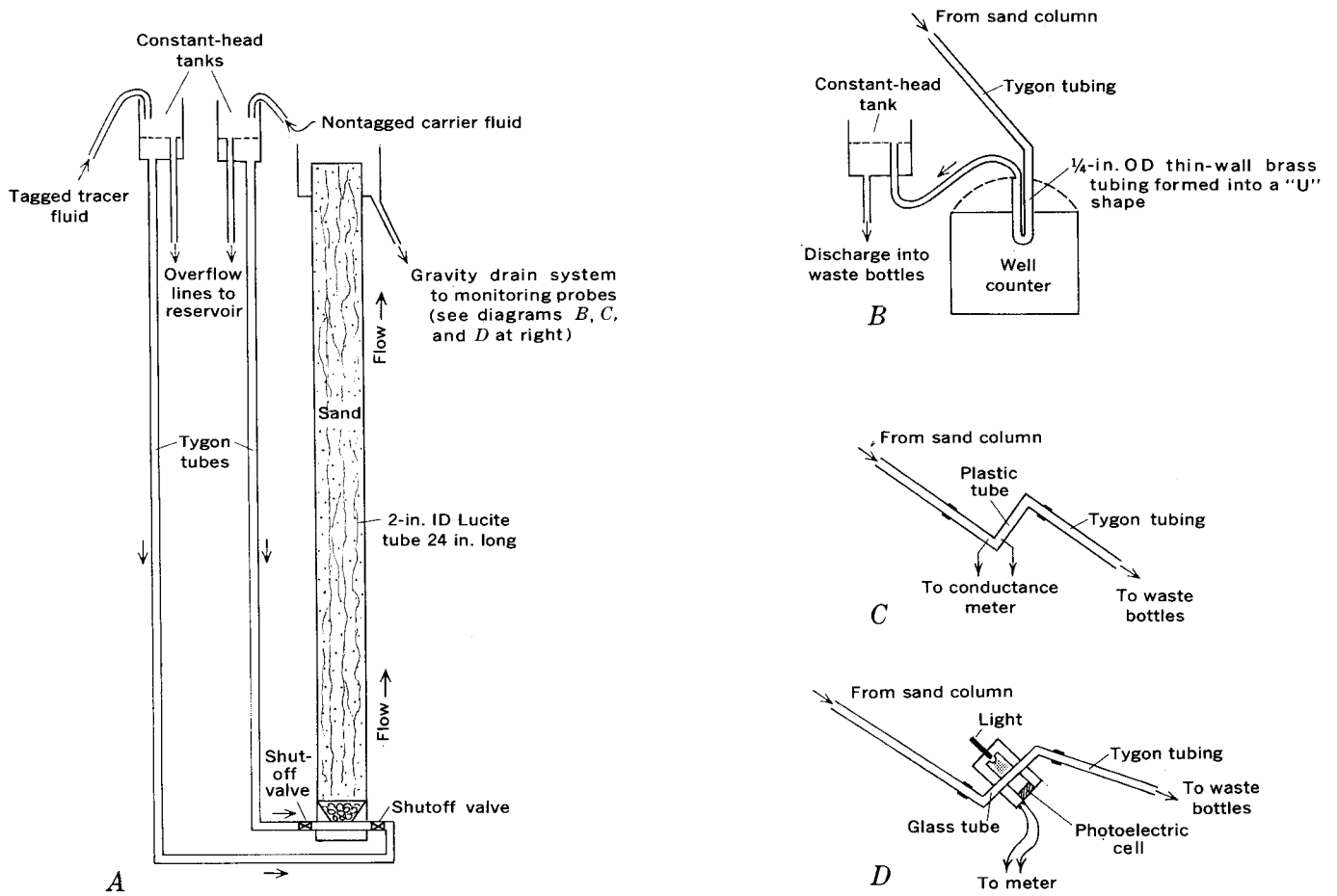


FIGURE 1.—Diagram of equipment used in experiment. Effluent from the sample column (*A*) is monitored with: (*B*) radiation probe, (*C*) conductivity probe, and (*D*) photoelectric-cell probe (not to scale).

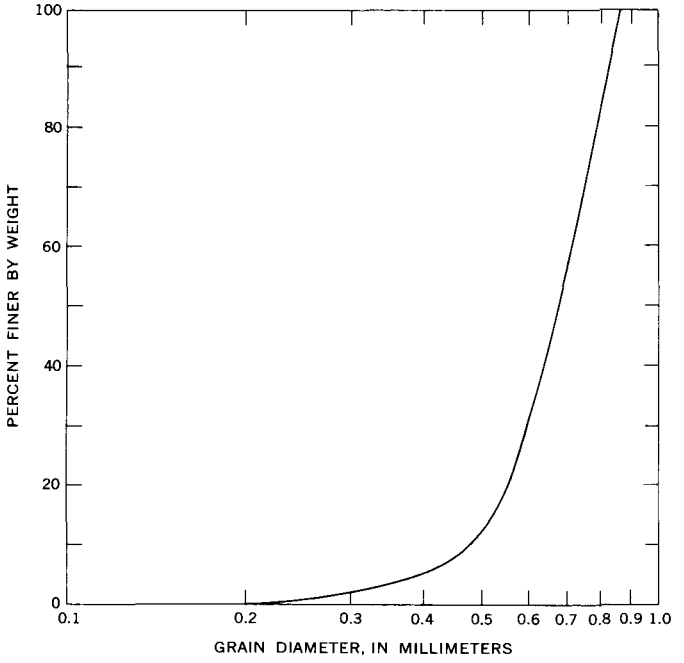


FIGURE 2.—Grain-size distribution curve of sand used in sample column.

sitometer (fig. 1*D*) and was continuously recorded. This measurement was made as the fluid passed through a glass tube of uniform thickness.

Figure 3 shows the rating curves for the three tracer solutions, measured with the previously described equipment. The radiotracer shows a linear relationship between radioactivity and meter deflection on a radiation analyzer. On the other hand, the salt solution and the dye-colored fluid show nonlinear relationships between concentration and meter deflection. The apparent reason for the relatively small changes in meter deflection that represent some large changes in salt and dye tracer concentrations lies in the nature of the probing elements in the monitoring circuits. Thus,

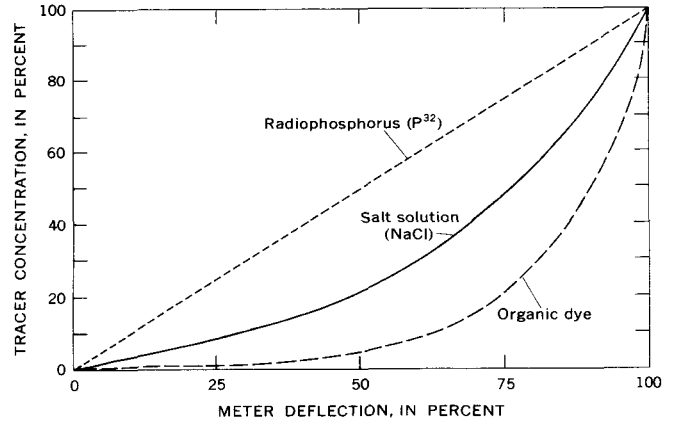


FIGURE 3.—Rating curves for the detection of tracer concentration.

at low salt concentrations there is less chance for the chloride ions to form a conductive path between the probe electrodes and hence, there is little flow of electric current. As the salt concentration increases and more ions are available to form conductive paths an increase in the flow of electric current is evident but the increase is not necessarily linear with respect to salt concentration. Similarly, for low concentrations of dye tracer the only filtering of the light beamed toward the photoelectric cell (probe) is due to the random scattering of the few dye molecules in solution. As the dye concentration increases there is less chance for the light source to reach the photoelectric cell, but again the relationship is not linear. The radiotracer measurements are much more precise in both the upper and lower ranges of the concentrations used in the test.

Each test using $P^{32}$ of dye was designed to minimize the exchange potential by making the tagged fluid as chemically like the untagged fluid as possible, and by running the untagged fluid through the sand column steadily and for a long enough period before the test for exchange equilibrium to be reached. For the radiotracer, 0.3*N* phosphoric acid solution was circulated through the sand column, before the radiophosphorus tracer was introduced, for a length of time sufficient to allow exchange equilibrium between the liquid and solid to be attained. After exchange equilibrium was reached a 0.1*N* phosphoric acid solution carrying the radiophosphorus tracer was introduced into the column. Because the sand material had previously been saturated with nonradioactive phosphorus, the delay in tracer breakthrough (point in time at which the tracer appears at virtually full strength in the effluent) was due only to the exchange between radioactive phosphorus and the nonradioactive phosphorus on the sand.

Since the fluid which carries the green organic-dye tracer is a mixture of glycerine and water, an uncolored but otherwise identical mixture of glycerine and water was circulated through the porous medium before the green tracer fluid was introduced into the column. This minimized the exchange effects between the liquid and the matrix, and eliminated any density difference between tracer fluid and preexisting fluid.

In accord with the procedure used by Kaufman and Orlob (1956), the column used to evaluate the breakthrough of the sodium chloride solution was prepared by circulating only clear tap water through the porous medium before introduction of the tracer. The salt tracer consisted of 10 grams of common table salt per liter of clear tap water.

In each test run and for all tracer fliuds the fluid used initially to saturate the column was displaced

with the fluid containing the tracer. The displacement phase was continued until the column effluent indicated a tracer-fluid concentration of 100 percent. At this point the tracer fluid was in turn flushed out, using the fluid that had initially saturated the column. For example, the 0.3*N* solution of phosphoric acid was used to flush from the column the 0.1*N* solution of phosphoric acid carrying the $P^{32}$.

## EXPERIMENTAL RESULTS

The results of the test runs are shown in figures 4 and 5. The curves in figure 4 represent the breakthrough of the tracers, measured at a given point in the effluent stream and plotted against the quantity of tracer fluid passed through the sand column. A single flow rate was used throughout the experiment. The quantities of fluid flow are defined in terms of multiples of the total pore volume of the column. The curve for the radiophosphorus tracer depicts an average of two tracer runs through the sand column. The curves for the organic dye and weak salt solutions are for averages of three runs each.

Because the tracers were introduced onto the samples at a single rate, the generally parallel nature of the graphs in figure 4 indicates that all tracers passed through the sand column at about the same rate. Moreover, the parrallelism of the concentration-distribution curves for the organic-dye and radiophosphorus tracers, until they reach a point of 80-percent tracer-fluid concentration, suggests that little or no exchange of either the radiotracer or the dye takes place until the higher concentration range is reached.

The results of the flushing phase are shown by the elution (point in time at which the tracer virtually disappears from the effluent) curves in figure 5. These curves represent averages of 2 flushing runs for the radiotracer and 3 each for the salt and organic-dye solutions. Because a single flow rate was used, the elution curves in figure 5 show that the 1-percent concentration of tracer fluid was reached more quickly for the salt solution than for the other two tracers. The experiment with the organic-dye tracer required the longest time and hence the largest volume of fluid to reach the 1-percent concentration of tracer fluid. The elution curves for the radiotracer and the dye suggest that exchange reactions took place between these tracers and the sand. When about 1.1 sand-pore volumes of fluid had passed through the columns, more than 50 percent of the tracer fluids had been flushed out. However, in the region of the graph where the tracer concentrations are 10 percent or less there are definite rises in the curves that could be explained by the longer time required for the flushing fluid to reverse the exchange reactions between the tracer and the sand.

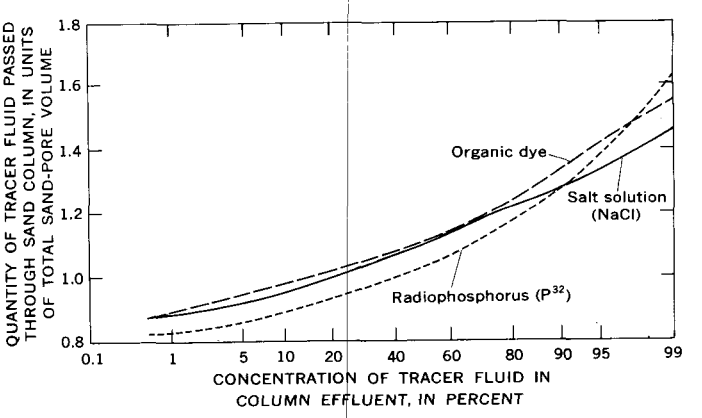


FIGURE 4.—Changes in concentration of tracer in effluent from column of silica sand with passage of tagged fluid through column.

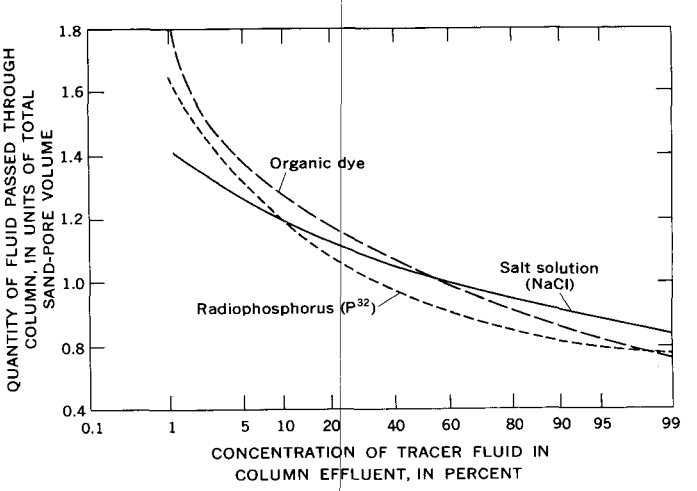


FIGURE 5.—Changes in concentration of tracer in effluent from column of silica sand when tracer fluid is flushed from column.

## CONCLUSIONS

Under the conditions of the breakthrough experiments, for the concentration ranges studied there appears to be little difference among the three tracer fluids except in the higher parts of the concentration ranges. At the higher concentrations, significant differences between the tracers are indicated (fig. 4) by the apparent greater time (reflected by greater volume) required for the radiotracer and dye solutions to pass through the sand columns and to reach virtually full strength in the effluent. These differences may be due to (1) the nonlinearity of the relations between concentration of salt or dye in a tracer, and the meter reading; or (2) the increase in ion exchange and adsorption potential with higher tracer-fluid concentrations. However, the curves drawn for the elution experiments (fig. 5) suggest that the latter reason is more likely, by virtue of the longer time required to flush the radiophosphorus and dye tracers from the sand columns.

Additional study is needed to define the extent to which exchange potentials are reduced by observing

the special precautions described. In addition, the particular influence of velocity of tracer-fluid movement and surface area of sand grains in contact with the tracer fluid should be evaluated. This could be done by establishing a fluid flux through the sand column for a series of experiments covering a range of fluid velocities and tracer concentrations. The effect of the surface area of sand grains could be studied by using several samples which have comparable particle-size distribution curves but different median grain diameters.

## REFERENCES

Kaufman, W. J., and Orlob, G. T., 1956, An evaluation of groundwater tracers: Am. Geophys. Union Trans., v. 37, no. 3, p. 297–306.

Ogata, Akio, 1964, The spread of a dye stream in an isotropic granular medium: U.S. Geol. Survey Prof. Paper 411-G, 11p.

Rose, Arthur and Rose, Elizabeth, 1956, The condensed chemical dictionary, 5th ed.: New York, Reinhold Publishing Corp., 1200 p.

Sheppard, C. W., 1962, Basic principles of the tracer method: New York, John Wiley and Sons, Inc., 282 p.

Skibitzke, H. E., 1960, Radioisotopes in the laboratory for Studying ground-water flow: Internat. Assoc. Sci. Hydrology Comm. of Subterranean Water, Helsinki, Finland, pub.52, p. 513–523.

# TRUCK-MOUNTED HYDRAULIC-LIFT SURVEYING TOWER

By HUGH B. LOVING and WALTER L. SAPPINGTON, Washington, D.C.

*Abstract.*—A surveying tower mounted on a 1-ton truck equipped with a newly developed hydraulic-lift system has highway-speed mobility and can be raised quickly in a confined area by one man. The tower has basically the same inner- and outer-unit design as that developed and reported on in 1962, but it is mounted on a truck rather than a trailer and can be extended to a height of 76 feet. The tower is hinged at the base to a supporting structure that is mounted on the rear of the truck, and is raised hydraulically. A stabilization system eliminates the need for guy wires. The observation platform is equipped with supports for an electronic distance-measuring instrument and flashing lights, and is designed to carry the weight of several men.

The development of a portable surveying tower for use in mapping by the Topographic Division of the U.S. Geological Survey was reported by Buckmaster and Murphy in 1962. This was a trailer-mounted tower that was towed by truck and raised and lowered with a hand winch. Its length was limited to 50 feet for towing. At that time, it was realized and pointed out that truck-mounted towers would have definite advantages—increased height, faster transportation, and ease and rapidity in erection. Consequently, design efforts were continually directed to this end.

The latest model surveying towers designed and used by the U.S. Geological Survey are truck mounted. Furthermore, hydraulic power has replaced the hand winch. The new tower has increased height (adjustable to a maximum of 76 feet) and highway-speed mobility, and is easily raised and lowered in a relatively confined space. The trailer-mounted tower took 2 experienced men at least an hour to set up, whereas the new truck-mounted tower can be raised or lowered, fully assembled, in 1 minute by 1 man. A built-in stabilization system permits use of the tower without securing it with guy wires.

The detailed description that follows covers the four components of the unit: transporting truck, hydraulic lift, surveying tower, and stabilization system.

## TRANSPORTING TRUCK

The truck used for transporting the tower and the hydraulic lift is a standard 1-ton model truck equipped with single or dual wheels and a 4-speed transmission. Two girders supporting a flatbed are installed on the truck chassis. A storage bin is provided under the flatbed for extra straight-tube parts of the tower for use when a higher tower is required. Two tool boxes (*1*, fig. 1) also are installed under the bed of the truck.

A support assembly (*2*, fig. 1) is mounted on the front of the truck to support the top portion of the tower when in transit. The tower is not fastened to the front support, but rests on it, thus eliminating the transfer of torsional stresses from the truck frame to the tower. The front support is designed to give maximum support to the tower and to provide the best visibility for the driver.

The overall height of the truck and the tower, when lowered, is approximately 11½ feet. For long-distance moves the tower is disassembled to a length of 32 or 38 feet, for which a special permit is not required for highway travel. For short moves between stations, where roads permit, the tower can be transported fully assembled.

## HYDRAULIC LIFT

Hydraulic power was chosen because (1) the necessary forces are obtained in equipment that occupies less space than other prime movers; (2) hydraulic components are uncomplicated by gear and clutch mechanisms, and are readily serviced; and (3) hydraulic operation is easily controlled, smooth, and not affected by variations in load.

The hydraulic cylinders (*1*, fig. 2) are double acting to provide the force necessary for lowering as well as raising the tower. The overall closed length of the cylinders is 49 inches. With 1,000 pounds per square inch line pressure, the lift capacity per cylinder is about 7,000 pounds.

The hydraulic pump (*1*, fig. 3) has a 2¼-horsepower electric motor of ball-bearing construction. The motor (*2*, fig. 3) may be operated on 12 or 24 volts d.c.; hence, the truck battery can furnish the external power for the motor. A gear pump having a capacity of 3

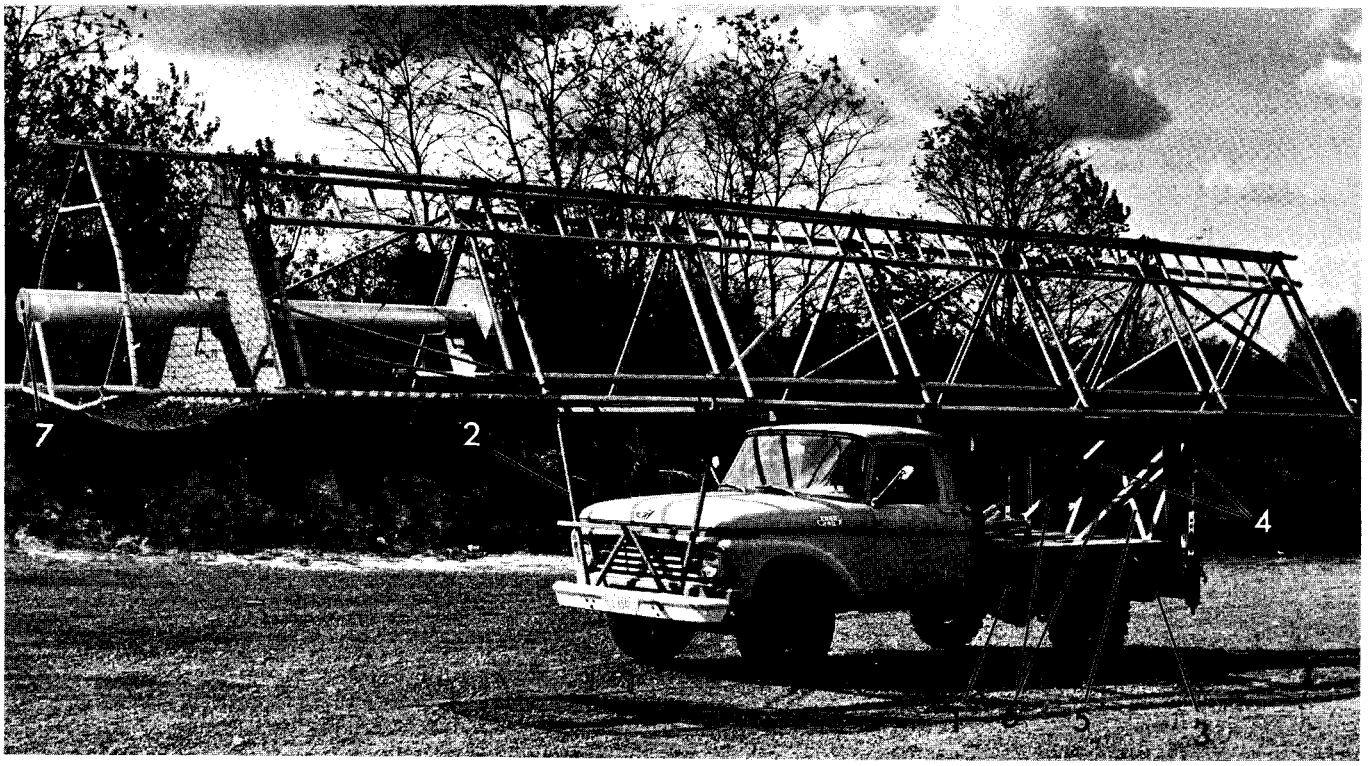


*1*, Tool box.
*2*, Front-support assembly.
*3*, Hydraulic-fluid storage reservoir and control box.
*4*, Posts.
*5*, Cross braces.
*6*, Reinforcing beams.
*7*, Instrument mount.

FIGURE 1.—Tower and truck ready for transit. (Without stabilization system.)

gallons per minute at 1,000 psi was selected for optimum volumetric efficiency.

The control valve for raising and lowering the tower is a self-centering plunger; when the lever (*3*, fig. 3) is released, it returns to neutral and the position of the boom is held. The capacity of the valve is 16 gpm with a pressure of 1,250 psi. Furthermore, the control valve has a built-in relief valve that prevents it from locking and prevents unequal pressures from forming in the hydraulic system. The control valve and the switch for the hydraulic-pump motor are at the rear of the truck so that the operator can watch the erecting operation and see the area in which the tower is to be centered. The valve and switch are mounted in a box on top of the 5-gallon storage reservoir for the hydraulic fluid (*3*, fig. 1).

The lift assembly consists of twin steel booms (*2*, fig. 2) fastened to the outer unit of the tower. It is hinged to a supporting structure mounted on the rear of the truck. The supporting structure is made up of 2 steel posts (*4*, fig. 1) attached to the flatbed girders and 2 steel cross pieces (*9*, fig. 2) attached across the top and bottom of the posts; cross braces (*5*, fig. 1) between the posts and 2 steel reinforcing beams (*6*, fig. 1) attached to the girders at approximately a 30° angle make the structure rigid.

Two lateral outriggers (*3*, fig. 2) are mounted on each side of the supporting structure for added support and ease in plumbing the surveying tower. Each outrigger can be extended horizontally approximately 30 inches to increase the base of support to 130 inches. To compensate for variations in the terrain, the outriggers are designed with a 36-inch adjustment for height (see fig. 4).

## SURVEYING TOWER

The lightweight surveying tower is basically the same as that described earlier by Buckmaster and Murphy (1962). It consists of an inner unit (*4*, fig. 2) and an outer unit (*5*, fig. 2), both similar in appearance and made from tubular aluminum. The inner unit, physically separate from the outer unit, supports the theodolite while the outer unit supports the observer's platform. Thus the theodolite is not affected by

797-218 O—66——15

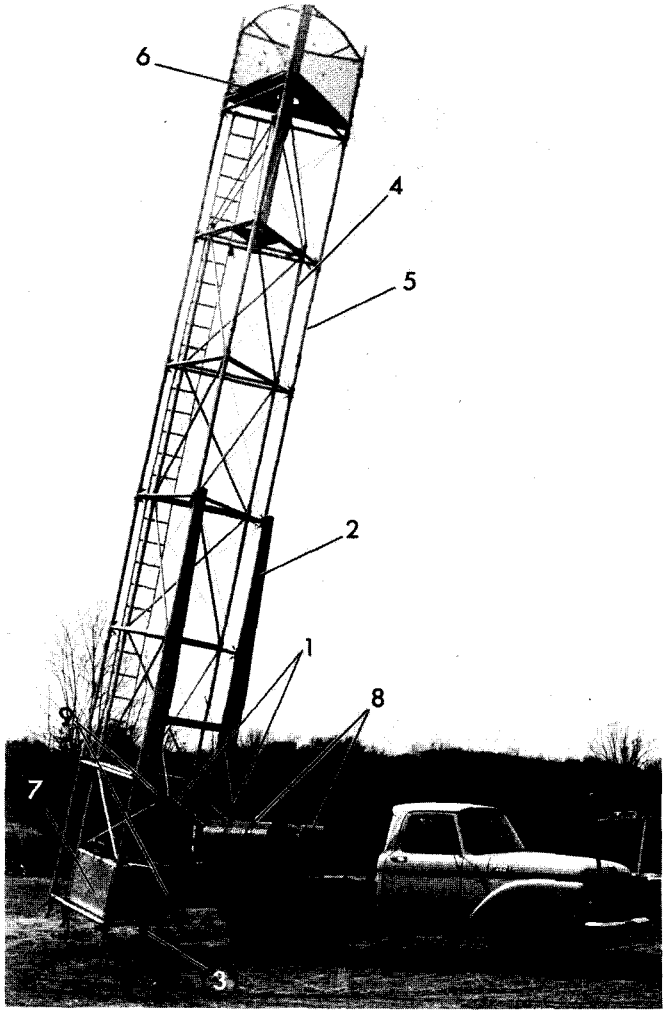


*1*, Hydraulic cylinder.
*2*, Boom assembly.
*3*, Lateral outrigger.
*4*, Inner unit of tower.
*5*, Outer unit of tower.
*6*, Platform.
*7*, Stabilization tank.
*8*, Storage tanks for stabilization-tank fluid.
*9*, Cross pieces.

FIGURE 2.—Tower equipped with stabilization tank.

movements of the observer. The weight of each unit is approximately 5 pounds per foot of length. The height of the tower can be varied from 10 to 76 feet in 6-foot increments by bolting on or removing 6-foot sections before it is raised. The tower can be set up in an open area roughly equal to the width of the truck and the length of the tower.

The outer unit is diagonally braced by crossed wire rope to give a maximum strength-to-weight ratio. In addition to being a support for the observer's platform, it is equipped with supports for electronic distance-measuring instruments and flashing lights. The platform (*6*, fig. 2), which is reached by an attached ladder, is designed to carry the weight of several men. Surrounding the platform is a nylon-mesh net for the safety of the observers and the instruments.

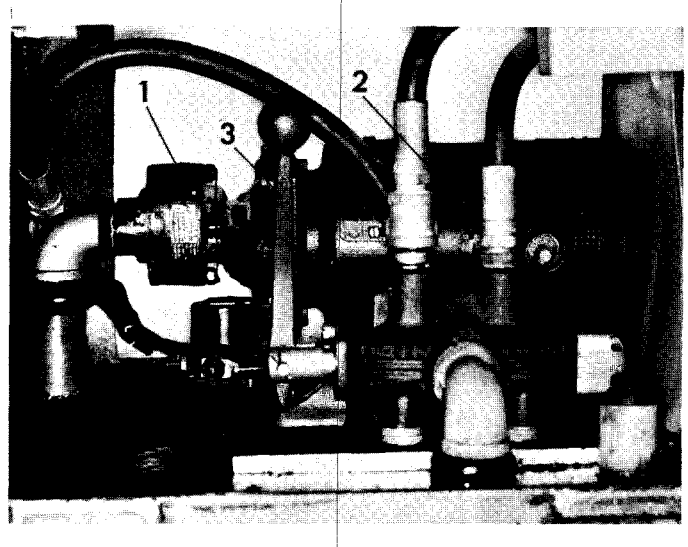


*1*, Hydraulic pump.
*2*, Electric motor.
*3*, Control-valve lever.

FIGURE 3.—Electric hydraulic pump and control valve.

The inner unit of the tower is diagonally braced by aluminum tubing. Attached to the top of the unit is a hollow aluminum column (*7*, fig. 1), 80 inches in length and 6 inches in diameter, which extends through the outer unit platform and acts as a pedestal for the theodolite. The column is adjustable in height to accommodate individual observers; it may be completely depressed while the tower is in transit. Hollow tubing is used because it is lightweight and yet will withstand large torques.

Since the outer unit supports the electronic distance-measuring instrument and the inner unit supports the theodolite, the distances and the angles can be read simultaneously by two observers.

The inner unit is plumbed by adjustable legs and footscrews; the outer unit is plumbed by one adjustable leg and the lateral outriggers. Footplates, attached under each footscrew of the inner unit, are curved at each end, similar to skis, so that during erection of the tower the legs will not dig into the ground. The outer unit is bolted to the boom assembly of the hydraulic lift.

## STABILIZATION SYSTEM

An improvement over the previous tower design is the addition of a built-in stabilization system. This system is designed to eliminate movement of the inner unit during observations. When wind velocities were high, the inner unit of the trailer-mounted tower, which was guyed by wires, moved considerably. The truck-mounted tower is stabilized by a liquid-filled tank mounted on the bottom section of the inner unit (*7*, fig. 2). Two storage barrels (*8*, fig. 2) and an

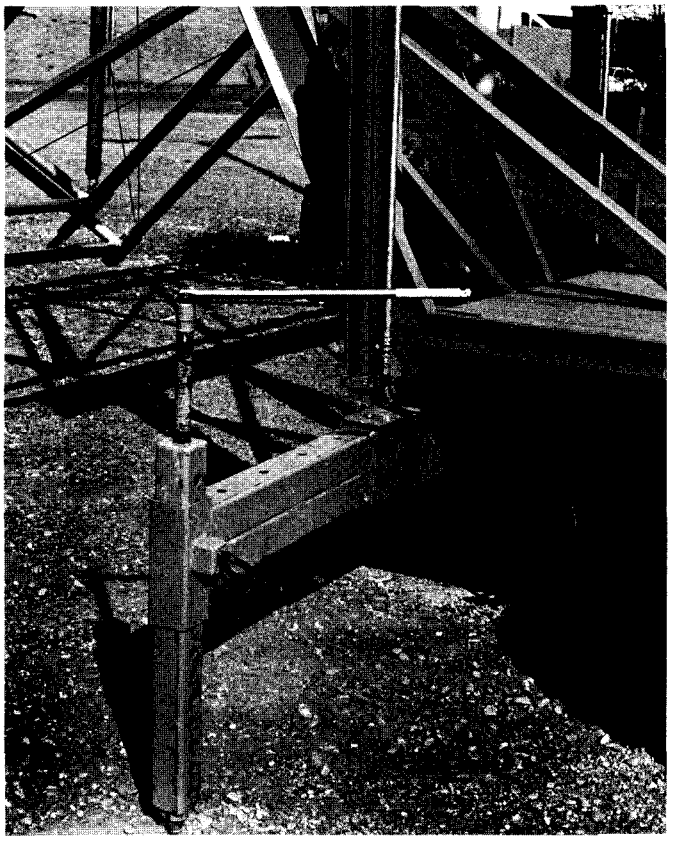

FIGURE 4.—Lateral outrigger adjustable for variations in terrain. (Without footplate.)

electric-powered water pump complete the stabilization system.

The tank is an aluminum triangular container whose sides are 54 inches long and 24 inches high. It has a 12-inch-diameter opening in the center through which the station point can be seen for centering the instrument. A 2-inch-diameter reinforced rubber hose connects the tank to the two storage barrels. When filled with liquid, the stabilization tank weighs approximately 1,000 pounds. When the tower is plumbed and centered over a station point, ethylene glycol and water solution is pumped to the stabilizing tank. The liquid is transferred back to the storage barrels when the tower is lowered.

The two storage barrels are located on the flatbed of the truck. A prototype system used gravity feed to transfer the liquid to and from the stabilization tank. However, when the tower was being lowered, the weight of the liquid-filled tank caused the inner and outer units to rub together; therefore, an electric-powered pump was installed to transfer the liquid to the storage barrels before the tower was lowered.

Further studies of the stabilization system to increase its effectiveness are underway, and an improved system for suspending the inner unit when the tower is lowered is in the design stage at the present time.

## REFERENCE

Buckmaster, J. L., and Murphy, W. D., 1962, Portable surveying tower: Art 217 *in* U. S. Geol. Survey Prof. Paper 450–E, p. E131–E132.

# SUBJECT INDEX

[For major headings such as "Economic geology," "Geophysics," "Paleontology," see under State names or refer to table of contents]

# AUTHOR INDEX





U.S. GOVERNMENT PRINTING OFFICE : 1966 O—797-218